Concepts and Models of Cosmology

VXPhysics.com

Cosmology: Study of the Entire Universe, Its Origin, Evolution, & Ultimate Fate

In the Beginning God Said

Genesis 1:1 "*In the beginning God created the heavens and the earth.*"
Genesis 1:3 "*And God said, Let there be light: and there was light.*"
Genesis 15:5 God said *"Look toward heaven, and number the stars."*
Psalms 19:1 "*The heavens declare the glory of God and the expanse proclaims the work of his hands. Day after day they pour out speech; night after night they communicate knowledg*e."
Romans 1:20 "*For His invisible attributes, that is, His eternal power and divine nature, have been clearly seen since the creation of the world, being understood through what He has made."*

Purpose: Abstracting Mathematical Models of Fundamental Cosmological Concepts

The purpose of this work is to survey, reconstruct, and evaluate the established mathematical framework of modern cosmology, with particular emphasis on the Λ–Cold Dark Matter (ΛCDM) concordance model. This manuscript does not present original theoretical results; rather, it reflects a personal investigation aimed at understanding how the standard equations, assumptions, and observational constraints of cosmology fit together as a coherent and testable framework. Foundational literature, observational data sets, and the canonical equations of relativistic cosmology are reviewed and restated in explicit, computable form.
To reproduce standard cosmological observables, this work employs the Python-based Code for Anisotropies in the Microwave Background (CAMB), a widely used linear Einstein–Boltzmann cosmology solver that evolves perturbations about a FLRW background. CAMB is used to generate cosmic microwave background anisotropy spectra, matter power spectra, and related quantities directly from ΛCDM parameter inputs, following established conventions used by Planck, WMAP, and large-scale structure analyses. The degree of empirical support and internal consistency of the standard model is illustrated through explicit equations, numerical reconstructions, and parameter plots.

"*The first principle is not to fool yourself – and you are the easiest person to fool.*" Richard Feynmann

"*The popular notion that the sciences are bodies of established fact is entirely mistaken. Nothing in science is permanently established, nothing unalterable, and indeed science is quite clearly changing all the time, and not through the accretion of new certainties.*" Karl Popper

"T*he progress of science is strewn, like an ancient desert trail, with the bleached skeletons of discarded theories which once seemed to possess eternal life*." Arthur Koestler

"*Time and again the passion for understanding has led to the illusion that man is able to comprehend the objective world rationally by pure thought without any empirical foundations – in short, by metaphysics*." Albert Einstein

"*[I]nflationary cosmology, as we currently understand it, cannot be evaluated using the scientific method.*"
Paul Steinhardt, (Co-developer of the Theory of Inflation.)

"*Science cannot produce any final answers on the subject of origins*." Alexander Williams and John Hartner

"*All models are wrong, but some are useful*." George E. P. Box

Tom Kotowski
Dec. 26, 2025

Methodology: Generative Computational Physics (GCP)

Using Python/Spyder + ChatGPT + Equation Editor together forms a powerful hybrid workflow—each tool covers limitations of the others, and together they create a complete ecosystem for theory → computation → interpretation → visualization → documentation.

Complementary Strengths: Structured breakdown of the advantages.

Python/Spyder

Excellent for numerical simulation, optimization, Monte Carlo work.
Access to scientific libraries (NumPy, SciPy, SymPy, Matplotlib, QuTiP, AstroPy).
Scales well to large datasets and high-performance computation.
Good for automation, loops, GPU acceleration, parallel physics models.

Equation Editor (Mathcad, Maple Flow, CalcTree, or Word Formula Editor)

Best suited for symbolic presentation of formulas, units-aware calculation.
Produces engineer-friendly notebooks with readable math—ideal for reports.
Handles dimensional units automatically, reducing physical-unit mistakes.
Useful for parametric sweeps, engineering designs, CMB or cosmology expressions formatted visibly.

ChatGPT

Generates code, explains equations, finds conceptual mistakes.
Derives programming on request
Accelerates debugging, provides reasoning behind steps.
Converts ideas into working code or documentation quickly.

Together:

Python = Math Engine
Beautiful Presentations and Documentation via an Equation Editor: Mathcad, Maple, Maple Flow, CalcTree, Word
ChatGPT = Cognitive assistant bridging the two.

For Example See Section: XXIII B Python ΛCDM Six-Parameter Base Model - GCP

Workflow Advantages

Stage	Python	ChatGPT	Math Editor	Combined Advantage
Derive equations	Can verify numerically	Symbolic manipulation, explanation	Beautiful presentation	**ChatGPT produces derivation → Mathcad displays → Python validates**
Run simulations	Fast computing	Can generate code quickly	Limited internally	**Python runs solvers, Mathcad interprets results**
Units & physical correctness	Manual handling	Can suggest units	**Automatic dimensional control**	**Fewer mistakes in constants, cgs/SI mixing, cosmology units**
Visualization	Plots via Matplotlib	Can refine style/analysis	Engineering plots	**Dual view: Python = dynamic, Mathcad = polished**
Documentation	Comments + code	Writes technical summary	Printable worksheets	**Papers, notebooks, and code inline**

ABSTRACT

This work presents a comprehensive survey and mathematical reconstruction of the foundational concepts, observational evidence, and theoretical framework of modern cosmology with emphasis on the Λ Cold Dark Matter (ΛCDM) model, it successes, its tensions, and its philosophical implications.
Using a functional-programming approach to document equations, the core equations of cosmology—from the Friedmann equations and distance measures to the cosmic microwave background (CMB) power spectrum and the matter power spectrum —are restated in explicit, computationally verifiable form. Observational pillars including baryon acoustic oscillations (BAO), large-scale structure (LSS), weak gravitational lensing, nucleosynthesis, and the distance ladder are analyzed and reproduced through mathematical modeling.

The study also evaluates major challenges to the concordance model, including the Hubble tension, early galaxy formation anomalies from JWST, dark matter and dark energy uncertainties, the lithium problem, and the entropy and horizon problems of the early universe. Updated cosmological data sets are incorporated (Planck, WMAP, SDSS, DES, eBOSS, DESI, and JWST).

A second part of this work addresses epistemological and theological dimensions of cosmology. These sections examine the limits of scientific inference, the philosophy of mathematics, the role of metaphysics in cosmological models, and the historical relationship between Christian theology and scientific cosmology. The discussion integrates classical theological insights on creation, rationality, and the intelligibility of the universe as understood through the Imago Dei. Overall, this document serves as both a technical cosmology reference and a philosophical commentary on the nature, origin, and coherence of the universe.

EXECUTIVE SUMMARY

Purpose of the Work

This manuscript has three primary goals:

1. To survey and reconstruct the mathematical structure of modern cosmology using explicit, computable models.
2. To critically evaluate the ΛCDM concordance model, discussing both its successes and unresolved tensions.
3. To explore philosophical and theological implications related to cosmology, scientific reasoning, and the origin of the universe.

Scope of Analysis

The work encompasses the entire structure of cosmology:

- General Relativity & the Friedmann–Lemaître–Robertson–Walker, FLRW, model
- Friedmann equations
- Composition of the universe (baryons, cold dark matter, radiation, dark energy)
- Distance ladder calibration
- Cosmic microwave background anisotropies
- Baryon acoustic oscillations
- Large-scale structure and matter power spectra
- Weak gravitational lensing
- Nucleosynthesis constraints
- Reionization, early structure formation, and high-redshift galaxies
- Cosmological tensions (H_0, S_8, lithium anomaly)
- Early universe physics (inflation, reheating, baryogenesis

Key Findings — Strengths of ΛCDM

- Accurate prediction of the acoustic peak structure in the CMB
- Remarkably successful fit to BAO measurements
- Correct large-scale matter distribution shape
- Consistent results across multiple data sets (CMB, SN Ia, BAO, LSS)
- Predictive framework for light-element abundances

Major Challenges

- Hubble tension (~5–9% discrepancy between early- and late-universe values)
- S_8 tension (weak lensing vs CMB growth-of-structure mismatch)
- Early massive galaxies in JWST (orders of magnitude earlier star formation)
- Lithium problem (BBN prediction exceeds measurement by factor 3–4)
- Fine-tuning in inflation and cosmological constant
- Dark matter and dark energy remain unobserved in laboratory physics

Mathematical Reconstruction

The paper includes full Math implementations for:

The equations for:

- Hubble Equation *H(a),*
- *a* is the scale factor, describes the expansion rate of the universe
- *T*otal energy density of the universe *ρ(a),*
- *CM*B Temperature Scale Factor Relation *T(a),*
- *A*ngular diameter distance to an object, relating its physical size to observed angular size on the sky. $d_A(z)$
- Luminosity distance to an object at a given redshift, $d_L(z)$,

Friedmann equations solved under multiple cosmological assumptions
Reproduction of the TT spectrum using transfer functions
Matter power spectrum *P(k)* from Eisenstein–Hu
BAO sound horizon calculations
Weak lensing convergence
Nucleosynthesis abundance modeling

Epistemology & Theology

This work recognizes that cosmology sits at the boundary of science and metaphysics.
Topics include:

- Popper's falsifiability
- The limits of inference for singular origins
- The philosophy of mathematics
- Interpretive frameworks for Genesis
- Classical Christian perspectives on the intelligibility of the universe
- The fine-tuning of physical constants

Conclusion

Cosmology is now a high-precision discipline, yet profound conceptual questions remain. The ΛCDM model is both powerful and incomplete. Mathematics continues to be the bridge between human understanding and cosmic structure, raising deep philosophical questions about the origin and nature of the universe.

Section by Section Summary

I. Some Key Historical Events and Investigative Methods

This section surveys the historical development of cosmology from early astronomical models to modern observational science, emphasizing how measurement techniques evolved alongside theory. It highlights the transition from geometric descriptions of the cosmos to physics-based models grounded in spectroscopy, photometry, and relativistic gravity, establishing observation as the arbiter of cosmological theory.

II A. GLOSSARY: ΛCDM Model, Distance Ladder and Key Observational Probes

II B. Λ CDM or Lambda-Cold Dark Matter Model of Cosmology

Introduces the ΛCDM model as the current concordance framework, specifying its principal components: baryons, cold dark matter, radiation, neutrinos, and dark energy (Λ). The section emphasizes ΛCDM's role as a phenomenological model constrained by data rather than a fundamental theory, summarizing its core assumptions and successes.

III. Mathematical Basis of Big Bang Cosmology: Einstein's General Relativity (GR), FLRW & GR Tests

Presents the mathematical foundation of cosmology via Einstein's field equations and their reduction under the assumptions of homogeneity and isotropy to the FLRW metric. Observational tests of GR on cosmological scales—gravitational lensing, perihelion precession, and time dilation—are briefly reviewed.

IV. The Equation of State

Defines the equation of state parameter $w=p/\rho$ for different cosmic components and explains how it governs the evolution of energy densities with scale factor. The section connects equations of state to acceleration, deceleration, and the interpretation of dark energy.

V. Distances in Cosmology

Introduces comoving, proper, luminosity, and angular-diameter distances, emphasizing their geometric meaning in expanding spacetime. The section clarifies how observational quantities depend on cosmological parameters and redshift through integrals of the Hubble parameter.

VI. Newtonian Energy Derivation of, H_0, the Rate of Galactic Expansion

Uses a Newtonian energy argument to derive a Friedmann-like expansion equation, illustrating the concept of critical density and escape velocity. This heuristic derivation provides intuition for cosmic expansion prior to full relativistic treatment.

VII. Equations for Cosmological Parameters

Defines the principal cosmological parameters—H_0, Ω_m, Ω_Λ, Ω_r, and curvature—and shows how they enter the Friedmann equations. Time evolution and scaling relations are discussed in both analytic and numerical form.

VIII. Steps in the Development of the ΛCDM Model

Traces the historical progression from early expanding-universe models to the modern ΛCDM framework, highlighting why cold dark matter and dark energy were introduced. The section emphasizes observational motivations rather than theoretical preference.

IX. Stellar Classification Systems

Reviews stellar spectral classification and the Hertzsprung–Russell diagram, explaining how stellar temperature, luminosity and evolution are inferred from spectra. These systems are presented as foundational tools for astrophysical distance estimation.

X. Measurement of Cosmic Distances: Trigonometric Parallax. The Standard Candle Initial Mass Function
Discusses geometric parallax as the most direct distance measurement and introduces the concept of standard candles anchored by stellar evolution and the initial mass function. The role of calibration in extending distances beyond the Milky Way is emphasized.

XI. Cosmic Distance Scale
Develops the hierarchical distance ladder, showing how parallax, Cepheids, and secondary indicators are linked. Sources of systematic uncertainty and error propagation across rungs of the ladder are discussed.

XII. Modeling the Dynamics of a Cepheid Variable: Find the Period, Solve for Oscillation
Presents physical and mathematical models of Cepheid pulsations, connecting stellar structure equations to observed periodic luminosity variations. The κ-mechanism and simplified oscillation equations are introduced.

XIII. A. Standard Candle #2
Introduces Type Ia supernovae as a second standard candle, outlining their physical origin and empirical standardization. The section explains why they are critical for measuring cosmological expansion at high redshift.

XIV. 1929 Hubble's Original Observations of Galaxy Recession & Hubble Constant Calculation
Reviews Hubble's original redshift–distance data and methodology, emphasizing calibration limitations and early overestimates of H_0. The historical context highlights the evolution of measurement precision.

XV. Stellar Flares Introduction – Dynamics of Stellar Flares – Exoplanet Light Curve Source Files
Explores stellar flare physics and their impact on photometric observations, particularly exoplanet transit light curves. The section connects stellar activity modeling to observational systematics.

XVI. Evolution of Galaxy Structure over Cosmic Time
Describes morphological and dynamical evolution of galaxies, including mergers, star-formation histories, and feedback processes. Observational trends with redshift are discussed in relation to structure formation models.

XVII. Various Estimates of Age, Mass, and Density of the Universe
Presents multiple independent methods for estimating cosmic age, mass, and density, including expansion history, stellar populations, and CMB constraints. Agreement and tension among methods are highlighted.

XVIII. Entropy Evolution of Universe
Discusses entropy production and growth in an expanding universe, including thermodynamic considerations of cosmic evolution. The section connects entropy increase to arrow-of-time arguments.

XIX. A. Planetary Data and Classical Newton's Calculation of Planetary Velocity
Uses classical mechanics and planetary motion as a pedagogical precursor to galactic dynamics. Newtonian velocity calculations establish a baseline for later discussion of anomalous rotation curves.

XX. Inference of Cold Dark Matter: Rotational Velocity Curves of Milky Way Galaxy
Analyzes observed galactic rotation curves and their deviation from Newtonian expectations based on luminous matter. The necessity of non-luminous mass (dark matter) is inferred quantitatively.

XXI. Evidence for Λ-CDM "Big Bang" Model
Summarizes the primary observational pillars supporting ΛCDM, including expansion, CMB, nucleosynthesis, and large-scale structure. Consistency among independent probes is emphasized.
XXII. Λ-CDM Model Theory and Parameters Provides a consolidated overview of ΛCDM parameters and their physical meaning, including spectral indices, optical depth, and matter fractions. Parameter estimation techniques are briefly discussed.

XXIII. Planck Microwave Anisotropy Probe CMB Angular Temperature Power Spectrum (TT)
Explains the origin and interpretation of the CMB temperature power spectrum, including acoustic peaks and damping tails. The sensitivity of the TT spectrum to cosmological parameters is highlighted.

XXIV. Measurement Advances and Technology in the Measurement of the Hubble Constant
Reviews technological and methodological improvements in measuring H_0, including space-based telescopes and time-delay lenses. The section connects instrumentation to reduced systematic uncertainty.

XXV. Mathematica CMBquick: Simulation of CMB Temperature Power Spectrum
Introduces numerical simulation of CMB spectra using simplified Boltzmann solvers, emphasizing pedagogical understanding of parameter dependence. Computational modeling is framed as an interpretive tool.

XXVI. Calculation of CMB Power Spectra from Model Parameters
Develops the calculation of CMB spectra from cosmological parameters, highlighting how changes in density, curvature, and ionization history alter predicted anisotropies.

XXVII. A. The Discovery of the Accelerating Universe (2011)
Reviews supernova evidence for cosmic acceleration and the inference of dark energy. Observational methodology and statistical significance are emphasized over theoretical interpretation.

XXVIII. Look-Back Time & Age of Universe vs. z. 2024 Metal-Poor JADES-GS-z14-0 Galaxy @ z=14.32
Discusses look-back time calculations and their application to high-redshift galaxies observed by JWST. The section highlights tensions between early structure formation and standard timelines.

XXIX. Early Universe Models: Quark–Gluon Era
Explores theoretical descriptions of the quark–gluon plasma epoch, emphasizing speculative extrapolation beyond direct observation. Connections to particle physics and thermodynamics are discussed.

XXX. Some Key Problems of the ΛCDM Cosmology
Summarizes unresolved issues such as small-scale structure problems, parameter tensions, and model extensions. The section distinguishes observational challenges from theoretical incompleteness.

XXXI. Three Analyses of the Flatness Problem – The Fine-Tuning Problem
Presents multiple formulations of the flatness problem, examining why near-critical density appears finely tuned. The section introduces inflationary and non-inflationary responses.

XXXII. One of the Biggest Successes and Weaknesses of the ΛCDM Theory: The Theory of Inflation
Reviews inflation as both a solution to horizon and flatness problems and a source of theoretical ambiguity. Predictions such as scalar tilt and primordial perturbations are discussed alongside unresolved issues.

XXXIII. Proof of the Borde–Guth–Vilenkin (BGV) Theorem – Proof that the Universe had an Origin
Explains the BGV theorem as a statement about geodesic incompleteness in expanding spacetimes, clarifying its assumptions and implications. The distinction between mathematical past-incompleteness and physical origin is emphasized.

XXXIV. Modified Gravity Theories

XXXV. In the Realm of Hubble Tension - A Review of Solutions

I. Introduction: Key Historical Events, Measurements, & Math Models

Key Mathematical Concepts for Correct Modeling of Planetary Motion

127 AD: Ptolomy proposed epicycle geocentric model of universe. This theory holds for 1500 years.
1543: Copernicus prosed the Heliocentric Model of the Universe. Galileo's telescope verifed this from the orbit of Venus.
1605: Kepler's Laws describe the Elliptical Model for Planet's Orbits. Lunar Conic Model, Time of Flight, Polar Model.
1686: Newton's Laws (supercede Kepler's) and Einstein's GR gives value for the precession of the perihelion of Mercury.

Key Concepts and Discoveries (Measurements) of Cosmology of Galaxies

1. Birth of Cosmology: Mathematical Basis of ΛCDM Cosmology: **Einstein's General Theory of Relativity (GR)**
In 1917 Einstein developed his General Theory of Relativity (GR), the general tool of Modern Cosmology.

2. 1912 Vesto Slipher, using spectroscopy, discovered the redshift of galaxies. Used Doppler Effect to calculate velocities.

3. **In 1922 Friedmann developed a solution of GR** that showed that the universe is not static, but predicted that the universe will expand. In 1927 Lemaitre came up with a model that included mass density and pressure. He showed a linear relationship between expansion of the universe and distance. This relationship was verified by redshift measurements by Slipher & Hubble's measurement of distance to galaxies. Hubble made the correlation between velocity and distance.

4. In 1929, measurements of the distance and the velocity of how fast galaxies are moving away from us were made by Edwin Hubble. The correlation he discovered between distance and velocity is know as **Hubble's Law**.
In 1932, **Einstein and de Sitter** solved GR for an expanding ($\lambda = 0$), Hubble H_o, finite mean density, flat universe.

4. In 1948 prediction of existence of Cosmic Microwave Background Radiation (**CMB**) made by George Gamow.

5. In 1950's it was thought that the light elements, such as hydrogen and helium. were formed in stars. However, the observed **% of helium was too high to be formed from the interior temperatures of stars**. The percentage of Helium can be explained by the BBT, i.e., the universe was so hot that it could produce a high percentage of helium.

6. In 1964 Penzias and Wilson, while calibrating a radio telescope accidentally **discovered this (CMB)**. Based on GR, the discovery of CMB, and Hubble's Law the **ΛCDM Theory was proposed**. To verify that the CMB originated from a BB, in **1989 the COBE** spacecraft was launched to determine if the temperature variations of the CMB were consistent with the ΛCDM cosmological framework. The uniformity of CMB agreed with BBT predictions.

7. Observations of rotational velocity of galaxies **implied the existence of a new form of matter**: **Cold Dark Matter.**

8. 1960's: The **Development of the ΛCDM** (Lambda Cold Dark Matter) Model

9. In the 1980s the **Concept of Inflation** was proposed to explain the fine tuning of the universe. Cosmic inflation, cosmological inflation, or just inflation, is a theory of exponential expansion of space in the early universe. The inflationary epoch is believed to have lasted from 10^{-36} seconds to between 10^{-33} and 10^{-32} seconds after the ΛCDM. It requires significant fine tuning, degree depends on model. XIX discusses the serious problems with the validity of this theory.

10. 1992: Discovery of the **anisotropic nature** of the universe in the **CMB**. Requires corrections to FRW model.

11. In 1998, it was observed that the **rate of expansion of the universe increase**d. This increase was attributed to a new form of energy called **dark energy**. In 2022, it was found to increase **5% to 9% even faster than thoug**ht.
The Greek letter Λ (lambda) is used to represent the cosmological constant, which is currently associated with a vacuum energy or dark energy in empty space that is used to explain the contemporary accelerating expansion of space against the attractive effects of gravity. A cosmological constant has negative pressure.

Satellite Space Telescopes: 1989 NASA COBE, 1990 NASA and ESA Hubble, 2009 Planck, 2021 JWST.

The High-Precision Era of Cosmology

\This refers to the period starting in the **late 1990s and early 2000s** when cosmology transitioned from a largely theoretical field with significant uncertainties to a **precise, data-driven science**. This transformation was driven by high-resolution observations of the cosmic microwavec (CMB), large-scale galaxy surveys, and supernova studies.

Key Milestones of the High-Precision Era

Cosmic Microwave Background (CMB) Measurements:

Hubble Space Telescope (1990) (90-2,500 nm):
Hubble contributed to precision measurements of the Hubble constant through distance-ladder observations.
NASA COBE (1989):
First detected CMB anisotropies, confirming early universe structure formation.
BOOMERANG & MAXIMA (1998–2000):
Provided detailed maps of the CMB power spectrum.
WMAP (2003–2013):
Precisely determined key cosmological parameters (age, composition, curvature).
Planck (2009–2018):
Achieved even higher precision, refining the standard cosmological model.
Type Ia Supernovae & Dark Energy (1998–1999):
James Webb Space Telescope Probing the Early Universe 2021--- (Infrared 600-28,500 nm):
While not specifically dsesigned to probe the CMB, it contributes significantly by the Discovery of Ancient Galaxies: JWST has observed galaxies that existed approximately 290 million years after the ΛCDM, providing insights into the formation and evolution of the earliest cosmic structures ***z > 10-15.*** It was designed to last at least 5 and 1/2 years.
Identification of Massive Early Galaxies: The telescope detected six massive galaxies formed between 500 to 700 million years post-ΛCDM. These galaxies challenge existing theories of galaxy evolution due to their substantial mass & density.
Observations from the Supernova Cosmology Project and the High-Z Supernova Search Team showed that the universe's expansion is accelerating.
This led to the discovery of dark energy, now estimated to make up ≈68% of the universe's energy budget.

Large-Scale Galaxy Surveys:
Sloan Digital Sky Survey (SDSS) (2000–present): Mapped millions of galaxies, measuring large-scale structure and baryon acoustic oscillations (BAOs).
2dF Galaxy Redshift Survey (1995–2002) or 2dFGRS: 2dF used the two-degree field spectroscopic facility on the Anglo-Australian Telescope out to z ~ 0.2. Provided key constraints on matter density and galaxy clustering.
ΛCDM Model Confirmation:

The Lambda Cold Dark Matter (ΛCDM) model became the standard framework, describing a universe composed of ≈68% dark energy, ≈27% dark matter, and ≈5% normal matter.
Baryon Acoustic Oscillations (BAOs) & Precision Distance Measures:
BAOs, detected in galaxy clustering patterns, provided an independent "standard ruler" for measuring cosmic expansion.

Impacts of the High-Precision Era

Cosmological Parameters Now Known to Percent-Level Accuracy:
Age of the Universe: 13.8 billion years
Hubble Constant (H_0): 67 to 74 km/s/Mpc (some tension remains between Planck and local measurements)
Matter Density (Ω_m): 0.31, Dark Energy Density ($\Omega\Lambda$): 0.69

Shift from High Precision Parameter Estimation to Fundamental Physics:

Questions about the nature of dark energy, dark matter, and potential physics beyond ΛCDM.

The Universe is big in both space and time, and for much of human history it has been largely beyond the reach of our boldest ideas and most powerful instruments. The birth of modern cosmology was roughly 100 years ago. Albert Einstein had introduced General Relativity, the first theory of gravity and space-time capable of describing the entire Universe, and the first cosmological solutions had been found (e.g., the de Sitter, Friedmann, and Lemaître solutions as well as Einstein's static model). At about the same time, George Ellery Hale and George Willis Ritchey invented the (modern) reflecting telescope, and Hale moved astronomy to the mountaintops of California—first Mount Wilson and, later, Palomar Mountain. With bold ideas and new instruments, astronomers were ready to explore the Universe beyond our own Milky Way galaxy and began to discover and understand the larger picture.

Hale's second big reflector, the 100-inch Hooker telescope, enabled Edwin Hubble to discover that galaxies are the building blocks of the Universe today and that it is expanding—the signature of its big bang beginning. While it took a few years to connect the solutions of General Relativity to the observational data, the basics of the big bang model were in place.

.In 1972, years before Standard Model referred to the remarkable theory that describes quarks and leptons. This Standard Model (Weinberg's Classic "Gravitation and Cosmology") traces the Universe from a hot soup of hadrons at around 10^{-5} s through the synthesis of the light elements (largely ^{4}He with trace amounts of D, ^{3}He, and ^{7}Li) at a few seconds to the formation of neutral atoms and the last scattering of CMB photons at around 400,000 years after the big bang, and finally to the formation of stars and galaxies.

The triad of the expansion, the light-element abundances, and the blackbody spectrum of the CMB provided an equally strong observational foundation. Note: The deceleration parameter, q_0, is discussed here for historical context.

In 1970, Sandage summed up cosmology as the search for two numbers, H_0 and q_0. The expansion rate of the Universe, H_0, also sets the age of the Universe, $t_0 = aH_0^{-1}$, with the deceleration parameter q_0 determining the constant a. And for a universe made up only of matter, q_0 , the ratio of the matter density to the critical density (Ω_0), and the curvature radius of the universe are related: $q_0 = \Omega_0 /2$ and $Rc = H_0^{-1}/|\Omega_0 - 1|^{1/2}$. It would take until 2000 and the Hubble Space Telescope (HST) Key Project to pin down H_0 with a reliable **error estimate**:

$H_0 = 72 \pm 2 \pm 6$ km s^{-1} Mpc^{-1} (statistical and systematic).

"Low-precision" versus "High-precision" Cosmology

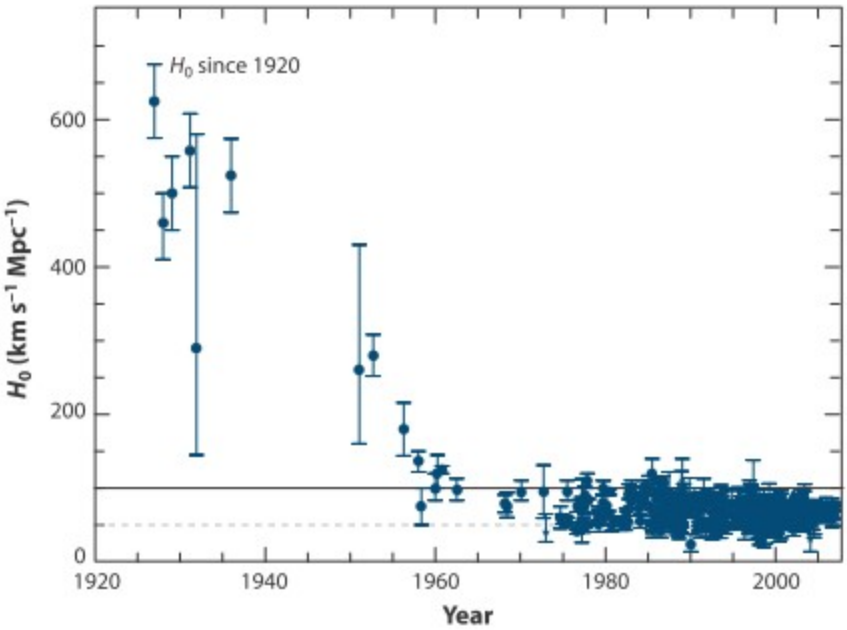

H_0 measurements from 1920 to 2020.

By 1970, most measurements were between 50 and 100 km s^{-1} Mpc^{-1}, but with unrealistically small error bars. The Hubble Space Telescope Key Project changed that with its 2000 determination, $H_0 = 72 \pm 2 \pm 6$ km s^{-1}Mpc^{-1}. As for q_0 it has been replaced by other cosmological parameters that better capture the physics and that can be measured with accuracy and precision.

Three Contrasting World Views Concerning the Validity of ΛCDM Singularity Hypothesis

#1: *An Introduction To Modern Cosmology*, Andrew Liddle

Four Observational Evidences for the ΛCDM Model:

1. The expansion of the universe according to Hubble's law (as indicated by brightness and redshifts of galaxies),
2. The discovery and measurement of the Cosmic Microwave Background Radiation (CMB),
3. The relative abundances of light elements produced by ΛCDM nucleosynthesis.
4. Observations of Galaxy formation and evolution and Agreement of Different Tests for the Age of the Universe

"The development of cosmology will no doubt be seen as **one of the scientific triumphs of the twentieth century**. At its beginning, cosmology hardly existed as a scientific discipline. By its end, the Hot ΛCDM cosmology stood secure as the accepted description of the Universe as a whole. The turn of the millennium saw the establishment of what has come to be known as the Standard Cosmological Model, representing an almost universal consensus amongst cosmologists as to the best description of our Universe."

#2. *Dismantling the ΛCDM, Reasons Why to Reject the Big-Bang Theory*, Alex Williams, J. Hartnett

The theory lacks a credible and consistent mechanism for the Origin of the Universe before the CMB.

"The big-bang universe begins in a singularity (entire universe crushed into a point of infinite density) and there is no known mechanism to start the universe expanding out of the singularity — the equations in the theory **only work after the expansion has begun**. It then requires a hypothetical period of stupendous inflation and stopping at a precise point to halt the universe from recollapsing. It further requires incredible fine tuning to maintain stability for a flat universe. Its mechanism for turning primordial energy into matter would produce equal amounts of matter and anti-matter but our universe is made only of matter. It is inconsistent with Thermodynamics. **It cannot explain the low entropy at the initial expansio**n." The detailed particle physics mechanism responsible for inflation is not known. It has to violate physical laws and appeal to unknown forces (dark energy) and substances (dark matter) to explain what we observe.

#3. Theological Arguments for Age of "Firmament"/Galaxy: God Created Firmament/Galaxy in 2 Days.

Epistemological Foundations and Assumptions (*The Lost World of Genesis One*, John Walton (ANE Texts)

1. Define a test for determining the Truth of a Proposition:
   The Law of Non-Contradiction: This law states that a truth proposition cannot be both statement A (what it is) and statement non-A (what it is not) at the same time and in the same relationship. One implication of this is that the vast corpus of Physics is self-consistent and thus passes the Law of Non-Contradiction.
2. 2 + 2 always equals 4. This is true for all time & everywhere in space. This establishes that Mathematics is always valid.
   For example, this law is true in the garden of Eden before the fall, in heavenly places, & everywhere in this universe. By extension, this implies that the Laws of Mathematics hold everywhere in space and for all time.
   With regard to math and logic, the above 2 + 2 always equals 4 implies that the logical mind of man (not necessarily his moral compass) is not impaired by the fall of Adam. Luther said truth comes from the Bible and Reason.
3. Law of Cause and Effect - As a generalization, the cause must always be greater than the effect. Cause for BBT.
4. Space and Time had a beginning. Refer to Section XXXIII Proof of the Borde-Guth-Vilenkin (BGV) Theorem.
5. **Moses Observed:** sky above, ground below, & a horizon (**firmament** above), with water surrounding ground, above the firmament, and below the ground (the deep). **Genesis 1:1-2**: "In the beginning God created the sky and the land. ... And the Spirit of God moved upon the face of the waters". **Gen 1:6-8** "And God said, Let there be a firmament in the midst of the waters, and let it divide the waters from the waters. And God made the firmament, and divided the waters which were under the firmament from the waters which were above the firmament: and it was so. And God called the firmament Heaven. And the evening and the morning were the second day." God Created the Firmament in two Days.
6. Physicist Eugene Wigner wrote a paper on the "*The Unreasonable Effectiveness of Mathematics in the Natural Sciences*." One of the implications of this is the wonder that the mind of man can understand the depths of the laws of Physics. A theological explication of this mystery is given in the Book of Genesis 1:27: "*So God created man in his own image, in the image of God he created him; male and female he created them*." Thus man, being made in the image of God (Imago Dei), is thus capable by God's design to understand the Laws of Physics and Math, as created by God.
7. Lifetimes: The sun has enough nuclear fuel to run for about 10 billion years and about half of it has been used up. The half-life of Uranium 238 is measured to be about 4.5 billion years. Elements heavier than UR have short half-lives.

The Nature of Science: Physics or Metaphysics - Limits to the Legitimate Realm of Physics

Unspoken Assumptions

Most people today believe because they have been taught it is so, that physics can explain the Origin of the universe. This is the Assumptions of Naturalism: The idea that matter is all there is. Upon this rests the current orthodoxy of cosmology.

What is Science? The Era of Post Empirical Science

The philosopher Karl Popper argued that what distinguishes a scientific theory from pseudoscience and pure metaphysics is the possibility that it might be falsified on exposure to empirical data.
In other words, a theory is scientific only if it has the potential to be proved wrong.
Some argue we live in the era of post empirical science. Major Concepts such as a Multiverse, Bouncing Universe, or 24 Dimensional String Theory can never be falsified. By Popper's criteria, these concepts do not constitute areas of legitimate scientific inquiry. One can hold the position that String Theory is manifestly false. It fails all predictions.

***Lost World of Genesis*, John Walton: There are Conceptual Limits to Science**

"**Based on the concept of the Scientific Principle, Science can only study things that happen more than once**. By this definition, many areas of Cosmology can never be verified or falsified. These areas would be in the **realm of speculati**on. To explain something means to describe the unknown in terms of the known. **Unknown concepts such as Dark Energy or Cold Dark Matter do not do well to further elucidate area of inquiry.** They are **more in the arena of Metaphysics rather than Physics.**The deeper we look into Physics and also the Biological Structure of the human cell, the deeper we see into a perhaps never ending depth of complexity."

Distinguishing Between the Realms of Myth, Philosophy, Explanations, Metaphysics, and Science

One case where science crosses over into religion is **The Beginning of Our Universe**. Physicists have put forward many theories for it: a ΛCDM, a big bounce, a collision of higher-dimensional membranes, a gas of strings, a network, a 5-dimensional black hole, and many more. But the scientifically correct answer is, that we don't know how the universe came into existence. There are good reasons to think we will never know. A greater cause, that transcends the physical realm, may be the origin. Many are unwilling to accept this as a possibility. Many fill this knowledge gap with tall tale creation myths, written in the language of Mathematics, such as a landscape of multiverses populated with googles of string topologies.
Einstein's quote from first page:

"*Time and again the passion for understanding has led to the illusion that man is able to comprehend the objective world rationally by pure thought without any empirical foundations – in short, by metaphysic*s."

The Origin, Purpose, and Destiny of the Universe: Perceived Tension Between Cosmology and Christianity

Christianity is consistent with the Big Bang Theory. Genesis 1:3 And God said "*Let there be light*" and there was light. Genesis is consistent with the Ex Nihilo creation of the cosmos. Chronologically, the different concepts men have had about the nature of the universe were: First Pagan God Centered, then Earth Centered, then Sun Centered, then the Great Enlightenment Material Centered, and presently, the latest Science of Cosmology Centered. The telescope was the instrument that falsified a number of astronomical world views. With respect to origin, what is the greatest possible cause, the Universe or God? With respect to these, what is the greatest possible explanation for our reality: Explanations for the physical properties and interactions of matter/energy or a Transcendent Being? Which is the more Transcendent origin? Our Perceptions and Theories about the Physical or God? The Law of Cause and Effect: The cause must always be greater than the effect. Who or What is a Self-Consistent cause to explain the creation of time?
Which is the more real? Abstract Field Theories about Matter, Tensor Field Equations, and Singularities or the Spiritual Influence of a Creator God who is the Creator of the Esoteric Field Theories of Physics, Math, and the Imago Dei Mind? Philosophically, the only ultimate origin is God who transcends a mere physical universe.

In the end, only a Supreme Law Giver, is the creator of the Laws of Physics and Mathematics. He is, by Definition, the Great Lawgiver of the Universe. He is the one explanation for the fine-tuning of the laws of Physics and cosmology. All truth, including the physical, is God's truth. **Thus there is no tension between Material Cosmology and the Biblical Old and New Testaments** as long as the Biblical Account of Creation is not interpreted out of the context of the age and culture in which it was written. For Genesis, it is in the context of the age, culture, and World View of Moses and **the children of Abraham coming out of Egypt seeing Only the Milky Way Galaxy stars, sun, and moon.**

Is Mathematics the Invention of Man or the Mind of God?

The question of whether mathematics is an invention of man or alternatively, a reflection of the mind of God. This is a profound philosophical and theological quandary. There are two main perspectives on this issue:

1. Mathematics as a Human Invention (Secular Theories)

- This view holds that mathematics is a creation of human intellect, developed over time to describe patterns, relationships, and logical structures. Other Philosophical Categories: Reductionism, Empiricism, Logicism, Intuitionism, and Formalism.
- Numbers, symbols, and mathematical systems (e.g., algebra, calculus) are seen as constructs designed to help us understand and manipulate the world. Different cultures have developed different mathematical systems, which suggests that mathematics is shaped by human experience and necessity.

2. Mathematics as the Mind of God (Platonist/Theistic View)

- This perspective sees mathematics as something discovered rather than invented, reflecting the order and rationality of God ’s creation. Mathematics is a reflection of the fact that man was made in the image of God. We are the mind of God.
- Many theologians and philosophers believe that mathematical truths exist independently of human thought, much like moral or logical truths.
- Biblical passages suggest that God established order in the universe (e.g., Job 38:4-5, where God speaks of measuring the foundations of the earth).
- The precise mathematical laws governing nature—such as the Fibonacci sequence, the fine-tuning of physical constants (See Sections XXXI, XXXII), Intelligibility of Cosmology, and the structure of DNA—point to a divine intelligence.

Until late 19th century, scientists were typically Christians who saw no conflict between their science and faith.

- Mathematicians like Johannes Kepler saw their work as "thinking God’s thoughts after Him."
- Galileo said "The laws of Nature are written in the language of mathematics."
- Pascal provided a famous 'wager' in which he gives a probabilistic argument for choosing to believe in God.
- Descartes provided two theistic proofs of God in his Meditations (Descartes 1976).
- Newton believed strongly in a Designer who worked through mathematical laws. "The most beautiful system of sun, planets and comets, could only proceed from the counsel and dominion of an intelligent and powerful Being."
- Leibniz regarded mathematical theorems as 'primarily and continuously thought by God', and when a mathematician discovers them, 'this knowing is a repetition of the primary divine knowing'.
- Bernoulli was a strong Calvinist and reflected on the theological implications of his discoveries in probability theory.

In the late 19th century, several intellectual, scientific & philosophical developments contributed to a fracture between a predominantly theistic view among many scientists and biblical literalism. Some key factors include:

1. Rise of Positivism and Empiricism – Thinkers like Auguste Comte promoted the idea that only observable, empirical evidence should be used to understand the world, reducing the role of theology in scientific explanations.
2. Darwin’s Theory of Evolution (1859) – Charles Darwin’s "On the Origin of Species" provided a naturalistic explanation for the diversity of life, challenging traditional religious interpretations of creation.
3. Advancements in Physics & Cosmology – Theories in thermodynamics and the mechanistic view of the universe led some scientists to see the cosmos as an **eternal self-sustaining system**, reducing the perceived need for divine intervention.
4. Higher Criticism of the Bible – Scholars began applying historical-critical methods to the Bible, which led to questioning of traditional theological interpretations.
5. Secularization of Education - Harvard, Yale, Dartmouth, UPenn, and Princeton, were founded as Schools of Divinity. Universities & scientific academies increasingly promoted secular approaches to knowledge, leading to a decline in explicitly religious perspectives in academic science: Now there was no meaning to life. Everyone is their own god.

Biblical, Philosophical, and Cosmic Support for Mathematics as Divinely Inspired

Psalm 19:1 – "The heavens declare the glory of God; the skies proclaim the work of his hands." (The universe follows mathematical laws.) Colossians 1:16-17– "In him all things were created… He is before all things, and in him, all things hold together." (Mathematical order is part of God's sustaining power.) *The Mind of Man*- Imago Dei.

Cosmic Paradigm Shift: In 1965 Penzias and Wilson discovered the CMB, the echo of the ΛCDM. The eternal universe had a beginning. This beginning is outside the realm of Science. Thus, Cosmology is not a threat to Christianity, instead the origin of this Mathematical Representation of the Cosmos is within the eternal realm --- *the Mind of God.*

II A. GLOSSARY: ΛCDM Model, Distance Ladder and Key Observational Probes

ΛCDM Model

H_0	Hubble constant today	km s⁻¹ Mpc⁻¹
$H(z)$	Hubble parameter at reds z	km s⁻¹ Mpc⁻¹
$a(t)$	Scale factor	dimensionless
z	Redshift	dimensionless
Ω_m	Total matter density fraction	dimensionless
Ω_b	Baryon density fraction	dimensionless
Ω_c	Cold dark matter density fraction	dimensionless
Ω_r	Radiation density fraction	dimensionless
Ω_Λ	Dark energy density fraction	dimensionless
Ω_k	Curvature density fraction	dimensionless
w	Dark-energy equation-of-state	dimensionless

Distances

Symbol	Meaning	Units
$D_C(z)$	Comoving distance	Mpc
$D_M(z)$	Transverse comoving distance	Mpc
$D_A(z)$	Angular diameter distance	Mpc
$D_L(z)$	Luminosity distance	Mpc
r_s	Sound horizon	Mpc
$D_V(z)$	Volume-averaged BAO distance	Mpc

Perturbations & Power Spectra

Symbol	Meaning	Units
k	Wavenumber	h Mpc⁻¹
$P(k)$	Matter power spectrum	(Mpc/h)³
$T(k)$	Transfer function	dimensionless
n_s	Scalar spectral index	dimensionless
A_s	Primordial amplitude	dimensionless
σ_8	RMS fluctuations in 8 h⁻¹ Mpc spheres	dimensionless

CMB Quantities

Symbol	Meaning	Units
ℓ	Multipole moment	dimensionless
C_ℓ	Angular power spectrum	μK²
$D_\ell = \ell(\ell+1)C_\ell/2\pi$	Rescaled CMB spectrum	μK²
τ	Optical depth to reionization	dimensionless
θ_s	Sound horizon angular scale	radians

Friedmann & Density Quantities

Symbol	Meaning	Units
ρ	Energy density	kg m⁻³
ρ_c	Critical density	kg m⁻³
$\rho_m, \rho_b, \rho_\Lambda$	Matter, baryon, dark-energy densities	kg

ΛCDM: The Standard Model of Cosmology

1. FLRW SPACETIME (Geometry)
Metric:

$$ds^2 = -c^2dt^2 + a^2(t)\left[\frac{dr^2}{1-kr^2} + r^2d\Omega^2\right]$$

- $a(t)$: scale factor
- $k = -1, 0, +1$: curvature
- Spatial symmetry: homogeneous, isotropic

Vector Graphic Element:
A sphere grid expanding over time (3 concentric shells showing increased scale factor).

2. FRIEDMANN EQUATION (Dynamics)

$$H^2(a) = H_0^2[\Omega_r a^{-4} + \Omega_m a^{-3} + \Omega_k a^{-2} + \Omega_\Lambda]$$

- Radiation dominates early universe
- Matter dominates intermediate
- Λ dominates today

Vector Graphic Element:
Stacked colored curves for each component vs. $a$or z.

3. ENERGY BUDGET OF THE UNIVERSE
Pie chart:

- **Dark Energy:** 68%
- **Dark Matter:** 27%
- **Baryons:** 5%
- **Photons + Neutrinos:** < 0.01%

(Values optional; use Planck 2018 best fit.)
Vector Graphic Element:
Clean pie graphic with 4 wedges.

4. EXPANSION HISTORY H(z)

$$H(z) = H_0\sqrt{\Omega_m(1+z)^3 + \Omega_r(1+z)^4 + \Omega_\Lambda}$$

Plot:

- x-axis: redshift z
- y-axis: $H(z)$line increasing toward early universe.

5. DISTANCES
Comoving Distance

$$D_C(z) = c\int_0^z \frac{dz'}{H(z')}$$

Angular Diameter Distance

$$D_A(z) = \frac{D_C(z)}{1+z}$$

Luminosity Distance

$$D_L(z) = (1+z)D_C(z)$$

Integrated Sachs–Wolfe Effect (ISW)

A contribution to the Cosmic Microwave Background (CMB) temperature anisotropy caused by time-varying gravitational potentials encountered by photons as they travel from the surface of last scattering to the observer. If gravitational potentials evolve—such as during radiation domination or late-time cosmic acceleration—photons experience a net energy shift, producing additional large-scale (low-ℓ) temperature anisotropy. The ISW effect provides an independent probe of dark energy through correlations between the CMB and large-scale structure.

$$\left(\frac{\Delta T}{T}\right)_{\mathrm{ISW}} = 2\int_{\eta_{\mathrm{ls}}}^{\eta_0} \dot{\Phi}(\eta)\, d\eta$$

The Sachs–Wolfe plateau corresponds to $10 \lesssim \ell \lesssim 30$.

where Φ is the Newtonian gravitational potential and η is conformal time.

Cosmological Significance:

The ISW effect enhances power at lowest multipoles of the CMB angular power spectrum and provides an independent observational probe of dark energy through correlations between CMB temperature maps and large-scale structure.

6. PRIMORDIAL POWER SPECTRUM

$$P(k) = A_s k^{n_s}$$

Nearly scale-invariant spectrum from inflation.

Vector Graphic Element:

Straight line with small tilt.

7. MATTER POWER SPECTRUM TODAY

$$P(k) = P_{\mathrm{prim}}(k)\, T^2(k)\, D^2(z)$$

- BAO Wiggles
- Turnover at equality

Vector Graphic Element:

P(k) curve with BAO oscillations.

8. CMB POWER SPECTRUM (TT)

Peaks correspond to:

- acoustic oscillations
- baryon loading
- photon diffusion
- matter–radiation ratio

Vector Graphic Element:

Classic TT multipole plot with labeled 1st, 2nd, 3rd peaks.

9. KEY OBSERVATIONAL INPUTS

Icons or mini-graphics for:

- **Type Ia SNe** — distance ladder
- **BAO** — standard ruler
- **CMB** — initial conditions
- **Weak Lensing** — structure growth
- **Galaxy Clustering** — P(k)

10. ΛCDM PARAMETER SET

The model is fully defined by **6 parameters**:

1. $\Omega_b h^2$
2. $\Omega_c h^2$
3. θ_s
4. A_s
5. n_s
6. τ

Cosmological Distances and the Distance Ladder

Cosmology uses both geometric distances defined within the FLRW model and an observational 'distance ladder' constructed from astrophysical standard candles and rulers. This section summarizes both perspectives.

1. Model-Based Cosmological Distances

• Comoving distance $D_C(z)$: integral over $H(z)$ that gives the line-of-sight comoving separation.

• Angular diameter distance $D_A(z)$: relates physical size to observed angular size, important for BAO and CMB.

• Luminosity distance $D_L(z)$: relates intrinsic luminosity to observed flux; key for supernova cosmology.

• Proper distance: scale-factor–dependent versions of the above, often used conceptually rather than directly observed.

2. Observational Distance Ladder

• Parallax: direct geometric distances to nearby stars ($\lesssim$ kpc).

• Cepheid variables: period–luminosity relation extends distances to nearby galaxies ($\lesssim$ tens of Mpc).

• Tip of the red giant branch (TRGB): standard-candle method complementary to Cepheids.

• Type Ia supernovae: standardized candles used out to $z \approx 1–2$ to measure $D_L(z)$ and constrain cosmic acceleration.

• Surface brightness fluctuations, masers, and other secondary distance indicators refine local calibrations.

• BAO: a standard ruler (comoving sound horizon) imprinted in galaxy clustering, constraining $D_A(z)$ and $H(z)$.

Key Observational Probes

Cosmic Microwave Background (CMB): The CMB provides a snapshot of the Universe at recombination ($z \approx 1100$). Its temperature anisotropies encode information about the primordial fluctuation spectrum, the baryon and dark matter densities, the geometry, and the overall age and composition of the Universe. The acoustic peak pattern tightly constrains ΛCDM parameters.

Baryon Acoustic Oscillations (BAO): BAO arise from sound waves in the early photon–baryon plasma, leaving a preferred comoving scale (the sound horizon) in the late-time distribution of galaxies. Measuring the BAO feature in galaxy clustering yields constraints on $D_A(z)$ and $H(z)$, providing a robust standard ruler.

Type Ia Supernovae (SNe Ia): Type Ia supernovae act as standardizable candles, allowing measurements of luminosity distance as a function of redshift. Their discovery in the late 1990s revealed that the cosmic expansion is accelerating, motivating dark energy/Λ.

Weak Gravitational Lensing: Weak lensing measures the coherent distortion of background galaxy shapes by intervening mass. It probes the projected matter distribution and the growth of structure, complementing geometry-based probes like BAO and SNe.

Galaxy Clustering and Redshift Surveys: The large-scale distribution of galaxies, measured by redshift surveys, constrains the matter power spectrum $P(k)$, the bias between galaxies and dark matter, and the growth rate of structure. Redshift-space distortions further probe the velocity field and gravity on large scales.

More Detailed Cosmology Nonmenclature

$a(t)$	Scale factor of the Universe
$a_{\ell m}$	Multipole of $\Delta T/T$
C_ℓ	Spectrum $\langle \lvert a_{\ell m} \rvert^2 \rangle$ of CMB anisotropy
f	Occupation number
$g_{\mu\nu}$ (g_{ij})	Spacetime (space) metric tensor
h_{ij}	Gravitational wave amplitude
H (H_0)	Hubble parameter $\dot{a}/a$ (present value)
k $(\mathbf{k})$	Comoving wavenumber (wave vector)
L $(\mathcal{L})$	Lagrangian (Lagrangian density)
n	Number density
$n_{\rm s}$	Spectral index of ζ
N	Hubble times of observable inflation
P	Pressure
$\mathbf{p}$ (p) (p^μ)	Momentum (magnitude of) (4-momentum)
$\mathcal{P}_g$	Spectrum of a perturbation g
r	Tensor fraction $\mathcal{P}_h/\mathcal{P}_\zeta$
$T^{\mu\nu}$	Energy momentum tensor
$\mathbf{v}$	Fluid velocity
V	Fluid velocity scalar
$V(\phi)$	Scalar field potential
x (x^μ) (x^i)	Comoving distance (spacetime coordinates) (space coordinates)
w	Ratio P/ρ for a fluid
z	Redshift
δ	Density contrast $\delta\rho/\rho$
ϵ	Slow-roll flatness parameter $\frac{1}{2}M_{\rm P}^2(V'/V)^2$
ζ	Primordial curvature perturbation
η	Slow-roll flatness parameter $M_{\rm P}^2 V''/V$
η	Conformal time $d\eta = dt/a$
$\eta_{\mu\nu}$	Metric tensor (Minkowski coordinates)
ρ (ρ_0)	Energy density (of present Universe)
Π	Anisotropic stress scalar
ϕ	Scalar field
Φ	Newtonian peculiar gravitational potential
Φ, Ψ	Metric perturbations
φ	Conformal inflaton field perturbation $a\delta\phi$
$\Omega_{\rm s}$	Present $\rho_{\rm s}/\rho$ of species 's"
R_c	Radius Hubble Sphere (Region where galaxies recede subliminally)
$g_{\mu\nu}$	The Metric $g_{\mu\nu}$. A rank two symmetric tensor that encodes information about geometry.
$T_{\mu\nu}$	Einstein Stress-energy Tensor which describes matter and energy distributions.
$R^{\delta}_{\mu\nu}$	Riemann Tensor is a math construct used to characterize the curvature of space-time.
$R_{\mu\nu}$	The Ricci Tensor is a contraction of the Riemann Tensor.
R	The Ricci Scalar is a contraction of the Ricci Tensor.
$G_{\mu\nu}$	The Einstein tensor $G\mu\nu$ is defined in terms of the Ricci tensor and scalar.

IIB. The ΛCDM or Lambda-CDM Concordance Model of Cosmology

See Section XXII: Λ-CDM Model Theory and Parameters

The ΛCDM or Lambda-Cold Dark Matter Model is a **parameterization of the ΛCDM cosmological model** in which the universe contains three major components: first, a cosmological constant denoted by Lambda associated with dark energy; second, the postulated cold dark matter; and third, ordinary matter. **A Concordance cosmology is a model of the universe that assumes a minimum number of parameters**, especially the Lambda-CDM model, which has 6 parameters: physical baryon density parameter; physical dark matter density parameter; the age of the universe; scalar spectral index; curvature fluctuation amplitude; and reionization optical depth. Different sorts of measurements — each using different kinds of instruments to look at completely different kinds of objects, all involving different kinds of physical processes, give completely consistent results. It is frequently referred to as the Standard Model of ΛCDM Cosmology because it is

The Simplest Model that provides a reasonably good account of the following properties of the cosmos:

- the existence, structure, uniformity, and magnitudes of anisotropies of the cosmic microwave background
- the large-scale structure in the distribution of galaxies
- the observed abundances of hydrogen (including deuterium), helium, and lithium
- the accelerating expansion of the universe observed in the light from distant stars, galaxies and supernovae.

This model assumes that General Relativity (GR) is the correct theory of gravity on cosmological scales. It emerged in late the 1990s as a concordance cosmology, after a period of time when disparate observed properties of the universe appeared mutually inconsistent, and there was no consensus on the makeup of the energy density of the universe. The ΛCDM model can be extended by adding cosmological inflation, quintessence, and other elements that are current areas of speculation and research in cosmology. This model does not explain baryon asymmetry..
The model includes **a single originating event, the "ΛCDM", a singularity,** which was not an explosion, but the abrupt appearance of expanding spacetime containing **radiation at temperatures of around 10^{15}** K. This was immediately (within 10^{-29} seconds) followed by an **exponential expansion of space by a scale multiplier of 10^{27}** or more, known as cosmic inflation. The early universe remained hot (above **10,000 K) for several hundred thousand years**, a state that is **detectable** as a residual cosmic microwave background, or **CMB**, a very low energy radiation emanating uniformly from all parts of the sky.

IIC. Hypothesized Thermal History of the Universe

We will briefly summarize the hypothetical thermal history of the universe, from the Planck era to the present. As we go back in time, the universe becomes hotter and hotter and thus the amount of energy available for particle interactions increases. As a consequence, the nature of interactions goes from those described at low energy by long range gravitational and electromagnetic physics, to atomic physics, nuclear physics, all the way to high energy physics at the electroweak scale, grand unification (perhaps), and finally quantum gravity. The last two are still uncertain since we do not have any experimental evidence for those ultra high energy phenomena, and perhaps Nature has followed a different path.

In principle, one can theoretically trace the evolution of the universe from its origin till today. According to the best accepted view, the universe must have originated at the Planck era (10^{19} GeV, 10^{-43} s) from a quantum gravity fluctuation. Needless to say, we don't have any experimental evidence for such a statement: Quantum gravity phenomena are still in the realm of physical speculation. However, it is plausible that a primordial era of cosmological inflation originated then. Its consequences will be discussed below. Soon after, the universe may have reached the Grand Unified Theories (GUT) era (10^{16} GeV, 10^{-35} s). Quantum fluctuations of the inflaton field most probably left their imprint then as tiny perturbations in an otherwise very homogenous patch of the universe. At the end of inflation, the huge energy density of the inflaton field was converted into particles, which thermalized and became the origin of the hot ΛCDM as we know it. Such a process is called reheating of the universe.
Since then, the universe became radiation dominated. It is "probable" (although by no means certain) that the asymmetry between matter and antimatter originated at the same time as the rest of the energy of the universe, from the decay of the inflaton. This process is known under the name of baryogenesis since baryons (mostly quarks at that time) must have originated then, from the leftovers of their annihilation with antibaryons.

II D. ΛCDM Model Cosmological Eras for the Early Universe

To describe the conditions of the early universe quantitatively, recall the relationship between the average thermal energy of particle (E) in a system of interacting particles and equilibrium temperature (T) of that system where k_B and $\hbar$ are Boltzmann and Planck constants. Then we can calculate the Energy Values, E for the different eras.

$k_B := 1.380649 \cdot 10^{-23} \cdot \frac{J}{K}$ $\quad eV := 1.6 \cdot 10^{-19} C \cdot volt$ $\quad GeV := 10^9 \cdot eV$ $\quad G := 6.67 \cdot 10^{-11} N \cdot m^2 \cdot kg^{-2}$

$\hbar := 4.13 \cdot 10^{-15} eV \cdot s$ **Convert Energy to Temp (K):** $E(T) := k_B \cdot T$ **Temp (K) to Energy:** $T(E) := \frac{E}{k_B}$

Planck Era: Derived from Fundamental Constants Scale for Quantum Effects on Gravity. Create Mini Black Holes?

Planck Length

$l_{pl} := \sqrt{\frac{\hbar \cdot G}{c^3}}$ $\quad l_{pl} = 4.045\, m \cdot 10^{-35}$

Planck Time

$t_{pl} := \frac{l_{pl}}{c}$ $\quad t_{pl} = 1.349\, s \cdot 10^{-43}$

Planck Energy, Temp, Mass, Density

$E_{pl} := \frac{\hbar}{2\pi \cdot t_{pl}}$ $\quad E_{pl} = 4.872 \times 10^{18} \cdot GeV$

$T(E_{pl}) = 5.646 \times 10^{31} K$

$M_{pl} := \sqrt{\frac{\hbar \cdot c}{G}} = 5.45 \times 10^{-8} kg$

$\rho_{pl} := \frac{M_{pl}}{\frac{4}{3} \cdot \pi \cdot {l_{pl}}^3} = 1.97 \times 10^{95} \frac{kg}{m^3}$

GUT Era: $E_{GUT} \approx 10^{16}\ GeV$ $\quad T(10^{16} GeV) = 1 \times 10^{29} K$

See **XXIX. Early Universe Models: Quark-Gluon Plasma**

Nucleons: Form at energies ≈ rest mass of a proton, or 1 GeV.

$T(1 GeV) = 1 \times 10^{13} K$

Atoms: Atoms form at an energy equal to the ionization energy of ground-state hydrogen (13 eV). The effective temperature for atom formation is therefore

$T(13eV) = 1.507 \times 10^5 K$

Photons: The formation of atoms in the early universe makes these atoms less likely to interact with light. Therefore, photons that belong to the CMB must have separated from matter at a temperature T associated with 1 eV (the approximate ionization energy of an atom). The temperature of the universe at this point was

$T(1eV) = 1.159 \times 10^4 K$

Recombination: Recombination is not instantaneous and photons keep re-ionizing hydrogen until the photon to baryon ratio drops enough.

The Saha equation describes the ionization equilibrium between electrons, protons, and neutral hydrogen:

- m_e is the electron mass $\quad m_e := 9.10938\, 10^{-31} kg$
- E_{ion} =13.6 V is the ionization energy of H.
- n_e is the electron density
- n_b is the baryon density, n_H Hydrogen density
- $n_b = n_e + n_H$ is the total baryon number density (protons + neutral hydrogen) and χ_e is their ratio.
- $n_\gamma(z)$ is the photon number density. @T=2.7K, n_γ ~410 cm^{-3}
- $\eta \sim 6*10^{-10}$ is the baryon to photon ratio.
- At recombination, the universe becomes ~50% ionized, so take $X_e \sim 0.5$
- $\xi(3)$ is the value of the Riemann zeta function at 3

$$\frac{n_e \cdot n_p}{n_H} = \left(\frac{2\pi \cdot m_e \cdot k_B \cdot T}{h^2}\right)^{\frac{3}{2}} \cdot e^{\frac{-E_{ion}}{k_B \cdot T}}$$

$$\frac{{\chi_e}^2}{1 - \chi_e} \cdot n_b = \left(\frac{2\pi \cdot m_e \cdot k_B \cdot T}{h^2}\right)^{2} \cdot e^{\frac{-13.6eV}{k_B \cdot T}}$$

$$n_b(T) := \left(\frac{2\pi \cdot m_e \cdot k_B \cdot T}{h^2}\right)^{\frac{3}{2}} \cdot e^{\frac{-13.6eV}{k_B \cdot T}}$$

$$\xi(n) := \sum_{n=1}^{\infty} \frac{1}{n^3} \qquad n_b(z) = \eta \cdot \frac{2\,\xi(3)}{\pi^2} \cdot \left(\frac{k_B \cdot T_{rec}}{h \cdot c}\right)^3$$

Putting it all together and solving for Trec gives:

$T_{rec} := 2970K$ $\quad z_{rec} := 1100$

$T_{recx} := \frac{13.6eV}{54 \cdot k_B}$ $\quad T_{recx} = 2919\, K$

Reionization:

Reionization refers to a change in the intergalactic medium from neutral hydrogen to ions. The neutral hydrogen had been ions at an earlier stage in the history of the universe, thus the conversion back into ions is termed a reionization. The reionization was driven by energetic photons emitted by the first stars and galaxies. We will use a combination of observational data and cosmological modeling.

We ask the question: **What was the time or redshift for the Reionization Era**

Mega Parsec, Mpc:

$Mpc := 3 \cdot 10^{19} km$

See Section XXII: Optical Depth - Reionization Optical Depth Parameter, τ

$$\tau = c \cdot \sigma_e \cdot \int_{t_{zcmb}}^{t_0} n_e(t)\, dt \qquad \tau = c \cdot \sigma_e \cdot \int_{t_{zcmb}}^{t_0} n_e(t) \cdot \left(\frac{d}{dz} t\right) dz \qquad \tau = \frac{2 \cdot c \cdot \sigma_T \cdot n_{e0}}{3 H_0} \cdot \sqrt{\Omega_m} \cdot \left[\left(1 + z_{re}\right)^{\frac{3}{2}} - 1 \right]$$

- $n_e(z)$ is the free electron density,
- σ_T is the Thomson cross-section,
- dt/dz depends on the cosmology

$H_0 := 67.4 \frac{km}{s} \cdot Mpc^{-1}$ $\quad \Omega_m := 0.315$ $\quad \tau := 0.054$

$\sigma_T := 6.652 \cdot 10^{-29} m^2$ $\quad n_{e0} := 2 \cdot 10^{-7} cm^{-3}$

Estimation Method for Redshift at Reionization

For a rough estimate using CMB optical depth τ, you can invert the equation assuming instantaneous reionization

Solving for z_{re} you get

$$z_{re} := \left(\frac{3 H_0 \cdot \tau}{2 \cdot c \cdot \sigma_T \cdot n_{e0} \cdot \sqrt{\Omega_m}} + 1 \right)^{0.66} - 1 \qquad z_{re} := 7.7$$

Estimate the temperature of the universe at reionization, we use the fact that the temperature of the cosmic microwave background (CMB) scales with redshift as:

Given Current CMB Temperature: $T_{cmbr} := 2.725K$ $\quad T_z(z) := T_{cmbr} \cdot (1 + z)$ $\quad T_z(7.7) = 23.707\,K$

CMB: $\mu eV := 10^{-6} eV$ $\quad E(T_{cmbr}) = 235.142 \cdot \mu eV$

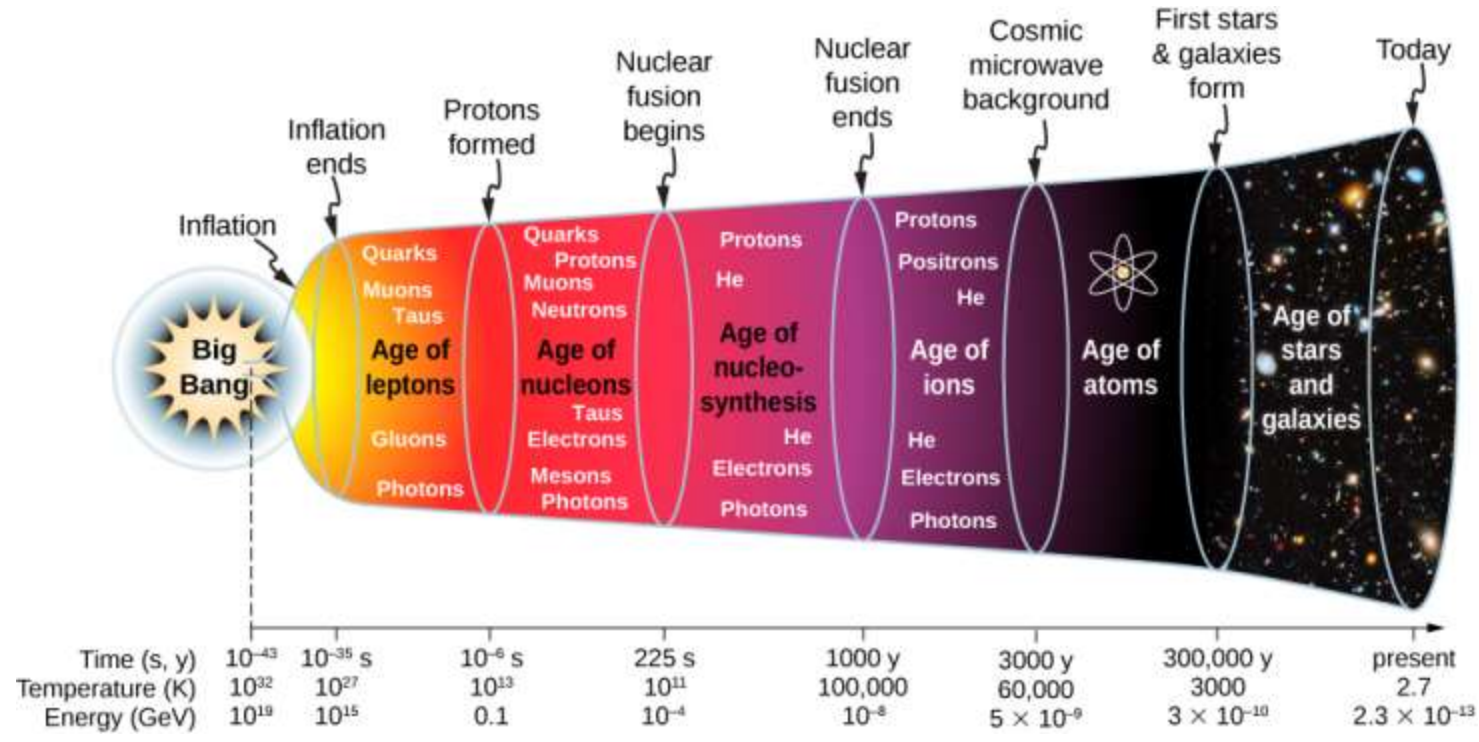

Hypothetical and Observable Thermal Sequence For the ΛCDM Theory

https://universe-review.ca/F02-cosmicbg01.htm

The relics and observables are physical facts,

while the interpretations of the events are mostly theories or conjectures. **See XXXII for Plot of Time Evolution of Eras.**

At any given time, **temperature translates** to a **characteristic mass** of particles ($\mathbf{kT \approx mc^2}$), which dominate that epoch.

Era	Time @ end of era	Size (observable) @ end of era	Energy/Temp	Relics & Observables	Events (as re-constructed from theories)
Planck era (???)	< 5.4×10^{-44} sec	< 1.6×10^{-33} cm	> 1.2×10^{19} Gev	(3+1)D space-time; Cosmic Expansion	Expansion started from a point to Planck scale; all forces united into one
GUT era	<10^{-35} sec	< 10^{-26} cm	> 10^{14} Gev > 10^{27} K	High energy cosmic rays; fundamental interactions	Separation of spacetime and matter; separation of gravitational, strong, and electroweak forces
Inflation (Rate of Expansion >>> c)	< 10^{-32} sec	< 30000 cm	10^{14} Gev	Un-observable universe; large scale structures	Reheating; Unstable vacuum; quantum fluctuations
Top Quark era Electro-weak era Quark-Gluon era QCD Domain	≈ 10^{-25} sec < 10^{-11} sec ≈ 10^{-10} sec ≈ 10 µsec	< 10^{14} cm	> 8 Tev > 300 Gev > 150 Gev > 200 Mev	Radiation; excess of matter over anti-matter; separation of force (bosons), and matter (fermions) fields	Radiation released in reheating; baryon asymmetry; separation of weak and E-M forces; origin of mass
Hadron era	< 1 sec	< 10^{20} cm	> 1.7 Mev	Formation of hadrons	Axion as dark matter
Weak decoupling	< 4 min	< 4×10^{20} cm	> 100 kev	neutron/proton ratio fixed	Neutrinos decouple
Nucleosynthesis	< 1/2 hour	< 10^{21} cm	> 40 Kev	Fraction of Light elements	Nuclear reactions freeze out, stable nuclei form
Radiation era Matter era	< 0.24 My	< 2×10^{27} cm	> 0.6 ev	Mass density fluctuations	Matter density finally exceeds radiation density
General Cosmology Time Era: Astronomical Observable, Relics, and Measureable					
Recombination $p^+ + e^- \rightarrow H + \gamma$	< 0.3 My	< 3×10^{27} cm	> 3000°K	CMBR 1965 Penzias and Wilson	e- and p+ recombine into H atoms, universe became transparent to light
----- Redshift----- *z = 1100 to 30* Dark Ages	< 1 Gy	< 2×10^{28} cm	> 100°K	21 cm radio emission, First stars, heavy elements	mass fluctuations grow, first small objects coalesce, reionization
Galaxy formation	< 2 Gy	< 2.5×10^{28} cm	> 70°K	Stars, quasars, galaxies	Collapse to galactic systems
Bright age of Galactic Clusters	< 12 Gy	< 4.5×10^{28} cm	> 3°K > 0.00025 ev	Solar system; decline of stellar formation from peak	dark energy became dominant; formation of clusters of galaxies
Present era	~ 13.7 Gy	~ 4.7×10^{28} cm	~ 2.73°K	Supercluster	Large scale gravitational instability

II E. List of Challenges with the ΛCDM Big Bang Theory (ΛCDM) - See Section XXXI for More Details

The ΛCDM Theory is a Concordance Model. It is derived by fitting six parameters to minimize errors. It is a parameterized phenomelogical model with strong predictive consistency across multiple observables.

Methodology of ΛCDM: . It's origin is using six parameters to curve fit the model to known measurements. When faced with discrepancies between theory and observation, cosmologists habitually react by adjusting or adding these parameters to fit observations, propose additional hypotheses, or even propose "new physics" and ad hoc solutions that preserve the core assumptions of the existing model.

The ΛCDM is based on the unverified core assumptions of the Cosmological Principle, namely that,

- ♦ The universe is isotropic and homogenous space at sufficiently large scales > 100 Mpc (MegaParsec).
- ♦ However, The Cosmological Principle is manifested false within the distance scales that can be verified.

ΛCDM Violates the Second Law of Thermodynamics: How did the universe start with such a Low Entropy?

The unknown nature and existence of Cold Dark Matter. The unknown nature and existence of Dark energy

Without the above sources of matter, the universe would be younger than the oldest stars, which is a contradiction.

Value of Cosmological Constant is one of the hugest inconsistencies in Physics. Off by 120 orders of magnitude!

Inflation Theory that requires initial conditions so unlikely that the probability that it happened purely by chance is greater than the probability of expansion by the Theory of Inflation.

Inflation requires a density 20 times higher than that implied by nucleosynthesis.

Postulates that the universe springs from a singularity. A singularity is a point of infinite density, infinite pressure, infinite temperature, and zero volume. At best, an extremely unstable state that is beyond the known laws of physics.

There is no known science that covers this, that is, no known physical laws.

At best it is veiled by the Planck era. A singularity is a thermodynamic dead end. Cannot return to other states.

None of Laws/Forces of Nature apply to Inflation, including GR. No event horizon around it. No spatial direction.

Friedmann Model breaks down at a singularity. No shell in which to define density. There is no space to put matter.

String Theory (M-Theory): Particles consist of one dimensional or two dimensional (called "branes") entities.

Absence of magnetic monopoles.

Assumption is that the only force on a cosmological scale is gravity. The force of gravity is 10^{-39} times smaller than E-M, but huge magnetic fields in space and indication of huge voltages and charge differences.

There is no explanation for the absence of anti-matter.

Expansion from a Singularity cannot produce rotational momentum required for galaxies and planets.

Confined gas molecules will produce a turbulence, destructive to a flat universe.

Latest Conflict with ΛCDM Theory - Latest Discoveries from the James Webb Telescope

The James Webb telescope, looking back to 400,000 years after the ΛCDM, has discovered at least five massive galaxies. These massive galaxies would have to grow 20 times faster than the Milky Way. For these young galaxies, the ΛCDM predicts galaxies 10 to 100 times smaller. There are various ways to account for these new discoveries.

The Tenuous Link of the Stellar Distance Ladder

One of the Core Principles of the Current ΛCDM Theory of the Universe is the Validity of the use of Stellar Distance Ladders to measure the distance to galaxies. However, less than 1% of the visible universe has a Distance Ladder that is verifiable by direct measurement.

Inconsistencies and Challenges -Cosmological "Tensions" Hubble Value See Sections XXII and XXXII

Differences in measured values of Hubble Constant from Redshift vs. Recession Velocity and CMB Uniformity

High redshift galaxy observations predict a higher star formation efficiency then BBT Planck CMB.

"Population of surprisingly massive galaxy candidates with stellar masses of order of 10^9 x Mass of the Sun, $M_\odot$.

See this Review Article for an Up-to-date Summary of the Challenges and "Tensions" facing the ΛCDM:

Challenges for ΛCDM: An update, L. Perivolaropoulos and F. Skara, arXiv:2105.05208v3 6 Apr 2022

Successes of the ΛCDM Model

The ΛCDM model has been remarkably successful in explaining most properties of a wide range of cosmological observations including the accelerating expansion of the Universe (Perlmutter et al. 1999; Riess et al. 1998), the power spectrum and statistical properties of the cosmic microwave background (CMB) anisotropies (Page et al. 2003), the spectrum and statistical properties of large scale structures of the Universe.

III. Mathematical Basis ΛCDM Cosmology: Einstein's General Relativity, FLRW & GR Tests

In 1915, Einstein developed his **General Theory of Relativity (GR)**. GR consists of a number of field equations that relate the geometry of spacetime to the distribution of matter within it. GR provides a deep physical and geometrical description of how mass/energy determines the dynamics of the universe.
The space-time evolution of the universe is guided by the Einstein Field Equation.

$$R_{\mu\nu} - \frac{1}{2} g_{\mu\nu} R = \frac{1}{M_{\rm pl}^2} T_{\mu\nu}$$

where the spacetime metric $g_{\mu\nu}$ and its corresponding Ricci tensor $R_{\mu\nu}$ and Ricci scalar R are related to energy content expressed through the Einstein Symmetric, order-2, Energy-Momentum Tensor $\boldsymbol{T_{\mu\nu}}$. Briefly, the Einstein equations equate the matter that's present in a spacetime with the spacetime's geometry.

In 1917, Schwarzschild solved the Einstein equations under the assumption of spherical symmetry, two years after their publication. The most obvious spherically symmetric problem is that of empty space outside a planet or star. The mass curves space-time and thus affects the particles moving nearby. The space-time interval in spherical coordinates in the Schwarzschild solution is.

$$ds^2 = (1 - \frac{2GM}{c^2 r}) c^2\, dt^2 - \frac{dr^2}{(1 - \frac{2GM}{c^2 r})} - r^2\, d\theta^2 - r^2 \sin^2\theta\, d\psi^2$$

General Relativity Test #1: Schwarzschild Equation Prediction of the Formation of a Black Hole

The definition of **proper time**, τ (tau), is the time interval for an **observer at rest**. In Minkowski space time $ds^2 = dt^2 - dx^2$, **for $dx = 0$, $dt = d\tau$**. Similarly in the Schwarzschild Metric if we have an observer at rest then dr = 0...etc and then proper time should be $dt = d\tau$ (like in the SR case giving ds = (1−2M/r)dt = (1−2M/r)$d\tau$

the first term T_{00} in the Einstein $T_{\mu\nu}$ Tensor is T_{tt}. If you take the distance r to be equal to $r_s = 2\frac{G \cdot M}{c^2}$ then the time factor, T_{tt}, which is equal to 1 - 2GM/c^{2}r in ds^2 becomes 0, so the value of ds^2 is undefined. It becomes a singularity. This value of the **radius = r_s** is called the **Schwarzschild radius**.

From the Schwarzschild Metric, if we plot the passage of time, $\Delta\tau$, versus the distance to the center, r, the relation is:

$$\Delta\tau(r) := 1 - 2\frac{GM}{r} \qquad E\text{-}R(\chi) := \chi \cdot e^{\frac{\chi}{2}} + \Theta$$

See Plots Below for Passage of Time $\Delta\tau(r)$ and Space (ER) in Schwarzschild Black Hole

The Plot below show that at the Event Horizon that the passage of proper time, τ, slows to 0, that is, time stops.

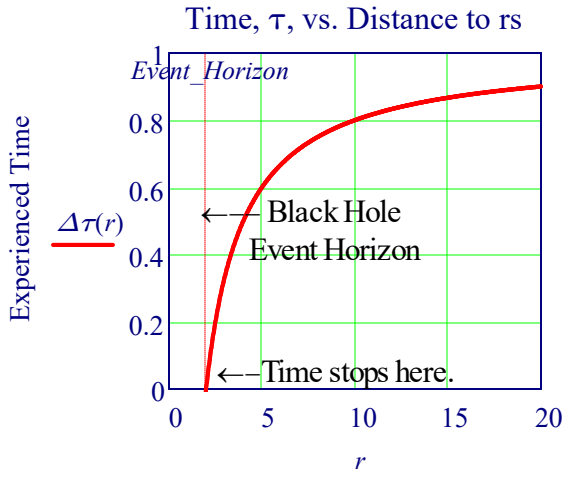

Schwarzschild Black Hole
Math 3D Surface Plot of Einstein-Rosen Bridge*

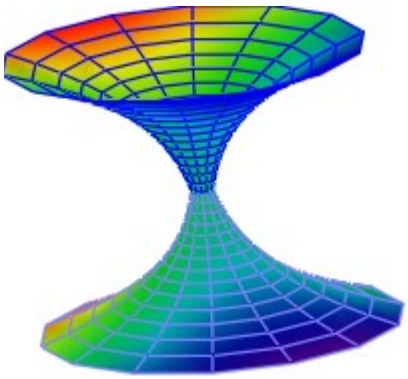

Theoretically, this connects two asymptotically flat "universes."

Image of the Event Horizon Captured by the EVLI Event HorizonTelescope

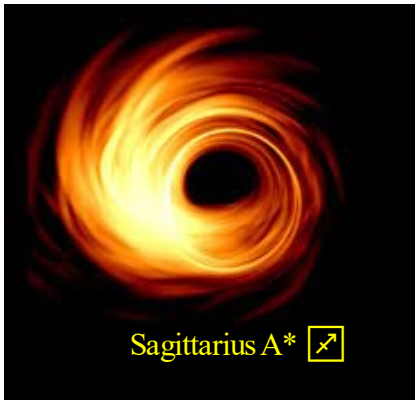

* Physikalische Zeitschrift. XVII: 448; Einstein & Rosen 1935, Phys. Rev. 48 73

General Relativity Test #2: GR Calculation of Precession of Mercury's Orbit

Reference: *The Precession of Mercury's Perihelion*, Owen Biesel, https://sites.math.washington.edu

Our First Test is the Calculation of the Precession of the Perihelion of Mercury. Newton's Theory says it 532 arcseonds per century, but the observed value is 43 arcseconds per century.

We will apply a General Relativistic treatment of geodesics in the Schwarzschild metric, and show that an "orbit" matches the observed Mercury's shift of approximately **43 arcseconds per century**. We assume that the particle is a test particle traveling along a geodesic through spacetime. Geodesics can also be described as stationary points of the integral

$$I = \int \langle \dot{\mathbf{x}}, \dot{\mathbf{x}} \rangle \, d\tau$$

Assume that the metric that similar to the above Schwarzschild Solution, we assume that the solar system is spherically symmetric, static, and asymptotically flat, so that the metric can be represented as follows:

$$ds^2 = -e^{2\alpha(R)}dT^2 + e^{2\beta(R)}dR^2 + e^{2\gamma(R)}d\Omega^2,$$

where the $d\Omega^2 = d\theta^2 + \sin^2\theta d\varphi^2$ term comes from spherical symmetry and T is the coordinate produced by the timelike Killing vector field. Then the **Euler-Lagrange Equations** for φ and T are

$$0 = \frac{d}{d\tau}\left(2r^2\dot{\phi}\right)$$

$$0 = \frac{d}{d\tau}\left(-2\left(1 - \frac{R_S}{r}\right)\dot{T}\right)$$

Binding Energy per Unit Mass, -E

$$-E = \frac{1}{2}\left(\dot{r}^2 + r^2\dot{\phi}^2\right) - \frac{GM}{r}$$

Now r(φ) is periodic with period 2π.

where $R_S = 2GM$ is the Schwarzschild radius of the sun.

The above implies that $L = r^2\dot{\varphi}$ and $E = \dot{T}(R_S/r - 1)$ are two constants of the motion. Then the relation $\mathcal{L} = -1$ gives us:

$$(\dot{r})^2 = (E^2 - 1) + \frac{R_S}{r} - \frac{L^2}{r^2} + \frac{R_S L^2}{r^3}$$

Now we introduced the notation $R\pm$ for the nonzero roots of the quartic polynomial in terms of the closed orbit r'

Now the requirement that of a closed orbit with $(r')^2 \geq 0$ imposes some constraints on L, E, and R_S; we need a connected component of $\{r : r' \geq 0\}$ to be a compact subset of R_+.

This means there exist at least two values R_+ and R_- where $r' = 0$, i.e. aphelion and perihelion. For Mercury

$$M_\odot := 1.989 \cdot 10^{30} kg \qquad R_+ := 69.8 \cdot 10^6 km \qquad R_- := 46 \cdot 10^6 km \qquad R_s := 2.95 km$$

Then the angle shift from R_- to R_+ is given, as in the Classical case, by:

$$\phi_+ - \phi_- = \int_{R_-}^{R_+} \frac{dr}{\sqrt{\frac{E^2-1}{L^2}r^4 + \frac{R_S}{L^2}r^3 - r^2 + R_S r}}.$$

Define D, ε:

$$D := \frac{R_+ \cdot R_-}{R_+ + R_-}$$

$$\varepsilon := \frac{R_s}{1 + R_s \cdot D^{-1}}$$

Now use the Taylor series expansion $(1 - \varepsilon/r)^{-1/2} \approx 1 + \varepsilon/2r$. This gives

$E := 0$

$$\phi_\pm = \phi_+ - \phi_- = \sqrt{\frac{L^2}{1 - E^2}} \int_{R_-}^{R_+} \frac{1 + \mathcal{E}}{r\sqrt{(R_+ - r)(r - R_-)}} + \frac{\varepsilon/2}{r^2\sqrt{(R_+ - r)(r - R_-)}} dr$$

$$\phi_\pm := \frac{\pi}{\sqrt{1 - \frac{R_s}{D}}} \cdot \left(1 + \frac{1}{4}\frac{R_s \cdot D^{-1}}{1 - R_s \cdot D^{-1}}\right) + \frac{\pi}{\sqrt{1 - \frac{R_s}{D}}} \cdot E$$

$$\phi_\pm - \pi = 0$$

The above $\phi_\pm$ equation is a trustworthy estimate of $\varphi_+ - \varphi_-$ (half a revolution, in radians)

Since Mercury completes 415.2 revolutions each century, and there are $360 \cdot 60 \cdot 60/2\pi$ arcseconds per radian, we find that General Relativity predicts that Mercury's perihelion advances by

$$\left(\phi_\pm - \pi\right) \cdot \frac{360 \cdot 60 \cdot 60}{\pi} \cdot 415.2 = 42.938 \quad \textbf{arcseconds per century.}$$

This calculated value from General Relativity agrees with the observed value of 43.1 ± 0.5 arcseconds per century.

GR Test #3: Predict Clock Difference Between GPS Satellite & Surface of Earth

The difference between a clock on the surface of earth and a clock in a Global Position Satellite in orbit above the earth is 38 microseconds per day. Does General Relativity predict this value of 38 microsecond difference?

Two Things Affect the Net Time Dilation (Note: This also applies to distant starlight. See Section XXIB):

Gravitation and Velocity. Velocity of Satellite slows satellite time down relative to earth, but the Earth's Gravitational Field Slows down clocks on earth for different heights.

G is Universal Gravitational Constant

$G := 6.674 \cdot 10^{-11} \cdot m^3 \cdot kg^{-1} \cdot s^{-2}$

$v_{eq} := 0.465 \frac{km}{s} = 1040.175 \cdot \frac{mile}{hr}$

GPS Period is 12 hours

$v_s := 3697 \frac{m}{s} = 8269.953 \cdot \frac{mile}{hr}$

M is mass of the earth

$g = 9.807 \frac{m}{s^2}$

$r_{eq} := 6378 km$

$alt_s := 20200 km$

$alt_s = 12551.698 \cdot mile$

c is the speed of light

$c = 2.99792458 \times 10^8 \frac{m}{s}$

$M_e := 5.97 \cdot 10^{24} \cdot kg$

Scale Factor, Micro, μ

$\mu := 10^{-6}$

Special and General Relativity Gives the Amount of Time Dilation as:

General Relativity: Schwarzschild Metric Gravitational Time Dilation Per Day

The Einstein Field Equation

Gives the Schwarzschild Metric

$$R_{\mu,\nu} - \frac{g_{\mu,\nu} R}{2} - \lambda \cdot g_{\mu,\nu} = \kappa \cdot T_{\mu,\upsilon}$$

The Schwarzschild Metric, describes space-time in the vicinity of a non-rotating massive spherically symmetric. It gives the change in time, $\Delta\tau\_\Delta t_{gravity}$ for altitude, alt.

$$\Delta\tau\_\Delta t_{gravity}(alt) := \left[\sqrt{1 - \frac{2 \cdot G \cdot M_e}{(alt + r_{eq}) \cdot c^2}} - \sqrt{1 - \frac{2 \cdot G \cdot M_e}{r_{eq} \cdot c^2}}\right] \cdot 24 \cdot 60 \cdot 60 s$$

Δτ for Satellite at Altitude: $\Delta\tau\_\Delta t_{gravity}(alt_s) = 45.643\, s \cdot \mu$

Special Relativity: Velocity Time Dilation Per Day

$$v_{orbit}(r) := \sqrt{\frac{G \cdot M_e}{r}} \qquad \Delta\tau\_\Delta t_{velocity}(r) := 1 - \frac{1}{\sqrt{\left(1 - \frac{v_{orbit}(r)^2}{c^2}\right)}}$$

$$\Delta t_{velocity\_day} := \Delta\tau\_\Delta t_{velocity}(alt_s + r_{eq}) \cdot 24 \cdot 60 \cdot 60 s = -7.206\, s \cdot \mu$$

Total Time on Earth Per Day is (Dilated) Longer by microseconds:

$$Total\ GPS\ Clock\ Dilation := \Delta\tau\_\Delta t_{gravity}(alt_s) + \Delta t_{velocity\_day}$$

$$Total\ GPS\ Clock\ Dilation = 38.438\, s \cdot \mu$$

Twice a Day the Time for a Satellite is Slowed by (19 μs) to match time on Earth
If not Corrected the Position Error Per Day Would be:

Two Satellite GPS Distance Error = Time Error x Speed of Light, c

$$Total\ GPS\ Clock\ Dilation \cdot c = 7.16 \cdot mile$$

IV. The Equation of State for a Simple Fluid Model

• Usually written as $P = w\,\rho$ P is the Pressure and ρ is the density.
• Note that this relationship is the simplest model. The actual model may be more complex.
• This is not necessarily the best way to describe matter/energy density; it implies a fluid of some kind
This may be acceptable for the matter and radiation we know,
but maybe it is not an optimal description for the dark energy
• Define Special values:
w = 0 means P = 0, e.g., non-relativistic matter
w = 1/3 is radiation or relativistic matter
w = −1 looks just like a cosmological constant
… but it can have in principle any value, and it can be changing in redshift

Evolution of the Density, ρ

Generally: $\rho \approx a^{-3(w+1)}$

- Matter dominated (w = 0):
- Radiation dominated (w = 1/3):
- Cosmological constant (w ≈ –1):
- Dark energy with (w < –1) e.g., w = –2:
  – Energy density increases as is stretched out!
  – Eventually would dominate over even the energies holding atoms together! ("Big Rip")

Continuity Equation
(Specifies that matter is conserved.)

$$\frac{\partial \rho}{\partial t} + \nabla \cdot (\rho\, \boldsymbol{v}) = 0$$

$\rho_m \approx a^{-3}$ Continuity Equation: $\rho \approx a^{-3}$
$\rho_r \approx a^{-4}$ Wavelength stretched with z
$\rho_\Lambda = constant$ Constant Vacuum Energy
$\rho_{dm} \approx a^{+3}$

$$\rho_m(t) = \rho_{m,0}\, a^{-3}(t)$$
$$\rho_r(t) = \rho_{r,0}\, a^{-4}(t)$$
$$\rho_v(t) = \rho_v = \text{const.}$$

See Sections VII & XXVIII for Density Plot

In a mixed universe, different components ρ_m, ρ_r, ρ_Λ will
dominate the global dynamics at different times →
Note in principle, it could be a function of time, density, etc

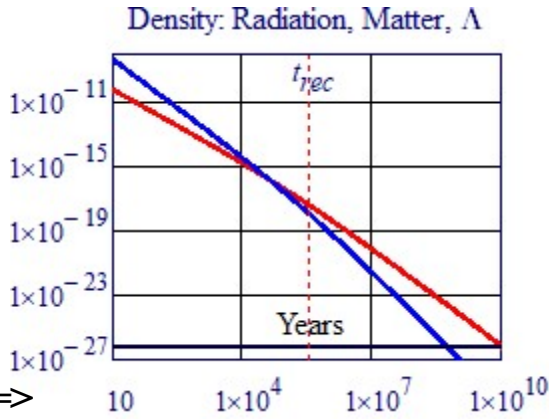

• Radiation density decreases the fastest with time
– Must increase fastest on going back in time
– Radiation must dominate early in the Universe
• Dark energy with w ≈ –1 dominates last; it is the dominant component now, and in the future

Models With Both Matter & Radiation ⟹

However, to good approximation, assume that K = 0 and either **radiation** or **matter** dominate

"α" is the symbol for *proportional to*

	γ-dom	m-dom	Λ-dom
	$a(t)$	$\alpha\ t^{1/2}$	$\alpha\ t^{2/3}$
• Matter (m) dominated (w = 0):	$\rho_m\ \alpha\ a^{-3}$	$\alpha\ t^{-3/2}$	$\alpha\ t^{-2}$
• Radiation (γ) dominated (w = 1/3):	$\rho_\gamma\ \alpha\ a^{-4}$	$\alpha\ t^{-2}$	$\alpha\ t^{-8/3}$

• Cosmological Constant (Λ) (w = -1): ----------> $\Lambda \approx a^{-\lambda t}$

Density of radiation today is mostly determined by the Temp of CMB.

$$z_{eq} \simeq 3612\,\Theta_{2.7}^{-4}\left(\frac{\Omega_{m0}h^2}{0.15}\right) \qquad \Theta 2.7 = T_{cmb}/2.75mK$$
$$T_{eq} = T_{CMB}(1 + z_{eq}) \qquad T_{eq} \simeq 5.65\,\Theta_{2.7}^{-3}\,\Omega_{m0}h^2\ \text{eV}$$

w = 1/3 radiation dominated $a(t) \propto t^{1/2}$
w = 0 matter dominated $a(t) \propto t^{2/3}$
w = -1 vacuum dominated $a(t) \propto e^{Ho\,t}$

In 1922 Friedmann–Lemaître–Robertson–Walker (FLRW) proposed a Relativistic Space-Time Metric that is the basis for an exact solution of Einstein's field equations of General Relativity; it is based on the assumption of a **homogeneous, isotropic, and expanding** (or otherwise, contracting) universe. The general form of the metric follows from the assumption of **homogeneity and isotropy** of space in the universe; Under these set of assumptions, Einstein's field equations are only needed to derive the scale factor of the universe as a function of time.

If we model the universe as a homogeneous, isotropic with spherical coordinates, we obtain the the Friedmann metric. **By defining a cosmic scale factor, "*a(t)*"**, which is a **function of time**. This scale factor parametrizes the **expansion of space**. The radius, r, is transformed to a comoving coordinate. **Furthermore, the radius of curvature** is also affected by cosmic expansion so it can be expressed in terms of the scale factor and a constant k

The Friedmann–Lemaître–Robertson–Walker (FLRW) Relativistic Space-Time Metric in terms of "a" is:

$$ds^2 = -c^2dt^2 + a^2(t)\left[\frac{dx^2}{1-\kappa\frac{x^2}{R^2}} + x^2d\Omega^2\right] \qquad \text{where} \quad Kt = \frac{k}{a^2t}$$

Note: "***a***" is NOT the acceleration, it is the Scale Factor $R(t)/R(t_0)$.

Based on this metric and its solution of the **Einstein's Field Equations** give the **Two Friedmann Equations**.
The assumption given the Field Equation: $R_{00} = T_{00}$

The first Equation is:

$$\frac{\dot{a}^2 + kc^2}{a^2} = \frac{8\pi G\rho + \Lambda c^2}{3} \qquad H^2 = \frac{8\pi \cdot G \cdot \rho + \Lambda \cdot c^2}{3} - \frac{k \cdot c^2}{a^2}$$

The Second Equation is: the Evolution of the Cosmic Scale Factor, *a*.

$$\frac{\ddot{a}}{a} = -\frac{4\pi G}{3}\left(\rho + \frac{3p}{c^2}\right) + \frac{\Lambda c^2}{3}$$

where ***a* is the scale factor**, *G, Λ, and c* are universal constants. *G* is Newton's gravitational constant, *Λ* is the cosmological constant with dimension length^{-2}, and c is the speed of light in vacuum. *ρ* and *P* are the volumetric mass density and the pressure, respectively. *k* is constant throughout a particular solution, but may vary from one solution to another. The symbol "*a*" is defined as the scale factor which changes with time, *ρ and p* are the volumetric mass density and pressure. They may vary from one solution to another. The expansion of the universe (***ȧ/a***) can be measured.
In the Friedmann model, **H ≡ ȧ/a and is defined as the Hubble parameter, which evolves with time.**

Hubble's Law, Expansion, and Redshift

The Friedmann equation allows us to explain Hubble's discovery that recession velocity is proportional to the distance. The velocity of recession is given by $\vec{v} = d\vec{r}/dt$ and is in the same direction as $\vec{r}$, allowing us to write

$$\vec{v} = \frac{|\dot{\vec{r}}|}{|\vec{r}|}\vec{r} = \frac{\dot{a}}{a}\vec{r}.$$

The last step used $\vec{r} = a\vec{x}$, remembering that the comoving position $\vec{x}$ is a constant by definition. Consequently, Hubble's law $\vec{v} = H\vec{r}$ tells us that the proportionality constant, the Hubble parameter, should be identified as **H ≡ ȧ/a**

$$H = \frac{\dot{a}}{a}$$

and the value as measured today can be denoted with a subscript '0' as H_0. Because we measure Hubble's constant to be positive rather than negative, we know that the Universe is expanding rather than contracting.
We notice from this that the phrase Hubble's constant is a bit misleading. Although certainly it is constant in space due to the cosmological principle, there is no reason for it to be constant in time. In fact, using it as a more compact notation, we can write the Friedmann equation as an evolution equation for *H(t)*. as

$$H^2 = \frac{8\pi G}{3}\rho - \frac{k}{a^2}$$

It is best to use the phrase 'Hubble parameter' for this quantity as a function of time, reserving 'Hubble constant' for its present value. Normally the Hubble parameter decreases with time, for instance as the expansion is slowed by the gravitational attraction of the matter in the Universe.

Expansion and Redshift

The redshift of spectral lines that we **used to justify the assumption of an expanding Universe** can also be related to the scale factor. In this derivation we'll make the simplifying assumption that light is passed between two objects which are very close together, separated by a small distance *dr*. We've drawn the objects as galaxies, but we really mean two nearby points. According to Hubble's law, their relative velocity *dv* will be

$$dv = H\,dr = \frac{\dot{a}}{a}\,dr$$

where $d\lambda$ is going to be positive since the wavelength is increased. The time between emission and reception is given by the light travel time $dt = dr/c$, and putting all that together gives

$$\frac{d\lambda}{\lambda_e} = \frac{\dot{a}}{a}\frac{dr}{c} = \frac{\dot{a}}{a}\,dt = \frac{da}{a}$$

Integrate and we find that $\lambda = \ln a + \text{constant}$, that is $\lambda \propto a$

where λ is now the instantaneous wavelength measured at any given time.

Although as we've derived it this result only applies to objects which are very close to each other, it turns out that it is completely general. It tells us that as space expands, wavelengths become longer in direct proportion. One can think of the wavelength as being stretched by the expansion of the Universe, and its change therefore tells us how much the Universe has expanded since the light began its travels. For example, if the wavelength has **doubled**, the Universe must **have been half its present size** when the light was emitted. Redshift observed is the wavelength from the emitted source.

The redshift as defined in the equation below is related to the scale factor by

$$1 + z = \frac{\lambda_{obs}}{\lambda_{em}} = \frac{a(t_{obs})}{a(t_{em})} \qquad z = \frac{\lambda_{obs} - \lambda_{em}}{\lambda_{em}}$$

where λ_{em} and λ_{obs} are the wavelengths of light at the points of emission (the galaxy) and observation (us).

In order to solve the Friedmann Equation, **we need to define the behavior of the mass/energy density, ρ(a)** of any given mass/energy component. Recall the basic

General Relativity paradigm relating to Cosmology:

Density Determines the Expansion
Expansion Changes the Density

Λ Density Parameter

$$\Omega_\Lambda = \frac{\rho_\Lambda}{\rho_{crit}}$$

Matter Density Parameter

$$\Omega_M = \frac{\rho_M}{\rho_{crit}}$$

Density Components: Each component will lead to a different evolution in redshift and a different Model

Matter, Radiation, Λ: $\rho_m(t) = \rho_{m0}\cdot a^{-3}(t)$ $\rho_{rad}(t) = \rho_{rad0}\cdot a^{-4}(t)$ $\rho_\Lambda(t) = \rho_\Lambda = constant$

$$\rho_0 = \frac{3\cdot H_0^{\,2}}{8\cdot\pi\cdot G}$$

Seconds in a Billion (Giga) Years, Gyr

$$Gyr := 3600\cdot 24\cdot 365.24\cdot 10^9\cdot s = 3.156\times 10^{16}\,s$$

MegaParSec (Mpc)

$$Mpc := 3\cdot 10^{19}\,km$$

Estimate of Hubble H_0

$$H_0 := 73\,\frac{km}{s}\cdot(Mpc)^{-1}$$

$$\Omega_M = \frac{8\pi G\cdot\rho}{3\cdot H_0^{\,2}} \qquad \Omega_\Lambda = \frac{\Lambda\cdot c^2}{3\cdot H_0^{\,2}}$$

When $a_0 = 1$

$$H_0^{\,2}\cdot\Omega_\Lambda = \Lambda\cdot c^2\,3$$

Models in Cosmology

In General: $\frac{8\pi G\rho}{3} = H_0^{\,2}\left(\Omega_{\Lambda,0} + \Omega_{m,0}a^{-3} + \Omega_{\gamma,0}a^{-4}\right)$

$\frac{1}{H_0} = 13.023 \cdot Gyr$

Example of Models

Einstein de Sitter Matter Only (γ, Λ = 0) Model **See Section VIII.**

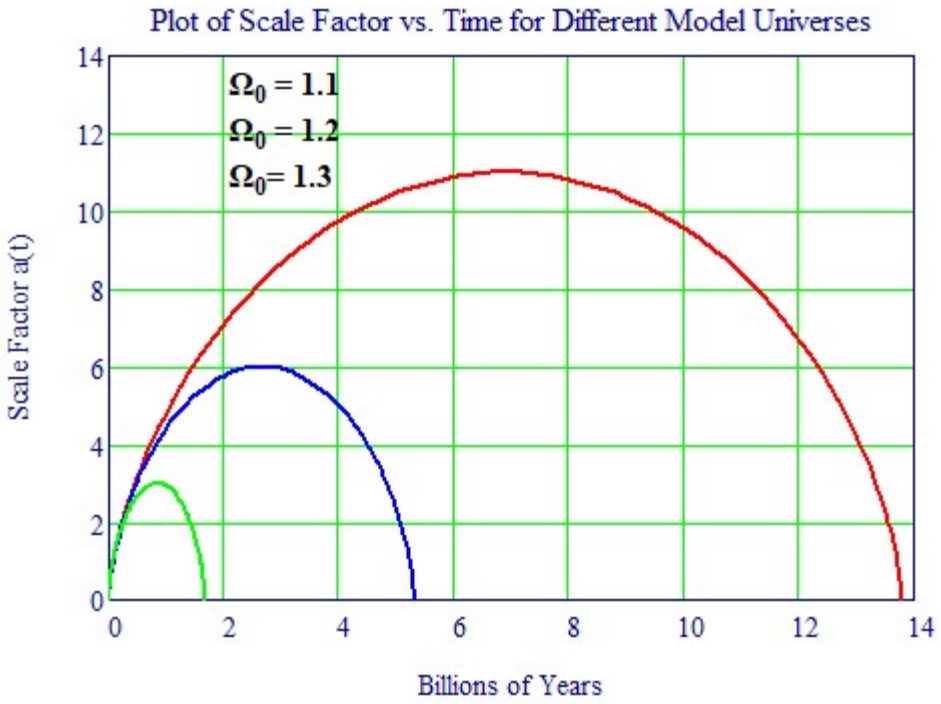

Consider Several Simple Models

Refer to Section VIII for Model Details

- k = 0, matter dominated, **Einstein de Sitter**
- k = 0, radiation dominated
- k < 0, ρ = 0, Milne Model
- k < 0, ρ > 0
- k > 0
- Λ dominated

k is the curvature of space

w=1/2 radiation dominated $a(t) \propto t^{1/2}$

w=0 matter dominated $a(t) \propto t^{2/3}$

w = -1 vacuum dominated $a(t) \propto e^{Ho\,t}$

De Sitter Universe has a constant curvature surface embedded in Minkowski space-time (two-dimensional case)

The Milne Model Universe is simply a piece of Minkowski spacetime described in expanding coordinates.

Where dr^2 is transformed to $d\chi^2$

$$ds^2 = dt^2 - t^2(d\chi^2 + \sinh^2\chi\, d\Omega^2)$$

Classification of Models

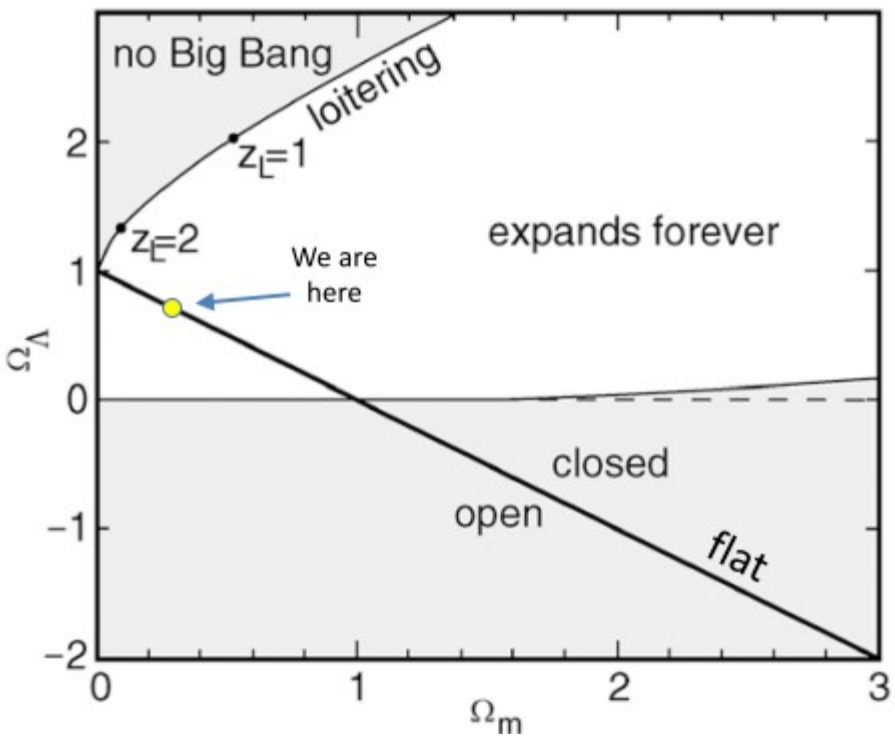

(Ignoring Ω_{rad}, since it is negligible for most of the history of the universe)

V. Distances in Cosmology: The Basic Goal of Cosmology and Hubble's Law

Hubble's law, also known as the **Hubble–Lemaître law**, is the observation in physical cosmology that galaxies are moving away from Earth at speeds proportional to their distance. In other words, the farther they are, the faster they are moving away from Earth. The velocity of the galaxies has been determined by the change in the wavelength, redshift (z), is a shift of the light they emit toward the red end of the visible spectrum.

The announcement of **Hubble's law in 1929** marks the **birth of Observational Cosmology**. It is considered **the first observational basis for the expansion of the universe**, and today it serves as one of the pieces of evidence most often cited in support of the ΛCDM model.

Hubble's Law: The motion of astronomical objects due solely to this expansion is known as the Hubble flow. It is described by the equation $v = H_0 x D$, with H_0 the constant of proportionality—the Hubble constant—between the **"proper distance" *D*** to a galaxy. The proper distance, *D*, can change over time, unlike the comoving distance, and its **speed of separation *v***, that is, the **derivative of proper distance with respect to the cosmological time coordinate**. The proper distance can also be defined as the separation between two objects at a **specific moment (simultaneously)** in cosmological time.

Suppose ***R(t)* (or a(t)) is called the scale factor** of the universe, and increases as the universe expands in a manner that depends upon the cosmological model selected. t_0 is some reference time, t. Its meaning is that all measured **proper distances *D(t)*** between co-moving points increase proportionally to R selected. All measured proper distances $D(t)$ between co-moving points increase proportionally to R. (The co-moving points (gravitationally bound) are not moving relative to each other except as a result of the expansion of space.)

Various Measures of Distance. Refer to Sections V and IX.

Flux is the amount of energy from a source in W/m^2. Luminous flux, *Lm*, is a measure of the **perceived power of visible light** produced by a light source or light fitting. **Its value is independent of an observer's distance from an object.** The luminous flux accounts for the sensitivity of the eye by weighting the power at each wavelength with the **luminosity function, lx,** which represents the eye's response to different wavelengths. ***Lm = lx / Area***

Scale Factor, a(t)

$$\frac{D(t)}{D(t_0)} = \frac{R(t)}{R(t_0)}$$

Hubble Parameter, *H(t)*

$$\frac{H}{H_0} = H(t) = \frac{\frac{d}{dt}R(t)}{R(t)}$$

Proper Distance

$$s(t) = a(t) \cdot r$$

Comoving Distance (z)

$$D_c = D_H \int_0^z \frac{1}{E(z)}\, dz$$

Luminosity Distance, D_L

$$d_L = \sqrt{\frac{L}{4\pi f}}$$

Hubble Unit:

$$D_H = c \cdot H_0$$

$$D_c = \frac{s(t)}{a}$$

$$E(Z) = \sqrt{\Omega_k \cdot (1+z)^2 + \Omega_{0m} \cdot (1+z)^3 + \Omega_{0r} \cdot (1+z)^4 + \Omega_{0\Lambda}}$$

The parameters that appear in Hubble's law, *velocities* and *distances*, are *not directly measured*.

In reality we determine, say, a supernova brightness, which provides information about its distance, and the redshift $z = \Delta\lambda/\lambda$ of its spectrum of radiation. **Hubble correlated brightness** and parameter z.

Calculating Luminosity Distance versus Redshift in FLRW Cosmology via Homotopy Perturbation Method

$d_L = (L/4\pi f)^{1/2}$

$$d_L = c(1+z) \int_o^{\tilde{}} \frac{dz'}{H_0 E(z')}$$

$$H^2 = H_0^2 \{\Omega_r a^{-4} + \Omega_m a^{-3} + \Omega_k a^{-2} + \Omega_\Lambda\}$$

So far, we've found out how to compute different cosmological models. But what good are they?

The basic goal of cosmology is to figure out in what model universe do we live.

Models are basically distinguished by their history of the expansion rate, how their scale factor changes as a function of time.

If we can figure out which curve of those we live on, we know we'll know about cosmological parameters.

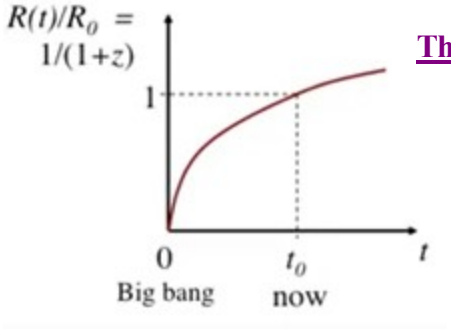

This relation is arguably the single most important equation in Cosmology

$$R_0 dr = \frac{c}{H(z)}\,dz \qquad R(t)/R_0 = 1/(1+z)$$

$$= \frac{c}{H_0}\left[(1-\Omega)(1+z)^2 + \Omega_v + \Omega_m(1+z)^3 + \Omega_r(1+z)^4\right]^{-1/2} dz.$$

Comoving Distance, D_C

$$D_C(z, \Omega_{0m}, \Omega_{0\Lambda}, \Omega_{0r}) := \int_{(1+z)^{-1}}^{1} \frac{1}{\sqrt{\Omega_{0m}\cdot a\xi + \Omega_{0\Lambda}\cdot a\xi^4 + \Omega_{0r}}}\,da\xi$$

The expansion **Scale Factor R(t) is simply related to redshift, z**, that is an observable quantity, and that's an easy part. The other axis is the time axis. Now unfortunately, this them galaxies do not carry gigantic clocks on them. Lookback time can only be inferred from a model. So it's very hard to figure out what is the look back time between us in some distant point, in a way that can be measured. So instead of that, what we do is we do **we transform coordinates,**

instead of the look back time, we can use distance which is simply time multiplied by the speed of light.

Distances in principle can be measured so we flipped the star Game and instead of expansion factor R(t), we use the redshift, which is an observable quantity. And instead of the time we use a distance, which we can figure out how to measure in some way. NOTE: Different redshifts correspond not only to different times, but also to different places.

So essentially, all cosmological tests boil down to this

We have to s**omehow measure a set of distances to a points as a function of redshift.** And because the whole thing just scales with Hubble constant, we only need to determine the shape of that curve.

So let's figure out how to measure distances in cosmology. A convenient unit of distance is Hubble distance, which is simply speed of the light divided by the Hubble constant. The Hubble constant has dimensions of one over time.

The Basis of Cosmological Tests

From ΛCDM Scale Factor Past, a(0), to Now(t_0) **From Now $D(z_0)$ at Distance $D(z_{past})$**

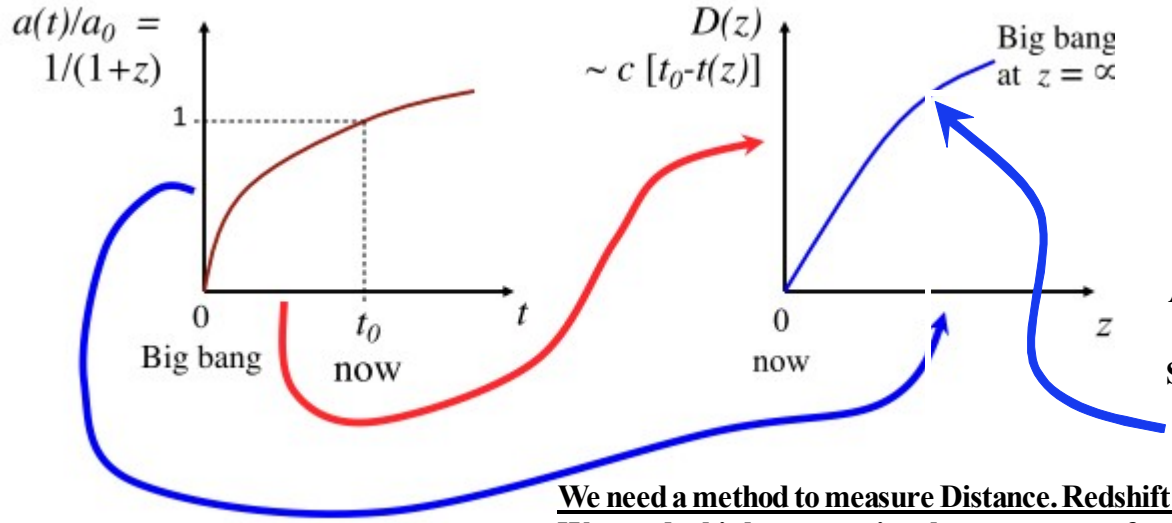

All Cosmological Tests essentially consist of comparing some measure of (relative) distance, $D(z) = c*(t_0-t_z)$ *(or look*-back time) to redshift, *z*. Absolute distance scaling is given by the H_0. **So that all we need is the shape of the *D(z)* curve** because it scales with H_0.

We need a method to measure Distance. Redshift z can be measured. We can do this by measuring the *Luminosity* of an object. See XVII

Cosmological Tests: The Why and How

- Model equations are integrated, and compared with the observations
- The goal is to determine the global geometry and the dynamics of the universe, and its ultimate fate
- The basic method is to somehow map the history of the expansion, and compare it with model predictions
- A model (or a family of models) is assumed, e.g., the Friedmann-Lemaitre models, typically defined by a set of parameters, e.g., H_0, $\Omega_{0,m}$, $\Omega_{0,\lambda}$, q_0, Λ, etc.
- Model equations are integrated, and compared with the observations

V. Distances in Cosmology

A convenient unit is the Hubble distance or radius, $D_H = c\ H_0 = 4.283\ h_{70}^{-1}$ Gpc $= 1.322\ 10^{28}\ h_{70}^{-1}$ cm

and the corresponding Hubble time, $t_H = 1/H_0 = 13.98\ h_{70}^{-1}$ Gyr $= 4.409\ 10^{17}\ h_{70}^{-1}$ s $= 13.02$ Gyr

At low z's, distance D ≈ z D_H.

But more generally, the **comoving distance, D_C** to a redshift z is:

$$D_C = D_H \int_0^z \frac{1}{E(z)}\, dz$$

This integral is not solvable analytically and must be calculated numerically.

The Hubble Parameter $H/H_0 = E(Z)$:

$$E(Z) = \sqrt{\Omega_k \cdot (1+z)^2 + \Omega_{0m} \cdot (1+z)^3 + \Omega_{0r} \cdot (1+z)^4 + \Omega_{0\Lambda}}$$

The Hubble Parameter at a Given Distance is then:

$H(z) = H_0\, E(z)$

Note: All Distances and Time scale linearly with the Hubble Constant, H

The Curvature is determined by Ω_k: $\Omega_k = 1 - \Omega_r - \Omega_m - \Omega_\Lambda$

Λ-CDM Model Parameters (Flat Space k = 0)

$\Omega_{r0} := 8.7 \cdot 10^{-5}$ $\quad \Omega_{m0} := 0.317$ $\quad \Omega_{\Lambda 0} := 0.683$ $\quad \Omega_{\Lambda 0} + \Omega_{m0} + \Omega_{r0} = 1$

Dynamical Equation Specifying the Evolution of the Hubble Factor of Our Universe

$$\frac{H}{H_0} = H\_H_0(z) := \sqrt{\Omega_{m0} \cdot (1+z)^3 + \Omega_{r0} \cdot (1+z)^4 + \Omega_{\Lambda 0}}$$

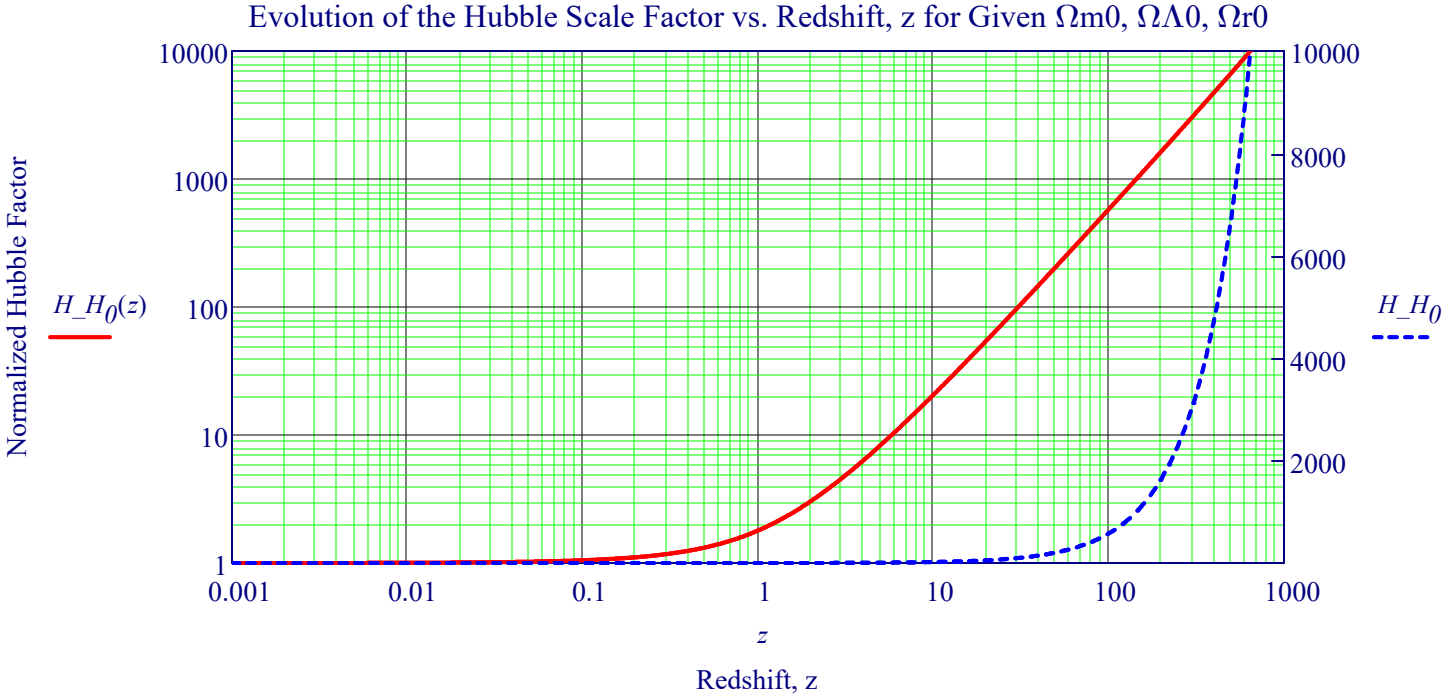

Cosmological Distances: The Horizon Problem

There are fundamentally Two Kinds of Coordinates in a GR cosmology:

Proper coordinates: Stay Fixed, Space Expands Relative to Them.

Examples:

- Sizes of atoms, molecules, solid bodies
- Gravitationally bound systems, e.g., Solar system, stars, galaxies …

Comoving coordinates: Expand with the Universe.

Examples:

- **Unbound systems**, e.g., any two distant galaxies
- **Wavelengths of massless quanta**, e.g., photons
- **Stretches relative to** the Proper Coordinates

We introduce a **scale factor**, commonly denoted as ***R(t)*** **or** ***a(t)***: **a spatial distance between** any two unaccelerated frames which move with their **comoving coordinates.**

Computing a(t) and various derived quantities **defines the cosmological models**.
This is accomplished by solving the Friedmann Equation

1. Proper Distances

We define a proper distance, as the distance between two events, A and B, in a reference frame for which they **occur simultaneously** ($t_A = t_B$).

$$(ds)^2 = (cdt)^2 - a^2(t)\cdot\left[\frac{dr^2}{\left(1-kr^2\right)} + r^2\cdot\left(d\theta^2 + \sin(\theta)^2\cdot d\phi^2\right)\right]$$

and set $d\theta = d\varphi = 0$ and $dt = 0$, so that

$$s(t) = \int_0^s 1\, ds' = a(t)\cdot\int_0^\tau \frac{1}{\sqrt{1+kr^2}}\, d\tau$$

The proper distance has solution *s(t)*,

where *k* is a curvature factor.

$$s(t) = a(t)\cdot\begin{cases} \frac{1}{\sqrt{k}}\sin^{-1}(r\sqrt{k}) & \text{for } k > 0 \\ r & \text{for } k = 0 \\ \frac{1}{\sqrt{|k|}}\sinh^{-1}(r\sqrt{|k|}) & \text{for } k < 0 \end{cases}$$

In a flat universe, the proper distance to an object is just its **coordinate distance,**

$$s(t) = a(t)\cdot r.$$

Because $\sin^{-1}(x) > x$ and $\sinh^{-1}(x) < x$,

Universe Contracts (Closed) or Universe Expands (Open)

in a closed universe (k > 0)
the proper distance to an object is greater than its coordinate distance,
while in an open universe (k < 0)
the proper distance to an object is less than its coordinate distance.

The Horizon

The proper distance to the **furthest observable point** - the particle horizon - at time t is:

Horizon Distance: $s_h(t)$

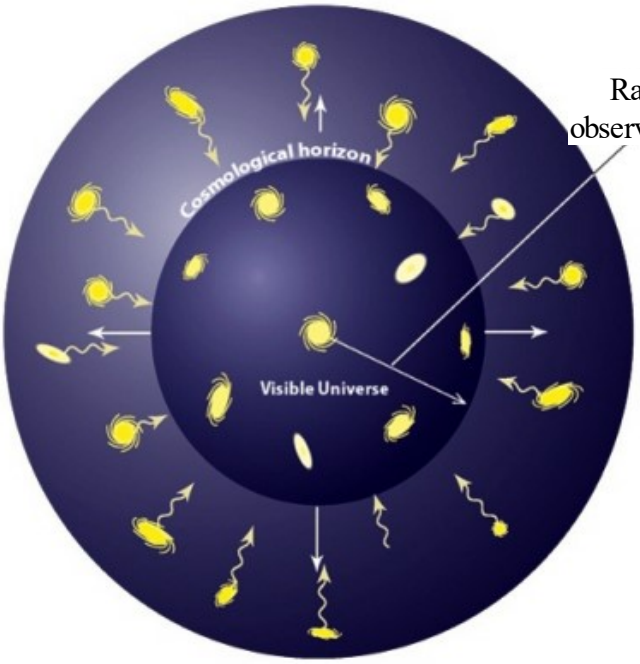

As the universe expands and ages, **an observer at any point is able to see increasingly distant objects** as the light from them has time to arrive. This means that, **as time progresses, increasingly larger regions of the universe come into causal contact with the observer.**

The proper distance to the furthest observable point, the particle horizon— at time t is the **horizon distance, $s_h(t)$.**

Again we return to the Robertson-Walker metric, placing an observer at the origin (r = 0) and let the particle horizon for this observer at time t be located at radial coordinate distance r_{hor}.

This means that a photon emitted at t = 0 at r_{hor} will reach our observer at the origin at time t.

Since photons move along null geodesics, ds = 0. Considering only radially traveling photons (dθ = dφ = 0), we find

$$\int_0^t \frac{1}{a(t)}\,dt = \frac{1}{c}\cdot\int_0^{\tau_{hor}} \frac{1}{\sqrt{1+kr^2}}\,d\tau$$

for k = 1 $\quad \sin\left(c\cdot\int_0^t \frac{1}{a(t)}\,dt\right)$ $\qquad$ for k = 0 $\quad c\cdot\int_0^t \frac{1}{a(t)}\,dt$

The lookback time $t_L(z)$ to a source at any redshift z is the **time photons needed to travel with speed c** from the source to the observer at z = 0. In a homogeneous universe, this global quantitity is just the sum of the small locally measured proper times dt. In terms of the scale factor *a* and $H = d\,ln(a)/dt$, it is.

$$t_L = \int_0^1 \frac{1}{a'\cdot H(a')}\,da' \qquad t_L(z) = \int_0^z \frac{1}{(1+z')\cdot H(z')}\,dz'$$

If the scale factor evolves with time as $a(t) = t^{\alpha}$, we can see that the above time integral diverges as we approach t = 0, if α > 1. **This would imply that the whole universe in is causal contact.**

However, α=1/2 and 2/3 in the radiation and matter-dominated regime, so there is a horizon.

The proper distance from the origin to r_{hor} is given by:

for k = 0 $\qquad s_{hor}(t) = a(t)\cdot\int_0^{\tau_{hor}} \frac{1}{\sqrt{1+kr^2}}\,d\tau = a(t)\cdot\int_0^t \frac{c}{a(t)}\,dt$

So $s_{hor}(t) = 2ct$ in the radiation-dominated era and $s_{hor}(t) = 3ct$ in the matter-dominated era. Notice that these distances are **larger than ct, the distance travelled by a photon in time t**. How could this be? The reason lies in our definition of proper distance, as the distance between two events measured in a frame of reference where those two events happen at the same time.

To understand this, consider a photon in emitted at comoving radial coordinate r_{hor} at time t = 0. We want to know what is the proper distance of that photon from ***our*** position, at r = 0, at a later time t. The coordinate of the photon at time t may be found by integrating

$$\int_0^t \frac{c}{a(t)}\,dt = \int_0^{\tau_{hor}} \frac{1}{\sqrt{1+kr^2}}\,d\tau$$

As before, we consider zero curvature models. Substituting for a(t) we obtain: $r = r_{hor} - \frac{2c}{H_0}\cdot\left(\frac{t}{t_0}\right)^{\frac{1}{3}}$

where $\mathbf{t_0 = 2t_H/3}$ **is the present age of the universe**. Recalling that $\mathbf{r_{hor} = 2c/H_0}$, and that **the proper distance** in a flat universe is just $\mathbf{s(t) = a(t) \cdot r}$, we find that the proper distance of the photon from Earth as a function of time is

$$s(t) := \frac{2c}{H_{0.}}\cdot\left[\left(\frac{t}{t_{0.}}\right)^{\frac{2}{3}} - \frac{t}{t_{0.}}\right] \qquad \text{for } k = 0$$

Proper distance as a function of tinie of a photon emitted from the present particle horizon at the time of the ΛCDM. The proper distance is expressed as. function of $2c/H_0$, the present horizon distance in a flat universe.

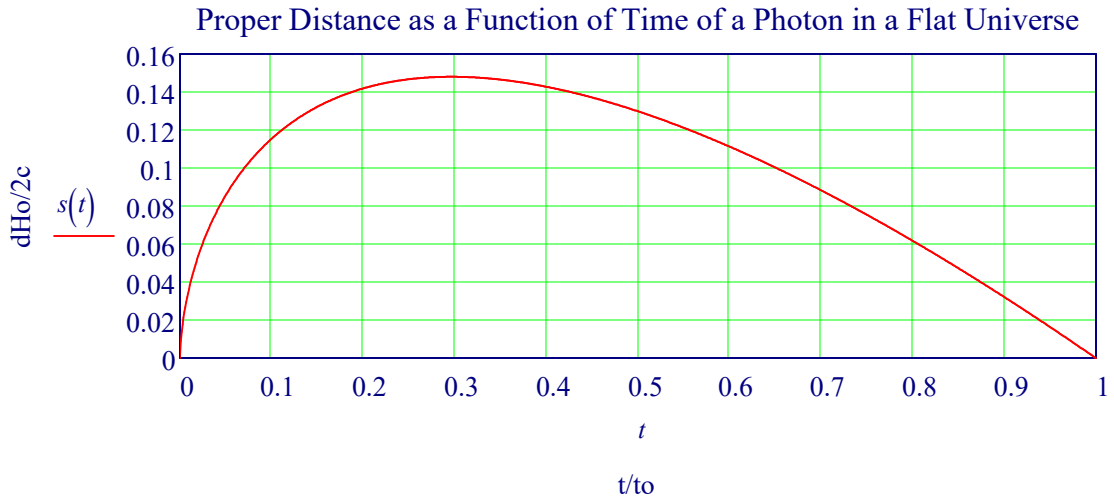

We can now see that **the initial expansion actually carried the photon away from Earth.** Although the photon's co-moving coordinate was always decreasing from an initial value r_{hor} towards Earth's position at r = 0, the scale factor a(t), (or R(t)), increased so rapidly that **at first the proper distance between the photon and Earth increased with time**.

Expansion and the Hubble's Law

Consider a point at a **comoving distance x**. At some time t it will be at a radial distance r(t) = a(t) x , where a(t) is the expansion factor. We will designate values for "here and now" with a subscript 0, t_0 = now, and $a_0 = a(t_0) = 1$. The recession velocity is:

$$\boldsymbol{v}(\boldsymbol{r},t) = \frac{\mathrm{d}}{\mathrm{d}t}\boldsymbol{r}(t) = \frac{\mathrm{d}a}{\mathrm{d}t}\boldsymbol{x} \equiv \dot{a}\,\boldsymbol{x} = \frac{\dot{a}}{a}\boldsymbol{r} \equiv H(t)\,\boldsymbol{r}$$

Where $H(t) := \frac{\dot{a}}{a}$ is the normalized expansion rate

$$\Delta\boldsymbol{v} = \boldsymbol{v}(\boldsymbol{r} + \Delta\boldsymbol{r}, t) - \boldsymbol{v}(\boldsymbol{r}, t) = H(t)\,\Delta\boldsymbol{r}$$

Which is the same as the Hubble's law: $v = H_0\,D$

H_0 is the value of the **expansion rate here and now**.
Note that it is not a constant, but it depends on a(t).

Cosmological Distance Tests for Expanding vs. Static Universe

The James Webb Space Telescope (JWST) is capable of detecting objects at record-breaking redshifts, $z \approx 15$. This is a crucial advance for observational cosmology, as at these redshifts the

differences between alternative cosmological models manifest themselves in the most obvious way.

Cosmological Tests

We shall focus primarily on the angular size–redshift relationship, θ(z), such as the Tolman surface-brightness test, the cosmological time dilation; number density–redshift relationship.

Cosmological models can be divided in two groups:

1. Expanding universes based on the Friedmann–Lemaitre–Robertson–Walker (FLRW) metric with a time-dependent scale factor;
2. static universes based, e.g., on the metric including a scale factor in metric's time component.

The commonly accepted model of the first type is the standard ΛCDM cosmological model, which best fits observational data among other expanding-Universe models

Compare Different Cosmological Models: Expanding Universe ΛCDM vs. Static

Comoving, $D_{CM}(z)$, Luminosity Distance, $d_L(z)$, Angular Diameter Distance, $D_A(z)$

$\Omega_{0m} := 0.3 \qquad \Omega_{0\Lambda} := 0.7$

$$D_{CM}(z) := \int_{(1+z)^{-1}}^{1} \frac{1}{\sqrt{\Omega_{0m} \cdot a\xi + \Omega_{0\Lambda} \cdot a\xi^4}}\, da\xi$$

$1\,Gpc = 3.26\,GLightYear$

Flat Universe: Einstein de Sitter (EDS)

$d_L(z) := (1+z) \cdot D_{CM}(z) \qquad D_A(z) := \frac{D_{CM}(z)}{1+z}$

Angular Diameter Model

$D_{Ads}(z) := \ln(1+z)$

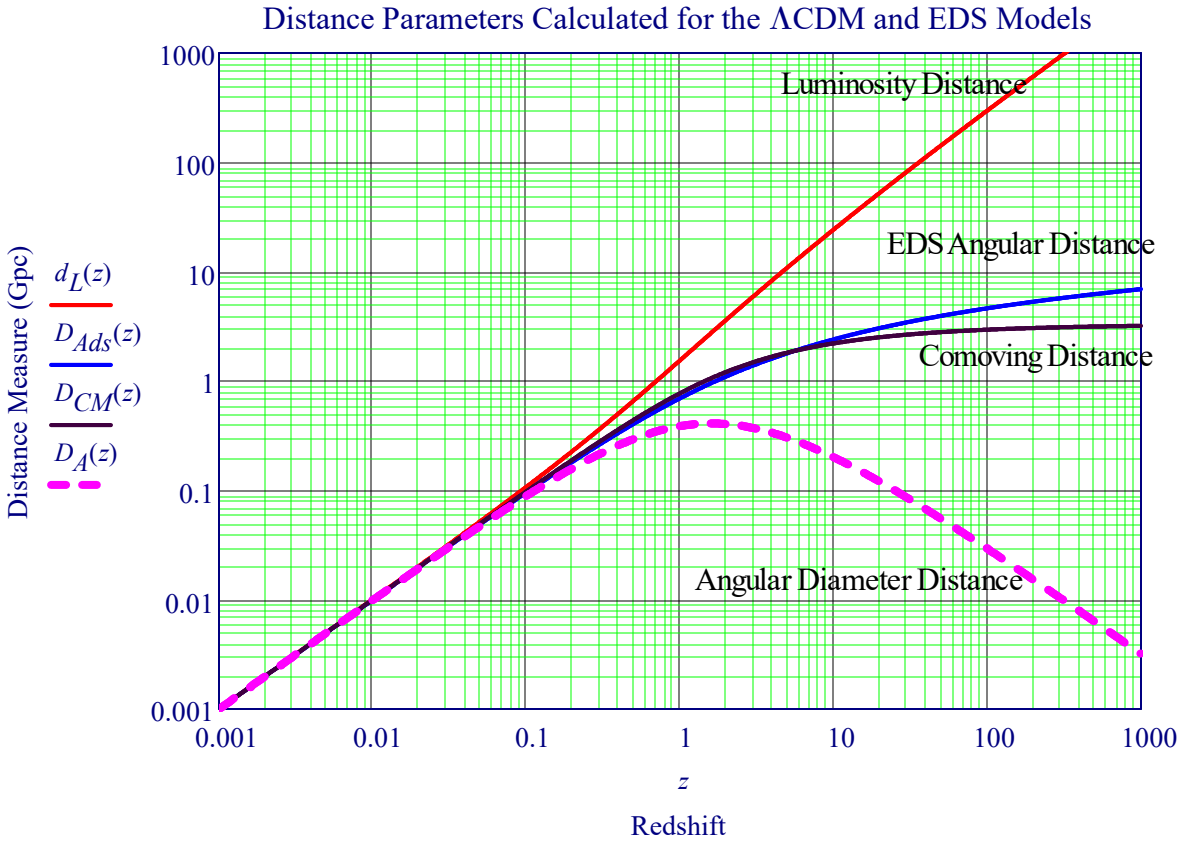

Distance Formulas: Light Travel D_{ltt}, Present D_{now}, Angular D_A and Luminous D_L

Astronomy 140 Lecture Notes, Edward L. Wright, 2008, https://astro.ucla.edu/~wright/intro.html

$$D_{now} = R_\circ \psi = \int \frac{cdt}{a} = \int_{1/(1+z)}^{1} \frac{cda}{a\dot{a}} \qquad D_{ltt} = \int cdt = \int_{1/(1+z)}^{1} \frac{cda}{\dot{a}} \qquad D_A = \frac{cZ(z)}{H_\circ} \frac{J([1-\Omega_{tot}]Z^2)}{1+z} \qquad D_L = (1+z)^2 D_A$$

Fitting these formulae to the existing supernova data gives a set of contours of $\Delta\chi^2$ as a function of Ω_{mo} and Ω_{vo} (ψ is the hyperbolic angle)

Four Simple Cases and One Hard Case:

For Each:

D_{now}

D_{llt}

D_A,

D_L

One of the 5 Cases

$\Omega = 0$

$\Omega_m = 1$

$\Omega_r = 1$

$\Omega_\nu = 1$

Only D_A and D_L

$\Omega_m = 2$

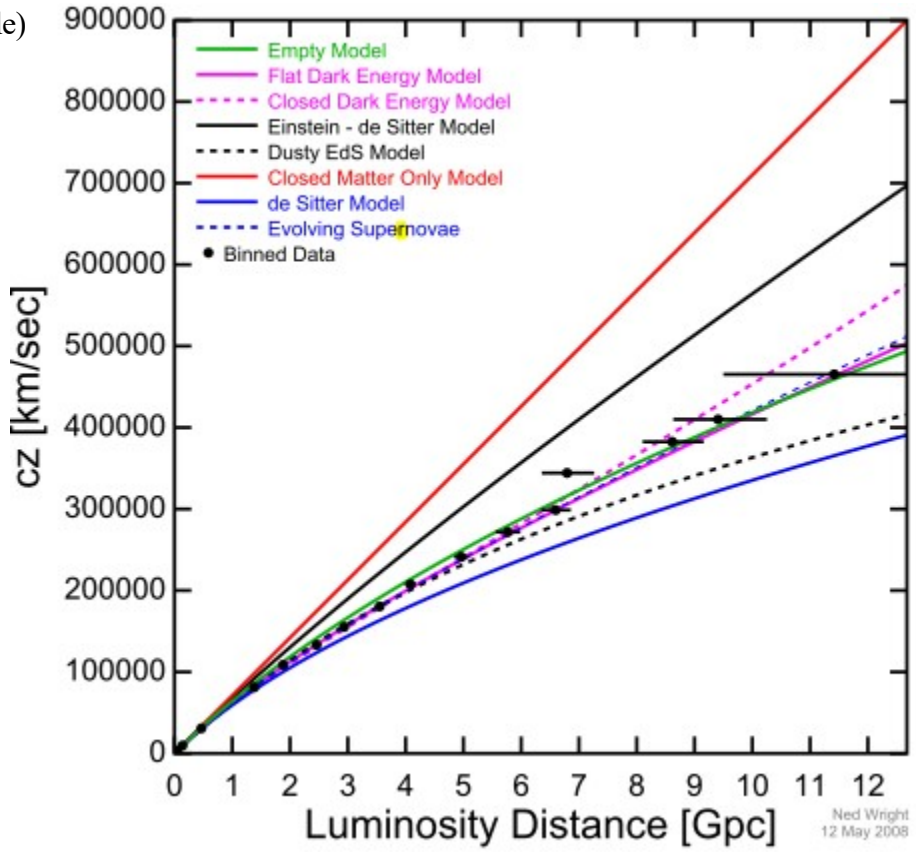

Luminosity distance vs. redshift for high redshift Type Ia supernovae.

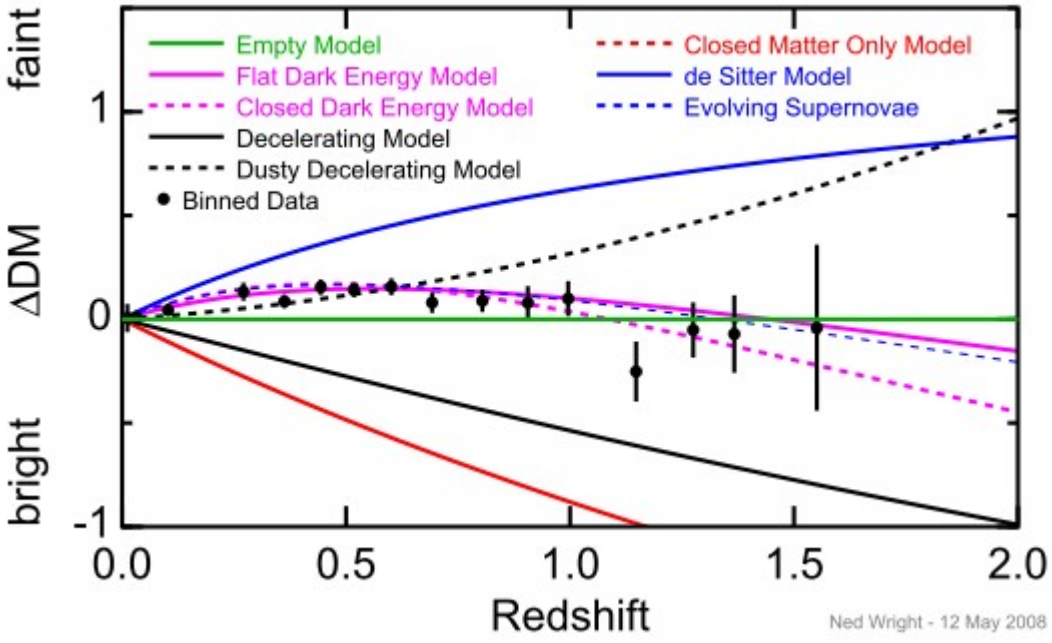

Distance modulus ($m - M$) relative to an $\Omega = 0$ model vs. redshift for high redshift Type Ia supernovae. The data points are binned values from the Kowalski et al. (2008, arXiv:0804.4142) union catalog of supernovae.

VI. Newtonian Energy Derivation of the Rate of Expansion, H

Consider a test particle of mass m as part of an expanding spherical shell of radius r & total mass M.

$$r(t) = a(t)\cdot x \qquad x = \frac{r(t)}{a(t)} \qquad v(r,t) = \frac{d}{dt}r(t) = \frac{da}{dt}x = \frac{da}{dt}\cdot\frac{r}{a} = \frac{a}{a}\cdot r = \frac{\dot{a}}{a}(t)\cdot r$$

Note: **"a"** is NOT the acceleration, it is the Scale Factor.

Note:

In the Newtonian Model Space is Euclidean and Gravity is a Force that causes massive bodies to accelerate, while in the Einsteinian View, Gravity is a manifestation of the Curvature of Spacetime. In the limit of weak spatial curvature or small $(v/c)^2$, the Newtonian View gives approximately the same results.

By Conservation of Energy, E = Constant

$$Energy = \frac{1}{2}m\cdot v^2 - \frac{GMm}{r}$$

$$\frac{1}{2}\left(\frac{d}{dt}r\right)^2 - \frac{GM}{r} - \frac{Energy}{m} = 0$$

$$M = \frac{4}{3}\pi r^3\cdot\rho \qquad r(t) = a(t)\cdot\frac{x}{r}$$

$$\frac{1}{2}\left(\frac{1}{r}\cdot\frac{d}{dt}r\right)^2 - \frac{G\cdot M}{r^3} - \frac{Constant}{r^2}$$

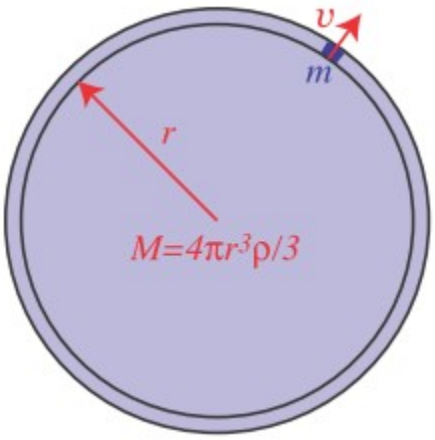

Rearrange to Friedmann Equation:

$$\left(\frac{\dot{a}}{a}\right)^2 = \frac{8\pi G}{3}\rho - \frac{kc^2}{a^2}$$

$$H^2 = \frac{8\pi\cdot G}{3}\cdot\rho - \frac{2\cdot Energy}{a^2}$$

Note: $\dot{a}$ is a contracting sphere if $\dot{a} < 0$ and k is proportional to Energy.

- **If k = 0 (flat universe):** $\dot{a}^2 > 0$, universe expands for ever, but as $a \to \infty$, $\dot{a} \to 0$
- **If k < 0 (open universe):** $\dot{a}^2 > 0$, universe expands for ever, but $\dot{a}^2 \to c$
- **If k > 0 (closed universe):** the expansion peaks when: $\dot{a}^2 = 0$.

The Two Friedmann Equations can be reduced to:

$$H^2 = \frac{8\pi G_N}{3}\rho - \frac{k}{a^2} + \frac{\Lambda}{3}$$

Expansion = Density - Curvature

$$\rho_\Lambda \equiv \frac{\Lambda}{8\pi G_N}$$

ρ_Λ = Cosmological Constant Energy Density

$$\rho_{tot} \equiv \rho + \rho_\Lambda$$

ρ_{tot} = Total Energy Density

For a given value of H, there is a special value of the density which would be required in order to make the geometry of the Universe flat, that is, k = 0. This is known as the critical density ρ_c

Note that to get the results in the FWLR form, we replaced the Energy Density term $\varepsilon_c(t)$ with the mass density, ρ.

$$\varepsilon_c(t) = \rho_c\cdot c^2 \qquad \rho_c \equiv \frac{3H^2}{8\pi G_N}$$

Sources of Matter and Energy

In General Relativity, all of the sources of matter and energy are included and contribute to the total energy density, ρ_{tot}. **The energy density today of each component is Normalized to the Critical Density, ρ_c,** (See below: $\Omega_{component}$) that is used in the definition of the corresponding "Omega parameter", **Ω.**

$$\Omega_{component} = \frac{\rho_{component}}{\rho_{c\_z0}}$$

Thus we have: $\Omega = \Omega_{baryon} + \Omega_{cdm} + \Omega_{radiation} + \Omega_{DE}$

Here Ω_{baryon} is the baryon content, Ω_{cdm} is the amount of cold dark matter, $\Omega_{radiation}$ is the radiation content, and Ω_{DE} is the contribution from dark energy. If $\Omega = 1$ that means the density is equal to the critical density, ρ_c, at z = 0, so we have a flat Universe (k = 0).

VII. Equations and Values of Constants for Cosmological Parameters:

Hubble & Scale Factors, z, Ωs, Density, Temp, V

Definitions and Equations below came from: *Introduction to Cosmology*, by Barbara Ryden[2]

Plots of these Cosmic Parameters are on the Following Pages

Define Constants

$c = 299792.458 \cdot \frac{km}{s}$ $\quad G := 6.67 \cdot 10^{-11} \frac{m^3}{kg \cdot s^2}$ $\quad H_0 := \frac{1}{4.355 \cdot 10^{17} s}$

Seconds per Billion (Giga) Years

$Gyr := 3600 \cdot 24 \cdot 365.24 \cdot 10^9 \cdot s$

$H_0 = 68.886 \cdot \frac{km}{s} \cdot (Mpc)^{-1}$

Create an Exponential Time: Order of Magnitude, OM, Scale Factor ai, Spanning 26 Orders of Magnitude:

$N26 := 10^{-26}$ $\quad OM := 26$ $\quad i := 0 .. 100 \cdot OM + 400$ $\quad a_i := 10^{0.01 \cdot i - OM}$ $\quad a_0 = 1 \cdot N26$ $\quad a_{3000} = 10000$

Densities and Curvature of our Universe

Critical Density

In flat universe total density ρ = critical density ρ_0

$\rho_0 = \frac{3 \cdot H_0^2}{8 \cdot \pi \cdot G}$ $\quad \rho_0 = 8.644 \frac{kg}{m^3} \cdot 10^{-27}$

Normalized radiation energy density for photons + neutrinos

$\Omega_{r0} := \frac{4.005 \cdot 10^{-14}}{\rho_0 \cdot c^2} \cdot (1 + 0.69) \cdot \frac{J}{m^3}$ $\quad \Omega_{r0} = 0$

Dark matter + baryonic matter

$\Omega_{m0} := 0.268 + 0.049$ $\quad \Omega_{m0} = 0.317$

Curvature Parameter

$\Omega_{\Lambda 0} := 1 - \Omega_{r0} - \Omega_{m0}$ $\quad \Omega_{\Lambda 0} = 0.683$

DEFINE: Ω, H, da_dt, Proper time, t, Diameter, Velocity, Mass Ratios, H(z)

Inflation, i

Dark energy for flat universe

$H_i \approx t_{GUT}^{-1} \approx 10^{36} \text{ sec}^{-1}$

Hubble Parameters

$H_i := H_0 \cdot \sqrt{\frac{\Omega_{r0}}{(a_i)^4} + \frac{\Omega_{m0}}{(a_i)^3} + \Omega_{\Lambda 0}}$

Scale Factor, a

$a(t) = \frac{1}{1 + z}$

Redshift,

$z = \frac{1}{a} - 1$ $\quad a = \frac{1}{z + 1}$

Friedmann equation for a flat universe
after inflation ends
and radiation epoch begins

$\dot{a} = H_\circ \left(\Omega_{k\circ} + \Omega_{v\circ} a^2 + \Omega_{m\circ}/a + \Omega_{r\circ}/a^2\right)^{1/2}$

$\frac{d}{dt} a = da\_dt(a) := H_0 \cdot \sqrt{\frac{\Omega_{r0}}{a^2} + \frac{\Omega_{m0}}{a} + \Omega_{\Lambda 0} \cdot a^2}$

Calculate the Cosmic Proper Time (t) and Lookback time (tL). Inflation Epoch Ends at 10^- 33 seconds

Distance to a galaxy is defined as the **proper distance $d_p(t)$**. The length of time light has traveled $t_0 - t_e$ is **lookback time**, t_L.

Inflation Era 10^{-35} to 10^{-33}

$$t_i := \int_0^{a_i} \frac{1}{da\_dt(a)}\, da \qquad t_{L_i} := \int_0^{z_i} \frac{1}{(1+z\varepsilon)\cdot H(z\varepsilon)}\, dz\varepsilon$$

$$\frac{t_{100\cdot OM}}{Gyr} = 13.096 \qquad \frac{t_{3000}}{Gyr} = 165.792$$

$$X33 := 10^{-33} \qquad t_1 = 2.443\, s\cdot X33 \qquad t_{3000} = 165.792\cdot Gyr \qquad Now := t_{100\cdot OM}\cdot s^{-1}$$

Numerical Integration: Integral_dD (a, b, n)

$$dD(a) := \frac{2\cdot c}{a\cdot da\_dt(a)}$$

$$Integral\_dD(a,b,n) := \begin{cases} \left[\frac{dD(a)+dD(b)}{2}\cdot(b-a)\right] & \text{if } n \le 1 \\ \text{otherwise} \\ \quad \left| \begin{array}{l} h \leftarrow \frac{b-a}{n} \quad \text{if } n > 1 \\ \frac{h}{2}\cdot\left[dD(a) + \left(2\cdot\sum_{i=1}^{n-1} dD(a+i\cdot h)\right) + dD(b)\right] \end{array} \right. \end{cases}$$

Calculate the Diameter, D, in Meters of Observable Universe Dou = 2*comoving distance

$$dD(a) := \frac{2\cdot c}{a\cdot da\_dt(a)} \qquad Initial := 1\cdot 10^{-100} \qquad da\_dt_i := da\_dt(a_i)$$

$$Dou_i := Integral\_dD(Initial, a_i, 500) \qquad Dou_0 = 279.757\, m \qquad \frac{Dou_{100\cdot OM}}{c\cdot Gyr\cdot s} = 88.602\,\frac{1}{s}$$

D = Scaled Up Diameter of Universe that was formerly observable at 10^{-33} second

$$D_i := \frac{a_i}{a_0}\cdot Dou_0 \qquad D_0 = 279.757\, m \qquad \frac{D_{100\cdot OM}}{Dou_{100\cdot OM}} = 33.375$$

$$Recombination\_Time := 3600\cdot 24\cdot 365.24\cdot 370000$$

Calculate Recessional Velocities

$$vrou_i := H_i\frac{Dou_i}{2} \qquad Vou := \frac{4\pi}{3}\cdot\left(\frac{Dou}{2}\right)^3$$

$$V_i := \left(\frac{a_i}{a_0}\right)^3\cdot Vou_0 \qquad vr_i := H_i\cdot\frac{D_i}{2}$$

Temperature (K)

$$T_{emp_i} := \frac{2.725}{a_i}$$

Mass Densities: Radiation, Mass, Λ, and Total. See Density (ρ) Plots in Section XXVIII

$$\rho r_i := \frac{\Omega_{r0}}{(a_i)^4}\rho_0 \qquad \rho m_i := \frac{\Omega_{m0}}{(a_i)^3}\rho_0 \qquad \rho\Lambda_i := \Omega_{\Lambda 0}\rho_0 \qquad \rho := \rho r + \rho m + \rho\Lambda$$

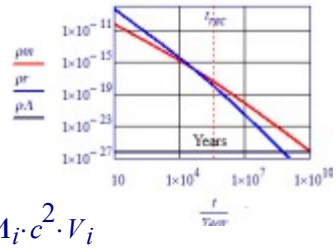

Mass (Mou) and Energy (Eou) of Dark and Baryonic Matter and Energy

$$Mou_i := \rho m_i \cdot Vou_i \qquad Erou_i := \rho r_i \cdot c^2 \cdot Vou_i \qquad Emou_i := \rho m_i \cdot c^2 \cdot Vou_i \qquad E\Lambda_i := \rho\Lambda_i \cdot c^2 \cdot V_i$$

$$M_{\rho v_i} := \rho m_i \cdot V_i \qquad Er_i := \rho r_i \cdot c^2 \cdot V_i \qquad Em_i := \rho m_i \cdot c^2 \cdot V_i \qquad E\Lambda ou_i := \rho\Lambda_i \cdot c^2 \cdot Vou_i$$

$$Eou := Erou + Emou + E\Lambda ou \qquad E := Er + Em + E\Lambda$$

Radiation - Matter Equality

$$arm := \frac{\rho r_{700}}{\rho m_{700}}$$

Matter - Lambda Equality

$$am\Lambda := \sqrt[3]{\frac{\rho m_{2600}}{\rho\Lambda_{2600}}} \qquad am\Lambda = 0.774$$

$$ar_i := \sqrt[4]{4\cdot\Omega_{r0}}\cdot(H_0\cdot t_i)^{\frac{1}{2}} \qquad am_i := \sqrt[3]{2.25\cdot\Omega_{m0}}\cdot(H_0\cdot t_i)^{\frac{2}{3}} \qquad a\Lambda_i := am\Lambda\cdot e^{\sqrt{1-\Omega_{m0}}\cdot H_0\cdot t_i}$$

$$C_{inf} = 8\pi G\cdot\frac{f}{3} + \frac{\Lambda}{3} \qquad a_{inflation}(t) = e^{\sqrt{C_{inf}}\cdot t} \qquad One\_Year := 3600\cdot 24\cdot 365 \qquad Now := t_{100\cdot OM}\cdot s^{-1}$$

Plots of the Ratio of Lookback time to H0 (tL_tH0) and the Ratio of Time to H0, (t_tH0)

$$tL\_tH0(z,\Omega_{0m},\Omega_{0\Lambda},\Omega_{0r}) := \int_0^z \frac{1}{(1+z\xi)\cdot\sqrt{\Omega_{0m}\cdot(1+z\xi)^3 + \Omega_{0\Lambda} + \Omega_{0r}\cdot(1+z\xi)^4}}\,dz\xi$$

$$tL\_tH0(1000, 0.3089, 0.6911, 0.001) = 0.952$$

$$t\_tH0(z,\Omega_{0m},\Omega_{0\Lambda},\Omega_{0r}) := \int_0^{(1+z)^{-1}} \frac{a}{\sqrt{\Omega_{0m}\cdot a + \Omega_{0\Lambda}\cdot a^4 + \Omega_{0r}}}\,da$$

$$t\_tH0(1000, 0.1, 0.7, 0.2) = 0$$

Comoving Distance

$$z = \frac{1}{a} - 1$$

$$D_{Cz}(z,\Omega_{0m},\Omega_{0\Lambda},\Omega_{0r}) := \int_{(1+z)^{-1}}^{1} \frac{1}{\sqrt{\Omega_{0m}\cdot a\xi + \Omega_{0\Lambda}\cdot a\xi^4 + \Omega_{0r}}}\,da\xi$$

Apparent Magnitude-Redshift Relation (Mukhanov) Eq 2.81 (See Section X of this Paper)

For Comoving Distance, χ_{em}

$$\chi = \int_{t_{em}}^{t_0} \frac{dt}{a(t)} \qquad \chi_{em}(z,\Omega_m) := \int_0^z \frac{1}{\sqrt{\Omega_m\cdot(1+z\xi)^3 + (1-\Omega_m)}}\,dz\xi$$

$$\Phi^2(\chi_{em}) = \begin{cases} \sinh^2\chi, & k=-1; \\ \chi^2, & k=0; \\ \sin^2\chi, & k=+1. \end{cases}$$

photon emitted at time t_{em}

Note: For k = 0

$$\Phi(\chi_{em}) = \chi_{em}$$

Bolometric Flux is the Flux Integrated over Entire Spectrum
Then the Bolometric Magnitude for k=0 is Given by:

$$m_{bol}(z,\Omega_m) := 5\log(1+z) + 5\log(\chi_{em}(z,\Omega_m)) + 25$$

Exploring the Behavior of Some Cosmology Models by Plotting Their Parameters Given by the Definitions in Section VII.

Plots of Cosmic Density Components, Scale Factor, Recession Velocity, Hubble Factor Cosmic Scale Factor, Components of the Energy of the Universe

Recombination Time (s)

$\rho_0 := 8.644 \frac{kg}{m^3} \cdot 10^{-27}$ $\Omega_{m0} := 0.317$ $\Omega_{r0} := 0$ $\Omega_{\Lambda 0} := 0.683$ $t_{rec} := 3 \cdot 10^5$ $t_{hadron} := 1$ $One := 1$

Cosmic Density: Total, Mass, Radiation, Lambda and Temperature vs Time (sec)

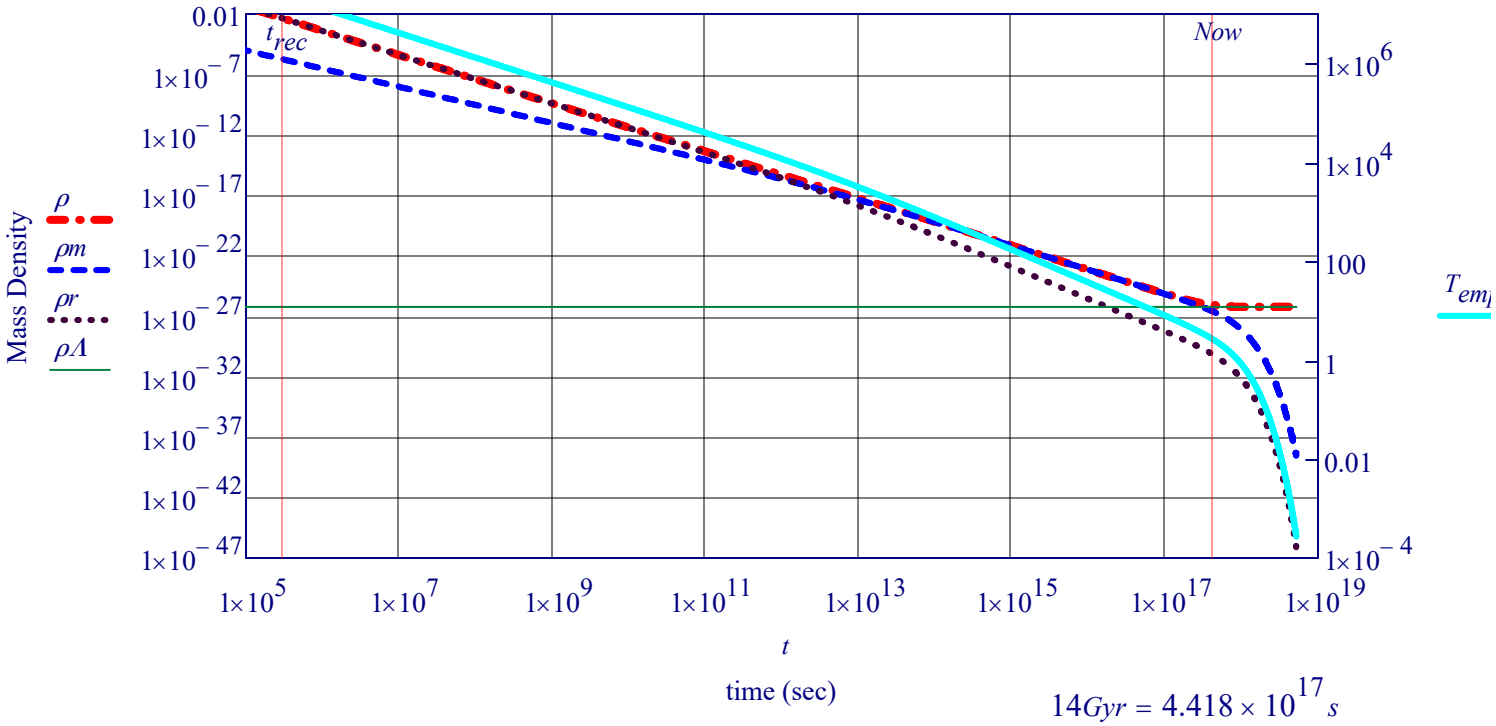

$14Gyr = 4.418 \times 10^{17}\, s$

Cosmic Density: Total, Mass, Radiation, Lambda and Scale Factor vs Time (sec)

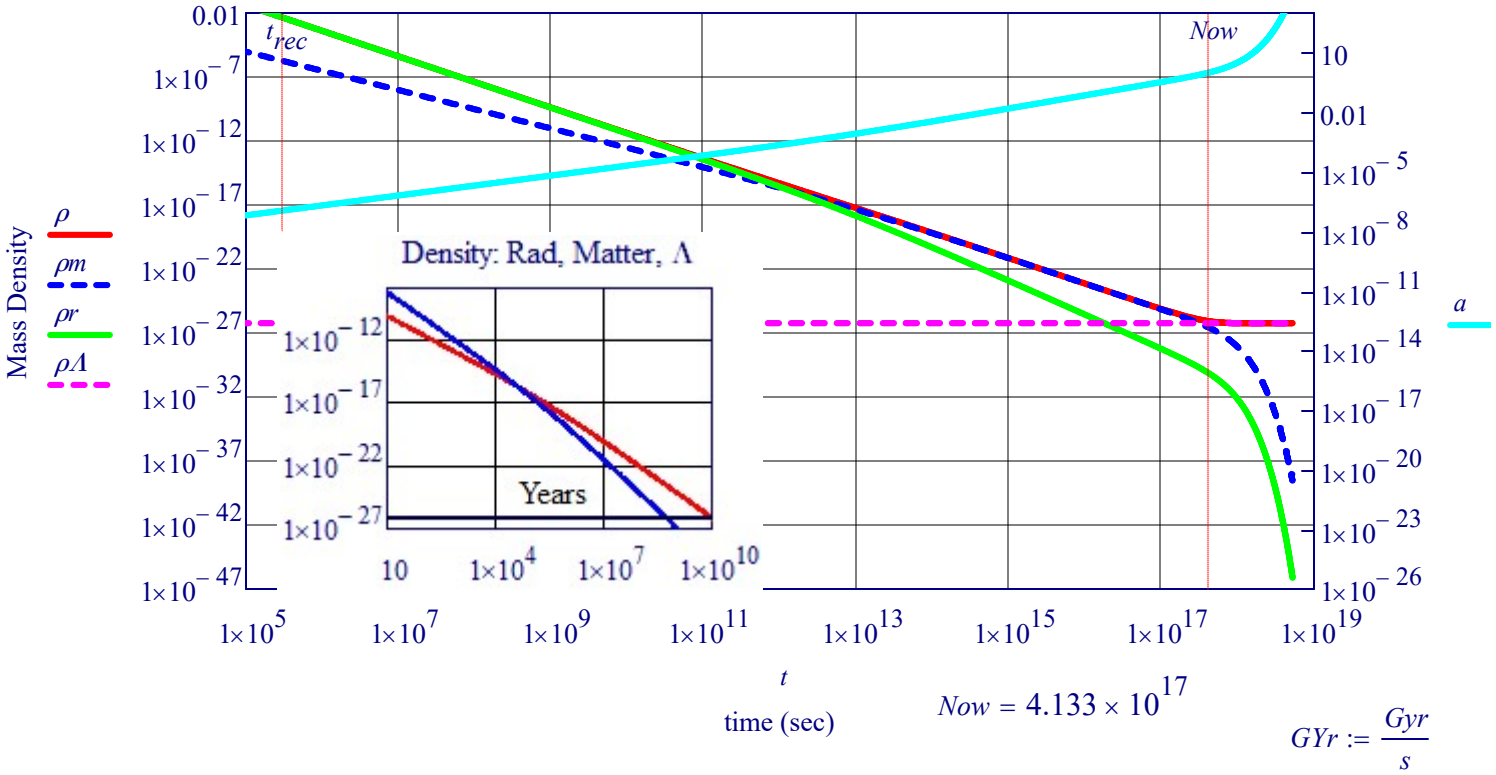

$Now = 4.133 \times 10^{17}$

$GYr := \frac{Gyr}{s}$

Cosmic Scale Factor and Doubling vs. Time(GYear)

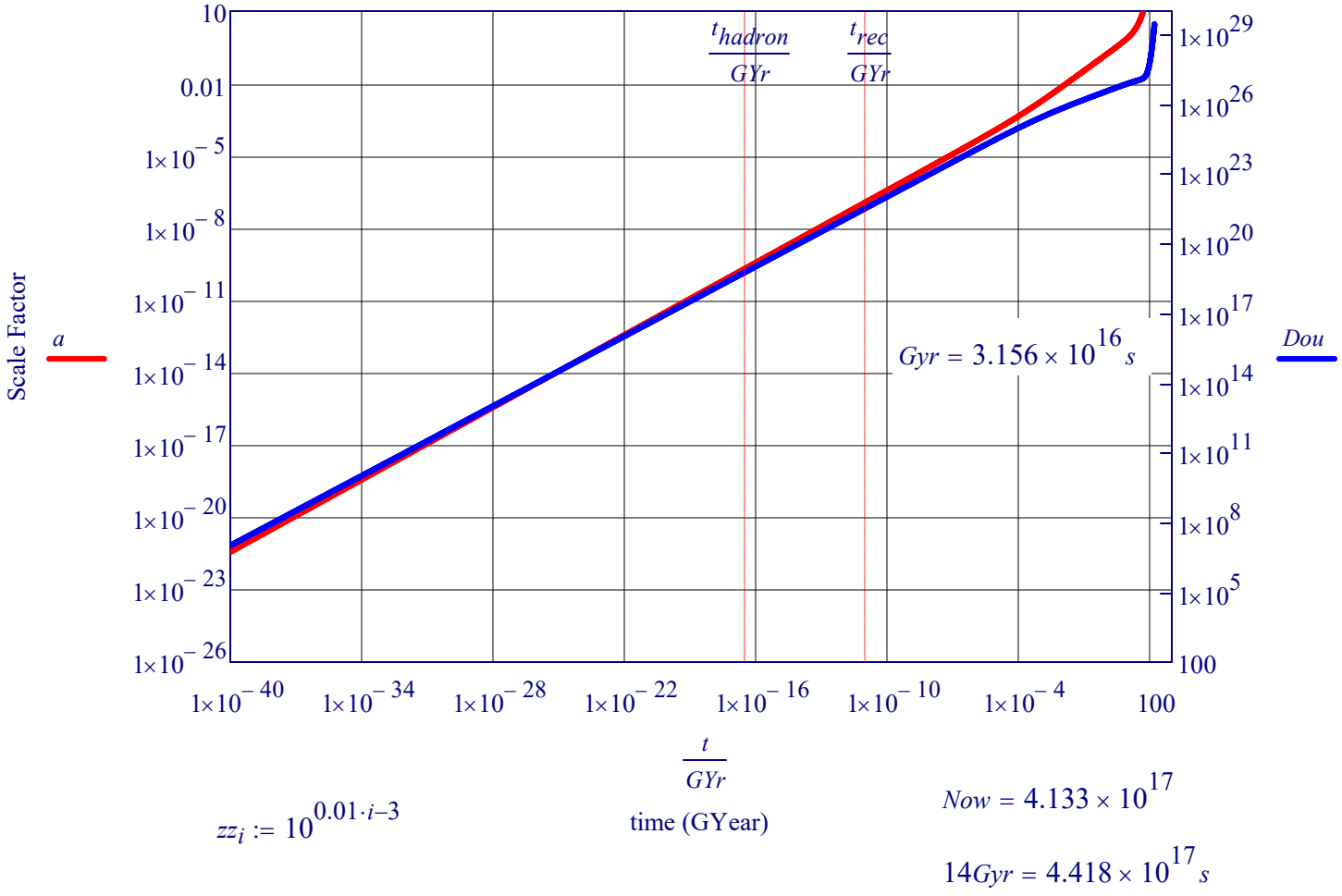

$zz_i := 10^{0.01 \cdot i - 3}$

$Now = 4.133 \times 10^{17}$

$14Gyr = 4.418 \times 10^{17}\ s$

Recession Velocity vs. Time (Units of Velocity of Light)

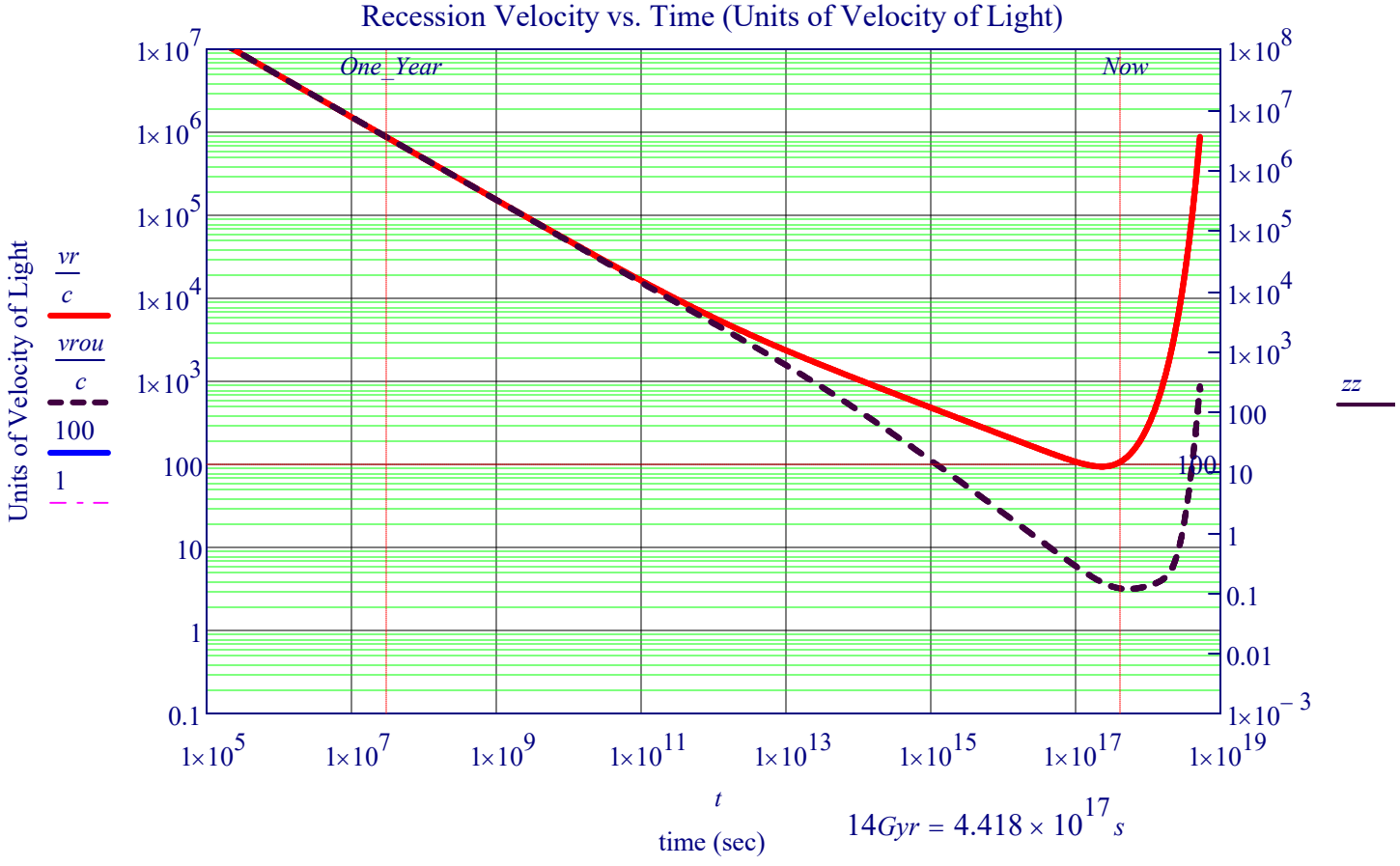

$14Gyr = 4.418 \times 10^{17}\ s$

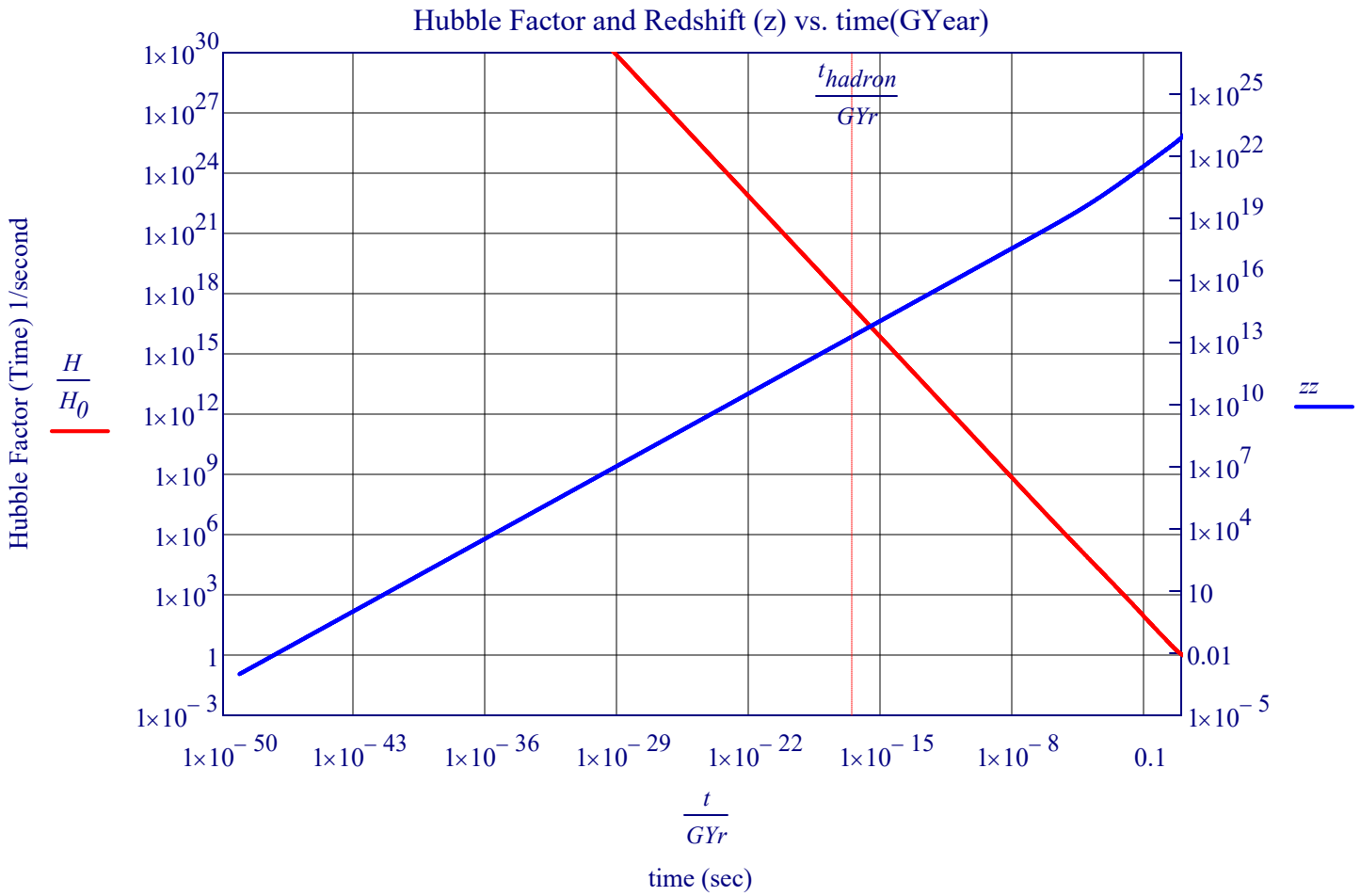
Hubble Factor and Redshift (z) vs. time(GYear)
Hubble Factor (Time) 1/second
H / H0
zz
t hadron / GYr
1×10^30
1×10^27
1×10^24
1×10^21
1×10^18
1×10^15
1×10^12
1×10^9
1×10^6
1×10^3
1
1×10^−3
1×10^25
1×10^22
1×10^19
1×10^16
1×10^13
1×10^10
1×10^7
1×10^4
10
0.01
1×10^−5
1×10^−50
1×10^−43
1×10^−36
1×10^−29
1×10^−22
1×10^−15
1×10^−8
0.1
t / GYr
time (sec)

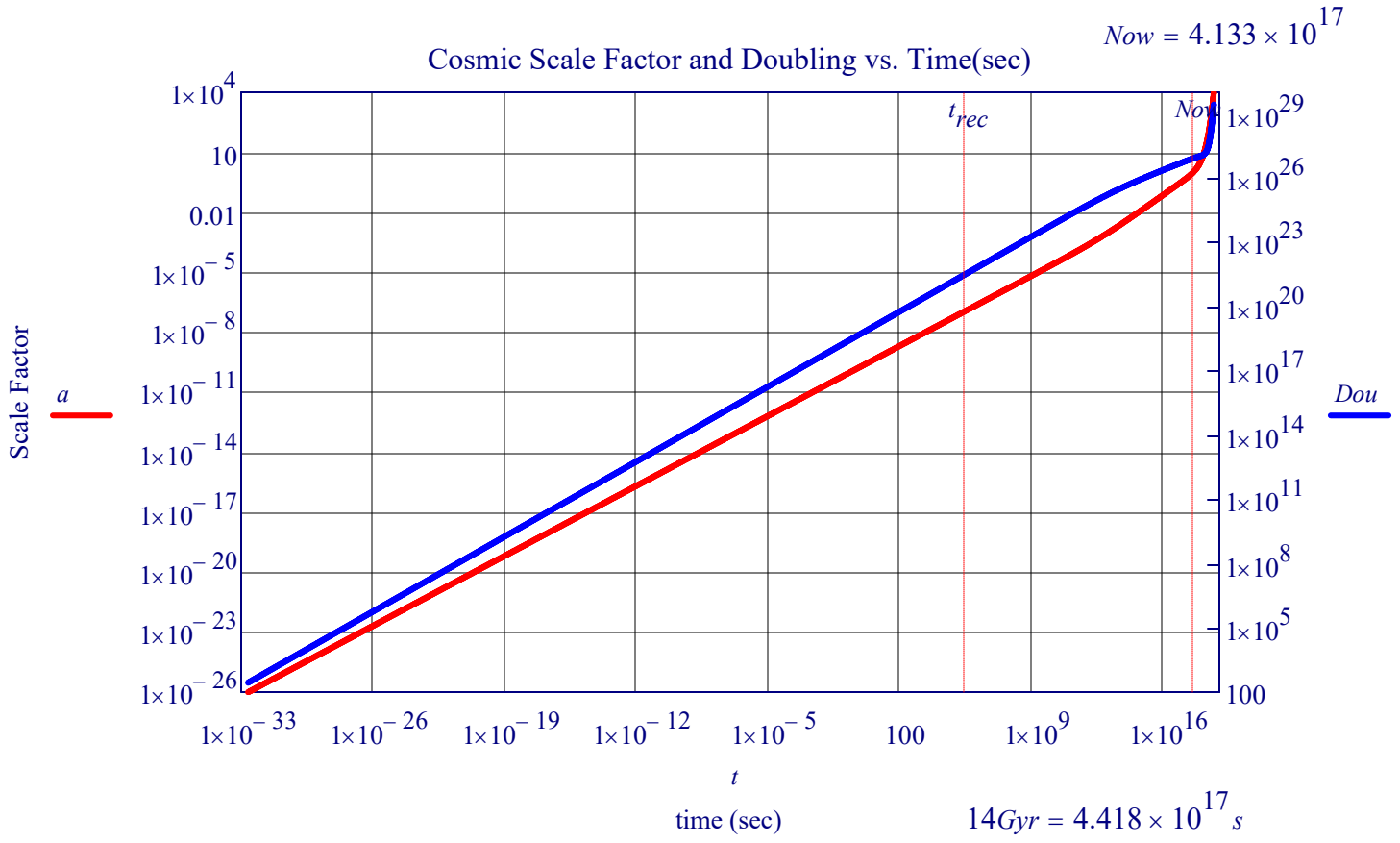
Now = 4.133 × 10^17
Cosmic Scale Factor and Doubling vs. Time(sec)
Scale Factor
a
Dou
t rec
Now
1×10^4
10
0.01
1×10^−5
1×10^−8
1×10^−11
1×10^−14
1×10^−17
1×10^−20
1×10^−23
1×10^−26
1×10^29
1×10^26
1×10^23
1×10^20
1×10^17
1×10^14
1×10^11
1×10^8
1×10^5
100
1×10^−33
1×10^−26
1×10^−19
1×10^−12
1×10^−5
100
1×10^9
1×10^16
t
time (sec)
14Gyr = 4.418 × 10^17 s

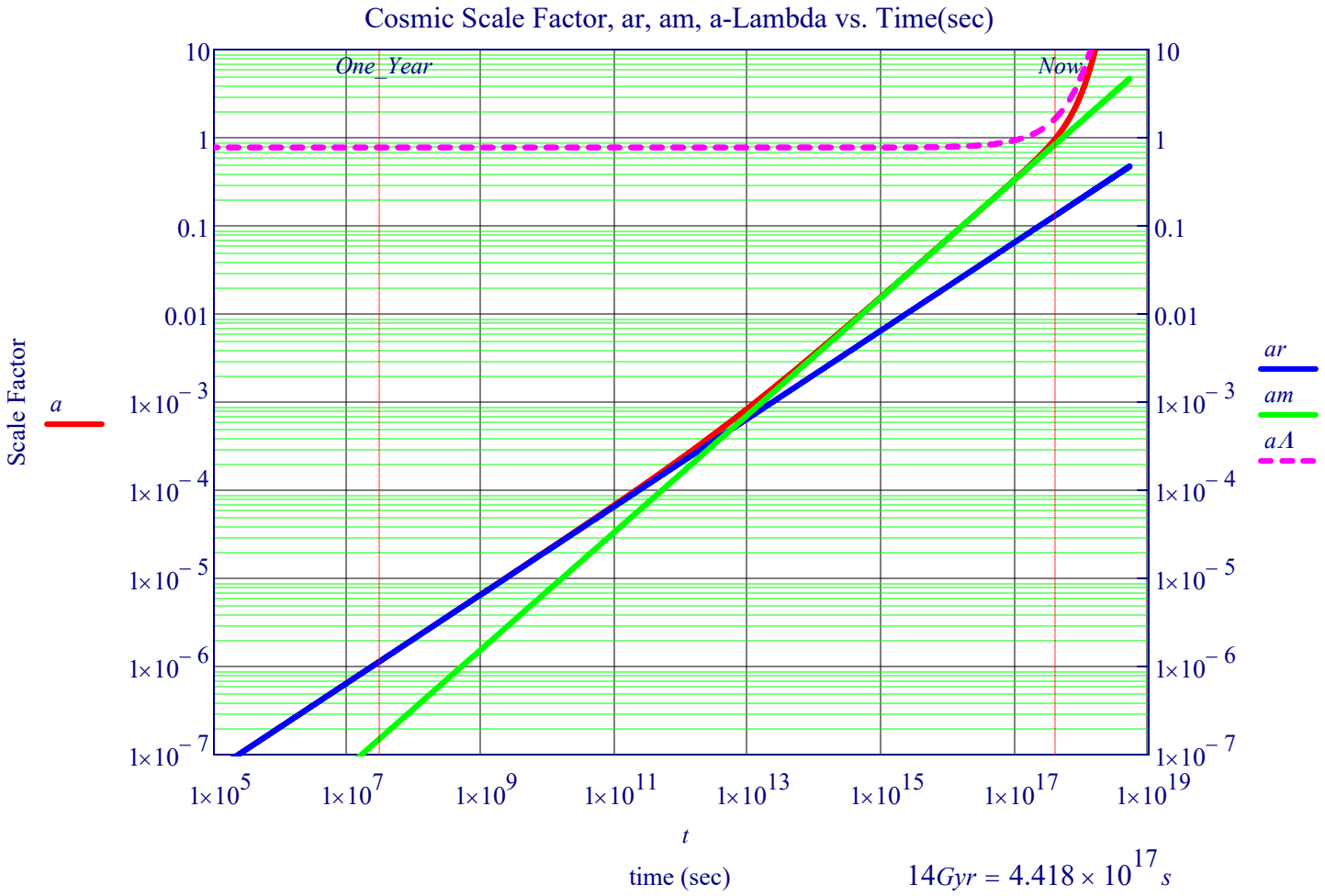
Cosmic Scale Factor, ar, am, a-Lambda vs. Time(sec)
One_Year
Now
Scale Factor
a
ar
am
aΛ
t
time (sec)
14Gyr = 4.418 × 10^17 s

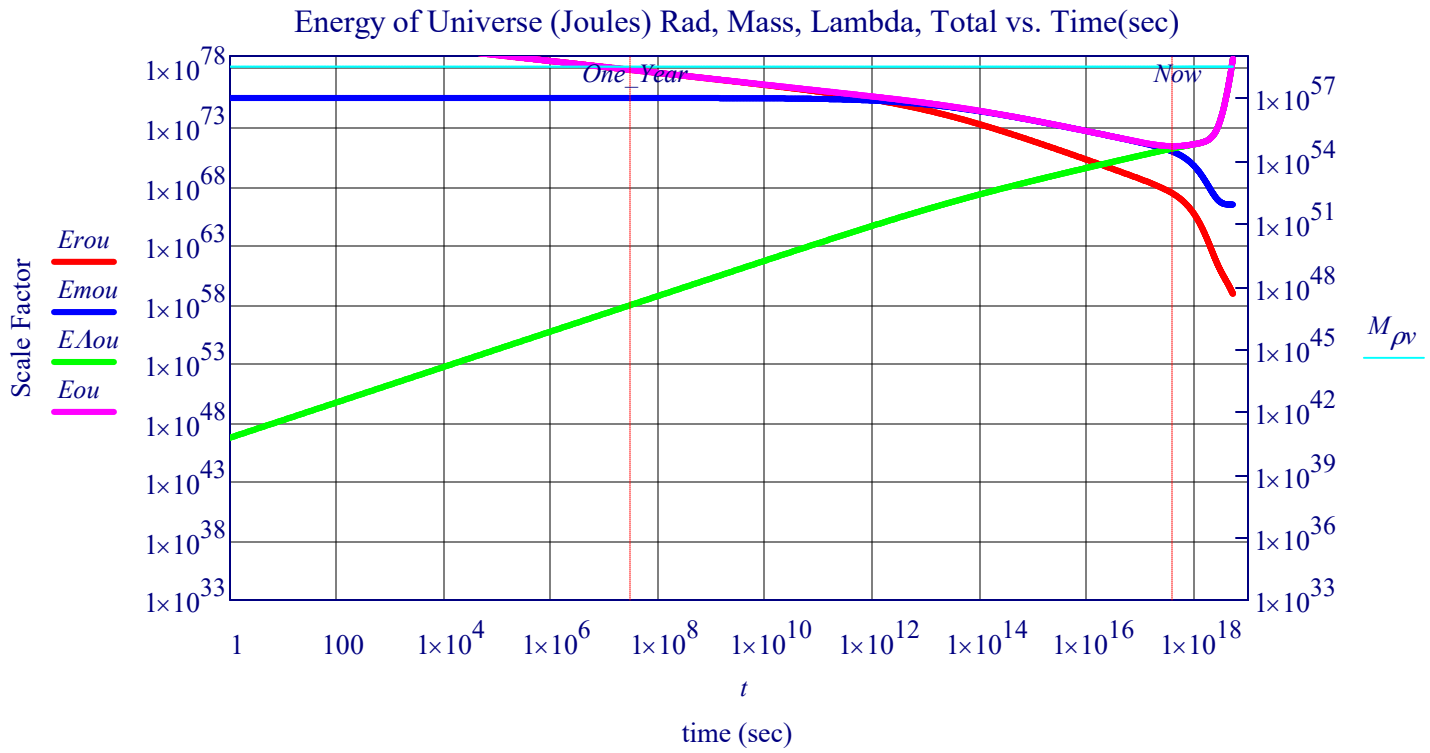
Energy of Universe (Joules) Rad, Mass, Lambda, Total vs. Time(sec)
One_Year
Now
Scale Factor
Erou
Emou
EΛou
Eou
Mρv
t
time (sec)

Plot in GYears

For a radiation-dominated critical density Universe, H0 = 1/2t

$$h_{bar} := 6.62607015 \cdot 10^{-34}\, m^2 \frac{kg}{2\pi \cdot s}$$

Planck Time, t_{Pl} $\quad t_{Pl} = \dfrac{h}{2\pi \cdot m_{Pl} \cdot c^2}$ $\quad t_{Pl} := \dfrac{h_{bar}^{\frac{1}{2}} \cdot G^{\frac{1}{2}}}{c^{\frac{5}{2}}}$ $\quad t_{Pl} = 5.39\, s \cdot 10^{-44}$

Density at Planck Time, ρ_{crit}

$$\rho_{crit} := \frac{3 \cdot H^2}{8 \cdot \pi G} \qquad H = \frac{1}{2t} \qquad \rho_{time}(t) := \frac{3}{32 \pi G \cdot t^2} \qquad \rho_{Pl} := \rho_{time}(t_{Pl}) \qquad \rho_{Pl} = 1.54 \times 10^{95} \frac{kg}{m^3}$$

$$\rho_{1ns} := \frac{3}{32 \cdot \pi \cdot G \cdot \left(10^{-9}\, s\right)^2} = 4.474 \times 10^{26} \frac{kg}{m^3} \qquad \Delta\rho_{1ns} := \rho_{1ns} + 0.5 \frac{kg}{m^3}$$

$$GYr := 3.156 \cdot 10^{16} \qquad NowGyr := \frac{Now}{GYr}$$

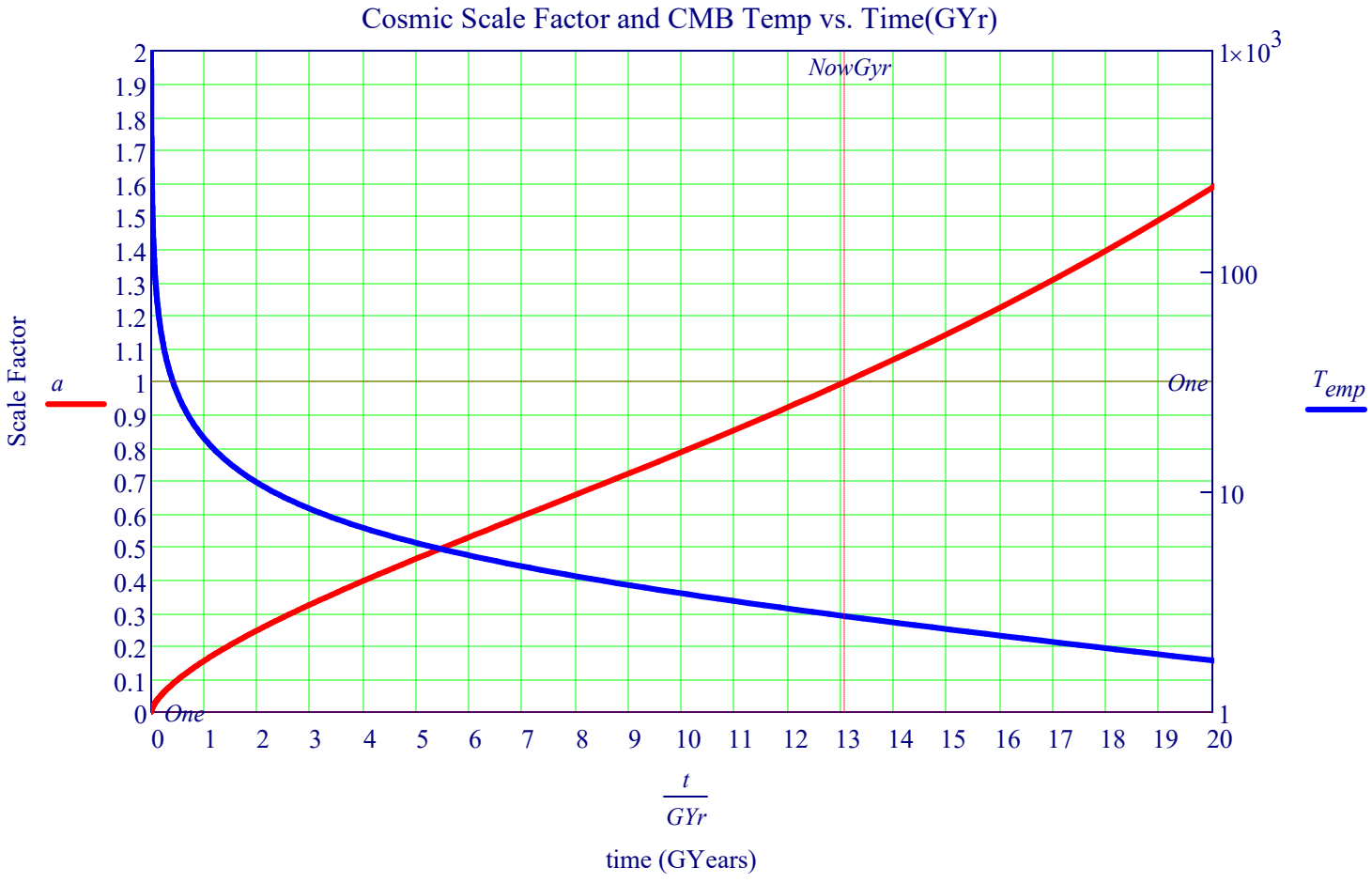

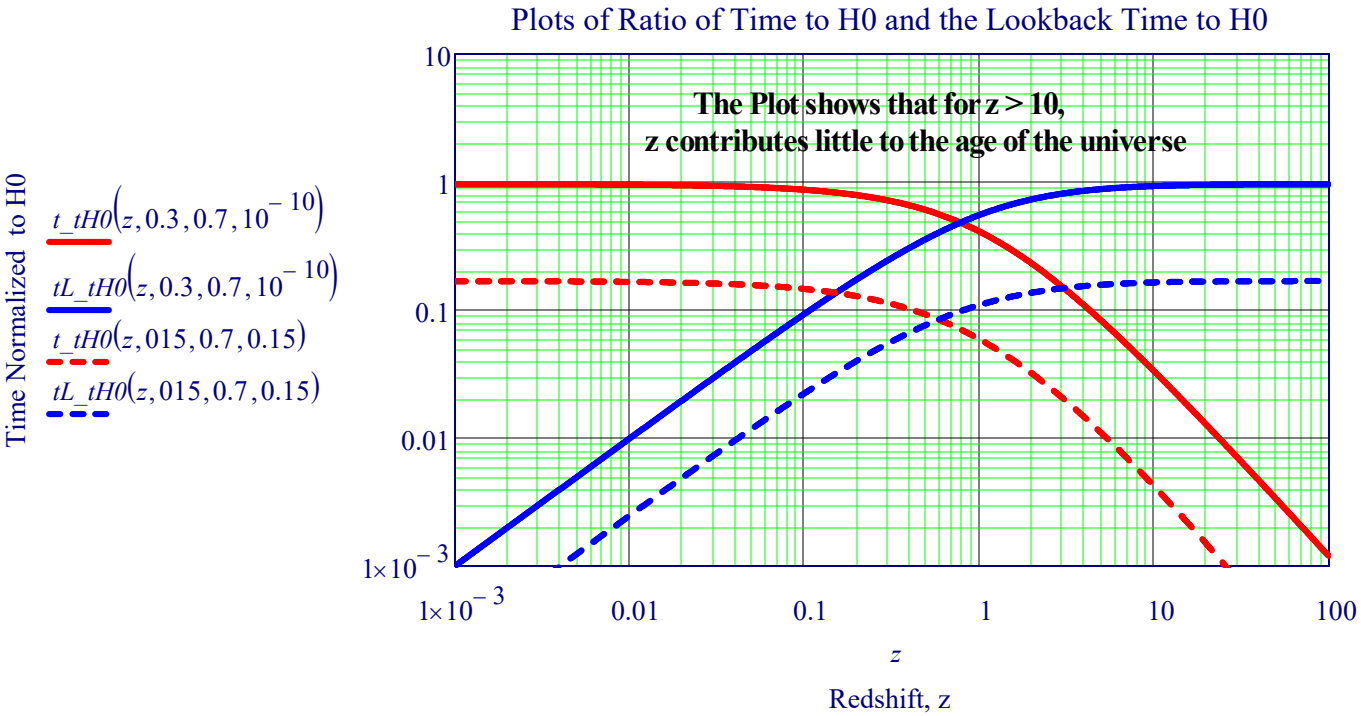

2023 Estimate z=10 is 13.30 Gyr

$t_{BB} := 13.8 Gyr$

$t_{BB} \cdot tL\_tH0\left(10, 0.3, 0.7, 10^{-10}\right) = 12.844 \cdot Gyr$ $\qquad z = \frac{1}{a} - 1$

Dynamics of the expansion

To the observer, the evolution of the scale factor is most directly characterized by the change with redshift of the Hubble parameter and the density parameter; the evolution of ***H(z)*** and ***Ω(z)*** is given immediately by the **Friedmann Equation** in the form $H^2 = 8\pi G\rho/3 - kc^2/R^2$. Inserting the above dependence of **ρ** on ***a*** gives

$$H^2(a) = H_0^2 \left[\Omega_v + \Omega_m a^{-3} + \Omega_r a^{-4} - (\Omega - 1)a^{-2}\right].$$

$$H_0 = \left.\frac{\dot{a}}{a}\right|_{t=t_0} \qquad \mathbb{E} \equiv H/H_0 \qquad dt = da/aH$$

This is a crucial equation, which can be used to **obtain the Relation between Redshift and Comoving Distance.**
The radial equation of motion for a photon is $R\,dr = c\,dt = c\,dR/R_{dot} = c\,dR/(RH)$.

With $R = R_0/(1+z)$, this gives

$$R_0 dr = \frac{c}{H(z)}\,dz$$
$$= \frac{c}{H_0}\left[(1-\Omega)(1+z)^2 + \Omega_v + \Omega_m(1+z)^3 + \Omega_r(1+z)^4\right]^{-1/2} dz.$$

This relation is arguably the single most important equation in cosmology, since it shows how to **relate comoving distance to redshift**, Hubble constant and density parameter.

The comoving distance determines the apparent brightness of distant objects, and the comoving volume element determines the numbers of objects that are observed. These aspects of observational cosmology are discussed in more detail below.

Lastly, using the expression for $H(z)$ with $\Omega(a) - 1 = kc^2/(H^2 R^2)$ gives

the redshift dependence of the total density parameter:

$$\Omega(a) - 1 = \frac{\Omega - 1}{1 - \Omega + \Omega_v a^2 + \Omega_m a^{-1} + \Omega_r a^{-2}}.$$

This last equation is very important.

It tells us that, at high redshift, all model universes apart from those with only vacuum energy will tend to look like the $\Omega = 1$ model.

This is not surprising given the form of the Friedmann equation: provided $\rho R^2 \to \infty$ as $R \to 0$, the $-kc^2$ curvature term will become negligible at early times.
If $\Omega \neq 1$, then in the distant past $\Omega(z)$ must have differed from unity by a tiny amount: the density and rate of expansion needed to have been finely balanced for the universe to expand to the present.

This tuning of the initial conditions is called the flatness problem and is one of the motivations for the applications of quantum theory to the early universe.

Evolution of the Hubble Factor: Mass Conservation of non-relativistic matter implies $\rho_m \propto a^{-3} = (1+z)^3$.
In the ΛCDM model, dark energy is assumed to behave like a cosmological constant: $\rho_\Lambda \propto a^0 = (1+z)^0$.
The density of radiation (and massless neutrinos) scales as $\rho_r \propto a^{-4} = (1+z)^4$ because the number density of photons is $\propto a^{-3} = (1+z)^3$ and the mass $E/c^2 = h\nu/c^2$ of each photon scales as $E \propto \lambda^{-1} \propto (1+z)^1 \propto a^{-1}$.

Calculated Values

$\Omega_{r0} = 0$
$\Omega_{m0} = 0.317$
$\Omega_{\Lambda 0} = 0.683$

Dynamical Equation Specifying the Evolution of the Hubble Factor of Our Universe

$$\frac{H}{H_0} = H\_H_0(z) := \sqrt{\Omega_{m0}\cdot(1+z)^3 + \Omega_{\Lambda 0} + \Omega_{r0}\cdot(1+z)^4}$$

***R(t)* is the Scale Factor**

$R(t_0) = 1$

$$H(t) = \frac{\frac{d}{dt}R(t)}{R(t)}$$

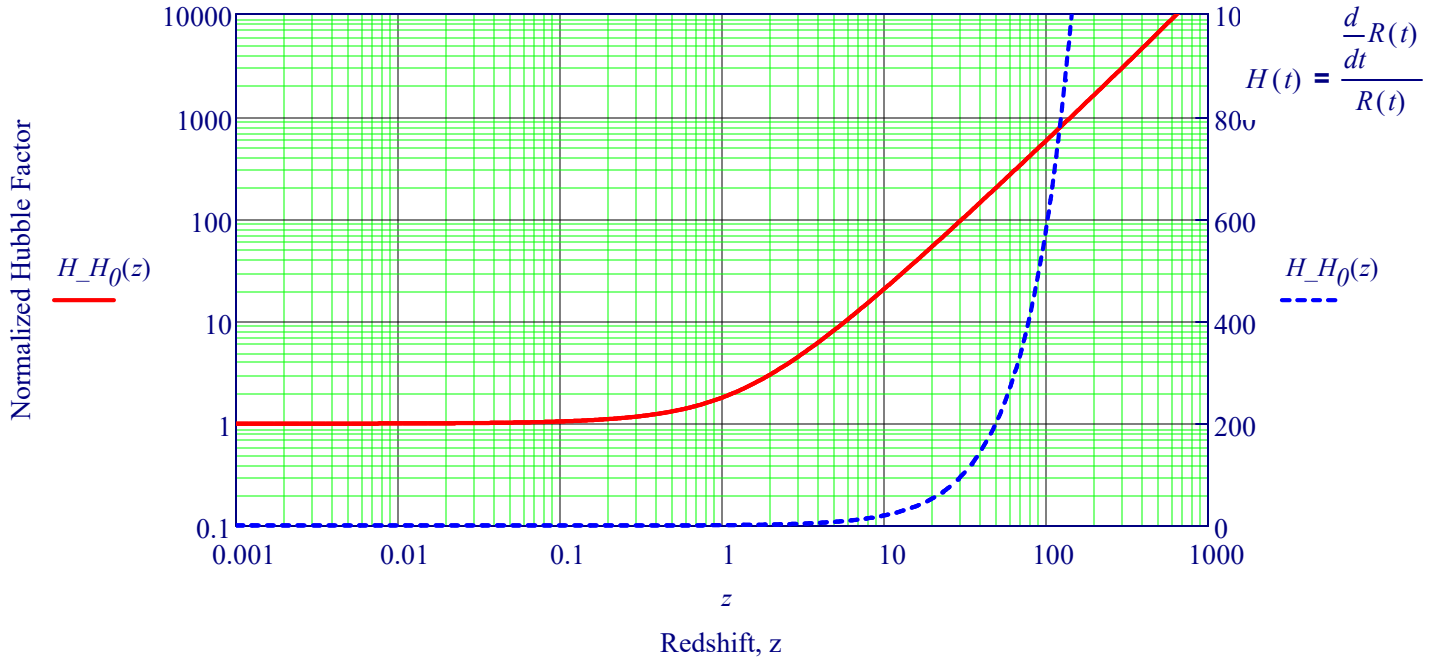

VIII. Multiple-Component Universes: Parameter (t_0H_0) Contour Vs. Densitites

ASTROPHYSICS AND COSMOLOGY

Juan Garcıa-Bellido, Theoretical Physics Group

Define $y = \frac{a}{a_0}$ $\qquad \tau = H_0 \cdot (t - t_0)$

Then Friedmann's Equation can be written:

$$\frac{d}{d\tau} y = \sqrt{1 + \left(\frac{1}{y} - 1\right) \cdot \Omega_M + \left(y^2 - 1\right) \cdot \Omega_\Lambda} \qquad \text{Equation 56}$$

With Initial Conditions

$$y(0) = 1 \qquad \frac{d}{d\tau} y(0) = 1$$

Therefore, the present age t_0 is a function of the other parameters,

$t_0 = f(H_0, \Omega_M, \Omega_\Lambda)$, determined from

$$t0H0(\Omega_M, \Omega_\Lambda) := \int_0^1 \frac{1}{\sqrt{1 + \left(\frac{1}{y} - 1\right) \cdot \Omega_M + \left(y^2 - 1\right) \cdot \Omega_\Lambda}}\, dy \qquad t0H0(0.3, 0.7) = 0.964$$

$\dot{a}^2 = H_0^2[\Omega_m a^{-1} + (1 - \Omega_m)a^2]$ and the time relationship $H_0 t(a) = \int_0^a \frac{x\, dx}{\sqrt{\Omega_m x + (1 - \Omega_m)x^4}}$

Calculate a Matrix $Time_0H_0$ (t0H0) of Values:

of t0H0 for Ω_M and Ω_Λ Ranging from 0 to 1.5

```
Time0H0 := | TML ← (0 0 0)
           | m ← 0
           | l ← 0
           | for mm ∈ 0, 1 .. 170
           |     m ← m + 0.01
           |     l ← 0
           |     for ll ∈ 0, 1 .. 100
           |         th ← t0H0(m, l)
           |         tml ← (m l th)
           |         l ← l + 0.01
           |         TML ← stack(TML, tml)
           | TML
```

$min(Time0H0^{\langle 0 \rangle}) = 0$

$min(Time0H0^{\langle 1 \rangle}) = 0$

$min(Time0H0^{\langle 2 \rangle}) = 0$

$max(Time0H0^{\langle 0 \rangle}) = 1.71$

$max(Time0H0^{\langle 1 \rangle}) = 1$

$max(Time0H0^{\langle 2 \rangle}) = 2.062$

$rows(Time0H0) = 17272$

Assemble Contour Line Points of Curves with Given t_0H_0 Values

Find Those Contour Values of **Density Parameters**, Ω_M and Ω_Λ,
of Matrix $Time_0H0$ that Give a t_0H_0 values (T) ranging from 0.65, 0.7 ... up to 1.2

$$TH(T) := \left| \begin{array}{l} R \leftarrow 0 \\ TH \leftarrow \begin{pmatrix} 0 & 0 & 0 \end{pmatrix} \\ \text{for } r \in 0, 1 .. 17000 \\ \quad \text{if } \left(Time0H0_{r,2} < T + 0.001 \right) \wedge Time0H0_{r,2} > T - 0.00 \\ \quad\quad \left| \begin{array}{l} out \leftarrow \begin{pmatrix} Time0H0_{r,0} & Time0H0_{r,1} & Time0H0_{r,2} \end{pmatrix} \\ TH \leftarrow stack(TH, out) \end{array} \right. \\ TH \end{array} \right.$$

$$\Omega_\Lambda(T) := TH(T)^{\langle 1 \rangle} \qquad \Omega_M(T) := TH(T)^{\langle 0 \rangle}$$

$$t0H0(1, 0) = 0.667$$

$$t0H0(0.01, 1) = 2.062$$

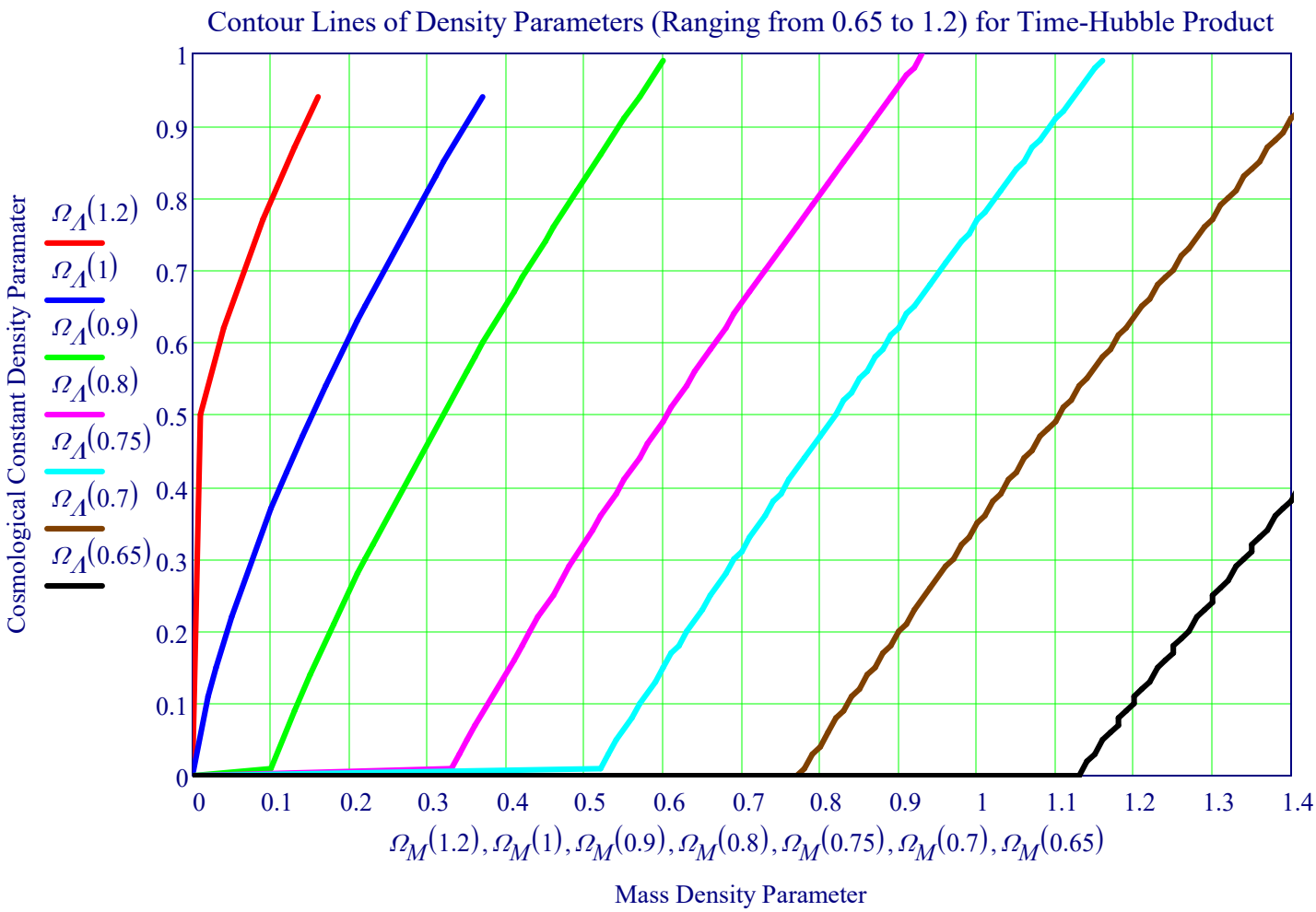

Einstein-de Sitter (EdS) Model Universe: Flat and Matter-Only FLRW Universe

The Einstein–de Sitter universe is a model of the universe proposed by Albert Einstein and Willem de Sitter in 1932. On first learning of Edwin Hubble's discovery of a linear relation between the redshift of the galaxies and their distance, **Einstein set the cosmological constant to zero** in the Friedmann equations, resulting in a model of the expanding universe known as the Friedmann–Einstein universe. In 1932, Einstein and De Sitter proposed an even simpler cosmic model by assuming a **vanishing spatial curvature as well as a vanishing cosmological constant**. In modern parlance, the Einstein–de Sitter universe can be described as a **Cosmological Model for a Flat Matter-Only** Friedmann–Lemaître–Robertson–Walker metric (FLRW) universe.

In the model, Einstein and de Sitter derived a simple relation between the average density of matter in the universe and its expansion according to $H_0^2 = \kappa\rho/3$, where H_0 is the Hubble constant, ρ is the average density of matter and κ is the Einstein gravitational constant. The cosmic time t as a function of scale factor, a, is given by

$$a_{eds}(t) := c \cdot e^{\sqrt{\frac{8\pi \cdot G \cdot \rho_0}{3}} \cdot t} \qquad t_0 := \frac{2}{3 \cdot H_0} = 9.2 \cdot Gyr \qquad t_0 := \frac{t_0}{Gyr} \qquad a_{E\_D}(t) := \left(\frac{t}{t_0}\right)^{\frac{2}{3}}$$

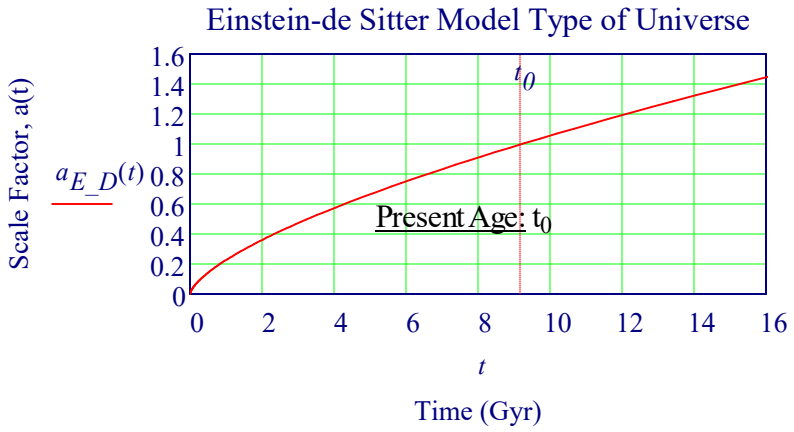

EdS: The cosmic time t as a function of the scale factor, a, is given by the Expression:

$$a_{EdS}(\eta, \Omega_0) := \frac{1}{2} \cdot \frac{\Omega_0}{1 - \Omega_0} \cdot (\cosh(\eta) - 1) \qquad t_{EdS}(\eta, \Omega_0) := \frac{1}{2H_0 \cdot \frac{Gyr \cdot km}{Mpc}} \cdot \frac{\Omega_0}{(1 - \Omega_0)^{\frac{3}{2}}} \cdot (\sinh(\eta) - \eta)$$

$ii := 0 .. 200 \qquad \eta_{ii} := \frac{2 \cdot \pi \cdot ii}{100}$ Time Normalized to $\Omega_0 = 0.9$ $\qquad t_{EdS0} := t_{EdS}(2\pi, 0.9)$

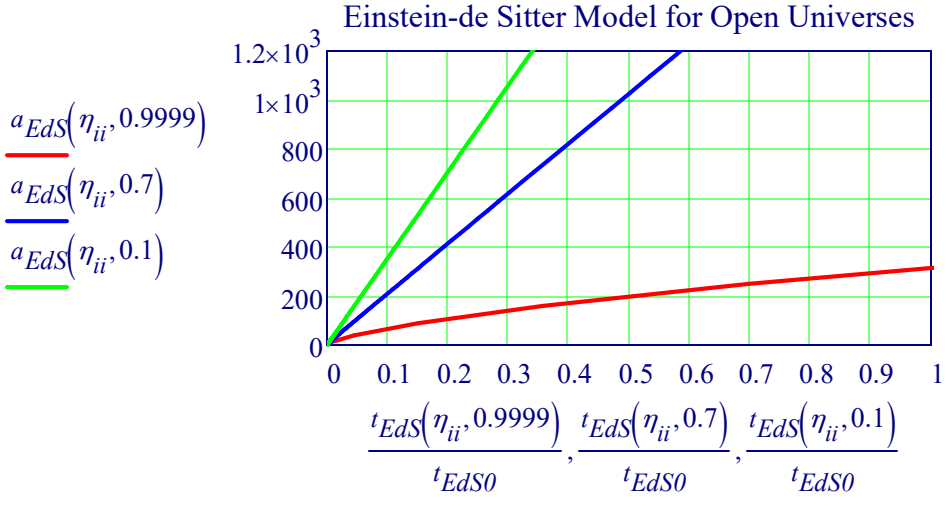

Plots of $a(t)$ versus t for the closed universes with $\Omega_0 = 1.1, 1.2, 1.5,$

$$a_{EdS}(\eta, \Omega_0) := \frac{1}{2}\cdot\frac{\Omega_0}{\Omega_0 - 1}\cdot(1 - \cos(\eta))$$

$$t_{EdS}(\eta, \Omega_0) := \frac{1}{2H_0\cdot\frac{Gyr\cdot km}{Mpc}}\cdot\frac{\Omega_0}{(\Omega_0 - 1)^{\frac{3}{2}}}\cdot(\eta - \sin(\eta))$$

$ii := 0 .. 100 \qquad \eta_{ii} := \frac{2\cdot\pi\cdot ii}{100}$

$t_{EdS0} := t_{EdS}(2\pi, 1.1)$

See Section XXXII on the Fine Tuning Flatness Problem

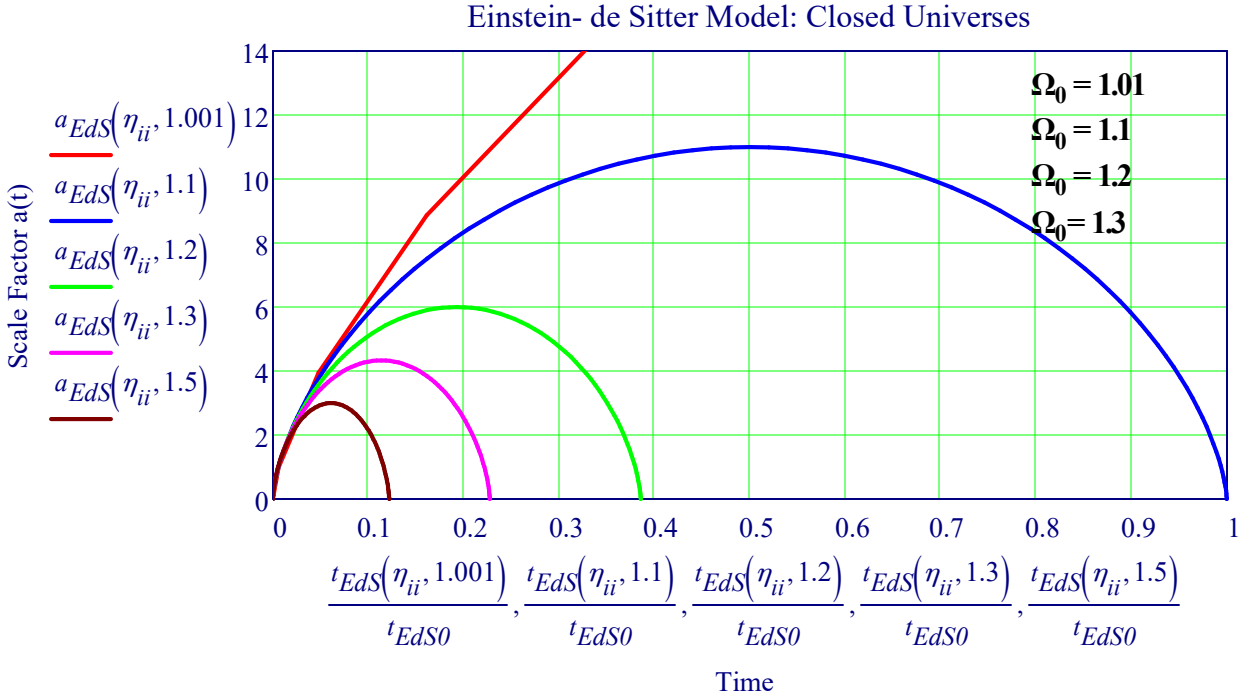

Temperature Jumps at Phase Transitions. Temperature at Recombination, E_{th}.

A New Version of the Lambda-CDM Cosmological Model, with Extensions and New Calculations, Journal of Modern Physics, 2024, 15, 193-238, Jan Helm

$\eta := 1.1$

$E_{th0} := -0.001$

Rate of Change of Eth with scale factor a, ΔEthΔa

$$\Delta Eth\Delta a = \frac{d}{da}Eth \qquad \Delta Eth\Delta a(a) := \frac{-E_{th0}}{a^{\eta}} \qquad T_{eV} := \frac{1eV}{k_B} \qquad T_{eV} = 1.2\times 10^4 K$$

Temperature after Recombination vs. Scale Factor, a, in electron volts, eV

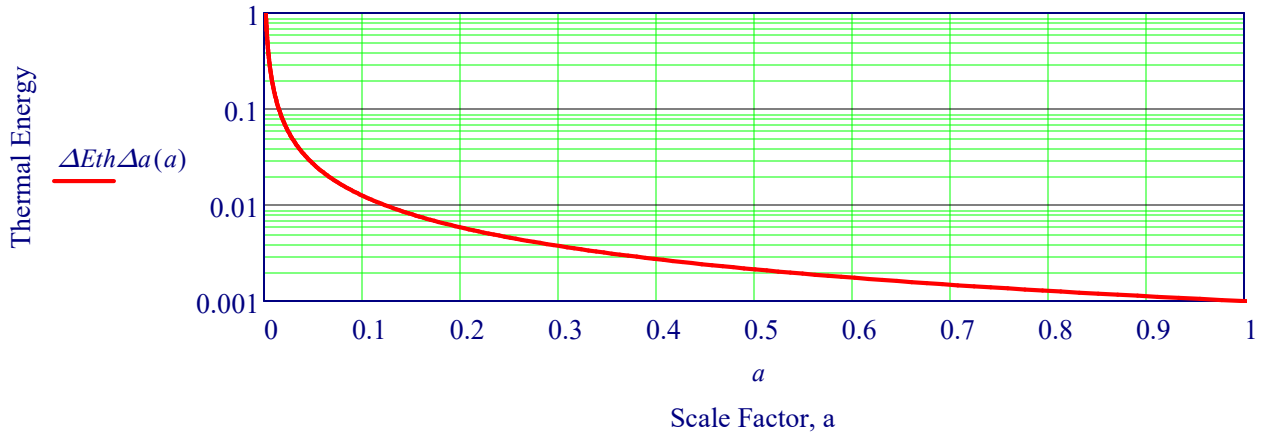

Measuring Cosmological Parameters

Cosmologists would like to know the scale factor *a(t)* for the universe. For a model universe whose contents are known with precision, the scale factor can be computed from the Friedmann equation. Finding *a(t)* for the real universe, however, is much more difficult. The scale factor is not directly observable; it can only be deduced indirectly from the imperfect and incomplete observations that we make of the universe around us. If we knew the **Energy Density ε** for each component of the universe, we could use the Friedmann equation to find the **scale factor *a(t)***. The argument works in the **other direction, as well**; if we could determine *a(t)* from observations, we could use that knowledge to find ε for each component. Let's see, then, what constraints we can put on the scale factor by making observations of distant astronomical objects.

Since **determining the exact functional form of a(t) is difficult**, it is useful, instead, to do a **Taylor series expansion** for a(t) around the present moment. Keeping the first three terms of the Taylor expansion, the scale factor in the recent past and the near future can be approximated as

$$a(t) = a(t_0) + \left.\frac{da}{dt}\right|_{t=t_0}(t-t_0) + \frac{1}{2}\left.\frac{d^2a}{dt^2}\right|_{t=t_0}(t-t_0)^2 + \cdots$$

Using the normalization $a(t_0) = 1$, the expansion can be written: $$a(t) \approx 1 + H_0(t-t_0) - \frac{1}{2}q_0H_0^2(t-t_0)^2$$

the parameter q_0 is a dimensionless number called the deceleration parameter, defined as

$$q_0 \equiv -\left(\frac{\ddot{a}a}{\dot{a}^2}\right)_{t=t_0} = -\left(\frac{\ddot{a}}{aH^2}\right)_{t=t_0}$$

Although H_0 and q_0 are themselves free of the theoretical assumptions underlying the Friedmann and acceleration equations, we can use the acceleration equation to predict what q0 will be in a given model universe. If our model universe contains N components, each with a different value of the equation-of-state parameter w_i, the acceleration equation can be written

$$\frac{\ddot{a}}{a} = -\frac{4\pi G}{3c^2}\sum_{i=1}^{N}\varepsilon_i(1+3w_i) \qquad -\frac{\ddot{a}}{aH^2} = \frac{1}{2}\left[\frac{8\pi G}{3c^2H^2}\right]\sum_{i=1}^{N}\varepsilon_i(1+3w_i)$$

The relation between the deceleration parameter q_0 and the density parameters of thedifferent components of the universe

For the current BB Model:

$$q_0 = \frac{1}{2}\sum_{i=1}^{N}\Omega_{i,0}(1+3w_i) \qquad q_0 = \Omega_{r,0} + \frac{1}{2}\Omega_{m,0} - \Omega_{\Lambda,0} \qquad q_0 := 0.53$$

1. In principle, determining H_0 should be easy. For small redshifts, the relation between a galaxy's distance d and its redshift z is linear Equation: $\boldsymbol{c\,z = H_0\,d}$ where $\boldsymbol{z = 1/a(t_e) - 1}$

Thus, if you measure the distance d and redshift z for a large sample of galaxies, and fit a straight line to a plot of cz versus d, the slope of the plot gives you the value of H_0. In practice, the distance to a galaxy is not only difficult to measure, but also somewhat difficult to define. The proper distance *dp(t)* between two points was defined as the length of the spatial geodesic between the points when the scale factor is fixed at the value a(t). The proper distance is perhaps the most straightforward definition of the spatial distance between two points in an expanding universe. We can get an approximate form by taking the first two terms of the Taylor expansion.

$$d_p(t_0) = c\int_{t_e}^{t_0}\frac{dt}{a(t)} \qquad d_p(t_0) \approx c(t_0 - t_e) + \frac{cH_0}{2}(t_0 - t_e)^2$$

where $c\,(t_0 - t_e)$ is the proper distance in a static universe.

substituting the $dp(t_0)$ equation into the Taylor Expansion gives: $$d_p(t_0) \approx \frac{c}{H_0}\left[z - \left(1 + \frac{q_0}{2}\right)z^2\right] + \frac{cH_0}{2}\frac{z^2}{H_0^2} = \frac{c}{H_0}z\left[1 - \frac{1+q_0}{2}z\right]$$

Light-cone structure of the FLRW space

$$ds^2 = -c^2dt^2 + a^2(t)\left(\frac{dr^2}{1-Kr^2} + r^2d\Omega^2\right)$$

Let us consider the K = 0 case, for simplicity. Moreover, consider also $d\Omega = 0$. In this case, the radial coordinate is also the distance. Then, putting $ds^2 = 0$ in the FLRW metric gives the following light-cone structures.

Cosmic time-comoving distance

From the above FLRW metric, the condition $ds^2 = 0$ gives us:

$$\frac{cdt}{dr} = \pm a(t)$$

We put our observer at r = 0 and t = t_0 . The plus sign in the above equation then describes an outgoing photon, i.e. the future light-cone, whereas the negative sign describes an incoming photon, i.e. the past-light cone, which is much more interesting to us. So, let us keep the negative sign and discuss the shape of the light-cone. Assume that a(0) = 0. Therefore, the slope of the past light-cone starts as −a(t 0), which we can normalise as −1, i.e. locally the past light-cone is identical to the one in Minkowski space. However, a goes to zero, so the light-cone becomes flat, encompassing more radii than it would for Minkowski space. See Figure below . We can show this analytically by taking the second derivative of the above with the minus sign.

$$\frac{c^2d^2t}{dr^2} = -\dot{a}\frac{cdt}{dr} = a\dot{a}$$

Space Time Diagram Comoving Distance and Normal Time

Cosmic Age/Lookback Time - Comoving distance

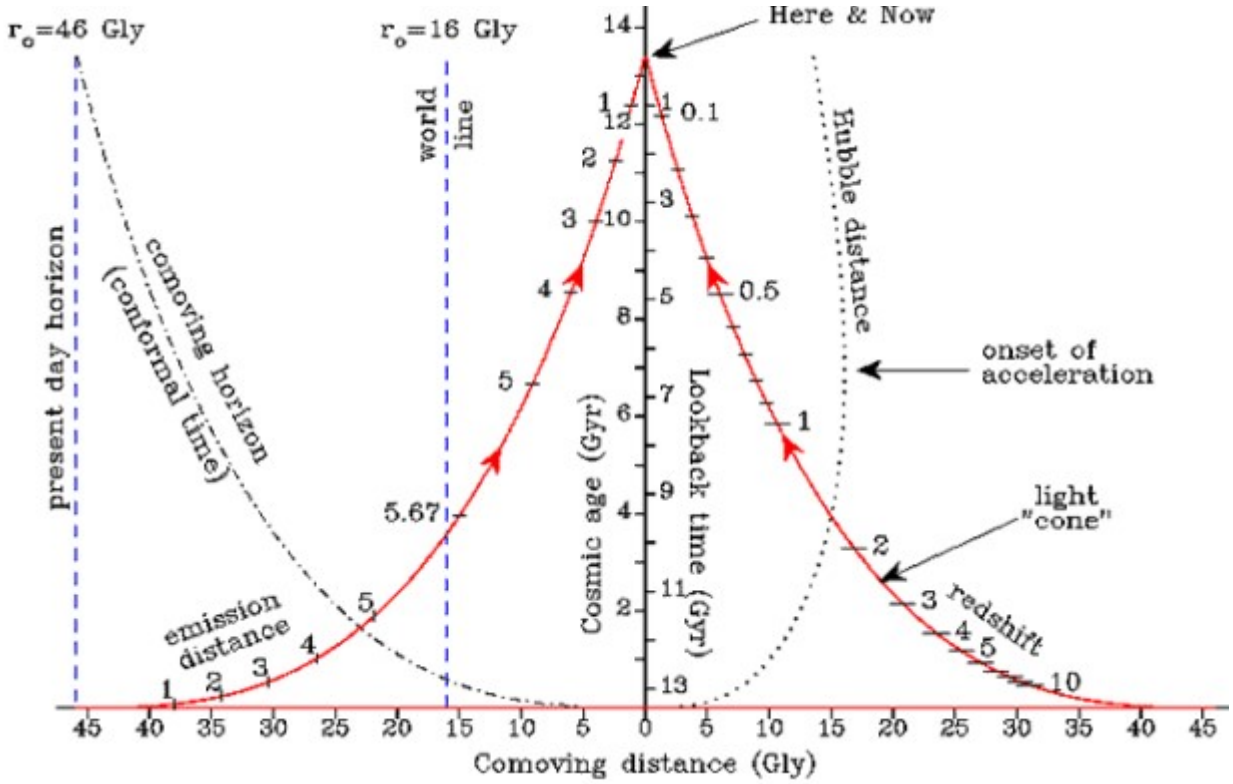

Space-time diagram and light-cone structure for the FLRW metric

The Constancy of the Laws of Nature - Variation of the Fine Structure Constant

The Value of the Fine Structure Constant Over Cosmological Times, C M Gutierrez and M. L´opez-Corredoira, The Astrophysical Journal , 713:46–51, 2010 April 10 doi:10.1088/0004-637X/713/1/46

In Jeremiah 33:25, God declares, "*I have established…the fixed laws of heaven and earth.*"
This is just one of several Scripture passages demonstrating that for thousands of years the Bible has been on record as stating that the laws of physics do not vary.

The one constant of physics most amenable to this testing technique is the fine structure constant, which characterizes the strength of the electromagnetic interaction. The fine structure constant has the additional advantage of being directly related to several other physical constants. For example, it is the ratio of the elementary electron charge to the Planck charge; the ratio of the velocity of the electron in the Bohr model of the atom to the velocity of light; the ratio of the energy needed to overcome the electrostatic repulsion between two electrons separated by distance D to the energy of a single photon at wavelength, $\lambda = 2\pi D$. It is the dimensionless coupling constant for electromagnetism, $\alpha \sim 1/137$.

Consequently, testing the constancy of the fine structure constant also test the constancy of several other physical constants. The principal assumption made in this work is that the difference in wavelengths divided by their sum is proportional to the fine-structure constant squared. The analysis is done by measuring the position of the fine structure lines of the [Oiii] doublet (λλ4959 and λλ5008) in QSO (Quasistellar Object, Quasar) nebular emission.

This method is based on fine structure splitting. The splitting ratio $(\lambda_2 - \lambda_1)/(\lambda_2 + \lambda_1)$ at two different epochs gives the relative difference in he relative difference in α between these two epochs. It is shown (Uzan 2003) that

$$\frac{\Delta\alpha}{\alpha}(z) = \frac{1}{2}\left\{\frac{[(\lambda_2 - \lambda_1)/(\lambda_2 + \lambda_1)]_z}{[(\lambda_2 - \lambda_1)/(\lambda_2 + \lambda_1)]_0} - 1\right\}$$

where λ_2 and λ_1 are the wavelengths of the pairs of the doublet, and the subscripts z and 0 refer to the values at redshift z and locally, respectively. Analyzed a sample of 1,568 quasars in the Sloan Digital Sky Survey Data Release 6.

Results of Analysis Matrix αz: Redshift Min, Max, Δα/α 10^{-5}, 1σ Errors

$\alpha_z := READPRN("Fine Structure Constant vs Redshift.txt")$

$za := 0 .. 8$ $\quad cols(\alpha_z) = 4$

$z_{avg_{za}} := mean(\alpha_{z_{za,0}}, \alpha_{z_{za,1}})$

$\Delta\alpha\_\alpha_{max} := \alpha_z^{\langle 2\rangle} + \alpha_z^{\langle 3\rangle}$ $\quad \Delta\alpha\_\alpha_{min} := \alpha_z^{\langle 2\rangle} - \alpha_z^{\langle 3\rangle}$

$\Delta\alpha\_\alpha_{mean} := \alpha_z^{\langle 2\rangle}$

$\Delta\alpha\_\alpha_{avg} := mean(\alpha_z^{\langle 2\rangle})$

$\Delta\alpha\_\alpha_{avg} = 3.533$

$\chi := line(z_{avg}, \Delta\alpha\_\alpha_{mean})$

$\Delta\alpha\_\alpha(z) := \chi_0 + \chi_1 \cdot z$

$\chi_0 = 3.852$

$\chi_1 = -1.235$

Change in the Fine Structure Constant Over Cosmological Times

Δα/α x 10-5 vs. Redshift, z

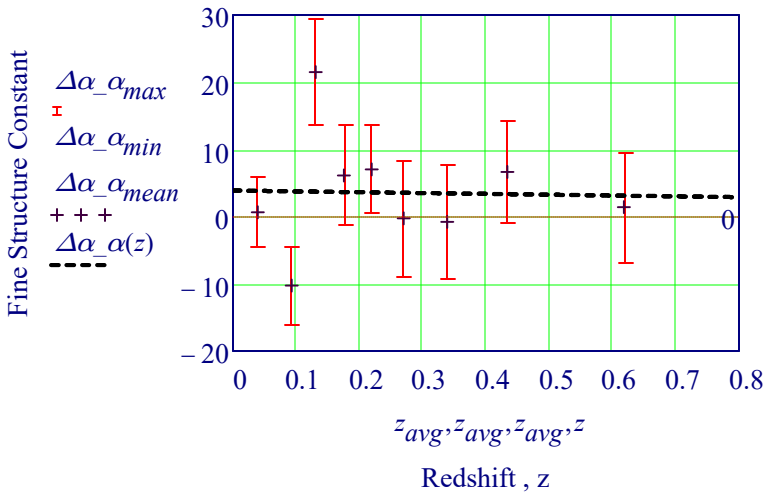

Δα/α = (+2.4 ± 2.5) × 10^{-5}
in the range of redshifts
z ~ 0 to 0.8

The range in redshift is a maximum look-back time of 6.6 Gyr, and a mean of 3.0 Gyr. See XXIV.

$$\frac{2.4 \cdot 10^{-5}}{3.3 Gyr} = 0.7 \cdot 10^{-14} \cdot yr^{-1}$$

The mean variation compatible with our results is: 1/t Δα/α = (0.7 ± 0.7) × 10^{-14} yr^{-1}

This gives at a confidence level of better than 99 percent that the value of the **Fine Structure Constant** has **Not Changed over the past seven billion years by any more than three parts per hundred trillion per year.**

IXA. Stellar Classification Systems - MK, Harvard, Hertzsprung–Russell

Luminosity Defins. - Absolute & Apparent Magnitudes, Distance Modulus, Luminous Flux

Magnitude, in astronomy, is a measure of the **brightness** of a star or other celestial body.
The distance modulus, μ, is a **way of expressing distances** that is often used in astronomy. It describes distances on a **logarithmic scale** based on the astronomical magnitude system. The **apparent magnitude, *m***, of a star is the magnitude it has **as seen by an observer on Earth.** The distance modulus, ***μ***, is defined as ***μ = m - M*** (ideally, corrected from the effects of interstellar absorption) where ***M***, is the a**bsolute magnitude,** of an astronomical object.

Luminous flux is a measure of the **power of visible light** produced by a light source or light fitting. It is measured in lumens (lm). **Luminosity**, in astronomy, the amount of light emitted by an object in a **unit of time**, or its power (W). For example, the luminosity of the Sun is 3.846×10^{26} watts. **Luminosity is an absolute measur**e of **radiant power**; that is, **its value is independent of an observer's distance from an object**

$$L_{\odot} := 3.846 \cdot 10^{26}\, W$$

Irradiance (or flux density) is a term of radiometry and is defined as the radiant flux received by some surface per unit area. In the SI system, it is specified in units of W/m^2.

Absolute magnitude M is defined as the **apparent magnitude** of an object when seen at a **distance of 10 parsecs**. If a light source has luminosity *L(d)* when observed from a **distance of d parsec**s, and luminosity *L(10)* when observed from a distance of 10 parsecs, the inverse-square law is then written like:

$$L(d) = \frac{L(10)}{\left(\frac{d}{10}\right)^2}$$

The apparent m and absolute magnitude M

$$m = -2.5 \log_{10} F(d)$$
$$M = -2.5 \log_{10} F(d = 10)$$

Estimating Distance to Star from Apparent Brightness and Hertzprung-Russell Diagram
One can use **detailed observations of nearby stars** to provide a means to measure distances to **more distant stars**. Using spectroscopy, one can measure precisely the colour of a nearby star; using photography, one can also measure its apparent brightness.

Using the apparent brightness, m, the distance, and inverse square law, one can **compute the absolute brightness** of these stars. Ejnar Hertzsprung (1873-1967) and Henry Russell (1877-1957) plotted this **absolute brightness against colo**r for thousands of nearby stars in 1905-1915. This yields the famous Hertzprung-Russell diagram. See Section IX. **Once one has this diagram, one can use it in reverse to measure distances to more stars than parallax methods can reach.** For any star, one can measure its colour and its apparent brightness and **from the Hertzprung-Russell diagram, one can then infer the Absolute Brightness**. From the apparent brightness and absolute brightness, **one can solve for distance**.

The distance modulus $m - M$ can be used to **determine the distance** to a star using the equation:

$$M = m - 5 \log(d/10)$$

M = -2.5 log(F(d))

Magnitudes of Some Cosmological Light Sources

Sun	-26.5
Full Moon	-12.5
Venus	-4.3
Mars or Jupiter	-2
Sirius (α CMa)	-1.44
Vega (α Lyr)	0.0
Alnair (α Gru)	1.73
Naked-eye limit	6.5
Binocular limit	10
Proxima Cen	11.09
Visual limit through 20 cm telescope	14
QSO at redshift $z = 2$	≈ 20
Cepheid in galaxy M100 observed with HST	26
Galaxy at $z = 6$ observed with Gemini 8.1 m telescope	28
Limit for James Webb Space Telescope	≥ 30

Luminosity Distance

The most fundamental distance scale in the universe is the Luminosity Distance,

Luminosity Distance: $d_L = (L/4\pi f)^{1/2}$

where f is the observed flux (sun = 1368 W/m^2) of an astronomical object and L is its luminosity.

In relativistic cosmologies, observed flux (bolometric, or in a finite bandpass) is:

$$f = L/\left[(4\pi D_L^2)(1+z)^2\right]$$

One factor of (1 + z) is due to the energy loss of photons, and one is due to the time dialation of the photon rate.

A **luminosity distance** is defined as $D_L = D\,(1 + z)$, so that $f = L/(4\pi D_L^2)$.

For a specific flux, however,

$$S_\lambda = \frac{1}{(1+z)}\,\frac{L_{\lambda/(1+z)}}{L_\lambda}\,\frac{L_\lambda}{4\pi D_L^2}$$

As shown by Terrell the luminosity distance and absolute magnitudes can be written for each case of the deceleration parameter (q_0) and is often expressed as:

"*The luminosity distance equation in Friedmann cosmology*", Terrell, James

$$E(z, \Omega_r, \Omega_m, \Omega_\Lambda, \Omega_k) := \sqrt{\Omega_k\cdot(1+z)^2 + \Omega_m\cdot(1+z)^3 + \Omega_r\cdot(1+z)^4 + \Omega_\Lambda}$$

Luminosity Distance (Model Dependent)

$$\Omega_K(0, 0.05, 0) = 0.95$$

$$\Omega_K(0, 0.2, 0.8) = 0$$

$$\Omega_K(0, 1, 0) = 0$$

$$\Omega_K(\Omega_r, \Omega_m, \Omega_\Lambda) := 1 - \Omega_r - \Omega_m - \Omega_\Lambda$$

$$d_L(z, \Omega_r, \Omega_m, \Omega_\Lambda, \Omega_k) := (1+z)\cdot\int_0^z \frac{1}{E(z, \Omega_r, \Omega_m, \Omega_\Lambda, \Omega_k)}\,dz$$

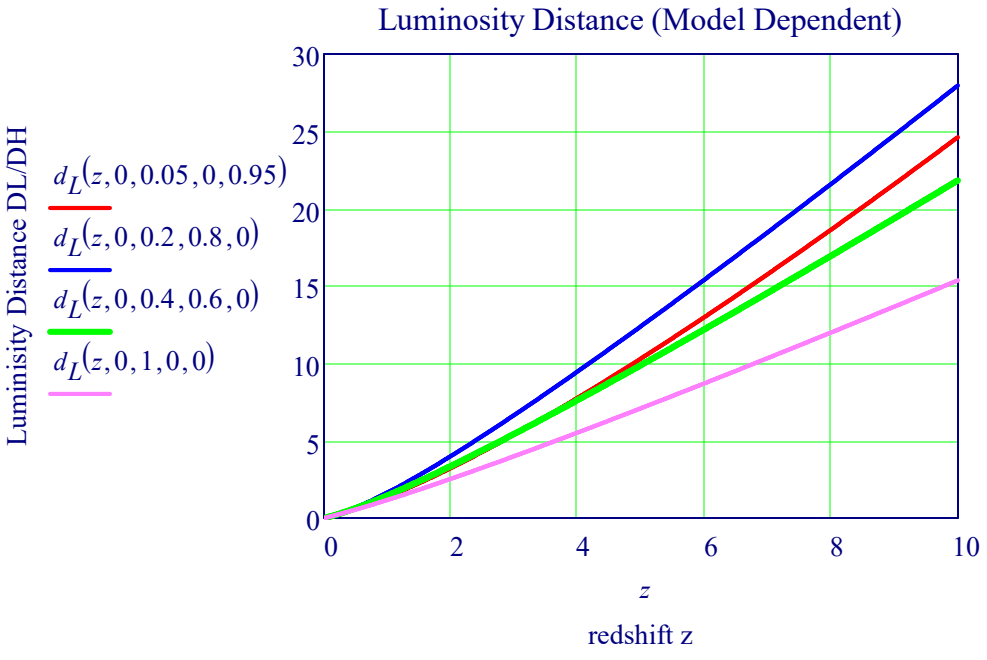

Stellar Classification Systems - MK, Harvard, Hertzsprung–Russell

Wikipedia - "In astronomy, stellar classification is the classification of stars based on their **spectral characteristics**. Electromagnetic radiation from the star is analyzed by splitting it with a prism or diffraction grating into a spectrum exhibiting the rainbow of colors interspersed with spectral lines. Each line indicates a particular chemical element or molecule, with the line strength indicating the abundance of that element. The strengths of the different spectral lines vary mainly due to the temperature of the photosphere, although in some cases there are true abundance differences. The spectral class of a star is a short code primarily summarizing the ionization state, giving an objective measure of the photosphere's temperature.

Most stars are currently classified under the Morgan–Keenan (MK) system using the letters O, B, A, F, G, K, and M, a sequence from the hottest (O type) to the coolest (M type). Each letter class is then subdivided using a numeric digit with 0 being hottest and 9 being coolest (e.g., A8, A9, F0, and F1 form a sequence from hotter to cooler). The sequence has been expanded with classes for other stars and star-like objects that do not fit in the classical system, such as class D for white dwarfs and classes S and C for carbon stars.

In the MK system, a luminosity class is added to the spectral class using Roman numerals. This is based on the width of certain absorption lines in the star's spectrum, which vary with the density of the atmosphere and so distinguish giant stars from dwarfs. Luminosity class 0 or Ia+ is used for hypergiants, class I for supergiants, class II for bright giants, class III for regular giants, class IV for subgiants, class V for main-sequence stars, class sd (or VI) for subdwarfs, and class D (or VII) for white dwarfs. The full spectral class for the Sun is then G2V, indicating a main-sequence star with a surface temperature around 5,800 K.

Harvard spectral classification

The Harvard system is a one-dimensional classification scheme by astronomer Annie Jump Cannon, who re-ordered and simplified the prior alphabetical system by Draper (see History). Stars are grouped according to their spectral characteristics by single letters of the alphabet, optionally with numeric subdivisions. Main-sequence stars vary in surface temperature from approximately 2,000 to 50,000 K, whereas more-evolved stars can have temperatures above 100,000 K[citation needed]. Physically, the classes indicate the temperature of the star's atmosphere and are normally listed from hottest to coldest."

A simple chart for classifying the main star types using Harvard classification

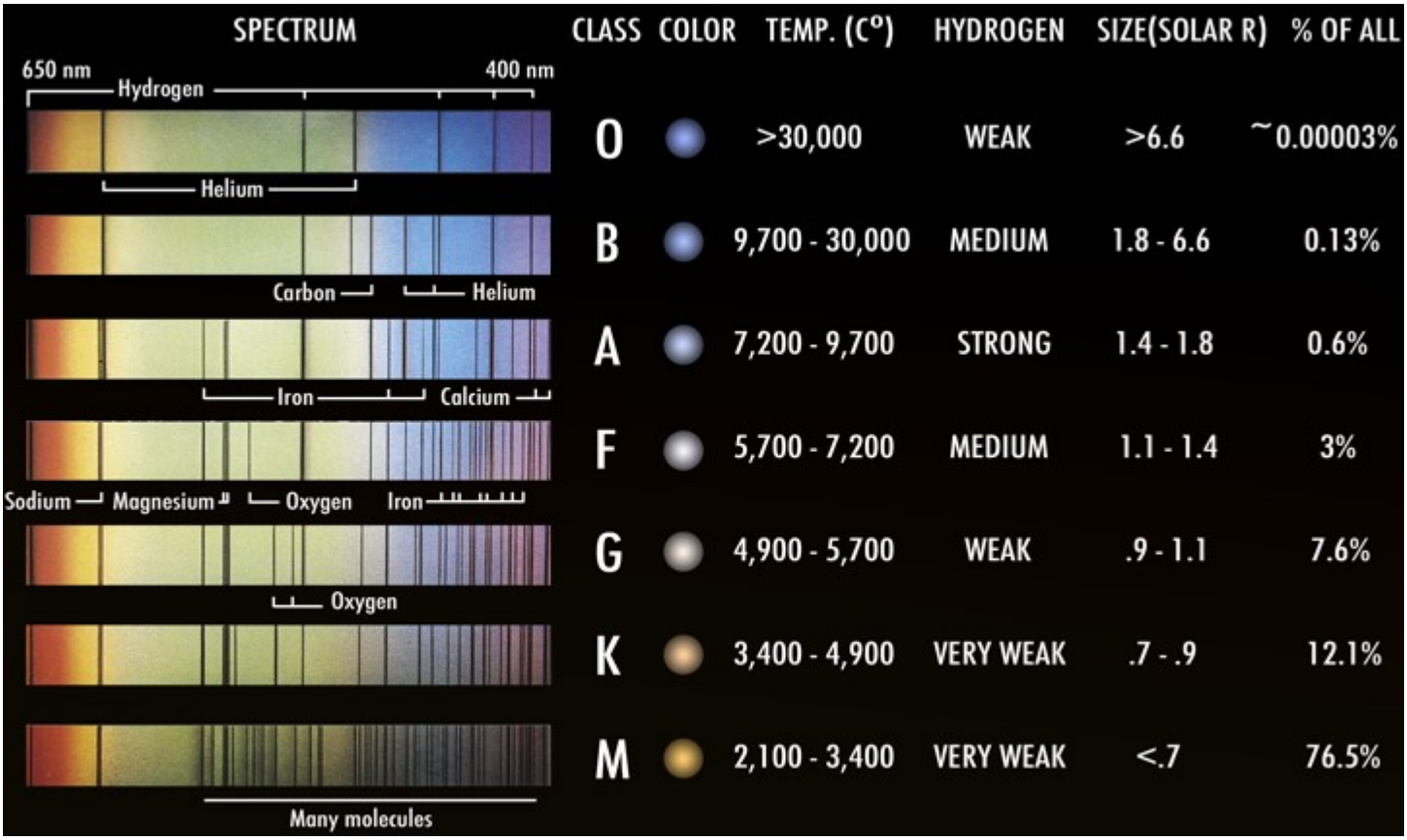

The Hertzsprung–Russell (H-R) diagram: Absolute Magnitude vs. Classification

Is a **scatter plot** of stars showing the relationship between the stars' **absolute magnitudes** or **luminosities versus their stellar classifications or effective temperatures**. The diagram was created in 1911 and represented a major step towards an understanding of stellar evolution. The H-R diagram is quite easy to understand if you can interpret what each axis means. The horizontal axis measures the surface temperature of the star in Kelvin. Stars on the right of the horizontal axis are cooler and redder in colour than the stars on the left, with temperatures of around 3000 Kelvin as opposed to 25,000 Kelvin upwards. The vertical axis on the left measures **luminosity using the Sun as our comparison**. So, a luminosity of one is equal to one Sun. The vertical axis on the right measure's absolute magnitude, or brightness, crucially considering a star's distance. The bottom axis identifies spectral type, or, spectral class of a star, which is another way to describe the colour and temperature. **Plotting Cepheids, RR Lyrae, Mira and Semiregular pulsating variable stars** on the H-R diagram is **not a single plot** like non-pulsating stars. During their evolution through the instability strips they are pulsationally **unstable – expanding and brightening,** then **contracting and become dimmer**. The instability strips for Miras and Cepheids are especially elongated because of these expansions and contractions. Some pulsating variable stars change in temperature by two spectral classes during one cycle from max to min. To show the entire cycle of change for individual variable stars, it is necessary to plot them twice on the H-R diagram – both at max and min absolute magnitude.

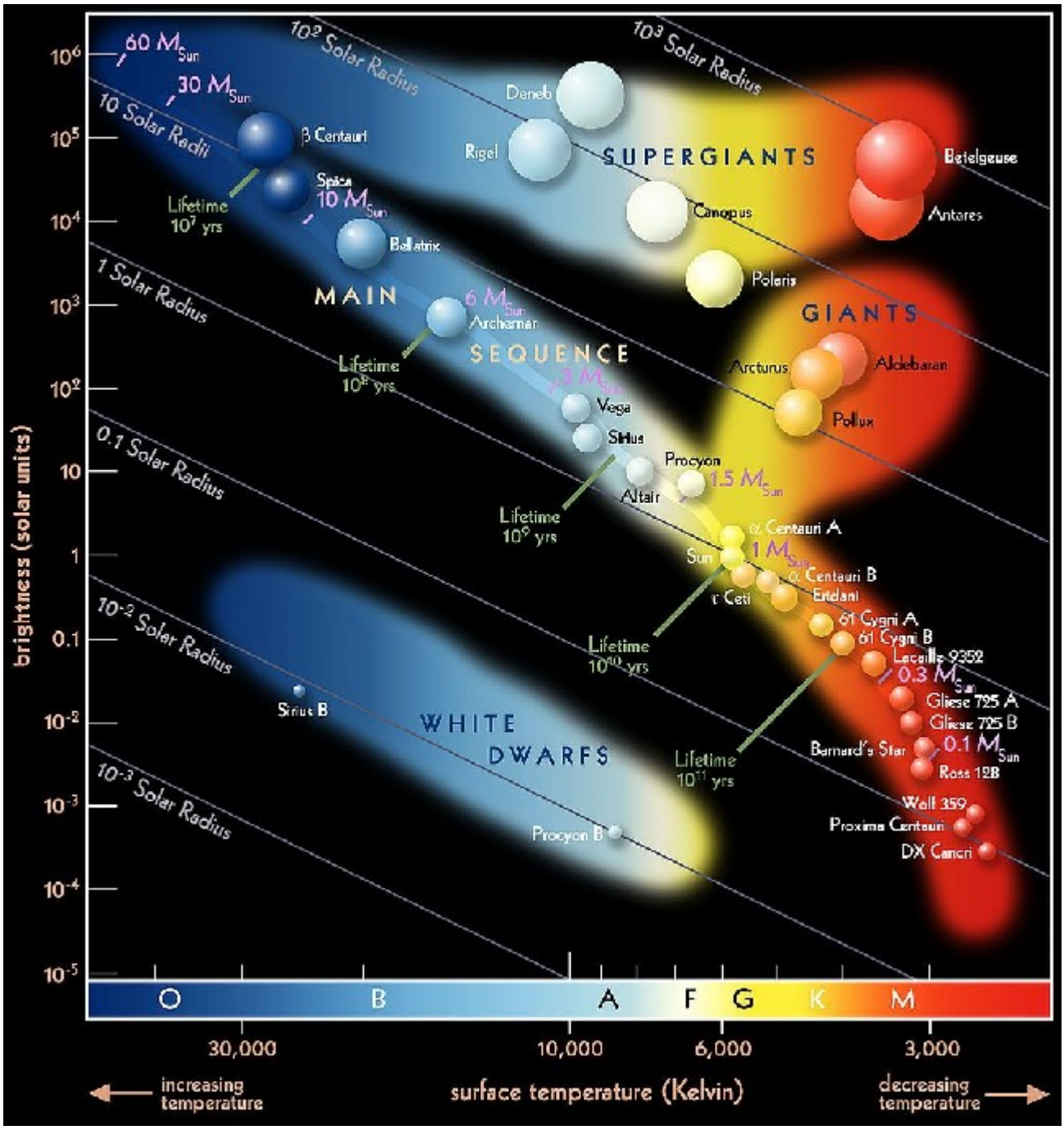

Spectral Analysis of Different Types of Stars

Dwarf Stars: Main Sequence stars of low class V **Luminosity.** Dwarf stars are fainter than giant stars. **Blue** (Types O and B), **Yellow** (mass like sun - Type G), **Orange** (K-type), **Red** (cooler - low mass K to M). **White** (remains of a dead star, electron degenerate, **not massive enough** to be Neutron Star), **Black** a **White** dwarf cooled so no longer emits visible light. Universe not old enought for Black dwarfs. **Brown** dwarf: substellar object not massive enough to fuse hydrogen to helium.

Main Sequence Star Types by Temperature

Our Bright Astronomers Frequently Generate Killer Mnemonics!

Type	Absorption lines	Temperature	Example
O	(H I, He I,) He II, N III , O III, Si IV	> 30000	
B	H I, He I, O II,Si III	> 10000	Orion's Belt
A	**H I**, Mg II,Si II, (Fe II, Ti II, Ca II)	> 7000	Sirius
F	H I, Ca II, Fe I, Ti I, Fe II, Ti II	> 6000	Procyon
G	(H I,) **Ca II**, Fe I, Ti I, etc., CH	> 5300	Sun
K	Ca II, **Ca I**, etc., TiO	> 4000	Arcturus
M	Ca I, TiO, etc.	> 2000	Betelgeuse

Get Star Data From PV Light House Spectral Irradiance Measurement Library

https://www2.pvlighthouse.com.au/resources/optics/spectrum%20library/spectrum%20library.aspx

B Type Star Spectral Irradiance Measurements

$StarTypeB5 := READPRN("B5\ Star\ Spectrum.txt")$ $\lambda_{sB} := StarTypeB5^{\langle 0 \rangle}$

G Type Star Spectral Irradiance Measurement

$StarTypeG := READPRN("G\ Star\ Spectrum3.txt")$ $\lambda_{sG} := StarTypeG^{\langle 0 \rangle}$

Note: For these particular Type B and G stars, the peaks are consistent with Type, but shapes are different.

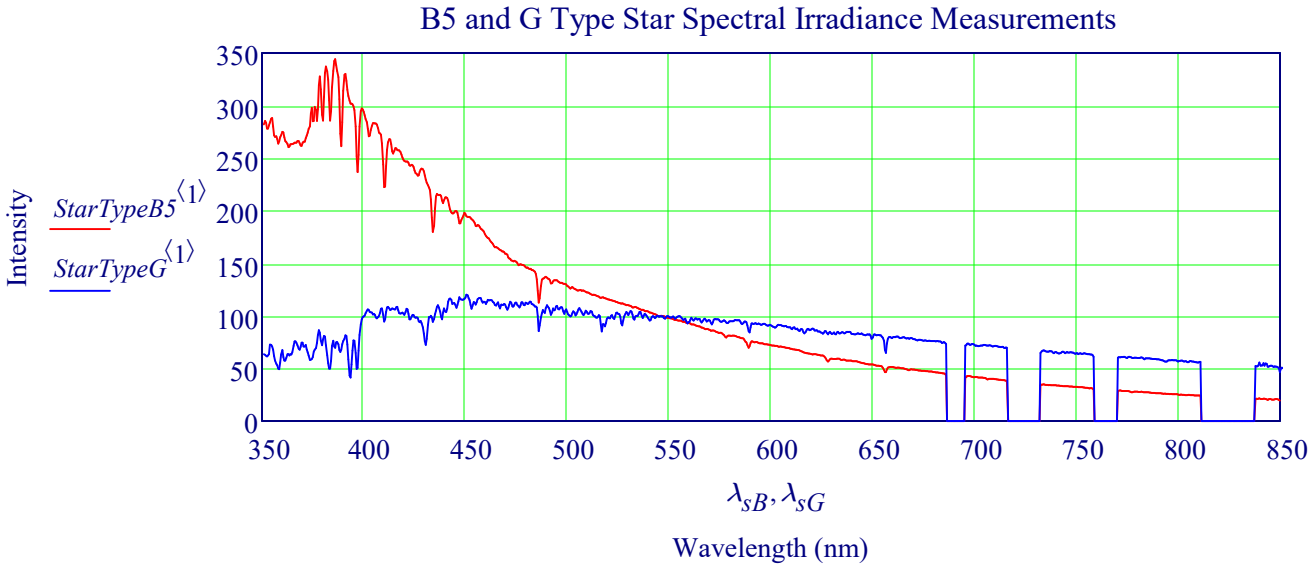

G Type Star (Sun) Spectral Irradiance Data - Sun AM0 & AM1.5

Get Star Spectral Irradiance Data From Spectrum Library

https://www2.pvlighthouse.com.au/resources/optics/spectrum%20library/spectrum%20library.aspx

AM0 and AM1.5 Correspond to the Sunlight at the Top of Atmosphere and at Sea Level, Respectively.

$SolarSpec_0 := READPRN("Solar AM0 Spectrum 280 -2500 2nm.txt")$ $SS_0 := SolarSpec_0$

$SolarSpec_{1.5} := READPRN("Solar AM1-5g Spectrum 280 -2500 2nm.txt")$ $SS_{1.5} := SolarSpec_{1.5}$

Planck's Spectral Radiation Law, B(λ,T)

$h := 6.6260693 \cdot 10^{-34} \cdot joule \cdot sec$ $k_b := 1.3806505 \cdot 10^{-23} \cdot \frac{joule}{K}$ $\lambda_s := SolarSpec_0^{\langle 0 \rangle}$

$$B(\lambda, T) := \frac{2h \cdot c^2}{(nm \cdot \lambda)^5} \cdot \frac{1}{e^{\frac{h \cdot c}{nm \cdot \lambda \cdot k_b \cdot T}} - 1}$$

$T_{sun} := 5777K$

Normalize Units B(λ,T): $Units := 2 \cdot B(500, T_{sun})^{-1}$ $B_N(\lambda) := B(\lambda, T_{sun}) \cdot Units$

Find Peak Wavelength for the AM0 Sun from its Blackbody Spectrum

$max(SolarSpec_0^{\langle 1 \rangle}) = 2.075$ $match(max(SolarSpec_0^{\langle 1 \rangle}), SolarSpec_0^{\langle 1 \rangle}) = (91)$

$(SolarSpec_0^{\langle 0 \rangle})_{91} = 462$ $\lambda_{peak} := 462$ $B_N(462) = 1.967$

The Sun's peak wavelength is between 483-504 nm (Green)

Wien's Displacement Law: Peak Wavelength Law

$$\lambda_{max}(T) := \frac{0.2898 cm \cdot K}{T}$$ $\lambda_{max}(T_{sun}) = 501.644 \cdot nm$

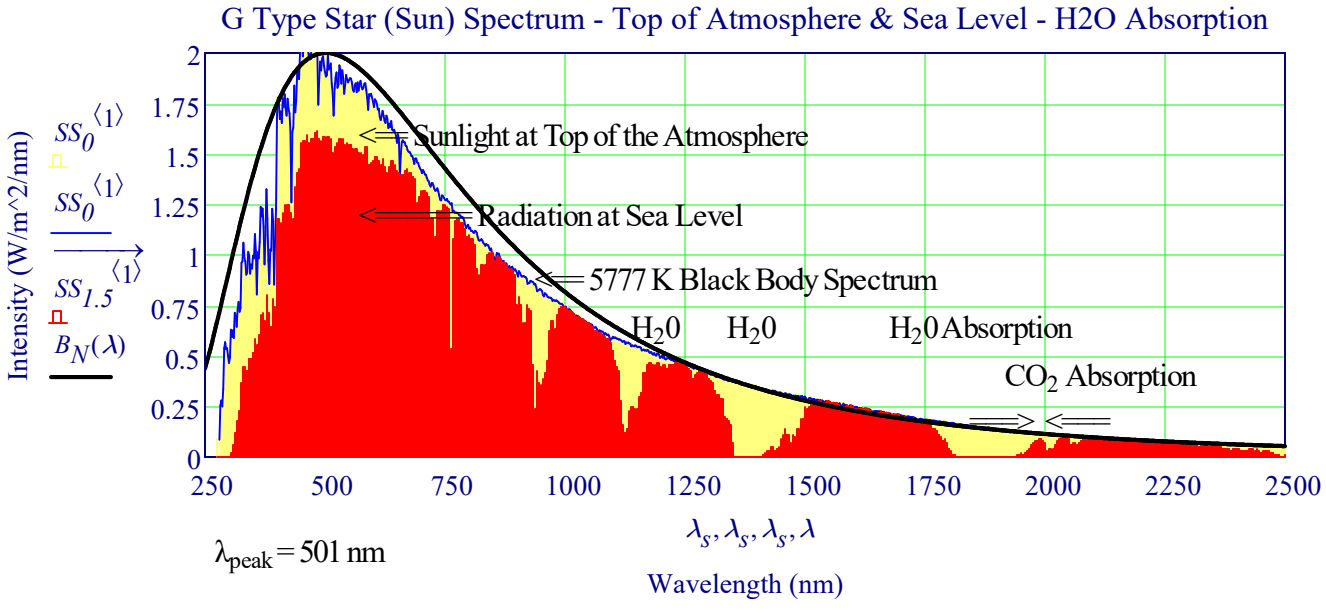

IXB.The Scale of the Universe

The Hubble Length, $D_H =$ equals c/H_0, and the Hubble time, t_H equals $1/H_0$, gives the approximate spatial and temporal scales of the universe.

H_0 is a scale parameter and is independent of the "shape parameters" (expressed as density parameters) Ω_m, Ω_Λ, Ω_k w, etc., which govern the global geometry and dynamics of the universe.

Distances to galaxies, quasars, etc., scale linearly with H_0, $D \approx c\,z\,/H_0$. They are necessary in order to convert observable quantities for example, fluxes, angular sizes into physical ones (luminosities, linear sizes, energies, masses, etc.)

Distance Ladder: Methods

Methods yielding absolute distances:

Parallax (trigonometric. secular. and statistical)
The moving cluster method - has some assumptions
Baade-Wesselink method for pulsating stars
Expanding photosphere method for Type ll SNe Mfidel
Sunyaev-Zeldovich effect <== Model dependent!d
Gravitational lens time delays <== Model dependent!

Telescope Resolution:
Hubble 0.05 arcseconds
Very-long-baseline interferometry (VLBI) 25 μarcsecs

Secondary distance indicators:

"**standard candles**, **requiring a calibration** from an absolute method applied to local objects -

The Distance Ladder:

Pulsating variables: Cepheids. RR Lyrae.
Main sequence titling to star clusters, Brightest red giants
Planetary nebula luminosity function
Globular cluster luminosity function
Surface brightness fluctuations
Tully-Fisher, D_a - σ, FP scaling relations for galaxies
Type 1a Supernovae

kpc
Mpc
Gpc

Diameter of our Local Group of galaxies is ≈3 megaparsecs, and it contains at least 80 galaxies, most of which are dwarf galaxies

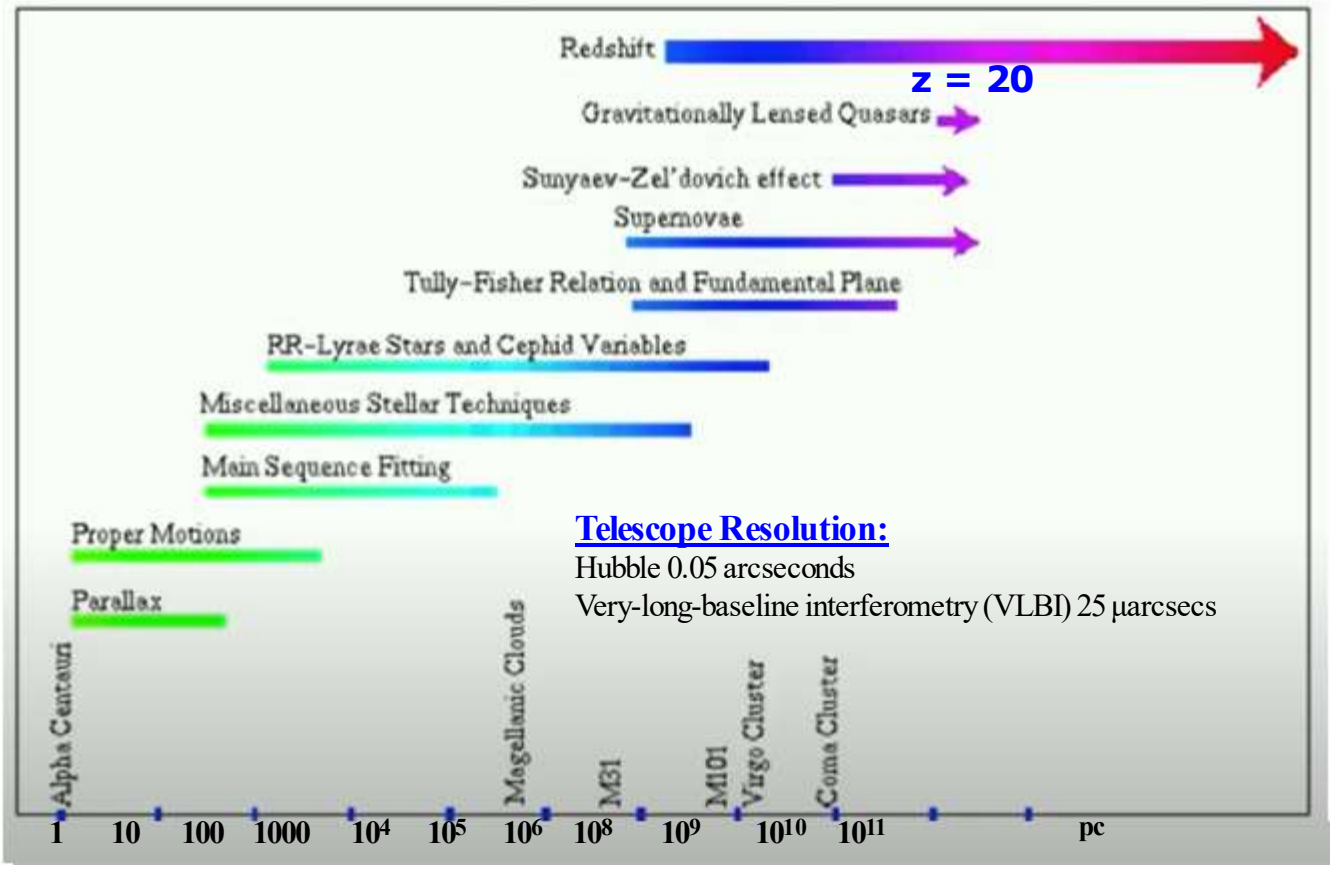

Telescope Resolution:
Hubble 0.05 arcseconds
Very-long-baseline interferometry (VLBI) 25 μarcsecs

Main Sequence Fitting for Star Clusters

Luminosity (distance dependent) vs. temperature or color (distance independent)

- Can measure distance to star clusters (open or globular) by fitting their main sequence with clusters with known distances from Gaia.
- The apparent magnitude difference gives the ratio of distances, as long as we know the reddening(extinction)!
- For globular clusters we use parallaxes to nearby subdwarfs (metal-poor main sequence stars)

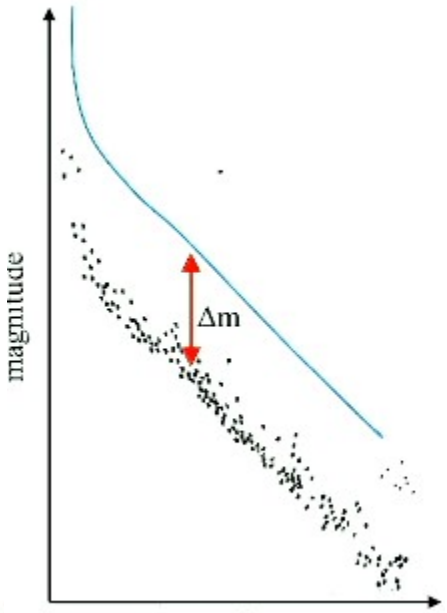

Pulsating Variables

- Stars in the instability strip in the HR diagram.
- All obey empirical period - luminosity distance independent vs.dependent) relations which can be calibrated to yield distances.
- Different types (in different branches of the HRD, different stellar populations) have different relation.
- Cephelds are high-mass, luminous, upper MS, Pop. I stars.
- RR Lyrae are low-mass, rnetal-poor (Pop. II), HB stars, often found in globulars.
- Long-period variables (e.g., Miras) pulse in a fashion that is less "well understood."

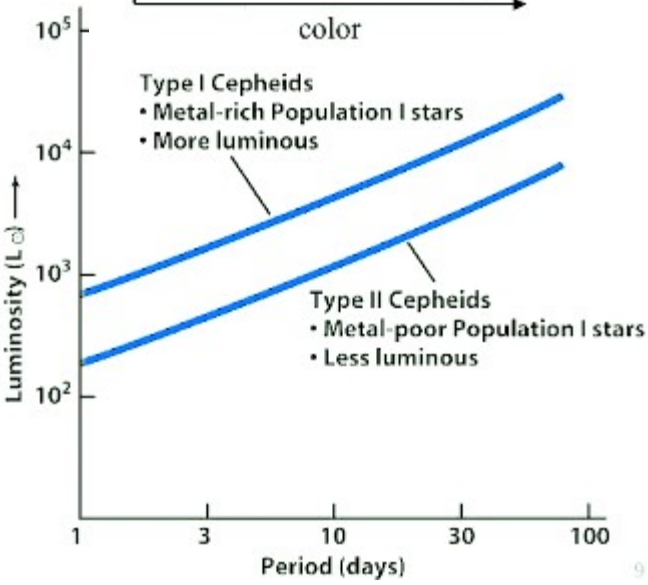

Cepheids

- Luminous (M ≈ -4 to -7 mag), pulsating variables high mass stars on the instability strip in the H-R diagram. Henrietta Leavitt (1912) found in a period-luminosity relation for Cepheids in the SMC: brighter ones have longer periods

- **Advantages**:

Bright and easily seen in galaxis(out to ≈25 Mpc with the HST, stellar plusation is well understood.

- **Disadvantages**:

Relatively rare, period may depend en rnetallicity or color, need runlet epoch observations found near star forming regions, so extinction corrections are necessary.

- Redder bands have smaller scatter, but also shallower slope.
- Calibrated using parallaxes on the II-R diagram

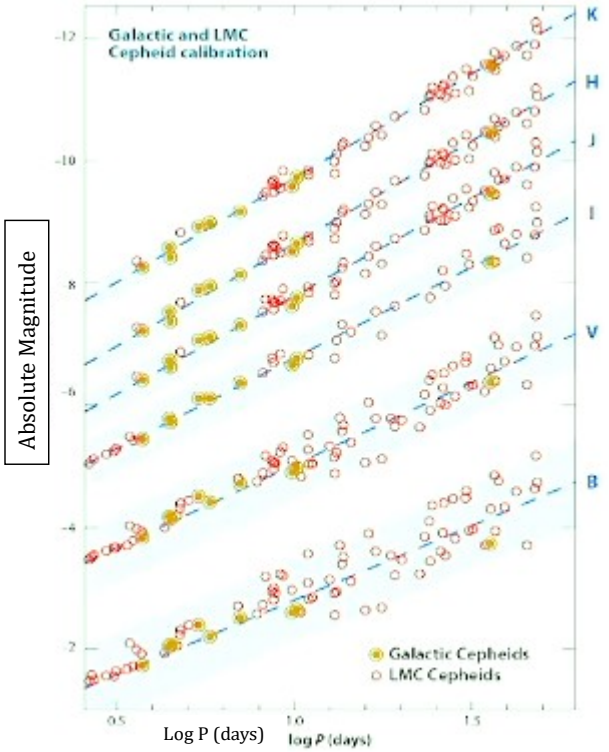

The Baade-Wesselink Method

$$L = \sigma R^2 T^4$$

Luminosity from the Stephan-Boltzmann formula
Consider a pulsating star at a minimum, with
a measured temperature T_1 and observed flux f_1
with radius R_1 , then:

$$f_1 = \frac{4\pi R_1^2 \sigma T_1^4}{4\pi D^2}$$

At a maximum, with a measured temperature T_2 and observed flux f2 with radius R2

$$f_2 = \frac{4\pi R_2^2 \sigma T_2^4}{4\pi D^2}$$

Note: T_1, T_2, f_1, f_2, are directly observable! Just need the radius. So, from spectroscopic observations we can get the photospheric velocity v(t), from this we can determine the change in the radius are

$$R_2 = R_1 + \Delta R = R_1 + \int_{t_1}^{t_2} v(t)\, dt$$

3 equations, 3 unknowns, solve for R1, R2, and D
Difficulties: the effects of the stellar atmospheres
(not a perfect black body), and deriving the true radial velocity from what we observed.

Galaxy Scaling Relations

Once a set of distances to galaxies of some type is obtained, one finds correlations between distance-dependent quantities that is, luminosity, radius and distance-independent ones, for example, rocational speeds for discs, or velocity dispersions from ellipticals and bulges, surface brightness, etc.
These are called **distance indicator relations**. Examples:

- **Tully-Fisher relation** for spirals (luminosity versus rotation speed).
- **Fundamental Plane** relationships from ellipticals radius versus a combination of velocity dispersion and surface brightness.
- These relations must be calibrated locally using other distance indicators, Cepheids or surface brightness fluctuations; then they can be extended into the general Hubble flow regime.
- Their origins-and thus there universality -are not yet well understood. There may be some systematic variations.

The basic idea:

- Need a correlation between a distance-independent quantity "X", for example, temperature or color for stars in the H-R diagram, or the period for the Cepheids, and a distance-dependent one.
Why for example, stellar absolute magnitude, M.

- Two sets of objects at different distances will have a systemic shift in the apparent versions of why that is,
stellar apparent magnitude, am from which we can deduce the relative distance.

- This works for stars, main sequence fittings,.-Luminosity relations,
we can we find such relationships for galaxies?

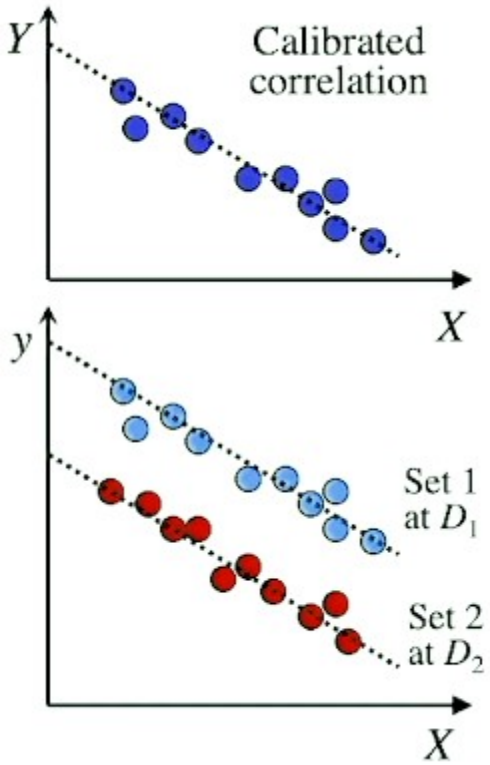

The Tulley-Fisher Relationship - Galaxy Distance vs Kinematic Rotational Speed

A new method of determining distances to galaxies, Tulley, Fisher, Astron and AstroPhys, Vol.54, p.661-673, 1977

Tulley -Fisher is a correlation that holds for galaxies with disks (spiral galaxies) stabilized by rotation, between the **intrinsic luminosity L of the galaxy** in optical or near-infrared bands and the **rate of rotation W**.

- A well-defined **Luminosity versus Rotational Speed** often measured as H1 21 cm line with **relation for spirals**:

$$L \approx v_{rot}^{\gamma}, \quad \gamma \approx 4 \text{ varies with wavelength.}$$

Or: $M = b \log(W) + c$, where:

- **M** is the absolute magnitude
- **W** is the **Doppler broadened line** with, typically measured using the HI 21 cm line, corrected for inclination,

$$W_{true} = W_{obs}/\sin(i)$$

- Both the **slope b** in the **zero-point c** can be measured from the set of nearby spiral galaxies with well-known distances.
- The slope b can also be measured from any set of galaxies with roughly the same distance-for example, galaxies in the cluster-even if that distance is not known.
- *Scatter* is approximately 10 to 20% at best, which limits the accuracy.
- Problems include dust extinction, so working in the redder bands is better.

XXIV. The Calibration of Tully-Fisher Relations and The Value of The Hubble Constant

THE ASTROPHYSICAL JOURNAL, 529:698È722, 2000 February 1

Photometric and Kinematical Data for Tulley Fisher Calibrators for Different Color Bands of 21 cm H I Line

B_T^c (mag) V_T^c (mag) R_T^c (mag) I_T^c (mag) $H_{-0.5}^c$ (mag) $\log W_{20}^c$ (km s^{-1}) $\log W_{50}^c$ (km s^{-1}) i_I^a (deg) $\bar{i}^a$ (deg)

$M := READPRN("Tulley Fisher Data A-Org4.txt")$ $W_{20} := M^{\langle 10 \rangle}$ $W := W_{20}$ $cols(M) = 18$

Tulley Fisher: -Mag vs. Log(W) - Blue

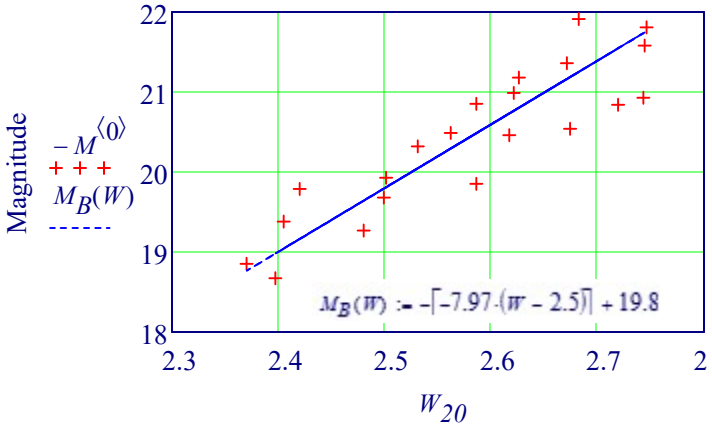

Tulley Fisher: -Mag vs Log(W) - Violet

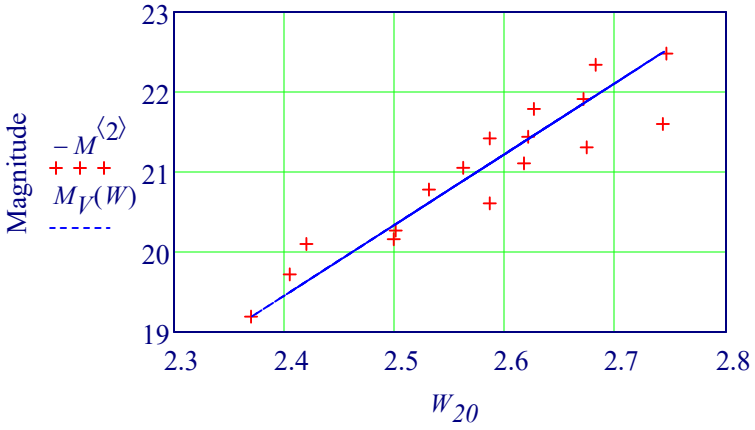

Tulley Fisher: -Mag vs Log(W) - Red

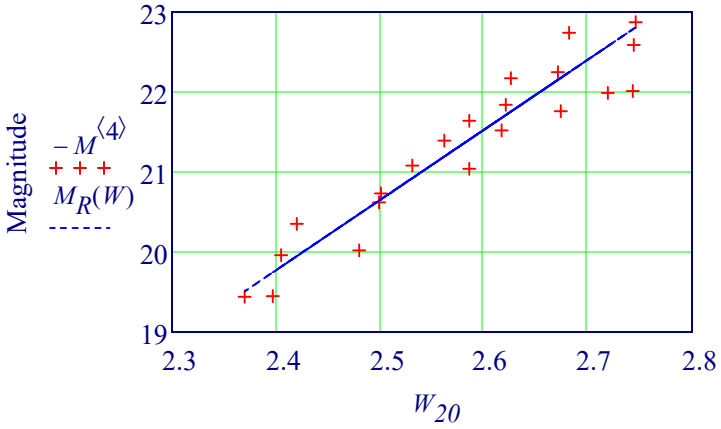

Tulley Fisher: -Mag vs Log(W) - InfraRed

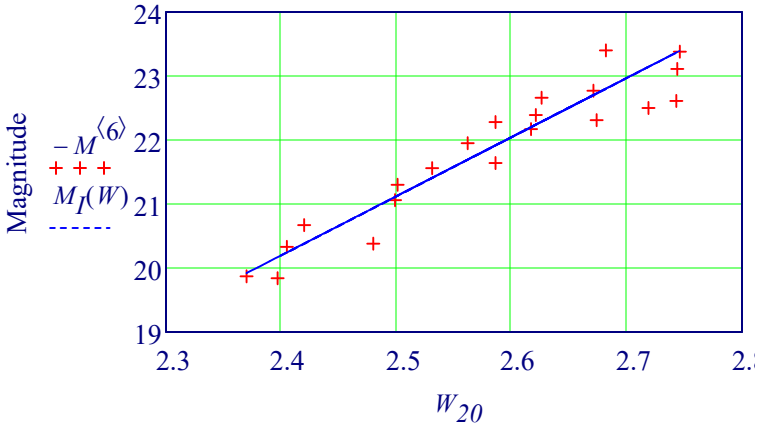

The Tully-Fisher Relation and Its Historical Importance

The Tully-Fisher empirical correlation between the **luminosity and rotational velocity of spiral galaxies** serves as a **distance indicator** to measure distances **independent of redshift**. **Possible Mechanism:** Rotational Velocity related to Mass, which is related to Luminosity. The Tully-Fisher relation has played an important role in Hubble constant measurements since its inception. In 1977 Brent Tully and Richard Fisher published their paper, They used only inclined spiral galaxies and proposed the usage of the linear relation between H I (21-cm neutral hydrogen (H I) emission line) profile and absolute magnitude as a distance indicator. The publication of the Tully-Fisher relation and the proposal to use it as a distance indicator was significant in many different ways. Firstly, it provided a robust new tool for measuring distance at redshifts that other methods such as Cepheid variable stars cannot. Secondly, Tully and Fisher measured the Hubble constant H_0 to be 80 km s^{-1}Mpc^{-1} from the Virgo cluster and Ursa Major. This value was the first to deviate from the two mainstream values. It was also used to probe the distribution and properties of dark matter in galaxies.

I-band Tully-Fisher

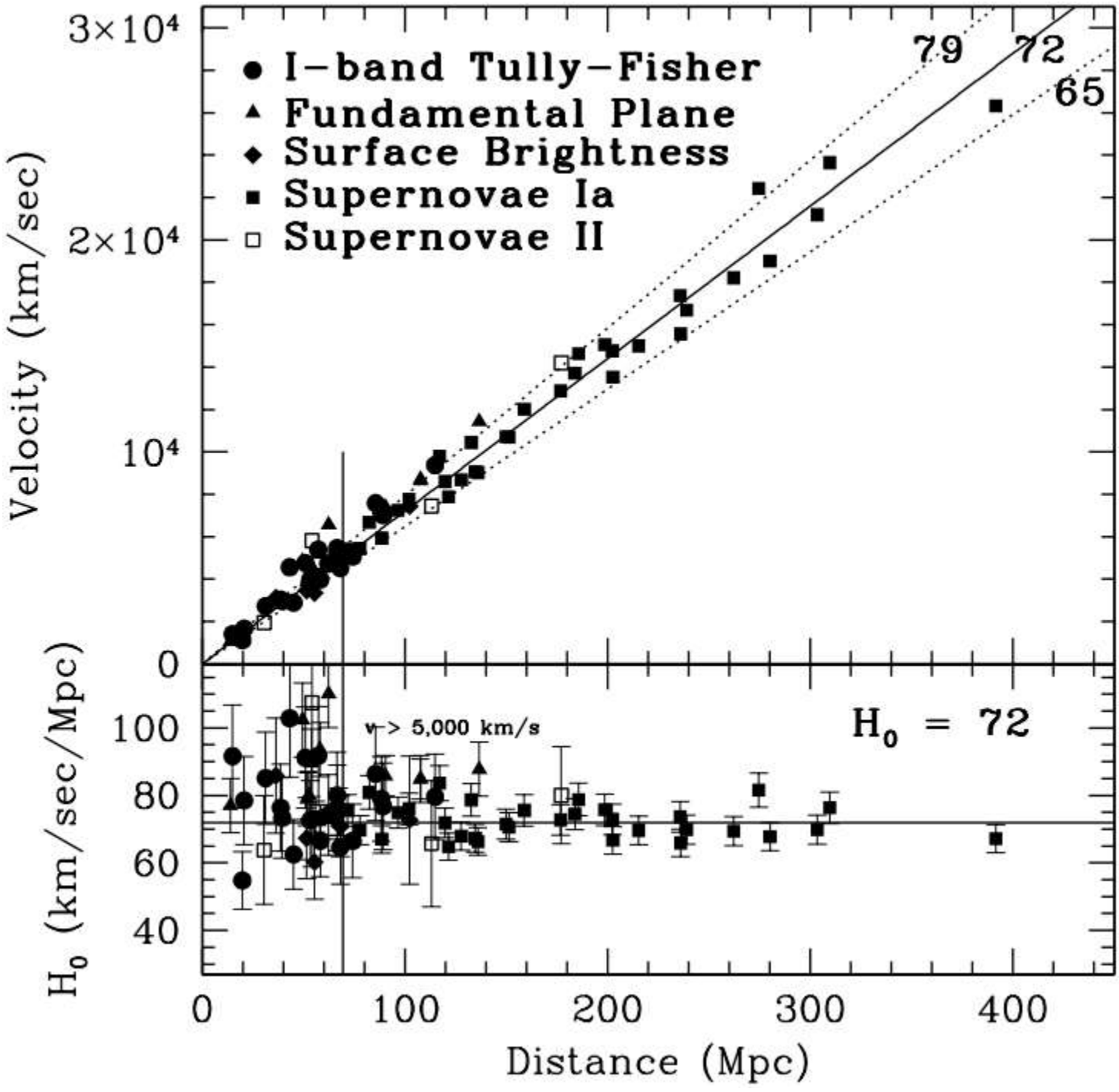

Stellar Mass, Luminosity, and Lifespan

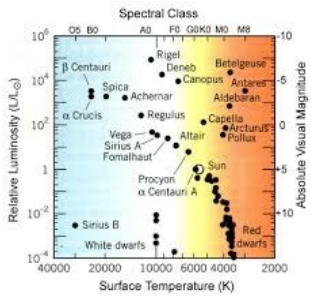

The H-R diagram is a plot of the luminosity up and down, versus temperature left and right with increasing temperature going to right to the left, and cooler stars on the right, hotter stars on the left, dimmer stars at the bottom and, and brighter stars (more luminous) at the top. Importnat: The main sequence is composes up to 80% of all the stars. Giants, supergiants, and white dwarfs are a minority.

Data Source: Accurate masses and radii of normal stars: Modern results and applications, G. Torres

"We have identified 95 detached binary systems containing 190 stars (94 eclipsing systems, and α Centauri) that satisfy our criterion that the mass and radius of both stars be known to an accuracy of ± 3% or better."

Binary Star Data Table:	P(d)	Mass	±	Radius	±	Teff	±	log g	±	log L	±	MV	±
	Vmax	(M⊙)	(M⊙)	(R⊙)	(R⊙)	(K)	(K)	(cgs)	(cgs)	(L⊙)	(L⊙)	(mag)	(mag)

Vmax is the Apparent Visual Magnitude

$L_{\odot} := 3.846 \cdot 10^{26} W$

Read in Data from File: $ObsParam := READPRN("Observed Parameters - Final.txt")$

$Mass := ObsParam^{\langle 1 \rangle}$ $Radius := ObsParam^{\langle 3 \rangle}$ $Teff := ObsParam^{\langle 5 \rangle}$ $logL := ObsParam^{\langle 9 \rangle}$ $M_v := ObsParam^{\langle 11 \rangle}$

Dependence of stellar radius on mass for **Main-Sequence** stars. Actual measurements show that the radius increases nearly in proportion to the mass over much of the range (as indicated by the straight line drawn through the data points). Most stars are members of binary systems—where two stars orbit one another, bound together by gravity. Here we describe—in an idealized case where the relevant orbital parameters are known—how we can use the observed orbital data, together with our knowledge of basic physics, to determine the masses of the component stars

Plot Stellar Data for Binary Stars from Above Torres Paper

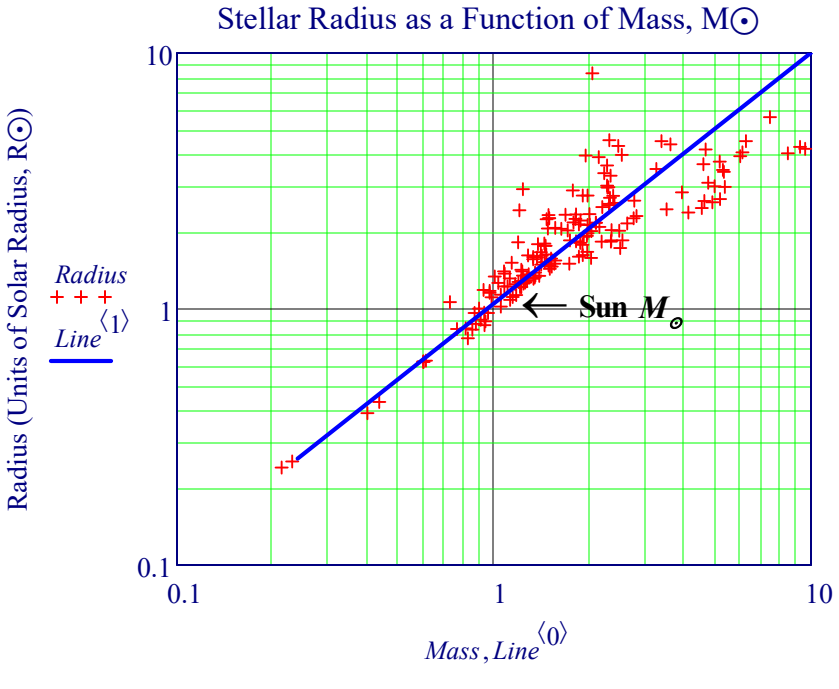

Binary Star Mass Relationship:

Given Mass M, Period P, and semimajor axis A, then Kepler's Law can be used to deduce relationships about binary star masses:

$$M_1 + M_2 \approx \frac{a^3}{p^2}$$

Example Sirius Binaries A & B

- orbital period = 50 years
- seimi-major axis = 20 AU
- $M_a + M_b = 3.2\ M_\odot$
- further study reveals: $M_a = 2.1\ M_\odot$ and $M_b = 1.1\ M_\odot$

For Main Sequence Stars,

the Stellar plot shows that relative to the Sun, with a mass of 1 $M_\odot$ and a size of 1 $R_\odot$, the mass and radius of Main Sequence Stars is only 0.1X to 10X relative to the sun.

But for Luminosity:

$$L = 4\pi \cdot R^2 \cdot \sigma \cdot T^4$$

$$\frac{L}{L_\odot} \approx \left(\frac{M}{M_\odot}\right)^4 \qquad L_{sun}(M_s) := \log\left(M_s^{3.8}\right)$$

Stellar Masses of Main Sequence

The following **Luminosity vs. Mass** plot shows a huge variation of 7 orders of magnitude of Luminiosity versus about 1.5 orders of magnitude of change for the Mass. This also suggests there must be a large variation with temperature verus mass. Mass is the Main Determinate of where a star will lie on the Main Sequence.

Plot Binary Stellar L vs Mass Data from Above Torres Paper

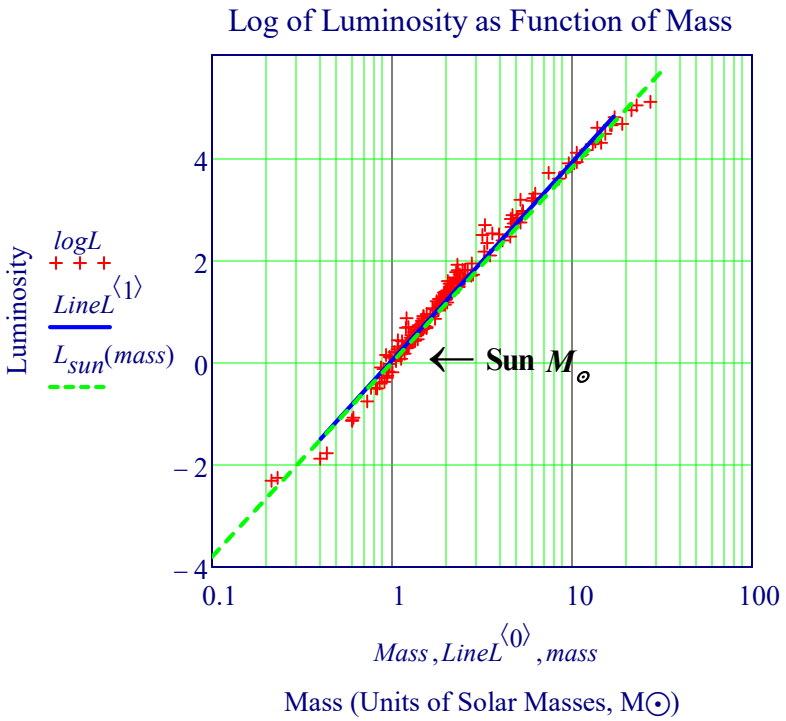

The Mass-Luminosity Relation from End to End

The Components of Close Binary Stars
ASP Conference Series, Vol. 318, 2004, Todd Henry

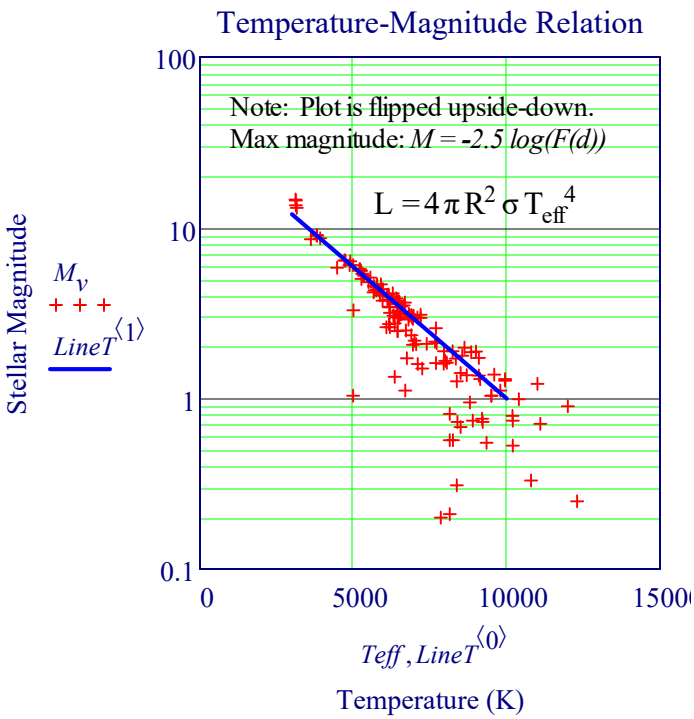

Plot Binary Stellar Magnitude vs. Mass from Above Torres Paper

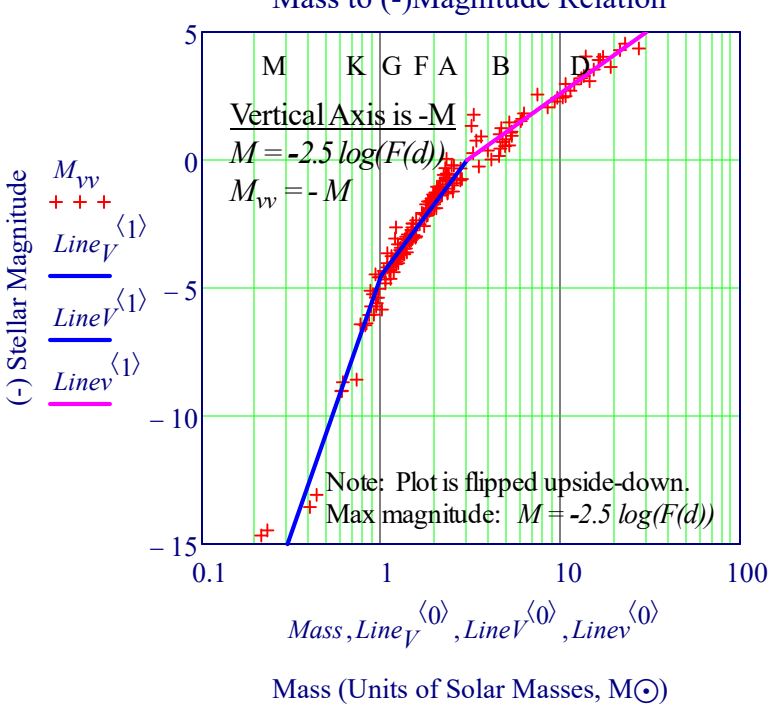

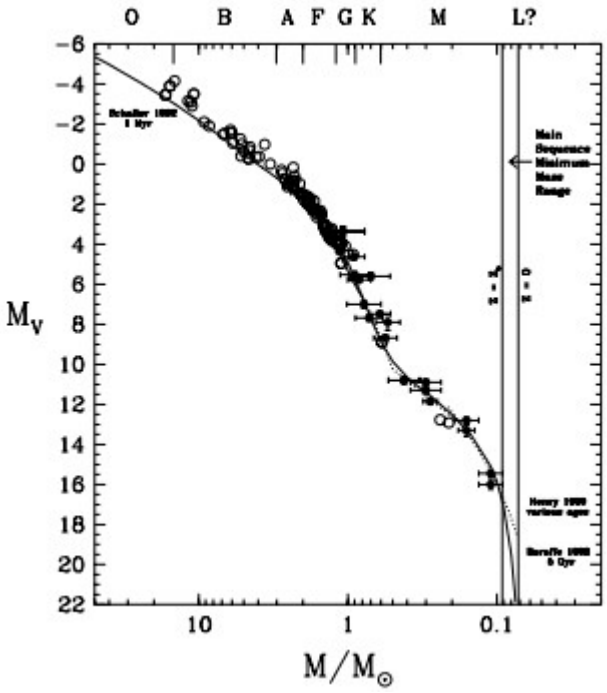

Stellar Lifetimes

Luminosity increases as Mass^3 for massive main-sequence stars and Mass^4 for more common main-sequence stars
Total fuel to burn in star is the mass. Therefore:

A 5 solar mass, $M_\odot$, star has only five times more hydrogen fuel than the Sun,

but (the star's luminosity)/(the Sun's luminosity) = $(5/1)^4 = 625$!

Its lifetime = $1/(5/1)^{(4-1)} \times 10^{10}$ years = $(1/125) \times 10^{10}$ years = 8.0×10^7 years.

More massive stars burn up fastest and have shortest lives since the luminosity increases as the cube of the mass for the most massive stars.

The Luminosity Density

Ay21 Lecture 7: The Contents of the Universe

https://sites.astro.caltech.edu/~george/ay21/Ay21_Lec07.pdf

The Contents of the Universe Evolve

The relative abundances of different components change in time, due to their different EOS behavior:

Integrate galaxy luminosity function (obtained from large redshift surveys)
to obtain the mean luminosity density at $z \approx 0$

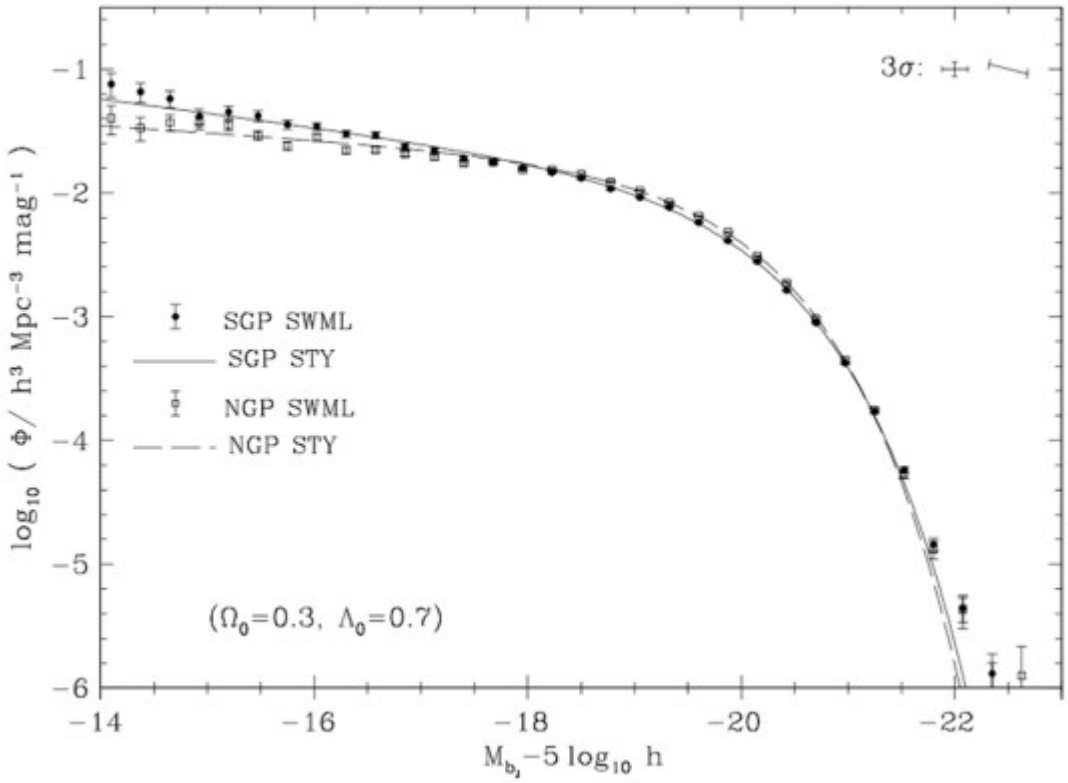

SDSS, *r* band: $\rho_L = (1.8 \pm 0.2) \times 10^8 \, h_{70} \, L_\odot/\mathrm{Mpc}^3$

2dFGRS, *b* band: $\rho_L = (1.4 \pm 0.2) \times 10^8 \, h_{70} \, L_\odot/\mathrm{Mpc}^3$

The Local Mass Density of the Luminous Matter in Galaxies: $\Omega_{0,lum}$

$$\rho_{lum} = \rho_L \times \langle M/L \rangle \times \langle 1 + f_{gas} \rangle \approx (7 \pm 2) \times 10^8 \, h_{70} \, M_\odot/\mathrm{Mpc}^3$$

$$\rho_{lum} \approx (4.7 \pm 1.3) \times 10^{-32} \, h_{70} \ \mathrm{g\ cm^{-3}}$$

Recall that $\rho_{0,crit} = 3H_0^2/(8\pi G) = 0.921 \times 10^{-29} \, h_{70}^2 \ \mathrm{g\ cm^{-3}}$

$\Omega_{0,lum}$ Luminous Baryon Density $\approx$ **(0.0051 0.0015) h_{70}^{-1}**

All of the visible matter amounts to only half a percent
of the total mass/energy content of the universe!

(Interestingly, this may be about the same as the contribution
from the massive cosmological neutrinos…)

Luminosity Function of Galaxies -The Schechter Luminosity Function

Definition of the luminosity function. The luminosity function specifies the way in which the members of a class of objects are distributed with respect to their luminosity. More precisely, the luminosity function is the number density of objects (here galaxies) of a specific luminosity. ϕ(M) dM is defined as the number density of galaxies with absolute magnitude in the interval |M, M + dM|. **The total density of galaxies is then**

$$\nu = \int_{-\infty}^{\infty} dM\ \Phi(M)$$

Accordingly, **ϕ(L) dL is defined as the number density of galaxies with a luminosity between L and L+ dL** . It should be noted here explicitly that both definitions of the luminosity function are denoted by the same symbol, although they represent different mathematical functions, i.e., they describe different functional relations. It is therefore important (and in most cases not difficult) to deduce from the context which of these two functions is being referred to.

Problems in determining the luminosity function of Galaxies

At first sight, the task of determining the luminosity function of galaxies does not seem very difficult. The history of this topic shows, however, that we encounter a number of problems in practice. As a first step, the determination of galaxy luminosities is required, for which, besides measuring the flux, distance estimates are also necessary. For very distant galaxies redshift is a sufficiently reliable measure of distance, whereas for nearby galaxies the methods discussed earlier have to be applied. Another problem occurs for nearby galaxies, namely the large-scale structure of the galaxy distribution. To obtain a representative sample of galaxies, a sufficiently large volume has to be surveyed because the galaxy distribution is heavily structured on scales of 100^{h-1} Mpc and more. On the other hand, galaxies of particularly low luminosity can only be observed locally, so the determination of $\phi(L)$ for small L always needs to refer to local galaxies. Finally, one has to deal with the so-called *Malmquist bias*; in a flux- limited sample luminous galaxies will always be overrep- resented because they are visible at larger distances (and therefore are selected from a larger volume). A correction for this effect is always necessary, and was applied to the Figure below.

The Schechter Luminosity Function

An Analytic Expression For The Luminosity Function For Galaxies. Paul Schechter

The global galaxy distribution can be roughly approximated by the Schechter luminosity function →

$$\Phi(L) = \left(\frac{\Phi^*}{L^*}\right)\left(\frac{L}{L^*}\right)^{\alpha} \exp\left(-L/L^*\right)$$

where L^* is a characteristic luminosity above which the distribution decreases exponentially, α is the slope of the luminosity function for small L, and ϕ^*_s specifies the normalization of the distribution. A schematic plot of this function, as well as a fit to early data, is shown in the Figure below. Expressed in magnitudes, this function appears much more complicated. Considering that an interval dL in luminosity corresponds to an interval dM in absolute magnitude, with $dL/L = -0.4 \ln 10\ M$, and using $\phi(L)\ dL = \phi(M)\ dM$, i.e., the number of sources in these intervals are of course the same, we obtain

$h := 0.74$

$\phi_s := 1.6 \cdot 10^{-2} h^3 \cdot Mpc^{-3}$ $\quad \phi_{ss} := 1000$

$M_{sB} := -19.7 + 5\log(h)$ $\quad \alpha := -1.07$ $\quad \phi(M) := 0.921\,\phi_s \cdot 10^{0.4\cdot(\alpha+1)\left(M_{sB}-M\right)} \cdot e^{\left[-10^{0.4\left(M_{sB}-M\right)}\right]}$

$M_{sB} = -20.354$

$L_{sB} := 1.2 \cdot 10^{10} \cdot h^{-2} \cdot L_s$

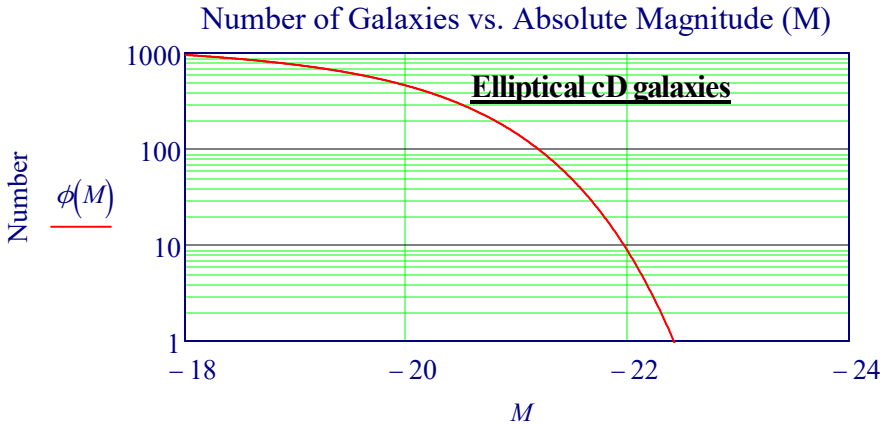

Elliptical cD Type Galaxies

These are extremely luminous (up to MB -25) and large (up to R < 1 Mpc) galaxies that are only found near the centers of dense clusters of galaxies. Their surface brightness is very high close to the center, they have an extended diffuse envelope, and they have a very high M/L ratio. It is not clear whether the extended envelope actually 'belongs' to the galaxy or is part of the galaxy cluster in which the cD is embedded, since such clusters are now known to have a population of stars located outside of the cluster galaxies.

X. Measurement of Cosmic Distances - Trigometric Parallax

The most important fundamental distance measurements come from trigonometric parallax. As the Earth orbits the Sun, the position of nearby stars will appear to shift slightly against the more distant background. When a star is observed from two points separated by a distance ***b***, the star's apparent position will shift by an angle ***θ***. If the baseline of observation is perpendicular to the line of sight to the star, the parallax distance will be

$lightyear := 9.46 \cdot 10^{12} km$ $pc := 3.261 lightyear$ $arcsec := \frac{°}{3600}$

An astronomical unit (AU, or au), a unit of length effectively equal to the average, or mean, distance between the Earth and the sun.

$b := 2AU$ Earth's orbit (b = 2 AU) as a baseline, b

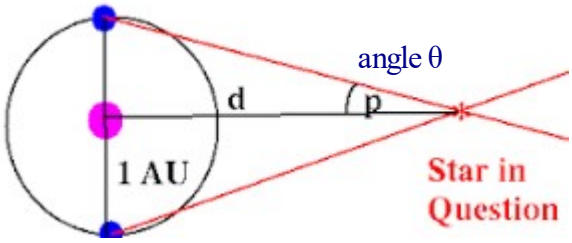

Parallax Distance, d_π

$$d_\pi(\theta, b) := 3.261 lightyear \cdot \left(\frac{b}{1AU}\right) \cdot \left(\frac{\theta \cdot °}{1 arcsec}\right)^{-1}$$

Measuring the distances to stars (galaxies are far too distant to be located by parallax) using the Earth's orbit ($b = 2\,AU$) as a baseline is a standard technique. Since the size of the Earth's orbit is known with great accuracy from radar measurements, the accuracy with which the parallax distance can be determined is limited by the accuracy with which ***θ*** can be measured. The Hipparcos satellite, launched by the European Space Agency in 1989, found the parallax distance for ~ 10^5 stars, with an accuracy of ~ 1 milliarcsecond.

Two decades after the end of the Hipparchos mission, another breakthrough arrived. In 2013, ESA launched a telescope called Gaia that charts the positions, parallaxes, and proper motions of more than one billion stars. That number represents only about 1% of the actual number of stars in the galaxy, but that's enough for astronomers to extrapolate the observations to understand how the Milky Way behaves as a whole. Using Gaia data, they could, for the first time, create a dynamic movie of the galaxy's life over billions of years, uncovering past events but also projecting what will happen in the future.
"Hipparcos had a detector with only one pixel and could only observe one star at a time," said de Bruijne, who is ESA's deputy project scientist for the Gaia mission. "Gaia, on the other hand, has nearly a billion pixels in its detectors and can observe thousands of stars at the same time."
Gaia's mirrors are 20 times larger and therefore it collects light much more efficiently than its predecessor, seeing much deeper into the galaxy.

In terms of absolute maximum distances, **Very Long Baseline Interferometry (VLBI)** can push these limits even further, potentially up to around **30,000 light years** with current technologies if the parallax measurement precision can be maintained at about (10 thousands of an arc second). Uses radio wavelengths 90 cm to 3 mm.
See Section XIX B. Our Galactic Home - The Milky Way

The **Event Horizon Telescope (EHT)** is a large telescope array consisting of a global network of radio telescopes. The EHT project combines data from several very-long-baseline interferometry (VLBI) stations around Earth, which form a combined array with an angular resolution sufficient to observe objects the size of a supermassive black hole's event horizon. The project's observational targets include the two black holes with the largest angular diameter as observed from Earth: the black hole at the center of the supergiant elliptical galaxy Messier 87 (M87*, pronounced "M87-Star").

Parallax Distance: $d_\pi\left(10 \cdot 10^{-3} arcsec, b\right) = 37368 \cdot lightyear$

An Improved Distance to NGC 4258, The Astrophysical Journal Letters, 2019 December 1
This paper claims a distance estimate of 7.6 Mpc or **24 Million Lightyears** for NGC 4258.

Measurement of Cosmic Distances - The Standard Candle

MEASURING COSMOLOGICAL PARAMETERS

The current proper distance to a galaxy, $dp(t_0)$, is not a measurable property

Since cosmology is ultimately based on observations, if we want to find the distance to a galaxy, we need some way of computing a distance **from that galaxy's observed properties**. Let's focus on the properties that we can measure for objects at cosmological distances. We can measure the flux of light, *f*, from the object, in units of watts per square meter. The complete flux, **integrated over all wavelengths** of light, is called the **bolometric flux**. (A bolometer is an extremely sensitive thermometer capable of detecting electromagnetic radiation over a wide range of wavelengths.)

Cosmologists would like to know the scale factor *a(t)* for the universe. For a model universe whose contents are known with precision, the scale factor can be computed from the Friedmann equation. Finding *a(t)* for the real universe, however, is much more difficult. **The scale factor is not directly observable**; it can **only be deduced** indirectly from the **imperfect and incomplete observations** that we make of the universe around us.

The Standard Candle

One way of using measured properties to assign a distance is the standard candle method. A standard candle is an object whose luminosity *L* is known. For instance, if some class of astronomical object had luminosities which were the same throughout all of space-time, they would act as excellent standard candles – if their unique luminosity *L* were known. For instance, if some class of astronomical object had luminosities which were the same throughout all of space-time, they would act as excellent standard candles – if their unique luminosity *L* were known. Nowadays, the bolometric apparent magnitude of a light source is defined in terms of the source's bolometric flux, *m*,

$$m \equiv -2.5 \log_{10}(f/f_x) \qquad \text{Reference Flux: } f_x := 2.53 \cdot 10^{-8} \cdot \frac{W}{m^2}$$

where the reference flux f_x is set at the value $f_x = 2.53 \times 10^{-8}\ watt\ m^{-2}$. Thanks to the **negative sign** in the definition, a small value of m corresponds to a large flux *f*. For instance, the flux of sunlight at the Earth's location is f = 1367 watts m^{-2} ; the Sun thus has a bolometric apparent magnitude of m = −26.8.
The bolometric absolute magnitude of a light source is defined as the apparent magnitude that it would have if it were at a **luminosity distance** of $d_L = 10$ pc. Thus, a light source with luminosity *L* has a bolometric absolute magnitude, *M*. Luminosity of the sun: $L_{M\odot}$

Reference Luminosity: $L_{\odot} := 3.846 \cdot 10^{26} W$ $\qquad L_x := 78.7 \cdot L_{\odot}$ $\qquad M \equiv -2.5 \log_{10}(L/L_x)$

Since that is the luminosity of an object which produces a flux $f_x = 2.53 \times 10^{-8}\ watt\ m^{-2}$ when viewed from a distance of 10 parsecs. The bolometric absolute magnitude of the Sun is thus M = 4.74.

Given the definitions of apparent and absolute magnitude, the relation between an object's **apparent magnitude, *m*,** and its absolute magnitude, *M*, can be written in the form

$$M = m - 5 \log\left(\frac{d_l}{10pc}\right)$$

The Distance Modulus is Defined as *m − M*, and is related to the luminosity distance by the relation

$$m - M = 5 \log\left(\frac{d_l}{10pc}\right) + 25$$

Using standard candles to determine the Hubble constant is the method used by Hubble himself.
The recipe for finding the Hubble constant is a simple one:

- Identify a population of standard candles with luminosity *L*.
- Measure the redshift **z** and flux ***f*** for each standard candle.
- Compute $dL = (L/4\pi f)^{1/2}$ for each standard candle.
- Plot c_z versus *dL* .
- Measure the slope of the c_z versus *dL* relation when $z << 1$; the slope gives H_0 .

Initial Mass Function, IMF

The properties and evolution of a star are closely related to its mass.

In astronomy, the initial mass function (IMF) is an **empirical function** that describes the **initial distribution of masses for a population of stars** during star formation. IMF not only describes the formation and evolution of individual stars, it also serves as an important link that describes the **formation and evolution of galaxies**. The mass of a star can **only be directly determined** by applying **Kepler's third law into binary stars system**. However, the number of binary systems that can be observed is low, thus **not enough samples to estimate** the initial mass function. Therefore, **stellar luminosity function is used to derive a mass function** (present-day mass function, PDMF) by applying mass–luminosity relation. the luminosity function requires accurate determination of distances, and the most straightforward way is by measuring stellar parallax within 20 parsecs from the earth. The IMF is often stated in terms of a **series of power laws**, where $\xi(m)\Delta m$, **the number of stars with masses in the range** m **to** $m + dm$ within a **specified volume** of space, is proportional to $m^{-\alpha}$.

$$\xi(\log m) = \frac{d(N/V)}{d\log m} = \frac{dn}{d\log m}$$

Note: The vertical axis for the Initial Mass Function $\xi(m)$ is **SCALED** so that **for** m **greater than** $M_\odot$ it is $(m/M_\odot)^{-2.35}$

Edwin E. Salpeter (1955) was the first astrophysicist who attempted to **quantify IMF by applying power law** into his equations. ξ_0 is a constant relating to the local stellar density

$M_\odot := 1.989\cdot 10^{30}\,kg$ $\quad \xi_0 := 1$ $\quad \xi(m,\Delta m) := \xi_0\cdot\left(\frac{m}{M_\odot}\right)^{-2.35}\cdot\left(\frac{\Delta m}{M_\odot}\right)$ $\quad \xi_S(m) := \xi_0\cdot\left(\frac{m}{1}\right)^{-2.35}$

Kroupa (2001)

$$\xi_K(m) := if\left[m < 0.08, m^{-0.3}\cdot 15, if\left[(m \ge 0.08)\wedge(m \le 0.5), 1.3\cdot m^{-1.3}, m^{-2.35}\right]\right]$$

***Intro to Cosmology*, 2nd. Ed., Ryden 2016 Equation 7.3**

$$\xi_r(M) := 2.5\cdot\frac{1}{M}\cdot exp\left[\frac{-(log(M) - log(0.2))^2}{2\times 0.5^2}\right] \qquad \xi_R(M) := if\left(M \ge 1, M^{-2.35}, \xi_r(M)\right)$$

Chabrier (2003) gave the following expression for the density of individual stars in the Galactic disk, in units of parsec^{-3}

The vertical axis is not ε(m), but is a scaled version $(m/M_\odot)^{-2.35}$

$$\xi_{chab}(M) := 55\cdot\frac{0.158}{M\cdot ln0(10)}\cdot exp\left[\frac{-(log(M) - log(0.08))^2}{2\times 0.69^2}\right] \qquad \xi_{Chab}(M) := if\left(M \le 1, \xi_{chab}(M), M^{-2.35}\right)$$

Mass ranges corresponding to the standard stellar spectral types O through M are indicated.

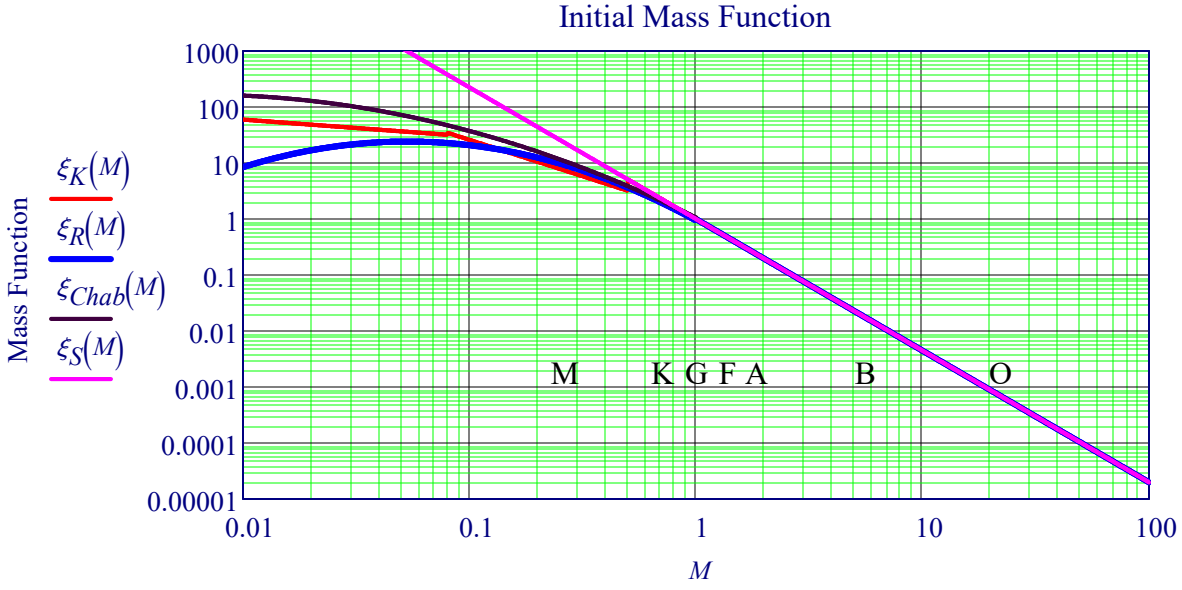

Initial Mass Function

Massive O stars are **extremely luminous**, they are also **short-lived**. An O star with a mass $M = 60\,M_\odot$ will run out of fuel for fusion in a time $t \approx 3$ Myr; it will then explode as a type II supernova.

Note:
$\Omega_{stars} \approx 0.3\%$

XI. Cosmic Distance Scale - Standard Candle 1: Cepheid Variables

The Standard Candle

To move outward in distance one starts One, with trigonometric parallaxes, then observes the same object with the other types of less precise parallaxes to calibrate and scale them. Once this is done one has the distance ladder reaching about 10,000 pc – **halfway across the Milky Way**. At this point one must put aside the parallax method and use other methods. With few exceptions, distances based on direct measurements are available only out to about a thousand pc, which is a modest portion of our own Galaxy. For distances beyond that, measurements are going to **depend upon physical assumptions**, that is, **knowledge of the object** in question. One must recognize the object and assume the **class of objects is homogeneous enough** that its members can be used for a meaningful estimation of distance – a standard candle as it were.

Almost all of the remaining rungs on the ladder are standard candles of one kind or another. A standard candle is an object that belongs to some class that has a **known brightness** (i.e., all members of the class have the same brightness). By comparing the **known luminosity of the latter to its observed brightness**, the distance to the object can be computed using the inverse square law.

Two problems exist for any class of standard candle. **The principal one is calibration**, determining exactly what the absolute magnitude of the candle is. This includes defining the class well enough that members can be recognized, and finding enough members with well-known distances that their true absolute magnitude can be determined with enough accuracy. The **second lies in recognizing members of the class**, and not mistakenly using the standard candle calibration upon an object which does not belong to the class. At extreme distances, which are where one most wishes to use a distance indicator, **this recognition problem can be quite serious.**

Standard Candle #1: Cepheid Variables

Cepheids were first noticed in 1784 in the constellation Cepheus in the northern sky, so these stars became known as "Cepheid variables." Cepheids are stars that periodically dim and brighten. In 1908 Henrietta Leavitt noticed a relationship between the brightness (or "luminosity") of a Cepheid variable star and its period for its pulsations in luminosity. They have a **unique waveform** and we can measure their period independent of how far away they are.

In the 1950s, astronomer Walter Baade discovered that the **nearby Cepheid variables used to calibrate the standard candle were of a different type than the more distant ones used to measure distances to nearby galaxies.** The nearby Cepheid variables were young, massive stars with much higher metal content than the distant old, faint ones. As a result, **the old stars were actually much brighter than believed,** and this had the ultimate effect of **doubling the distances** to the globular clusters, the nearby galaxies, and the diameter of the Milky Way.

Cepheids are luminous variable stars that **radially pulsate**. The strong direct relationship between a Cepheid's luminosity and its pulsation period makes them an important standard candle for Galactic and extragalactic sources. **Type I Cepheids** undergo pulsations with **very regular periods** on the order of days to months.

A relationship between the **period and luminosity for Type I Cepheids** was discovered in 1908 by **Henrietta Swan Leavitt** in her investigation of thousands of variable stars in the Magellanic Clouds. To use them as standard candles, one **observes the pulsation period to get the luminosity (absolute magnitude)**. By then measuring the apparent brightness (value observed at Earth) one has everything needed to use the **distance modulus** $\boldsymbol{m - M}$. The work was so important that Leavitt was considered for the Nobel Prize, but she died before her name could be submitted.

In addition, using data from the **HIPPARCOS astrometry satellite**, astronomers calculated the distances to many Galactic Cepheids using the trigonometric parallax technique. The resultant period-luminosity relationship for Type 1 Cepheids was:

$$\mathbf{M_V = 2.81 \log(P) - (1.43 \pm 0.1)}$$

where $\mathbf{M_V}$ is the absolute magnitude and P is the period in days.

XII. Modeling the Dynamics of a Cepheid Variable

There are **two classifications** of variable stars, RR Lyrae and Oepheid Variables. BB Lyrae have approximately a Solar mass and are yellow-white giants with luminosities on the order of 100 times that of the Sun. **Cepheid Variables** are **yellow supergiants** with several Solar masses and luminosities on the order of 20,000 times that of the Sun. These stars pulsate as the result of a special relationship between **pressure and gravity**. One idea is that as radiation emanates from the star, some of the He^{+} ionized into He^{2+} leading the surface of the star become more opaque. As the surface darkens, less energy is able to escape therefore heating the gas within the star. As the gas heats it pushes outward expanding the staris radius. As the star grows in volume, the gas cools allowing the pressure inside to drop (He^{+2} converts back to He^{+}) and gravity to once again dominate by pulling everything inward. The cycle then is able to begin again.

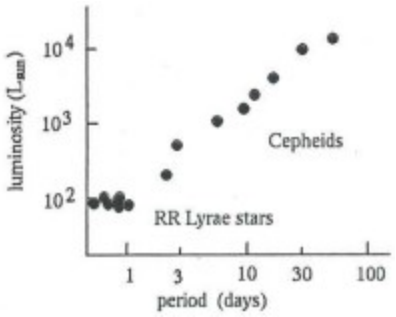

Find The Period of a Cepheid Variable Star

From Newton's Second Law:

$$m\cdot\frac{d^2}{d\tau^2}R = \frac{-G\cdot M\cdot m}{R^2} + 4\pi R^2\cdot P$$

In Equilibrium R is constant

$$\frac{G\cdot M\cdot m}{R^2} = 4\pi R^2\cdot P$$

Let $R = R_0 + \delta R$ $P = P_0 + \delta P$

$$4\pi R_0\cdot P = \frac{G\cdot M\cdot m}{R_0^3}$$

$$m\cdot\frac{d^2}{d\tau^2}(R_0+\delta R) = \frac{-G\cdot M\cdot m}{(R_0+\delta R)^2} + 4\pi(R_0+\delta R)^2\cdot(P_0+\delta P)$$

First Order Approximation: (Taylor Series Expansion)

$$\frac{1}{(R_0+\delta R)^2} = \frac{1}{R_0^2}\cdot\left(1-2\cdot\frac{\delta R}{R_0}\right)$$

$$m\cdot\frac{d^2}{d\tau^2}(\delta R) = \frac{-G\cdot M\cdot m}{R_0^2} + \frac{2G\cdot M\cdot m}{R_0^3} + 4\pi R_0^2\cdot P_0 + 8\pi R_0\cdot P_0\cdot\delta R + 4\pi R_0^2\cdot\delta P$$

Substitute $\frac{G\cdot M\cdot m}{R^2} = 4\pi R^2\cdot P$

$$m\cdot\frac{d^2}{d\tau^2}(\delta R) = \frac{2G\cdot M\cdot m}{R_0^3} + 8\pi R_0\cdot P_0\cdot\delta R + 4\pi R_0^2\cdot\delta P$$

For the adiabatic expansion of a gas: $P_0\cdot V_0^{\gamma} = P\cdot V^{\gamma}$ $P\cdot V^{\gamma} = Constant$ $V = \frac{4}{3}\pi\cdot R^3$

This Equation has the form of an Wave/Oscillation

$P\cdot R^{3\gamma} = Constant$ $\frac{\delta P}{P_0} = -3\gamma\cdot\frac{\delta R}{R_0}$ $\frac{d^2}{d\tau^2}(\delta R) = -(3\gamma-4)\cdot\frac{G\cdot M}{R_0^3}\cdot\delta R$ $M := 10^6$

Find the Period for this simple harmonic oscillation:

The Period, T, is $T_{Cepheid} = \frac{2\pi}{\omega}$

Mass, M, and Radius, R, of Sun

$M_{\odot} := 1.989\cdot10^{30}kg$ $R_{\odot} := 6.96\cdot10^{8}m$ $\gamma := \frac{5}{3}$

$\delta R(\tau) = A\cdot\sin(\omega\cdot\tau)$ $\omega^2 = (3\gamma-4)\cdot\frac{G\cdot M}{R_0^3}$

For a Cepheid 10X Mass & 30X Radius of Sun

$$T_{Cepheid} := \frac{2\pi}{\sqrt{(3\gamma-4)\cdot\frac{G\cdot 10M_{\odot}}{(30R_{\odot})^3}}}$$

$T_{Cepheid} = 6.024\cdot day$

Modeling the Dynamics of a Cepheid: Solve for δ Radii, Velocity, and Pressure

Newton's Second Law **Use the Greek letter *thau τ* to represent the symbol for time (t)**

$$m\cdot\frac{d^2}{d\tau^2}R = \frac{-G\cdot M\cdot m}{R^2} + 4\pi R^2\cdot P \qquad P_0\cdot V_0{}^{\gamma} = P\cdot V^{\gamma} \qquad V = \frac{4}{3}\pi\cdot R^3 \qquad P = P_0\cdot\left(\frac{R_0}{R}\right)^{3\gamma} \qquad R = R_0\cdot r$$

$$3\cdot\gamma = 5 \qquad P = P_0\cdot\left(\frac{1}{r}\right)^5 \qquad m\cdot R_0\cdot\frac{d^2}{d\tau^2}r = \frac{-G\cdot M\cdot m}{R_0{}^2\cdot r^2} + 4\pi R_0{}^2\cdot r^2\cdot P \qquad \frac{d^2}{d\tau^2}r = \frac{-G\cdot M}{R_0{}^3\cdot r^2} + \frac{4\pi R_0{}^2\cdot r^2\cdot P}{m}$$

$$P_0 := 56\cdot kPa$$

$$\frac{d^2}{d\tau^2}r + \frac{G\cdot M}{R_0{}^3\cdot r^2} - \frac{4\pi R_0{}^2\cdot P}{m\cdot r^3} = 0 \qquad \alpha_0 := \frac{G\cdot 10M_\odot}{\left(30R_\odot\right)^3} \qquad \beta_0 := \frac{4\pi\left(30\cdot R_\odot\right)^2\cdot P_0}{10M_\odot}$$

$$\alpha_0 = 1.457\times 10^{-10}\,\frac{1}{s^2} \qquad \beta_0 = 1.542\times 10^{-8}\cdot\frac{km}{s^2}$$

$$\frac{d^2}{d\tau^2}r + \frac{\alpha}{r(\tau)^2} - \frac{\beta}{r(\tau)^3} = 0 \qquad \alpha := 1.4\cdot 10^{-10} \qquad \beta := 1.2\cdot 10^{-10}$$

Solve Differential Equation for Cepheid Oscillations

Ordinary Differential Equation Solver

Given $r''(\tau) + \frac{\alpha}{r(\tau)^2} - \frac{\beta}{r(\tau)^3} = 0$ $r(0) = 1$ $r'(0) = 0$

$r := Odesolve(\tau, 10000000)$

$Day := 24\cdot 3600$ $D := Day$

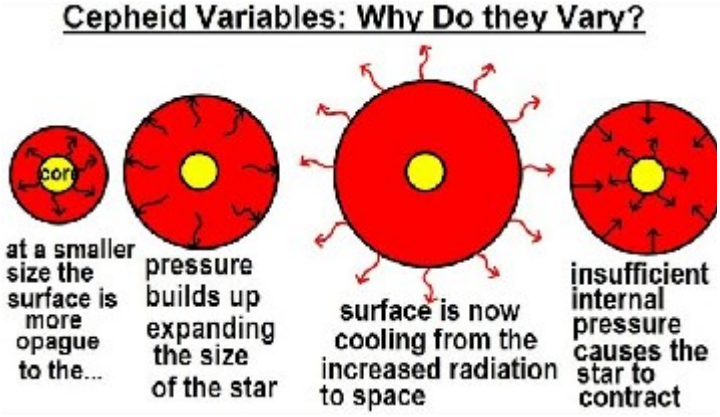

Below are Plots for Solution of Radius, Vel, Pressure

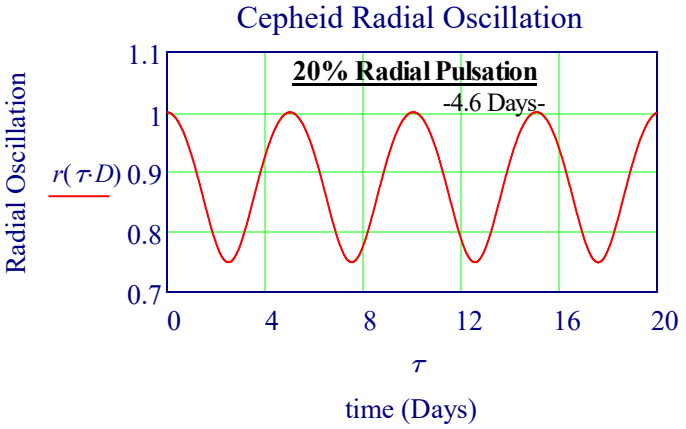

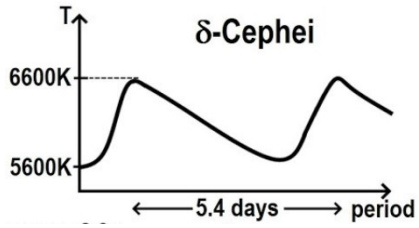

Definitions of Velocity, *v(τ)*, and Pressure, *P(τ)*

$$v(\tau) := \frac{d}{d\tau}r(\tau) \qquad P_{init} := 5.6\cdot 10^4 \qquad P(\tau) := \frac{P_{init}}{r(\tau)^5}$$

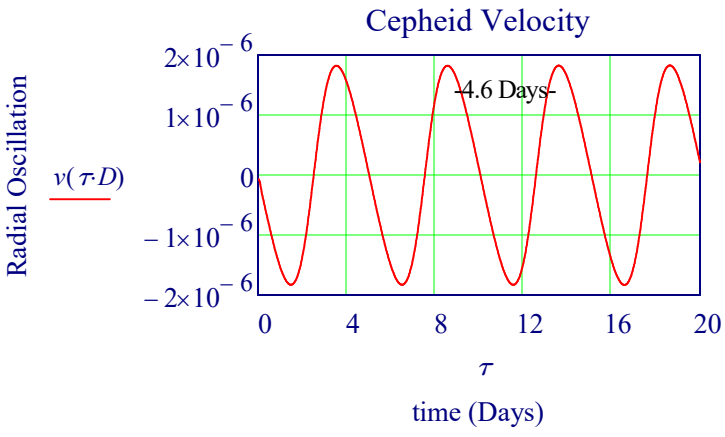

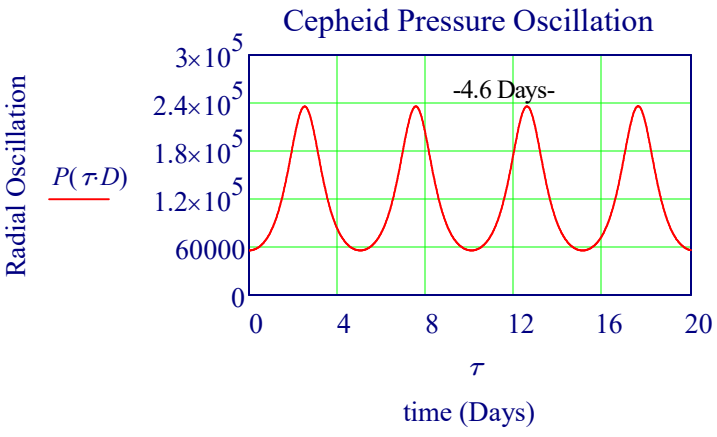

Calibrating Cepheid period-luminosity relation from the infrared surface brightness

Astronomy & Astrophysics 534, A95 (2011) **https://www.aanda.org/articles/aa/pdf/2011/10/aa17154-11.pdf**

The Cepheid period-luminosity (P-L) Relation is fundamental to the calibration of the extra-galactic distance scale and thus to the determination of the Hubble constant.

DATA: Distances & absolute magnitudes Large Magellanic Clouds (LMC) Cepheids calculated using precepts

ID#	log(P)	d (kpc)	σ(d) (kpc)	$(m-M)_0$ (mag)	σ(m−M) (mag)	M_V (mag)	M_I (mag)	M_J (mag)	M_H (mag)	M_K (mag)	W_{VI} (mag)	W_{JK} (mag)	E(B−V) (mag)	Δφ	Δ(m−M) (mag)

Read In Cepheid Data from File: $CPL := READPRN("Distances and absolute magnitudes for the LMC Cepheids.txt")$

$P := CPL^{\langle 1 \rangle}$ $M_K := -CPL^{\langle 10 \rangle}$ $M_V := -CPL^{\langle 6 \rangle}$ $ab := line(P, M_K)$ $MP(p) := ab_1 \cdot p + ab_0$

$AB := line(P, M_V)$ $Mp(p) := AB_1 \cdot p + AB_0$ $ab_0 = 2.401$ $ab_1 = 3.315$ $AB_0 = 1.225$ $AB_1 = 2.774$

Read Small Magellanic Clouds: $CPL_s := READPRN("Distances and absolute magnitudes for the SMC Cepheids.txt")$

$P_s := CPL_s^{\langle 1 \rangle}$ $M_{Ks} := -CPL_s^{\langle 10 \rangle}$ $M_{Vs} := -CPL_s^{\langle 6 \rangle}$

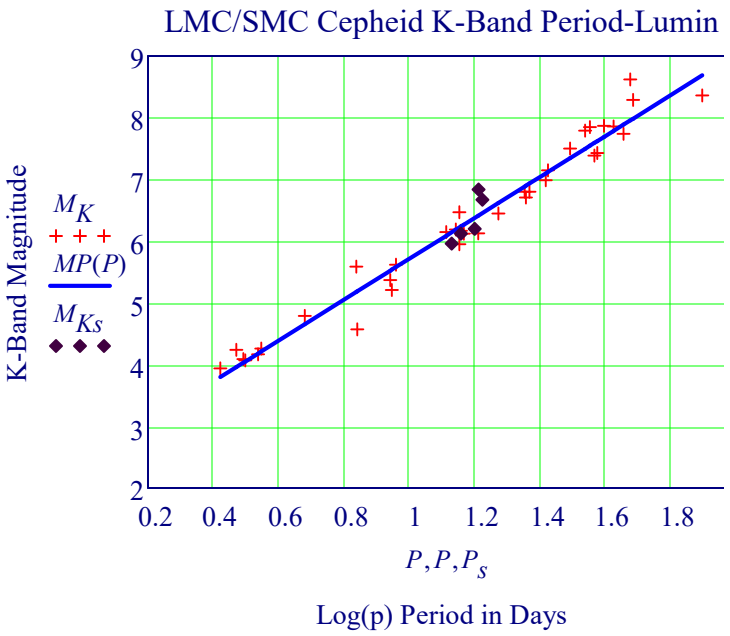

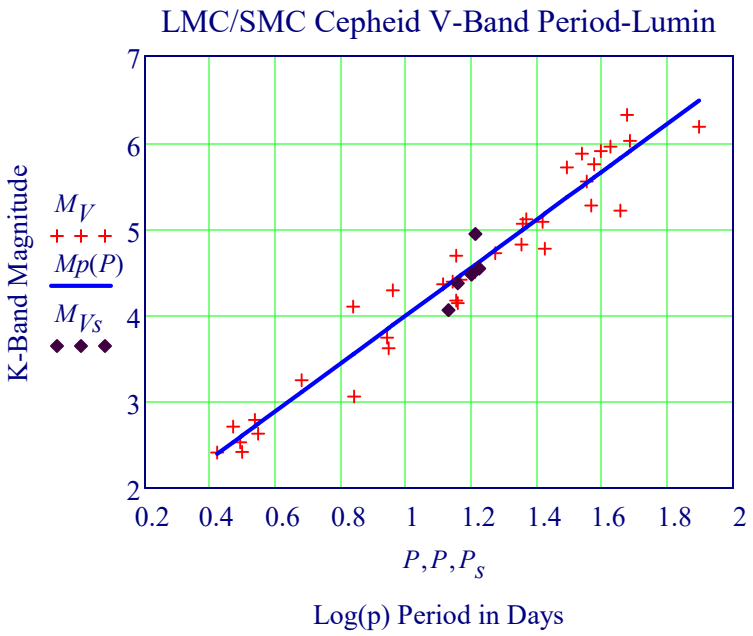

Calibrating Cepheid period-luminosity relation, **Conclusion- J. Storm, W. Gieren, P. Fouqué:**

The emerging conclusion based on our data and analysis is that for accurate distance measurements to galaxies the **K-band Cepheid Period-Luminosity** is the best suited tool: it is metallicity-independent both regarding the slope and the zero point, it is very insensitive to reddening, and it has a smaller intrinsic dispersion than any optical PL relation.

Apparent Brightness

Describe how bright a star seems as seen from Earth by its apparent brightness. This is often called the **intensity** of the starlight. Sometimes it is called the **flux of light**. The apparent brightness is how much energy is coming from the star per square meter per second, as measured on Earth. The units are watts per square meter (W/m_2).

- the distance d to the star,
- the apparent brightness b of the star, and
- the luminosity L of the star.
- All of the energy produced by the star per second must cross a sphere of radius d.
- The study of geometry tells us that area of this sphere is $4 \pi d^2$

$$b = \frac{L}{4\pi d^2}$$

$$L = \left(4\pi d^2\right) b$$

XIII A. Standard Candle 2: *Type 1a Supernovae (SN)*

$q_0 := -0.53$

***Introduction to Cosmology*, Ryden, pg. 116 (Ryden's Distance Equation for Distance Modulus, Dmod)**

"To determine the acceleration of the universe, we need to view standard candles for which the relation between d_L and z deviates significantly from the linear relation that holds true at lower redshifts. In terms of H_0 and q_0, the equations for **luminosity distance d_L** and **distance modulus $D_{mod}(z)$** at small redshift ($z < 1$) is, (Ryden 2nd Ed. Eq. 6.51),

$$d_L(z) := \frac{c}{H_0} z \cdot \left[1 + \left(\frac{1 - q_0}{2}\right) z\right] \qquad D_{mod}(z) := 43.23 - 5\,log\left(\frac{H_0}{68 km \cdot s^{-1} Mpc^{-1}}\right) + 5\,log(z) + 1.086\left(1 - q_0\right)z$$

At a redshift z = 0.2, for instance, the luminosity distance d_L in the Benchmark Model (with $q_0 = -0.53$) is 5 percent larger than dL in an empty universe (with $q_0 = 0$).

For a standard candle to be seen at $d_L > 1000$Mpc, it must be very luminous. In recent years, the standard candle of choice among cosmologists has been type *Ia supernovae*. A supernova may be loosely defined as an exploding star. Early in the history of supernova studies, when little was known about their underlying physics, supernovae were divided into two classes, on the basis of their spectra. Type I supernovae **contain no hydrogen absorption lines in their spectra**; type II supernovae contain strong hydrogen absorption lines. Gradually, it was realized that all type II supernovae are the same species of beast; they are massive stars
($M > 8 M_\odot$) whose cores collapse to form a black hole or neutron star when their nuclear fuel is exhausted. During the rapid collapse of the core, the outer layers of the star are thrown off into space. Type I supernovae are actually two separate species, called type Ia and type Ib. Type Ib supernovae, it is thought, are massive stars whose cores collapse after the hydrogen-rich outer layers of the star have been blown away in strong stellar winds. Thus, type Ib and type II supernovae are driven by very similar mechanisms – their differences are superficial, in the most literal sense. **Type Ia supernovae**, however, are something completely different. They **begin as white dwarfs**; that is, stellar remnants that are supported against gravity by the quantum mechanical effect known as electron degeneracy pressure. The maximum mass at which a white dwarf can be supported against its self-gravity is called the Chandrasekhar mass; the value of the Chandrasekhar mass is $M \approx 1.4\ M_\odot$. A white dwarf can go over this limit by merging with another white dwarf, or by accreting gas from a stellar companion. If the Chandrasekhar limit is approached or exceeded, the white dwarf starts to collapse until its increased density triggers a runaway nuclear fusion reaction. The entire white dwarf becomes **a fusion bomb**, blowing itself to smithereens; unlike type II supernovae, type Ia supernovae do not leave a condensed stellar remnant behind.

Within our galaxy, type Ia supernovae occur roughly **once per century**, on average. Although type Ia supernovae are not frequent occurrences locally, they are **extraordinarily luminous**, and hence can be seen to large distances. The luminosity of an average type Ia supernova, at peak brightness, is $L = 4 \times 10^9\ L\ M_\odot$; that's **100,000 times more luminous than even the brightest Cepheid**. For a few days, a type Ia supernova in a moderately bright galaxy can **outshine all the other stars in the galaxy combined**. Since moderately bright galaxies can be seen at $z \approx 1$, this means that type Ia supernovae can also be seen at $z \approx 1$.

So far, type Ia supernovae sound like ideal standard candles; very luminous and all produced by the same mechanism. There's one complication, however. Observation of supernovae in galaxies whose distances have been well determined by Cepheids reveals that **type Ia supernovae do not have identical luminosities**. Instead of all having $L = 4 \times 10^9\ L_\odot$, their peak luminosities lie in the fairly broad range $L \approx (3 - 5) \times 10^9\ L_\odot$. However, it has also been noted that the peak luminosity of a type Ia supernova is tightly correlated with the shape of its light curve. Type Ia supernovae with luminosities that shoot up rapidly and decline rapidly are less luminous than average at their peak; supernovae with luminosities that rise and fall in a more leisurely manner are more luminous than average. Thus, just as the period of a Cepheid tells you its luminosity, **the rise and fall time of a type Ia supernova tells you its peak luminosity."** **Refer to the Two Classes of Light Curve Graphs Below**

Compare Supernovae Types: Characteristics and Light Curve Differences

Two Basic Scenarios of Stellar Death:

Ia. Thermonuclear runaway at degenerate conditions (drives the destruction of white dwarf stars in Type Ia Sne)
II. Implosion of stellar cores (associated with what is called core-collapse supernovae (CCSNe) of Types II, Ib/c

Type Ia supernova, needs several very specific events to push the white dwarf over the Chandrasekhar limit. Type II events occur during the regular course of a massive stars evolution.

Type Ia Supernovae
Pretty Good Standard Candles, Mv ~ -19.3. Believed to be caused by accretion of material from binary companion star to a white dwarf (WD), pushing it over its Chandrasekhar limit, causing its collapse.

Type II Supernovae
Formed by collapse of massive stars (also Type Ib). Not good standard candles, but we can measure their distance using the Baade-Wesselink method of measuring the expansion of the outer envelope. Not as bright as Type Ia's.

Type Ia

- **No H, He in spectrum**
- No visible progenitor (WD)
- Kinetic Energy: 10^{51} erg
- Total EM Radiation: 10^{49} erg
- Likely no neutrino burst
- Rate: 1/300 yr in Milky Way
- Occur in spirals and ellipticals
- No remnant
- most of the explosion energy is in **heavy element synthesis** and kinetic energy of the ejecta

Type II

- **Both H, He in spectrum**
- Supergiant progenitor
- Kinetic Energy: 10^{51} erg
- Total EM Radiation: $10^{48\text{-}49}$ erg
- Neutrinos: 10^{53} erg
- Rate: 1/50 yr in Milky Way
- Occur mainly in spiral galaxies
- Remnant: NS or BHs
- vast majority of the energy is in neutrino emission

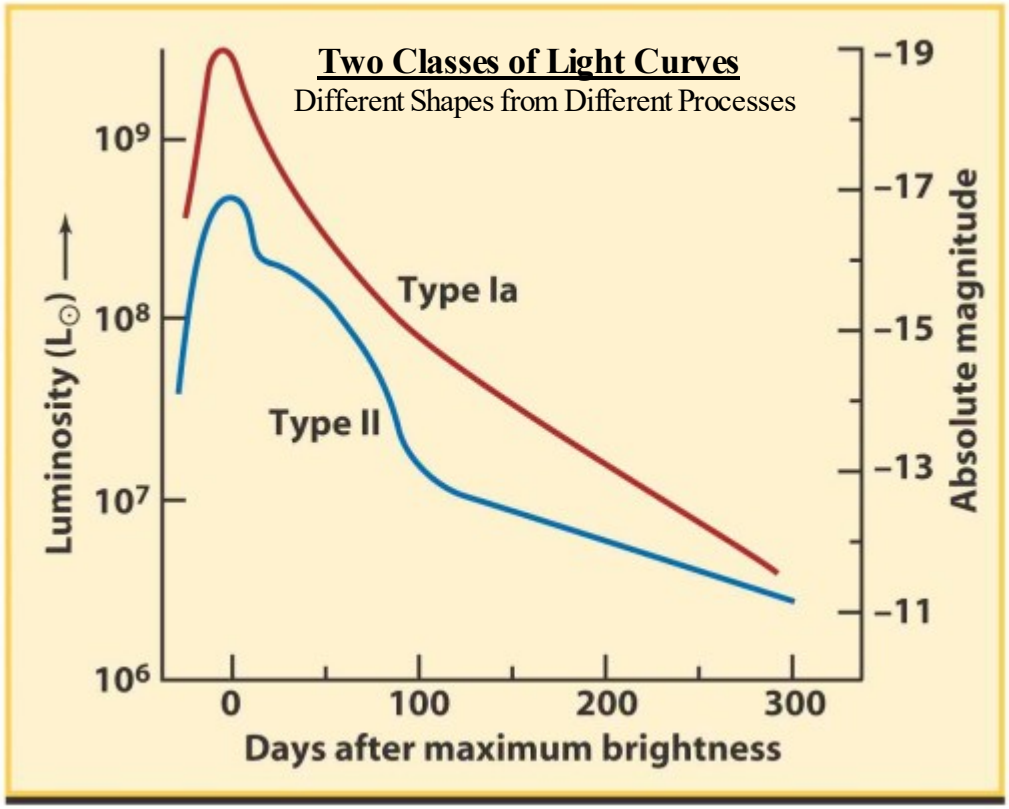

Source: https://www.astro.umd.edu/~richard/ASTR480/A480_supernova_remnants_2016_lec1.pdf

Cosmic Distance Scale Summary

- Local measurements of the H_0 are now good to ≈5%, and may be improved in the future
- Concept of distance ladder; many uncertainties & calibration problems, model dependence, etc
- Cepheids as the key local distance indicator
- SNe as a bridge to the far-field measurements
- Far-field measurements (SZ effect, lensing, CMB)
- Ages of oldest stars (globular clusters), white dwarfs, heavy elements consistent with CMB age
- CMB provides more precise determinations of the H_0 and other cosmological parameters.
- However, **persistent discrepancy between the CMB based & Cepheid based measurements**.

This may be a sign of a new physics.

XIV. A. 1929 Hubble's Original Observations Galaxy Recession & Hubble Constant Calculation

The relationship between the expansion of the universe & the distance, H_0, was discovered by Edwin Hubble in 1929 from astronomical observations of Cepheid Variables, and is known as Hubble's Law. Hubble estimated velocity from redshift, z, where He assumed that z = v/c. The distance, d, is measured from parallax or a luminosity of a standard candle. Then $\mathbf{v = H_0 * r}$. Hubble thought that the redshift, z, was from the Doppler effect, v/c. He estimated the value of H_0 as 500 km/s per Mpc. Which is grossly in error because he **underestimated the distance to the galaxies**. The large number from the redshift velocity divided by a too small distance. Note: H = r/v. Therefore H is the reciprocal of time from expansion.

$$H_{HubbleData} := READPRN("Hubble Dataset.txt")$$

Distance Data (Mpc)

$$d_{recH} := H_{HubbleData}^{\langle 0 \rangle}$$

Recessional Velocity (km/s) Data from Redshift, r

$$v_{recH} := H_{HubbleData}^{\langle 1 \rangle}$$

$$ab4 := line(d_{recH}, v_{recH})$$

$$H_{fitH}(d) := ab4_0 + ab4_1 \cdot d$$

$$H_{Hubble} := ab4_1$$

$$H_{Hubble} = 500 \frac{km}{s} \cdot Mpc^{-1}$$

Hubble's original estimate estimate from Cepheids was in error. The current value is H_0 is 73 ± 1 km/sec/Mpc

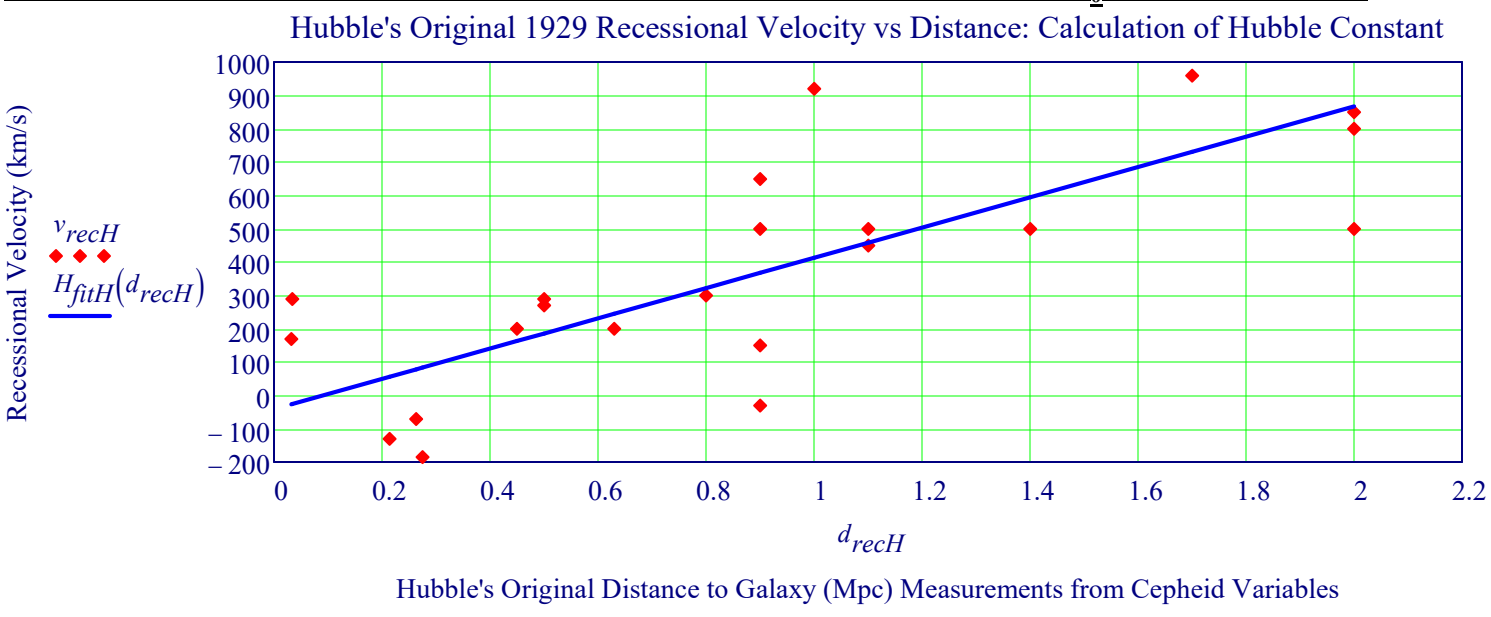

The Physical Meaning of the Hubble Constant in terms of Expansion Rate per Distance:
The Hubble constant tells us how quickly any two distant points in the universe are moving apart per unit distance. For example, if H_0 equals 2.3 *10^{-18} m s^{-1} , it means that for every meter between two points, the separation increases by 2.3 *10^{-18} meters per second.

Standard Candle #2: Type Ia supernova For example, **all observations seem to indicate that Type Ia supernovae that are of known distance have the same brightness** (corrected by the shape of the light curve); however, the possibility that the distant Type Ia supernovae have different properties than nearby Type Ia supernovae exists. The use of Type Ia supernovae is crucial in determining the correct cosmological model. If indeed the properties of the Type Ia's are different at large distances, i.e. if the extrapolation of their calibration to arbitrary distances is not valid, ignoring this variation can dangerously bias the reconstruction of the cosmological parameters.

$parsec := 3 \cdot 10^{13} \cdot km$ $\quad Mpc := 3 \cdot 10^{19} km$ $\quad v = H_0 \cdot r$ $\quad H_0 := 73 \frac{km}{s} \cdot (Mpc)^{-1}$

NASA/IPAC EXTRAGALACTIC DATABASE of Type IA Supernova (3645 Distance Measurements)

Read Data for 3,716 distances to 1,210 galaxies with v < 1/8 c

https://ned.ipac.caltech.edu/level5/NED1D/ned1d.html

$H_{NASA} := READPRN("Galaxy NED-1D d \& v Only.txt")$

Number of Data Points

$rows(H_{NASA}) = 3645$

Galaxy Luminal Distance (Mpc) $\quad d_{rec} := H_{NASA}^{\langle 0 \rangle}$

Recessional Velocity (km/s) $\quad v_{rec} := H_{NASA}^{\langle 1 \rangle}$

Redshift z $\quad z := \frac{v_{rec} \cdot km}{c \cdot s}$

Corrected for Redshift $\quad d_{recz} := \frac{\overrightarrow{d_{rec}}}{1 + z}$

Current Estimate of Hubble's Constant:

Find Slope of Recessional Velocity (km/s) to Corrected Distance (Mpc)

Fit Line to Data: $ab := line(d_{recz}, v_{rec})$

$H_{fit}(d) := ab_0 + ab_1 \cdot d$ $\quad ab_0 = 23.882$

$H_{twk} := ab_1 \cdot \frac{km}{s} \cdot Mpc^{-1}$

Calculated H_{twk} within less than a 2% Error.

$H_{twk} = 68.55 \cdot \frac{km}{s} \cdot Mpc^{-1}$

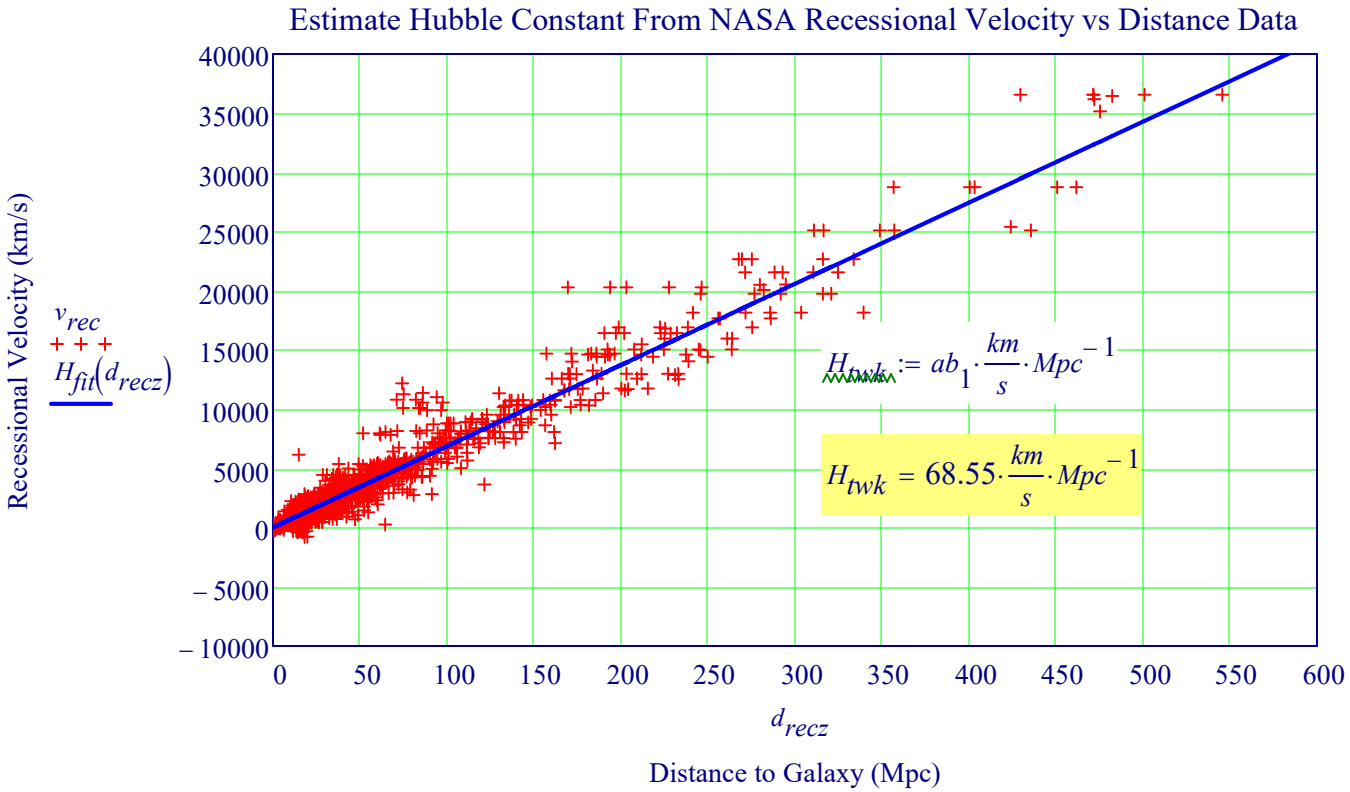

Standard Candle 2: *Hubble Space Telescope Light Curves Of Type 1a SN*

Supernova Cosmology Project

"Amanullah et al. (The Supernova Cosmology Project), Ap.J., 2010
https://supernova.lbl.gov/Union/figures/SCPUnion2_mu_vs_z.txt

$q_0 := -0.53$

$mu\_z := READPRN("mu\_vs\_z - No Name No OL.txt")$ $mu\_z := csort(mu\_z, 0)$ $z_{mu} := mu\_z^{\langle 0 \rangle}$

Fit Straight Line, Fit(z), to Data: $\chi := line\left(log(z_{mu}), mu\_z^{\langle 1 \rangle}\right)$ $Fit(z) := \chi_0 + \chi_1 \cdot z$

Power Function Fit $m_{fit}(z) := a \cdot z^b + c$

Modern Version of the SN Hubble Diagram

The solid line represents the best fitted cosmology for a flat Universe including the CMB and BAO constraints.

Distance Modulus vs Redshift for Type Ia Supernovae

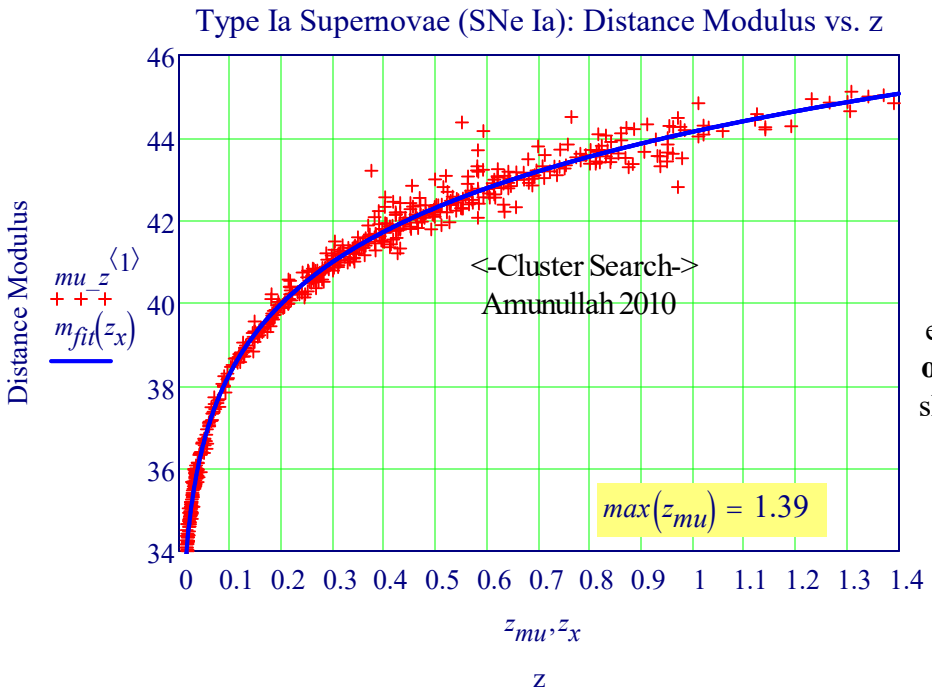

Type Ia Supernovae

are believed to be caused by the thermonuclear explosions of a carbon-oxygen white dwarf in a binary system. The process involves mass transfer to the white dwarf from the companion. When the white dwarf reaches the Chandrasekhar mass, the explosion occurs. **Since the explosions occur at the same mass**, the explosions should be **nearly identical**. Furthermore, luminosity evolution should not occur since the **physics of the explosion is the same in the past.**

Fit a Line to Modern Version of Hubble Diagram

$D_{mod}(z)$ is Ryden's Equation (See below), which is an approximation for the Distance Modulus for small redshift. The deviation from the straight line Fit(z) tells us that the expansion of the universe is **speeding up**.

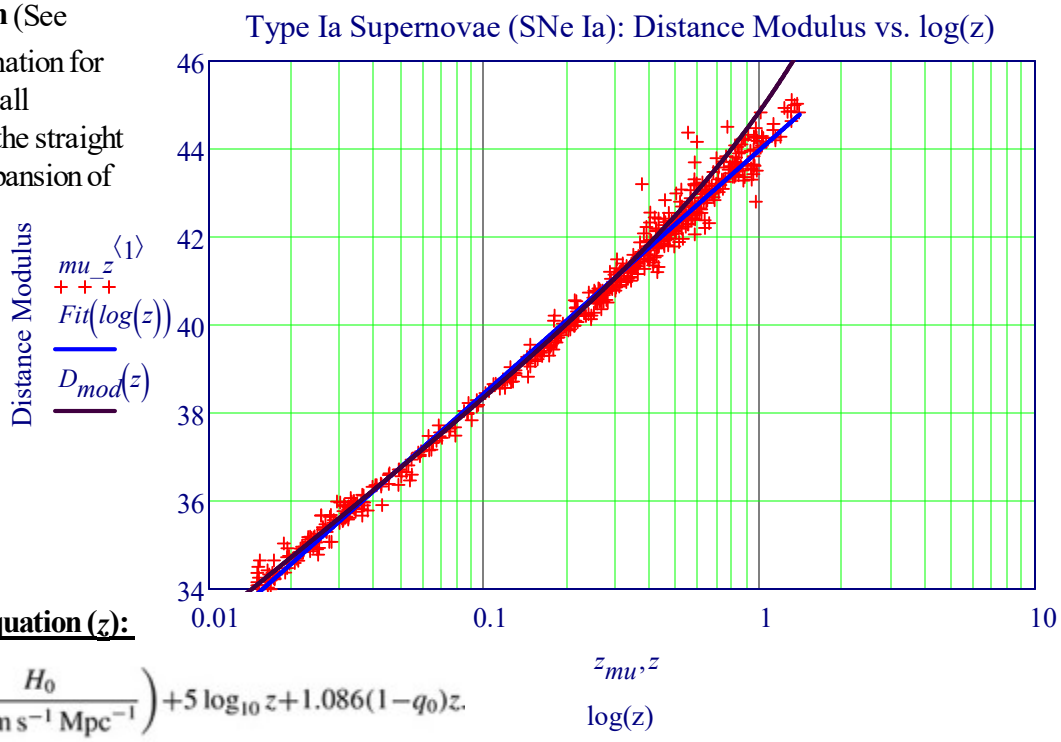

Ryden's Distance Modulus Equation (z):

$$m - M \approx 43.23 - 5\log_{10}\left(\frac{H_0}{68\ \mathrm{km\ s^{-1}\ Mpc^{-1}}}\right) + 5\log_{10} z + 1.086(1 - q_0)z.$$

B. Reconstructing Cosmic History: *JWST-Extended Mapping of the Hubble Flow from z~0 to z~7.5 with HII Galaxies* https://arxiv.org/html/2404.16261v1

Abstract

Over twenty years ago, Type Ia Supernovae (SNIa) observations revealed an accelerating Universe expansion, suggesting a significant dark energy presence, often modelled as a cosmological constant, Λ. Despite its pivotal role in cosmology, the standard ΛCDM model remains largely underexplored in the redshift range between distant SNIa and the Cosmic Microwave Background (CMB). **This study harnesses the James Webb Space Telescope's** advanced capabilities to extend the Hubble flow mapping across an unprecedented redshift range, from $z \approx 0$ **to** $z \approx 7.5$. Utilising a dataset of 231 HII galaxies and extragalactic HII regions, we employ the $L-\sigma$ relation, correlating the luminosity of Balmer lines with their velocity dispersion, to define a competitive technique for measuring cosmic distances. This approach **maps the Universe's expansion over more than 12 billion years, covering 95% of its age**. Our analysis, using Bayesian inference, constrains the parameter space

$$\{h, \Omega_m, w_0\} = \{0.731 \pm 0.039, 0.302^{+0.12}_{-0.069}, -1.01^{+0.52}_{-0.29}\}$$

(statistical) for a flat Universe. These results provide new insights into cosmic evolution and suggest uniformity in the photo-kinematical properties of young massive ionizing clusters in giant HII regions and HII galaxies across most of the Universe's history.

In the pursuit of a more versatile analysis framework, we have also established an h-free likelihood function. This involves a **rescaling of the luminosity distance (d_L)** through the introduction of a **dimensionless luminosity distance**, $D_L(z,\theta)$, defined as:

$$D_L(z,\theta) = (1+z)\int_0^z \frac{dz'}{E(z',\theta)}$$

In this formulation, d_L is expressed as $d_L = cD_L/H_0$. This rescaling technique is employed to ascertain cosmological parameters independently of the Hubble constant. Here $E(z,\theta)$ for a flat Universe is given by:

$$E^2(z,\theta) = \Omega_r(1+z)^4 + \Omega_m(1+z)^3 + \Omega_w(1+z)^{3y}\exp\left(\frac{-3w_a z}{1+z}\right)$$

with $y = (1+w_0+w_a)$ and Ω_r the radiation density parameter such that we can define $\Omega_w = 1-\Omega_m-\Omega_r$

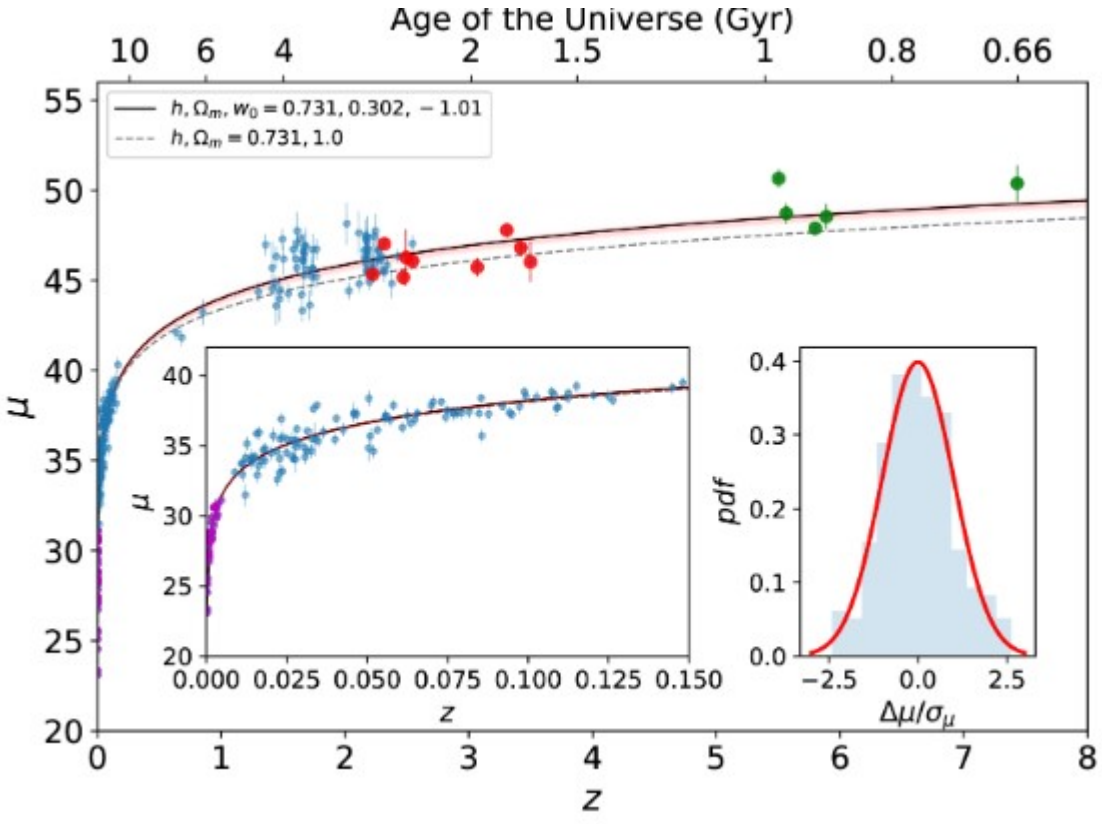

Overview of the Rungs of the Cosmic Distance Ladder

1. Geometric Methods (Nearby)

Parallax

The most fundamental method. As Earth orbits the Sun, nearby stars shift slightly against background stars.
Works reliably out to a few thousand light years (Gaia extends this to hundreds of millions of stars).
Radar ranging Distances within the solar system are measured by bouncing radio signals off planets.

2. Standard Candles in the Milky Way

Cepheid Variable Stars

Their pulsation period is directly related to intrinsic luminosity. Calibrated by parallax.

RR Lyrae Variables

Fainter but numerous, useful for globular clusters and nearby galaxies.

3. Extragalactic Standard Candles

Type Ia Supernovae

Explosions of white dwarfs reaching a critical mass. They have nearly uniform peak luminosity, making them "standardizable candles." Used out to redshifts z ~ 1–2.

Tip of the Red Giant Branch (TRGB)

The brightness of the brightest red giants is nearly constant; good for nearby galaxies.

4. Standard Rulers

Baryon Acoustic Oscillations (BAO)

Imprints from sound waves in the early universe provide a "standard ruler" visible in the large-scale distribution of galaxies.

CMB Acoustic Peaks

Fluctuations in the CMB at $z \approx 1100$ encodes the size of the sound horizon, a fundamental calibration scale.

5. Redshift–Distance Relation

Hubble's Law

Beyond a few hundred million light years, galaxies' redshift can be related to distance via the Hubble constant, once it has been calibrated with the lower rungs..

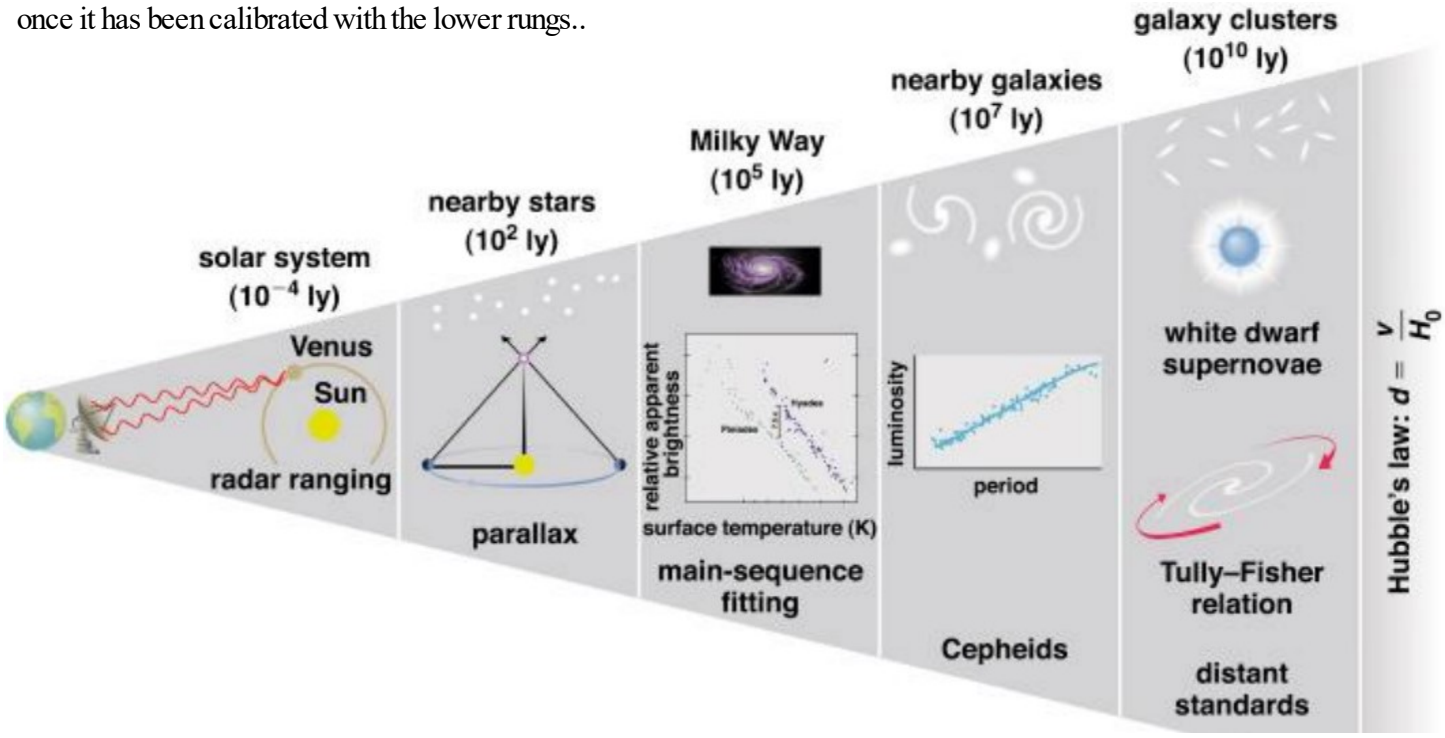

Three Redshift, z, regimes that can be used to determine the Hubble Constant

1. Low-Redshift Hubble Law (Linear Regime)

The original Hubble's Law is:

$$v = H_0\, d \quad \text{or} \quad z \approx \frac{H_0 d}{c} \quad \text{for small } z$$

This relation is strictly linear only for z ≲ 0.1.

At higher redshift, cosmological effects (dark energy, matter density, curvature) change the relation between redshift and distance, so assuming a simple linear Hubble law introduces systematic errors.

☞ Largest redshift for "direct" Hubble Law use: about z ≈ 0.1 (sometimes z ≈ 0.2 at most).

2. Intermediate Redshifts (0.1 ≲ z ≲ 2)

Beyond z ~ 0.1, the Universe's expansion history deviates from a straight line. To determine H_0 at these distances, one **must assume a cosmological model** (ΛCDM, with Ω_m, $\Omega\Lambda$, etc.). Methods like Type Ia supernovae or BAO (Baryon Acoustic Oscillations) use model-dependent fitting of the expansion curve to infer H_0.

3. High Redshift (z ≳ 1000, CMB)

The Cosmic Microwave Background (CMB, z ≈ 1100) is often used to measure H_0, but this requires assuming a full cosmological model and extrapolating forward to today's expansion. This is not a "direct" measurement of H_0, but an indirect, **model-dependent inference**.

Summary:

Direct Hubble Law (linear): reliable only for z ≲ 0.1.
Intermediate z (0.1–2): requires ΛCDM assumptions (supernovae, BAO).
Very high z (CMB at z ~ 1100): indirect inference, strongly model-dependent.
plot of the redshift–distance relation showing where it stays nearly linear (z < 0.1) and how it curves away at higher z?

So the largest redshift for using Hubble's Law in its simplest, nearly linear form is about z ~ 0.1.
If one allows cosmological modeling, then effectively any redshift can be used—including z ≈ 1100 from the CMB.

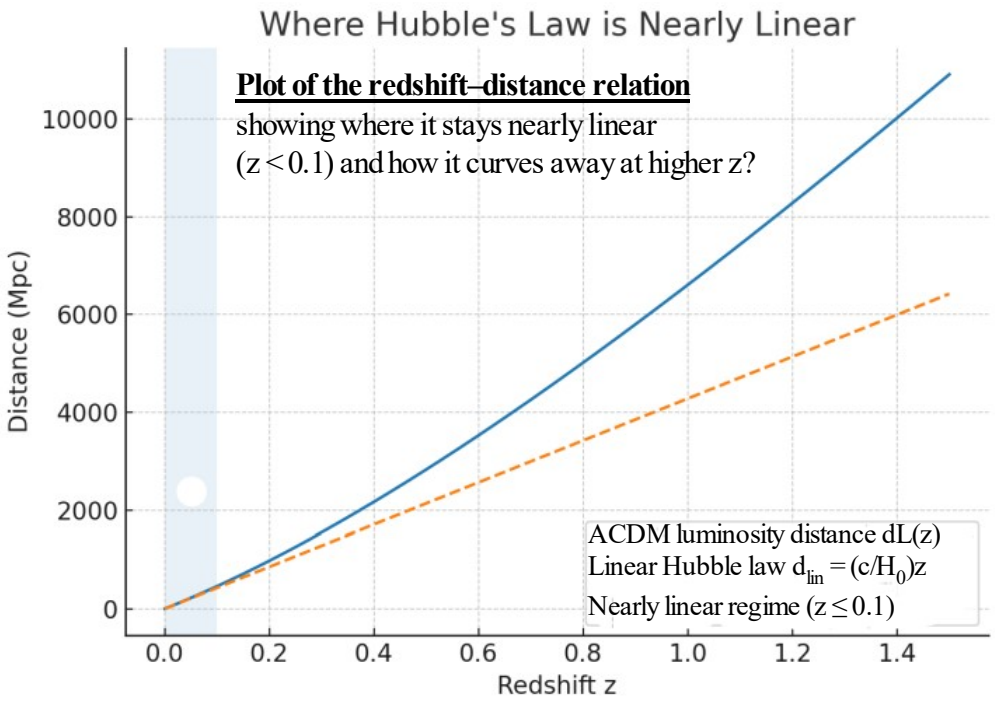

Deviation from linear Hubble law
(ΛCDM, H0=70, Ωm=0.3, ΩΛ=0.7)

z	d_L (Mpc)	Linear d (Mpc)	Fractional deviation
0.02	87	85.655	0.01539
0.05	222	214.137	0.03807
0.1	460	428.275	0.07478
0.2	980	856.55	0.1442
0.5	2833	2141.37	0.32295
1	6608	4282.75	0.54285
1.5	10910	6424.12	0.69823

Above Figures:
Hubble diagram for GEHRs and HIIGs, here z is the redshift and μ is the distance modulus. In magenta we present the 'anchor' sample of 36 GEHRs which have been analysed in [26], in blue we present the full sample of 181 HIIGs which have been analysed in [18], **while in red we present the 9 new HIIGs** from [27] and in **green the 5 new HIIGs studied with JWST** by [28]. The black line is the cosmological model that best fits the data with the red shaded area representing the 1σ uncertainties to the model, while the grey dashed line is a flat cosmological model without dark energy. The inset at the left shows a close-up of the Hubble diagram for $z \leq 0.15$. The inset at the right presents the pulls probability density function (pdf) of the entire sample of GEHRs and HIIGs and the red line shows the best Gaussian fit to the pdf.

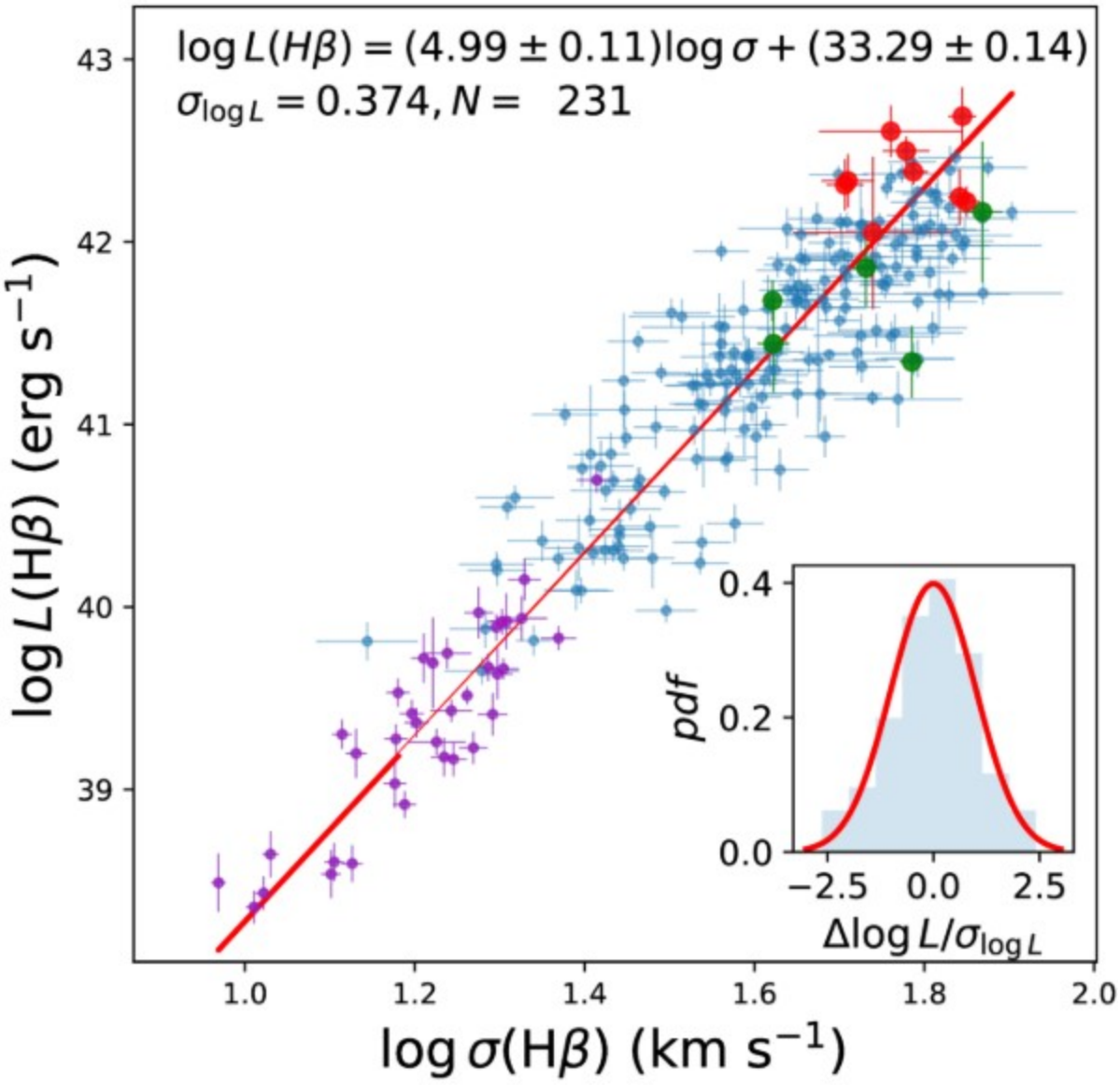

The $\boldsymbol{L-\sigma}$ relation of GEHRs and HIIGs. The data points follow the same color code for the different samples as in the previous figure. The red line shows the best linear fit to the data, including the uncertainties in both axis. At the top of the figure we present the values of the slope and intercept of the best fit including their uncertainties. We also show the standard deviation of the ***log L*** around the best fit and the total number of objects in the sample. The inset shows the pulls distribution of the entire sample of GEHRs and HIIGs and the red line shows the best Gaussian fit to the distribution.

[18] González-Morán, A. L. et al.Independent cosmological constraints from high-z H II galaxies: new results from VLT-KMOS data.MNRAS 505, 1441–1457 (2021).
[26] Fernández Arenas, D. et al.An independent determination of the local Hubble constant.MNRAS 474, 1250–1276 (2018).
[27] Llerena, M. et al.Ionized gas kinematics and chemical abundances of low-mass star-forming galaxies at z ~ 3.A&A 676, A53 (2023).

C. Using Gravitational Waves to Find Hubble's Constant, Hg

The gravitational wave signal emitted by the merger of two compact objects can be used as a self-calibrating standard candle. Unlike the methods to Measure the Hubble Constant, H_0, in the followings Section X, the LIGO measurement does not use a "distance ladder". By detecting gravitational waves from merging binary neutron stars or black holes, LIGO can provide a measurement of the distance to the source and the rate at which it is movingaway from us. There are now operational detectors at LIGO Hanford and LIGO Livingston in the USA, Virgo in Italy, and KAGRA in Japan. The detectors measure the strain amplitude of a gravitational wave by using laser inferometry to detect the minuscule changes in the length of perpendicular beams as a wave passes by. The purpose of the two sites in the USA is to later out local seismic vibrations. The wave amplitude is related to the chirp mass M_c which is in turn derivable from the waveform calculated for a merger. A implied form of the relevant equations are:

LIGO Parameters

$$\mathcal{M} = \frac{(m_1 m_2)^{3/5}}{(m_1+m_2)^{1/5}} = \frac{1}{G}\left[\frac{5}{96}\pi^{-8/3} f^{-11/3}\dot{f}\right]^{3/5}$$

$$\mathcal{M}_z = (1+z_{\rm obs})\mathcal{M}$$

$$h(t) = \frac{\mathcal{M}_z^{5/3} f(t)^{2/3}}{d_L} F(\theta, i)\cos\Phi(t)$$

For Definitions of Parameters See Sections V, VII, XII, XXIC, XXID.

Compare the Theoretical Magnitude-Redshift to Perlmutter 1999 SB 1A

Given the Luminosity Red Shift Relation (for k > 0):

$$D_L(z) = \frac{c(1+z)}{H_0\sqrt{\Omega_K}} \sinh\left[\sqrt{\Omega_K}\int_0^z \frac{H_0}{H(z')}\,dz'\right]$$

$$m_{bol}(z, \Omega_m) := 5\,log(1+z) + 5\,log(\chi_{em}(z, \Omega_m)) + 24$$

where the Luminosity Distance, $D_L(z)$ is given as the red shift integral of the Hubble parameter $H(z)$, and the Hubble constant H_0. f is the frequency, m_1 and m_2 the merging masses, Φ(t) the phase, and Rh(t) the measured dimensionless strain of the strongest harmonic (Abbott et al. 2016). The rest-frame chirp mass is red shifted by zcobs, and F is a function of the angle between the sky position of the source and detector arms, and the inclination I between the binary orbital plane and line of sight.

The LIGO-Virgo detector network had a detection horizon of ~ 190 Mpc for binary neutron star (BNS) events (Abbott et al. 2017a), For example, the counterpart associated with GW170817 had brightness ~ 17 mag in the I band at 40 Mpc

When a **binary neutron star** (BNS) system merges, there is an **accompanying burst of light from matter outside** the combined event horizon. For this reason, it is known as a "**bright siren**". If the ash can be observed, the host galaxy is identified and one can use its redshift in the above equation.

The **event GW170817** was just such a BNS merger. Given the search region, an optical counterpart was found in NGC 4993 at a distance, d_L, of ~ 40 Mpc. Around $f_c = 3000$ cycles of the wave resolved the chirp mass in the detector frame as $M_c = 1.197\,M\odot$ to accuracy of 1 part in 10^3, consistent with a BNS merger. The main remaining uncertainty is then the inclination angle I. The Black Hole Merger, GW150914, was 1.3 Billion Light-Years away.

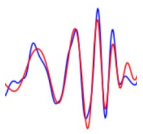

$f_c = 3000Hz$

$M_z = 1.197 M_\odot$

$d_L = 43.8Mpc$

$$H_g = H_g(M_z, f, d_L, F, \Phi)$$

This Gives: $H_g = 70\,\frac{km}{s}\cdot Mpc^{-1}$

Abbott, B. P., et al. 2017a, PRL, 119, doi:10.1103/PhysRevLett.119.161101

—. 2017b, ApJL, 848, doi:10.3847/2041-8213/aa920c

—. 2017c, ApJL, 848, doi:10.3847/2041-8213/aa91c9

MEASURING THE EXPANSION OF THE UNIVERSE WITH GRAVITATIONAL WAVES https://www.ligo.org/science/Publication-GW170817Hubble/flyer.pdf

D. Real Time Measurement of Cosmic Expansion Within Our Lifetime

A Measurement of the Cosmic Expansion Within our Lifetime, Fulvio Melia, arXiv:2112.12599v1

Methodology: Measurement of Spectroscopic Velocity Shifts - Redshift Drift

The goal is to measure Incremental Changes in red shift, δz, over a "short" time interval, δt. Because of the small magnitude of the drift of redshift with time, measurements must be made over many decades.

Introduction: Objects receding from us with the general Universal expansion become fainter with time, and their spectra are redshifted according to their distance. The rate at which these quantities change is characterized by the expansion speed and acceleration, but is scaled to the age of the Universe ($t_0 \approx 13.5$ Gyr), which is considerably longer than a human lifetime. It would therefore be farfetched to even consider 'watching the Universe expand in real time. And yet, there is great interest at the prospect of actually measuring the evolving redshift of distant sources via a campaign lasting several decades. For example, using the European Extremely Large Telescope for observations.

Red Shift Drift

Cosmology today is based on the Friedmann-Lemaıtre-Robertson-Walker (FLRW) metric (**See Section IV**) for a spatially homogeneous and isotropic three-dimensional space, expanding or contracting according to a time-dependent expansion factor, $a(t)$: This form of the FLRW metric is written using the coordinates of a comoving observer, for whom t is the cosmic time (and is the same everywhere), r is the comoving radius, which remains fixed for any source lacking so-called peculiar motion. Every physical distance in FLRW should be product of a fixed comoving radius r and $a(t)$.

Cosmic Acceleration

The most reliable information on $a(t)$ comes in EM waves, shifted in frequency, ν, by the combined effects of kinematic and gravitationally induced redshift effects. The null geodesic equation describing the propagation of such waves along the $-\hat{}$r direction, with fixed θ and φ, is obtained from the equation: $cdt = -a(t)\,dr$

Thus, an electromagnetic signal emitted at r_e, at time t_e, will reach the observer at time t_0 given by

$$\int_{t_e}^{t_0} \frac{dt}{a(t)} = r_e$$

See Section V. Distances in Cosmology

this equation tells us how t_0 changes as a function of t_e due to the evolution of $a(t)$ between these two times. For example, if we consider the emission and detection of two crests of the wave, one a t_e and t_0, and the second at

$t_e + \delta t_e$ and $t_0 + \delta t_0$, then $\int_{t_e+\delta t_e}^{t_0+\delta t_0} \frac{dt}{a(t)} = \int_{t_e}^{t_0} \frac{dt}{a(t)}$

By definition: $z \equiv \frac{\lambda_0 - \lambda_e}{\lambda_e}$

Doppler Shift

substituting $\nu = c/\lambda$ and $\frac{\nu_e}{\nu_0} = \frac{\delta t_0}{\delta t_e}$, gives $1 + z = \frac{a(t_0)}{a(t_e)}$

$$1 + z = \sqrt{\frac{1 + v/c}{1 - v/c}}$$

this relation gives us the redshift corresponding to cosmic evolution over millions and billions of years. It is hardly useful as a probe of the change occurring over a mere human lifetime. It is necessary for us to derive from this Equation

an expression yielding the incremental changes in z expected during a much shorter time interval δt_0.

Differentiating the above equation for $1 + z$ with respect to the observer's time δt_0, we find that

$$\frac{dz}{dt_0} = [1 + z(t_0)]H(t_0) - \frac{a(t_0)}{a(t_e)^2}\frac{da(t_e)}{dt_e}\frac{dt_e}{dt_0}$$

Given Hubble Parameter: $H(t) = \frac{1}{a(t)}\frac{da(t)}{dt}$ and $dt_0 = [1 + z(t_0)]\,dt_e$

this finally gives: $$\frac{dz}{dt_0} = (1+z)H_0 - H(z)$$

During a monitoring campaign, the surveys will measure the spectroscopic velocity shift, Δv, defined in terms of the redshift drift Δz over an observation time Δt. The goals is to measure spectroscopic velocity shifts of < 1 cm s^{-1} yr^{-1}. Then the redshift drift can then be used to determine the real time values of the standard ratios for mass, radiation and dark energy:

$$H\_H_{0\nu}(z, \Omega_m) := \sqrt{\Omega_m \cdot (1+z)^3 + \Omega_{r0} \cdot (1+z)^4 + \Omega_{\Lambda 0}}$$

Refer to Section V. Distances in Cosmology

For example, in the simplified approach of assuming a spatially flat Universe (i.e., $k = 0$) and dark energy in the form of a cosmological constant Λ (with $w_{de} = -1$),

the monitoring of Δv should provide a direct measurement of Ω_m, and therefore of $\Omega_{de} \equiv \Omega_\Lambda = 1 - \Omega_m$.

To illustrate the potential for carrying out this groundbreaking work, we show in the Figure below the variation of $\Delta v/\Delta t$ (in units of cm s^{-1} yr^{-1}) with redshift and the matter density Ω_m.

$$dvdt(z, \Omega_m) := c \cdot \frac{\left[(1+z) - H\_H_{0\nu}(z, \Omega_m)\right] \cdot H_0}{(1+z) \cdot cm \cdot s^{-1} \cdot yr^{-1}}$$

Plot Below Shown *with Ω_m values of 0.1, 0.2, 0.315, and 0.5*

Example of How Measurement of Universe's Real Time Cosmic Expansion by Spectroscope drift can be used to Fit Cosmological Model Parameter Values to these Measurements of Cosmic Drift (Δv/Δt cm/sec /year)

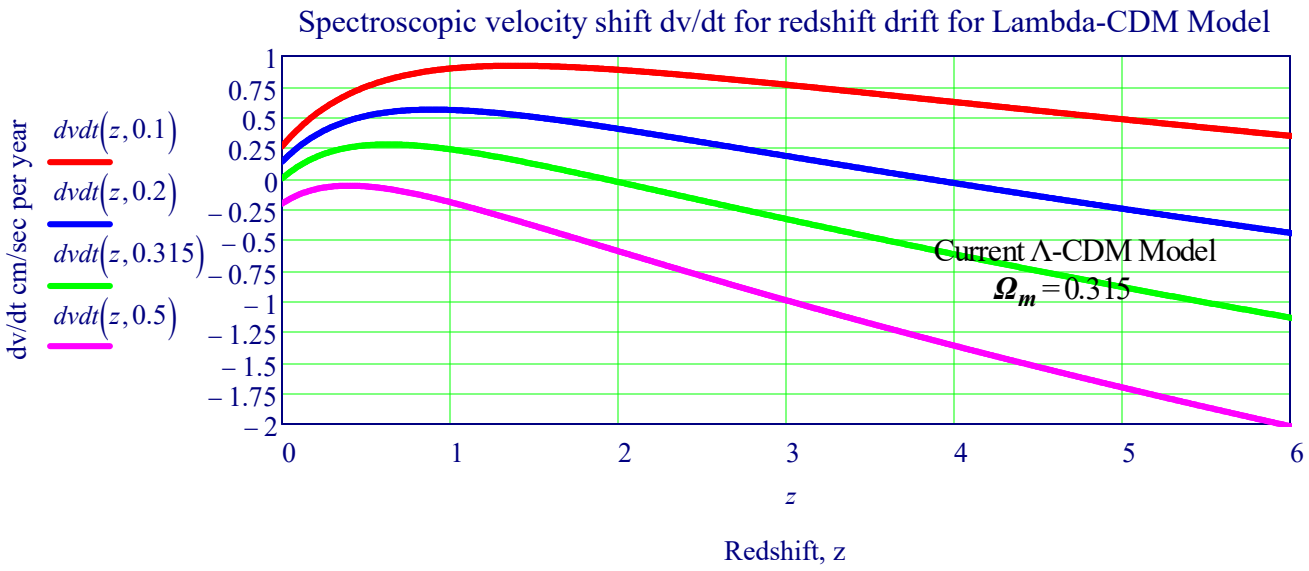

Spectroscopic velocity shift $\Delta v/\Delta t$ associated with the redshift drift predicted by the Planck-ΛCDM model ($k = 0, \Omega_m = 0.315, H_0 = 69.8$ km s^{-1} Mpc^{-1} ; thick black line), and several variations with alternative values of Ω_m (indicated in the plot).

In every case, dark energy is assumed to be a cosmological constant, Λ, with $w_{de} = -1$ and $\Omega_\Lambda = 1 - \Omega_m$.

Notice, e.g., that the redshift drift with time is positive at low redshifts, and then turns negative or the more distant sources. This **unambiguous prediction by the standard model** is simply based on the temporal evolution of the matter (ρ_m) and dark-energy (ρ_{de}) densities, which sees the Universe dominated by ρ_m at $z > 0.7$, giving way to the latter towards the present. In ΛCDM, dark energy functions as an agent of acceleration, whereas a matter-dominated cosmos is always decelerating. Planck-ΛCDM has been quite successful in accounting for a broad range of cosmological observations, but careful scrutiny reveals several major fundamental problems with its theoretical foundation.

There are few instances in science when the anticipated impact of an experiment carries this much weight.

XV. Stellar Flares Introduction:

Stellar Flares: Power bursts of energy from stars resulting from magnetic fields. Almost all stars in the Universe with convection zones produce stellar flares - bursts of energy emitted from the star that are thought to be caused by magnetic reconnection.

Light Curve File: Time series data for a target pixel file of a specific star that shows the change in brightness. Light curves are saved as text files, with 10 columns and two header lines.

A Light Curve flare characteristic is a **rapid rise followed by a slow decline process**.

Our Sun is a G-type star, or "yellow dwarf." It has a rotational period approximately 25 days at its equator, but varies depending on latitude, with the polar regions taking longer to rotate, reaching up to 35 days; this phenomenon is called differential rotation. G defined by strong absorption lines from ionized calcium; more generally, absorption lines from metals are stronger in G-type stars than in hotter stars (such as F-type stars) and weaker than in cooler stars (such as K-type stars). G-type stars have typical (effective) temperatures between around 5200 Kelvin (K) and 6000 K. Our sun is an old star ≈ 10 GYr.

Red dwarfs (or M-dwarf) are by far the most common type of fusing star in the Milky Way. A red dwarf is the smallest kind of star on the main sequence with
2000 to 3,900 K temperature and 0.08 to 0.6 $M_\odot$ mass. M-dwarfs make up 75% of nearby stars.

Flare Properties of Small Stars

The amplitude of stellar flares from small stars (such as red dwarfs or other low-mass stars) tends to decrease with increasing mass and temperature for several reasons. This phenomenon is related to the way magnetic activity, which drives stellar flares, is influenced by the star's mass and internal properties. Explosion of stellar flares can release enormous energy, mainly caused by the magnetic reconnection process in the coronal region.

1. Magnetic Activity and Stellar Mass:

Low-Mass Stars (Red Dwarfs):
Low-mass stars are typically more active magnetically. These stars have stronger magnetic fields relative to their size, which means they are more prone to flare activity. The magnetic dynamo in low-mass stars (the process that generates their magnetic field) operates more efficiently due to their relatively slower rotation rates, higher levels of magnetic flux, and a more vigorous convective envelope.

High-Mass Stars:
Higher-mass stars (such as G-type or A-type stars) have weaker magnetic fields and less intense convection, which means they generate fewer flares. Their magnetic dynamos tend to be less efficient, and because they rotate faster, the magnetic activity is often more evenly spread out over the star's surface, preventing highly energetic flares. Essentially, these stars are less magnetically active overall.
Effect on Flare Amplitude: Low-mass stars (e.g., red dwarfs) experience frequent, intense flares because of their strong magnetic fields, higher-mass stars experience fewer, less intense flares due to weaker magnetic activity.

2. Temperature and Stellar Activity:

Cooler Stars:

Cooler, lower-mass stars (like red dwarfs) have deeper convection zones. These convection zones, combined with the star's relatively slow rotation, create large, localized magnetic fields that can produce powerful flares. The cool Temperature allow for more pronounced magnetic field interactions at the surface, leading to stronger flares.

Hotter Stars:

As a star's mass increases, it tends to be hotter, and this increases its luminosity and temperature.
For these hotter stars (e.g., F-type, G-type), the convective regions are smaller and less dynamic, which means that the magnetic field generation is weaker. Hotter stars also tend to rotate more quickly, which can cause their magnetic fields to become less concentrated in localized regions and reduce flare activity.

Effect on Flare Amplitude: As temperature increases, the star's magnetic field becomes less effective at producing high-amplitude flares. The smaller convection zones in hotter stars limit the intensity of the magnetic activity that drives flares.

Rotation Rate: Slower Rotators:

Small, low-mass stars **like red dwarfs** typically rotate **more slowly** compared to more massive stars. This **slower rotation** allows for a **more stable and concentrated magnetic field**, which can result in more frequent and intense flare events.

Faster Rotators:

More massive stars tend to rotate faster. The fast rotation leads to a more diffuse magnetic field, which, while still present, is not as concentrated in specific regions. This reduces the likelihood of intense flare events since the magnetic field is more spread out and less prone to the localized instabilities that cause flares.

Effect on Flare Amplitude:

The slower rotation in low-mass stars helps build up stronger magnetic fields that can lead to large, energetic flares. In higher-mass stars, the faster rotation leads to more spread-out, weaker magnetic fields, and hence weaker flares.4. Star's Life span and Magnetic Activity:Red Dwarfs

Low-Mass Stars:

These stars have long lifetimes, often on the order of tens to hundreds of billions of years. Their magnetic fields remain active throughout their long lives, and they continue to experience flares. They are also more prone to "flare events" because of their strong, active magnetic dynamos.

Higher-Mass Stars:

These stars have shorter life spans, and their magnetic activity typically wanes more quickly as they age. As they exhaust their nuclear fuel, the mechanisms that generate strong magnetic fields become less effective. Thus, their flare activity decreases with age.

Mass and Temperature Effects:

As stellar mass and temperature increase, the star's magnetic activity decreases because:
More massive stars have weaker magnetic fields and less efficient magnetic dynamos.
Hotter stars have smaller convection zones, which limits the dynamo's efficiency and reduces flare activity.
Faster rotation in more massive stars results in more diffused magnetic fields, leading to weaker flares.

Thus, the amplitude of stellar flares tends to decrease as both stellar mass and temperature increase: Primarily due to the diminished strength of the magnetic activity that drives flare events in these stars.

Light curves for Exoplanet Survey Data

For a comprehensive description of all known Exoplanets refer to the NASA Exoplant Archive:
https://exoplanetarchive.ipac.caltech.edu/cgi-bin/TblView/nph-tblView?app=ExoTbls&config=PS&constraint=default_flag=1&constraint=disc_facility+like+%27%25TESS%25%27

Exoplanet light curve
https://exoplanets.nasa.gov/exoplanet-watch/about-exoplanet-watch/background/
A light curve can show the change in brightness of a star when an exoplanet passes in front of the star. We can't see the exoplanet directly using the transit method, but we can see the effect the exoplanet has on its star's brightness as it transits.

The horizontal part of the light curve is the baseline brightness of the star when there are no exoplanets passing in front of it. The dip in the light curve shows the star's light blocked by the exoplanet during the transit. The deeper the dip, the more light is blocked, the bigger the planet. If you observe the same star over many nights, you can see how often the star's light is blocked by a transiting exoplanet. The more frequently these transits occur, the shorter the year is for the exoplanet, and the hotter the planet is. By looking at light curves, you can even tell whether the planet has a thick atmosphere.

When we create light curves, we compare the brightness of the target star with the brightness of a few nearby comparison stars, or comp stars. It's important to choose comp stars that are not variable stars (stars whose brightness changes over time), so we use star charts from the American Association of Variable Star Observers (AAVSO) to help us identify stars with stable brightness to compare with our target star.

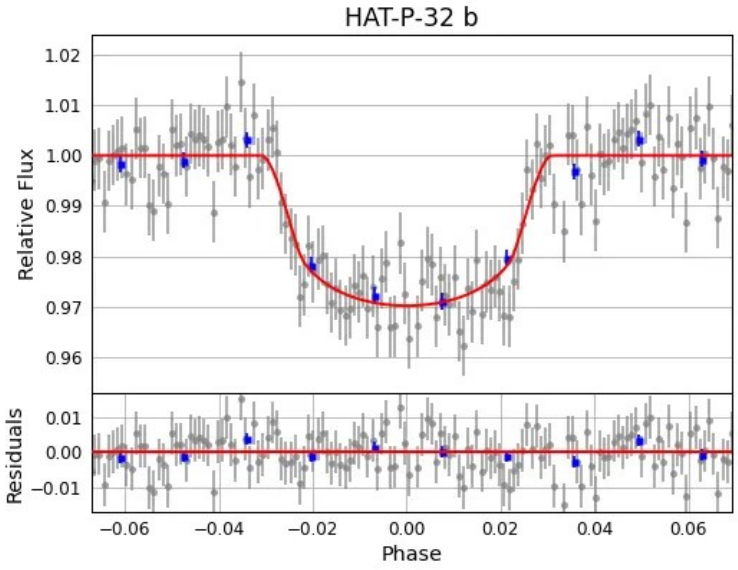

"Detrending data" means to **remove any noticeable trend or pattern (usually a linear increase or decrease)** from a dataset, effectively **leaving behind only the fluctuations around that trend**, allowing for a **more focused analysis on the variability** within the data **without the influence of the overall trend line;** this is typically achieved by **fitting a line to the data** and **subtracting that fitted line** from the original data points.

The flare energy is calculated using the following equation

$$E_{\text{flare}} = 4\pi R_*^2 \sigma_{\text{SB}} T_*^4 \int F_{\text{flare}}(t)\mathrm{d}t$$

Mikulski Archives - Space Telescopes

The Mikulski Archive for Space Telescopes (MAST) is an astronomical data archive focused on the optical, ultraviolet, and near-infrared. MAST hosts data from over a dozen missions like Webb, Hubble, Kepler, Transiting Exoplanet Survey Satellite (TESS), and in the future Rome.
TESS's two-year all-sky survey would focus on nearby G-, K-, and M-type stars with apparent magnitudes brighter than magnitude 12 and 1,000 of the closest red dwarfs.

MAST TESS Transients Light Curve Files

https://tess.mit.edu/public/tesstransients/pages/readme.html
TESS periodically reads out entire frame of all four cameras, nominally every 30 minutes (below says 10 minutes).

MAST Light Curve File Text Format

BTJD TJD cts_per_s e_cts_per_s mag e_mag bkg

TJD	TESS Julian date, equal to Julian Data, JD - 2457000
BTJD	Barycentric TESS Julian Date (Day + Fraction of Day) - Relativistic coordinate time scale
cts_per_s	Flux light curve in counts per second (photoelectrons per second).
e_cts_per_s	Uncertainty in cts_per_s (1-sigma).
mag	Light curve in TESS magnitudes (see Flux Calibration).
e_mag	Uncertainty in mag (1-sigma). A value of 99.9 marks a 3-sigma upper limit.
bkg	Local background in differential counts.

Get Data: $LCF := READPRN("lc\_2022sfe\_cleaned No Header.txt")$

$cols(LCF) = 7 \qquad rows(LCF) = 3760$

$Mag := LCF^{\langle 4 \rangle} \qquad Time := LCF^{\langle 1 \rangle} - 2797 \qquad Days := Time_{3759} - Time_0 = 27.16$

Choose 12 Days to View

$Time_{1900} = 14.264$

$Time_{2800} = 20.597$

TESS Measurement Interval: $(Time_1 - Time_0) \cdot 24 \cdot 60 min = 9.994 \cdot min$

Sample 12 Days of Data: $LCF_{12} := submatrix(LCF, 0, 1700, 0, 6) \qquad Time_1 := LCF_{12}^{\langle 1 \rangle}$

$min(LCF_{12}^{\langle 2 \rangle}) = -17.002 \qquad max(LCF_{12}^{\langle 2 \rangle}) = 67.942$

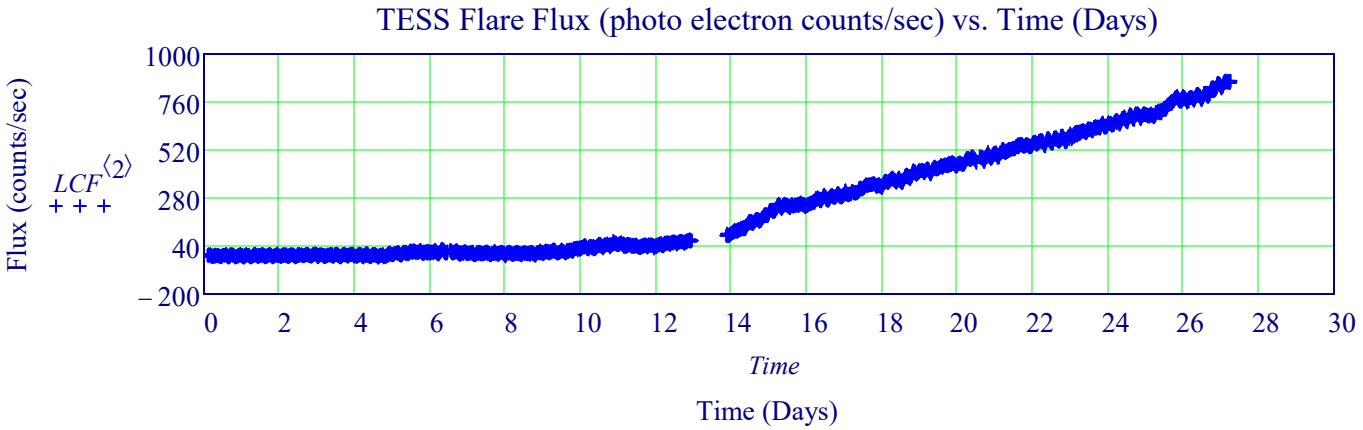

Detrend Data Reference Line: $Flux_{line}(tt) := 210 + 50 \cdot (tt - 15)$

Use Median Value to Smooth Flux Curve $SFlux := medsmooth(LCF^{\langle 2 \rangle}, 3)$

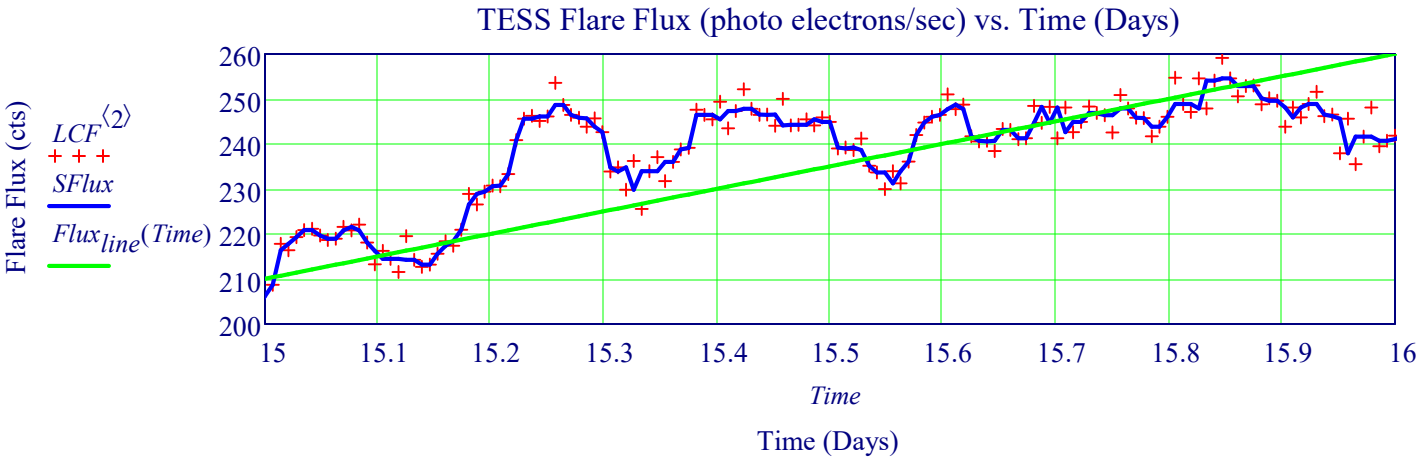

Flare Magnetic Activity and Physical Parameters of Exoplanet Host Stars

Based on LAMOST DR7, TESS, Kepler, and K2 Surveys,

The Astrophysical Journal Supplement Series, 261:26 (20pp) , 2022 August

Data Columns: **ID Peak Time Begin End Duration Amplitude Teff Radius Energy**

$TDat := READPRN("Data\Flare Parameters of Exoplanet System of TESS.txt")$

$KDat := READPRN("Data\Flare Parameters of Kepler.txt")$

$K2Dat := READPRN("Data\Flare Parameters of K2.txt")$

$TK2 := stack(TDat, KDat, K2Dat)$ $\quad temp := TK2^{\langle 6 \rangle}$

$Radius := TK2^{\langle 7 \rangle}$ $\quad R := line(temp, Radius)$ $\quad Rad(t) := R_0 + R_1 \cdot t$

$Energy := TK2^{\langle 8 \rangle}$ $\quad E := expfit(temp, Energy)$ $\quad E_T(T) := E_0 \cdot exp(E_1 \cdot T) + E_2$

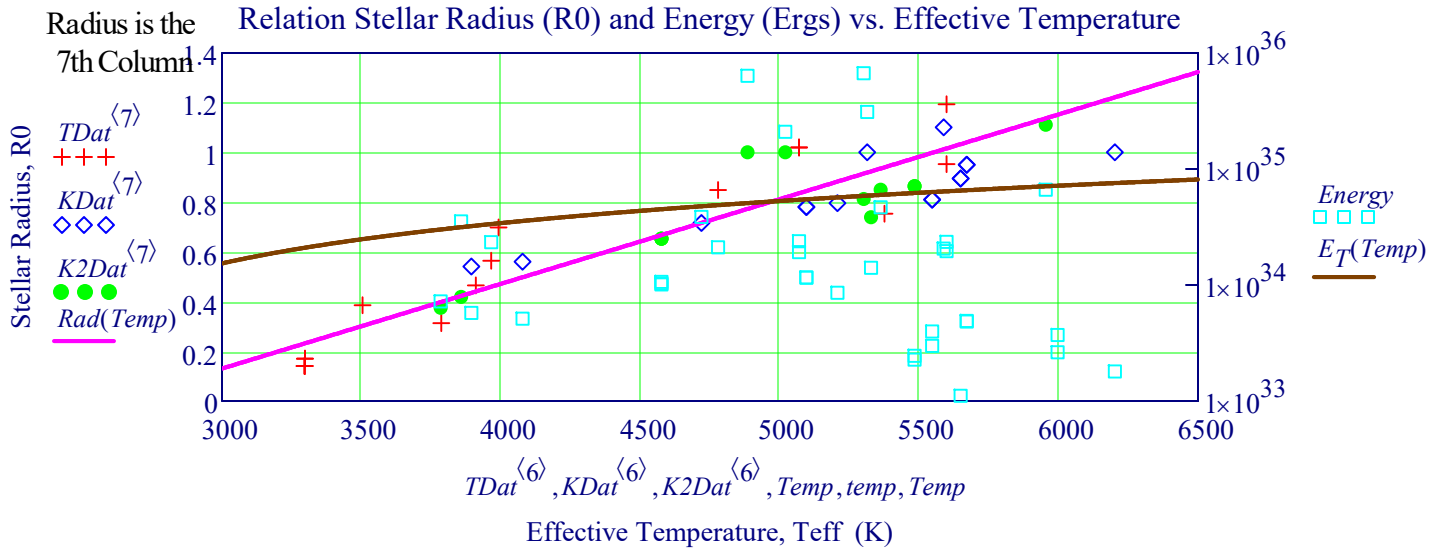

Intro to TESS

The Transiting Exoplanet Survey Satellite (TESS) is a NASA-sponsored Astrophysics Explorer-class mission that is performing a near all-sky survey to search for planets transiting nearby stars. TESS completed its primary mission in July of 2020, and has now entered its extended mission. The current extended mission will last until September 2022, and will continue to scan the sky for exoplanets and transient events. The TESS mission is now more community focused with a larger guest investigator (GI) program.

Over the last three years TESS has observed both the northern and southern hemispheres, with each hemisphere being split into ≈13 sectors. Each sector is observed for ≈27 days by TESS's four cameras.

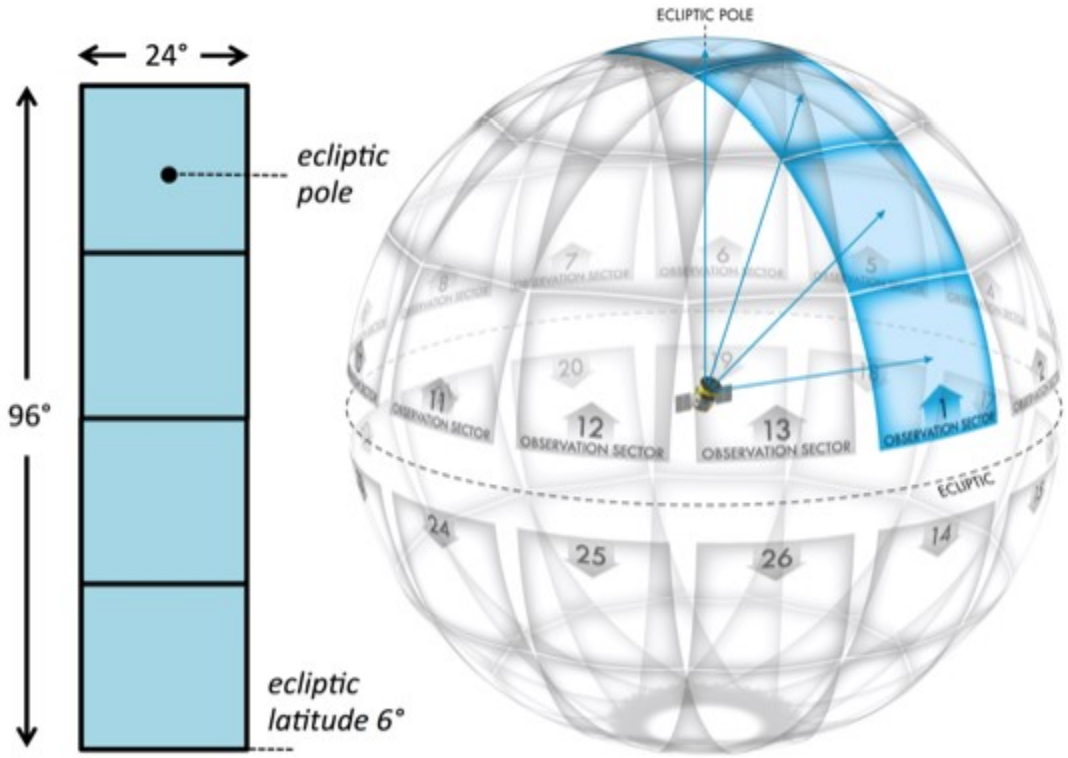

The main data products collected by the TESS mission are described below.

Full Frame Images (FFIs): The full sector images, with a cadence of 30-min (years 1 & 2) or 10-min (years 3 & 4).

Target Pixel Files (TPFs): Postage stamp cut outs from the FFIs, focused on a selected target of interest. Each stamp has a cadence of 2-min or 20-sec.

Light Curve Files (LCFs): The time series data produced for each 2-min or 20-sec TPF object.

Info on the TESS mission and its data products, available at TESS GI pages.

Light Curve Data Sources

https://exoplanetarchive.ipac.caltech.edu/

https://heasarc.gsfc.nasa.gov/docs/tess/TESS-Intro.html

Lightkurve

Lightkurve offers a user-friendly way to analyze time series data obtained by telescopes, in particular NASA's Kepler and TESS exoplanet missions. You can search for the various data products for TESS on MAST using the various Lightkurve functions for Full Frame Images, Target Pixel Files, or Light Files for Specific Objects.

https://github.com/lightkurve/lightkurve/blob/48b406a2133267fc03f09d115ecd5cd95a35c702/src/lightkurve/search.py#L723

XVI. Early Galaxy Formation and JWST Mass-Growth Tension

The formation and evolution of galaxies represent one of the most direct observational manifestations of cosmic structure growth and provide a critical testing ground for cosmological models. Within the standard ΛCDM framework, galaxies form hierarchically as small density perturbations in the primordial matter distribution grow through gravitational instability. Dark matter collapses first, forming virialized halos that act as gravitational potential wells into which baryonic matter falls. Gas accretion, radiative cooling, and angular momentum redistribution then enable the formation of rotationally supported disks and spheroidal stellar components. Over cosmic time, mergers, feedback processes, and secular evolution further shape galactic structure, leading to the diverse population of galaxies observed in the present-day Universe.

Observationally, galaxy evolution has been mapped across a wide range of redshifts through deep surveys conducted with ground-based telescopes and space observatories such as the Hubble Space Telescope. These studies have established robust trends in galaxy size, stellar mass, star formation rate, metallicity, and morphology as functions of redshift. At moderate redshifts ($z \lesssim 3$), galaxies are observed to grow steadily in stellar mass, with star formation rates that peak around $z \sim 2$ and decline toward the present epoch. Morphological transformations, including the emergence of bulge-dominated systems and quiescent ellipticals, are commonly associated with mergers, environmental effects, and feedback from supernovae and active galactic nuclei. Taken together, these observations have largely supported a picture of gradual, regulated galaxy growth embedded within an expanding Universe dominated by dark matter and dark energy.

From a theoretical perspective, the evolution of galaxy structure is governed by a complex interplay of physical processes operating across a wide range of spatial and temporal scales. Gas cooling and star formation occur on sub-kiloparsec scales, while halo growth and mergers unfold over cosmological volumes. Feedback mechanisms—such as stellar winds, supernova explosions, and radiation pressure—play a crucial role in regulating star formation efficiency and redistributing baryons within and beyond halos. As a result, galaxy evolution models rely on a combination of analytic prescriptions, numerical simulations, and semi-empirical scaling relations to connect fundamental cosmological parameters to observable galaxy properties. Despite these complexities, the ΛCDM paradigm has proven remarkably successful in reproducing the broad statistical properties of galaxies across most of cosmic history.

The advent of the James Webb Space Telescope has extended observational access to the earliest phases of galaxy formation, probing redshifts beyond $z \sim 10$ and into the first few hundred million years after the Big Bang. JWST observations have revealed candidate and spectroscopically confirmed galaxies at epochs previously thought to be dominated by small, chemically primitive systems. Some of these early galaxies appear unexpectedly luminous and massive given the limited cosmic time available for star formation and mass assembly. These findings highlight the importance of reassessing assumptions about star formation efficiency, gas accretion rates, feedback strength, and the initial conditions of galaxy formation in the early Universe.

Importantly, the detection of massive and luminous galaxies at very high redshift does not, by itself, imply a failure of the standard cosmological model. Rather, it underscores the need to carefully quantify the physical limits imposed by cosmic time, baryon availability, and feedback processes. At extreme redshifts, even modest changes in star formation efficiency or halo growth rates can lead to large differences in observable galaxy properties. Consequently, early galaxy observations provide a sensitive probe of the high-redshift regime where standard scaling relations may approach their limits of applicability.

In this context, simplified or "toy" models of early galaxy formation serve a valuable diagnostic role. By isolating key parameters—such as halo growth, baryon inflow, star formation efficiency, and outflow strength—such models allow one to explore the conditions under which early galaxies can assemble substantial stellar mass within a short time. These approaches do not seek to replace detailed numerical simulations, but rather to clarify the parameter space consistent with observations and to identify where tensions may arise. The implications of recent JWST discoveries for early galaxy growth, including quantitative mass–growth constraints inferred from high-redshift systems, are examined in detail in Section XXVIII.

A. Structural Measurement Methods: Non Parametric

Recent measurement technique involves the non-parametric method of measuring galaxy light distributions. Non-parametric methods of measuring galaxy structure began in the photographic era with attempts to quantify the light concentration in galaxies by Morgan (1962), although extensive quantitative measures were not done until the mid-1990s. At present, the most common methods for measuring galaxy structure in a non-parametric way is through the CAS system (e.g., Conselice 2003) and through similar parameters (Takamiya 1999). These parameters are designed to capture the major features of the underlying structures of these galaxies, but in a way that does not involve assumptions about the underlying form, as is done with the S´ersic fitting.

Asymmetry Index. One of the more commonly used indices is the asymmetry index(A) which is a measure of how asymmetric a galaxy is after rotating along the line of sight center axis of the galaxy by 180 deg (Figure 2). It can be thought of as an indicator of what fraction of the light in a galaxy is in non-symmetric components. The basic formula for calculating the asymmetry index (A) is given by:

$$A = \min\left(\frac{\Sigma|I_0 - I_{180}|}{\Sigma|I_0|}\right) - \min\left(\frac{\Sigma|B_0 - B_{180}|}{\Sigma|I_0|}\right)$$

Where I_0 represents is the original galaxy image, $\boldsymbol{I_{180}}$ is the image after rotating it from its center by 180°. The measurement of the asymmetry parameter however involves several steps beyond this simple measure. This includes carefully dealing with the background noise in the same way that the galaxy itself is by using a blank background area (B_0), and finding the location for the center of rotation. The radius is usually defined as the Petrosian radius at which $\eta(R) = 0.2$, although once out to large radius the measured parameters are remarkably stable. Operationally, the area B_0 is a blank part of the sky near the galaxy. Typical asymmetry values for nearby galaxies are discussed in Conselice (2003) with ellipticals having values A ~ 0.02 ± 0.02, while spiral galaxies are found in the range from A ~ 0.07 − 0.2, while for Ultra-Luminous Infrared Galaxies (ULIRGs), which are often mergers, the average is A ~ 0.32 ± 0.19, and for merging starbursts A ~ 0.53 ± 0.22

Galaxy Morphology and Structure allows a new way to compare with cosmologically based galaxy formation models, as well as those which include extensive physics such as starformation, AGN feedback and supernova in more detailed hydrodynamical models.

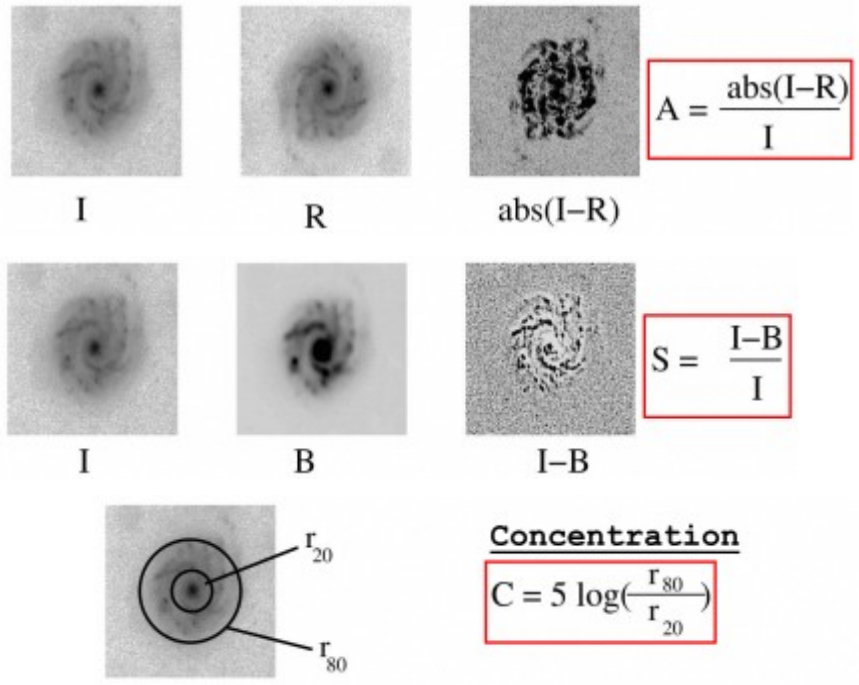

A graphical representation of how the concentration (C), asymmetry (A), clumpiness (S) are measured on an example nearby galaxy. Within the measurements for A and S, the value '***I***' represents the original galaxy image, while '***R***' is this image rotated by 180 deg. For the clumpiness S, 'B' is the image after it has been smoothed (blurred) by the factor $0.3 \times r(\eta = 0.2)$. The details of these measurements can be found in Conselice et al. (2000a) for asymmetry, A, Bershady et al. (2000) for concentration, C, and Conselice (2003) for the clumpiness index, S.

B. Galaxy Type Classification

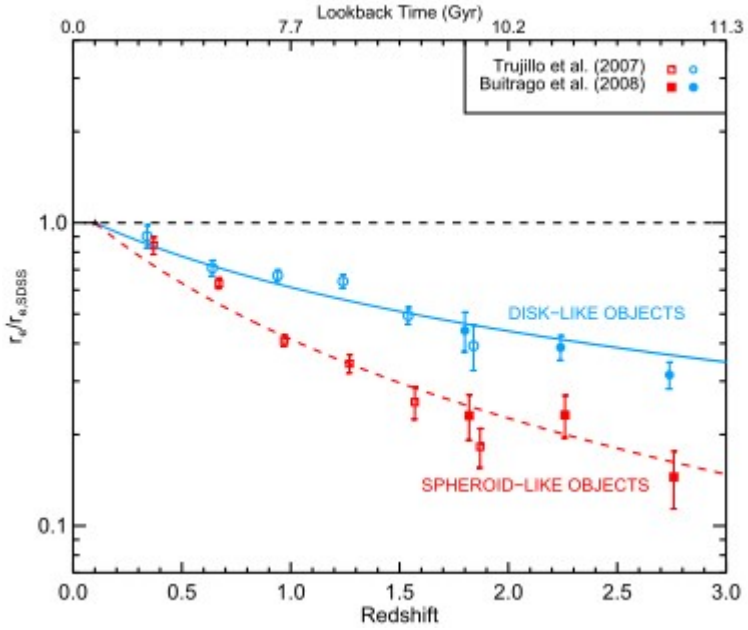

The average sizes of massive galaxies selected with Stellar Mass, $M* > 10^{11}$ $M_{\odot}$ as imaged in the POWIR (Conselice et al. 2007) $z < 2$ data and GNS > 1.5 images (Buitrago et al. 2008; Conselice et al. 2011). The size evolution is divided into galaxies with elliptical-like profiles, with Sersic indices (See below) $n > 2.5$, and disk-like profiles having $n < 2.5$. The measured effective radius, r_e , is plotted as a function of the ratio with the average size of galaxies at the same stellar mass measurements with $M* > 10^{11}$ $M_{\odot}$ at $z = 0$ from Shen et al. (2003).

The Sérsic Index controls the degree of curvature of the profile. The smaller the value, the less centrally concentrated the profile is and the shallower (steeper) the logarithmic slope at small (large) radii.

The average concentration (C), asymmetry (A), and clumpiness (SS) parameters for nearby galaxies as measured in the optical R-band (Conselice 2003).

Galaxy Type	Concentration (R)	Asymmetry (R)	clumpiness (R)
Ellipticals	4.4±0.3	0.02±0.02	0.00±0.04
Early-type disks (Sa-Sb)	3.9±0.5	0.07±0.04	0.08±0.08
Late-type disks (Sc-Sd)	3.1±0.4	0.15±0.06	0.29±0.13
Irregulars	2.9±0.3	0.17±0.10	0.40±0.20
Edge-on Disks	3.7±0.6	0.17±0.11	0.45±0.20
ULIRGs	3.5±0.7	0.32±0.19	0.50±0.40
Starbursts	2.7±0.2	0.53±0.22	0.74±0.25
Dwarf Ellipticals	2.5±0.3	0.02±0.03	0.00±0.06

The clumpiness (or smoothness) (***S***) parameter is used to describe the fraction of light in a galaxy which is contained in clumpy distributions. Clumpy galaxies have a relatively large amount of light at high spatial frequencies, whereas smooth systems, such as elliptical galaxies contain light at low spatial frequencies. Galaxies which are undergoing star formation tend to have very clumpy structures, and thus high S values.

The original image $\boldsymbol{I_{x,y}}$ is blurred to produce a secondary image, $\boldsymbol{I^{\sigma}_{x,y}}$ The size of the smoothing kernel σ is determined by the radius of the galaxy,

$$S = 10 \times \left[\left(\frac{\Sigma(I_{x,y} - I^{\sigma}_{x,y})}{\Sigma I_{x,y}} \right) - \left(\frac{\Sigma(B_{x,y} - B^{\sigma}_{x,y})}{\Sigma I_{x,y}} \right) \right]$$

Early Galaxy Formation (Toy Model)

Overview

Computations Python Program: **VXPhysics.com/Python/Early Galaxy Formation.py**

These figures illustrate a simplified ("toy") model of early galaxy formation in a ΛCDM cosmology, tracking the **coupled evolution of dark matter halos, baryonic gas, star formation, and chemical enrichment** from redshift $z \approx 25$ to $z \approx 6$.

Halo growth

Evolution of the dark matter halo mass as a function of redshift. The rapid growth at high redshift reflects the hierarchical nature of structure formation, where halos accrete mass efficiently due to the high cosmic density and merger rate in the early universe.

$$\dot{M}_{\rm halo} \approx K \left(\frac{M}{10^{12} M_\odot} \right)^{1.1} (1+z)^{2.5} \, M_\odot/\mathrm{yr}$$

Key physical idea:

Dark matter collapses first and provides the gravitational potential well that enables baryonic galaxy formation.

Baryon reservoirs

Evolution of the stellar mass (solid line) and cold gas mass (dotted line) within the halo. Gas is accreted from the halo, converted into stars through star formation, and depleted by stellar feedback-driven outflows.

Key physical idea:

Galaxy growth is governed by a competition between gas inflow, star formation, and feedback.

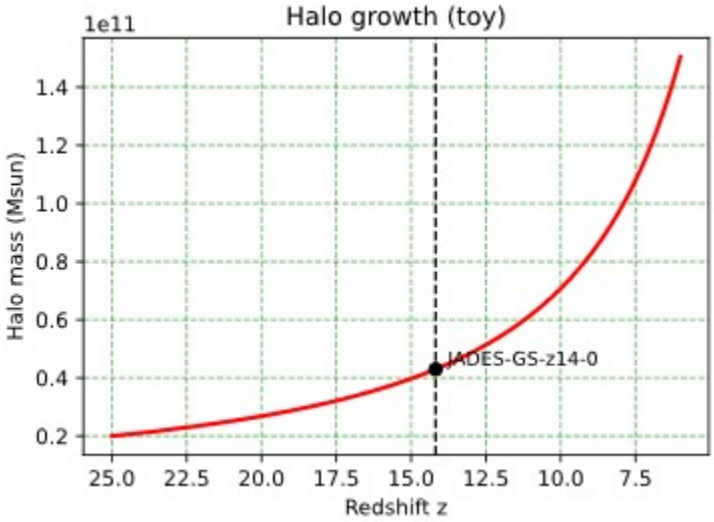

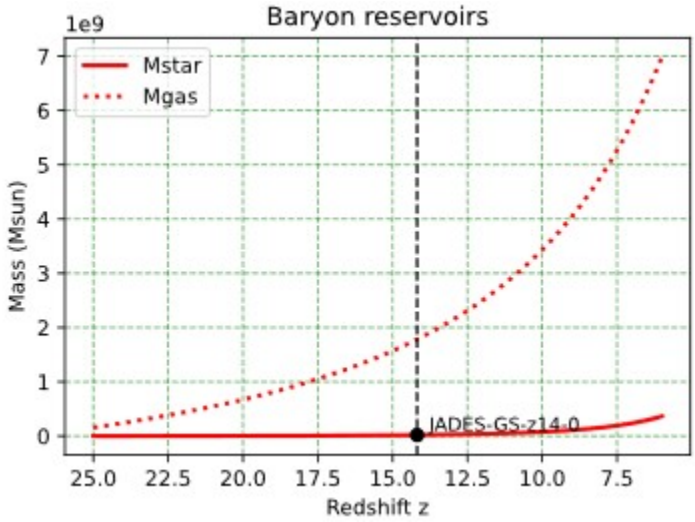

JWST Mass-Growth Tension: Galaxy Growth Dynamics

Dark matter halo formation (foundation)

What it represents

- The gravitational scaffolding where galaxies form
- Collapse of overdensities after recombination

Gas infall & cooling (first baryons)

What it represents

- Gas falling into dark matter halos
- Cooling via atomic hydrogen, molecular hydrogen (H_2)

What you can program

- Cooling time vs halo mass
- Virial temperature thresholds
- Gas accretion rates

$$t_{\rm cool} \sim \frac{3kT}{n\Lambda(T)}$$

Black hole seeds & early growth

Classic growth law: $M(t) = M_0 e^{t/t_E}$

How gas turns into stars when density exceeds a threshold

- Schmidt-Kennicutt laws
- Star-formation efficiency vs redshift
- Bursty vs steady star formation

Simple model $\dot{M}_\star = \epsilon \frac{M_{\rm gas}}{t_{\rm dyn}}$

Chemical enrichment (metals appear fast)

Gas Metallicity: What it represents

- Supernovae enriching gas with metals
- Transition from Pop III →Pop II stars
- Metallicity evolution
- Yield models
- Mixing timescales

$$Z(t) = \frac{M_Z(t)}{M_{\rm gas}(t)}$$

Dynamics with the Following Graphs

Star formation rate

Star formation rate (SFR) as a function of redshift, computed using a Schmidt-type star formation nal to the available cold gas mass. The elevated SFR at high redshift reflects the high gas densities and short dynamical times characteristic of early galaxies.

See Above: Cooling time Classic growth law Gas Metallicity

Key physical idea:

Early galaxies can form stars very rapidly, producing intense, bursty star formation episodes.

Gas metallicity (toy)

Evolution of the gas-phase metallicity, showing the progressive chemical enrichment of the interstellar medium by stellar nucleosynthesis. Metals are produced by short-lived massive stars and redistributed through feedback and gas flows.

Key physical idea:

Even very early galaxies can become chemically enriched on timescales of tens of Myr, consistent with metal detections in high-redshift JWST galaxies.

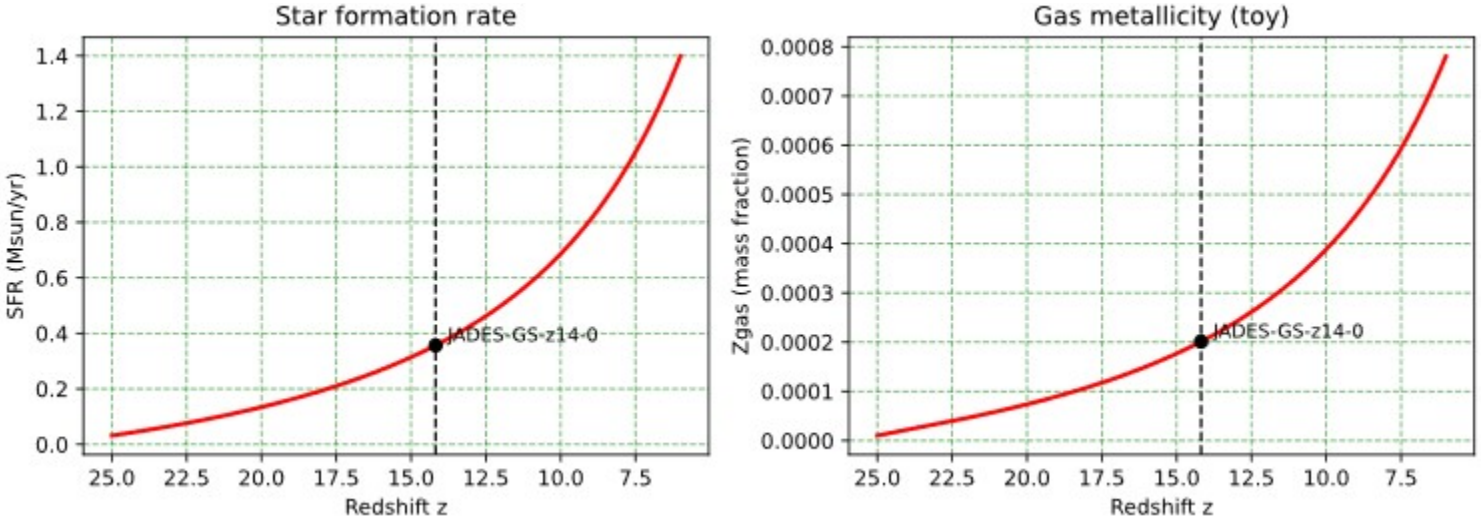

Computations Python Program: VXPhysics.com/Python/JWST Mass–Growth Tension.py

JWST Mass-Growth Tension Diagnostics

Diagnostic plots illustrating the "mass-growth tension" implied by very massive, UV-luminous galaxies at z ≈ 10–15. The panels quantify (i) the average star-formation rate required to assemble a given stellar mass within the available cosmic time, (ii) a toy upper envelope for star formation set by baryonic supply and a star-formation efficiency prescription, (iii) the exponential growth of black-hole seeds under Eddington or super-Eddington accretion, and (iv) the age of the Universe as a function of redshift in a flat ΛCDM cosmology. Together these show how inferred stellar or black-hole masses at high redshift translate into stringent constraints on formation redshift, duty cycle, accretion efficiency, and feedback-regulated baryon conversion.

Build M_* by z_{obs} — Required average SFR vs z_{form}

Required time-averaged star-formation rate $\langle \mathrm{SFR} \rangle$ needed to assemble a target stellar mass M_* by an observed redshift z_{obs}, as a function of the assumed onset of star formation z_{form}. The curve steepens rapidly for later z_{form} because the available cosmic time $\Delta t = t(z_{obs}) - t(z_{form})$ shrinks to tens of Myr at $z \gtrsim 10$. This panel highlights the basic "clock constraint": at fixed M_*, the inferred $\langle \mathrm{SFR} \rangle \propto 1/\Delta t$, so even modest increases in M_* or delays in z_{form} can require extreme SFRs or near-continuous duty cycles.

Toy SFR envelope at $z_{\rm obs}$ — Supply/efficiency limit

Toy upper envelope for the star-formation rate at $z_{\rm obs}$ as a function of halo mass, based on a simple baryon supply assumption $M_{\rm gas} \sim f_{\rm in} f_b M_{\rm halo}$ and a Schmidt-type scaling $\mathrm{SFR} \sim \epsilon\, M_{\rm gas}/t_{\rm dyn}$. The dashed horizontal line marks the required $\langle \mathrm{SFR} \rangle$ from panel (a) for a representative $z_{\rm form}$. Intersections (or lack thereof) illustrate whether the implied stellar buildup is plausible for a given halo mass without invoking unusually high baryon inflow, star-formation efficiency, or suppressed feedback. This panel reframes the tension as a comparison between required growth and available baryonic throughput.

JWST Mass-Growth Tension Diagnostics

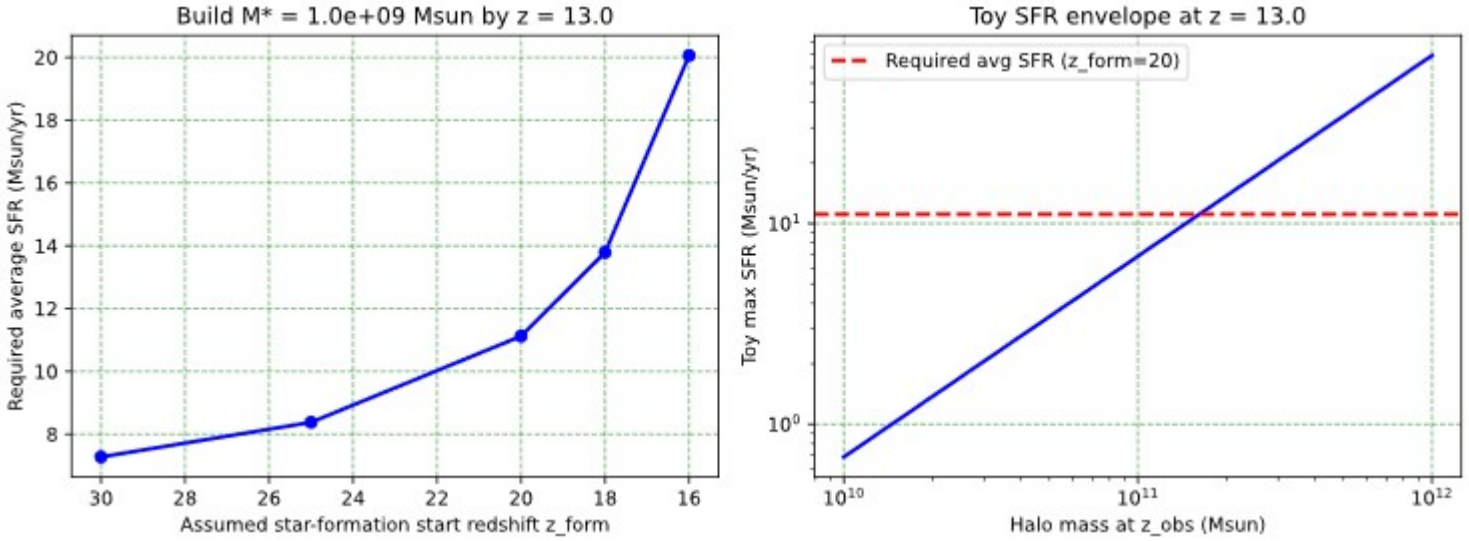

BH growth from $z_{\rm start}$ to $z_{\rm end}$ — Eddington constraint

Final black-hole mass achieved by seeds of different initial mass M_0 under sustained accretion at a fraction $f_{\rm Edd}$ of the Eddington rate, assuming radiative efficiency ϵ. Growth is exponential, $M(t) = M_0 \exp(\Delta t/t_{\rm Salp})$, where $t_{\rm Salp}$ is the Salpeter timescale. The strong sensitivity to $f_{\rm Edd}$ and M_0 illustrates why early supermassive black holes can be challenging: reaching $10^{8-9} M_\odot$ at high redshift may require heavy seeds (e.g., direct-collapse scenarios), super-Eddington phases, low radiative efficiency, or high duty cycle.

Cosmic time vs redshift (flat ΛCDM) — the time budget

Age of the Universe as a function of redshift in a flat ΛCDM cosmology, emphasizing that JADES-GS-z14-0 is observed only $\sim 280-300$ Myr after the Big Bang. The extremely short time intervals between $z \sim 20$ and $z \sim 14$ underpin the mass-growth tension: galaxies at these redshifts must form stars, enrich their gas, and build structure on timescales comparable to a single galactic dynamical time.

The Eddington constraint

states that there is a maximum luminosity—and therefore a maximum steady accretion rate—at which the outward force of radiation pressure on ionized gas exactly balances the inward force of gravity, limiting how rapidly mass can be accreted.

2. Physical balance behind the constraint

The Eddington limit arises from the balance between gravitational attraction acting on protons and radiation pressure acting primarily on electrons through Thomson scattering. When radiation pressure equals gravity, additional infalling material is prevented from accreting.

3. The Eddington luminosity

The Eddington luminosity is given by $L_{\rm Edd} = \frac{4\pi G M m_p c}{\sigma_T},$

which numerically evaluates to $L_{\rm Edd} \approx 1.26\times10^{38}\ (M/M_\odot)\ {\rm ergs}^{-1}$.

This represents the maximum steady luminosity for spherical accretion of ionized hydrogen.

4. Accretion rate associated with the Eddington limit

Relating luminosity to mass accretion via the Eddington accretion rate

where ϵ is the radiative efficiency, typically of order 0.1 for standard accretion disks.

$$L = \epsilon \dot{M} c^2,$$

5. The Eddington (Salpeter) timescale

If accretion proceeds continuously at the Eddington rate, mass grows exponentially with time. The characteristic e-folding timescale is known as the Salpeter time.

$$t_{\rm Salp} \approx 45\ {\rm Myr} \left(\frac{\epsilon}{0.1}\right).$$

6. Relevance to JWST-era galaxies

JWST observations reveal massive galaxies and black holes at redshifts $z \gtrsim 10$, when the Universe was only a few hundred million years old. The limited number of Eddington e-folding times available places strong constraints on how rapidly stars and black holes could have assembled.

7. Ways the constraint can be relaxed

The Eddington constraint is not absolute and may be alleviated through mechanisms such as super-Eddington accretion, reduced radiative efficiency, anisotropic radiation, high accretion duty cycles, or the presence of massive initial black-hole seeds formed by direct collapse.

8. Why it is a constraint rather than a strict law

The Eddington limit relies on simplifying assumptions, including spherical symmetry, steady accretion, and electron scattering opacity. Real astrophysical systems can temporarily exceed this limit, making it a useful benchmark rather than a strict physical prohibition.

Summary

The Eddington constraint provides a fundamental timescale and upper limit on mass growth by accretion, playing a central role in interpreting the rapid assembly of massive galaxies and black holes observed by JWST in the early Universe.

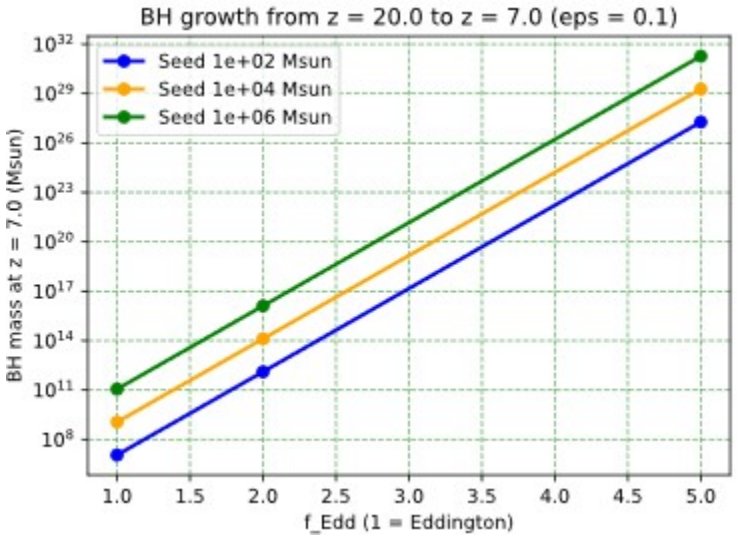

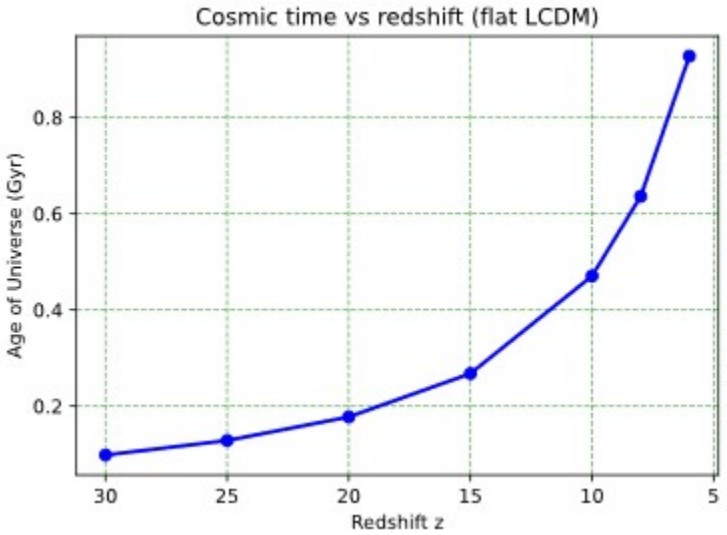

z14: Spectroscopically confirmed at z ≈ 14. Very luminous and extended for such an early time.

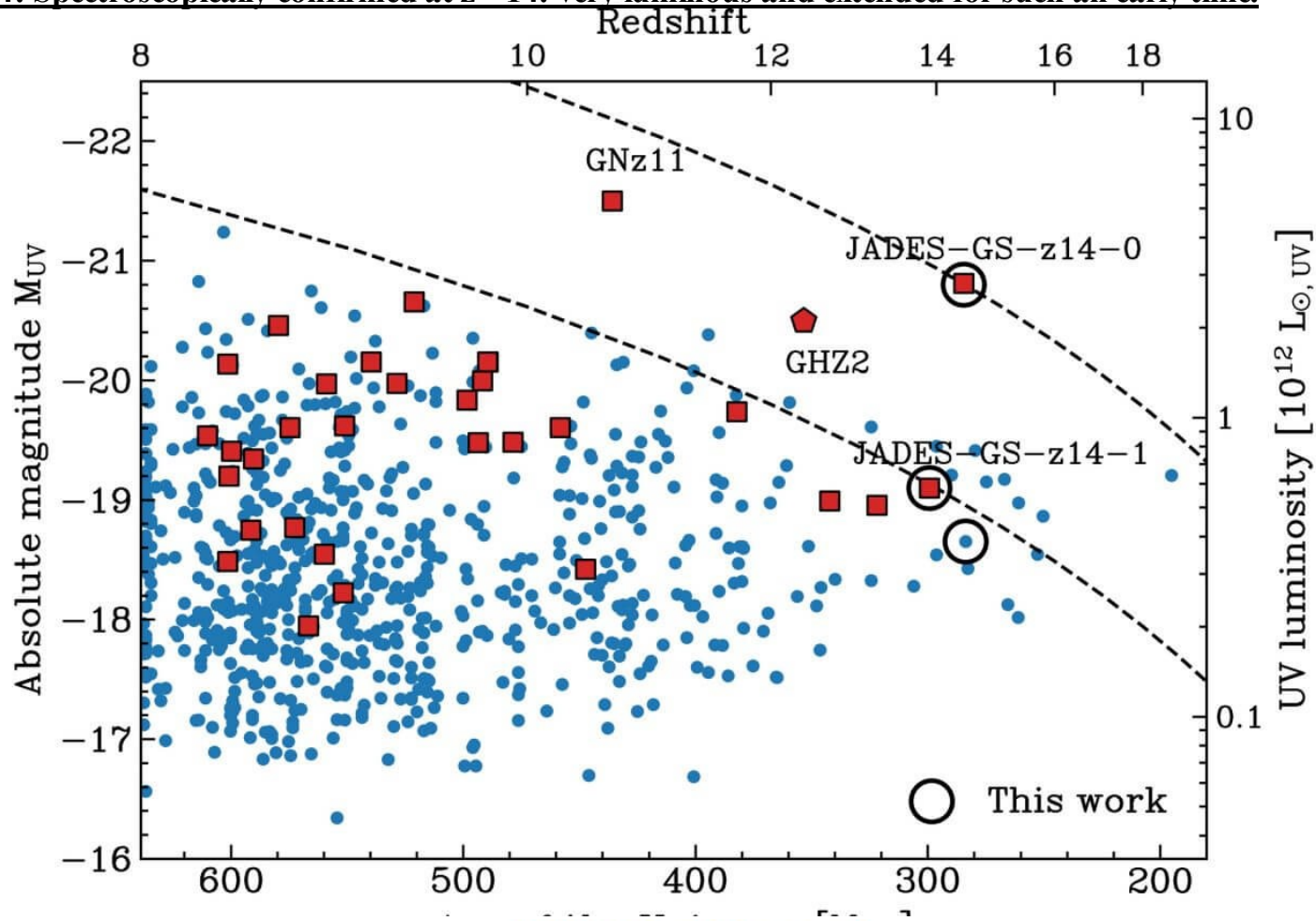

JADES-GS-z14-0

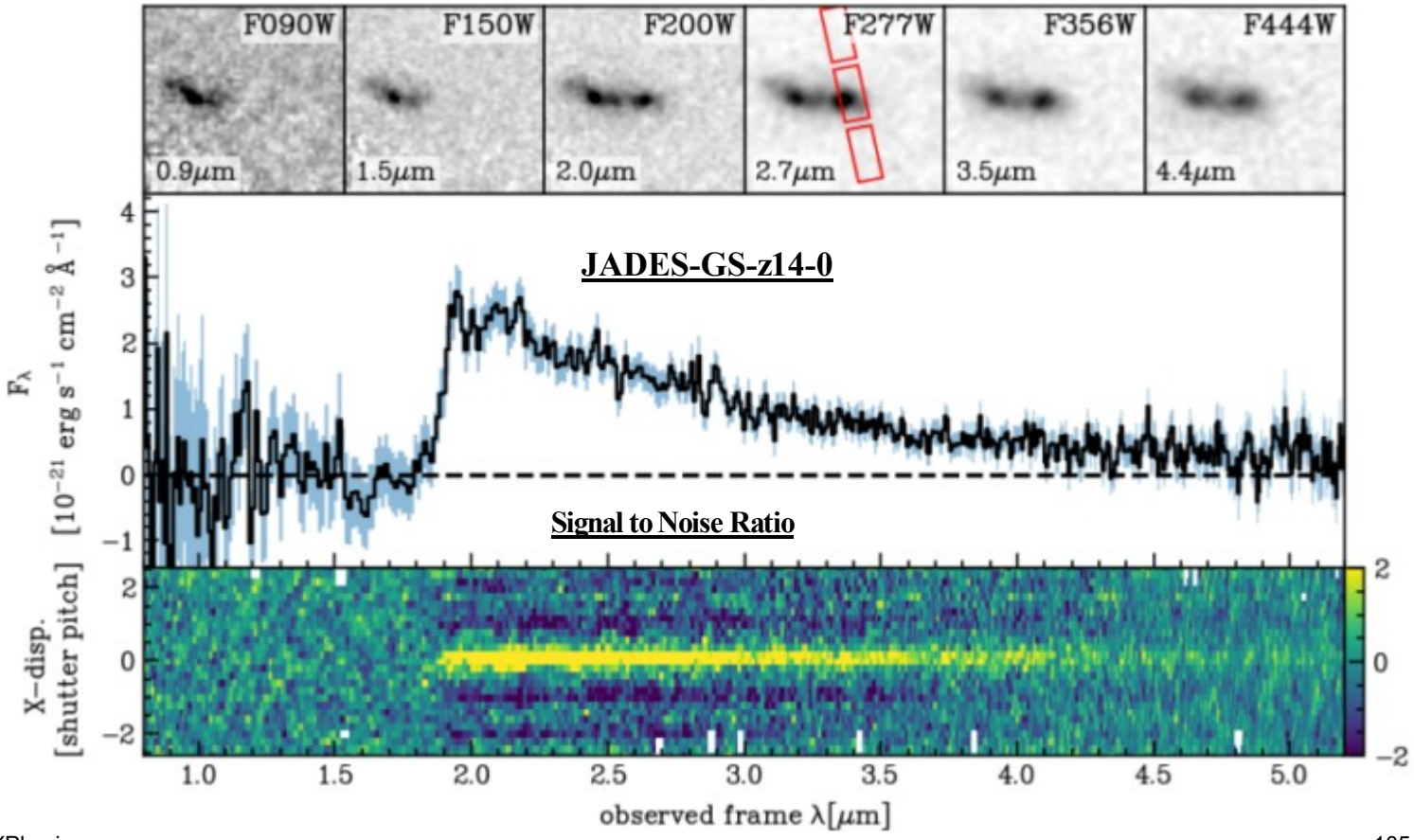

XVII. Various Estimates of Age, Mass, and Density of Universe

JADES CMB Mesurement*, H_{0JDC} $H_{0JDC} := 71 \frac{km}{s \cdot Mpc}$ $\frac{1}{H_{0JDC}} = 13.765 \cdot Gyr$

TWK Local Estimate, H_{twk}** $H_{twk} = 68.55 \cdot \frac{km}{s \cdot Mpc}$ $\frac{1}{H_{twk}} = 14.257 \cdot Gyr$

CMB Recombination Redshift/Cooling: $T_{rec}(z) := 2.7250 \cdot z$ $z_{CMB} := \frac{3000}{2.725}$ $z_{CMB} = 1101$

See Section IV. Equation of State $t_{CMB} := 13.8Gyr$

Critical Density, ρ_0 $\rho_0 := 8.6443584621592 \cdot 10^{-27} \cdot kg \cdot m^{-3}$

Matter-Radiation Equality: $H_{M\gamma}{}^2 = (8\pi G/3)\,\rho$ $H_{M\gamma} := \sqrt{\frac{8\pi G}{3}\rho_0}$ $\frac{1}{H_{M\gamma}} = 14.414 \cdot Gyr$

Hubble Constant from Gravitation Waves: $H_{grav} := 70 \frac{km}{s} Mpc^{-1}$ $Age_g := \frac{1}{H_{grav}}$ $Age_g = 13.962 \cdot Gyr$

See Section XV. Standard Candles

Estimate Lifetime of the Sun, $Age_\odot$ $Age_\odot := 10.8Gyr$

See Section XIIC. $M_{glxy} := 2 \cdot 10^{41} kg$ $r_{glxy\odot} := 26000Lyr$

***Sun's/Earth'a Galactic Years*, $GalYr_\odot$** $v_\odot := \sqrt{G \cdot \frac{M_{glxy}}{r_{glxy\odot}}}$ $GalYr_\odot := \frac{0.4 Age_\odot \cdot v_\odot}{2 \cdot \pi \cdot r_{glxy\odot}}$ $GalYr_\odot = 19\ Yrs_{glxy}$

Number of time the sun orbited Milky Way $v_\odot := 220 \frac{km}{s}$

Estimates of Age of Globular Clusters, Age_{GC} $Age_{GC} := 10Gyr$

See Section XIII.

Age of White Dwarfs from Cooling Curves of Local Galactic Disk*, Age_{WD}** $Age_{WD} := 8Gyr$

Numerical Modeling of Thermochemically Driven Fluid Flow With Non-Newtonian Rheology Applied to the Earth's Mantle, Age_{cool} $Age_{cool} := 4.5Gyr$

$t_{.est} := 4.8Gyr$

Half-Life of Uranium:

Percent Decay U_{238}, $PC_{U238} = N(t)/N_0$

$PC_{U238}(t) := \left(\frac{1}{2}\right)^{\frac{t \cdot Gyr}{t_{½Ur238}}} 100\%$ $\frac{PC_{U238}(t)}{\%}$

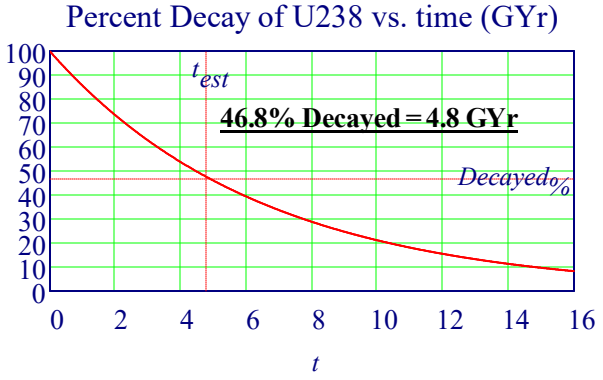

Half Life U238: $t_{½Ur238} := 4.47Gyr$

%U238 Decayed: $Decayed_\% := 46.8$

Roche Limit - Time of Recession of Moon **** $Age_{recession} := 1.3Gyr$

Parallax Distance, Event Horizon Telescope: Parallax Distance: $d_\pi(10 \cdot 10^{-3} arcsec, b) = 37368 \cdot lightyear$

See Section X. Black Hole, Messier M87*

* *XXIV. JADES: Lookback Time versus Red Shift and Age of Univ z = 13.2* Gyr

** *XIV. A. Current Value of Hubble's Law, H0. Data: NASA Galaxy Recession from 3645 Galaxies*, TWK

*** *The Cool White Dwarf Luminosity Function And the Age of the Galactic Disk*, S. K. Leggett

Measuring the of Age of the Universe - Globular Clusters

- Could place a lower limit from the **ages of astrophysical objects** (pref. the oldest you can find). e.g..
  - **1. Age of Globular clusters** in our Galaxy; known to he very old.
    Need stellar evolution isochrones to fit to color-magnitude diagrams
  - **2. Age of White dwarfs** from their observed **Luminosity Function** cooling theory and assumed star formation rate
  - **3. Age of Heavy elements**. produced in the first Supernovae; somewhat model-dependent
  - **4. Age-dating stellar populations in distant galaxies:**
    this is very tricky and requires modeling of stellar population evolution. with many uncertain parameters.
- Related to the **Hubble time** $t_H = 1/H_0$, but the exact value depends on the cosmological parameters

Ages of Globular Clusters

We measure the age of a globular cluster by measuring the **magnitude of the main sequence turnoff** or the difference between that magnitude and the level of the horizontal branch, and comparing this to stellar evolutionary models of which estimate the surface temperature and luminosity of stars as a function of time period
There are a fair number of uncertainties in these estimates, including errors and measuring the distances to the GC's, and uncertainties in the isochrones used to drive ages, that is, stellar evolutionary models.

Inputs to stellar evolution models include oxygen abundance [O/Fe] treatment of convection, He abundance, reaction rates of N + p O plus gamma. Heat diffusion, and conversions from theoretical temperatures and luminosity to observed colors and magnitudes, and opacities; and especially **distances.**

Wikipedia- Stellar Isochrone

"In stellar evolution, an isochrone is a curve on the Hertzsprung-Russell diagram, representing **a population of stars of the same age but with different mass**. The Hertzsprung-Russell diagram plots a star's luminosity against its temperature, or equivalently, its color. Stars change their positions on the HR diagram throughout their life. Newborn stars of low or intermediate mass are born cold but extremely luminous. They contract and dim along the Hayashi track, **decreasing in luminosity but staying at roughly the same temperature**, until reaching the main sequence directly or by passing through the Henyey track. Stars evolve relatively slowly along the main sequence as they fuse hydrogen, and after the vast majority of their lifespan, all but the least massive stars become giants. They then evolve quickly towards their stellar endpoints: white dwarfs, neutron stars, or black holes.
Isochrones can be used to date open clusters because their members all have **roughly the same age**. One of the first uses of an isochrone method to date an open cluster was by Demarque and Larson in 1963.

If the initial mass function of the open cluster is known, isochrones can be calculated at any age by taking every star in the initial population, **using numerical simulations to evolve it forwards** to the desired age, and plotting the star's luminosity and magnitude on the HR diagram. The resulting curve is an isochrone, which can be compared against the observational color-magnitude diagram to determine how well they match. If they match well, the assumed

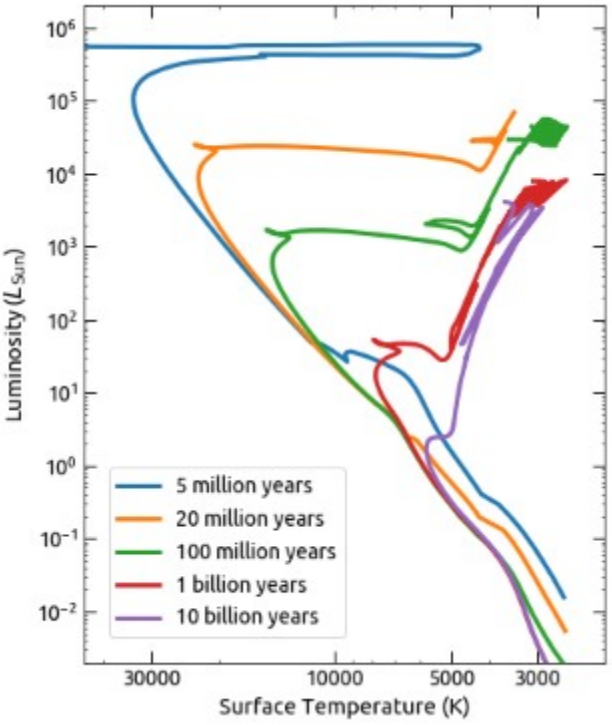

Theoretical isochrones for **near-solar metallicity** and a range of ages.

age of the isochrone is close to the actual age of the cluster."

Estimate Age using Hubble Time and Chemical Element Radioactive Decay

Imagine the Hubble expansion scenario playing like a movie in reverse. Instead of galaxies moving away from each other as time goes forward, galaxies would rush toward each other as time goes backward. Galaxies would be closer and closer together in the past, until at some time in the distant past the matter that makes up the galaxies would have been very close together. We can extrapolate back to this time, the beginning of the Universe. If we know the expansion rate for the Universe and assume that it has been constant, we can run the clock backwards and calculate how much time the Universe has been stretching.
The age of the universe is largely determined by the rate at which it expands, and the current value of the Hubble 'constant' fixes the Hubble time. The Hubble constant is an example of a stretching rate. The Hubble constant is generally expressed in units of km/s/Mpc due to how it is measured. However, both km and Mpc are units of distance and cancel out, so the Hubble constant, or any stretching rate, actually has units of 1/time. Again, assuming that the expansion rate has been constant, **we therefore have an expression for the age of Our Universe.**

$t_{twk\_age\_universe} := \frac{1}{H_{twk}}$ $billion := 10^{9}$ $t_{twk\_age\_universe} = 14.257 \cdot billion \cdot yr$

Estimate from Age of Chemical Elements Using Radioactive with Long Half Lives:
The Allende meteorite is well studied and has an age of 4.554 Gyr.

Estimate of Radius of Curvature of the Universe: (Einstein's Old Static Idealized Model)

Putting $\dot{a} = \ddot{a} = 0$ into the Friedmann Equation, gives the radius of curvature of space in the universe

$\rho_c := 8.644 \frac{kg}{m^3} 10^{-27}$ $light\_year := c \cdot yr$ $R_E := \frac{c}{\sqrt{4\pi \cdot G \cdot \rho_c}}$ $R_E = 11.77 \cdot light\_year \cdot billion$

XVIIC. Estimate the Lifetime of the Sun

Calculation is Based on the Intensity of Light from Sun and the Amount of Liberated Fusion Energy
Physics of the Sun, Dipak Basu, Chapter 11.3 *Proton Collision Rates in the Sun*

Power to Earth From Sun: $P_{sun\ earth} := 1357 W \cdot m^{-2}$ Total Area of Earth is $4\pi * d^2$

Rate Sun is Burning Energy = Sun's Luminosity: $L_{sun} := P_{sun\_earth} \cdot 4 \cdot \pi \cdot \left(92.027 \cdot 10^{6} mile\right)^2$ $L_{sun} = 3.74 \times 10^{26} \cdot W$

What Percent of Mass in Converted: One He atom has less than Mass of 4 H atoms

Particle	Proton	Neutron	2 Protons+2 Neutrons	Alpha	Difference
Units 10^{-27} kg:	1.672621637	1.674927211	6.695097696	6.64465620	0.050441496

$4 \cdot H = He + Energy$ $M_{4p} := 6.692 \cdot 10^{-27} kg$ $M_{He} := 6.644 \cdot 10^{-27} kg$

$M_{lost\_Percent} := \left(M_{4p} - M_{He}\right) \cdot M_{4p}^{-1}$ $M_{lost\_Percent} = 0.717 \cdot \%$

Estimate Sun's Lifetime: Life Time = Total Energy (Esun) to Burn/fuse = Esun / Burn Rate

Only 10% of the mass of the sun is at the core where it is hot enough for fusion to occur

Mass of Sun: $M_{\odot} := 1.989 \cdot 10^{30} kg$ $E_{sun} := 10\% \cdot M_{\odot} \cdot c^2 \cdot M_{lost\_Percent}$

$$Billion := 10^9 \qquad Life_{sun} := \frac{E_{sun}}{L_{sun}} \qquad Life_{sun} = 10.9 \cdot Billion \cdot yr$$

Evolution of the Sun

https://en.wikipedia.org/wiki/Sun

"Evolution of a Sun-like star. The track of a one solar mass star on the Hertzsprung–Russell diagram is shown from the main sequence to the post-asymptotic-giant-branch stage.

The Sun is about halfway through its main-sequence stage, during which nuclear fusion reactions in its core fuse hydrogen into helium. Each second, more than four billion kilograms of matter are converted into energy within the Sun's core, producing neutrinos and solar radiation. At this rate, the Sun has so far converted around 100 times the mass of Earth into energy, about 0.03% of the total mass of the Sun. The Sun will spend a total of approximately 10 to 11 billion years as a main-sequence star before the red giant phase of the Sun. At the 8 billion year mark, the Sun will be at its hottest point according to the ESA's Gaia space observatory mission in 2022.

The Sun is gradually becoming hotter in its core, hotter at the surface, larger in radius, and more luminous during its time on the main sequence: since the beginning of its main sequence life, **it has expanded in radius by 15%** and the surface has increased in temperature from 5,620 K to 5,772 K (9,930 °F), resulting in a **48% increase in luminosity** from **0.677 solar luminosities to its present-day 1.0 solar luminosity**. This occurs because the helium atoms in the core have a higher mean molecular weight than the hydrogen atoms that were fused, resulting in **less thermal pressure**. The core is therefore shrinking, allowing the outer layers of the Sun to move closer to the center, releasing gravitational potential energy. According to the virial theorem, half of this released gravitational energy goes into heating, which leads to a gradual increase in the rate at which fusion occurs and thus an increase in the luminosity. This process speeds up as the core gradually becomes denser. At present, it is increasing in brightness by about 1% every 100 million years. **It will take at least 1 billion years from now to deplete liquid water from the Earth from such increase**. After that, the Earth will cease to be able to support complex, multicellular life and the last remaining multicellular organisms on the planet will suffer a final, complete mass extinction."

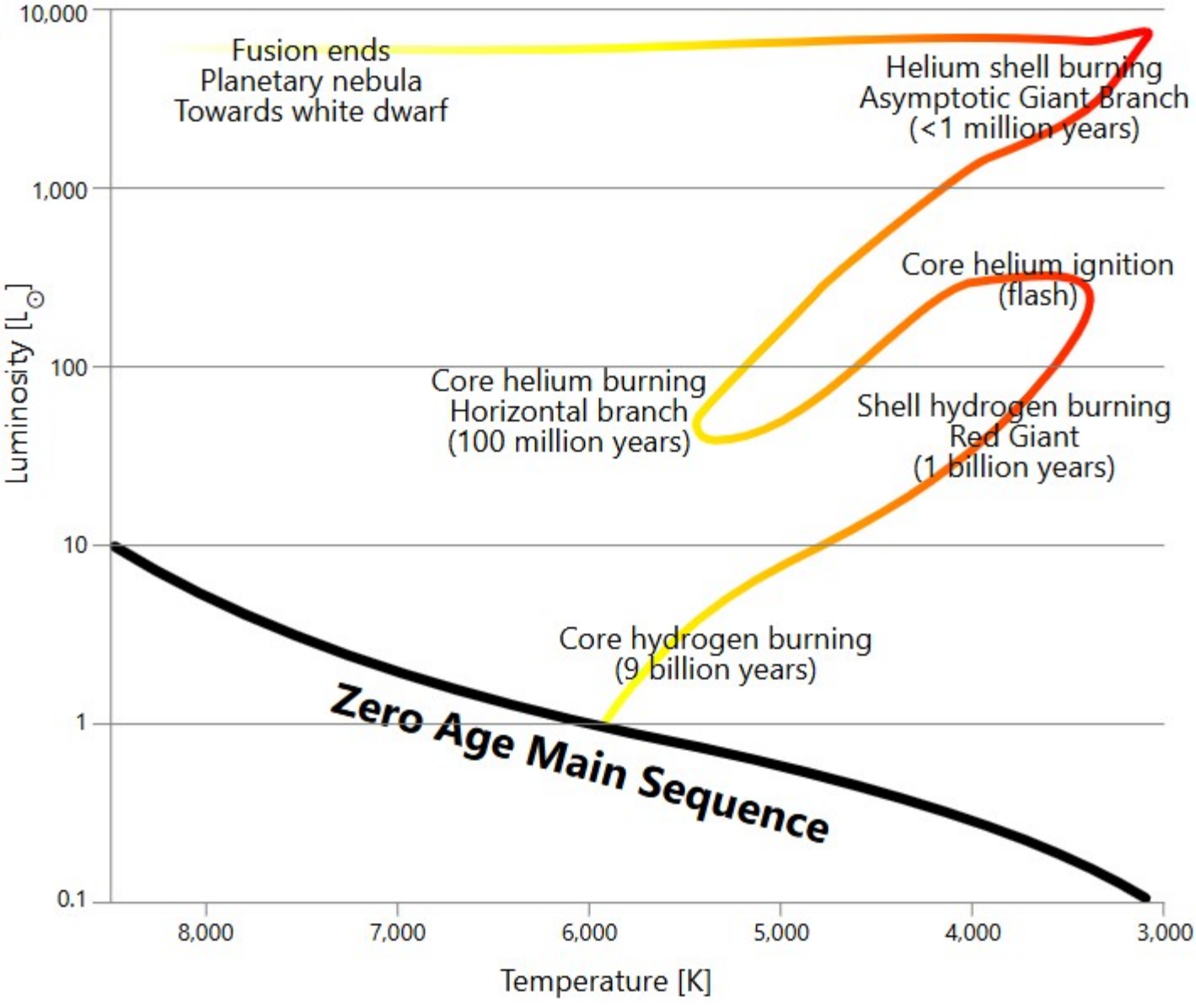

Diverse Estimates for Mass and Densities of Matter in the Universe

Estimating the amount of baryonic matter by the number of observable stars

Estimating the amount of baryonic matter in the universe from the number of stars involves several assumptions and simplifications. Stars make up a significant portion of the visible, or baryonic, matter in the universe, but they do not account for all of it. There's also interstellar gas, planets, and other components. Here's a basic approach to such an estimate:

Astronomical Estimate the Number of Stars in the Universe: Current estimates suggest that there are approximately N_{stars} stars in the observable universe. This range is based on the estimated number of galaxies in the observable universe and the average number of stars per galaxy. Number of stars in a typical galaxy (e.g. Milky

$N_{stars\_gal} := 100 \cdot 10^{9}$ $N_{galaxies} := 2 \cdot 10^{12}$ $N_{stars} := N_{stars\_gal} \cdot N_{galaxies}$ $N_{stars} = 2 \times 10^{23}$

Average Mass of a Star M_{star}: The mass of stars varies widely but for a rough estimate, you can use the mass of the Sun as an average value. $M_{\odot} = 1.989 \times 10^{30}\, kg$ $M_{tot\_stars} := N_{stars} \cdot M_{\odot}$

Baryonic Mass Inventory for GALAXIES and Rarefied Media

from Theory and **Observations of Rotation (RC) and Luminosity - 2023** $\rho_{BaryonGal\_2023RC} := 6 \cdot 10^{-25} \frac{kg}{m^3}$

Baryonic Content of Visible Universe, Persic, 1992 $\Omega_{b\_stars} := 0.002$ $\Omega_{b\_total} := 0.003$

ρ_{Baryon} for Universe: $\rho_{Baryon} := 3 \cdot 10^{-28} \frac{kg}{m^3}$ $\rho_{Baryon} \cdot \rho_c^{-1} = 0.035$

Adjust for Non-Stellar Baryonic Matter: Stars are not the only form of baryonic matter. There's also interstellar and intergalactic gas, planets, and other forms of matter. To account for this, you can adjust the total mass. Typically, the ***Mass*** of stars is estimated to be about **half** of the total baryonic matter,

$H_0 := 73 \frac{km}{s} \cdot (Mpc)^{-1}$ $M_{Baryon} := 2 \cdot M_{tot\_stars}$ $M_{Baryon} = 7.956 \times 10^{53}\, kg$

Estimate the Density of Matter, Mass, and Number of Atoms in the Universe

The critical density is that combination of matter and energy that brings the universe coasting to a stop at time infinity. Einstein's equations lead to the following expression for the critical density (ρ_{crit}). **A flat universe implies $\rho_{crit} = 1$.**

Equivalent to 10 Hydrogen atoms per m^3

$\rho_c := 3 \cdot \frac{H_0^2}{8\pi \cdot G}$ $\rho_c = 1.002 \frac{kg}{m^3} \cdot 10^{-26}$

Estimates Based on Observable Volume of Universe Give Unreasonable Results

Radius Universe, r_{Univ} $r_{univ} := 13 \cdot 10^{9} \cdot light\_year = 1.23 \times 10^{26}\, m$ $V_{univ} := \frac{4}{3}\pi \cdot r_{univ}^3$

Mass of Observable Universe: $Mass_{Univ} := V_{univ} \cdot \rho_c$ $Mass_{Univ} = 7.808 \times 10^{52}\, kg$ $V_{univ} = 7.792 \times 10^{81}\, L$

Mass Observable (Galaxies) Universe: $\rho_{galax} := 3 \cdot 10^{-28} \frac{kg}{m^3}$ $M_{galax} := \rho_{galax} \cdot V_{univ} = 2 \times 10^{51}\, kg$

Mass of Hydrogen:

$m_H := 1.67 \cdot 10^{-27}\, kg$ $Number_{atoms} := \frac{Mass_{Univ}}{m_H}$ $Number_{atoms} = 4.675 \times 10^{79}$

Fred Hoyle's Estimate

$M_{FH} := \frac{c^3}{2G \cdot H_0}$ $M_{FH} = 8.528 \times 10^{52}\, kg$

Mass from Observable Radius Fails Sanity Check

$\frac{M_{Baryon}}{Mass_{Univ}} = 10.19$ $\frac{\rho_{Baryon}}{\rho_c} = 2.994 \cdot \%$

Measuring Age of Universe from Abundance of Elements in Solar System

Nucleocosmochronology

Can use the radioactive decay of elements to age date the oldest stars in the Galaxy. Has been done with the half life of thorium 232 (half life of 14 giga years) and uranium 238 (half life of 4.5 giga years) and other elements. Measuring the ratio of various elements provides an estimate of the age of the universe given theoretical predictions of the initial abundance ratio This is difficult because thorium and uranium have weak spectral lines so this can only be done with enhanced thorium and uranium, (requires large surveys for metal poor stars) and unknown theoretical predictions for the production of R-process, (rapid neutron capture elements).

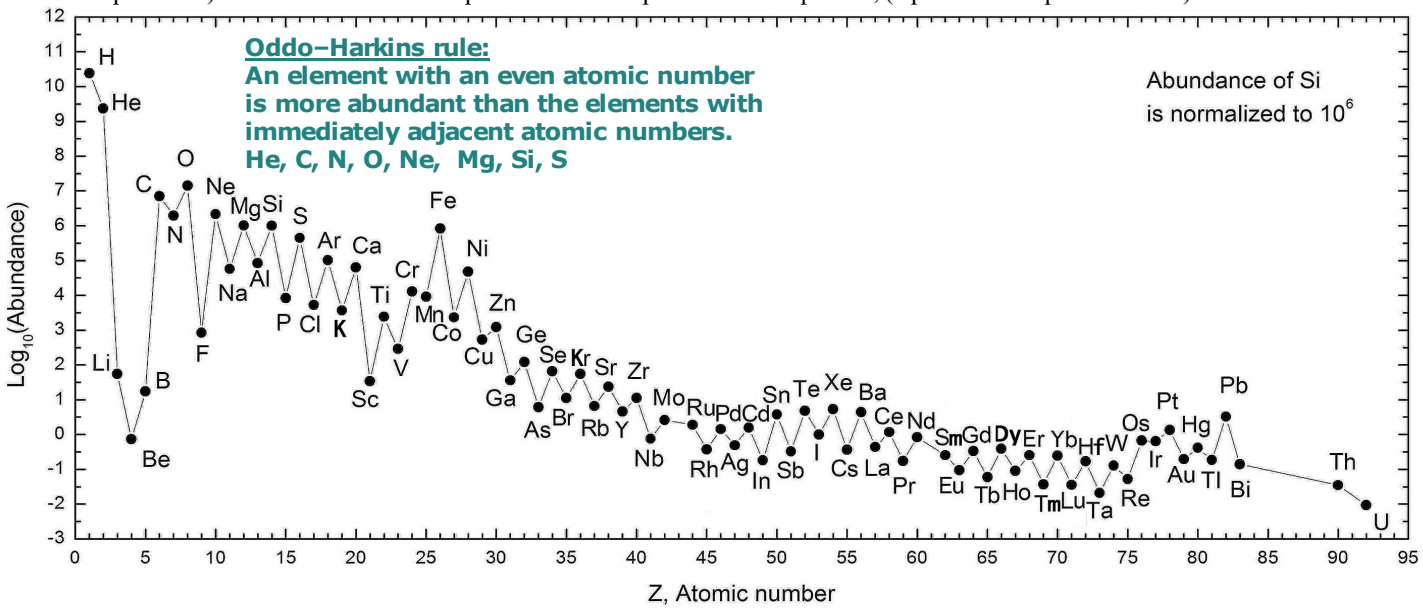

Abundance of elements in Earth's crust

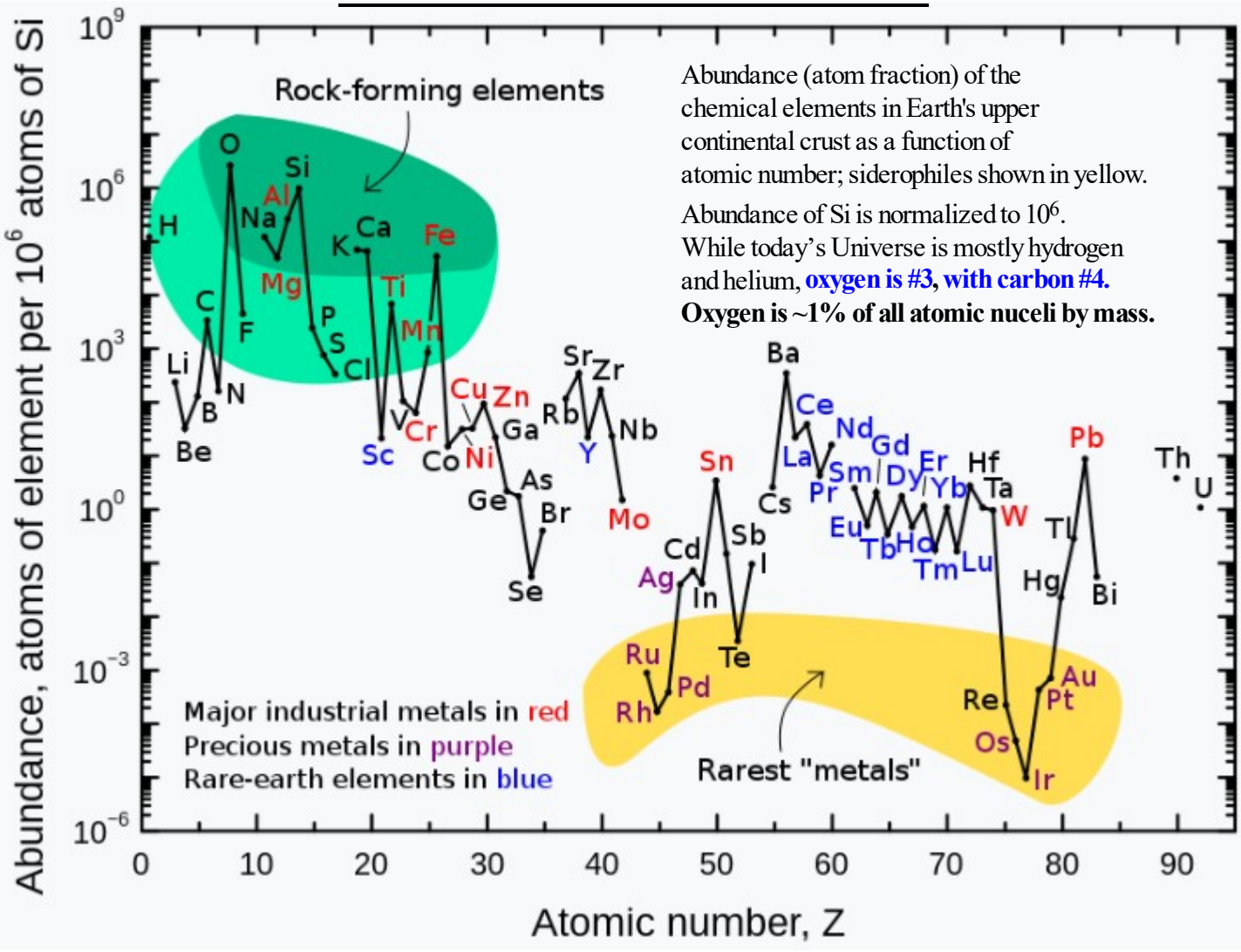

Graphs of abundance against atomic number can reveal **patterns relating abundance to stellar nucleosynthesis** and geo- chemistry. The alternation of abundance between even and odd atomic number is known as the Oddo–Harkins rule. The rarest elements in the crust are not the heaviest, but are rather the siderophile elements (iron-loving) in the Goldschmidt classification of elements. These have been depleted by being relocated deeper into the Earth's core; their abundance in meteoroids is higher. Tellurium and selenium are concentrated as sulfides in the core and have also been depleted by preaccretional sorting in the nebula that caused them to form volatile hydrogen selenide and hydrogen telluride.

There are 92 elements. All but the two of them are extremely anomalous, in terms of what we see in the crust of the earth, relative to what we see in Rocky material elsewhere in the universe. The two that are normative are manganese and iron. Everything else is anomalous, and in some cases, extremely anomalous. So for example, the crust of the earth is 630 times as much thorium 340 times as much uranium as what we see in Rocky material in the rest of the universe. And as thanks for that super abundance of uranium and thorium, our planet a long lasting hot core. And that hot liquid iron core, being circulated, has enabled our planet to have a strong magnetosphere and developing us that allows us to be protected from deadly solar and cosmic radiation. It also prevented the atmosphere and the oceans of the Earth from being sputtered away by the particle radiation from the sun.apacity. So we got 60 times less sulfur, that's what enables us to grow food, you're not going to grow any food or crops on Mars, because there's way too much sulfur there. But you can on the earth, so we're deficient by a factor of 60 times in sulfur. But were abundant by a factor of 60 times in aluminum, 90 times in titanium, which enables us to construct aircraft that can fly all over the world. These are light metals that have very high strength. And so we have in a very anomalous high abundance of these valuable elements. And they're 22 elements we see in the periodic table, that are what we call vital poisons. If they exist in the crust of the earth, at too high of an abundance level, it'll kill us, but too low of an abundant level, it will also kill us.

So we have to have just the right amount of molybdenum, and the crust of the earth, just the right amount of iron, just the right amount of arsenic. There's actually proteins in your body that need arsenic, but you only need a very, very tiny amount, and you get above that tiny amount, the arsenic will kill you. And it has to be at just the right level. And so all 22 of these vital poisons are extremely anomalous, and their abundance level here on planet Earth. And we don't see it anywhere else in the universe. So it really does look like somebody engineered it to get it just right. And astronomers again have discovered how this happened. How the early solar system formed in a gigantic cluster of about 20,000 stars that existed much closer to the center of the galaxy than the solar system exists today. And in that dense cluster of stars, the early emerging solar system got exposed to three different kinds of supernova eruption events. It got exposed to neutron stars merging together to make black holes, where the supernova and neutron star merging events happen at exactly the right time, and the right distance from the earth so that the earth was not destroyed. But on the other hand, got sufficiently enriched in all these elements and sufficiently depleted and elements be a problem. And then when all that enrichment depletion was accomplished, we got kicked out of the birth cluster and driven to a distance twice as far away from the center of the galaxy, what kicked us out, it was a gravitational slingshot, where our solar system was interfacing with four or five very massive stars that slung us out of the birth cluster. And then when we got to the ideal place for advanced life, we again engage another four or five, six massive stars that halted our movement. And so we were born in the most dangerous part of our galaxy. And we ended up in the safest part of our galaxy, but only after we got in rich. Now, it's also true that our planet **Earth is anomalous**, compared to all the other planets, and asteroids we see in in our solar system. And that's because our Earth formed, in a way incredibly different from the other planets, the other planets formed by gravitational accretion. And our solar system began with 10 planets, not eight, five gas giants and five rocky planets. Two of those rocky planets, so proto Earth and Thea collided with one another, when the Earth had oceans 1000s of kilometers deep, that very deep ocean cushion the collision, so the earth was not destroyed. In fact, what happened, most of the mass of thea got absorbed into the earth. So the earth became bigger, more massive and denser. There is a debris cloud around the new forming Earth, that condensed to make the moon. And so we have this relatively small planet, orbited by a gigantic moon that stabilizes the tilt of a rotation axis. It ensured that at the just right time for human beings, we have a rotation rate slowed down to 24 hours. And that this gas giant planet, it got kicked out by a gravitational interaction with Jupiter and Saturn. And that gravitational interaction basically slimmed down Mars from being a planet about twice the mass of Earth, down to a planet. That was only one night the mass of the Earth. This was called the Smar small Mars problem. It took 20 years for astronomers to determine how did Mars get to be so small, but we now recognize if it wasn't for that transformation of Mars, there'd be no possibility for advanced life to exist on planet Earth.

ESTIMATIONS OF TOTAL MASS AND ENERGY OF THE OBSERVABLE UNIVERSE

Dimitar Valev, Physics International 5 (1): 15-20, 2014

To determine gravitational and kinetic energy of the observable universe, information of the size and total mass of the universe are needed. There are different estimations of the mass of the observable universe covering very large interval from 3×10^{50} kg (Hopkins, 1980) to 1.6×10^{60} kg (Nielsen, 1997). Also the estimations of the size (radius) of the universe are from 10 Glyr (Hilgevoord, 1994) to more than of 78 Glyr (Cornish et al., 2004).

Estimate Mass of Universe by Dimensional Analysis

The fundamental parameters as the gravitational constant G, speed of the light c and the Hubble constant $H \approx 70$ km s^{-1} Mp_{s-1} (Mould et al., 2000) determine the global properties of the universe. Therefore, by means of these parameters, **a mass dimension** quantity m_{dim} related to the universe could be constructed:

$$m_{dim} = kc^{\alpha} G^{\beta} H_0^{\gamma}$$

where, k is a dimensionless parameter of the order of magnitude of a unit and α, β and γ are unknown exponents which have been found by means of analysis. Taking into account the dimensions of the quantities in the mx Equation we obtain the system of linear equations for unknown exponents Equations:

We use the determinant Δ of the system for the above mx Equation to find the parameters by Kramer's formula.

$$\alpha + 3\beta = 0 \quad -\alpha - 2\beta - \gamma = 0 \quad -\beta = 1 \qquad \Delta = \begin{vmatrix} 1 & 3 & 0 \\ -1 & -2 & -1 \\ 0 & -1 & 0 \end{vmatrix} = -1 \qquad \alpha = \frac{\Delta_1}{\Delta} = 3 \quad \beta = \frac{\Delta_2}{\Delta} = -1 \quad \gamma = \frac{\Delta_3}{\Delta} = -1$$

Check Exponent Values

This result gives the correct solution for exponent α,β,λ

$\alpha := 3$ $\beta := -1$ $\gamma := -1$

Compare this to the above estimate

$\alpha + 3\beta = 0$ $-\alpha - 2\beta - \gamma = 0$ $-\beta = 1$

Theoretical Estimate of the Maximum Number of Stars in Universe

Mass from Dimensional Analysis

$m_{dim} = kc^{\alpha} G^{\beta} H_0^{\gamma}$ $m_{dim} := \frac{c^3}{G \cdot H_0}$ $m_{dim} = 1.706 \times 10^{53}\ kg$

Mass from Critical Density, ρ_c

$Mass_{Univ} = 7.808 \times 10^{52}\ kg$

WMAP Estimate: $Pecent_{baryonic} := 0.046$

$$MassUniv_{baryonic} := Pecent_{baryonic} Mass_{Univ}$$

$$MassUniv_{baryonic} = 3.592 \times 10^{51}\ kg$$

The most common type of star turns out to be one with about 0.25 solar mass.

$$M_{typical} := 0.25 \cdot M_{\odot}$$

$$Num_{stars} := \frac{MassUniv_{baryonic}}{M_{typical}}$$

$$Num_{stars} = 7.223 \times 10^{21}$$

Entropy Evolution of the Universe

Planck Epoch

$t_{pl} := 10^{-43} sec$ $T_{planck} := 10^{32} K$

Planck Total Entropy Horizon Volume

$S_{Planck\_HV} := 10^{17} k_b$

Present-day CMB temperature $T_0 := 2.725K$

Approximate particle horizon today $d_H := 1.4 \cdot 10^{26} m$

Effective relativistic degrees of freedom after e+e- annihilation $g_{star\_ee} := 3.91$

Function: radiation entropy density [J/(m³·K)

$$s_{rad}(a) := \frac{2\pi^2}{45} \cdot g_{star\_ee} \cdot \frac{k_b^4}{\hbar^3 \cdot c^3} \cdot \left(\frac{T_0}{a}\right)^3$$

Radiation Entropy in Universe Today

$S_{rad}(a) := s_{rad}(a) \cdot \frac{4}{3}\pi \cdot d_H^3$ $S_{rad}(1) = 1.35 \times 10^{86} \cdot k_b$

Bekenstein-Hawking entropy formula for a black hole; AEH is the Area of the Event Horizon

$M_{BH} := 10^8 \cdot M_\odot$ $A_{EH} := 4\pi \left(\frac{2G \cdot M_{BH}}{c^2}\right)^2$ $S_{BH} := \frac{c^3 A_{EH} \cdot k_b}{4G \cdot \hbar}$

Galactic Growth $Growth(a) := 10^{12\left[(a-0.1)^{0.5}\right]}$

CMB Photons	Neutrinos	Stars/Barvons	Dark Matter	One Black Hole
$S_{CMB} := 10^{88} k_b$	$S_{Neut} := 2 \cdot 10^{87} \cdot k_b$	$S_{Baryons} := 1.4 \cdot 10^{80} k_b$	$S_{DM} := 10^{88} k_b$	$S_{BH} = 1.675 \times 10^{92} \cdot k_b$

Entropy of Single Black Hole At Galaxy Formation:

$$S_{BHgf}(a) := if\left(a < 0.1, 1 \cdot 10^{55}, \frac{S_{BH}}{k_b} \cdot 10^{-23} \cdot Growth(a)\right)$$

Assume 10^{11} Galaxies with BHs - Total Universe: $S_{BH\_Total} := 10^{11} \cdot S_{BH}$ $S_{BH\_Total} = 1.675 \times 10^{103} \cdot k_b$

Why is Entropy of Black Holes So Large? $S_{BH} \propto M^2$ Not just matter, M, but M^2. Maximally compresses matter. Gravitational Entropy dominates the universe today.

The Major Portion of the Entropy of the Universe after Galaxy Formation is in Black Holes

Time's arrow is intimately connected to gravitational collapse. Black holes represent the final "destination" of entropy growth.

Cosmic Components of Entropy (kb) vs. Scale Factor, a, of the Universe

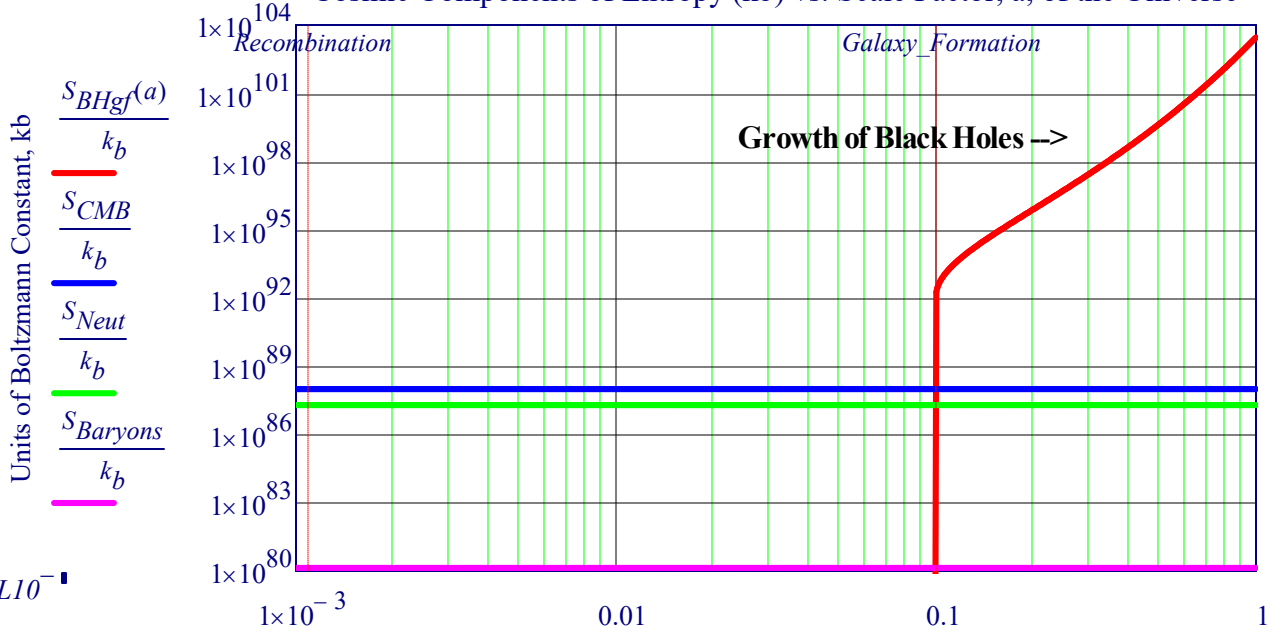

Planck Total Entropy Horizon Volume

$S_{Planck\_HV} := 10^{17} k_b$

History of Numbering of the Stars - Cosmology

We Live in a Time of Exponential Growth in Our Knowledge of the Universe (Cosmology)

Estimate of Order of Magnitude (# of Zeros) of Number of "Known Stars"

List Number of Stars that were Cataloged, Known, or Estimated Based on Observations.
Example: 2500 BC could only see about 3,000, Yerkes Observatory cataloged 13,655 stars in 1800.
We are interested only in obtaining the Order of Magnitude of the Known, Cataloged, or Estimated Stars.

$N_{stars} := READPRN("Num\ of\ Stars2.txt")$ $\quad Abraham := -2200$ $\quad Edwin\_Hubble := 1925$

$Zeros := log(N_{stars}^{\langle 1 \rangle})$ $\quad Year := N_{stars}^{\langle 0 \rangle}$ $\quad rows(N_{stars}) = 20$

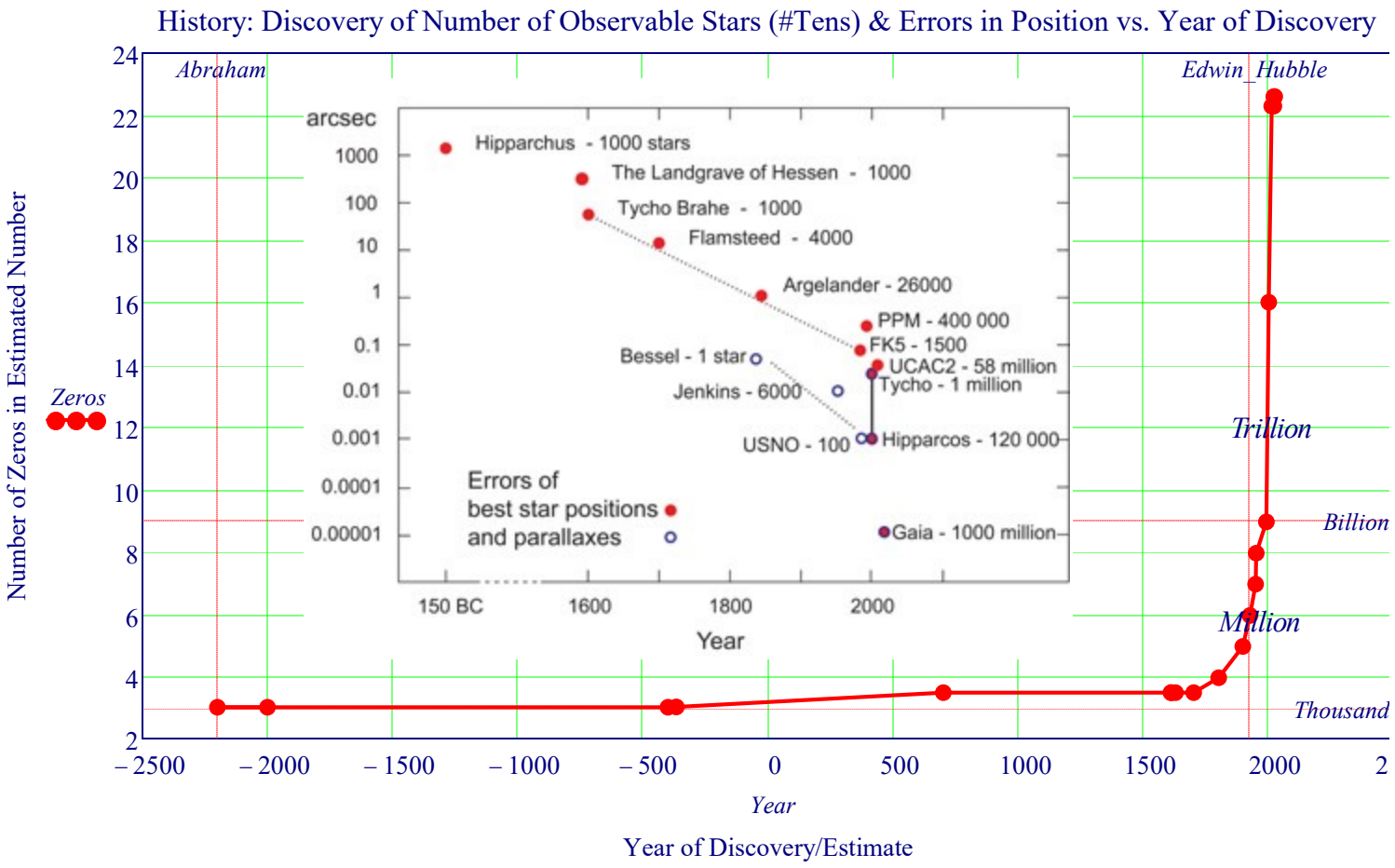

Ratio of Baryonic to Dark Matter

To calculate this ratio in a specific galaxy, astronomers **measure the rotation speed of the galaxy at various distances** from its center. They then create a rotation curve based on the visible matter (using the mass of stars, gas, etc.) and compare it with the observed rotation curve. The difference between these curves indicates the amount of dark matter. By integrating the mass profiles of both baryonic and dark matter, astronomers can estimate their respective contributions to the galaxy's total mass. While the exact ratio of dark matter to baryonic matter varies, a commonly cited average is that dark matter makes up about 85% of the total matter content in galaxies, with baryonic matter constituting about 15%. This implies a ratio of approximately 5.7:1 (dark matter to baryonic matter).

Applying this ratio gives for the total Matter in Universe $\quad Tot_{matter} := M_{Baryon} \cdot (1 + 5.7) = 5.331 \times 10^{54}\ kg$

XIX A. Planetary Data and Classical Newton's Calculation of Planetary Velocity

Read Planetary Data (MDD) and Compare to Calculated Velocity from Newton's Equation, vss

https://nssdc.gsfc.nasa.gov/planetary/factsheet/

$MDD := READPRN("Planets Mass Dist Density.txt")$ $MDD := MDD^T$

MERCURY VENUS EARTH MARS JUPITER SATURN URANUS NEPTUNE PLUTO

Mass Density Gravity EscapeVel Period Day Distance Perih, Aph, OrbPeriod OrbVelocity

$Mass := MDD^{\langle 0 \rangle}$ $Dist := MDD^{\langle 7 \rangle}$ $Vel_{Data} := MDD^{\langle 11 \rangle}$ $v_{Earth} := Vel_{Data_2}$

Analytic Estimate: Newton's Model Equation for Velocity vs. Distance, d

$M_\odot := 1.98 \cdot 10^{30} \cdot kg$ $v_{Newton}(d) := \sqrt{G \cdot \frac{M_\odot}{d \cdot 10^6 \cdot km} \cdot \frac{1}{\frac{km}{s}}}$ $d_{Earth} := Dist_2$

$v_{Newton}(6000) = 4.693$

Velocity vs Distance Curve, Falls Off Rapidly with Distance, is What is Expected for Galaxy Rotational Velocity

$d := 0, 10 .. 6000$

Note Excellent Agreement Between Planetary Velocity Data and Newton's Prediction

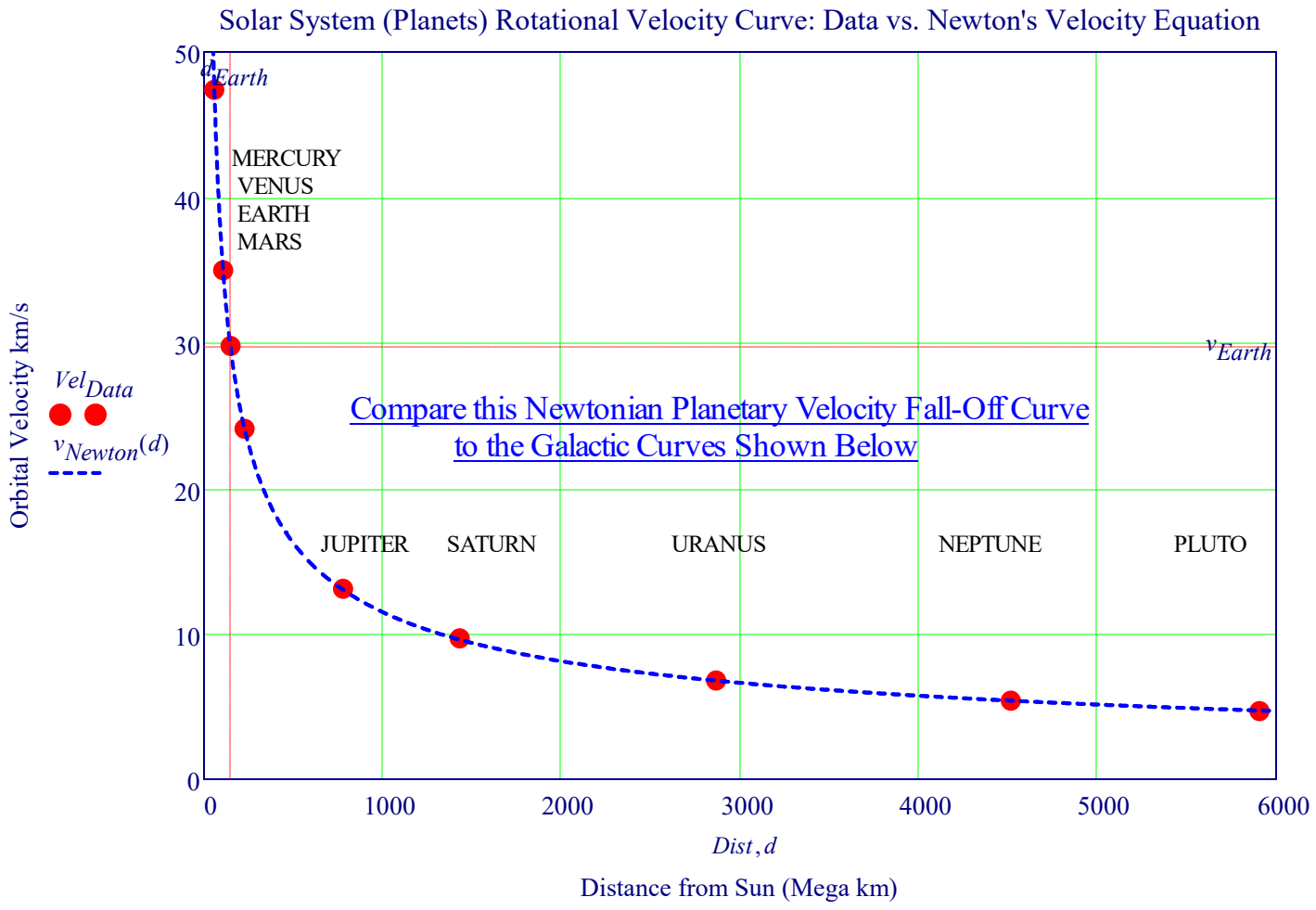

XIX B. Our Galactic Home - The Milky Way

The Milky Way is a spiral galaxy that contains our solar system and is made up of billions of stars, gas, and dust. It's estimated to be about 100,000 light years in diameter. At its core it has a Super Massive Black Hole: **Sagittarius A*** (Sgr A*, pronounced "Sagittarius A-Star"). It is the only galaxy which we are able to examine in great detail. We can resolve individual stars and analyze them spectroscopically. We can perform detailed studies of the interstellar medium (ISM), such as the properties of molecular clouds and star forming regions. We can quantitatively examine extinction and reddening by dust. Furthermore, we can observe the local dynamics of stars and gas clouds as well as the properties of satellite galaxies (such the Magellanic Clouds).
Finally, **VLBI** Paralax reveals that the Galactic center is at a distance of **only 26,000 light years.** This gives us the unique opportunity to examine the central region of a galaxy at very high resolution. Only through a detailed understanding of our own Galaxy can we hope to understand the properties of other galaxies. Of course, we implicitly assume that the physical processes taking place in other galaxies obey the same laws of physics that apply to us. If this were not the case, we would barely have a chance to understand the physics of other objects in the Universe, let alone the Universe as a whole.

It is found that the Galaxy consists of several distinct components:

- a thin disk of stars and gas with a radius of about 20 kpc and a scale height of about 300 pc, which also hosts the Sun;
- a ≈ 1 kpc thick disk, which contains a different, older stellar population compared to the thin disk;
- a central bulge, as is also found in other spiral galaxies;
- and a nearly spherical Halo which contains most of the globular clusters, some old stars, and gas with different densities and temperatures. The Figure below shows a schematic view of our Milky Way and its various components.

Schematic View of Milky Way Galaxy

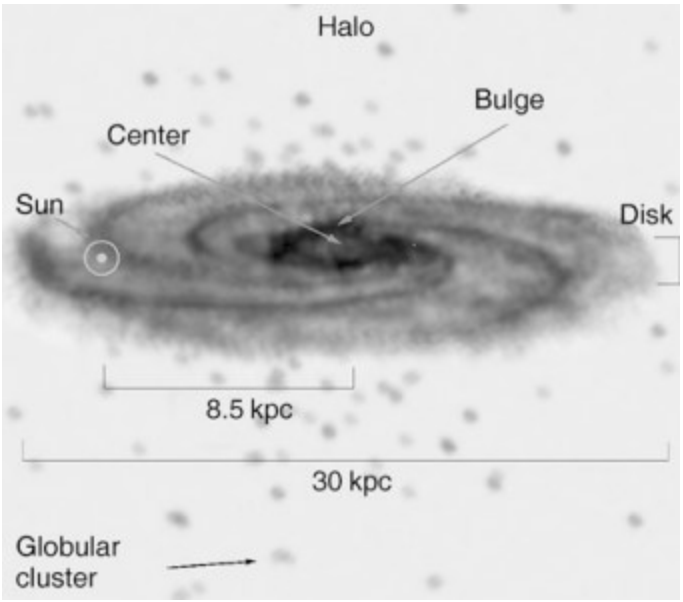

Refer to Rotation vs. Radius Plots on Next Page

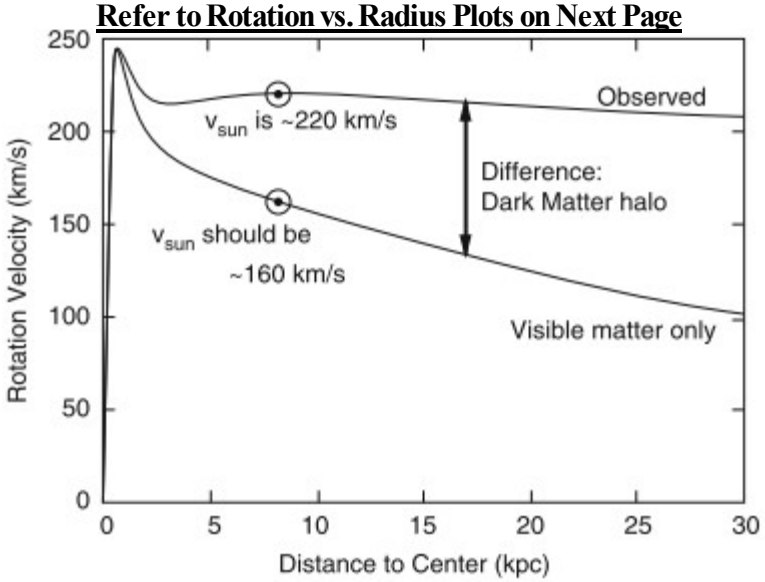

Schematic Structure of the Milky Way consisting of the disk, the central bulge with the Galactic center, and the spherical halo in which most of the globular clusters are located. The Sun orbits around the Galactic center at a distance of 8.5 kpc with orbital velocity of 220 km/s.

The upper curve is the observed rotation curve ***V(R)*** of our Galaxy, i.e., the rotational velocity of stars and gas around the Galactic center as a function of their galacto-centric distance. The lower curve is the rotation curve that we would predict based solely on the observed stellar mass of the Galaxy. The difference between these two curves is ascribed to the presence of dark matter, in which the Milky Way disk is embedded.

The observed rotational velocity V_0 of the Sun around the Galactic center is significantly higher than would be expected from the observed mass distribution. If $M(R_0)$ is the mass inside a sphere around the Galactic center with radius R_0 = 8.5 kpc, then V_0 from Newtonian Mechanics is:

$$V_0 = \sqrt{\frac{G\,M(R_0)}{R_0}}\,.$$

From the visible matter in stars we would expect a rotational velocity of 160 km/s, but we observe V_0 = 220 km/s. This indicates that the galaxy contains significantly more mass than is visible in the form of stars.

XX. Indication of Cold Dark Matter: Rotational Velocity Curves - Milky Way Galaxy

Observed Rotational Velocity of Galaxies - Velocity Does Not Falloff Rapidly Like Planets

Observing the rotational velocity of stars in galaxies is a fundamental tool to derive the mass distribution in the galaxy. Estimating the velocity of galaxy based on visible based on Classic Newton's or Kepler's Law's gives a velocity curve (VR_{Kep}) that falls off quickly with distance. The actual Galactic Velocity acts like there is a halo of matter around galaxy.

Cold Dark Matter constitutes about 26.5% of the mass–energy density of the universe. The remaining 4.9% comprises all ordinary matter observed as atoms, chemical elements, gas and plasma, the stuff of which visible planets, stars and galaxies are made. The great majority of ordinary matter in the universe is unseen, since visible stars and gas inside galaxies and clusters account for less than 10% of the ordinary matter contribution to the mass–energy density of the universe.

We want to calculate the Fraction of Cold Dark Matter in the Milky Way Galaxy

Bright Matter Mass of Milky Way Galaxy: $M_{mwg} := 6.3 \cdot 10^{41} \cdot kg \cdot 0.1$ $kpc := 3.08 \cdot 10^{16} km$

Radial Scale Length: $R_0 := 2.1 kpc$ $r_c := 16 kpc$ $M_o := 6 \cdot 10^{42} kg$

Expected Galactic Velocity Distribution (VKep) based on Keplerian type (Sun - Planetary) Mass Distribution

This is the type of falloff of velocity with distance we would expect to see from the mass of ordinary visible matter

$VR_{Kep} := READPRN("Galaxy Expected.csv")$ $R_{Kep} := VR_{Kep}^{\langle 0 \rangle} \cdot 4$ $X := 1 - 0.7 \frac{R_{Kep}}{100}$

$V_{Kepler} := \overrightarrow{\left(VR_{Kep}^{\langle 1 \rangle} \cdot X\right)}$ See Graph of Galaxy Velocity on Next Page

Determination of Amount of Dark Matter from Rotation Curve (RC) of Milky Way Galaxy

Radius (kpc), $V_{rotation}$ (kms/s), Std Dev (km/s)

DATA: Rotation Curve Parameters of the Milky Way and the Dark Matter Density, Yoshiaki Sofue, mdpi.com
Institute of Astronomy, Graduate School of Sciences, The University of Tokyo, Mitaka, Tokyo, Japan

Read Data for Rotation Curve: $RCMW := READPRN("Rotation curve of the Milky Way.txt")$

Milky Way Velocity: $V_{mwg} := RCMW^{\langle 1 \rangle}$ Let r_g be the radius of Galaxy: $r_g := RCMW^{\langle 0 \rangle}$ $n := 0 .. rows(RCMW) - 1$

Note the two prominent rotation velocity dips at radii 3 and 9 kpc.

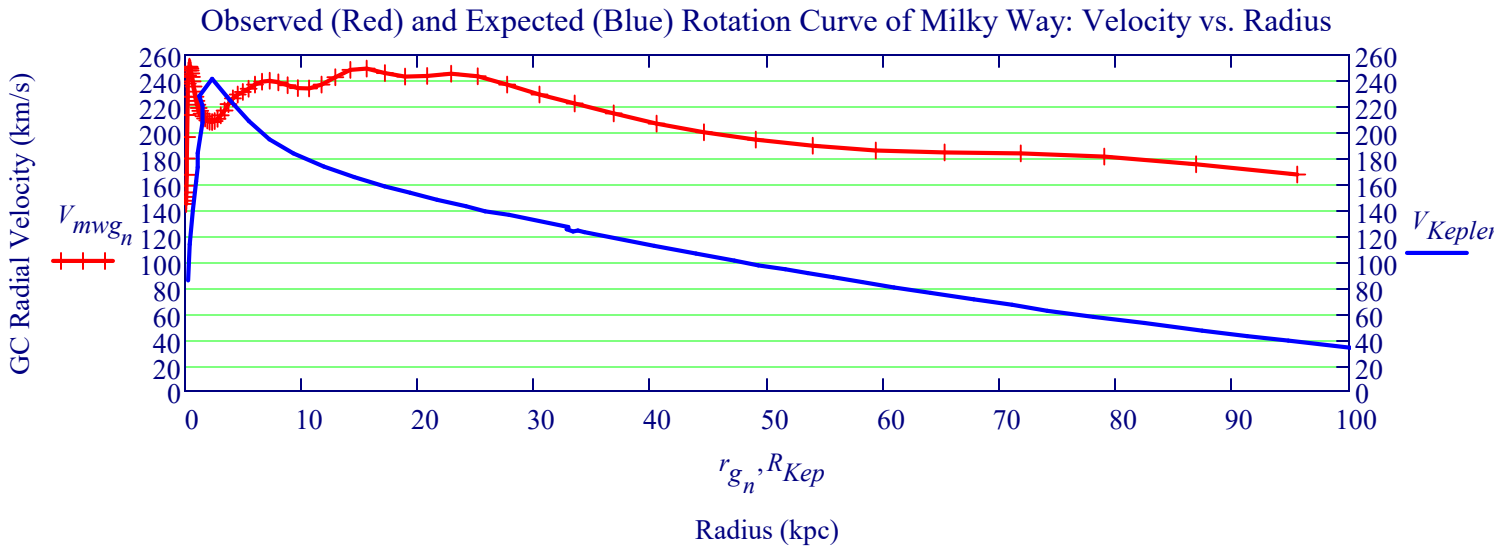

ROTATION CURVE OF THE MILKY WAY OUT TO ~200 kpc

https://iopscience.iop.org/article/10.1088/0004-637X/785/1/63/pdf

$MWB := READPRN("RC\ MILKY\ WAY\ 200\ kpc\ -Bhattacharjee.txt")$

$V_{mwb} := MWB^{\langle 1 \rangle}$ $r_{gb} := MWB^{\langle 0 \rangle}$ $u := 0, 1 .. rows(MWB) - 1$ $V_{mwbS} := ksmooth(r_{gb}, V_{mwb}, 12)$

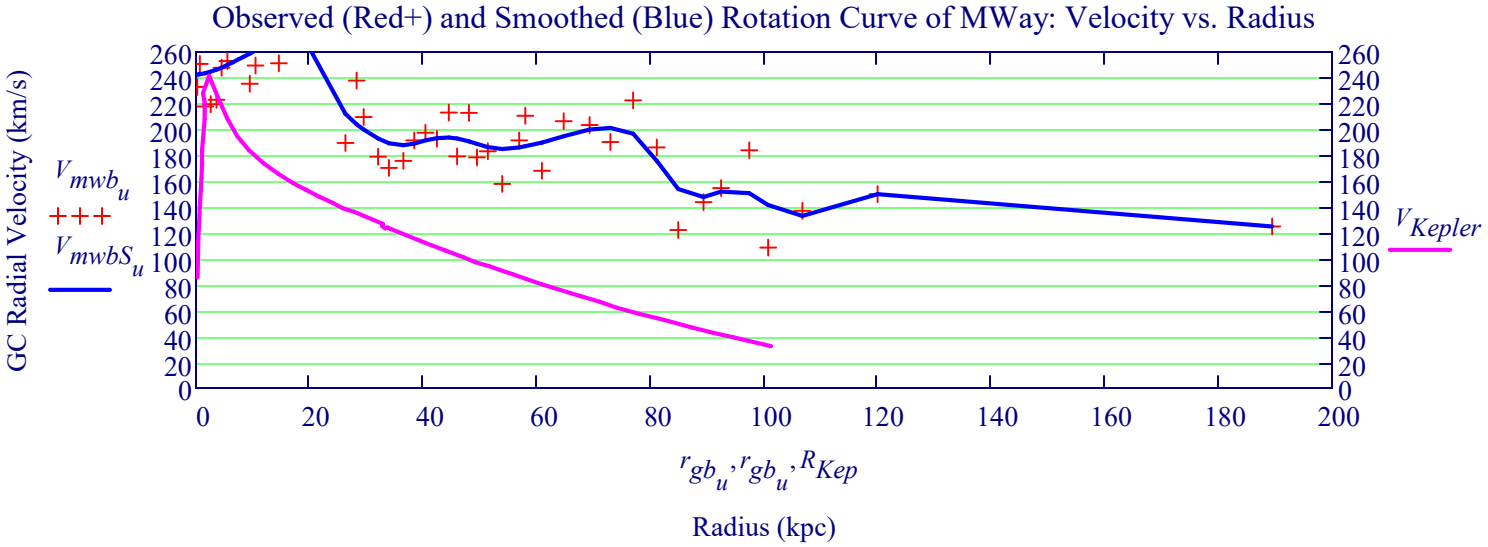

Composite Rotation Curve of Milky Way Galaxy Showing Mass Components

Composite Rotation Curve including the bulge, disk, spiral arms, and dark halo.
Yoshiaki Sofue, Mareki Honma , and Toshihiro Omodaka, PASJ 2018

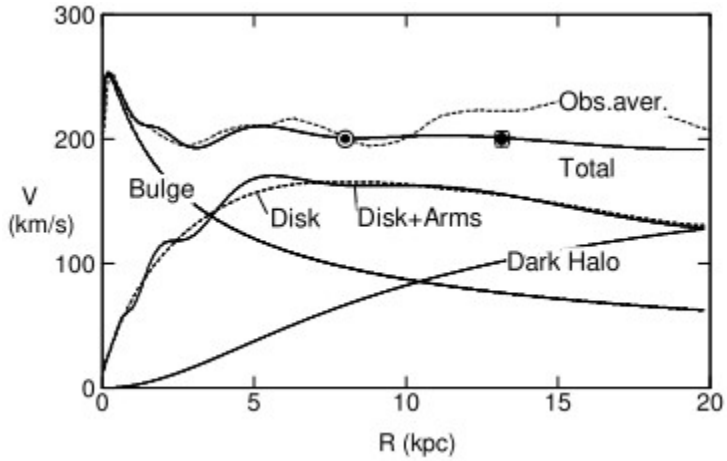

The rotation velocity is written by the gravitational potential as $V(R) = \sqrt{R \cdot \frac{\partial}{\partial R} \Phi}$

where $\Phi = \sum_i \Phi_i$

with Φi being the potential of the i-th mass component

Knowing that Vi(R) = R ∂ Φi / ∂ R, we have $V(R) = \sqrt{\sum_i V_i^2}$.

Mass Components

Below, the subscript BH represents black hole, b stands for bulge, d for disk, and h for the dark halo. The contribution from the black hole can be neglected in sufficiently high accuracy, when the dark halo is concerned.

$$V(R) = \sqrt{V_{BH}(R)^2 + V_b(R)^2 + V_d(R)^2 + V_h(R)^2}.$$

The **mass components** are usually assumed to have the following functional forms:

The GC of the **Milky Way** is known to **nest a massive black hole** of mass of MBH **~ 4×10^6 $M_\odot$**

The RC is assumed to be expressed by a curve following the Newtonian potential of a point mass at the nucleus. and the rest of total mass is what is called dark matter---material that does not emit any light (a small fraction of it is ordinary matter that is too faint to be detected yet) but has a significant amount of gravitational influence. The total mass of the galaxy, M_g, including the extended dark halo, has been measured by analyzing the outermost RC and motions of satellite galaxies orbiting the galaxy, and the **mass up to ~100–200 kpc** has been estimated to be **3×10^{11} $M_\odot$** ,

Mg = 0.3 Trillion Sun Masses

Where $M_\odot$ is the mass of Sun $M_\odot := 1.989 \cdot 10^{30} kg$ $M_g := 3 \cdot 10^{11} \cdot M_\odot$ $R_g := 8 kpc$

Fit a Curve, (VFit), to the Milky Way Rotation Curve

$V_{Fit} := ksmooth(r_g, V_{mwg}, 10)$

Simple Model for Milky Way Galaxy that Approximates Galaxy Rotation Curves

Galactic Model: *Simple Model for Explaining Galaxy Rotation Curves*, A. Wojnar, Sporea

Model Parameters: M_0 the total galaxy mass, R_0 the observed scale length of the galaxy, r_c the core radius and fitting parameters b and β

Galactic Velocity Curve Fitting Model, vmw, with Five Fitting Parameters, Mg, R0, rc, b, and β

$M_{gas} := 10^{9.68} \cdot M_\odot$ $M_s := 10^{9.76} \cdot M_\odot$ $R_0 := 2.6 kpc$ $r_c := 0.88 kpc$ $b := 0.352$ $\beta := 1$

$M_g = 5.967 \times 10^{41} kg$ $M_{tot} := M_{gas} + M_s$ $X_M := (M_{gas} + M_s) \cdot M_g^{-1}$

$$v_{model}(r) := \sqrt{\frac{G \cdot M_{tot}}{r} \cdot \left(\sqrt{\frac{R_0}{r_c}} \cdot \frac{r}{r + r_c} \right)^{3\beta} \cdot \left[1 + b \cdot \left(1 + \frac{r}{R_0} \right) \right]} \qquad v_{model}(20 kpc) = 202.875 \cdot \frac{km}{s}$$

The Dark Halo Density profile:

DM Model: ***Untied Rotation Curve of the Galaxy, Decomposition Bulge, Disk, Dark Halo,*** **Sofue**

ρ_{hc} and R_h are constants giving the central mass density (ρ_{hc}) and scale radius of the halo, respectively

$$\rho_{hc} := 0.03 \cdot M_{\odot} \cdot parsec^{-3} \qquad R_h := 5.5kpc \qquad light\_year := 0.000306kpc$$

$$\rho_{halo}(r) := \rho_{hc} \cdot \left[1 + \left(\frac{r}{R_h}\right)^2\right]^{-1} \qquad V_{inf} := \sqrt{4 \cdot \pi \cdot G \cdot \rho_{hc} \cdot R_h^{\,2}} \qquad V_{inf} = 221.258 \cdot \frac{km}{s}$$

Estimate of Dark Halo - Isothermal Spherical Distribution

$$V_{inf} := 150\frac{km}{s} \qquad V_{halo}(r) := V_{inf} \cdot \left(1 - \frac{R_h}{r \cdot kpc} \cdot atan\left(\frac{r \cdot kpc}{R_h}\right)\right) \cdot \frac{1}{\frac{km}{s}}$$

Sum of Keplerian and Dark Halo Distributions

$$v_{k\_d} := V_{Kepler} + \overrightarrow{V_{halo}(R_{Kep})}$$

Velocity Plots: Milky War Data (++), Vhalo of Dark Matter (Blue), vk_d Sum of Dark and Kepler, Galaxy Model (Purple), VFit Fit Curve to Data+ (Dashed Black), VKep Kepler Plot (Red)

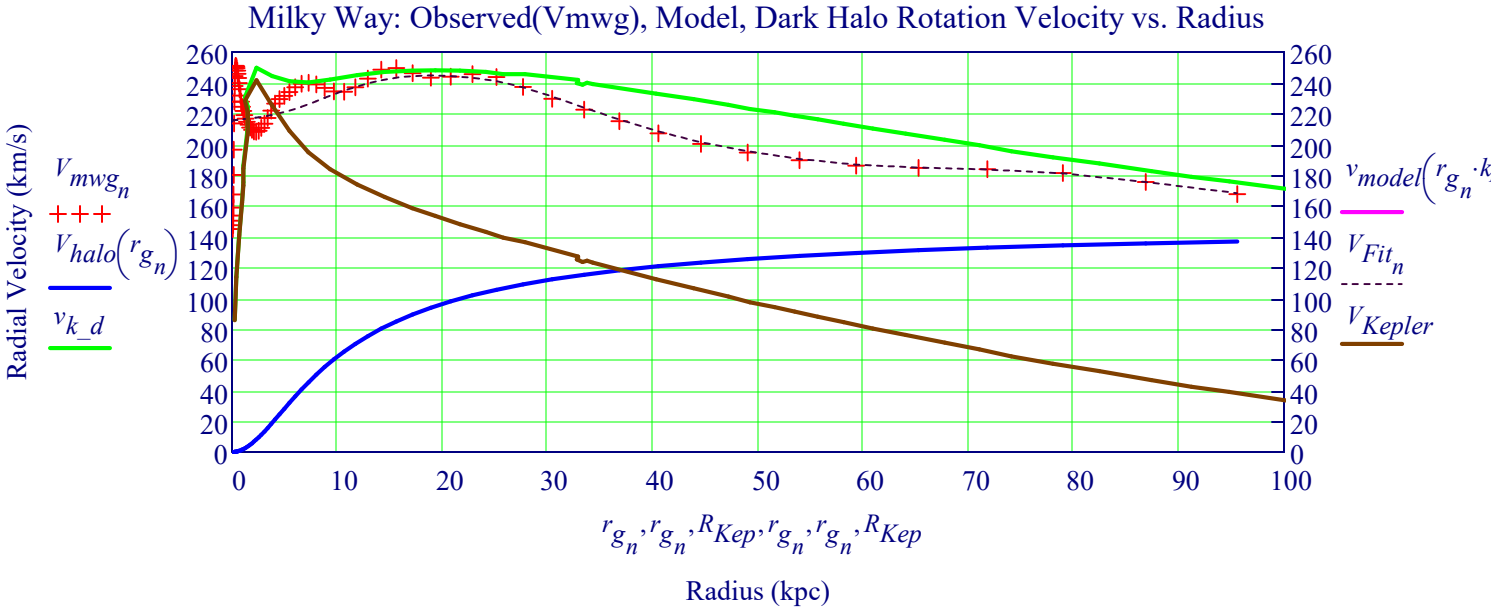

Milky Way Galaxy Effects on Earth and Sun

The motion of the Sun (and the entire solar system) around Sagittarius A*—the supermassive black hole at the Milky Way's center—does have gravitational effects, though they're typically very small at our distance.

Orbital Motion of the Solar System

The Sun orbits Sagittarius A* at a distance of about 26,000 light-years (or ~8 kpc).
Orbital speed: ~220–230 km/s.
Orbital period: about 230 million years.

Local Gravitational Effects

☑ Tidal forces
The gravitational tidal forces from Sagittarius A* at this distance are tiny compared to local gravitational effects (like those from the Sun or nearby stars). They're not significant for: Planetary orbits

Solar system stability

☑ No measurable frame-dragging
The frame-dragging (Lense-Thirring) effect of Sagittarius A*'s spin is negligible at the Sun's location.

Overall Galactic Potential

While the black hole itself contributes to the galactic gravitational potential, it's only a small part of the total mass (~4 million solar masses out of ~100 billion solar masses for the galaxy).
Most of the solar system's orbital motion is due to the gravitational pull of the Milky Way's stars and dark matter halo, not the black hole alone.

Does it affect Earth or life?

No significant direct effects:
Tides, orbital perturbations, or frame-dragging from Sagittarius A* are negligible for the Earth.
The motion around the galaxy defines our cosmic neighborhood and velocities, but not daily or yearly physics on Earth.

Summary

✔ The Sun's orbit around Sagittarius A* is real and well-documented, with spectacular implications for understanding galactic dynamics.
✔ Local gravitational effects on Earth (from Sagittarius A*) are incredibly small—no measurable impacts on the solar system's stability or everyday phenomena.

Gravitational Redshift / Blueshift (Cosmological Doppler Effect)

As the solar system orbits the galaxy's center:
Our motion relative to the CMB rest frame (~370 km/s) causes a dipole anisotropy in the CMB
— a measurable effect!
But locally (like within the solar system), the gravitational redshift due to Sagittarius A* is negligible because:

$M_\odot := 1.99 \cdot 10^{30} \cdot kg$ $M_{BH} := 200 \cdot 10^{6} \cdot M_\odot$

$r := 26000 \cdot LightYear$

Negligible Effect

$\frac{G \cdot M_{BH}}{c^2 \cdot r} = 0.012 \cdot 10^{-7}$

Angular Momentum

$J := \frac{G \cdot \left(200 \cdot 10^{6} \cdot M_\odot\right)^2}{c}$

$J = 3.527 \times 10^{58} \frac{m^2 \cdot kg}{s}$

Frame-Dragging (Lense-Thirring Effect)

Sagittarius A* spins and drags spacetime around it (frame-dragging).

Ω_{LT}

$\Omega_{LT} := \frac{2G \cdot J}{c^2 \cdot r^3}$

Effect on the Sun's orbit is:

$M_{blackHole} := 200 \cdot 10^{6} \cdot M_\odot$

Negligible: $\Omega_{LT} = 3.519 \cdot \frac{rad}{s} \cdot 10^{-30}$

XXIA. Evidence for Λ-CDM "Big Bang" Model

What are the strongest physical evidences for the big bang?

Thanks to technological advances, astronomers can measure the current temperature of radiation lingering from the cosmic origin event as well as the temperature of this radiation at various times in the past. As the figure below shows, actual temperature measurements match the cooling curve a ΛCDM model (creation model)predicts, given the age of the cosmos (≈13.8 billion years old) and its measured expansion rate. The most accurate of these past measurements is the one in the middle of the cooling curve. This measurement fits the curve so closely that its error bar can't be seen in this graph. Figure 2: Evidence of Cooling from the ΛCDM Creation Event. The curve is the predicted cooling of the universe according to the ΛCDM creation model with a cosmic age of 13.79 billion years and an average cosmic expansion rate at 68.65 kilometers/second/megaparsec.The dots and error bars are actual temperature measurements of the Cosmic Microwave Background Radiation.

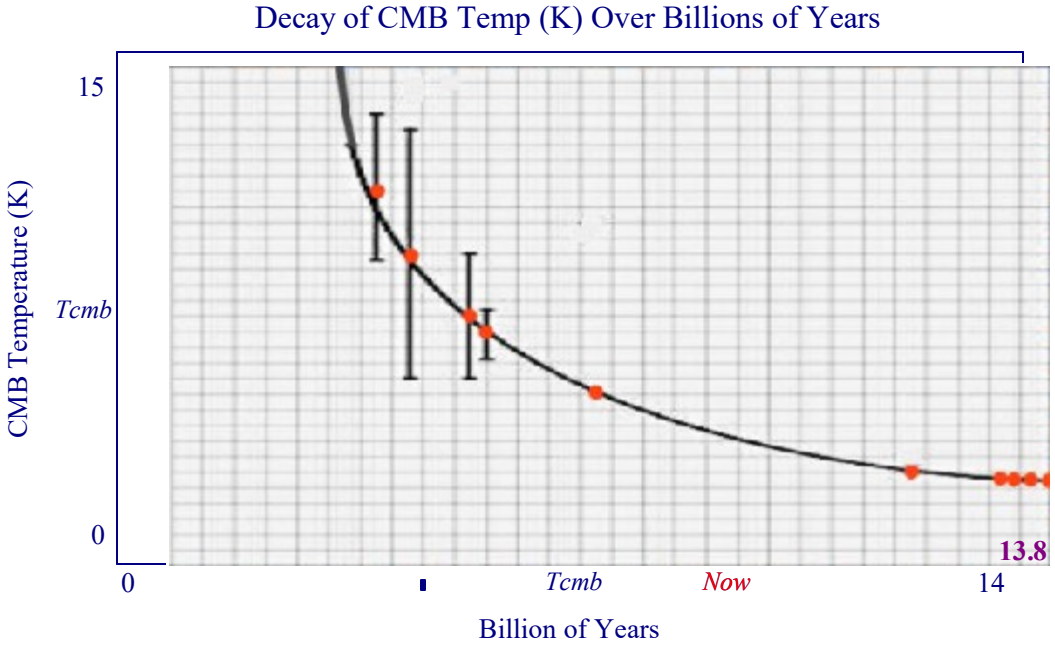

Does the Law of Conservation of Energy Apply to the ΛCDM.

As the Universe expands, Dark Energy is created. Energy by itself is not conserved. Energy can increase or decrease whenever space itself changes in time. Photons have an energy that is inversely proportional to their wavelength. As space expands, the wavelength of photons increases and it energy decreases. So where it go? This is why the Cosmic Microwave Background Radiation is so cold. In GR, we have a more complicated theory of Energy Conservation.

Generalized Energy Conservation

It Generalized Energy Conservation of Covariant Conservation Law of the Stress-Energy Tensor. The change in energy in the photon has to match the change in energy of space.

Test for Expansion: Comparison of Theoretical (Ideal) vs. Measured CMB Temp. from VLT

Data Source: *The evolution of the cosmic microwave background temperature Measurements of T CMB at high redshift from carbon monoxide excitation,* P. Noterdaeme , P. Petitjean , R. Srianand, C. Ledoux, and S. López

A milestone of modern cosmology was the prediction and serendipitous discovery of the cosmic microwave background (CMB), the radiation leftover after decoupling from matter in the early evolutionary stages of the Universe. A prediction of the standard hot Big-Bang model is the linear increase with redshift of the black-body temperature of the CMB (T_{CMB}). This radiation excites the rotational levels of some interstellar molecules, including carbon monoxide (CO), which can serve as cosmic thermometers. Using three new and two previously reported CO absorption-line systems detected in quasar spectra during a systematic survey carried out using Very Large Telescope,VLT / European Southern Observatory, UVES, we constrain the evolution of T_{CMB} to $z \approx 3$. Combining precise measurements with previous constraints, we obtain $T_{CMB}(z) = (2.725 \pm 0.002) \times (1+z)^{1-\beta}$ K with $\beta = -0.007 \pm 0.027$, a more than two-fold improvement in precision. The measurements are consistent with the standard (i.e. adiabatic, $\beta = 0$) Big-Bang model and provide a strong constraint on the effective equation of state of decaying dark energy (i.e. $w_{eff} = -0.996 \pm 0.025$).

$T_{cmbdat} := READPRN("Redshift vs Tcmb to z1 G Hurier 2014C.txt")$

Theoretical (Ideal) CMB Temperature vs Redshift z

$T_{cmb\_theo}(z) := 2.725 \cdot (1+z)$

Measured CMB Temperature vs Redshift z

$\beta := -0.007$ $\quad T_{cmb\_data}(z) := 2.725 \cdot (1+z)^{1-\beta}$

Measurements are based on the rotational excitation of CO molecules are represented by red dots.

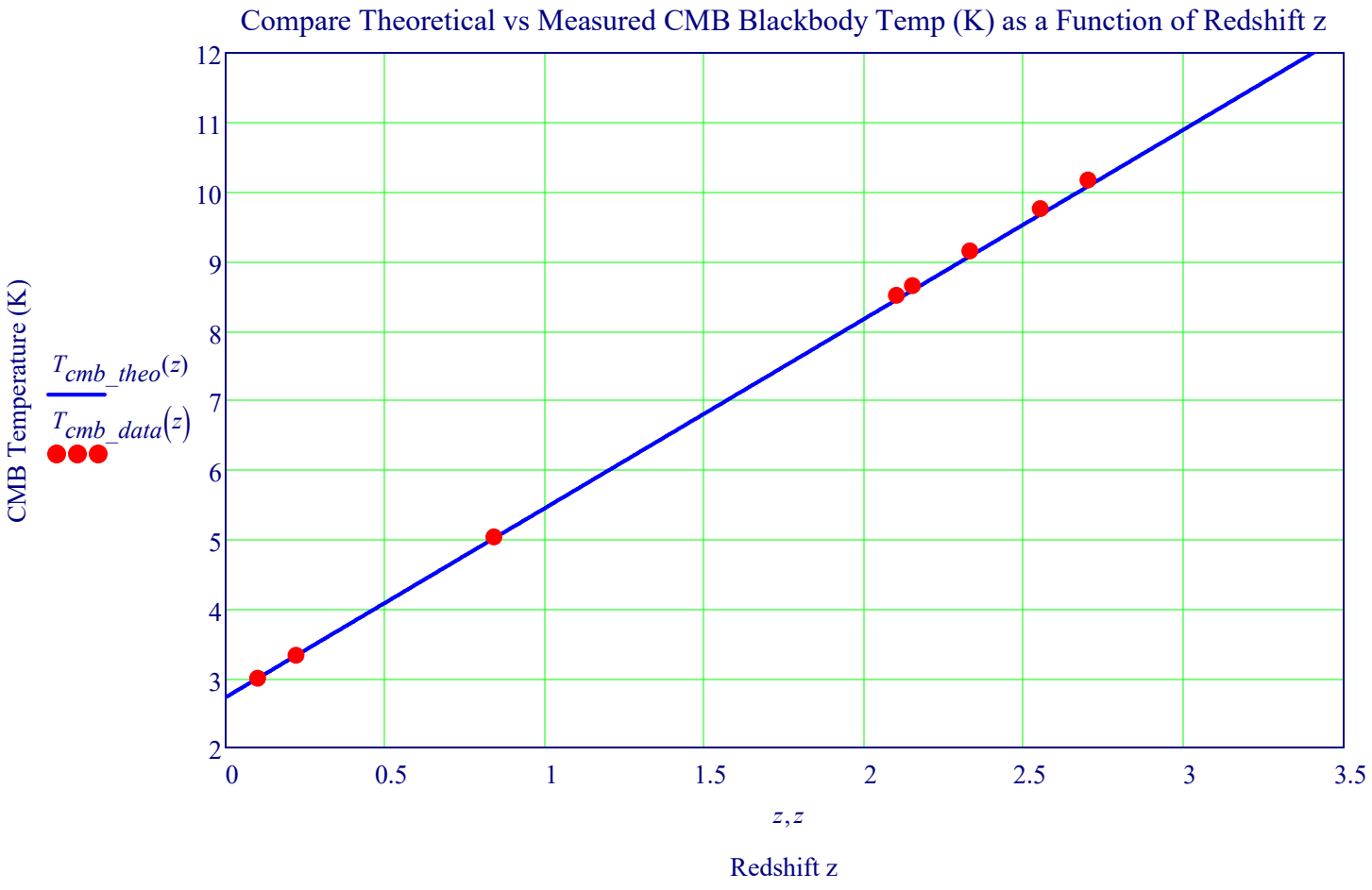

The evolution of the cosmic microwave background temperature (2011)

Measurements of TCMB at high redshift from carbon monoxide excitation

P. Noterdaeme1, P. Petitjean2, R. Srianand3, C. Ledoux4, and S. López

ABSTRACT

A milestone of modern cosmology was the prediction and serendipitous discovery of the cosmic microwave background (CMB), the radiation leftover after decoupling from matter in the early evolutionary stages of the Universe. A prediction of the standard hot Big-Bang model is the linear increase with redshift of the black-body temperature of the CMB (T_{CMB}). This radiation excites the rotational levels of some interstellar molecules, including carbon monoxide (CO), which can serve as cosmic thermometers. Using three new and two previously reported CO absorption-line systems detected in quasar spectra during a systematic survey carried out using VLT/UVES, we constrain the evolution of T_{CMB} to $z \sim 3$.

Combining our precise measurements with previous constraints, we obtain

$$T_{CMB}(z) = (2.725 \pm 0.002) \times (1+z)^{1-\beta}\ \mathrm{K}$$

with $\beta = -0.007 \pm 0.027$, a more than two-fold improvement in precision. The measurements are consistent with the standard (i.e. adiabatic, $\beta = 0$) Big-Bang model and provide a strong constraint on the effective equation of state of decaying dark energy (i.e. $w_{eff} = -0.996 \pm 0.025$).

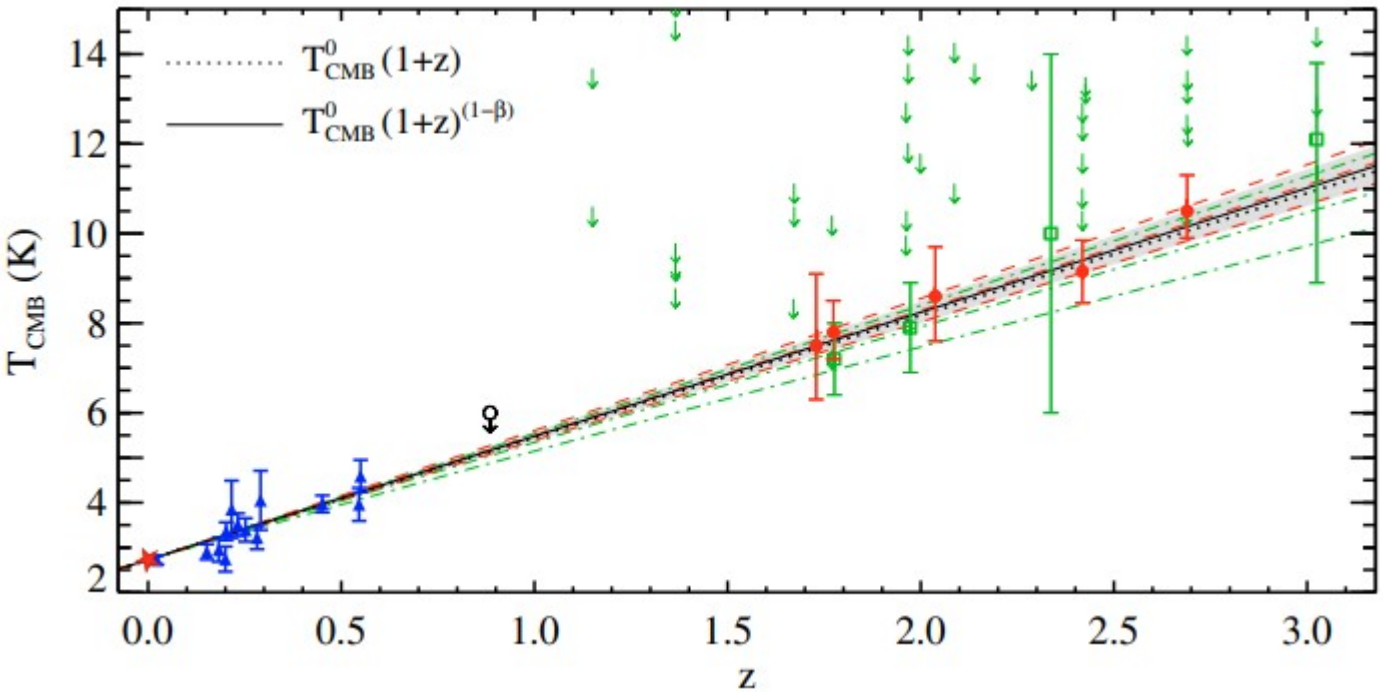

Black-body temperature of the cosmic microwave background radiation as a function of redshift. The star represents the measurement at $z = 0$ (Mather et al. 1999). Our measurements based on the rotational excitation of CO molecules are represented by red filled circles at $1.7 < z < 2.7$. Other measurements at $z > 0$ are based (i) on the S-Z effect (blue triangles at $z < 0.6$, Luzzi et al. 2009) and (ii) on the analysis of the fine structure of atomic carbon (green open squares: $z = 1.8$, Cui et al. 2005; $z = 2.0$, Ge et al. 1997; $z = 2.3$, Srianand et al. 2000; $z = 3.0$, Molaro et al. 2002). Upper limits come from the analysis of atomic carbon (from the literature and our UVES sample, see Srianand et al. 2008) and from the analysis of molecular absorption lines in the lensing galaxy of PKS 1830-211 (open circle at $z = 0.9$, Wiklind & Combes 1996).

The dotted line represents the adiabatic evolution of TCMB as expected in standard hot Big-Bang models. The solid line with shadowed errors is the fit using all the data and the alternative scaling of $T_{CMB}(z)$ (Lima et al. 2000) yielding $\beta = -0.007 \pm 0.027$. The red dashed curve (resp. green dashed-dotted) represents the fit and errors using S-Z + CO measurements (resp. S-Z + atomic carbon).

XXIB. Time Dilation in Type Ia Supernova Spectra at High Redshift - Tolman Test

Time Dilation in Type Ia Supernova Spectra at High Reshift, S. Bondi, Am. Astronomical Society, April 19, 2008

One of the **most straightforward and direct substantiations of the ΛCDM creation model** is a phenomenon referred to as **time dilation**. The time dilation test is based on Einstein's special theory of relativity. The redshift, z, is a fundamental observational quantity in Friedman-Lemaitre-Robertson-Walker (FLRW) models of the universe. **It relates the frequency of light emitted from a distant source to that detected by a local observer by a factor of 1/(1 + z).** One important consequence is that the **observed rate of any time variation** in the intensity of emitted radiation will also be **proportional to 1/(1 + z)** (see Weinberg 1972). This phenomenon is directly related to time dilation because the stretching of the wavelength corresponds to a stretching of the time intervals between the peaks of the light wave. The further away a galaxy is, the faster it appears to be receding from us due to the expansion of the universe. (There is also a 1+z stretching of the wavelength of radiation.) Due to their large luminosities (several billion times that of the Sun) and variability on short timescales (20 days from explosion to peak luminosity; Riess et al. 1999; Conley et al. 2006), Type Ia supernovae (SNe Ia) are ideally suited to probe these time dilation effects across a large fraction of the observable universe. The suggestion to u**se supernovae as cosmic clock**s and **tested on light curves** of low-redshift SNe Ia in the mid- 1970s (Rust 1974), but only since the mid-1990s has this effect been unambiguously detected in the light curves of high-redshift objects (Leibundgut et al. 1996; Goldhaber et al. 2001). These latter studies show that the **light curves of distant SNe Ia are consistent with those of nearby SNe Ia whose time axis is dilated by a factor of 1 + z.** However, there exists an intrinsic variation in the width of SN Ia light curves that is related to their peak luminosities (Phillips 1993), such that more luminous SNe Ia have broader light curves. This width-luminosity relation is derived using low-redshift SNe Ia for which the time dilation effect.

Time Dilation - Apparent aging rate vs. 1/(1 + z)

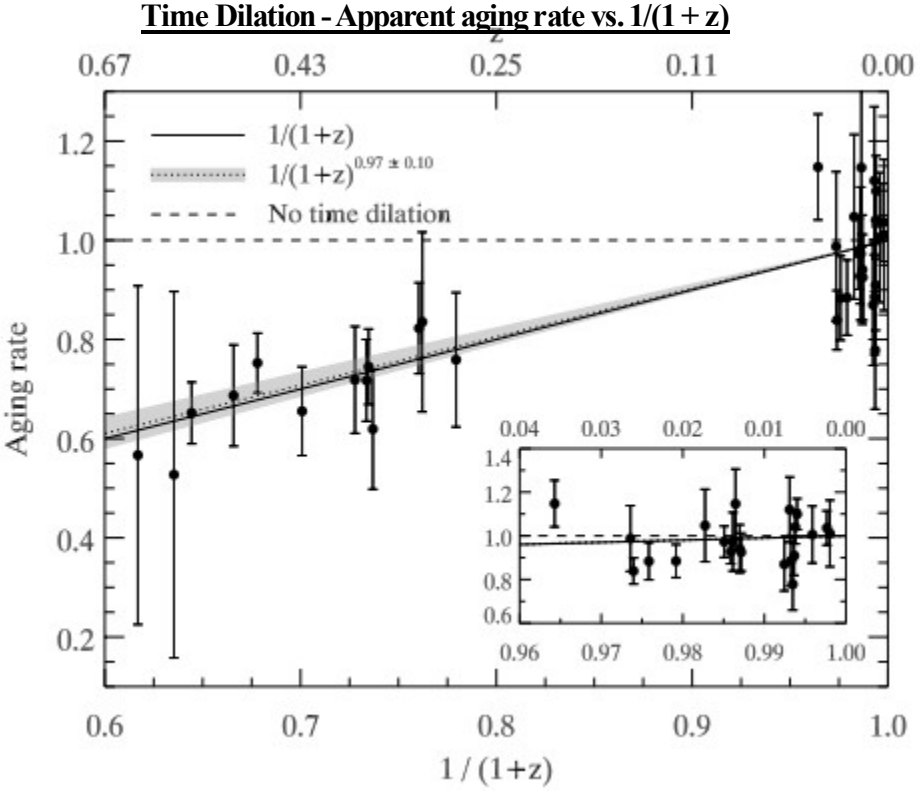

Photometry of Supernova Ia: Peaking of Light Curve

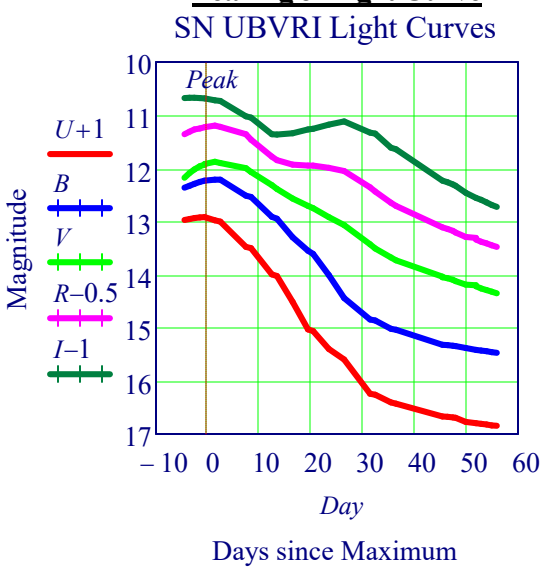

DATA: *OPTICAL LIGHT CURVE TYPE Ia SUPERNOVA.* SUNTZEFF, ASTRONOMICAL JOURNAL, 117, 1999 March

1. UBVRI PassBand Photometric System
2. Brighter stars have smaller Magnitude.

Apparent aging rate vs. *1/(1 + z)* for the 13 high-redshift ($0.28 < z < 0.62$) and 22 low-redshift (***z < 0.04***) SNe Ia in our sample. Overplotted are the expected 1/(1 + z) time dilation (solid line) and the best-fit $1/(1+z)^b$ model (with b =0.97; dotted line and gray area). The dashed line corresponds to no time dilation, as expected in the tired-light model, clearly inconsistent with the data. Inset: Close-up view of the low-redshift sample.

Using the standard definition of redshift, $z = (\lambda_0 - \lambda_1)/\lambda_1 = \nu_1/\nu_0 - 1$, we obtain a relationship between observed and rest-frame time intervals in a RW metric as a function of redshift z: $\frac{\delta t_0}{\delta t_1} = 1 + z$

The prediction of time dilation proportional to *1 + z* is generic to expanding universe models, whether the underlying theory be general relativity.

XXII. Λ-CDM Model Theory and Parameters

*Planck 2013 results. XVI. Cosmological parameter*s, arXiv:1303.5076v3 [astro-ph.CO] 20 Mar 2014

See Section IIC: Table of The Hypothesized Thermal History of the Universe
See Section XXVI D: CMB Matter Power Spectrum
See Section XXXII: Some Key Problems of the ΛCDM Cosmology

Introduction

Planck temperature power spectrum multipole, ℓ

The discovery of the cosmic microwave background (CMB) by Penzias & Wilson (1965) established the modern paradigm of the hot ΛCDM cosmology. Almost immediately after this seminal discovery, searches began for anisotropies in the CMB – the primordial signatures of the fluctuations that grew to form the structure that we see today. This describes the cosmological parameter results from the Planck temperature power spectrum. This model is based upon a spatially-flat, expanding Universe whose dynamics are governed by General Relativity and whose constituents are dominated by cold dark matter (CDM) and a cosmological constant (Λ) at late times. The primordial seeds of structure formation are Gaussian-distributed adiabatic fluctuations with an almost scale-invariant spectrum. This model is described by only six key parameters. The focus is to investigate cosmological constraints from the temperature power spectrum measured by Planck. XXIII summarizes some important aspects of the **Planck temperature power spectrum**; we plot this as $\boldsymbol{D \equiv \ell\,(\ell+1)C_l/2\pi}$ (a notation we will use throughout this paper) versus multipole $\boldsymbol{\ell}$. The **temperature likelihood** used in this paper is a hybrid: over the multipole range $\ell = 2 - 49$, the likelihood is based on a component-separation algorithm applied to 91% of the sky. **See XXVI:** Calculation of CMB Multiple Moments Power Spectra, $\boldsymbol{\ell}$.

Λ-CDM Theoretical model

We shall treat anisotropies in the CMB as small fluctuations about a Friedmann-Robertson-Walker metric whose evolution is described by General Relativity. We parameterize the **mass fraction in helium by Y_P**. The process of standard big bang **nucleosynthesis** (BBN) can be accurately modeled, and gives a predicted relation between Y_P, the photon-baryon ratio, and the expansion rate (which depends on the number of relativistic degrees of freedom).

Ionization history - Optical Depth due to Reionization (Thomson Scattering), τ and Ionization Fraction, x_e

To make accurate predictions for the CMB power spectra, the background ionization history has to be calculated to high accuracy. Although the main processes that lead to recombination at $\mathbf{z \approx 1090}$ are well understood, cosmological parameters from Planck can be sensitive to sub-percent differences in the **ionization fraction $\boldsymbol{x_e}$**. The process of recombination takes the Universe from a state of fully ionized hydrogen and helium in the early Universe, through to the completion of recombination with residual fraction $x_e \approx 10^{-4}$. Sensitivity of the CMB power spectrum to $\boldsymbol{x_e}$ enters through changes to the sound horizon at recombination, from changes in the timing of recombination, and to the detailed shape of the recombination transition, which affects the thickness of the last-scattering surface and hence the amount of small-scale diffusion (Silk) damping, polarization, and line-of-sight averaging of the perturbations. Cosmological parameters from Planck can be sensitive to sub-percent differences in the ionization fraction $\boldsymbol{x_e}$.

The background recombination model should accurately capture the ionization history until the Universe is reionized at late times via ultra-violet photons from stars and or active galactic nuclei. We approximate reionization as being relatively sharp, with the **mid-point parameterized** by a **redshift $\mathbf{z_{re}}$** (where $x_e = f/2$) the **Redshift of Half Reionization Width** parameter $z_{re} = 0.5$. Hydrogen reionization and the first reionization of helium are assumed to occur simultaneously, so that when reionization is complete $x_e = f = 1 + f_{He} \approx 1.08$, where **$\mathbf{f_{He}}$ is the helium - to-hydrogen ratio by number**.

In this parameterization, the optical depth is almost independent of z_{re} and the only impact of the specific functional form on cosmological parameters comes from very small changes to the shape of the polarization power spectrum on large angular scales. The second reionization of helium (i.e., $He^+ \rightarrow He^{++}$) produces very small changes to the power spectra ($\Delta\tau \approx 0.001$, where τ is the optical depth to Thomson scattering) and does not need to be modeled in detail. We include the second reionization of helium at a fixed redshift of $z = 3.5$ (consistent with observations of Lyman- a forest lines in quasar spectra, e.g., Becker et al. 2011), which is sufficiently accurate for the parameter analyses described in this paper.

Initial conditions: Curvature Power Spectrum

In our baseline model we assume purely adiabatic scalar perturbations at very early times, with a (dimensionless) **Curvature Power Spectrum** parameterized by

$$\mathcal{P}_{\mathcal{R}}(k) = A_s \left(\frac{k}{k_0}\right)^{n_s - 1 + (1/2)(dn_s/d\ln k)\ln(k/k_0)}$$

with **Scalar Spectrum Power-Law Index, n_s** and **Running of Spectral Index, $dn_s/d\ln k$** taken to be constant. For most of this paper we shall assume no "running", i.e., a power-law spectrum with $dn_s/d\ln k = 0$. The pivot scale, k_0, is chosen to be $\mathbf{k_0 = 0.05\ Mpc^{-1}}$, roughly in the middle of the logarithmic range of scales probed by Planck.

With this choice, n_s is not strongly degenerate with the **Amplitude Parameter A_s**.

The **Amplitude of the small-scale linear** CMB power spectrum is proportional to $e^{-2\tau} A_s$. Because Planck measures this amplitude very accurately there is a tight linear constraint between t and $\ln A_s$. For this reason we usually use $\ln A_s$ as a base parameter with a flat prior, which has a significantly more Gaussian posterior than A_s. A linear parameter re- definition then also allows the degeneracy between t and A_s to bewith n_s and $dn_s/d\ln k$ taken to be constant. For most of this paper we shall assume no "running", i.e., a power-law spectrum with $dn_s/d\ln k = 0$. The pivot scale, k_0, is chosen to be $k_0 = 0.05\ \mathrm{Mpc}^{-1}$, roughly in the middle of the logarithmic range of scales probed by Planck. With this choice, n_s is not strongly degenerate with the amplitude parameter A_s to be explored efficiently. (The degeneracy between τ and A_s is broken by the relative amplitudes of large-scale temperature and polarization CMB anisotropies and by the non-linear effect of CMB lensing.) We shall also consider extended models with a significant amplitude of primordial gravitational waves (tensor modes). Throughout this paper, the (dimensionless) tensor mode spectrum is parameterized as a power-law with

$$\mathcal{P}_t(k) = A_t \left(\frac{k}{k_0}\right)^{n_t}$$

We define $r_{0.05} = A_t/A_s$, the primordial tensor-to-scalar ratio at $k = k_0$. Our constraints are only weakly sensitive to the tensor spectral index, n_t (which is assumed to be close to zero), and we adopt the theoretically motivated single-field indication consistency relation $n_t = -r_{0.05}/8$, rather than varying n_t independently. We put a flat prior on $r_{0.05}$, but also report the constraint at $k = 0.002\ \mathrm{Mpc}^{-1}$ (denoted $r_{0.002}$), which is closer to the scale at which there is some sensitivity to tensor modes in the large- angle temperature power spectrum. Most previous CMB experiments have reported constraints on Ratio of tensor primordial power to curvature power at $k_0 = 0.05\ \mathrm{Mpc}^{-1}$, $\mathbf{r_{0.05}}$

Power spectra

Over the last decades there has been significant progress in improving the accuracy, speed and generality of the numerical calculation of the CMB power spectra given an ionization history and set of cosmological parameters.

Base parameters

The first section of Table 1 lists our base parameters that have flat priors when they are varied, along with their default values in the baseline model. When parameters are varied, unless otherwise stated, prior ranges are chosen to be much larger than the posterior, and hence do not affect the results of parameter estimation.

Derived parameters: θ_{MC} Approximation to r*/D A (CosmoMC)

Matter-radiation equality z_{eq} is defined as the redshift at which $\rho_\gamma + \rho_\nu = \rho_c + \rho_b$ (where ρ_ν approximates massive neutrinos as massless). The redshift of last-scattering, z_*, is defined so that the optical depth to Thomson scattering from $z = 0$ (conformal time $\eta = \eta_0$) to $z = z_*$ is unity, (Redshift for which the optical depth equals unity) assuming no reionization. The optical depth is given by

$$\tau(\eta) \equiv \int_{\eta_0}^{\eta} \dot{\tau}\, d\eta'$$

where $\tau = -a\, n_e\, \sigma_T$ (and n_e is the density of free electrons and σ_T is the Thomson cross section). We define the **angular scale of the sound horizon at last-scattering**, $\theta_* = r_s(z_*)/D_A(z_*)$, where r_s is the sound horizon.

$$r_s(z) = \int_0^{\eta(z)} \frac{d\eta'}{\sqrt{3(1+R)}}, \qquad \text{with } R \equiv 3\rho_b/(4\rho_\gamma).$$

Optical Depth of $r_* = 0.054$ means that about one CMB photon in 18 scatters from a free electron.

The parameter θ_{MC} (approximation to r*/D A (CosmoMC)) in Table 1 is an approximation to θ_* that is used in CosmoMC and is based on fitting formula given in Hu & Sugiyama (1996). Baryon velocities decouple from the photon dipole when Compton drag balances the gravitational force, which happens at $\tau_d \sim 1$, where

$$\tau_d(\eta) \equiv \int_{\eta_0}^{\eta} \dot{\tau}\, d\eta'/R.$$

Here, again, τ is from recombination only, without reionization contributions. We define a drag redshift z_{drag}, so that $\tau_d(\eta(z_{drag})) = 1$. The sound horizon at the drag epoch is an important scale that is often used in studies of baryon acoustic oscillations (BAO); we denote this as $r_{drag} = r_s(z_{drag})$. z_{drag} is the Redshift at which baryon-drag optical depth equals unity We compute z_{drag} and r_{drag} numerically from camb).

The characteristic wavenumber for damping, k_D, is given by

$$k_D^{-2}(\eta) = -\frac{1}{6}\int_0^{\eta} d\eta'\, \frac{1}{\dot{\tau}}\, \frac{R^2 + 16(1+R)/15}{(1+R)^2}$$

We define the angular damping scale, $\boldsymbol{\theta_D = \pi/(k_D D_A)}$, *where D_A is the comoving angular diameter distance to z_*.*

*For our purposes, the normalization of the pow*er spectrum is most conveniently given by A_s. However, the alternative measure σ_8 is often used in the literature, particularly in studies of large-scale structure. By definition, σ_8 is the rms fluctuation in total matter (baryons + CDM + massive neutrinos) in 8 h^{-1} Mpc spheres at z = 0, computed in linear theory. It is related to the dimensionless matter power spectrum, $\mathcal{P}_m$, by

$$\sigma_R^2 = \int \frac{dk}{k}\, \mathcal{P}_m(k) \left[\frac{3 j_1(kR)}{kR}\right]^2$$

where R = 8 h^{-1} Mpc and j_1 is the **spherical Bessel function of order 1**. In addition, we compute $\Omega_m h^3$ (matter density $\Omega_m/\rho_{critical}$) a well-determined combination orthogonal to the acoustic scale degeneracy in flat models; see e.g., Percival et al. 2002 and Howlett et al. 2012), $10^9 A_s e^{-2\tau}$ (which determines the small-scale linear CMB anisotropy power), $r_{0.002}$ (the ratio of the tensor to primordial curvature power at k = 0.002 Mpc^{-1}), $\Omega_m h^2$ (the physical density in massive neutrinos), and the value of Y_P from the BBN consistency condition.

Acoustic scale

The characteristic angular size of the fluctuations in the CMB is called the acoustic scale. It is determined by the comoving size of the sound horizon at the time of last-scattering, $r_s(z_*)$, and the angular diameter distance at which we are observing the fluctuations, $D_A(z_*)$. With accurate measurement of seven acoustic peaks, Planck determines the observed angular size $\theta_* = r_s/D_A$ (CosmoMC) to better than 0.1% precision at 1σ :

$$\theta_* = (1.04148 \pm 0.00066) \times 10^{-2} = 0.596724^\circ \pm 0.00038^\circ$$

BAO surveys measure the distance ratio d_z

$$d_z = r_s\left(\frac{z_{drag}}{D_V(z)}\right) \qquad D_V(z) = \left[(1+z)^2 D_A^2(z)\frac{cz}{H(z)}\right]^{1/3}$$

The tight constraint on θ_* also implies tight constraints on some combinations of the cosmological parameters that determine D_A and r_s. The sound horizon r s depends on the physical matter density parameters, and D_A depends on the late-time evolution and geometry. Parameter combinations that fit the Planck data must be constrained to be close to a surface of constant θ_*. This surface depends on the model that is assumed. For the base Λ CDM model, the main parameter dependence is approximately described by a 0.3% constraint in the three-dimensional $\Omega_m - h - \Omega_b h^2$ subspace:

$$\Omega_m h^{3.2}(\Omega_b h^2)^{-0.54} = 0.695 \pm 0.002$$

Reducing further to a two-dimensional subspace gives a 0.6% constraint on the combination

$$\Omega_m h^3 = 0.0959 \pm 0.0006$$

Hubble parameter and dark energy density - Fixed Parameter: Matter Density Parameter, $\Omega_m h^3$

The Hubble constant, H_0, and matter density parameter, Ω_m, are only tightly constrained in the Combination $\Omega_m h^3$ discussed above, but the extent of the degeneracy is limited by the effect of $\Omega_m h^2$ on the relative heights of the acoustic peaks. The projection of the constraint ellipse shown in onto the axes therefore yields useful marginalized constraints on H_0 and Ω_m (or equivalently Ω_Λ) separately. We find the 2% constraint on H_0 :

$H_0 = (67.4 \pm 1.4)$ km $^{s-1}$Mpc^{-1}. $\Omega_\Lambda = 0.686 \pm 0.020$ $\Omega_m h^2 = 0.1423 \pm 0.0029$

Optical depth - Reionication Optical Depth Parameter, τ

Small-scale fluctuations in the CMB are damped by Thomson scattering from free electrons produced at reionization. This scattering suppresses the amplitude of the acoustic peaks by $e^{-2\tau}$ on scales that correspond to perturbation modes with wavelength smaller than the Hubble radius at reionization. Planck measures the small-scale power spectrum with high precision, and hence accurately constrains the damped amplitude $e^{-2\tau} A$. With only unlensed temperature power spectrum data, there is a large degeneracy between t and A_s, which is weakly broken only by the power in large-scale modes that were still super-Hubble scale at reionization. However, lensing depends on the actual amplitude of the matter fluctuations along the line of sight. Planck accurately measures many acoustic peaks in the lensed tempera- ture power spectrum, where the amount of lensing smoothing depends on the fluctuation amplitude. Furthermore Planck's lensing potential reconstruction provides a more direct measurement of the amplitude, independently of the optical depth. The combination of the temperature data and Planck's lensing reconstruction can therefore determine the optical depth τ relatively well. The combination gives $\tau = 0.089 \pm 0.032$ (68%; Planck + lensing).
This provides marginal confirmation (just under 2σ) that the total optical depth is significantly higher than would be obtained from sudden reionization at z ~ 6, and is consistent with the WMAP-9 constraint, $\tau = 0.089 \pm 0.014$, from large-scale polarization.

$$\tau_* = \int_{t_*}^{t_0} \Gamma(t)dt = c\sigma_e \int_{t_*}^{t_0} n_e(t)dt.$$

Each free electron has a cross-section $\sigma_e = 6.65\ 10^{-29}$ m^2 for scattering with a photon given electron number density, n_e, resulting in optical depth, τ_*.

Spectral index

The scalar spectral index (see below) is measured by Planck data alone to 1% accuracy: $n_s = 0.9616 \pm 0.0094$ (68%; Planck). Since the optical depth t affects the relative power between large scales (that are unaffected by scattering at reionization) and intermediate and small scales (that have their power suppressed by $e^{-2\tau}$), there is a partial degeneracy with n_s. Breaking the degeneracy between t and n_s using WMAP polarization leads to a small improvement in the constraint: $n_s = 0.9603 \pm 0.0073$. Comparing the two values of n_s, it is evident that the Planck temperature spectrum spans a wide enough range of multipoles to give a highly significant detection of a deviation of the scalar spectral index from exact scale invariance (at least in the base ΛCDM cosmology) independent of WMAP polarization information.

$$\mathcal{P}_{\mathcal{R}}(k) = A_s \left(\frac{k}{k_0}\right)^{n_s - 1 + (1/2)(dn_s/d\ln k)\ln(k/k_0)}$$

Sachs-Wolfe Effect - Gravitational Potential ϕ, Integrated Sachs-Wolfe

The Gravitational Potential $\Phi(a)$

1. Definition and Gauge Choice

In linear cosmological perturbation theory, scalar metric perturbations about a Friedmann–Robertson–Walker background may be written in Newtonian (longitudinal) gauge as

$$ds^2 = -(1+2\Phi)\,dt^2 + a^2(t)(1-2\Psi)\,\delta_{ij}\,dx^i dx^j .$$

Here $\Phi(\mathbf{x},t)$and $\Psi(\mathbf{x},t)$represent the gravitational potentials associated with **time dilation and spatial curvature**, respectively. In the absence of significant anisotropic stress—as is an excellent approximation after recombination in ΛCDM—these two potentials are equal,

$$\Phi = \Psi.$$

The potential Φplays the role of the **relativistic generalization of the Newtonian gravitational potential**, governing both the motion of non-relativistic matter and the gravitational redshift experienced by photons.

---

2. Physical Meaning of Φ

The gravitational potential Φmeasures the depth of spacetime curvature wells created by density perturbations. Its physical effects include:

- **Time dilation:** clocks in potential wells run more slowly.
- **Gravitational redshift:** photons climbing out of wells lose energy.
- **Structure formation:** gradients of Φaccelerate matter, driving growth of overdensities.

For the Cosmic Microwave Background, Φdetermines how much energy CMB photons lose or gain both at last scattering and during their journey to the observer.

---

3. Relation to Density Perturbations

On sub-horizon scales, **Φis related to the matter density contrast δ through a relativistic Poisson equation,**

$$\nabla^2\Phi = 4\pi G a^2 \bar{\rho}\,\delta,$$

which shows that Φ encodes the gravitational influence of matter perturbations. On super-horizon scales, Φremains well defined and nearly constant for adiabatic initial conditions.

---

4. Evolution of ΦAcross Cosmological Epochs

Radiation Domination ($a \ll a_{\mathrm{eq}}$)

During radiation domination, relativistic pressure resists gravitational collapse. As perturbations enter the horizon, gravitational potentials decay. This early-time evolution is responsible for the **early Integrated Sachs–Wolfe effect**, though it contributes only modestly to the observed CMB anisotropy.

Matter Domination ($a_{\mathrm{eq}} \lesssim a \ll a_{\Lambda}$)

Once matter dominates the energy density of the universe, density perturbations grow as

$$D(a) \propto a,$$

and the gravitational potential becomes approximately constant:

$$\Phi(a) \propto \frac{D(a)}{a} \approx \text{constant}.$$

This constancy is a key result: it implies that photons traveling through matter-dominated spacetime experience **no net gravitational redshift along the line of sight**, and hence the Integrated Sachs–Wolfe effect vanishes during this epoch

Dark-Energy Domination ($a \gtrsim a_\Lambda$)
When dark energy begins to dominate, the expansion of the universe accelerates. The growth of structure slows, and density perturbations no longer grow as fast as a. Consequently,

$$\Phi(a) \propto \frac{D(a)}{a} \text{ decays with time.}$$

This decay of gravitational potentials is the physical origin of the **late-time Integrated Sachs–Wolfe effect**. Photons traversing decaying potential wells gain a small net amount of energy, producing additional temperature anisotropy on the largest angular scales.

---

5. Normalization and Interpretation of the Plot
In the figure, the potential is plotted in normalized form:

$$\Phi_{\mathrm{norm}}(a) = \frac{\Phi(a)}{\Phi(a=1)}.$$

This normalization emphasizes **relative evolution** rather than absolute amplitude:

- $\Phi_{\mathrm{norm}}(1) = 1$by construction.
- Deviations from unity at earlier times indicate how much deeper gravitational wells were in the past.
- The slope $d\Phi/da$directly controls the magnitude of the ISW contribution.

---

6. Connection to the Sachs–Wolfe and ISW Effects
The gravitational potential enters the observed CMB temperature anisotropy through

$$\frac{\Delta T}{T} = \frac{1}{3}\Phi(\eta_{\mathrm{ls}}) + 2\int_{\eta_{\mathrm{ls}}}^{\eta_0} \dot{\Phi}(\eta)\, d\eta.$$

- The **ordinary Sachs–Wolfe term** depends on the value of Φat last scattering.
- The **Integrated Sachs–Wolfe term** depends on the time derivative $\dot{\Phi}$.

Thus, the potential evolution shown in the figure is not merely a background quantity—it is the **direct source** of large-scale CMB anisotropies.

---

7. Why the Gravitational Potential Is a Sensitive Probe of Dark Energy
Unlike the expansion rate alone, the gravitational potential responds to both the background cosmology and the growth of structure. Its late-time decay provides:

- A test of cosmic acceleration independent of supernovae,
- A link between the CMB and large-scale structure via ISW cross-correlations,
- Sensitivity to deviations from ΛCDM, such as evolving dark energy or modified gravity.

For this reason, $\Phi(a)$occupies a central role in modern observational cosmology.

8. Summary
The gravitational potential $\Phi(a)$encodes the depth and evolution of spacetime curvature generated by density perturbations. Its near constancy during matter domination suppresses line-of-sight temperature shifts, while its decay during dark-energy domination generates the Integrated Sachs–Wolfe effect. The evolution of $\Phi(a)$therefore provides a direct physical bridge between the expansion history of the universe and the large-scale structure of the Cosmic Microwave Backgroun

Evolution of the Gravitational Potential $\Phi(a)$

Definition

The Newtonian-gauge gravitational potential Φdescribes scalar perturbations of the metric in the linear regime. In the absence of anisotropic stress, it governs both gravitational redshift and the growth of structure.

The quantity plotted is

$$\boxed{\Phi_{\mathrm{norm}}(a) = \frac{\Phi(a)}{\Phi(a=1)},}$$

so that the potential is normalized to unity at the present epoch.

Model for $\Phi(a)$

The potential is related to the linear growth factor $D(a)$by

$$\Phi(a) \propto \frac{D(a)}{a}.$$

The growth factor is approximated by

$$D(a) = \frac{5\Omega_m}{2}\, E(a) \int_0^a \frac{da'}{a'^3 E^3(a')}, E(a) = \sqrt{\frac{\Omega_r}{a^4} + \frac{\Omega_m}{a^3} + \Omega_\Lambda},$$

and is normalized such that $D(1) = 1$.

Physical Interpretation

- **Matter domination**
  When the universe is matter-dominated, $D(a) \propto a$, so $\Phi(a)$remains approximately constant and $\dot{\Phi} \approx 0$. In this case, the Integrated Sachs–Wolfe effect vanishes.
- **Dark-energy domination**
  As dark energy becomes dynamically important at late times, the growth of structure slows, causing gravitational potentials to decay. This time dependence ($\dot{\Phi} \neq 0$) generates the ISW contribution seen in the low-multipole power spectrum.

Connection to the Figure Above

The two figures are directly linked:

- **Figure B** shows the **cause**: time evolution of gravitational potentials.
- **Figure A** shows the **effect**: large-scale temperature anisotropies imprinted on the CMB.

A constant $\Phi(a)$produces a flat Sachs–Wolfe plateau, while a decaying $\Phi(a)$leads to enhanced power at the lowest multipoles.

Summary Description Sachs–Wolfe

Here ***Φ(ηls)*** denotes the Newtonian-gauge gravitational potential evaluated at the conformal time of last scattering, which determines the ordinary Sachs–Wolfe temperature anisotropy through $(\Delta T/T)_{SW} = \Phi(\eta_{ls})/3$.

$GP := READPRN("Phi\_of\_a\_normalized.csv")$

$a := GP^{\langle 0 \rangle}$ $\phi_{norm} := GP^{\langle 1 \rangle}$

$$\Phi_{\text{norm}}(a) = \frac{\Phi(a)}{\Phi(a=1)}$$

Φ(a) Newtonian-gauge gravitational potential evaluated at the time of last scattering z~ 1100. **Φ:** scalar metric perturbation describing gravitational potential wells

Time Domain (Cosmic History) Plot - Not Angular

The ISW Effect is controlled by $\dot{\Phi} \neq 0$

So in the $\Phi(a)$ plot:

- **ISW-active regions** → where $\Phi(a)$ $\dot{\Phi} \neq 0$ (changing)
- **No ISW** → where $\Phi(a)$ is flat

Visual rule of thumb

- Flat $\Phi(a)$ → no ISW
- Decaying $\Phi(a)$ → ISW present

In ΛCDM, the gravitational potential is computed via the growth factor:

Growth factor

$$\Phi(a) \propto \frac{D(a)}{a}$$

$$D(a) = \frac{5\Omega_m}{2} E(a) \int_0^a \frac{da'}{a'^3 E^3(a')} \quad \text{with} \quad E(a) = \sqrt{\frac{\Omega_r}{a^4} + \frac{\Omega_m}{a^3} + \Omega_\Lambda}$$

In the line-of-sight formalism, the Sachs–Wolfe contribution to the temperature transfer function is:

$$\Delta_\ell^{\text{SW}}(k) = \frac{1}{3} \Phi(\eta_{\text{ls}})\, j_\ell(k r_{\text{ls}})$$

j_l: spherical Bessel function

τ_{ls}: comoving distance to last scattering.

Figure B: Gravitation Potential Evolution

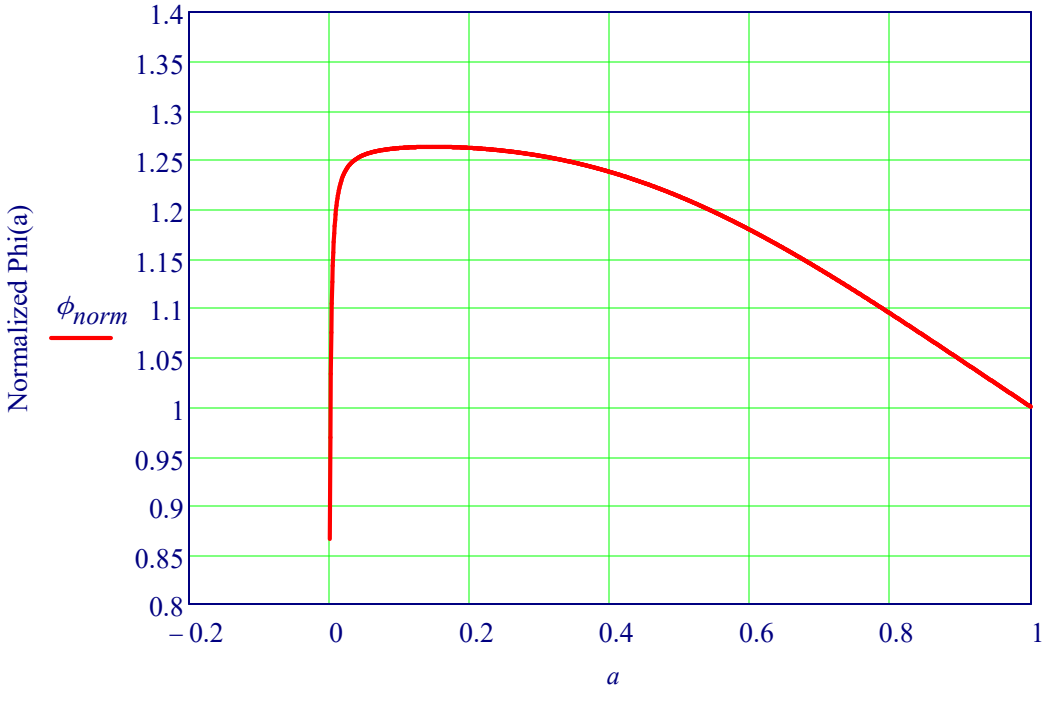

Scale Factor a

Integrated Sachs - Wolfe (ISW) Effect

Low-Multipole CMB Temperature Power Spectrum (Sachs–Wolfe + ISW)
Definition
The angular power spectrum of CMB temperature anisotropies is defined by the spherical-harmonic expansion

$$\frac{\Delta T}{T}(\hat{\mathbf{n}}) = \sum_{\ell m} a_{\ell m}\, Y_{\ell m}(\hat{\mathbf{n}}),$$

with

$$\langle a_{\ell m} a^{*}_{\ell' m'} \rangle = C_\ell\, \delta_{\ell \ell'} \delta_{m m'}.$$

The quantity plotted is

$$\boxed{D_\ell \equiv \frac{\ell(\ell+1)}{2\pi}\, C_\ell,}$$

which represents the contribution to the temperature variance per logarithmic interval in multipole moment.

Physical Content
At large angular scales ($\ell \lesssim 30$), temperature anisotropies are dominated by gravitational redshift effects rather than photon–baryon microphysics. Two mechanisms contribute:

1. **Ordinary Sachs–Wolfe effect**

$$\left(\frac{\Delta T}{T}\right)_{\mathrm{SW}} = \frac{1}{3}\,\Phi(\eta_{\mathrm{ls}}),$$

arising from photons climbing out of gravitational potential wells at the surface of last scattering.

2. **Integrated Sachs–Wolfe (ISW) effect**

$$\left(\frac{\Delta T}{T}\right)_{\mathrm{ISW}} = 2\int_{\eta_{\mathrm{ls}}}^{\eta_0} \dot{\Phi}\,(\eta)\, d\eta,$$

generated when gravitational potentials evolve with time as photons propagate to the observer.

Computed Spectrum
In line-of-sight form, the transfer function entering the power spectrum is

$$\Delta_\ell(k) = \frac{1}{3}\Phi(\eta_{\mathrm{ls}})\, j_\ell \quad (kr_{\mathrm{ls}}) + 2\int_{\eta_{\mathrm{ls}}}^{\eta_0} \dot{\Phi}\,(\eta)\, j_\ell \quad (kr(\eta))\, d\eta,$$

leading to

$$C_\ell = 4\pi \int \frac{dk}{k}\, P_\Phi(k)\, \Delta_\ell^2(k),$$

where j_ℓ are spherical Bessel functions and $P_\Phi(k)$ is the primordial potential power spectrum.

The Sachs–Wolfe plateau is: $\boxed{\ell(\ell+1)C_\ell \approx \text{constant} \quad \text{for } \ell \lesssim 30}$

Normalization
Because the absolute amplitude is not fixed in this reduced model, the spectrum is **normalized to the Sachs–Wolfe plateau**:

$$D_\ell^{\mathrm{norm}} = \frac{D_\ell}{\langle D_\ell \rangle_{10 \le \ell \le 30}}.$$

This normalization sets the mean plateau level to unity and highlights deviations due to the Integrated Sachs–Wolfe effect.

Interpretation

- A **nearly flat plateau** at low ℓ reflects scale-invariant primordial perturbations.
- Any **enhancement at the lowest multipoles** arises from late-time decay of gravitational potentials, providing a direct observational signature of dark energy.
- Acoustic peaks are absent because photon–baryon oscillations are not included in the Sachs–Wolfe treatment.

Plots Generated by Python Program:

Sachs–Wolfe + ISW - TWO PLOTS - Norm.py
Program Located at: VXPhysics.com/Python

$SW := READPRN("SW\_ISW\ \ Normalized.csv")$

Read Values: $l := SW^{\langle 0 \rangle}$ $D_l := SW^{\langle 1 \rangle}$

$$D_\ell = \frac{\ell(\ell+1)C_\ell}{2\pi} \quad \text{vs. } \ell$$

Figure A: Low-l Angular Power Spectrum (Sach's Wolfe +ISW)

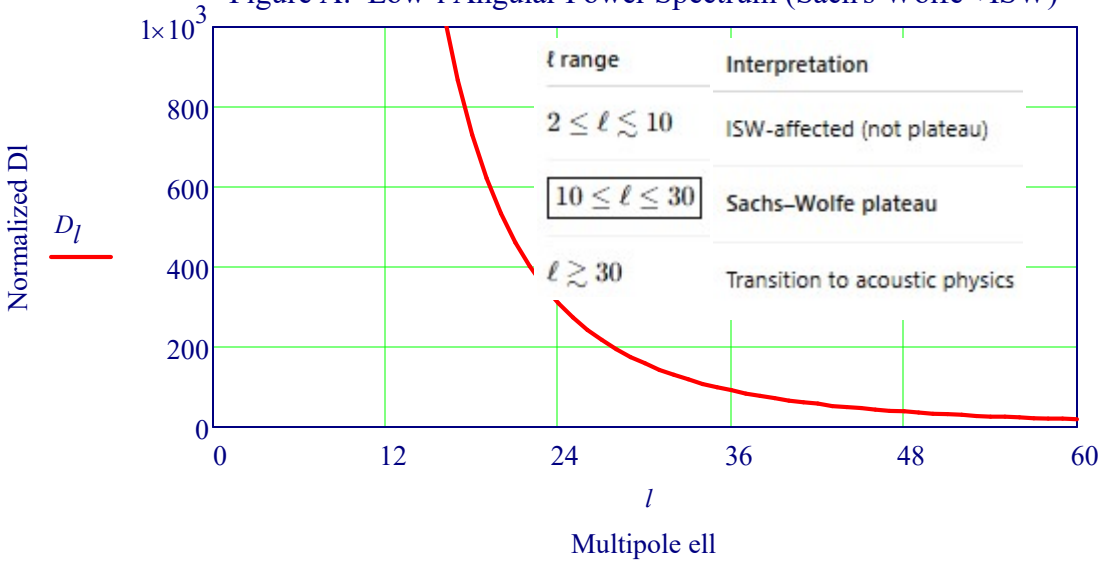

Summary:

The large-scale CMB temperature anisotropy arises from gravitational redshift at last scattering and from the subsequent evolution of gravitational potentials along the photon path. The Sachs Wolfe plateau reflects nearly scale-invariant primordial perturbations, while any low-multipole enhancement originates from the Integrated Sachs Wolfe effect driven by late-time cosmic acceleration. Together, the angular power spectrum and the gravitational potential history provide a direct link between the CMB and the expansion history of the universe.

The Real-Space Two-Point Correlation Function ξ(r) and the BAO Standard Ruler

1. Introduction

The real-space two-point correlation function, denoted ξ(r), is one of the most fundamental descriptors of large-scale structure. It quantifies how galaxies (or matter) are clustered relative to a uniform random field. While the power spectrum P(k) describes clustering in Fourier space, ξ(r) provides a complementary view in physical separation r, making it ideal for highlighting the Baryon Acoustic Oscillation (BAO) feature at ~105–110 Mpc/h.

Understanding ξ(r) unifies early-universe physics, CMB anisotropies, linear perturbation theory, and galaxy survey observations (e.g., 2dF, SDSS, BOSS, and DESI). In many ways, the BAO peak in ξ(r) is the direct fossil of acoustic waves propagating in the primordial photon-baryon fluid.

2. Definition of ξ(r)

Consider a galaxy survey with mean number density ⟨n⟩. The two-point correlation function is defined:

Definition of Real-Space Two-Point Correlation Function, ξ

$$\xi(r) = \frac{\langle n(\mathbf{x})\, n(\mathbf{x}+\mathbf{r})\rangle}{\langle n\rangle^2} - 1$$

$n(x)$ = number density galaxies at x
$\langle n\rangle$ = mean number density
$r = |\mathbf{r}|$ = Physical separation

It measures the excess probability of finding two galaxies separated by distance r.

The probability of finding a galaxy in volume dV_1 and another dV_2, separated by r, is

$$dP = n^2\,[1 + \xi(r)]\,dV_1\,dV_2$$

ξ(r) > 0 → clustering at scale r
ξ(r) = 0 → random distribution
ξ(r) < 0 → under-dense or void-like behavior

Relationship Between P(k) and ξ(r)

ξ(r) is the 3-dimensional Fourier transform of the matter power spectrum:

$$\xi(r) = \frac{1}{2\pi^2}\int_0^\infty k^2 P(k)\,\frac{\sin(kr)}{kr}\,dk$$

This integral reveals:

The broadband shape of ξ(r) comes from the general slope of P(k).
The oscillatory wiggles in P(k) (acoustic peaks) transform into a single broad BAO peak in ξ(r).
Large scales (small k) dominate behavior near the BAO radius.

This Fourier relationship is central: ξ(r) provides a complementary real-space visualization of physics encoded in P(k).

Physical Origin of the BAO Peak

Acoustic oscillations before recombination
Before z ≈ 1100, baryons and photons were tightly coupled. Overdensities launched spherical sound waves, propagating outward at

$$c_s \approx \frac{c}{\sqrt{3(1+R)}}, \quad R = \frac{3\rho_b}{4\rho_\gamma}$$

At recombination, photon pressure vanished and the wavefront "froze in" at the sound horizon: $r_s \approx 105\,h^{-1}\,Mpc$

Result in ξ(r)

A galaxy today is slightly more likely to have a neighbor at **~105 Mpc/h**, the radius of the primordial shell.
This produces a **broad peak** in ξ(r) centered near that separation.
The BAO peak serves as a **standard ruler** for measuring the expansion history

Typical Shape of ξ(r)

1. Small scales (r < 5 Mpc/h):
   Strong clustering; ξ(r) ≫ 1.
2. Intermediate scales (5–50 Mpc/h):
   ξ(r) decays roughly as a power law, often approximated by: $\xi(r) \approx \left(\frac{r}{r_0}\right)^{-1.8}$
3. BAO scale (~100–115 Mpc/h):
   A broad peak, amplitude of a few × 10^{-2}.
4. Large scales (>150 Mpc/h):
   ξ(r) → 0 or slightly negative (approaching homogeneity).
6. A Practical Fitting Model for ξ(r)
   For applications, ξ(r) is often approximated as:

ΛCDM-Like Analytic Model Approximation: $\xi_{model}(r)$

$$\xi(r) = A\, r^{-\alpha} e^{-r/r_d} + B \exp\left[-\frac{(r - r_{BAO})^2}{2\sigma^2}\right]$$

where:

- $A r^{-\alpha} e^{-r/r_d}$ → broadband clustering
- Gaussian term → BAO bump
- $r_{BAO} \approx 108\,\mathrm{Mpc}/h$
- $\sigma \approx 10-15\,\mathrm{Mpc}/h$ (Silk damping + nonlinear broadening)

$$\xi_{model}(r) := 4.8 \cdot 10^{4} \cdot r^{-1.73} \cdot e^{\frac{-r}{210}} + 43 \cdot exp\left[\frac{-(r-108.5)^2}{2(11.5)^2}\right] + \Xi$$

This model fits SDSS-III and BOSS DR12 ξ(r) data shown below eand matches the extracted points from the BAO figure.

Measurement in Galaxy Redshift Surveys

Modern surveys measure ξ(r) by:
Counting galaxy pairs at separation r → **D–D counts**
Comparing to random catalog pairs → **R–R**
Using the Landy–Szalay estimator of *ξ(r)* :

$$\xi(r) = \frac{DD - 2DR + RR}{RR}$$

This minimizes variance and corrects for survey geometry.

Key features measured:

Position of the BAO peak → gives $D_v(z)$, $H(z)$, $D_A(z)$
BAO peak height + width → growth of structure
Broadband slope → Ω_m, n_s, dark energy effects

What is a "galaxy pair": Landy–Szalay estimator

Take all the galaxies in a survey (e.g., SDSS, DESI).
For every pair of galaxies, compute their separation r.
Example: If galaxy A and galaxy B are 110 Mpc/h apart, that is one pair with separation 110.
A large survey may contain billions of such pairs.

D–D (Data-Data) = the number of galaxy pairs in the real data at separation r

"D" stands for Data — the actual observed galaxy positions. Count how many pairs of real galaxies have separations **in each bin** (e.g., 100–101 Mpc/h).
This measures:
how often real galaxies are found at distance r.

If the Universe were completely uniform,
DD(r) would follow a predictable curve (roughly ∝ r^2).
But clustering causes **excess counts**
at certain scales → that's ξ(r).

Why ξ(r) is Important

It is **the clearest observable imprint** of the **sound horizon in the late Universe**.
It provides a geometric standard ruler, independent of supernova systematics.
ξ(r) is less sensitive than P(k) to small-scale nonlinearities.
It directly connects CMB physics to galaxy clustering.

Many Superimposed Waves
Positions predicted once dark matter and baryon density is known.

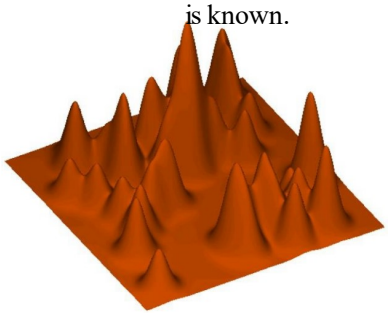

BAO measurements in ξ(r) contribute enormously to constraints on:

Dark energy equation of state w(z)
Curvature Ω_k
Hubble parameter H(z)
Matter density Ω_m

Example: BAO Data Extraction

Using the SDSS post-reconstruction plot in this paper, the extracted ξ(r) values show:

A declining broadband shape
A well-defined BAO bump near 108–110 Mpc/h
Slight negative dip near 140 Mpc/h
Rising toward 200 Mpc/h as nonlinear effects increase

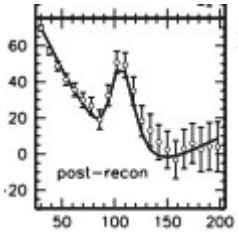

These values match the analytic model above and provide a real worked example.

Summary

The real-space correlation function ξ(r):
Encodes how galaxies cluster as a function of physical separation
Is the Fourier counterpart to the power spectrum P(k)
Contains a robust BAO peak from primordial acoustic waves
Serves as an essential tool for precision cosmology
Provides a direct geometric method for testing ΛCDM and probing dark energy

Incorporating ξ(r) and the BAO standard ruler into the broader framework of cosmological modeling completes the unified picture of how early-universe physics shapes present-day structure.

DETECTION OF THE BARYON ACOUSTIC PEAK

Having established the physical origin of the sound horizon and its role in setting the characteristic acoustic scale, it is useful to examine how this primordial feature manifests itself in present-day large-scale structure. The same oscillations imprinted in the early photon–baryon fluid leave a corresponding signature in the late-time matter distribution, producing a distinct bump in the real-space two-point correlation function ***ξ(r)*** at a comoving separation of roughly **105 h^{-1} Mpc**. **This "BAO peak"** provides a powerful standard ruler that connects the physics of recombination to the clustering of galaxies in the low-redshift Universe. To illustrate this connection explicitly, the following dataset and plot show ξ(r) over separations of 50–250 h^{-1} Mpc, highlighting the BAO feature predicted by ΛCDM and measured in surveys such as SDSS and BOSS.

Extended Baryon Oscillation Spectroscopic Survey (eBOSS),

https://arxiv.org/pdf/astro-ph/0501171

The acoustic peaks in the cosmic microwave background (CMB) anisotropy power spectrum have emerged as one of **the strongest cosmological probes**. They measure the contents and curvature of the universe Acoustic peaks occur because the cosmological perturbations excite sound waves in the relativistic plasma of the early universe. The recombination to a neutral gas at redshift z ~ 1000 abruptly decreases the sound speed and effectively **ends the wave propagation**. In the time between the formation of the perturbations and the epoch of recombination, **modes** of different wavelength can complete different numbers of oscillation periods. **This translates the characteristic time into a characteristic length scale &** produces a **harmonic series of maxima and minima in the anisotropy power spectrum**.

The data in the file: "SDSS-III BAO Measurements.txt"

gives a table that presents a theoretical estimate of the real-space two-point correlation function, ξ(r),

for comoving separations between 50 and 250 h^{-1} Mpc in a standard ΛCDM cosmology. This function quantifies the excess probability, relative to a random distribution, of finding pairs of galaxies separated by a distance r, and it **encodes key information about the large-scale clustering of matter in the Universe.**

Research Study:

The clustering of galaxies in the SDSS-III Baryon Oscillation Spectroscopic Survey: baryon acoustic oscillations in the Data Releases 10 and 11 Galaxy samples, MNRAS 441, 24–62 (2014)

BAO position in spherically averaged two-point measurements is fixed by the projection of the sound horizon at the drag epoch, r_d, and provides a measure of:

$$D_V(z) \equiv \left[cz(1+z)^2 D_A(z)^2 H^{-1}(z)\right]^{1/3}$$

Definition of Real-Space Two-Point Correlation Function, ξ

$$\xi(r) = \frac{\langle n(\mathbf{x})\, n(\mathbf{x}+\mathbf{r})\rangle}{\langle n\rangle^2} - 1$$

n(x) = number density galaxies at ***x***
⟨n⟩ = mean number density
r = |***r***| = Physical separation

Fetch the Correlation Data from the SDSS-III Paper ⟶

$Corr := READPRN("SDSS\text{-}III\ BAO\ Measurements.txt")$

$r_{sdss} := Corr^{\langle 0\rangle}$ $\quad \xi := Corr^{\langle 1\rangle}$ $\quad \xi_{smooth} := ksmooth(r_{sdss}, \xi, 6)$

$$\xi_{model}(r) := 4.8\cdot 10^4 \cdot r^{-1.73} \cdot e^{\frac{-r}{210}} + 43\cdot exp\left[\frac{-(r-108.5)^2}{2(11.5)^2}\right]$$

Example:
At r≈100Mpc/h,
ξ(r) has a small bump

Baryon Acoustic Oscillation, BAO

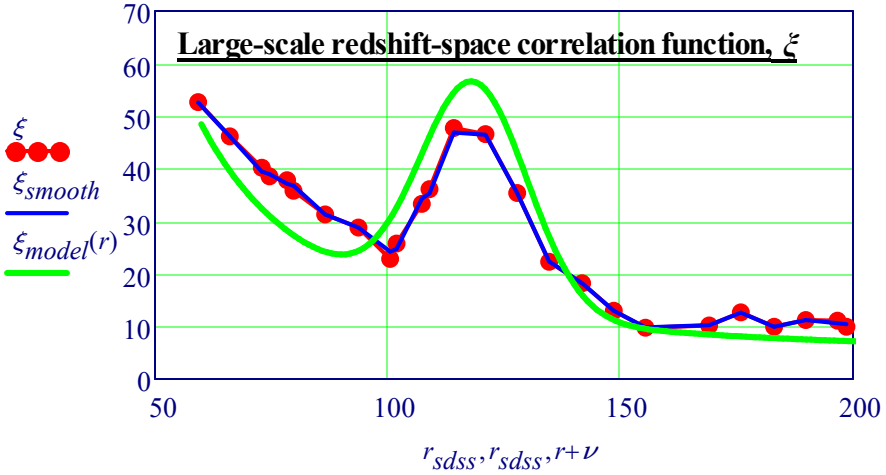

Comoving Separation, s (Mpc/h)

Introduction: Weak Gravitational Lensing

Weak gravitational lensing uniquely probes the growth of structure rather than cosmic geometry alone. Unlike supernovae and baryon acoustic oscillations, which primarily constrain distance–redshift relations, lensing directly measures the amplitude and evolution of matter fluctuations through the coherent distortion of background galaxies. As a result, weak lensing is particularly sensitive to the parameter combination,

$$S_8 = \sigma_8 \cdot \sqrt{\frac{\Omega_m}{0.3}}$$

making it a critical test of ΛCDM consistency at late cosmic times.

Variables

- shear γ
- convergence κ
- kernels W(z)

Conceptual Overview of Weak Gravitational Lensing and the Convergence Field

This diagram shown below illustrates the physical and observational basis of weak gravitational lensing in large-scale structure. Light from distant background galaxies is deflected by intervening foreground dark-matter halos along the line of sight, producing small but coherent distortions in observed galaxy shapes.

These distortions are quantified by the **shear field *γ*,** an observable extracted statistically from ensembles of galaxy ellipticities. Through line-of-sight integration and inversion techniques, **the shear field is used to reconstruct the convergence field *κ(θ)***, which traces the projected mass density.

The resulting κ maps and their angular power spectra encode information about the underlying matter power spectrum ***P(k)***, the matter density parameter Ω_m, and the growth of structure through the growth factor ***D(z)***.

To see how it relates to ΛCDM - Refer to Section:

XXIII B Python ΛCDM Six-Parameter Base Model - GCP

Introduction for CAMB_CMB_TT and _Lensing

Weak Gravitational Lensing

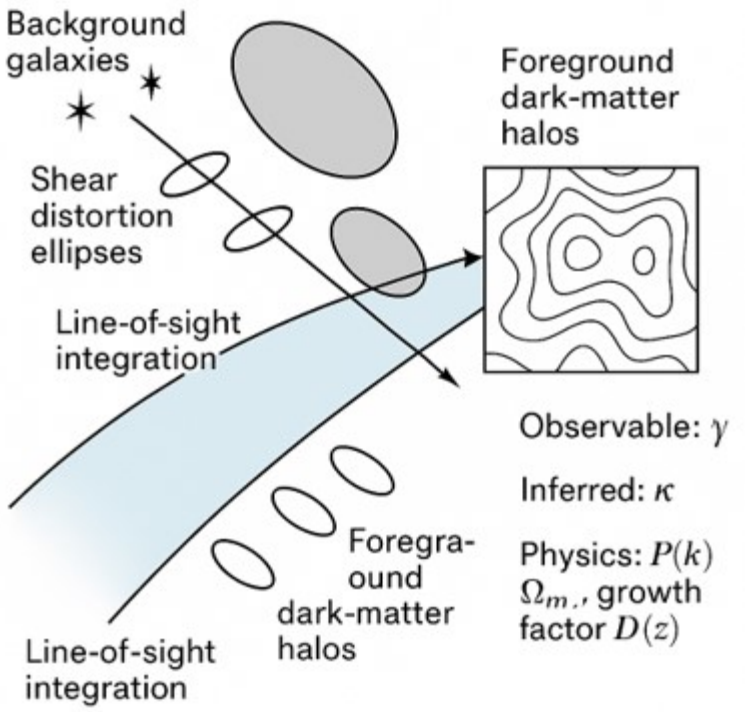

Core Observable Convergence $\kappa(\theta)$

κ is a weighted line-of-sight projection of the matter overdensity

- Depends on: Ω_m
- Growth of structure
- Geometry via distances
- Scale factor a(χ)

This connects weak lensing directly to ΛCDM parameters, not just observationally but mathematically.

Weak Gravitational Lensing - Key Equations

Convergence (line-of-sight projection):

$$\kappa(\theta) = \frac{3H_0^2\Omega_m}{2c^2}\int_0^{\chi_s} d\chi\, \frac{(\chi_s-\chi)\chi}{\chi_s\, a(\chi)}\, \delta(\chi,\theta)$$

Shear–convergence relation (Fourier space, flat-sky):

$$\gamma(\ell) = e^{2i\varphi_\ell}\, \kappa(\ell)$$

Convergence angular power spectrum (Limber approximation, flat universe):

$$C_\ell^{\kappa\kappa} = \int_0^{\chi_s} d\chi\, \frac{W^2(\chi)}{\chi^2}\, P_\delta\!\left(k = \frac{\ell+1/2}{\chi},\, z(\chi)\right)$$

Lensing efficiency (single source plane):

$$W(\chi) = \frac{3H_0^2\Omega_m}{2c^2}\, \frac{\chi}{a(\chi)}\, \frac{\chi_s-\chi}{\chi_s}$$

Rescaled spectrum often plotted:

$$D_\ell^{\kappa\kappa} \equiv \frac{\ell(\ell+1)}{2\pi}\, C_\ell^{\kappa\kappa}$$

S8 parameter (growth-of-structure diagnostic):

$$S_8 \equiv \sigma_8 \sqrt{\Omega_m/0.3}$$

Key Equations

Generic observable–parameter mapping:

$$\mathcal{O} = \mathcal{F}(\Omega_m, H_0, \sigma_8, w, \ldots)$$

Weak-lensing example $C_\ell^{\kappa\kappa} \propto S_8^2$

CMB example: $\theta_s = \dfrac{r_s(z_*)}{D_A(z_*)}$

What is labelled on the Weak Lensing Geometry

- *Observable:* **shear** γ (galaxy weak lensing)
- *Inferred:* **convergence** κ (mass reconstruction / CMB lensing)
- Source planes (galaxies vs CMB last-scattering surface)
- Foreground mass / halos
- Observer

Weak Lensing Geometry

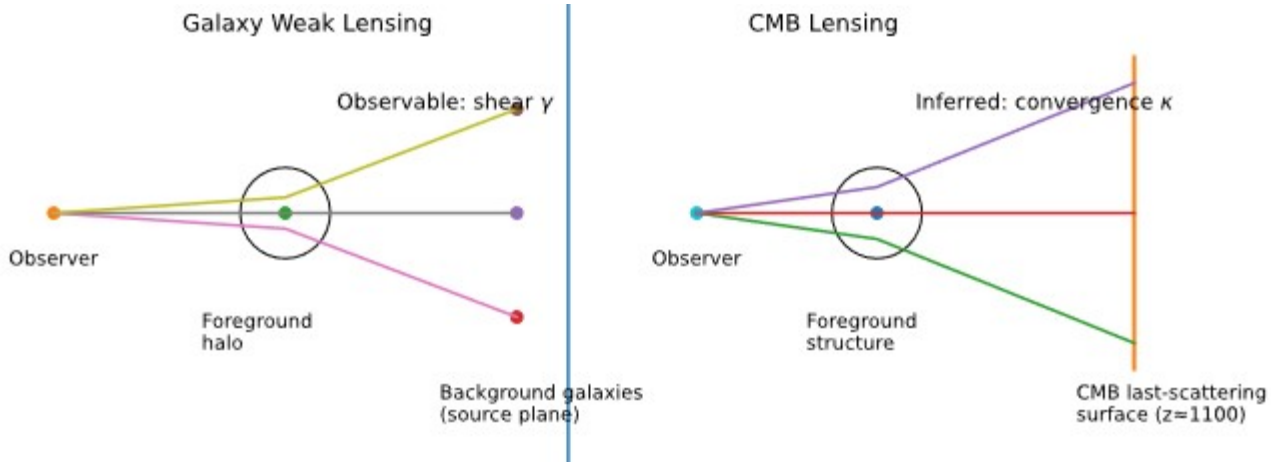

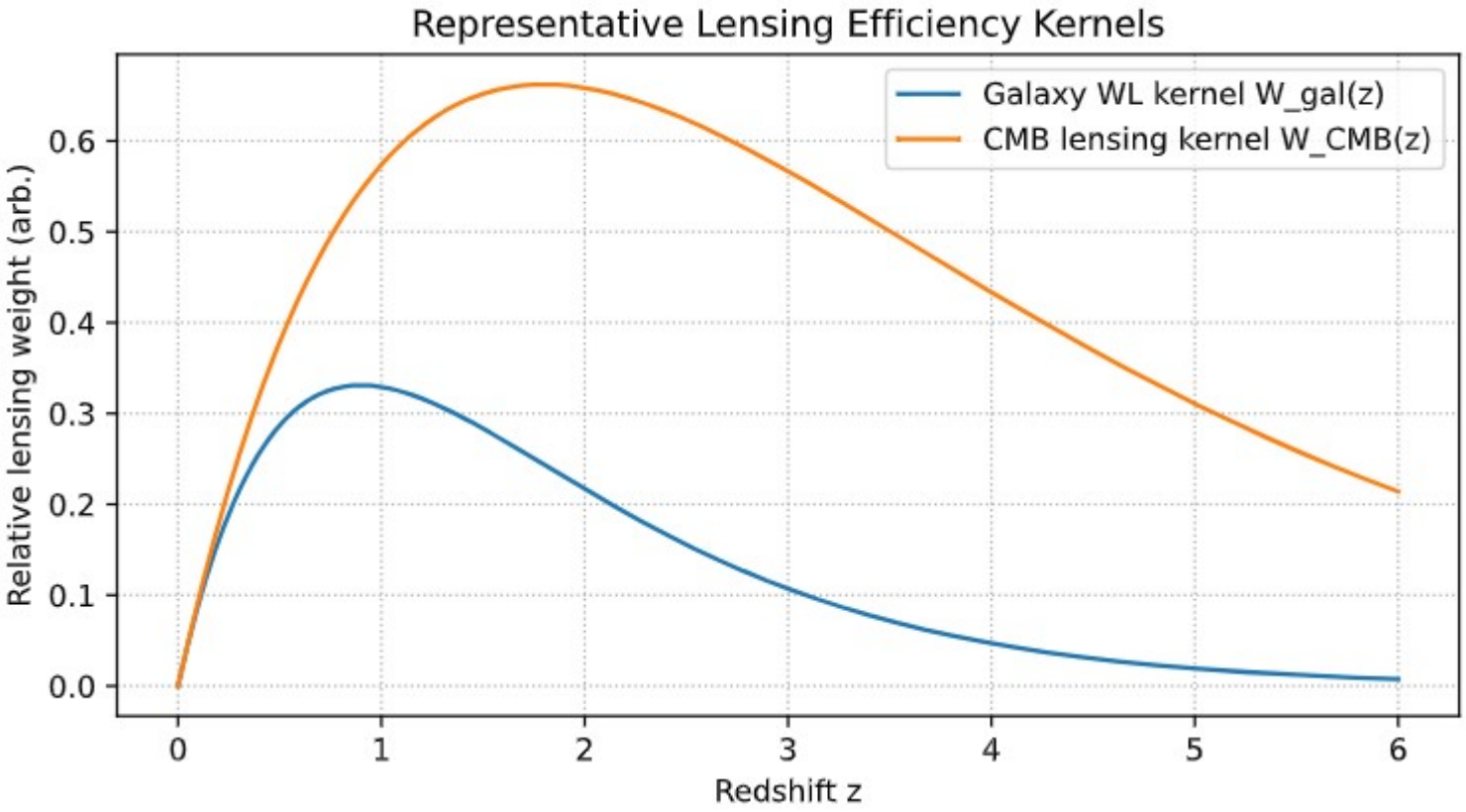

Weak Gravitational Lensing (Cosmic Shear)

Geometry → $\kappa(\theta)$ → C_l

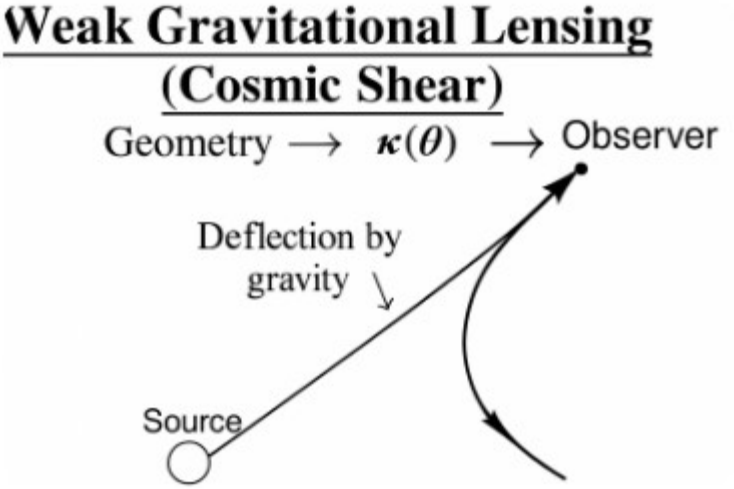

Weak gravitational lensing constrains the combined parameter S_8

Making it a uniquely sensitive probe of structure growth
and a key diagnostic for testing ΛCDM and its extensions.

Connection to Modified Gravity and Dark Energy

Implications for New Physics

The sensitivity of weak gravitational lensing to S_8 makes it a powerful probe of physics beyond the standard ΛCDM model. Measurements of S_8 from weak-lensing surveys such as DES, KiDS, and HSC are systematically lower than the value inferred from the Cosmic Microwave Background under ΛCDM assumptions, giving rise to the so-called S_8 *tension*.

This tension may reflect:

- **Modified gravity**, in which the growth of structure deviates from General Relativity while leaving background expansion largely unchanged.
- **Evolving dark energy**, which alters the growth factor $D(z)$ and suppresses structure formation at late times.
- **Massive neutrinos**, which damp small-scale power and reduce the lensing signal.
- **Astrophysical systematics**, such as baryonic feedback or intrinsic alignments.

Because weak lensing directly probes the growth of structure rather than only the background geometry, it provides a crucial complement to CMB and supernova measurements. Any successful extension of ΛCDM must simultaneously account for both the expansion history and the observed value of S_8.

Python Program to Generate "Toy" Plots: *weak_lensing_kappa_power_spectrum.py*

Compute a toy weak-lensing convergence power spectrum assuming Eisenstein–Hu ***P(k)*** and a single source redshift.

κ is a weighted line-of-sight projection of the matter overdensity

$$\kappa(\boldsymbol{\theta}) = \frac{3H_0^2\Omega_m}{2c^2}\int_0^{\chi_s}\frac{(\chi_s-\chi)\chi}{\chi_s a(\chi)}\,\delta(\chi,\boldsymbol{\theta})\,d\chi$$

κ is a weighted line-of-sight projection of the matter overdensity

Depends on:

- Growth of structure
- Geometry via distances
- Scale factor a(χ)
- $H_0 \rightarrow$ geometry
- $S_8 \rightarrow$ growth

Weak gravitational lensing primarily constrains the parameter combination

$$S_8 = \sigma_8\cdot\sqrt{\frac{\Omega_m}{0.3}}$$

which captures the dominant degeneracy between the amplitude of matter fluctuations and the matter density.

$$\gamma(\ell) = e^{2i\phi}\,\kappa(\ell)$$

Weak lensing surveys measure shear, which is mathematically inverted to recover the projected mass field.
Weak lensing uniquely measures the projected matter density
without relying on luminous tracers or galaxy bias assumptions.

Toy weak-lensing convergence power spectrum

Flat ΛCDM: H_0=70.0 km/s/Mpc, $\Omega_m = 0.3$, $\Omega_L = 0.7$, $n_s = 0.965$, $\sigma_8 = 0.8$, $z_s = 1.0$

Data: l Cl $D_l = l(l+1)\,C_l/(2\pi)$

Read Data from Python Program: $WLens := READPRN("kappa_power_spectrum-Data2.txt")$

$l := WLens^{\langle 0\rangle}$ $C_l := WLens^{\langle 1\rangle}$ $D_l := WLens^{\langle 2\rangle}$

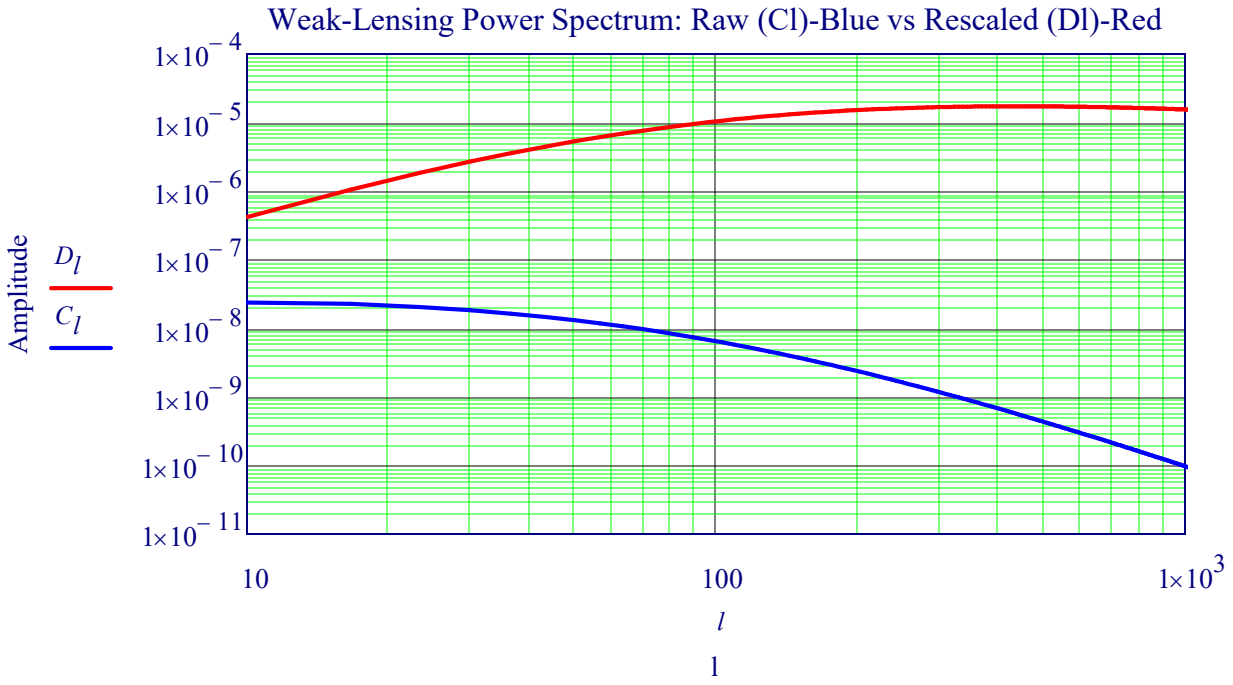

In the standard cosmological framework, weak gravitational lensing

encodes information about both the geometry of the Universe and the growth of structure. The convergence and shear fields depend on the matter power spectrum projected along the line of sight, making lensing sensitive to the total matter content and the amplitude of density fluctuations. Consequently, the lensing signal responds similarly to an increase in the matter density Ω_m or an increase in the fluctuation amplitude σ_8,

producing a degeneracy between these two parameters.

Rather than constraining Ω_m and σ_8 independently, weak-lensing data primarily constrain the combination

$$S_8 = \sigma_8 \sqrt{\Omega_m/0.3} \quad \Rightarrow \quad \sigma_8 = \frac{S_8}{\sqrt{\Omega_m/0.3}} \qquad \sigma_8(S_8, \Omega_m) := S_8 \cdot \left(\sqrt{\frac{\Omega_m}{0.3}}\right)$$

which traces the dominant direction of sensitivity in parameter space.

This behavior is illustrated in the following figure, where curves of constant S_8 define the characteristic degeneracy pattern observed in weak-lensing analyses.

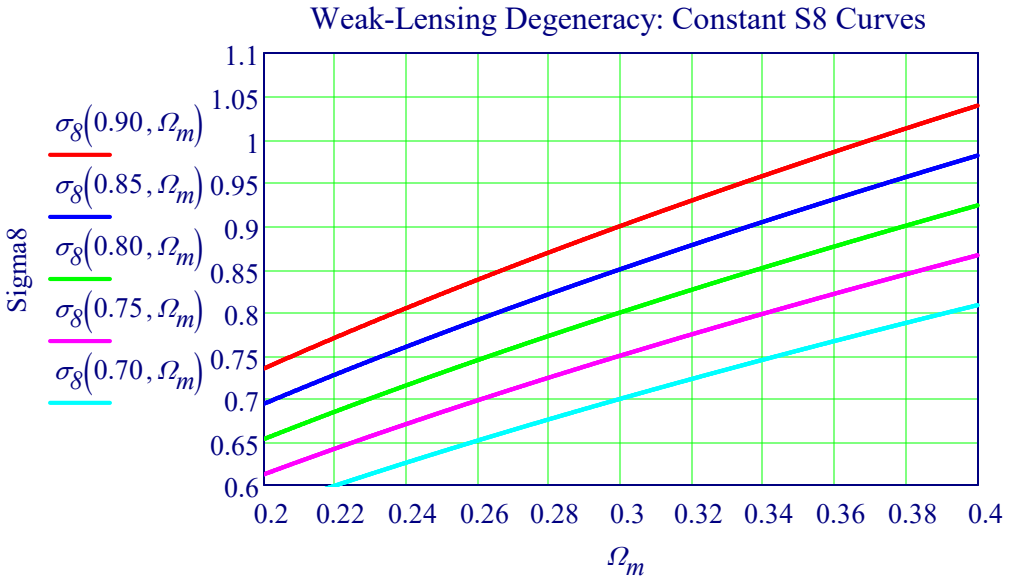

Overlay DES / KiDS / HSC Likelihood Contours

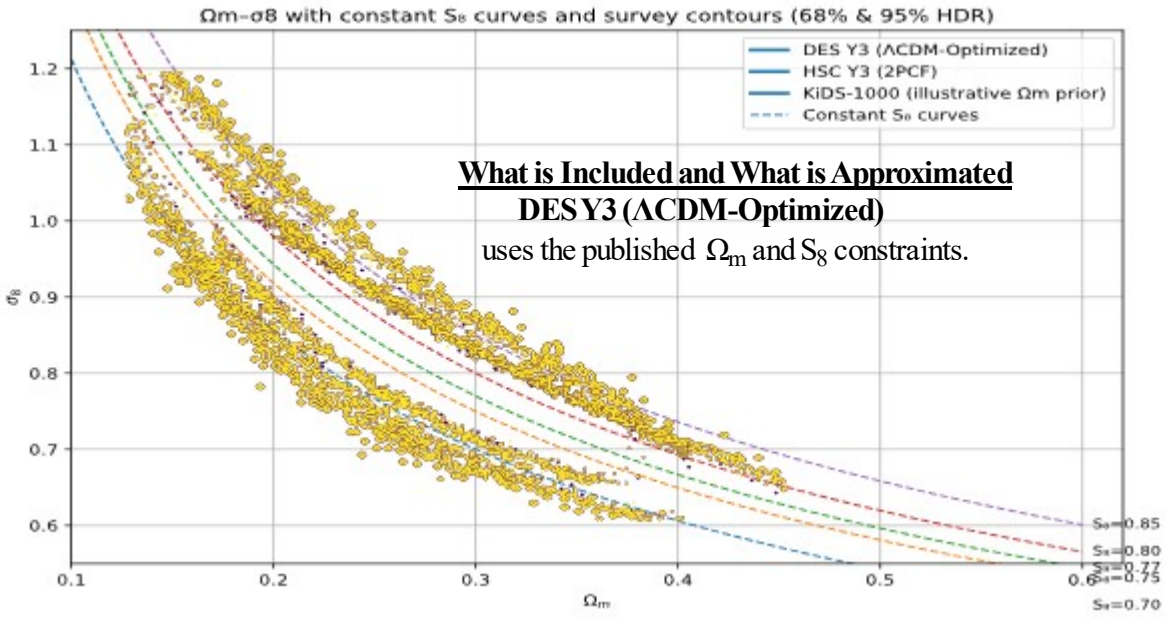

Degeneracy in Weak Gravitational Lensing

Weak gravitational lensing measurements probe the projected matter distribution through the coherent distortion of background galaxy shapes.
The amplitude of this signal depends on both the present-day normalization of matter fluctuations, σ_8, and the matter density parameter, Ω_m. As a result, cosmic shear surveys are most sensitive to the combined parameter

$$S_8 = \sigma_8 \cdot \sqrt{\frac{\Omega_m}{3}}$$

The Figure below illustrates the resulting degeneracy using an analytic likelihood constructed directly in the $\Omega_m - \sigma_8$ plane. The filled contours represent relative likelihood values, while the white curves indicate approximate 68% and 95% confidence regions.
The elongated shape of the contours reflects the fact that increases in Ωm can be partially compensated by decreases in σ_8, leaving the lensing signal approximately unchanged.
Although this figure is not derived from a full Markov-Chain Monte Carlo analysis, it reproduces the characteristic structure and orientation of weak-lensing constraints seen in surveys such as DES, KiDS, and HSC, making it useful for conceptual understanding and model comparison.

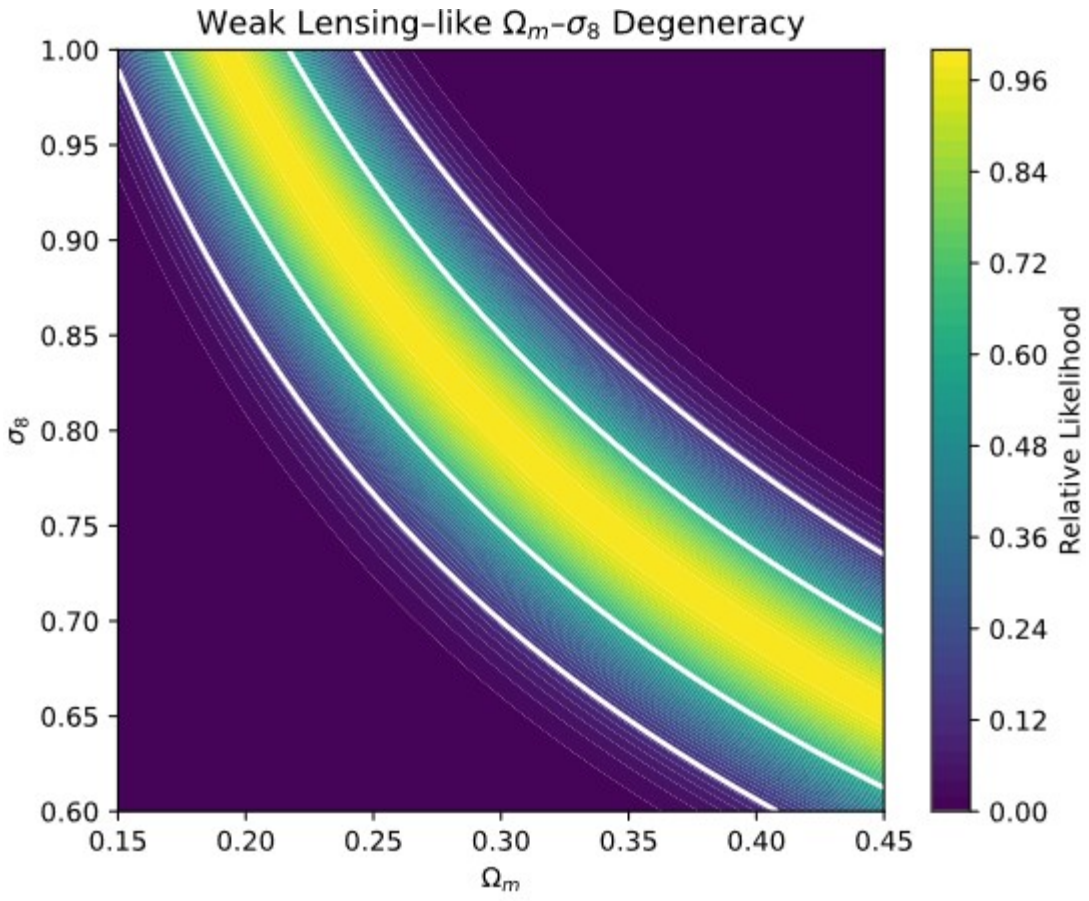

This figure is intended as a conceptual illustration;
full parameter constraints require detailed survey likelihoods, redshift distributions, and nonlinear modeling

Mollweide Toy Multimode Map

The Mollweide projection provides a **full-sky, equal-area representation of fields** defined on the celestial sphere and is widely used in cosmology to visualize Cosmic Microwave Background (CMB) temperature anisotropies, polarization patterns, and large-scale structure.
The figure mollweide_toy_multimode.svg presents a simplified, illustrative ("toy") sky map constructed from the superposition of multiple spherical harmonic–like modes. Rather than representing observational data, this visualization is designed to demonstrate how different angular scales and mode combinations manifest as coherent structures on the sphere when projected onto a two-dimensional map.

By combining low- and intermediate-order angular modes, the figure highlights key qualitative features such as large-scale hemispherical variations, nodal lines, and localized hot–cold regions that naturally arise in spherical decompositions. The Mollweide projection preserves relative area across the sky, allowing visual comparison of mode amplitudes and spatial correlations without distortion of surface weighting.

This toy multimode map serves as a pedagogical bridge between abstract harmonic coefficients $a_{\ell m}$ and their real-space sky patterns. It provides intuition for how power at different multipoles contributes to observed anisotropy maps and why full-sky projections are essential for interpreting angular correlations, power spectra, and symmetry properties in cosmological data analysis.

Uses the Python Program: mollweide_sphharm_and_lensing_kernel.py
Python Program is located: *VXPhysics.com/Python*

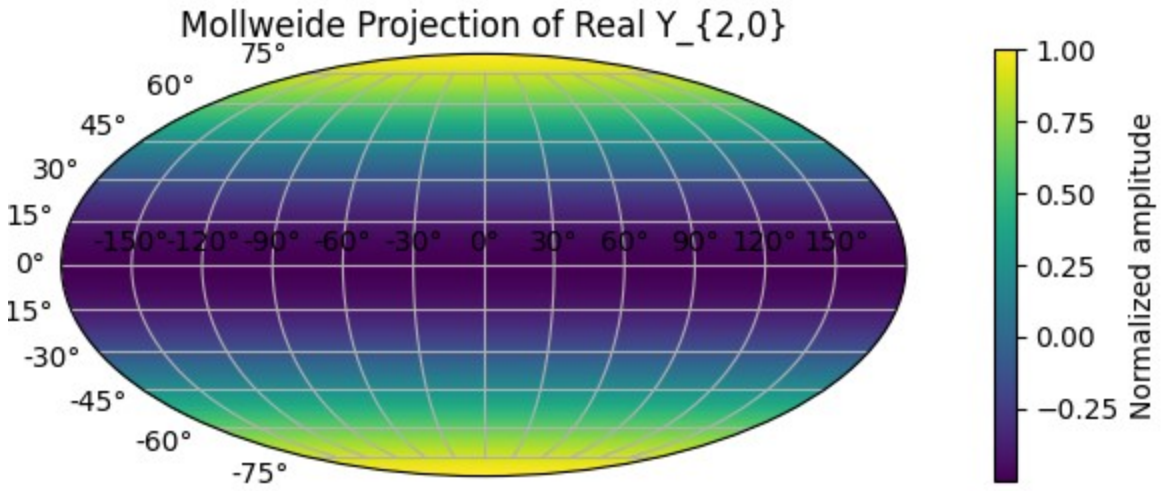

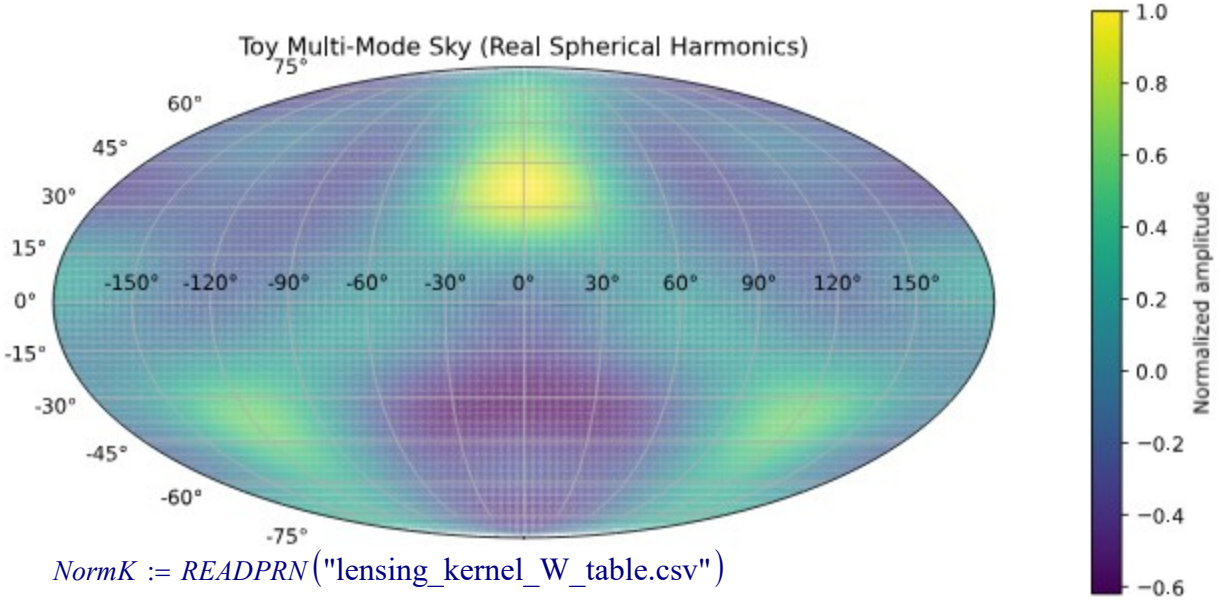

$NormK := READPRN("lensing\_kernel\_W\_table.csv")$

$z := NormK^{\langle 0 \rangle}$ $\chi_{cm} := NormK^{\langle 1 \rangle}$ $WLK := NormK^{\langle 2 \rangle}$

Radial Weak-Lensing Kernel vs Redshift, z

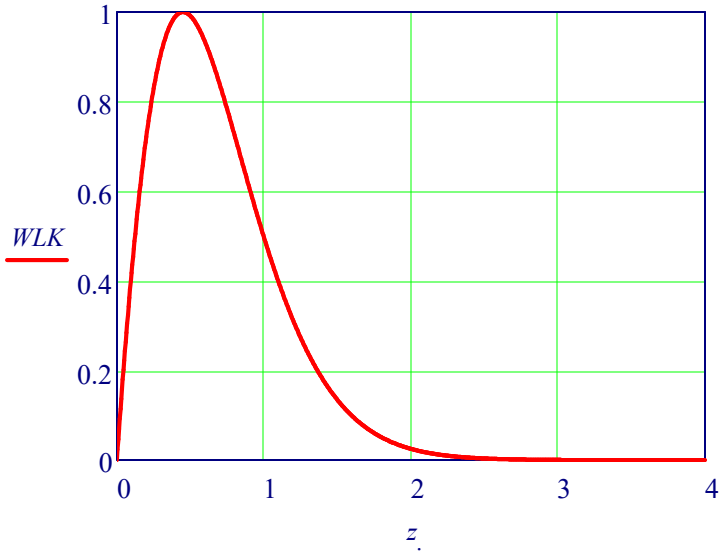

Radial Weak-Lensing Kernel vs x

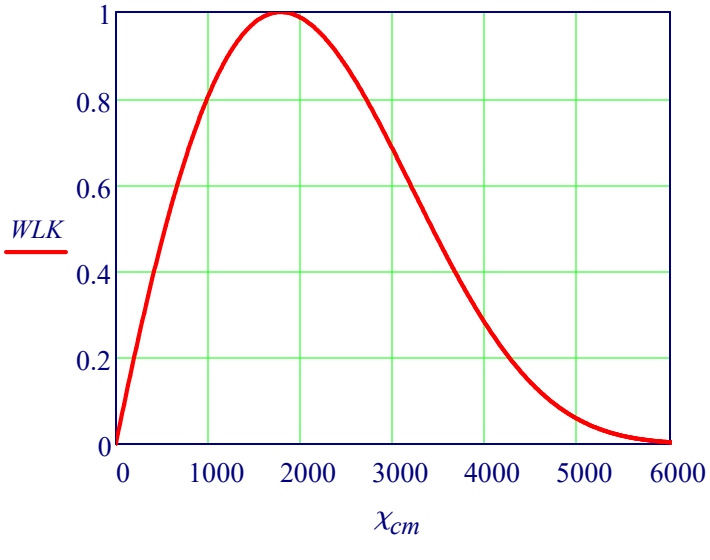

Planck Collaboration: Cosmological parameters

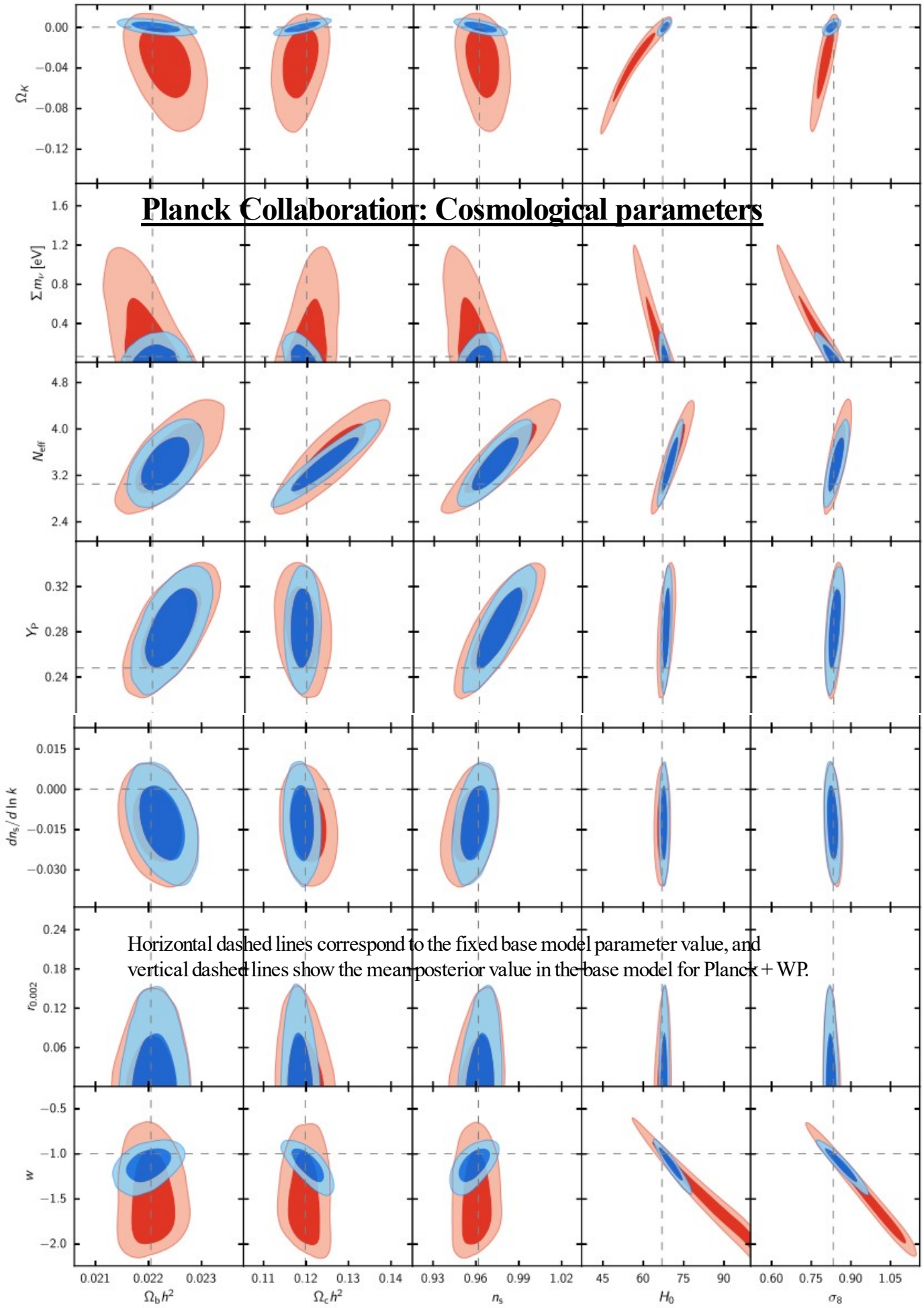

Horizontal dashed lines correspond to the fixed base model parameter value, and vertical dashed lines show the mean posterior value in the base model for Planck + WP.

Uniformity of the CMBR is Evidence for Istropic Expansion and the ΛCDM

1998 COBE Far Infrared Absolute Spectrophotometer Monopole Spectrum Measurements

Assess If the Origin of the Cosmic Microwave Background Radiation (CMBR) is from the ΛCDM

COBE Measurements of CMBR Spectrum - Test: Surface of Last Scattering (from Clouds)? Thermal Blackbody?

Column 1 = Reciprocal Wavelength, λ, from Table 4 of Fixsen et al., in units = cm^{-1}

Column 2 = Intensity of FIRAS monopole spectrum computed as the sum of column 3, units = MJy/sr

$CMBR := READPRN("iras\_monopole\_spec\_v1.txt")$ $T_{mw} := 2.7250K$

$\lambda := CMBR^{\langle 0 \rangle}$ $\lambda_6 = 4.99$ $I := CMBR^{\langle 1 \rangle}$ $n := 0, 1 .. rows(I) - 1$

$k_b := 1.3806505 \cdot 10^{-23} \cdot \frac{joule}{K}$ $h := 6.6260693 \cdot 10^{-34} \cdot joule \cdot sec$

Determine How Well COBE Spectrum Matches the Stretched Black Body Radiation at T = 2.750 K

Model: Equation for Intensity of Ideal Black Body Spectrum

$$B_\lambda(\lambda, T) := 2h \cdot c^2 \cdot \lambda^3 \cdot \left(e^{\frac{h \cdot c \cdot \lambda}{k_b \cdot T}} - 1 \right)^{-1}$$

Normalize Units at λ = 4.99

$$N_{unit} := I_6 \cdot B_\lambda\left(\frac{4.99}{cm}, T_{mw} \right)^{-1}$$

Wavelength of Light, λ, Stretches with Expansion

Stretches with the scale factor, a and λ stretch factor, z.

Given wavelength at emission, λ_o, λ today is

$$\lambda = \frac{1}{a(t)} \cdot \lambda_0 = (1 + z)\lambda_0$$

The CMBR has the most Perfect (Planckian) Black Body Spectral Curve known: T = 2.725 ± 0.001 K

Evidence: COBE CMB Radiation Black Body Spectrum is Perfect Fit for 2.725 K

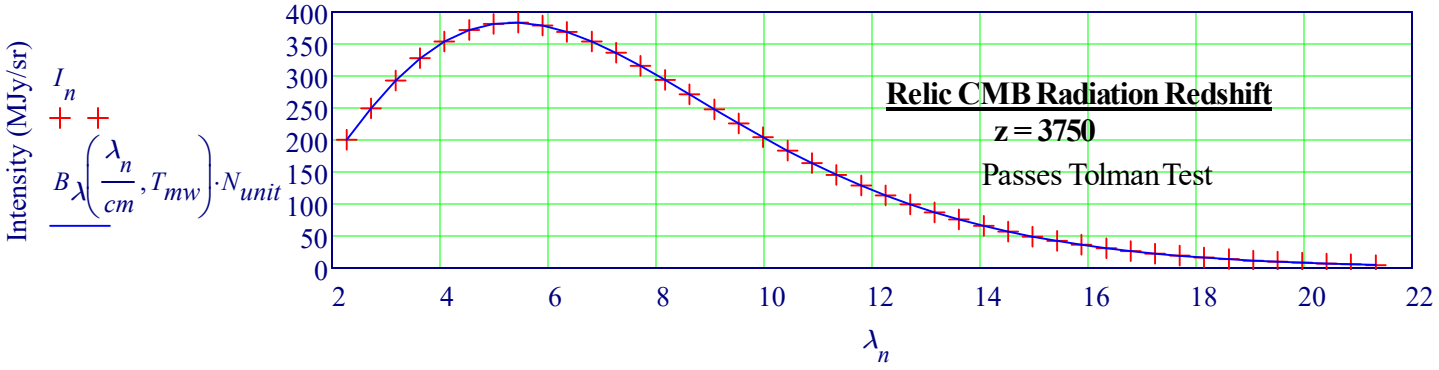

Frequency Measured as Reciprocal Wavelength (1/cm)

CMB Energy: $N19 := 10^{-19}$ $eV := 1.6 \cdot 10^{-19} C \cdot volt = 1.6 J \cdot N19$ $k_b \cdot 2.75K = 0 \cdot eV$

Measured Uniformity (Low Error) of CMBR Temperature Reveals An Almost Perfect 2.725K Spectrum

$$Error\% := \frac{1}{rows(I) \cdot 100} \left[\sum_n \left(I_n - B_\lambda\left(\frac{\lambda_n}{cm}, T_{mw} \right) \cdot N_{unit} \right) \right]$$

$Error\% = 3.0064 \times 10^{-5}$

Scaling ==> $Temp(t) = \frac{T_0}{a(t)}$ $\lambda := \frac{c}{\nu} \approx$ **a**

CONCLUSION - ORIGIN OF CMBR:

The CMB radiation was emitted 13.7 billion years ago, only a few hundred thousand years after the ΛCDM, **long before stars or galaxies ever existed**. Radiation's temperature is defined by the wavelength of the individual photons that make it up. **As the Universe expands**, not only does the radiation get **less intense**, but the **stretching of space** will stretch the wavelength of the photons from the ΛCDM, which **decreases the energy** of the photons to longer wavelengths, which correspond to the energy of **lower temperatures**. When neutral atoms form, the radiation can no longer interact, and simply flies in a straight line until it interacts with something. **13.8 billion years later, that something is our eyes** and instruments, revealing an **ultra-cold, uniform bath** of radiation at 2.725 K. This is **Evidence of radiation from a hot, dense phase** in the past that many had theorized as representing the origin of our expanding Universe.

Λ-CDM Model Parameters

Wikipedia

"The current standard model of cosmology, the Lambda-CDM model, uses the FLRW metric. By combining the observation data from some experiments such as WMAP and Planck with theoretical results of Ehlers–Geren–Sachs theorem and its generalization, astrophysicists now agree that the early universe is almost homogeneous and isotropic (when averaged over a very large scale) and thus nearly a FLRW spacetime. That being said, attempts to confirm the purely kinematic interpretation of the Cosmic Microwave Background (CMB) dipole through studies of radio galaxies and quasars show disagreement in the magnitude. Taken at face value, these observations are at odds with the Universe being described by the FLRW metric. Moreover, one can argue that there is a maximum value to the Hubble constant within an FLRW cosmology tolerated by current observations, $H_0 = 73 \pm 8$ km/s/Mpc

Hubble Tension - Difference Between Local and Global Determinations of H_0

H_0 from **Cepheids and SNIa** = 73.04 $kms^{-1}Mpc^{-1}$ **Planck CMB** = 67.4 ± 0.5 $km^{s-1}Mpc^{-1}$. Discrepancy is $\approx 5\sigma$

2018 Planck CMB Results

https://arxiv.org/abs/1807.06209

Planck Collaboration 2018 Results. VI. Cosmological Parameters

	Description	Symbol	Value
Independent parameters	Baryon density today	$\Omega_b h^2$	0.0224±0.0001
	Cold dark matter density today	$\Omega_c h^2$	0.120±0.001
	100 × approximation to r∗/DA (CosmoMC)	$100\theta_{MC}$	1.04089±0.00031
	Reionization optical depth	τ	0.054±0.007
	Log power of the primordial curvature	$\ln(10^{10}A_s)$	3.043±0.014
	Scalar spectrum power-law index	n_s	0.965±0.004
Fixed parameters	Total matter density today (inc. massive neutrinos)	$\Omega_m h^2$	0.1428 ± 0.0011
	Equation of state of dark energy	w	$w_0 = -1$
	Tensor/scalar ratio	r	$r_{0.002} < 0.06$
	Running of spectral index	$dn_s/d\ln k$	0
	Sum of three neutrino masses	$\sum m_\nu$	0.06 eV/c^2
	Effective number of relativistic degrees of freedom	N_{eff}	2.99±0.17
	Hubble constant	H_0	67.4±0.5 $km{\cdot}s^{-1}{\cdot}Mpc^{-1}$
Calculated Values	Age of the universe	t_0	$(13.787)\times10^9$ years
	Dark energy density parameter	Ω_Λ	0.6847±0.0073
	The present root-mean-square matter fluctuation, averaged over a sphere of radius $8h^{-1}$ Mpc	σ_8	0.811±0.006
	Redshift of reionization (with uniform prior)	z_{re}	7.68±0.79

CMB Data Analysis Methodology: Angular Temperature Power Spectrum (TT)

CMB Data Analysis Methodology

Data pipeline and radical compression. Maps are constructed for each frequency channel from the data timestreams, combined, and cleaned of foreground contamination by spatial (represented here by excising the galaxy) and frequency information. Bandpowers are extracted from the maps and cosmological parameters from the bandpowers. Each step involves a substantial reduction in the number of parameters needed to describe the data, from potentially 10^{10} —> 10 for the Planck satellite.

In every step of CMB data analysis the aim is to reduce the volume of data without losing information.

ipeline

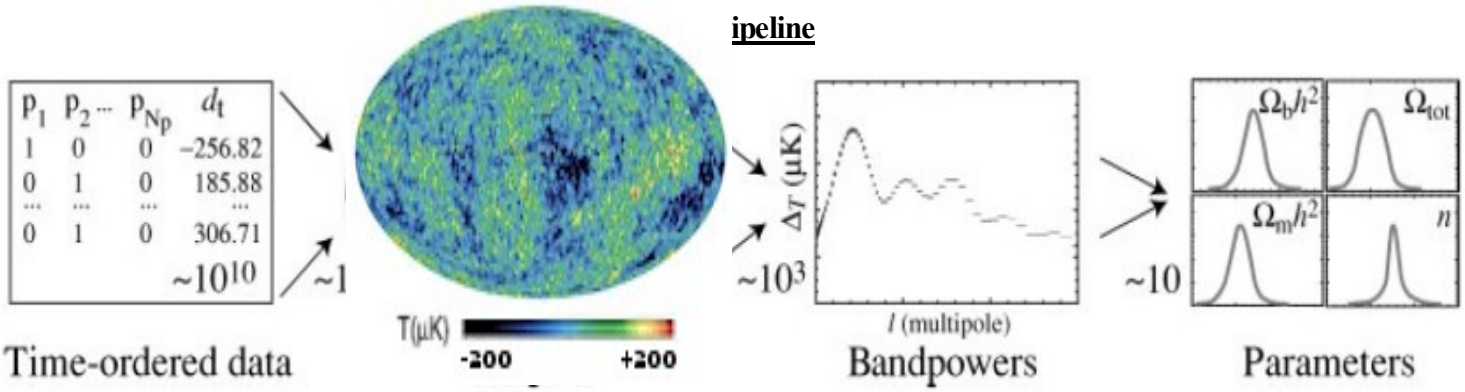

CMB temperature anisotropies are expressed in terms of multipoles:

If δT/T is expanded in terms of **Spherical Harmonics:** Y_{lm}

$$\frac{\delta T(\theta,\phi)}{T_0} = \sum_{l,m} a_{lm} Y_{lm}(\theta,\ \phi)$$

then the complex coefficients a_{lm}, in a homogeneous and isotropic universe, satisfy the condition

$$a_{lm} = \int \frac{\Delta T(n)}{T} \cdot Y_{lm}(n)\ dn$$

$$Y_0^0(\theta,\phi) = \frac{1}{2}\sqrt{\frac{1}{\pi}}$$

$$Y_1^{-1}(\theta,\phi) = \frac{1}{2}\sqrt{\frac{3}{2\pi}}\sin\theta\, e^{-i\phi}$$

$$Y_1^0(\theta,\phi) = \frac{1}{2}\sqrt{\frac{3}{\pi}}\cos\theta$$

$$Y_1^1(\theta,\phi) = -\frac{1}{2}\sqrt{\frac{3}{2\pi}}\sin\theta\, e^{i\phi}$$

It is the **variance of the temperature field** which **carries the cosmological information**, rather than the values of the individual $a_{\ell m}$s; in other words the power spectrum in ℓ fully characterizes the anisotropies. The power at each ℓ is $(2\ell+1)C_\ell/(4\pi)$, and a statistically isotropic sky means that all ms are equivalent.

Where a_{lm} follow the Gaussian (maximally randomized) distribution with zero mean and variance given by C_l :

$$\langle a^*_{l'm'} a_{lm}\rangle = \delta_{ll'}\,\delta_{mm'}\,C_l \qquad C_\ell \equiv \left\langle |a_{\ell m}|^2 \right\rangle$$

An unbiased estimator of C_l is defined as:

$$C_l = \frac{1}{2l+1}\cdot \sum_{m=-l}^{l} \left(a_{lm}\cdot a_{lm}\right)^*$$

CMB Likelihood

- CMB temperature and polarization observations can constrain cosmological parameters if the likelihood function can be computed exactly.
- Computing the likelihood function exactly in a brute force way is computationally challenging since it involves inversion of the covariance matrix i.e., $O(N^3)$ computation.
- In Cosmological parameter estimation a theoretical model is represented by its angular power spectrum C_l .
- For a set cosmological parameters we can compute the angular power spectrum C_l using publicly available Boltzmann codes like **CMBFAST** and **CAMB** (**Code for Anisotropies in the Microwave Background**) and try to fit that with observed C_l . **CMBquick** (Refer to Section XVI) is implemented in Mathematica.

XXIII A. Planck Microwave Anisotropy Probe CMB Angular Temp. Power Spectrum (TT)

The Wilkinson Microwave Anisotropy Probe (WMAP) was launched in 2001.
Planck, launched in 2009, images the sky with more than 2.5 times greater resolution than WMAP.

https://irsa.ipac.caltech.edu/data/Planck/release_3/ancillary-data/cosmoparams/

$Planck\_tt := READPRN("COM\_PowerSpect\_CMB-TT-binned\_R3.01.txt")$

$MM := Planck\_tt^{\langle 0 \rangle}$ $PS := Planck\_tt^{\langle 4 \rangle}$

CMB Table Has Peaks & Troughs
See CMB Table Below
CMB **Holds a Matrix of Values**

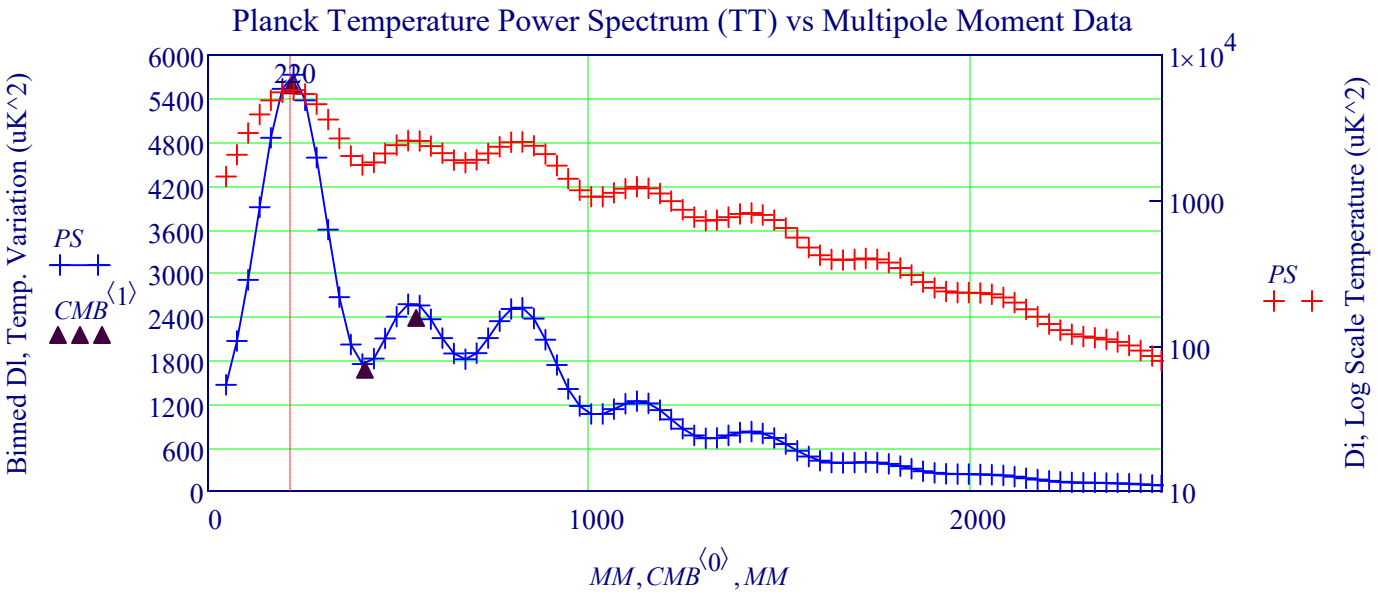

WMAP: TT AND TE ANGULAR POWER SPECTRUM PEAKS FOR ABOVE SPECTRUM

The Characteristics of the Above Spectrum Reveals the Values Needed to Model BB Cosmology

Baryonic fraction $M_{b+d} = M_{b+d+h} = 0.072$

CMB Peaks and Troughs Table

Quantity	Symbol	ℓ	ΔT_ℓ (μK)	ΔT_ℓ^2 (μK^2)	FULL ℓ	FULL ΔT_ℓ^2 (μK^2)
First TT peak	ℓ_1^{TT}	220.1 ± 0.8	74.7 ± 0.5	5583 ± 73	219.8 ± 0.9	5617 ± 72
First TT trough	$\ell_{1.5}^{TT}$	411.7 ± 3.5	41.0 ± 0.5	1679 ± 43	410.0 ± 1.6	1647 ± 33
Second TT peak	ℓ_2^{TT}	546 ± 10	48.8 ± 0.9	2381 ± 83	535 ± 2	2523 ± 49
First TE antipeak	ℓ_1^{TE}	137 ± 9	...	-35 ± 9	151.2 ± 1.4	-45 ± 2
Second TE peak	ℓ_2^{TE}	329 ± 19	...	105 ± 18	308.5 ± 1.3	117 ± 2

Based on the the spatial variation of the CMB and the Model Parameters of the Λ-CDM , astrophysicists predicted a Hubble Constant of 67.5 ±0.5 km/s per megaparsec.
This is different from the Hubble Constant value measured from the change of recessional velocity of galaxies with distance.

Python Scripts are available at: **VXPhysics.com/Python**

XXIII B Python ΛCDM Six-Parameter Base Model - GCP

CAMB: Code for Anisotropies in the Microwave Background, **Spyder**: The Scientific Python Development Environment

Model Name: Flat ΛCDM (Six-parameter base model) Python 3.9, Spyder 5.1.5

This is the standard cosmological model used by Planck, WMAP, and CAMB if you set no special extensions. Specifically, this Python script computes a vanilla, spatially flat ΛCDM CAMB spectrum with no curvature, no evolving dark energy, and a single massive neutrino (0.06 eV).

Python Script Name: ***cmb_tt_planck_camb Dec 1 25.py***

Output from Python CMB Model: $\Lambda CDM := READPRN("CMB\_TT\_model\_scaled.csv")$

Cosmological Parameters Used

Parameter	Value	Meaning
H_0	67.5 km/s/Mpc	Hubble constant today
Ω_b h²	0.022	Physical baryon density
Ω_c h²	0.122	Physical cold dark matter density
Ω_k	0	Curvature = 0 (flat universe)
m_ν	0.06 eV	Single massive neutrino (minimal normal hierarchy)

- $h = H_0/100 = 0.675$
- $\Omega_b = \frac{\Omega_b h^2}{h^2} \approx 0.048$
- $\Omega_c \approx 0.268$
- Ω_ν (from 0.06 eV) ≈ 0.0014

→ Total matter: $\Omega_m \approx 0.317$

Reinization Parameter: 0.06

$$\Omega_\Lambda = 1 - \Omega_m - \Omega_r - \Omega_k \qquad \Omega_\Lambda \approx 1 - 0.317 - 0.0001 \approx 0.683$$

Parameter	Value	Meaning
A_s	2.1×10^{-9}	Primordial amplitude at pivot scale
n_s	0.965	Scalar spectral index (tilt)
Pivot scale (CAMB default)	k_pivot = 0.05 Mpc⁻¹	

CMB Calculations	
Setting	**Value**
lmax	2500
CMB_unit	'muK' (CAMB returns Dℓ in μK²)
lens_potential_accuracy	0 (lensing off for speed

Why These Parameters?

- close to Planck 2018 best-fit parameters,
- fast for CAMB to compute,
- stable and do not trigger unit or convergence errors,
- produce a first peak near $\ell \approx 220$.
- scale the model so that $D_{220} \approx 6000\ \mu K^2$,
- matching my desired normal

Planck Temperature Power Spectrum (TT) Data vs Python CMB Model

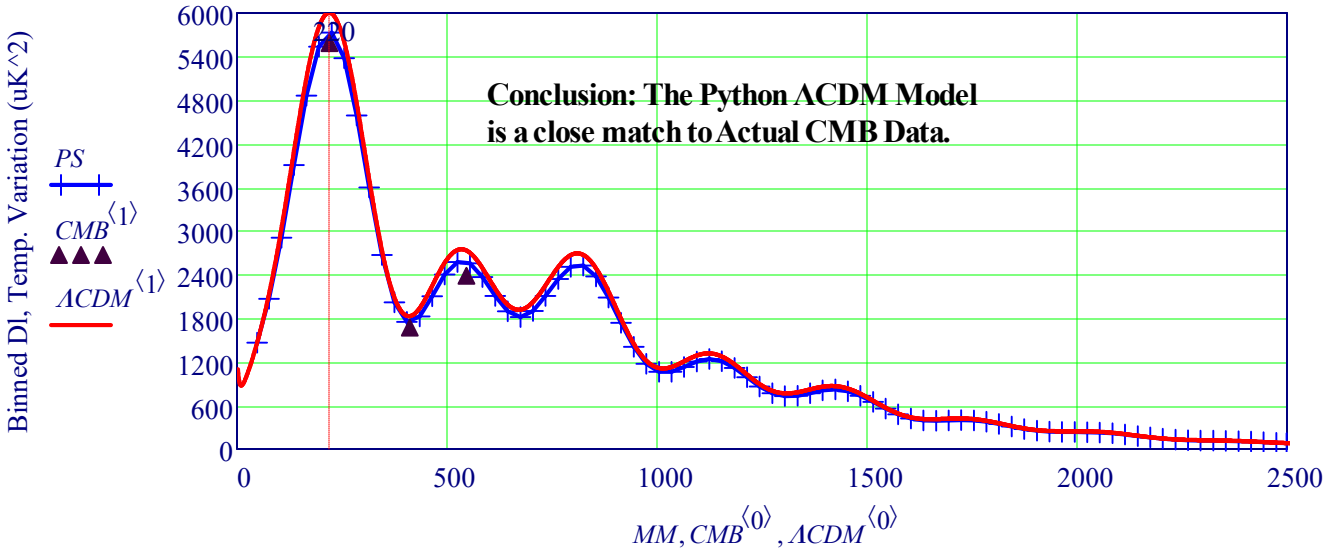

Multipole Moment, The Symbol for Multiple Moment is the letter "l"

Introduction for CAMB_CMB_TT and_Lensing

Python Program: CAMB_CMB_TT_and_Lensing_Example.py See: VXPhysics.com/Python

This program demonstrates how modern cosmology computes the cosmic microwave background (CMB) temperature anisotropy spectrum and **its modification by gravitational lensing** using the Boltzmann code CAMB (Code for Anisotropies in the Microwave Background).

Script solves the coupled EinsteinBoltzmann equations for a flat ΛCDM cosmology to generate both unlensed and lensed CMB power spectra. Gravitational lensing by large-scale structure between the surface of last scattering and the observer redistributes CMB power, smoothing acoustic peaks & transferring power from small to slightly larger angular scales.

In temperature (TT) anisotropies, this lensing effect is subtle and **typically only a few percent**, making it difficult to see on direct overlays. For this reason, the program also computes the CMB lensing potential power spectrum C_ℓ'3f^{φφ}, which directly encodes the projected matter distribution responsible for the deflections.

The outputs of this program illustrate three key ideas:

(1) the distinction between unlensed primordial anisotropies and lensed observed spectra,
(2) the physical role of gravitational lensing as a line-of-sight projection effect rather than a modification of early-universe physics, and
(3) the separation between directly observed quantities and model-dependent inferences in modern cosmology.

CAMB_CMB_TT_and_Lensing_Example.py

$CMB\_TT_{Spectra} := READPRN("cmb\_spectra\_TT\_EE\_Dl.csv")$ $l := CMB\_TT_{Spectra}^{\langle 0 \rangle}$

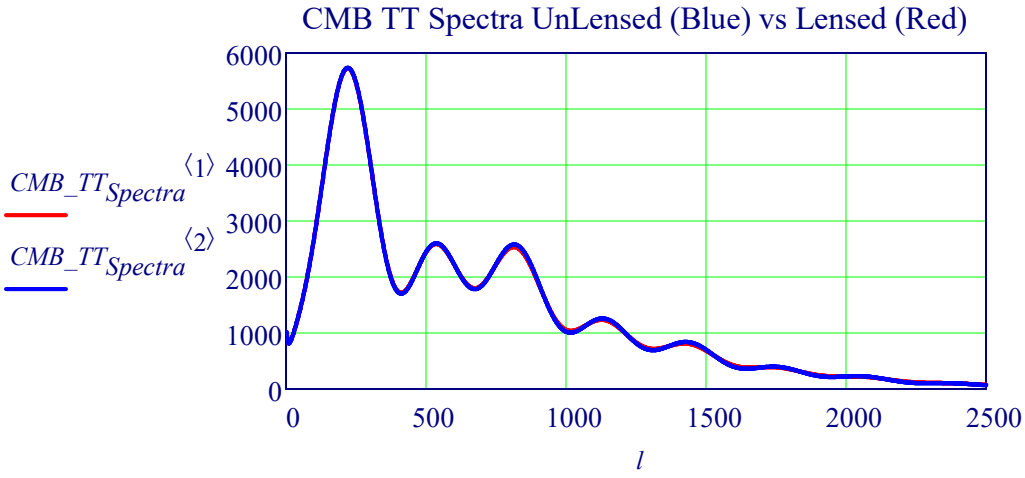

The ratio of lensed to unlensed CMB power spectra isolates the effect of gravitational lensing, revealing percent-level smoothing in temperature anisotropies and a significantly stronger signature in polarization

$CMB\_TT_{Ratio} := READPRN("TT\_lensing\_ratio.csv")$

CAMB_TT_EE_Ratio_to_CSV.py

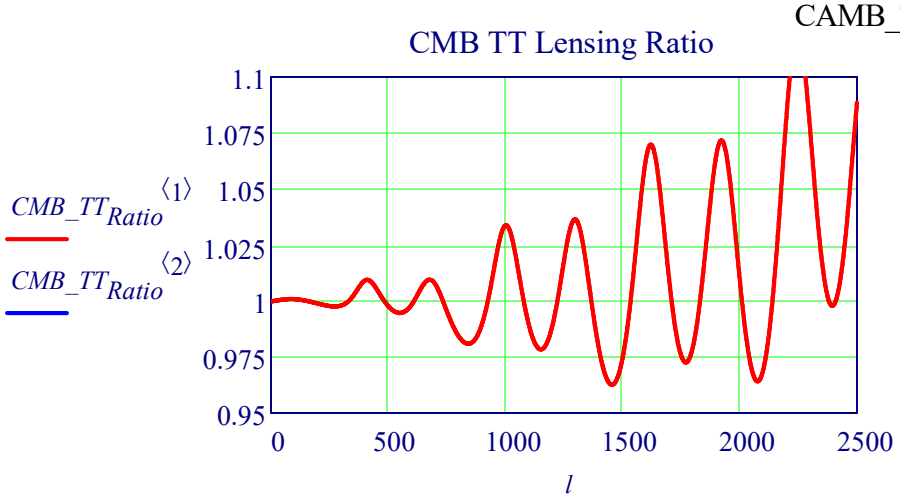

Introduction for CAMB_EE_with_Planck_Overlay

This program compares theoretical predictions for the **CMB E-mode polarization (EE) power spectrum**, computed using CAMB, with observational data from the Planck 2018 mission on a single, self-contained vector-graphic page.

Unlike temperature anisotropies, **CMB polarization is more strongly affected by gravitational lensing.** Deflections caused by large-scale structure partially mix E- and B-modes, producing a clearer and more easily detectable lensing signature in the EE spectrum. As a result, EE polarization provides one of the cleanest observational confirmations of CMB lensing.

The script computes both unlensed and lensed EE spectra for a Planck-consistent ΛCDM cosmology and overlays these model predictions with binned Planck EE data. This directly illustrates how modern cosmological parameters are constrained by matching theoretical models to observed polarization power spectra.

The resulting single-page SVG figure emphasizes three fundamental points:
(1) gravitational lensing is required to match observed EE spectra,
(2) polarization data provide stronger evidence for lensing than temperature anisotropies alone, and
(3) cosmological conclusions arise from fitting physical models to data rather than from direct observation of underlying quantities such as dark matter or spacetime curvature.

CAMB_CMB TT EE and Lensing_Example.py

$$CMB\_EE_{Spectra} := READPRN("cmb\_spectra\_TT\_EE\_Dl.csv") \quad l := CMB\_EE_{Spectra}^{\langle 0 \rangle}$$

Dl_TT_lensed_muK2Dl_TT_unlensed_muK2Dl_EE_lensed_muK2Dl_EE_unlensed_muK2Dl_TE_lensed_muK2Dl_TE_unlensed_muK2

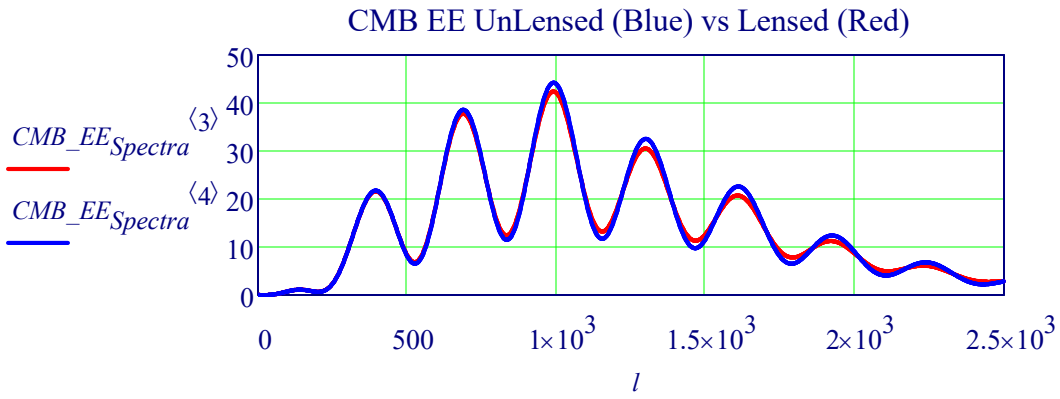

$$CMB\_EE_{Ratio} := READPRN("EE\_lensing\_ratio.csv")$$

CAMB_TT_EE_Ratio_to_CSV.py

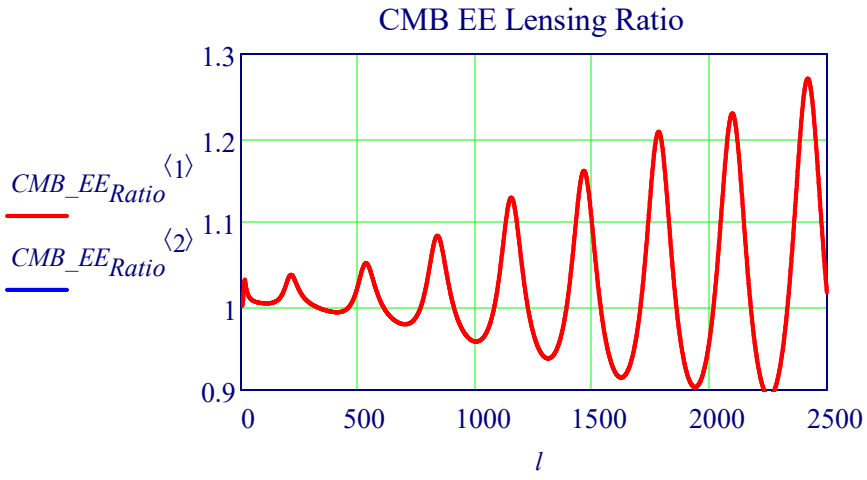

The CMB lensing potential power spectrum computed by CAMB

It is not a temperature or polarization spectrum;
it describes the projected gravitational potential that lenses the CMB.

What physical quantity is this?

Lensing potential $\phi(\hat{n})$

As CMB photons travel from the last-scattering surface to us, their paths are deflected by intervening large-scale structure. Those deflections are described by a scalar lensing potential ϕ

$$\vec{\alpha}(\hat{n}) = \nabla\phi(\hat{n})$$

- $\vec{\alpha}$ = deflection angle on the sky
- ϕ = line-of-sight integral of the gravitational potential

$C_\ell^{\phi\phi}$

- Angular multipole ℓ
- Roughly corresponds to angular scale $\theta \sim \frac{180^\circ}{\ell}$

- Power spectrum of the CMB lensing potential
- Dimensionless
- Encodes how much large-scale structure deflects CMB photons at each angular scale

$$D_\ell^{\phi\phi} = \frac{\ell(\ell+1)}{2\pi} C_\ell^{\phi\phi}$$

- A rescaled version used for plotting
- Makes power per logarithmic ℓ interval easier to see

How this differs from TT / EE / TE

Quantity	What it describes
TT	Temperature anisotropies at last scattering
EE	Polarization anisotropies
φφ	Gravitational lensing by intervening matt

TT and EE are affected by lensing
φφ is the lensing field itself

Why this spectrum is important

1. It directly traces matter

$C_\ell^{\phi\phi}$ depends on:

- Ωm
- growth of structure
- geometry of the Universe

Unlike TT:

- it is late-time
- it is sensitive to dark matter directly

2. It is what Planck actually reconstructs

Planck measures ϕ via:
4-point correlations of the CMB
then compares Cℓϕϕ to ΛCDM predictions

In harmonic space:

$$C_\ell^{\kappa\kappa} = \frac{\ell^2(\ell+1)^2}{4} C_\ell^{\phi\phi}$$

The CMB lensing potential power spectrum $C_\ell^{\phi\phi}$ quantifies the projected gravitational influence of large-scale structure on CMB photons and provides a direct probe of the matter distribution between recombination and the present epoch.

l, Cl_phi_phi, Dl_phi_phi

$\phi\phi := READPRN("lensing\_phi\_phi.csv")$ $DI := READPRN("cmb\_spectra\_Dl.txt")$ $l := \phi\phi^{\langle 0 \rangle}$

$C_{l\phi\phi} := \phi\phi^{\langle 1 \rangle}$ $D_{l\phi\phi} := \phi\phi^{\langle 2 \rangle}$

CMB Lensing Potential, Cl phi phi, l(L+1)Clphi phi/2 pi

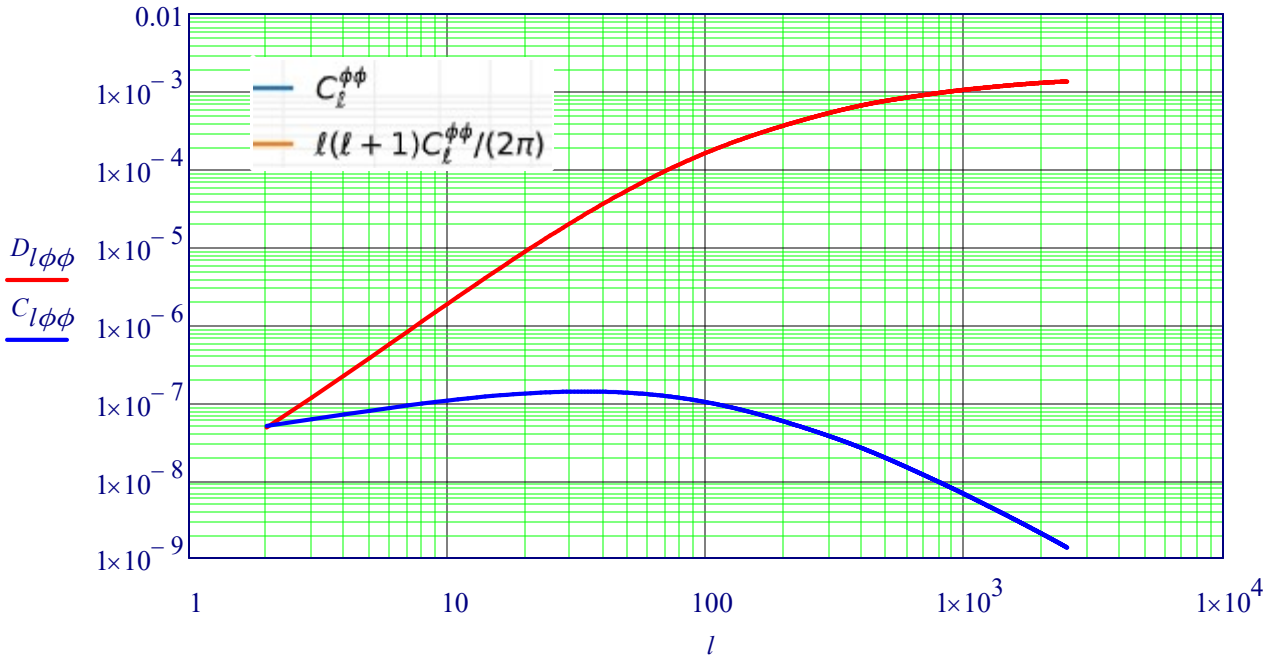

Cosmo LambdaCDB Model.py

lcdm_matter_Pk_camb

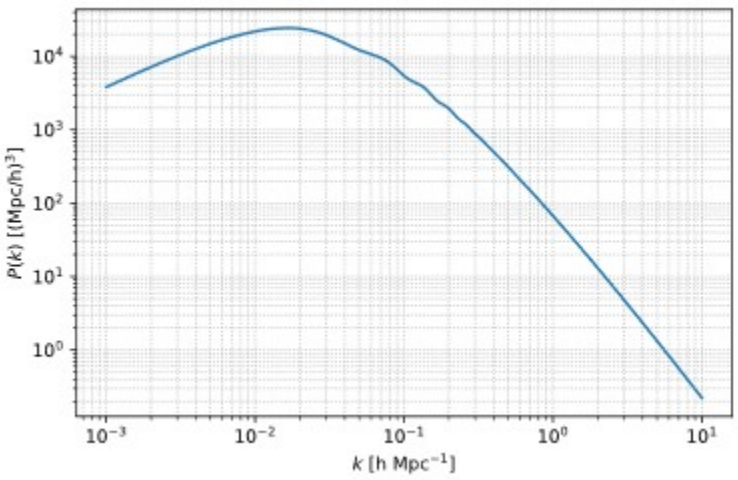

lcdm_CMB_TT_CAMB

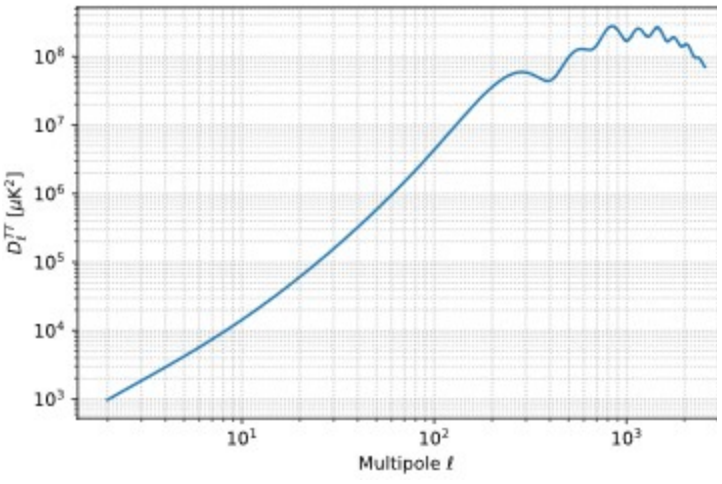

Lookback Time versus Red Shift and Age of Universe (See Section VIII)

Plot from: VII. Equations and Values of Constants for Cosmological Parameters

$$z = \frac{1}{a} - 1$$

ζ represents redshift

$t\_tH0(\zeta, 0.3, 0.7, 10^{-10})$

$tL\_tH0(\zeta, 0.3, 0.7, 10^{-10})$

$t\_tH0(\zeta, 015, 0.7, 0.15)$

$tL\_tH0(\zeta, 015, 0.7, 0.15)$

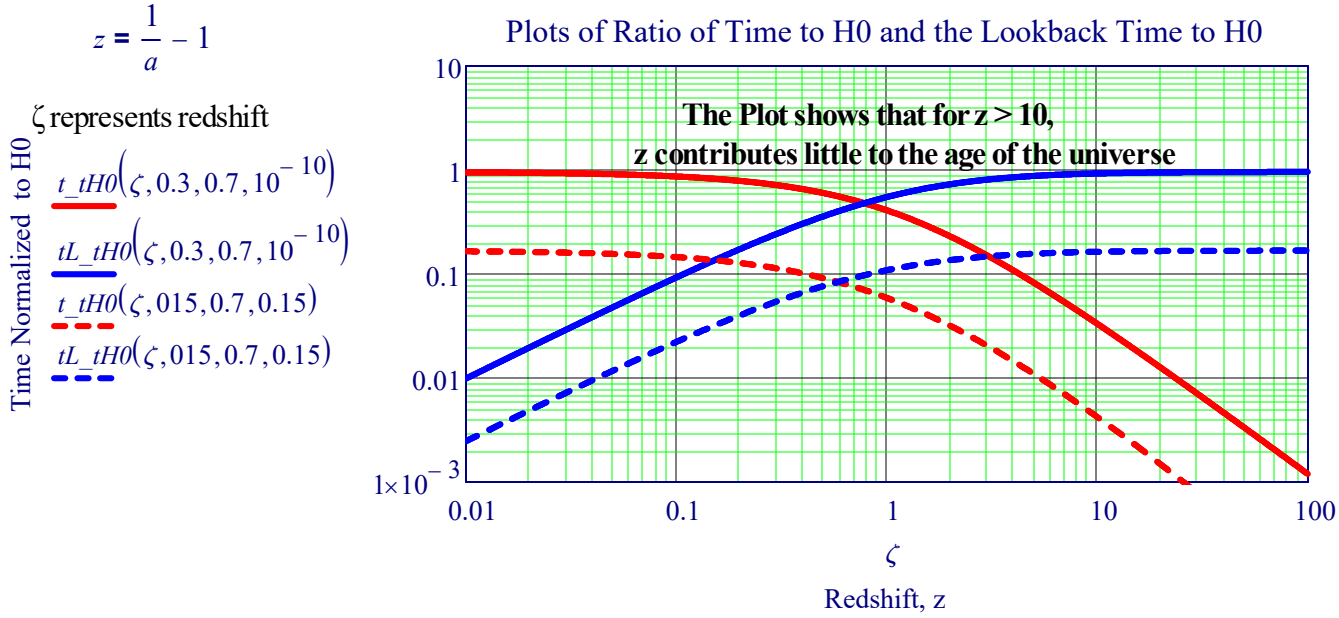

Evolution of the Hubble Factor:

Mass Conservation of non-relativistic matter implies $\rho_m \propto a^{-3} = (1+z)^3$.

In the ΛCDM model, dark energy is assumed to behave like a cosmological constant: $\rho_\Lambda \propto a^0 = (1+z)^0$.

The density of radiation (and massless neutrinos) scales as $\rho_r \propto a^{-4} = (1+z)^4$ because the number density of photons is $\propto a^{-3} = (1+z)^3$ and the mass $E/c^2 = h\nu/c^2$ of each photon scales as $E \propto \lambda^{-1} \propto (1+z)^1 \propto a^{-1}$.

Dynamical Equation Specifying the Evolution of the Hubble Factor of Our Universe

$$\Omega_{r0} := 8.7 \times 10^{-5}$$

$$\frac{H}{H_0} = H\_H_0(z) := \sqrt{\Omega_{m0}\cdot(1+z)^3 + \Omega_{\Lambda 0} + \Omega_{r0}\cdot(1+z)^4}$$

Red Line is Scale on Left (1 to 1000). Blue Dotted Line is scale on Right (1 to 10)

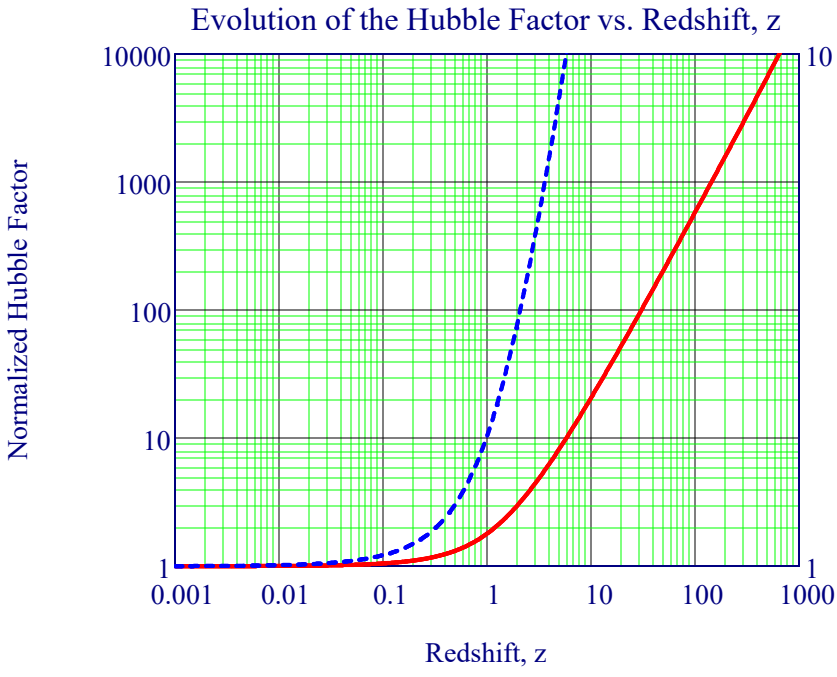

Different z, Different Time, & Different Place

It must always be remembered that **different redshifts** correspond not only to **different times**, but also to **different places**. Thus, when we presume to connect observations of galaxies at different redshifts to derive an overall picture of cosmic evolution, we are implicitly assuming homogeneity; i.e. that "back-then, over there" is basically the same as "back-then, over here". For this to be true it is crucial that surveys for high-redshift galaxies contain sufficient cosmological volume to be "representative" of the Universe at the epoch in question. As we shall see, at $z > 5$ this remains a key challenge with current observational facilities.

Cosmology does not directly measure parameters

It measures patterns in light

from which physically meaningful parameter combinations are inferred.

CMB Lensing and Galaxy Weak Lensing: Complementary Probes of Structure

Gravitational lensing provides a unique window into the distribution of matter in the Universe by tracing the deflection of light by gravitational potentials along the line of sight. Two distinct but complementary realizations of this effect are widely used in modern cosmology: weak lensing of distant galaxies and lensing of the Cosmic Microwave Background (CMB). While both phenomena arise from the same underlying physics, they probe different epochs, scales, and sources of uncertainty.

Galaxy weak lensing measures the coherent distortion of background galaxy shapes caused by foreground large-scale structure. Because galaxies span a broad range of redshifts, galaxy lensing primarily probes the late-time growth of structure, making it highly sensitive to parameters such as Ωm, $\sigma 8$, and the growth factor $D(z)$. In contrast, CMB lensing traces the cumulative deflection of photons originating from a single, well-defined source plane at redshift $z \approx 1100$. As a result, CMB lensing integrates matter fluctuations over nearly the entire cosmic history, providing a clean and complementary probe of the matter distribution.

Although the observable quantities differ—shear correlations for galaxy lensing and reconstructed lensing potential for the CMB—the underlying theoretical description is closely related. In both cases, the lensing signal is governed by a line-of-sight projection of the matter power spectrum weighted by a lensing efficiency kernel. However, the redshift dependence of these kernels differs substantially, leading to different sensitivities to cosmological parameters and systematics.

The combination of galaxy and CMB lensing therefore offers a powerful internal consistency test of the ΛCDM model. Agreement between the two probes supports the standard picture of structure growth, while discrepancies may indicate observational systematics or new physics affecting the growth of perturbations.

What Cosmology Actually Measures

From Observables to Parameters: What Cosmology Really Measures

Modern cosmology is often presented as a discipline that "measures" fundamental parameters such as the matter density Ωm, the Hubble constant $H0$, or the amplitude of density fluctuations σ_8. In practice, however, cosmological observations do not directly measure these quantities. Instead, t**hey measure statistical properties of observables**—angles, redshifts, brightness fluctuations, and correlations—which are then **mapped onto cosmological parameters through theoretical models.**

This indirect relationship between observation and inference is a defining feature of cosmology. Observables such as galaxy shapes, CMB temperature anisotropies, or galaxy clustering statistics depend on cosmological parameters in **coupled ways**, leading naturally to **parameter degeneracies**. As a result, experiments **often constrain** specific **combinations** of parameters rather than individual values. Well-known examples include the acoustic scale ***θs*** measured by the CMB and the parameter $S_8 = \sigma_8 \sqrt{\Omega_m / 0.3}$ ured by weak lensing

Rather than being a limitation, these degeneracies encode valuable physical information. They reflect how geometry, expansion history, and structure growth interact in shaping the observable Universe. Understanding which combinations of parameters are constrained by a given observation clarifies both the strengths and the limitations of each cosmological probe.

This perspective highlights cosmology as an inverse problem: light propagates through spacetime, interacts with matter, and produces observable patterns on the sky. Cosmological models provide the forward map from parameters to observables, while data analysis seeks to invert this map to recover the underlying physical description

XXIV. Advances in Measurement and Technology for Measuring Hubble Constant

Hubbles's original value in 1923 was 500 kms s^{-1} Mpc^{-1}. The high value was that he overestimated the distance. Unknown to him there are two classes of Cepheids: Type I Cepheids (δ Cepheus is a classical Cepheid) are population I stars with high metallicities, and pulsation periods generally less than 10 days. Type II Cepheids (W Virginis stars), are low-metallicity, population II stars, that are older, cooler, and redder, with pulsation periods between 10 and 100 days. Hubble had used Population I Cepheid variable stars to determine distances to spiral nebulae. Hubble had made the assumption that these Pop I Cepheid stars in distant spiral nebulae were similar to those observed in our galaxy. In fact, the stars Hubble was using to estimate distances were systematically brighter than the nearer comparison stars. When this was realized in the **1950s**, thanks to Baade's work, Hubble's distances were doubled and Ho halved from 500 to 250.

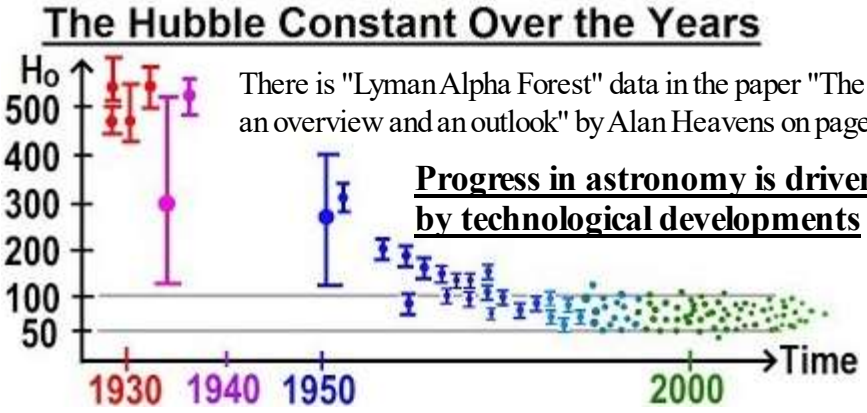

There is "Lyman Alpha Forest" data in the paper "The Cosmological Model: an overview and an outlook" by Alan Heavens on page 24

Progress in astronomy is driven by technological developments

Charge-coupled devices (CCDs) were first used in astronomy in **1976** by Jim Janesick and Brad Smith. Compared to photographics plates, they have better low-light performance, a wider (red) spectral range, and the ability to quickly convert photons into electrons. Photographic plates saturate and cannot discriminate brightness like CCDs. GigaPixel CCDs also improved the light gathering power of telescopes by nearly two orders of magnitude. These advances revolutionized astronomy by facilitating immediate data analysis and enabling practical space-based observations.

The Hubble Space Telescope was launched in **1990**, taken to space in the cargo bay of the space shuttle Discovery. Its main purpose was to figure out a distance scale of the Universe (how big it is) and where the elements present in space came from. **HST was optimized for 0.1 to 2.5 μm region.**

The Planck Space Telescope 2009, was designed to study the Cosmic Microwave Background (CMB) at **3-160 μm.**

The Goal of the JWST (Launched in 2021) is to see high redshift galaxies to observe farther into the universe than ever before. To observe the Cosmic Dawn. JWST Instruments capable of studying **0.6 to 28μm Infrared Region.**

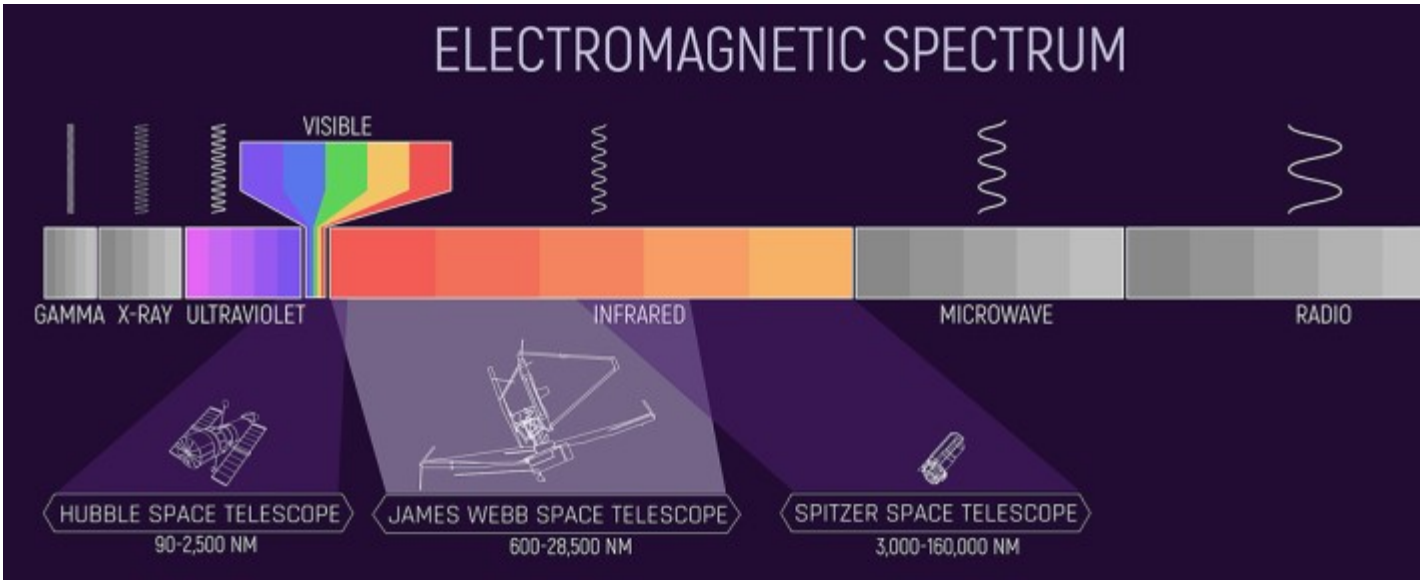

James Webb Space Telescope (JWST) - Infrared Deep Field Survey

The James Webb Space Telescope (JWST) is the scientific successor to both the Hubble Space Telescope (HST) and the Spitzer Space Telescope. It is envisioned as a facility-class mission. JWST aims to achieve science goals that can never be reached from even the largest envisioned groundbased telescopes. **HST Optimized for 0.1 to 2.5 µm region.**
It will be equipped with four instruments capable of studying the **0.6 to 28µm region** using both imaging and spectroscopic techniques. The instrument suite provides broad wavelength coverage and capabilities aimed at four key science themes:

$$z = (\lambda_{obs} - \lambda_{rest}) / \lambda_{rest} \qquad \text{Lyman-alpha break} = 121\ \text{nm}$$

1) The End of the Dark Ages: First Lig.ht and Reionization; finding the light from the first objects to coalesce after the Universe has cooled after the Big Bang
2) The Assembly of Galaxies; how do galaxies change from first light objects to the suite of morphologies and galaxy types that we see today. To unravel the birth and early evolution of star, from the earliest epochs ≲ 300 Myr after the Big Bang, through the Epoch of Reionization.
3) The Birth of Stars and Protoplanetary Systems;
4) Planetary Systems and the Origins of Life. NIRCam is the 0.6 to 5 micron imager for JWST, and it is also the facility wavefront sensor used to keep the primary mirror in alignment. JWST will work to unravel the birth and early evolution of stars, from infall onto dust-enshrouded protostars to the genesis of planetary systems. The Hubble Space Telescope (HST) has a highest resolution of about 0.03 arcseconds, while the Very Long Baseline Array (VLBA) makes images with a resolution smaller than 0.001 arcsec. The JWST at located at Lagrange 2, has 6.5 m mirror, and a resolution of 0.1 arcsec.

JWST Mid Infrared Instrument JWST Instruments

The JWST Mid-Infrared Instrument (**MIRI**) provides imaging and spectroscopic observing modes from ≈5 to 28µm.

JWST Near Infrared Camera

The JWST Near Infrared Camera (**NIRCam)** offers imaging, coronagraphy, wide field slitless spectroscopy, and time-series monitoring both in imaging and spectroscopy, as well as wavefront sensing measurements for JWST mirror alignment.
The JWSTprovides near-IR spectroscopy from 0.65.3 µm within a 3.4 ×3.6 arcmin field of view using a micro-shutter assembly (MSA), an integral field unit (IFU), and fixed slits (FSs).

JWST Near Infrared Imager and Slitless Spectrograph

The JWST Near Infrared Imager and Slitless Spectrograph (**NIRISS**) provides observing modes for slitless spectroscopy, high-contrast interferometric imaging, and imaging, at wavelengths between 0.6 and 5.0 µm over a 2.2' x 2.2' FOV.

JWST Near Infrared Spectrograph

The JWST Near Infrared Spectrograph (NIRSpec) provides near-IR spectroscopy from 0.6–5.3 µm within a 3.4 × 3.6 arcmin field of view using a micro-shutter assembly (MSA), an integral field unit (IFU), and fixed slits (FSs).

NIRISS pupil and filter wheels

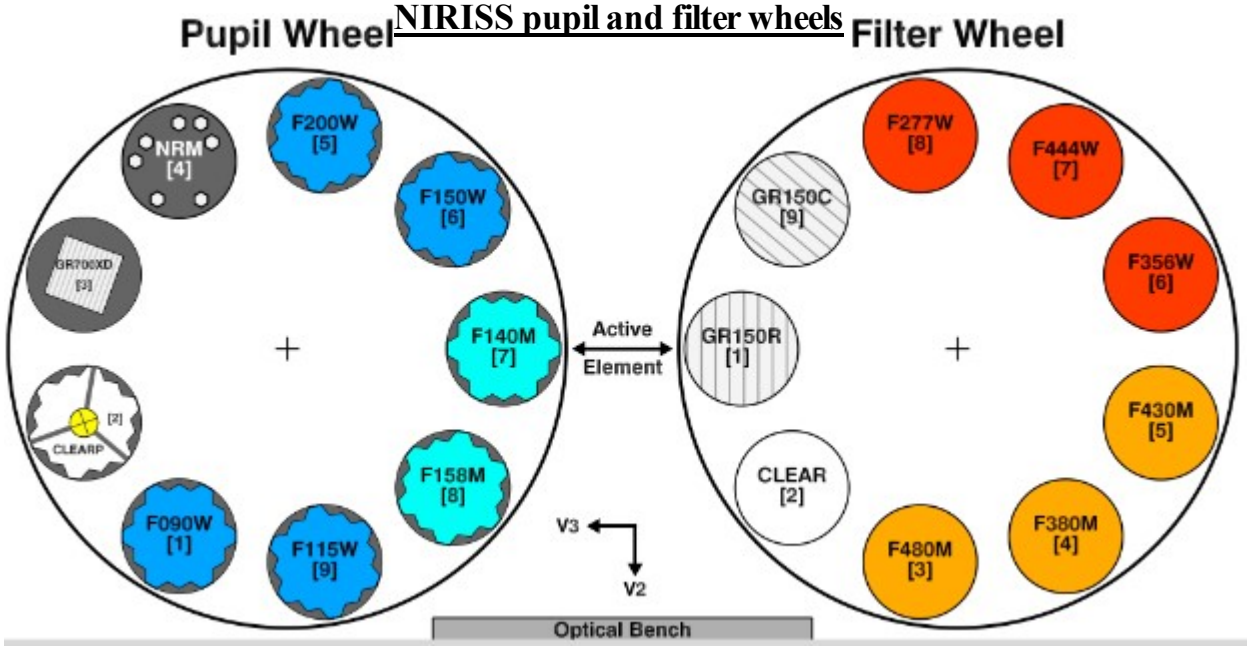

JADES: JWST Advanced Deep Extragalactic Survey Near-IR Spectroscopy Optics

JADES: Lookback Time versus Red Shift and Age of Univ z = 14.3 Gyr

Look-Back Time & Age of Unuv vs. z. 2024 Metal-Poor JADES-GS-z14-0 galaxy @z=14.3, Age: 290 million years

***The Value of the Cosmological Constant*, John D. Barrow, 2018**

"If you neglect the energy density of radiation and **consider that the universe is currently flat**, the following formula is derived from the Friedmann equation:"

$$H^2 = \frac{8\pi G}{3}\rho + \frac{\Lambda}{3} - \frac{K}{a^2},$$
$$\frac{\ddot{a}}{a} = -\frac{4\pi G}{3}(\rho + 3P) + \frac{\Lambda}{3}$$
$$\dot{\rho} + 3H(P + \rho) = 0,$$

$H_0 := 71 \frac{km}{s \cdot Mpc}$

$\Omega_{\Lambda 0} := 0.73$

$$dt = \frac{da}{H_0\left(\frac{\Omega_{m,0}}{a} + a^2\Omega_{\Lambda,0}\right)^{\frac{1}{2}}}$$

The subindices mean current values for the Hubble parameter (=71 Km /s Mpc), Omega matter (=0.27), Omega cosmological constant (=0.73). To get the age at a given redshift z, you have to integrate from a = 0, to a = 1/(1+z).

The fraction of the effective mass of the universe attributed to "dark energy" or the cosmological constant is $\Omega_{\Lambda 0}$ With 73% of the influence on the expansion of the universe in this era, the dark energy is viewed as the dominant influence on that expansion.

We assume that the matter source of the FLRW universe is a perfect fluid with energy density ρ and pressure P related by the barotropic, linear, and constant equation of state **P = wρ, w = const.**

$$z = \frac{\lambda_{observed} - \lambda_{expected}}{\lambda_{expected}}$$

Values of Some Constants

$Lyr := 1yr \cdot c$ $Lyr = 9.461 \times 10^{15}\, m$ $Mpc := 3.086 \cdot 10^6 Lyr$ $Gyr := 10^9 yr$ $w := 0.1 .. 1$

w: Ratio P/ρ for a fluid

Note: $t_L(z)$ factor should be 3/2. Used 1.45 to get a better match.

$$t_L(z) := \frac{3}{2H_0 \cdot 1.45}\cdot\left[1 - (1+z)^{-\frac{3}{2}}\right]$$

$$t_0(w) := \frac{2 \cdot H_0^{-1}}{3(w+1)\cdot\sqrt{\Omega_{\Lambda 0}}}\cdot ln\left(\frac{1+\Omega_{\Lambda 0}}{\sqrt{1-\Omega_{\Lambda 0}}}\right)$$

Some Results of JWST Advanced Deep Extragalactic Survey - Lookback Time

Age of Universe (tBB) from from 2021 Lambda-CDM concordance Model (Billion Years)

$t_{BB} := 13.737$ $BigBang := t_{BB}$

Furthest Observations of 2023 Metal-Poor JADES-GS-z14-0 galaxy @z=14.2, 290 Million Years Old

(Refer to Section VIII for Derivation of Lookback Time)

$t_{lb}(z) := t_{BB} \cdot tL\_tH0\left(z, 0.3, 0.7, 10^{-10}\right)$ $t_{age}(z) := t_{BB} \cdot t\_tH0\left(z, 0.3, 0.7, 10^{-10}\right) \cdot 1000$

$Furthest\_z := 14.3$ $\frac{1}{H_0} = 13.765 \cdot Gyr$ $j := 0, 0.01 .. 20$ $z_j := j$

Initial Galaxy Census from JWST 2023 (See Section X - IMF)

The study of galaxies at the highest redshifts is crucial to unveiling the earliest stages of galaxy formation and evolution

References: *The abundance of z 10 galaxy candidates in the HUDF using deep JWST NIRCam medium-band imaging*, Donnan et al 2023, Perez-Gonzalez et al. 2023

Read Data from JWT Observations:

Donnan est al 2023, Harikane et al 2022, McLeod et al 2016, Oesch et al 2018, Perez-Gonzalez et al. 2023 Bouwens et al. 2022

Similar Graph, ρ_{UV} *The Dearth of z ~ 10 Galaxies in All HST Legacy Fields — The Rapid Evolution of the Galaxy Population in the First 500 Myr*, Oesch, The Astrophysical Journal, 855:105 (12pp) , 2018 March

$Dat\rho_{UV} := READPRN("Luminosity density Galaxies per Volume vs z.txt")$

$\rho_{UV} := Dat\rho_{UV}^{\langle 1 \rangle}$ $z_{fit} := Dat\rho_{UV}^{\langle 0 \rangle} \cdot \frac{17}{16.5}$

Model Curve to UV Luminosity ρ

$fit(z) := log\left[(1+z)^{-4.2}\right] + 29.5$

Redshift Evolution of the UV Luminosity density, ρ_{uv} and Inferred Cosmic Star-Formation Rate Density, ρ_{SFR}

$\log10(\rho_{uv}/\text{ergs s}^{-1}\ \text{Hz}^{-1}\ \text{Mpc}^{-3})$ vs. Redshift, z

Initialize Second Unit Scale

$\rho_{SFR} := 1$

UV Luminosity Density, ρ_{UV}

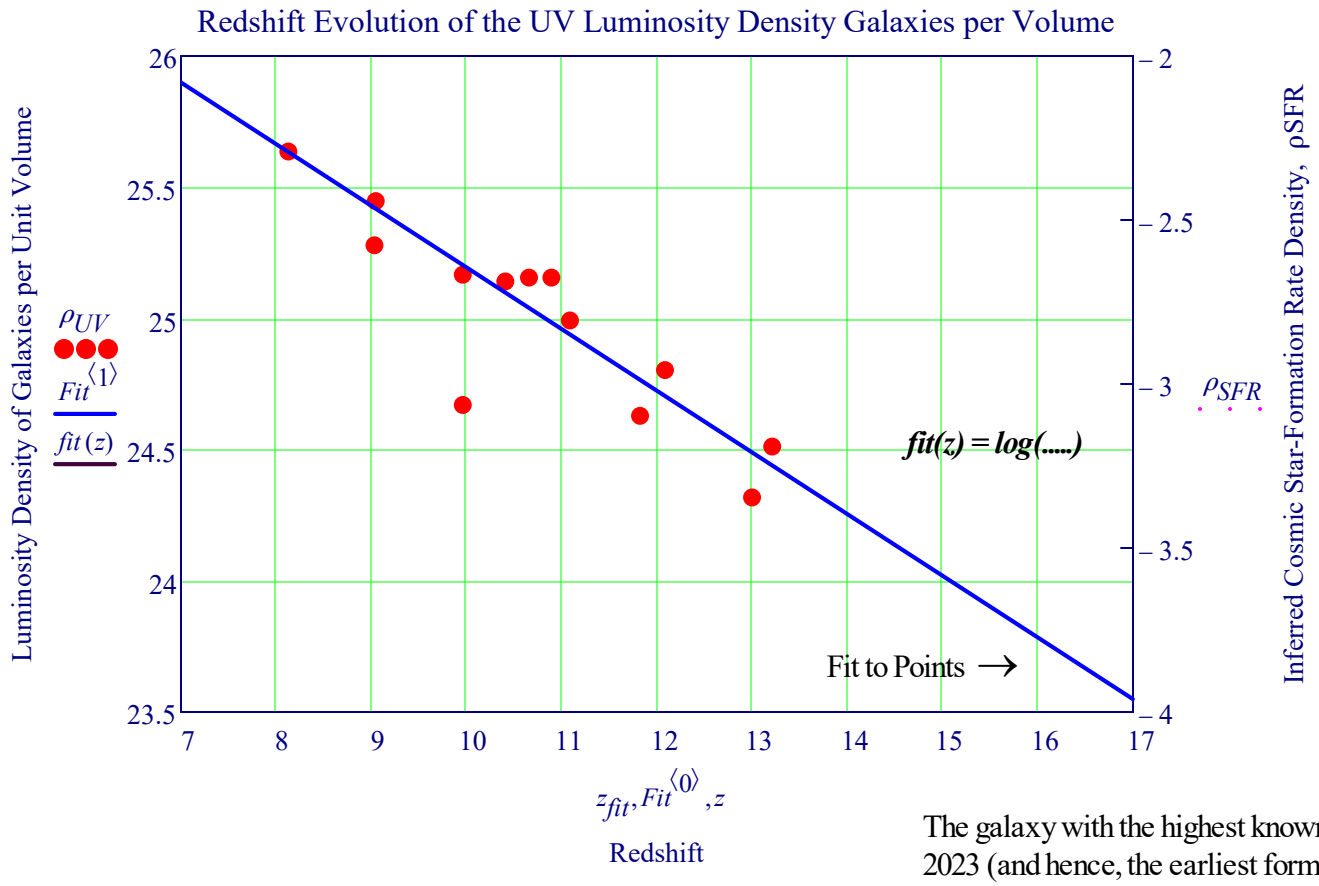

The galaxy with the highest known redshif 2023 (and hence, the earliest formed) is now JADES-GS-z13-0 at redshift 13.20, 400 million years after the Big Bang

Look-back Time by Redshift and Age of Universe

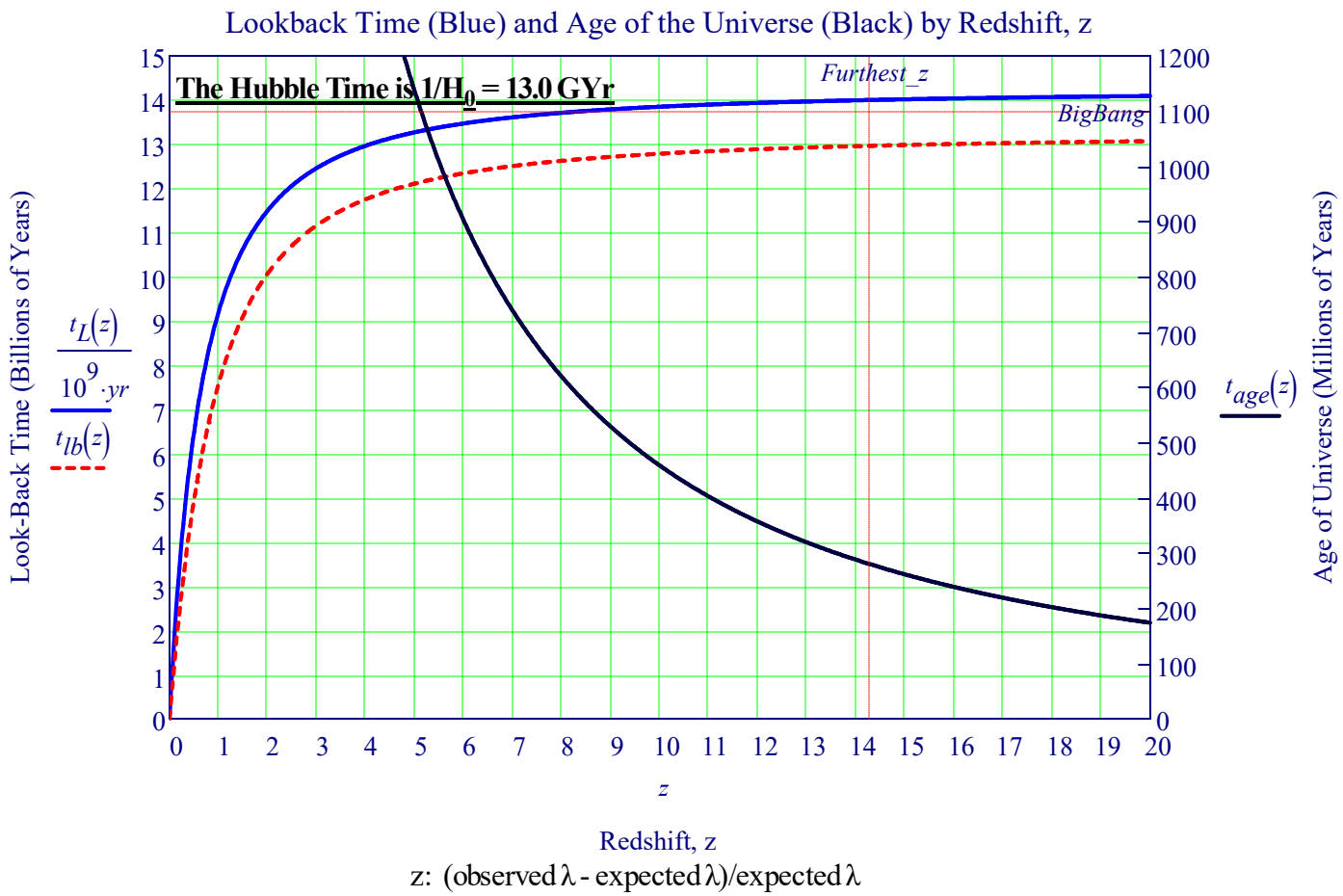

The mass-to-light ratios and the star formation histories of Disc Galaxies

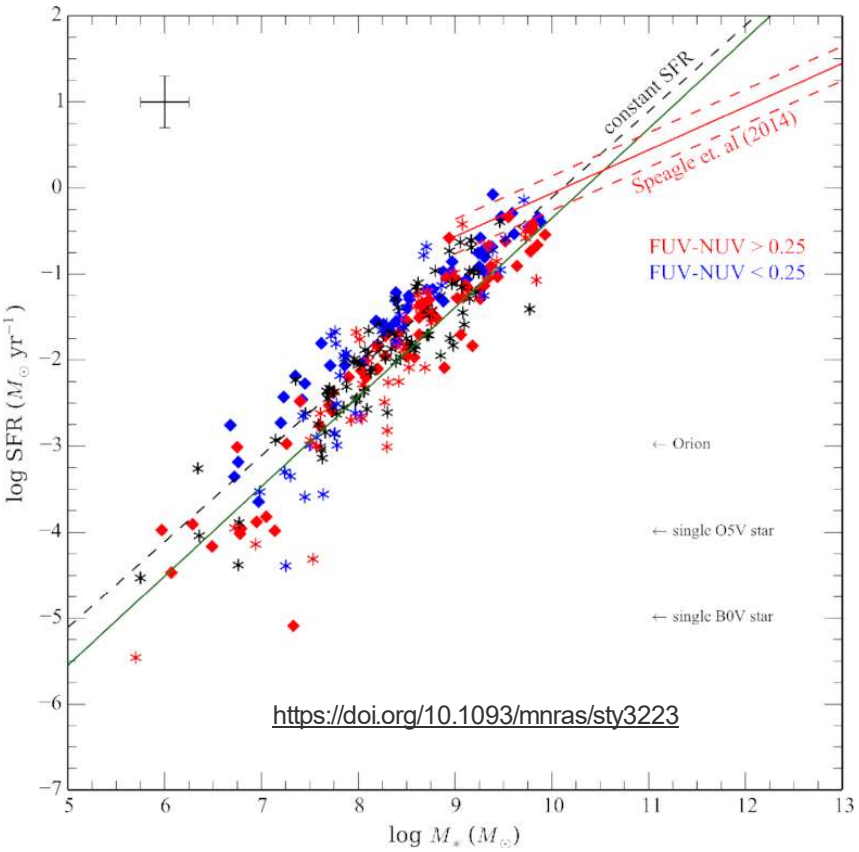

The main sequence for high- and low-mass star-forming galaxies.

Star Formation Rate, SFR, is the rate at which gas and dust is turned into stars. It is the total mass of stars formed per year. The term can be used in describing a galaxy or globular cluster. **Data: 2017**

The data sets from Cook et al. (the solid symbols) and LSB + SPARC (the starred symbols) are shown, colour coded by FUV–NUV color.
The green line is a fit to the LSB + SPARC sample (McGaugh, Schombert & Lelli 2017).
The dashed line is the line of constant star formation for a 13 Gyr Universe.
There is a clear trend for **blue FUV −NUV colors** to lie **above** the constant SFR line (rising SFR in the last 100 Myr) versus **red FUV −NUV color's below the line** (declining SFH).
The z = 0 relationship from Speagle et al. is shown for the high-mass spirals, along with 3σboundaries.
Also shown are the values for SFR that correspond to an Orion-sized complex, a single O star and a single B star.
SFR estimates below −4.5 are highly inaccurate.
A representative error is shown in the upper left, errors in SFR and stellar mass are from McGaugh, Schombert(2017).

XXV. Mathematica CMBquick: Simulation of CMB Temperature Power Spectrum

WMAP Temperature Power Spectrum (TT) vs Multipole Moment Modeling

This Analysis is Based on Cyril Pitrou's Mathematica tools for creating CMB Spectra.

https://www2.iap.fr/users/pitrou/

"CMBquick is a package for Mathematica in which tools are provided to compute the spectrum and bispectrum of Cosmic Microwave Background (CMB)... CMBquick is a slow but precise and pedagogical, tool which can be used to explore and modify the physical content of the linear and non-linear dynamics. Second, its is a tool which can help developing templates for nonlinear computations, which could then be hard coded once their correctness is checked. The number of equations for non-linear dynamics is quite sizable and CMBquick makes it easy (but slow) to manipulate the non-linear equations, to solve them precisely, and to plot them."

Below are the results of CMBquick Simulation to find the Temp Power Spectrum for WMAP

Compare The Analysis Results Below to the Analysis from the Previous Section, XV

WMAP Temperature Power Anistrophies Calculated from Mathematica (CMB quick)

$WMAP\_CMB := READPRN("CAMB\_WMAP\text{-}CMBquick.dat")$

$WMAP\_CMBq := READPRN("wmap\_CMBq.dat")$

$\Delta T_W := WMAP\_CMB^{\langle 1 \rangle}$ $\quad MPM_W := WMAP\_CMB^{\langle 0 \rangle}$

$\Delta T_{Wq} := WMAP\_CMBq^{\langle 3 \rangle}$ $\quad MPM_{Wq1} := WMAP\_CMBq^{\langle 0 \rangle}$

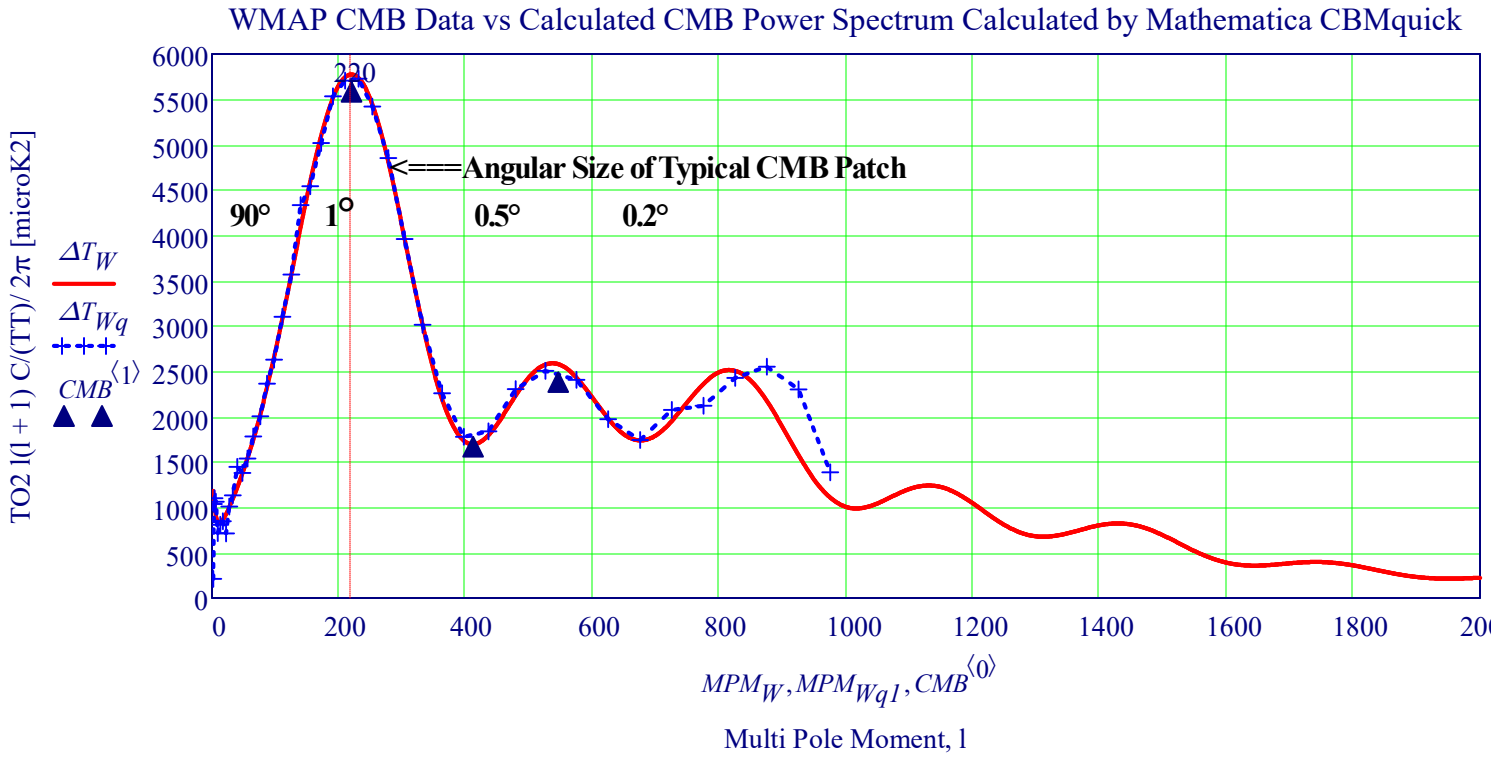

Angular Scale °, Curvature, and Projection Effects on CMB

The corresponding angle on the sky is approximately 100 / *l* degrees°

The Curvature of the Universe is Indicated by the Location of the First CMB Peak

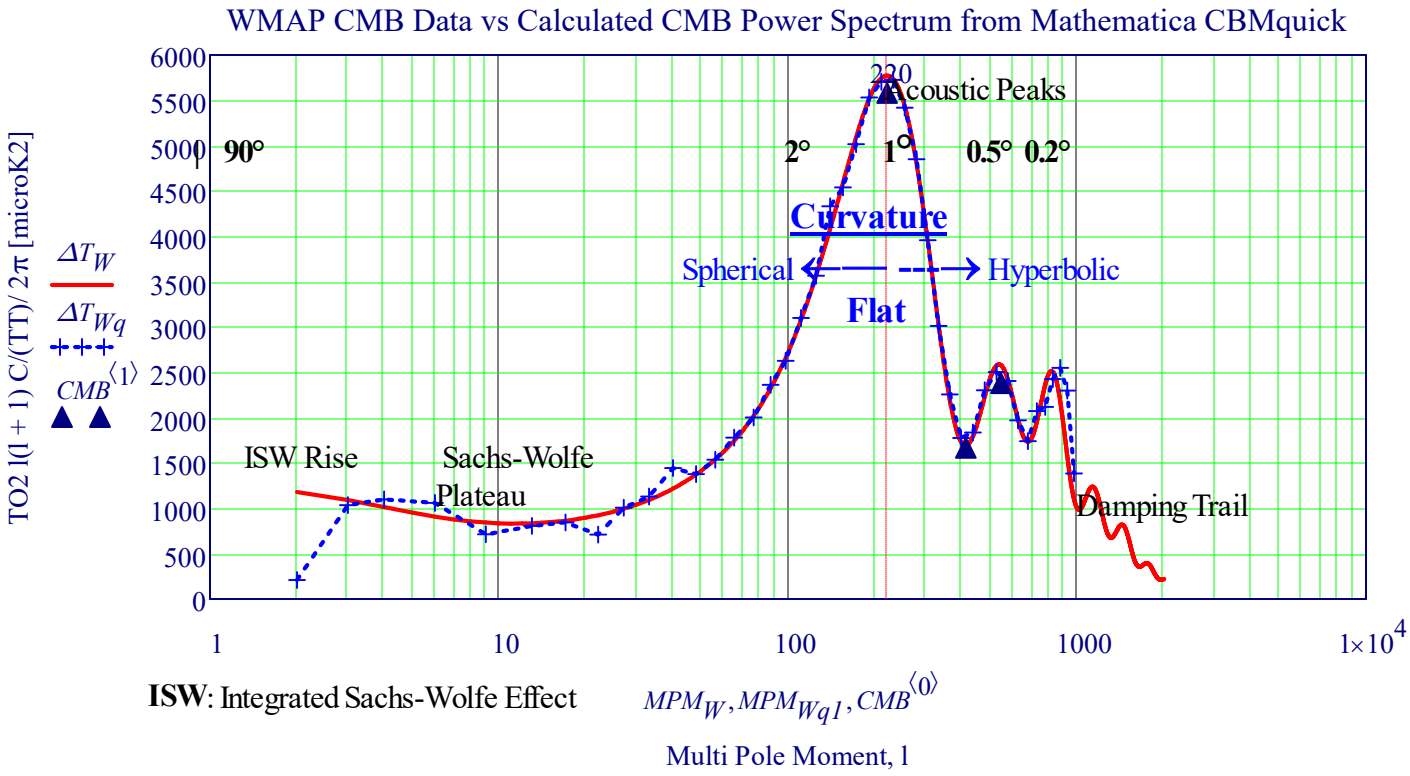

ISW: Integrated Sachs-Wolfe Effect $MPM_W, MPM_{Wq1}, CMB^{\langle 0 \rangle}$

Projection Effects

See Pages 9, 10 and 11 for Definitions

$$\rho_0 = \frac{3 \cdot H_0^2}{8 \cdot \pi \cdot G} \qquad \rho_0 := 8.6443584621592 \cdot 10^{-27} \cdot \frac{kg}{m^3} \qquad \rho_{crit} = 1.879\ \ 10^{-29}\ h^2\ g\ cm^{-3}.$$

$$\Omega_M = \frac{8 \pi G \cdot \rho}{3 \cdot H_0^2} \qquad \Omega_\Lambda = \frac{\Lambda \cdot c^2}{3 \cdot H_0^2} \qquad \Omega_0 = 1 \text{ Radiation Transfer Function}$$

The mass is usually parameterized by Ω_0 which is the energy density in units of the critical density

$$\Omega_0 = \frac{\rho_T}{\rho_{crit}} \qquad \Omega_\Lambda = \frac{\rho_\nu}{\rho_{crit}} \qquad \Omega_0 + \Omega_\Lambda = 1$$

ρ_v is the vacuum contribution

$\Omega_0 > 0.1$ to 0.3 $\qquad \Omega_0 := 0.15$ $\qquad$ The Baryon Fraction is $\Omega_b h^2 = 0.01$ to 0.02

For the acoustic contributions, the k modes that reach extrema in their oscillation at last scattering form a harmonic series of peaks related to the sound horizon. This in turn is approximately

$$\frac{\eta_{star}}{\sqrt{1 + C \cdot (1 + R(n_{star}))}} \qquad R(n_{star}) = 30 \Omega_b \cdot h^2 \qquad C := \sqrt{3} - 1$$

Since $\Omega_b h^2$ must be low to satisfy nucleosynthesis constraints, the sound horizon will scale roughly as the particle horizon . The particle horizon at last scattering itself scales as

$$\eta_{star} = \left(\Omega_0 \cdot h^2\right)^{\frac{1}{2}} \cdot f_R \qquad f_R = \sqrt{\left[1 + \left(24\,\Omega_0 \cdot h^2\right)^{-1}\right]} - \sqrt{24\,\Omega_0 \cdot h^2}$$

CMBquick Cosmology CPLP Planck Perturbation Parameters

We compute the cosmology k dependent Boltzmann Hierarchy

Variable	Value	Units	
Ω_{b0}	0.049169		Abundance of baryons
Ω_{c0}	0.26474		Abundance of CDM
Ω_{r0}	0.000092414		Abundance of radiation (massless ? 's and photons)
$\Omega_{\Lambda 0}$	0.686		Abundance of Λ
Ω_K	0		Abundance of curvature
T_0	2.7255	K	Temperature of CMB
N_ν	3.045		Number of massless neutrinos
h	0.6727		Reduced H constant
τ_{rei}	0.079		Optical depth of reionization
n_s	0.9645		Scalar perturbations spectral index
k_{eq}	0.010362	Mpc^{-1}	k at equivalence time
z_{rei}	10.701		Redshift at reionization
z_{eq}	3395.7		Redshift at equivalence
z_{LSS}	1061.2		Redshift at t-trei = ln(2)
z_{dec}	1090.3		Redshift at max of visibility function
z_*	1091.2		Redshift at t-trei = 1
$d_A(z_*)$	13910.	Mpc	Angular distance at z *
$d_A(z_{eq})$	14078.	Mpc	Angular distance at equivalence
D_H	4456.56	Mpc	Hubble distance today
t_0	13.8308	Gyears	Age of the Universe
t_*	371 312.	years	Age of universe at z *
$r_{hor}(z_{dec})$	280.58	Mpc	Radius of horizon at z dec
η_0	14191.	Mpc	Conformal time today
A_s^2	2.4736×10^{-9}		Primordial scalar perturbations amp at k = 0.002 Mpc
n_S	0.9645		Scalar spectral index
r	0		Tensor to Scalar ratio at k = 0.002 Mpc
n_T	1		Tensor spectral index
σ_8	0.84516		Relies on extrapolation of the matter power spectrum

XXVI A. Calculation of CMB Power Spectra from Model Parameters - CAMB Tool

Code for Anisotropies in the Microwave Background [CAMB].
An Online CAMB Calculation Routine to calculate CMB_Model ΛCDM Model Parameters is available at:
https://lambda.gsfc.nasa.gov/toolbox/camb_online.html

Cosmological Model Parameters for Model Input

Ω_b h² = 0.022600
Ω_c h² = 0.112000
Ω_ν h² = 0.000640
Ω_Lambda = 0.724000
Ω_K = 0.000000
Ω_m (1-Ω_K-Ω_L) = 0.276000
100 θ (CosmoMC) = 1.039532
N_eff (total) = 3.046000
1 η, g= 1.0153 m_nu*c²/k_B/T_nu0= 353.71 (m_nu= 0.060 eV)
Age of universe/GYr = 13.777
z* = 1088.75
r_s(z*)/Mpc = 146.38
100*θ = 1.039819
z_{drag} = 1059.70
$r_s(z_{drag})$/Mpc = 149.01
k_D(z*) Mpc = 0.1393
100*θ_D = 0.160248
z_EQ (if ν_nu=1) = 3216.47
100*θ_EQ = 0.847737
τ_recomb/Mpc = 284.72 τ_now/Mpc = 14362.3

Fake Model Params for Comparison

Ω_b h² = 0.05
Ω_c h² = 0.112000
Ω_ν h² = 0.000640
Ω_Lambda = 0.724000
Ω_K = 0.000000
Ω_m (1-Ω_K-Ω_L) = 0.276000
100 θ (CosmoMC) = 1.039532
N_eff (total) = 3.046000

Fake Model CMB Curve

$CMB\_Model_{Fake} := READPRN("Lensedcls-CMB Spectrum Om_b h2 050.txt")$

$\Delta T2K_{Fake} := CMB\_Model_{Fake}^{\langle 1 \rangle}$

$MPM_{Fake} := CMB\_Model_{Fake}^{\langle 0 \rangle}$

Use the Online CAMB Calculation Routine with Above CMB Parameters ==> ΛCDM Model

$CMB\_Model := READPRN("Lensedcls-CMB Spectrum.txt")$ $rows(CMB\_Model) = 2099$

$\Delta T2K := CMB\_Model^{\langle 1 \rangle}$ $MultiPoleMoment := CMB\_Model^{\langle 0 \rangle}$

Note: The Excellent Match Between Data and the Model

TO² l(l + 1) C/(TT)/ 2π [microK²]

CMB Data vs Calculated CMB Power Spectrum from Model

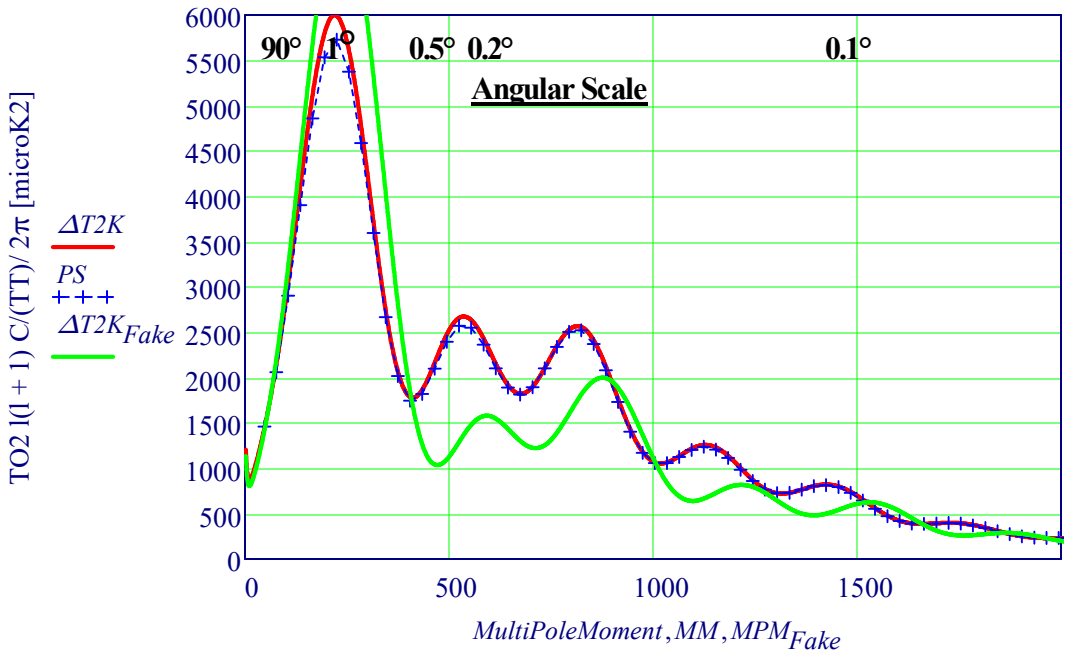

XXVI B. CMB Spherical Bessel Projection Approximation

Mathcad "Toy Model" To Investigate Use of Spherical Bessel Functions to Project 3D to 2D Sky

The spherical Bessel functions project these 3D oscillations onto the 2D sky. $j_\ell(k(\eta_0 - \eta))$

These Bessel functions, ***js_l*** naturally have oscillatory behavior.

$$C_\ell^{TT} \approx \int dk\, k^2\, S_k^2\, j_\ell^2(kr)$$

So, in our **Approximate Delta-Function Model:**

The oscillations ***in*** C_ℓ^{TT} directly come from the **Bessel functions**, j_ℓ and the source function's own oscillations.

In this approximation the source function is static in time—it's treated as if the entire contribution to the CMB anisotropy is **from a single conformal time (last scattering)**. This is known as the "Delta-Function Approximation": the time integral in the projection of $\Theta_l(k)$ is replaced by a single time (like a delta function at η_*).

A Sachs_Wolfe term was added given by the SW_plateau correction for Multipole Moments < 135.

Artifacts are a Possibility in Our Approximation. In real physics, the source function is not a delta function—it's spread over time, which smooths out some oscillatory features at high ℓ

It arises from **acoustic oscillations of the photon-baryon plasma** before recombination.

Spherical Bessel Function, js(m,z). This is a 1200 x 500 Multipole by k Table of Bessel Function Values

Factor to Normalize TT Spectrum ~ Unity

$\eta_0 := 1.4 \cdot 10^4$ $r := \eta_0$ $x := 0 .. 1199$ $\ell_x := x$ $Normalization := 2.2 \cdot 10^{-11}$

$n := 0 .. 499$ $ell\_values := \ell$ $k\_values_n := 0.0001 + 0.0006 \cdot n$ $max(k\_values) = 0.3$

$n\_ell := 1200$ $n\_k := 500$ $r := 14000$ Sachs-Wolfe plateau amplitude: $SW\_plateau := 1.9 \cdot 10^{-13}$

Generate Spherical Bessel Functions j-ell(k * r)

$SBF :=$ for $\ell \in 0 .. 1199$
  for $j \in 0 .. 499$
    $BM_{\ell,j} \leftarrow js(\ell, k\_values_j \cdot 14000)$
  BM

Source function for all k - Delta-Function Approximation

$S\_k(k) := k^{0.2} \exp\left(\frac{-k}{0.1}\right) \cdot \left|\sin(0.02 \cdot k \cdot r)\right|$

$n\_k := length(k\_values)$

$S\_vector_n := S\_k(k\_values_n)$

Compute approximate TT spectrum for each Multipole ℓ and Integrate

$TT\_Spectrum :=$ for $\ell \in 0 .. 1199$
  for $j \in 0 .. 499$
    $integrand_{\ell,j} \leftarrow (k\_values_j)^2 \cdot (S\_vector_j)^2 \cdot (SBF_{\ell,j})^2$
  $h \leftarrow k\_values_1 - k\_values_0$
  $sum \leftarrow 0$
  for $j \in 0 .. 499$
    $sum \leftarrow sum + integrand_{\ell,j}$
  $TTS_\ell \leftarrow \frac{h}{2} \cdot (integrand_{\ell,0} + 2 \cdot sum + integrand_{\ell,499})$
  $\ell \leftarrow TTS_\ell + SW\_plateau$ if $\ell < 135$
  $\frac{TTS}{Normalization}$

$ApproxCMB := ksmooth(\ell, TT\_Spectrum, 6)$

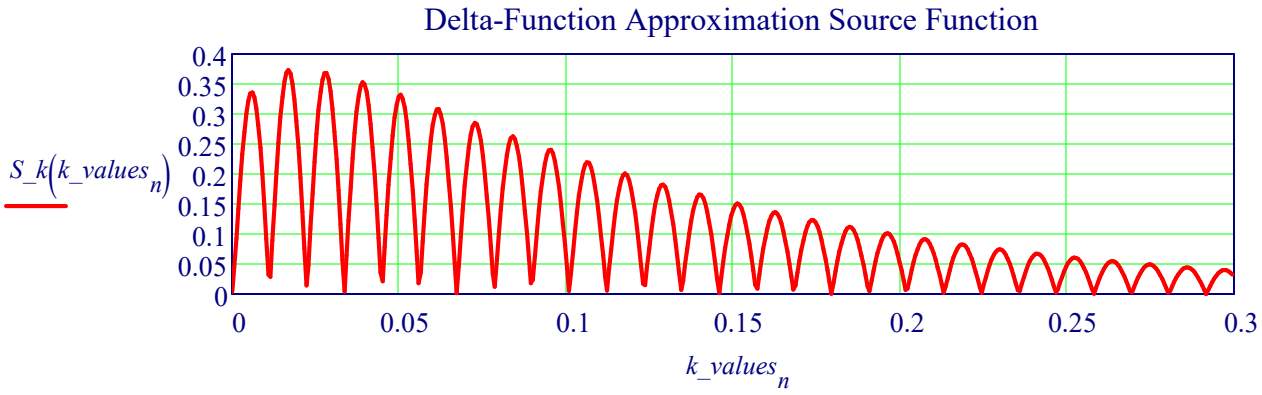

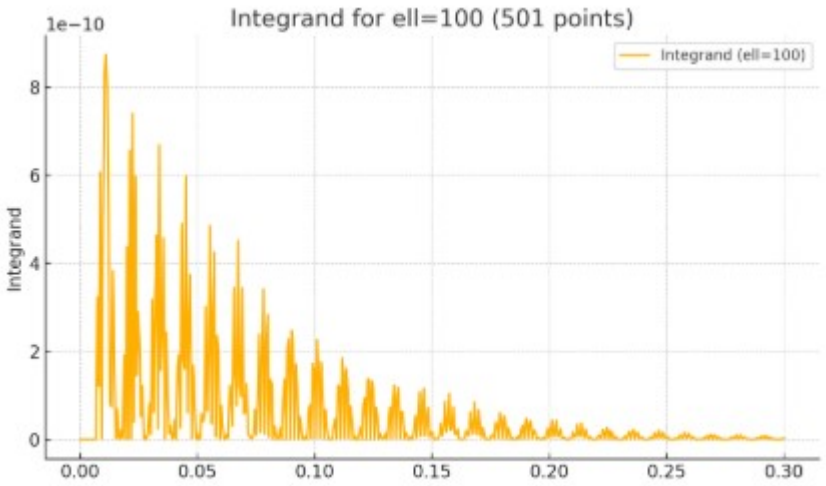

Spherical Bessel Function Projection Approximation to CMB TT Amplitude Multipole Distribution

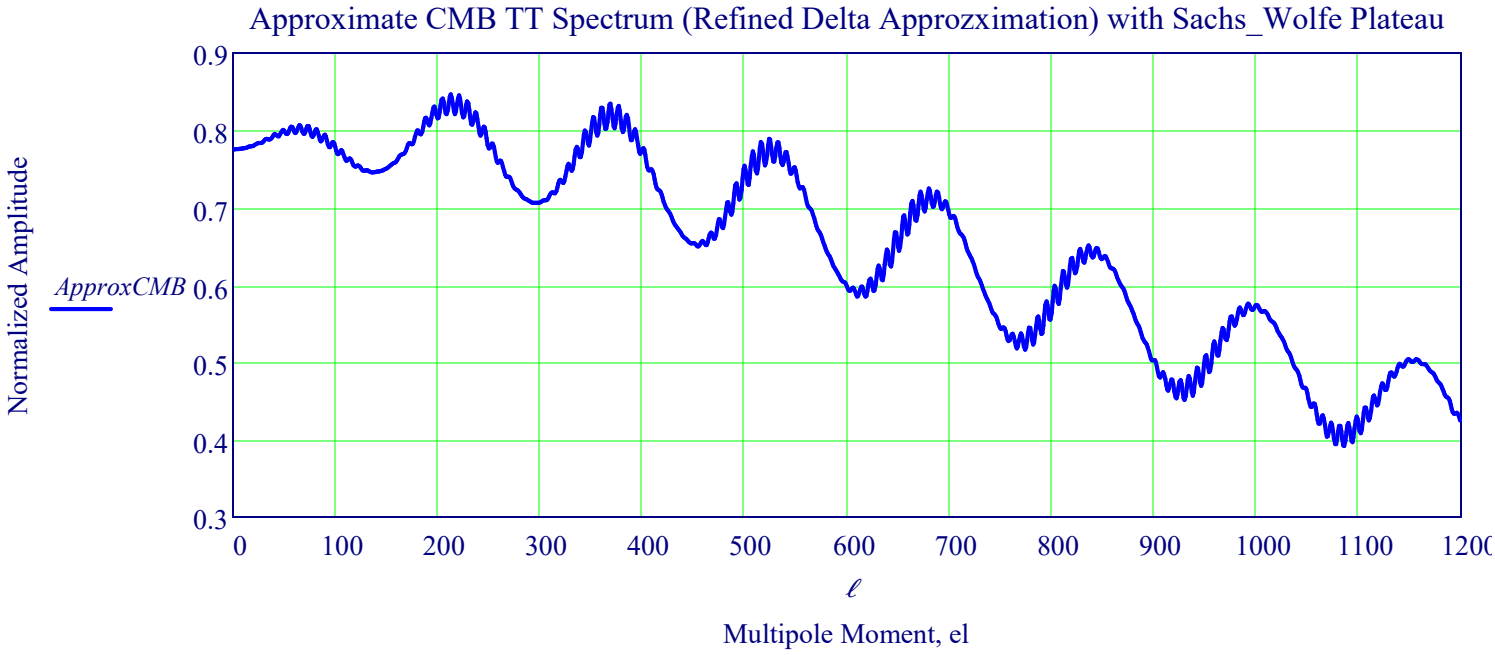

Reference: *SMALL SCALE COSMOLOGICAL PERTURBATIONS: AN ANALYTIC APPROACH,* Wayne Hu, arXiv:astro-ph/9510117v2

XXVI C. CMB TWK Empirical Gaussian TT Power Spectra Model

Features of This Model

The primordial seeds of structure formation are Gaussian-distributed adiabatic fluctuations with an almost scale-invariant spectrum. This model uses Gaussian Waveforms for each acoustic peak (localized power) and has an Excellent Match to Planck TT spectrum shape up to $\ell \sim 2400$,

TT Power Spectrum Plot Data Sources

Planck 2018 TT temperature power spectrum

Planck 2018 results. https://lambda.gsfc.nasa.gov/education/lambda_graphics/more/tt_spec

$C := READPRN("Planck CMB TT Spectra3.txt")$ $\ell := C^{\langle 0 \rangle}$ $D_{data} := C^{\langle 1 \rangle}$ $rows(\ell) = 111$

First Peak: $max(D_{data}) = 5793.4395$ $match(max(D_{data}), D_{data}) = (34)$ $\ell_{34} = 225.2$

First Peak: Corresponds to the largest acoustic oscillation in the photon-baryon plasma before recombination. The sound horizon—the maximum distance a sound wave (photon-baryon density wave) could travel in the early universe before photons decoupled from baryons (recombination). Sound Horizon at recombination $r_s \sim 144Mpc$

Second Peak: Second harmonic of acoustic oscillations of in the photon-baryon plasma. Maximum rarefraction.

Ratio of Peak Locations: $\frac{225}{538} = 0.418$ gives $\Omega_b h^2 \sim 0.022$

TWK Cosmological parameters to Match the Planck 2018 TT best-fit approximations

Multipole Amplitude Dispersion, Multipole Amplitude Dispersion, Multipole Amplitude Dispersion Multipole Amplitude Disp

$P12 := (225.2 \quad 5.793 \times 10^3 \quad 95 \quad 538 \quad 2.5 \times 10^3 \quad 90 \quad 810 \quad 2.5 \times 10^3 \quad 100 \quad 1.1 \times 10^3 \quad 1.2 \times 10^3 \quad 100)^T$

$P9 := (1.4 \times 10^3 \quad 850 \quad 120 \quad 1.7 \times 10^3 \quad 300 \quad 130 \quad 2 \times 10^3 \quad 200 \quad 200)^T$ $P := stack(P12, P9)$ $rows(P) = 21$

Gaussian TT Mathcad Model Function for Single Peak

$$Gauss(\ell, i) := P_{1+3 \cdot i} \cdot exp\left[-\left[\frac{(\ell - P_{0+3i})^2}{2 \cdot (P_{2+3 \cdot i})^2}\right]\right]$$

Seven Peak Gaussian Composite Model

$$Model(\ell) := \sum_{i=0}^{6} Gauss(\ell, i)$$

Excellent CMBR TWK Gaussian Empirical TT Power Spectra Match to Planck Data (Red).

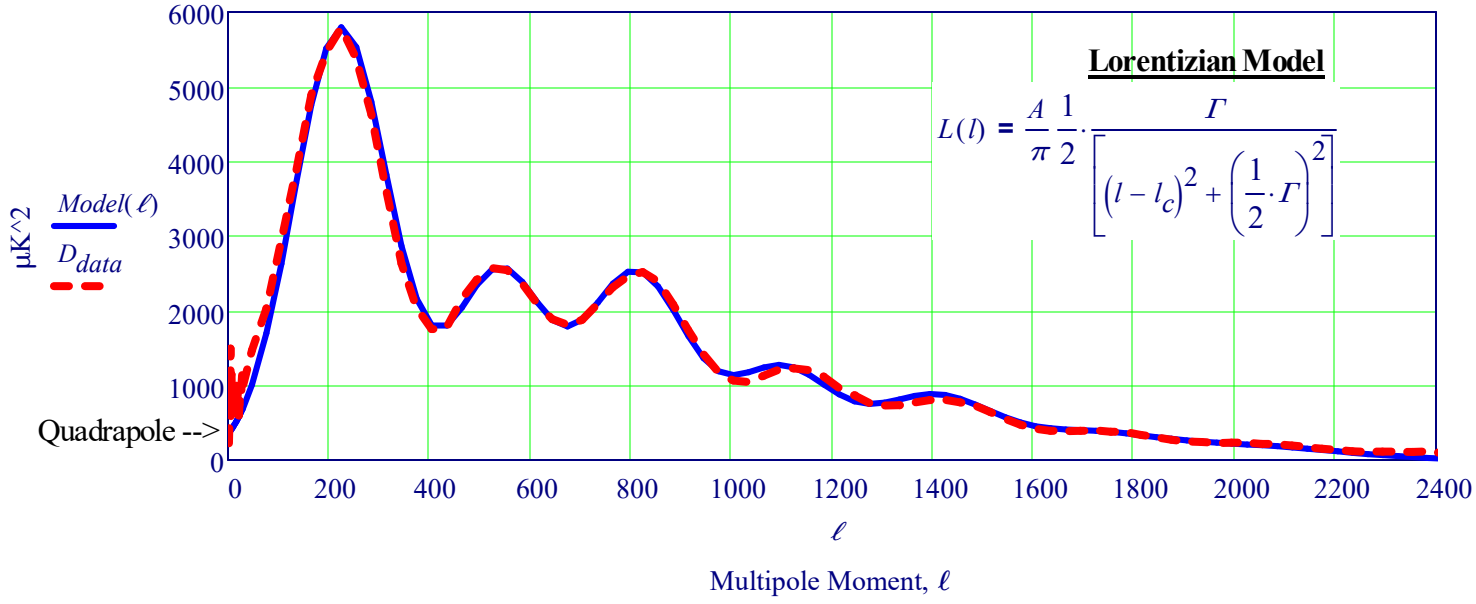

XXVI D. CMB Matter Power Spectrum

See XXII. Λ-CDM Model Theory and Parameters

Current Universe Matter Power Spectrum: Amplitude vs Scale

Linear Matter Power Spectrum at z = 0: P(k) vs. k in Log-Log Space

Key points about this plot

- The horizontal axis is wavenumber k(units typically $h\,\mathrm{Mpc}^{-1}$).
- The vertical axis is the power spectrum $P(k)$(units typically $(h^{-1}\mathrm{Mpc})^3$).
- On large scales (small k), $P(k)$rises roughly like a power law; on smaller scales (large k) it drops more steeply. For example, the asymptotic behaviours are approximately $P(k) \propto k^{n_s}$at very small $k$and $P(k) \propto k^{n_s-4}$at large $k$for a matter-dominated epoch (see e.g., the "linear matter power spectrum" discussion). NASA/IPAC Extragalactic Database+2Wikipedia+2
- A characteristic "turn-over" occurs at the scale corresponding to matter–radiation equality (typically $k_{\mathrm{eq}} \sim 2 \times 10^{-2}\ h\,\mathrm{Mpc}^{-1}$). Wikipedia+1

The Matter Power Spectrum

$P(k)$vs. k

- Horizontal axis: **comoving wavenumber** $k[h/\mathrm{Mpc}]$
- Vertical axis: **matter density fluctuation amplitude** $P(k)$
- Epoch: **today** (redshift $z = 0$)
- Physics it probes:
  - growth of **large-scale structure**
  - horizon scale at matter–radiation equality
  - dark matter clustering
  - small-scale suppression from transfer functions
- Typical shape:
  - **Power-law rise** at large scales (small k)
  - **Turnover peak** near $k \sim 0.02\ h/\mathrm{Mpc}$
  - **Decay** at small scales (large k)

This tells us how **matter is distributed today**.

How the Two Spectra Are Related

Both measure the same initial primordial power spectrum

but evolve it differently: $P_{\mathrm{prim}}(k) \propto k^{n_s}$

Quantity	Domain	Epoch	Sensitive to
CMB C_ℓ	angular multipoles ℓ	$z = 1100$	photon–baryon sound waves
Matter $P(k)$	spatial wavenumber k	$z = 0$	growth of structure under gravity

They are related by the **radiation transfer function** and **projection from 3D→2D sky**:

$$C_\ell = 4\pi \int \frac{dk}{k} P(k)\,|\Delta_\ell(k)|^2$$

This means:

- The CMB **is a 2D angular projection** of primordial 3D fluctuations.
- The **matter spectrum is the 3D distribution** after ~13.8 Gyr of growth.

CMB Angular Power Spectrum
Multiple peaks
Each peak encodes harmonic sound modes in the early universe
High-ℓ damping tail
Low-ℓ plateau

What is Labeled:

- Physics & geometry → photon propagation
- Observables: $\gamma, \kappa, \Delta T/T$
- Inferred parameters: S_8, Ω_m, θ_s

Information Flow Diagram

fig7_1_information_flow

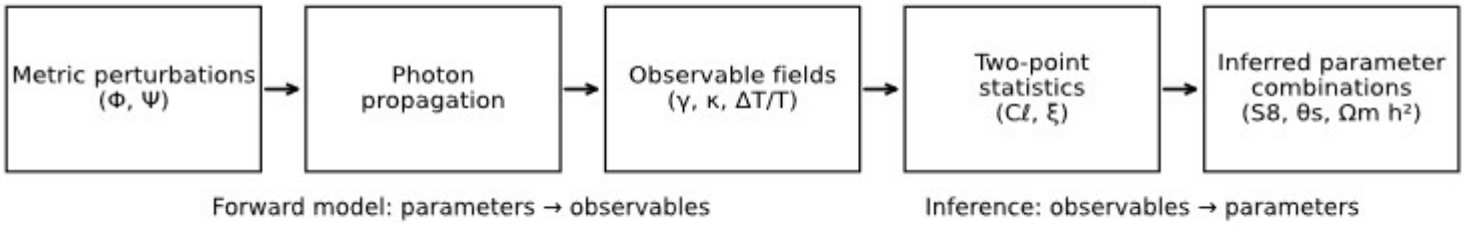

Kernels vs Transfer Functions (CAMB/Class)

In modern cosmology, predicted observables are constructed in two distinct steps: evolution and projection. These steps are encoded mathematically by transfer functions and kernels, respectively.

Transfer functions describe how primordial perturbations evolve with time and scale:
d(k, z) = T(k, z) d_prim(k)

Boltzmann codes such as CAMB and CLASS compute these transfer functions by solving the linearized Einstein–Boltzmann equations for matter, radiation, and metric perturbations. The resulting matter power spectrum is **P(k, z) = P_prim(k) T²(k, z).**

Kernels project evolved perturbations into observables by weighting contributions along the line of sight. For weak gravitational lensing, the convergence field is given by $\kappa(\hat{n}) = \int W(\chi)/\chi^2 \; \delta(\chi(\hat{n}, z)) d\chi$.

In harmonic space, kernels appear explicitly in angular power spectra:

$C_\ell^{\kappa\kappa} = \int [W^2(\chi)/\chi^2] \; P(k = \ell/\chi, z) \, d\chi$.

Rescaled spectrum $D_\ell^{\kappa\kappa} \equiv \frac{\ell(\ell+1)}{2\pi} C_\ell^{\kappa\kappa}$

In CAMB and CLASS, transfer functions govern physical evolution, while kernels govern geometric and observational projection into angular space.

Physically, what each "parameter" represents

ℓ Angular scale on the sky (small ℓ = large angles, large ℓ = small angles)

$C_\ell^{\kappa\kappa}$ → variance of projected mass fluctuations

$D_\ell^{\kappa\kappa}$ → variance per logarithmic interval in ℓ

References:
Dodelson, S. & Schmidt, F., Modern Cosmology, 2nd ed., Academic Press (2020).
Bartelmann, M. & Schneider, P., Weak Gravitational Lensing, Physics Reports 340, 291–472 (2001).
Seljak, U. & Zaldarriaga, M., A Line-of-Sight Integration Approach to Cosmic Microwave Background Anisotropies, Astrophysical Journal 469, 437 (1996).
Eisenstein, D. J. & Hu, W., Baryonic Features in the Matter Transfer Function, Astrophysical Journal 496, 605 (1998).
Ishak, M., Testing General Relativity in Cosmology, Living Reviews in Relativity 22, 1 (2019).

Matter Power Spectrum Data

Custom high-resolution plot log P(k) vs.log k using a standard Linear-Theory Transfer-Function (LTTF)
(e.g., from the CLASS or CAMB code) for ΛCDM-like cosmology. Y-axis P(k) normalized so that P(k = 0.2h/Mpc) = 1000. Shape is computed using a BBKS CDM transfer function with Planck-like parameters: **Ωm ≈ 0.315, *h* ≈ 0.67, ns ≈ 0.965Ω**

$Pk_{LTTF0} := READPRN("matter\ power\ spectrum\ table.txt")$ $Pk_{LTTF} := 1000 \cdot Pk_{LTTF0}^{\langle 1 \rangle}$

Consistent with Power Law Approximation: $Pk_{Power_n} := 35(k_n)^{-2.45}$ $k_{LTTF} := Pk_{LTTF0}^{\langle 0 \rangle}$

Matter Power Spectrum Data from Tegmark et al. 2003, BOSS
Tegmark 22 band-power measurements k from 0.02 to 0.3 h/Mpc
Galaxy clustering from SDSS main sample

$Pk_{tegmark} := READPRN("SDSS\_Tegmark2003\_Pk\_table.txt")$
$Pk_{BOSS} := READPRN("BOSS\_DR12\_excerpt\_Pk\_table.txt")$

Pk_{Lya} Data: *The Atacama Cosmology Telescope, ACT: A Measurement of The Primordial Power Spectrum*
See Next Page for the Matter Distribution

$Pk_{Lya} := READPRN("Lya\_digitized\_high\_k.txt"$

Current Matter Power Spectrum, P(k) versus Wavenumber

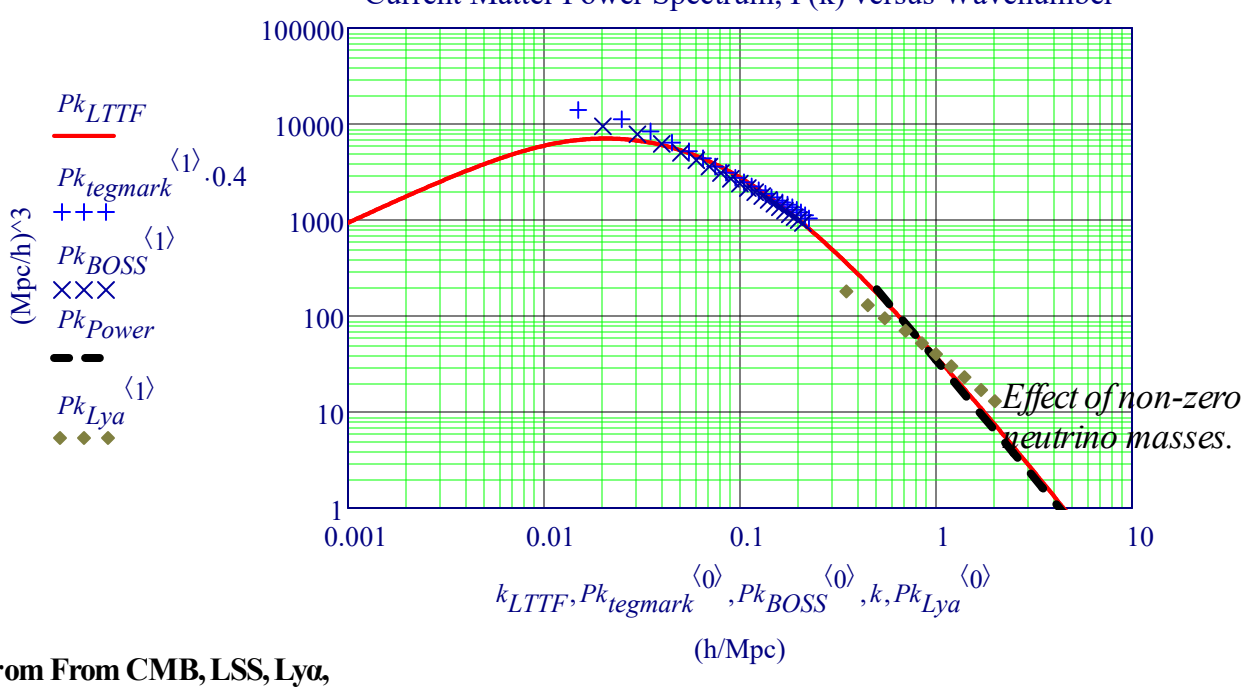

Data from From CMB, LSS, Lyα, cluster abundances and weak lensing

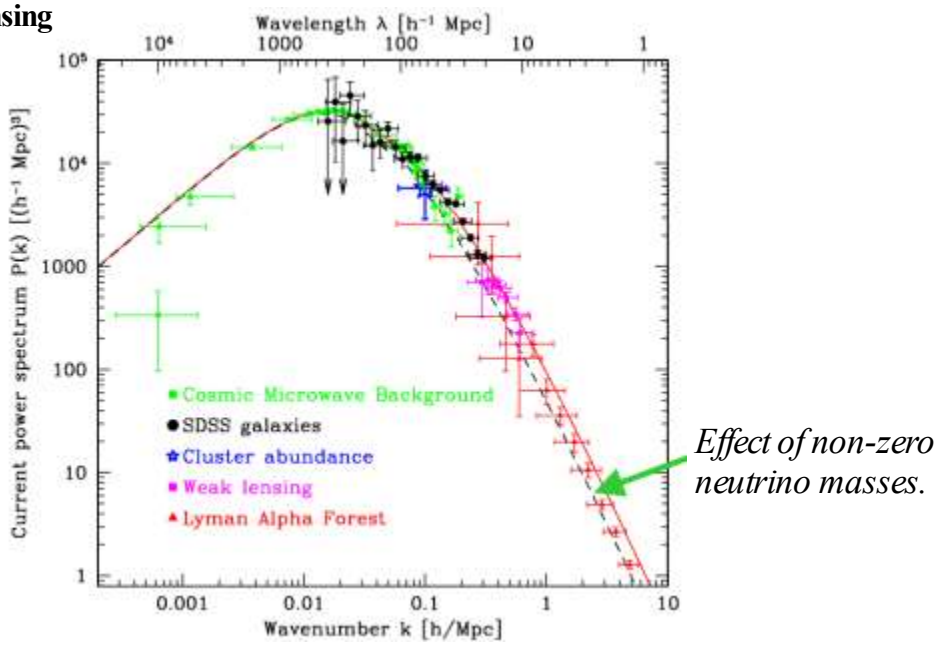

A Measurement of The Primordial Power Spectrum - Data from Atacama (ACT)

The Atacama Cosmology Telescope, ACT: A Measurement of The Primordial Power Spectrum, arXiv:1105.4887v1, Renee Hlozek, Joanna Dunkley1,2,3, Graeme Addison, John William Appe, October 10, 2018

Below is the primordial power spectrum of adiabatic fluctuations using data from the 2008 Southern Survey of the ACT. The angular resolution of ACT provides sensitivity to scales beyond $\ell = 1000$ for resolution of multiple peaks in the primordial temperature power spectrum, which enables us to probe the primordial power spectrum of adiabatic scalar perturbations with wavenumbers up to $k \approx 0.2\ \mathrm{Mpc}^{-1}$. We find **no evidence for deviation from power-law fluctuations** over two decades in scale. Matter fluctuations inferred from the primordial temperature power spectrum evolve over cosmic time and can be **used to predict the Matter Power Spectrum at late times**; we illustrate the overlap of the matter power inferred from CMB measurements (which probe the power spectrum in the linear regime) with existing probes of galaxy clustering, cluster abundances and weak lensing constraints on the primordial power. This highlights the range of scales probed by current measurements of the matter power spectrum.

Matter Distribution

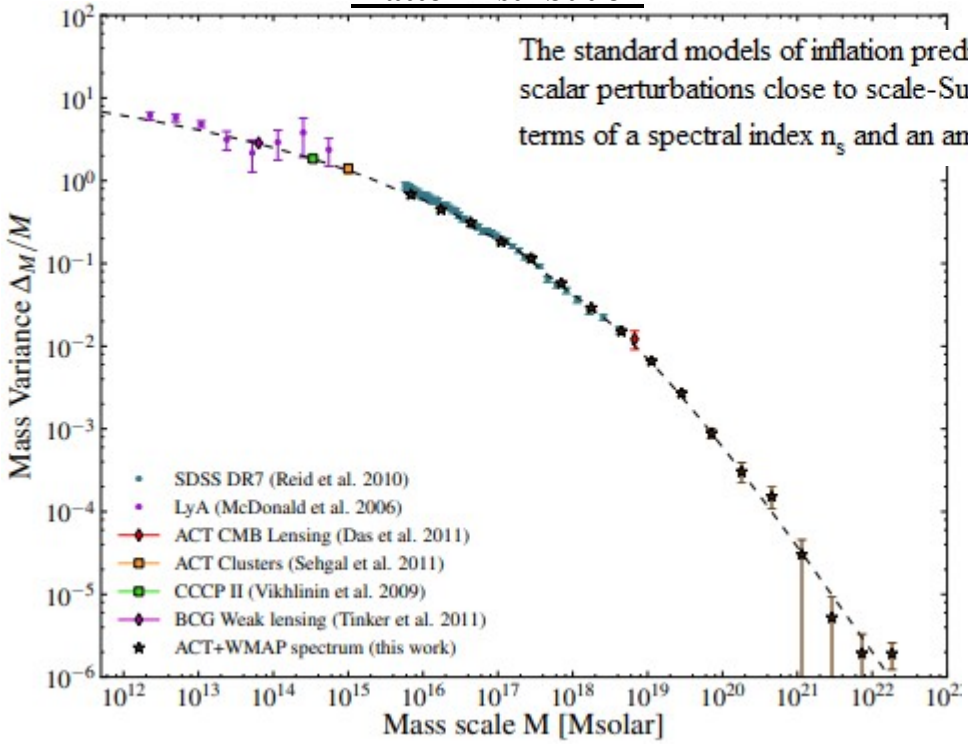

The standard models of inflation predict a power spectrum of adiabatic scalar perturbations close to scale-Such models are often described in terms of a spectral index n_s and an amplitude of perturbations Δ^2_R

$$\mathcal{P}(k) = \Delta^2_{\mathcal{R}} \left(\frac{k}{k_0}\right)^{n_s - 1}$$

Transforming from units Power Spectrum to Mass Variance

$\Delta_M/M = [P(k)k^3/(2\pi^2)]^{1/2}$, allows one to visualize directly the **relationship between mass scale and variance**. While $\Delta_M/M \approx 1$ for $10^6\ M_\odot$ galaxies, the variance decreases as the mass increases and we probe the largest scales, covering ten orders of magnitude in the range of masses of the corresponding probes.

The reconstructed matter power spectrum: the stars show the power spectrum from combining ACT and WMAP data (top panel). The solid and dashed lines show the nonlinear and linear power spectra respectively from the best-fit ACT ΛCDM model with spectral index of $n_s = 0.96$ computed using CAMB and HALOFIT (Smith et al. 2003). The data points between $0.02 < k < 0.19\ Mpc^{-1}$ show the SDSS DR7 LRG sample, and have been deconvolved from their window functions, with a bias factor of 1.18 applied to the data. This has been rescaled from the Reid et al. (2010) value of 1.3, as we are explicitly using the Hubble constant measurement from Riess et al. (2011) to make a change of units from h^{-1}Mpc to Mpc. The constraints from CMB lensing (Das et al. 2011), from cluster measurements from ACT, CCCP (Vikhlinin et al. 2009) and BCG halos, and the power spectrum constraints from measurements of the Lyman–α forest (McDonald et al. 2006) are indicated. The CCCP and BCG masses are converted to solar mass units by multiplying them by the best-fit value of the Hubble constant, $h = 0.738$ from Riess et al. (2011). The above panel shows the same data plotted on axes where we relate the power spectrum to a mass variance, Δ_M/M, and illustrates how the range in wavenumber k (measured in Mpc^{-1}) corresponds to range in mass scale of over 10 orders of magnitude. Note that large masses correspond to large scales and hence small values of k. This highlights the consistency of power spectrum measurements by an array of cosmological probes over a large range of scales

From Primordial Fluctuations to the Matter Power Spectrum

In the ΛCDM cosmological framework, the large-scale distribution of matter arises from primordial curvature perturbations generated during inflation and subsequently processed by well-understood microphysical effects in the early universe. While inflation predicts a nearly scale-invariant primordial power spectrum, the evolution through radiation domination and the coupling of baryons to photons significantly modify the growth of density perturbations after horizon entry. These effects imprint a characteristic turnover and a series of baryon acoustic oscillations (BAO) in the late-time matter power spectrum.

This section develops the connection between the primordial scalar power spectrum and the observed clustering of galaxies by introducing the linear transfer function ***T(k)***, with particular emphasis on the analytic **Eisenstein–Hu** (1998) formulation. The resulting **Matter Power Spectrum** $P_m(k)=P(k)T^2(k)$ provides a direct theoretical bridge between early-universe physics and large-scale structure measurements from galaxy surveys such as SDSS and DESI, which exploit both the broadband shape and the BAO feature as precision cosmological probes.

ΛCDM model incorporates:

8 Factors: $\Omega_m, \Omega_b, \Omega_{cdm}, \Omega_\Lambda, H_0, n_s, A_s, \tau$,

- $\mathbf{A_s}$ Primordial amplitude
- n_s "Scalar Spectral Index
- Pivot Scale, k_0

$A_s := 2.1\cdot 10^{-9}$

$n_s := 1.0$

$k_0 := 0.05\cdot Mpc^{-1}$

$P(k, n_s) := A_s\cdot\left(\frac{k\cdot Mpc^{-1}}{k_0}\right)^{(n_s-1)}$

$n_s = 1$: Scale-invarianat (Harrison-Zeldovich) Spectrum

The farther n_s is below 1, the steeper the downard "**Tilt**".

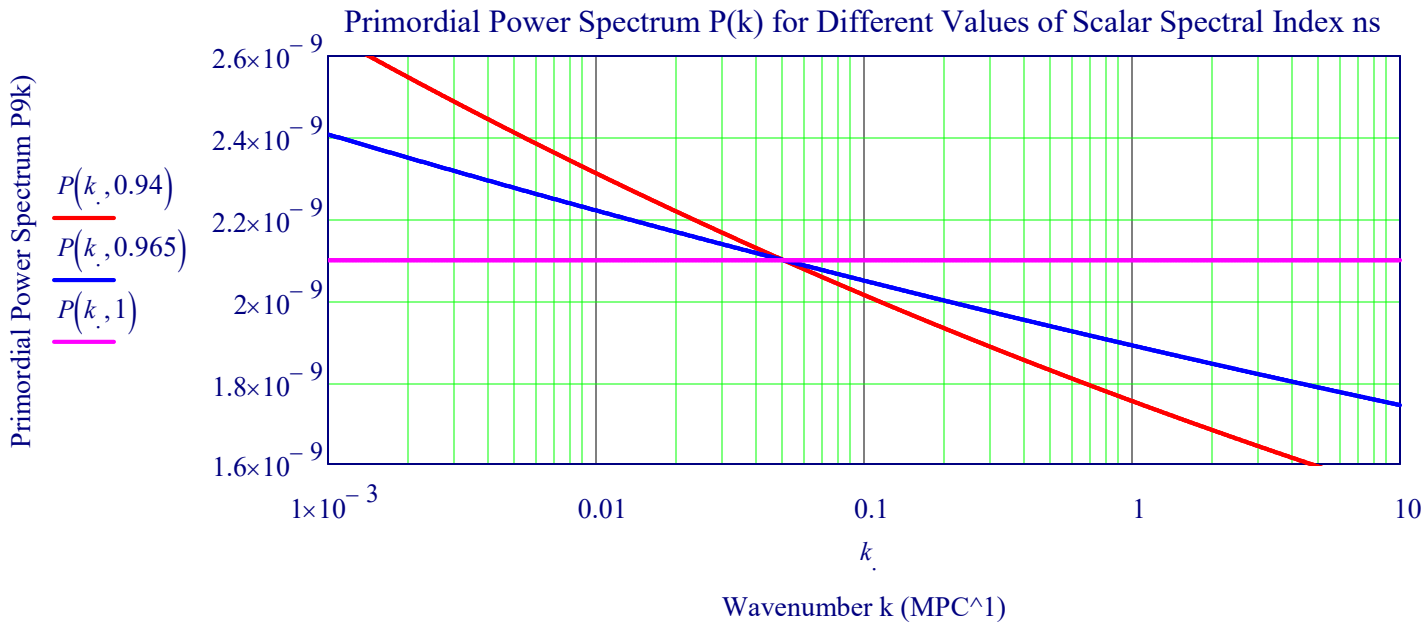

The primordial scalar power spectrum is modified by causal microphysical processes after horizon entry. These effects are encoded in the **transfer function *T(k)***

$P_m(k) = P(k)\cdot T^2(k)$

Late-time matter spectrum:

While inflation predicts a nearly scale-invariant spectrum, **radiation domination and baryon coupling suppress growth on small scales**, producing the characteristic turnover observed in galaxy surveys.

At early times $z > 3400$, the universe was radiation-dominated. Small-scale density perturbations enter the horizon during radiation domination, where radiation pressure and rapid expansion inhibit gravitational growth, while baryons remain coupled to photons until recombination, delaying their collapse and suppressing power on small scales.

Radiation domination: trying to form galaxies in a hurricane.

Eisenstein–Hu (1998) Transfer Function with BAO

The **linear matter power spectrum** is

$$\boxed{P_m(k,z) = A_s \left(\frac{k}{k_0}\right)^{n_s-1} T^2(k)\, D^2(z)}$$

where the **total transfer function** is

$$\boxed{T(k) = f_c\, T_c(k) + f_b\, T_b(k), \qquad f_b = \frac{\Omega_b}{\Omega_m},\ f_c = 1 - f_b}$$

All quantities below follow Eisenstein & Hu (1998).

1. Background Quantities

Define physical densities:

$$\omega_m = \Omega_m h^2, \omega_b = \Omega_b h^2$$

CMB temperature factor:

$$\theta = \frac{T_{\mathrm{CMB}}}{2.7}$$

2. Matter–Radiation Equality Scale

$$\boxed{k_{\mathrm{eq}} = 0.0746\ \frac{\omega_m}{\theta^2}\ \mathrm{Mpc}^{-1}}$$

Define the dimensionless variable:

$$q = \frac{k}{13.41\, k_{\mathrm{eq}}}$$

3. Drag Epoch and Sound Horizon

Drag redshift z_d

$$z_d = \frac{1291\ \omega_m^{0.251}}{1 + 0.659\ \omega_m^{0.828}}\left[1 + b_1\ \omega_b^{b_2}\right]$$

where

$$b_1 = 0.313\ \omega_m^{-0.419}(1 + 0.607\ \omega_m^{0.674})$$
$$b_2 = 0.238\ \omega_m^{0.223}$$

Sound horizon at drag epoch

$$\boxed{s = 44.5\ \frac{\ln(9.83/\omega_m)}{\sqrt{1 + 10\ \omega_b^{0.75}}}\ \mathrm{Mpc}}$$

4. CDM Suppression Parameters

$$\alpha_c = a_1^{-f_b}\ a_2^{-f_b^3}$$

with

$$a_1 = (46.9\ \omega_m)^{0.670}[1 + (32.1\ \omega_m)^{-0.532}]$$
$$a_2 = (12.0\ \omega_m)^{0.424}[1 + (45.0\ \omega_m)^{-0.582}]$$

and

$$\beta_c = [1 + 0.944\ f_b]^{-1}$$

The Eisenstein–Hu (1998) transfer function

Provides an analytic description of the linear evolution of density perturbations in a baryon–cold dark matter universe, accurately capturing both radiation-era suppression and baryon acoustic oscillations. By modeling the imprint of the photon–baryon sound horizon and Silk damping, it reproduces the essential features of the linear matter power spectrum and serves as a widely used **analytic framework for BAO analyses in galaxy surveys.**

5. Core CDM Shape Function

$$\boxed{T_0(k;\alpha,\beta) = \frac{\ln\quad(e+1.8\,\beta\,q)}{\ln\quad(e+1.8\,\beta\,q) + \left(\frac{14.2}{\alpha} + \frac{731}{1+62.5\,q}\right)q^2}}$$

6. CDM Transfer Function $T_c(k)$

$$\boxed{T_c(k) = f\,T_0(k;1,\beta_c) + (1-f)\,T_0(k;\alpha_c,\beta_c)}$$

where

$$f = \frac{1}{1+(k\,s/5.4)^4}$$

This interpolates between large-scale and small-scale CDM growth.

7. Silk Damping Scale

$$\boxed{k_{\text{Silk}} = 1.6\,\omega_b^{0.52}\,\omega_m^{0.73}[1+(10.4\,\omega_m)^{-0.95}]}$$

8. Baryon Transfer Function $T_b(k)$

First define the **effective sound horizon shift**:

$$\tilde{s} = \frac{s}{[1+(\beta_b/ks)^3]^{1/3}}$$

with

$$\beta_b = 0.5 + f_b + (3-2f_b)\sqrt{(17.2\,\omega_m)^2+1}$$

Then

$$\boxed{T_b(k) = \left[\frac{T_0(k;1,1)}{1+(k\,s/5.2)^2} + \frac{\alpha_b}{1+(\beta_b/ks)^3}\right]\frac{\sin(k\tilde{s})}{k\tilde{s}}\;e^{-(k/k_{\text{Silk}})^{1.4}}}$$

where

$$\alpha_b = 2.07\,k_{\text{eq}}\,s\,(1+R_d)^{-3/4}$$

and

$$R_d = 31.5\,\omega_b\,\theta^{-4}\left(\frac{1000}{z_d}\right)$$

9. Final Result

$$\boxed{T(k) = f_c\,T_c(k) + f_b\,T_b(k)} \Rightarrow \boxed{P_m(k) = P(k)\,T^2(k)}$$

Explicit Connection to SDSS & DESI

What surveys observe

Galaxy surveys measure:

$$P_g(k,z) = b^2(z)\,P_m(k,z)$$

What Eisenstein–Hu provides

- **Broadband shape** → turnover from radiation domination
- **BAO oscillations** → from $\sin(k\tilde{s})/(k\tilde{s})$
- **Silk damping** → exponential suppression at high k

Observational consequences

- **SDSS (BOSS/eBOSS)**
  Uses EH98 "wiggle" and "no-wiggle" templates to isolate BAO
- **DESI**
  Measures BAO with higher precision across multiple redshifts, constraining $D_A(z)$, $H(z)$, and Ω_m

PLOT SUMMARY

In ΛCDM, the Eisenstein–Hu (EH) transfer function encodes radiation-era suppression and baryon acoustic physics, producing both the turnover and the BAO oscillations observed in galaxy surveys such as SDSS and DESI.

Three EH98 Schematic Plots

These plots were made Using the Python Programs:

- Python-CAMB cross-validation (EH98 vs CAMB).py
- EH98_BAO_wiggle_program.py

These Programs are available at: VXPhysics.com/Python

$$T_{wiggle} := READPRN("EH98\_BAO\ \ fractional\ \ wiggles.csv")$$
$$k := T_{wiggle}^{\langle 0 \rangle} \qquad T_{kBAOFrac} := T_{wiggle}^{\langle 1 \rangle}$$

Fractional BAO Feature This plot isolates the baryon acoustic oscillation signal by dividing the full matter power spectrum by a smooth, no-wiggle reference spectrum. **The resulting fractional oscillation**s reveal the characteristic BAO scale that serves as a robust standard ruler in galaxy surveys such as SDSS and DESI.

$$P_{wig}/P_{nw} - 1$$

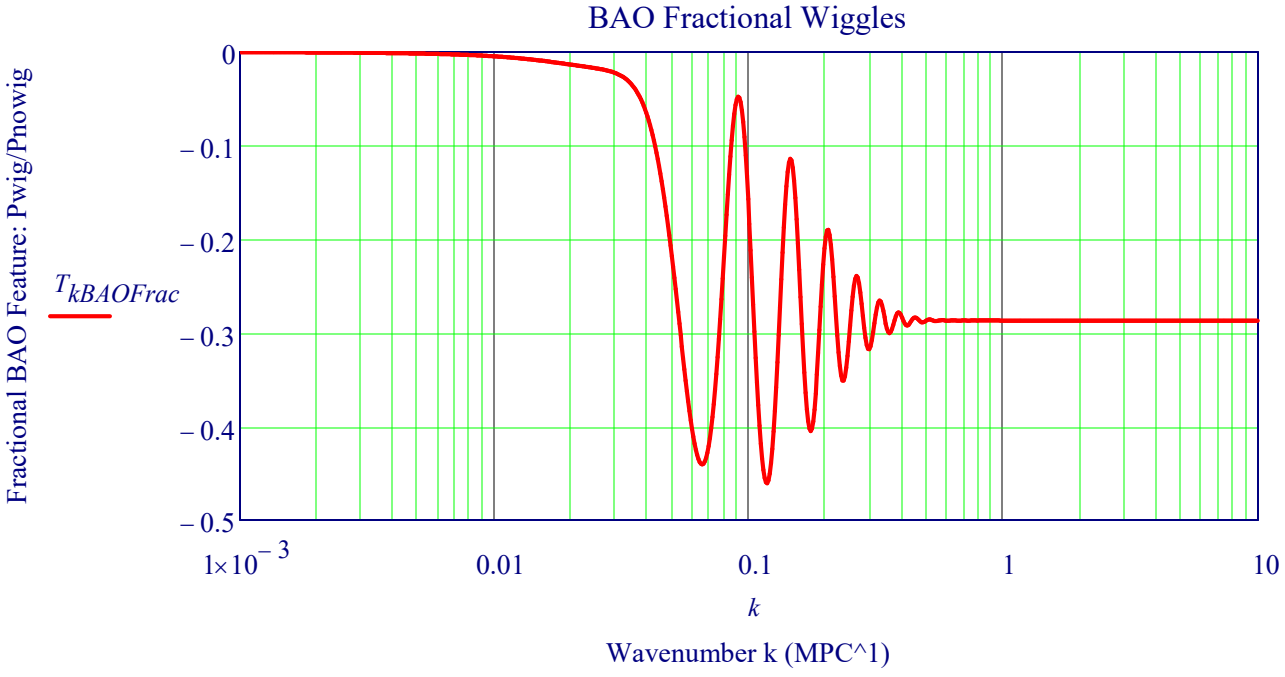

What this confirms (important)

- The plot you now see is exactly the intended Eisenstein–Hu BAO fractional feature:

$$\frac{P_{wig}(k)}{P_{nw}(k)} \to 1 \quad \Rightarrow \quad \frac{P_{wig}}{P_{nw}} - 1 \to 0$$

- The oscillations are present at the correct k-scales (around k ~ 0.05-0.3h Mpc^{-1}
- The amplitude is a few percent, as expected for linear BAO physics
- This is pure EH98 analytic physics, not CAMB, not data, not non-lear

Linear Matter Power Spectrum $P_m(k)$

The linear matter power spectrum $P_m(k) = P_{prim}(k)T^2(k)$ rates how primordial inflationary fluctuations are processed by early-universe physics, producing a characteristic turnover and BAO oscillations at intermediate scales. Smooth curve highlights the broadband shape, while the oscillatory deviations trace the baryonic imprint on large-scale structure.

$T_{wiggle} := READPRN("EH98\_matter\_power\_wiggle\_nowiggle.csv")$

$k := T_{wiggle}^{\langle 0 \rangle}$ $T_{kwiggle} := T_{wiggle}^{\langle 1 \rangle}$ $T_{kNowiggle} := T_{wiggle}^{\langle 2 \rangle}$

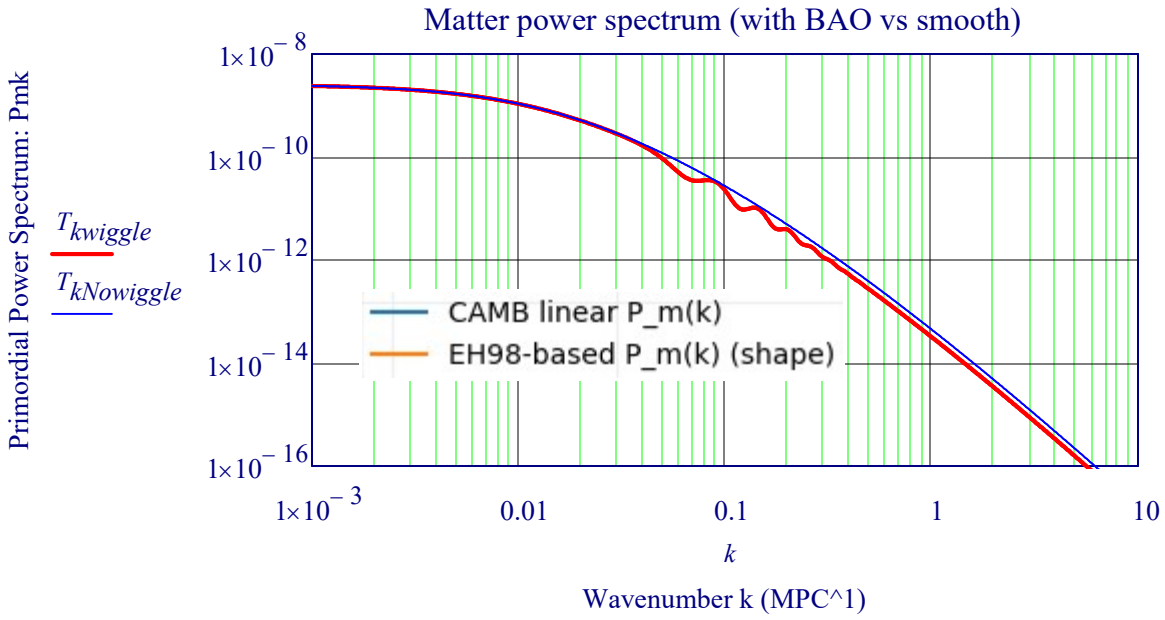

Transfer Function *T(k)*: Wiggle vs No-Wiggle

This plot shows **the Eisenstein–Hu linear transfer function *T(k)***, comparing the smooth suppression of power from radiation domination with the oscillatory modulation produced by baryon acoustic oscillations. The BAO features arise from sound waves in the photon–baryon fluid prior to recombination and are damped on small scales by photon diffusion.

$T_{tran\_fn} := READPRN("EH98\_transfer\_functions.csv")$

$k := T_{tran\_fn}^{\langle 0 \rangle}$ $T_{kBAO} := T_{tran\_fn}^{\langle 1 \rangle}$ $T_{kNoWig} := T_{tran\_fn}^{\langle 2 \rangle}$

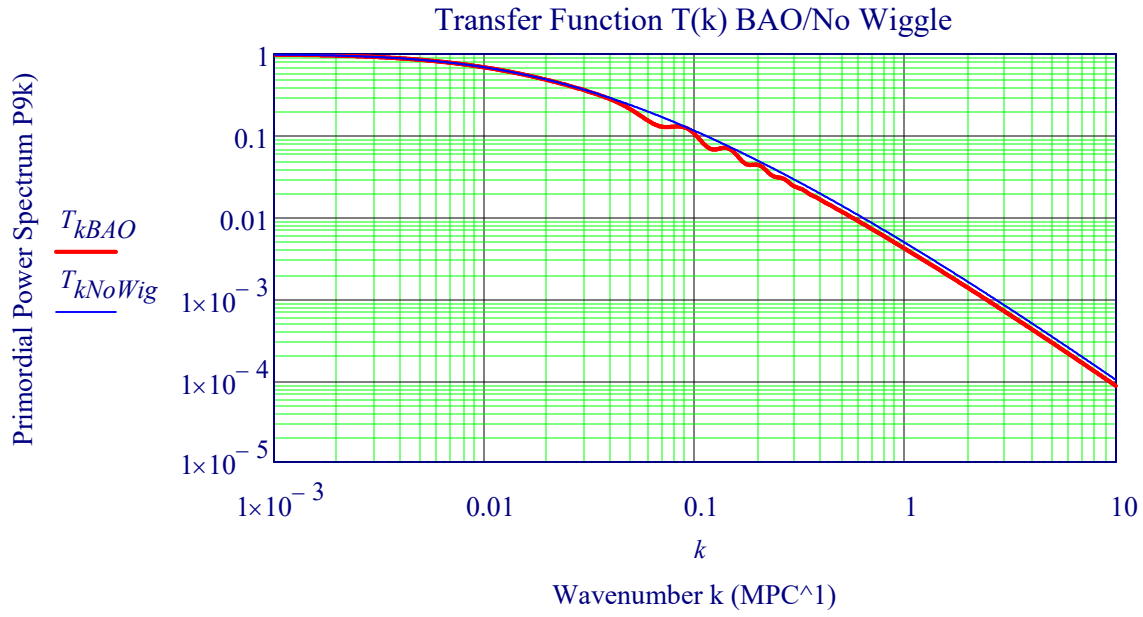

XXVIIA. The Discovery of the Accelerating Universe (2011)

What is the minimum redshift needed to determine if expansion of the universe is accelerating?

There isn't a single magic redshift, because it depends on (a) what you're measuring (SNe, BAO, cosmic chronometers), and (b) how strong your systematics are. But there is a clean physics answer:
What redshift scale contains "acceleration information"?
At very low redshift, the distance–redshift relation can be expanded as

$$d_L(z) \approx \frac{cz}{H_0}\left[1 + \frac{1-q_0}{2}z + \cdots\right]$$

The acceleration/deceleration parameter today, q_0, first appears at order z^2.

That means you need redshift large enough that the z^2 term is measurable, not buried in noise.

Minimum redshift in principle $z \gtrsim 0.1$ is the rough minimum where the curvature term $\propto z^2$ can start to become detectable in principle.

Minimum redshift in practice (what actually works)

- $z \gtrsim 0.3$ is a good practical minimum to get a statistically meaningful handle on acceleration from a Hubble diagram (e.g., Type Ia supernovae), because below that:
- peculiar velocities,
- local bulk flows,
- calibration systematics can dominate.

Best leverage for a clean "accelerating vs not" conclusion
$z \sim 0.5$ to 1 gives strong leverage, because the deviation between an accelerating and non-accelerating expansion history becomes much larger in the distance–redshift curve.

A useful rule of thumb
If the dataset only goes to only goes to $z \lesssim 0.2$, it's very hard to claim acceleration robustly.
If it reaches $z \gtrsim 0.5$, it's in the regime where the "curvature" of the Hubble diagram is clearly informative.

Saul Perlmutter (with the Supernova Cosmology Project, SCP) used Type Ia supernovae at redshifts extending to about $z \approx 0.8$, with the key acceleration signal coming from supernovae around $z \sim 0.4 – 0.7$.

What Perlmutter actually used (1998–1999)
📌 **Probe**
Type Ia supernovae as standardizable candles

📌 **Redshift range**
Low- z anxchor: $z < 0.1$ (nearby SNe for calibration)
High-z sample: up to $z \sim 0.83$
Critical leverage: $z \gtrsim 0.4$

Perlmutter's discovery of cosmic acceleration relied on Type Ia supernovae extending to redshift

$z \sim 0.5$ to 0.8,

where the curvature of the luminosity–distance relation becomes sensitive to the deceleration parameter.

Distance Modulus vs. Redshift for Type Ia Supernovae from the Supernova Cosmology Project

Lawrence Berkeley National Laboratory Data:
The Supernova Cosmology Project, SCP

Data from: https://supernova.lbl.gov/Union/figures/SCPUnion2.1_mu_vs_z.txt

$SCP := READPRN("SCPUnion mu vs z. Data Only.txt")$ $SCP := csort(SCP, 0)$

$z_{mu} := SCP^{\langle 0 \rangle}$ $M_{mu} := SCP^{\langle 1 \rangle}$ $vg := (1 \quad 1 \quad 1)^T$ $rows(SCP) = 580$

Fit a Logfit Function and a Straight Line to Magnitude vs. Redshift Data

$ab := logfit(z_{mu}, M_{mu}, vg)$ $M(z) := ab_0 \cdot ln(z + ab_1) + ab_2$

$ba := line(log(z_{mu}), M_{mu})$ $M_{line}(z) := ba_0 + ba_1 \cdot log(z)$

$Diff(z) := M(z) - M_{line}(z)$

Hubble Diagram: Supernova Type 1a Measurement - Distance Modulus vs. z

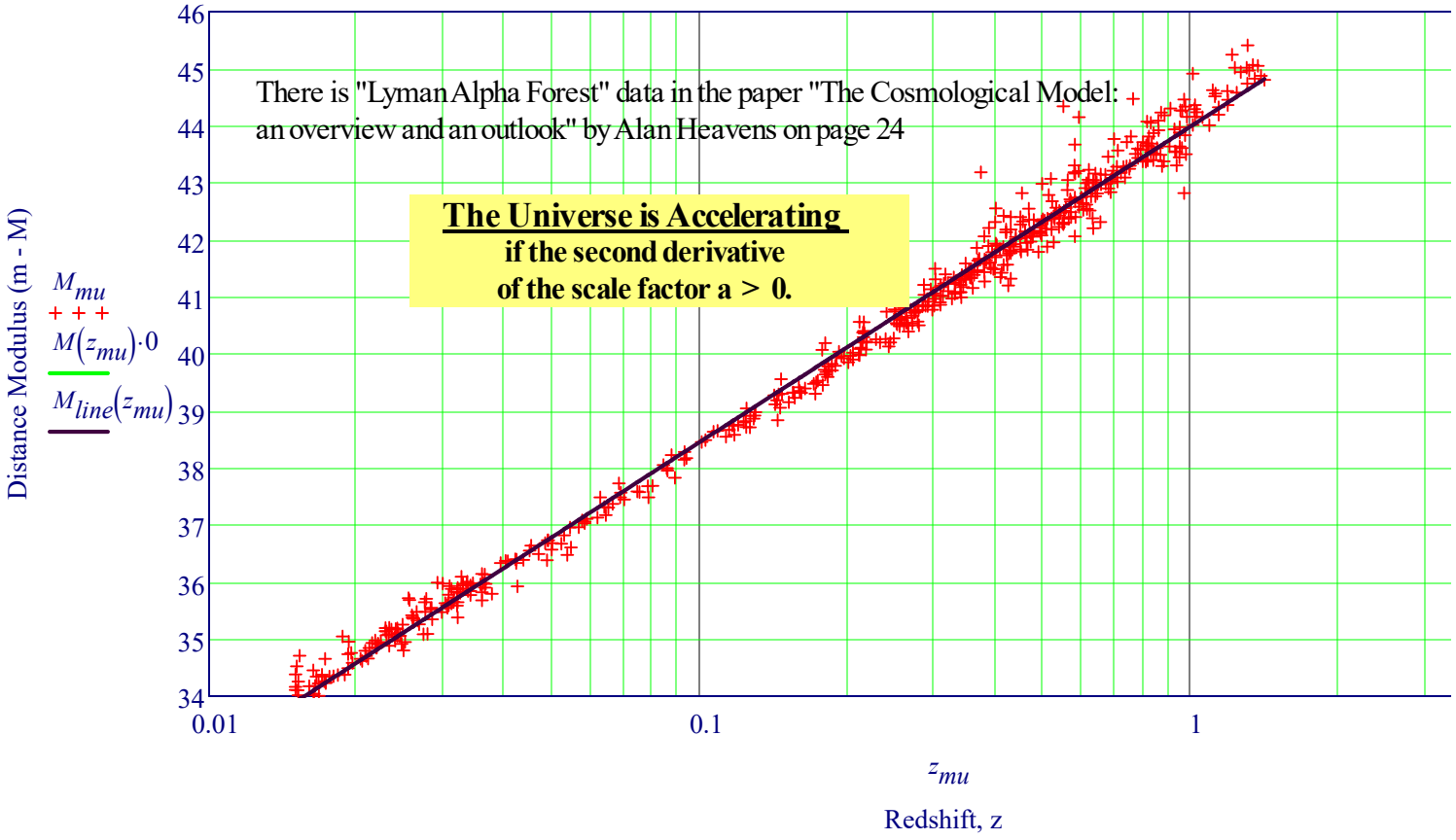

Find the Percent of z > 0.1 Supernovae that are above the Regression Line, Mline

$$PercentAbove := \left(\sum_{n=478}^{579} if\left(M_{mu_n} - M_{line}\left(z_{mu_n}\right) > 0, 1, 0\right) \right) \frac{1}{100}$$

$PercentAbove = 64 \cdot \%$

- $\ddot{a} > 0 \rightarrow$ accelerating
- $\ddot{a} < 0 \rightarrow$ decelerating

This 64% shows that the Velocities of the High z Galaxies are statistically increasing faster than the Hubble Constant. **The Expansion is Accelerating. Visually, the second derivative of the scale factor, a > 0.**

XXVIIB. The Discovery of the Accelerating Universe (1999)

Ω AND Λ FROM 42 HIGH-REDSHIFT SUPERNOVAE, Perlmutter et. al. (1999)

Named by Science magazine as the 'Scientific Breakthrough of the Year" for 1998.

The Supernova Cosmology Project, SCP

Attempts to measure the deceleration parameter Λ were stymied for **lack of high-redshift supernovae**. The Supernova Cosmology Project was started in 1988 to address this problem. The primary goal of the project is the determination of the cosmological parameters of the universe using the magnitude-redshift relation of type Ia supernovae. The Project developed techniques, including instrumentation, analysis, and observing strategies, that make it possible to systematically study high-redshift supernovae. As of 1998 March, more than 75 type Ia supernovae at redshifts **z = 0.18 to 0.86** have been discovered and studied by the Supernova Cosmology Project. (Perlmutter et al.)

$z \quad \sigma_z \quad m_X^{peak} \quad \sigma_X^{peak} \quad A_X \quad K_{BX} \quad m_B^{peak} \quad m_B^{eff} \quad \sigma_{m_B^{eff}}$

$ZD := READPRN("SCP SNE IA DATA - Perlmutter Data Only.txt")$ $rows(ZD) = 42$

$zd := READPRN("CALAN-TOLOLO SNE IA DATA.txt")$ $rows(zd) = 18$

Merge Data Files: $ZD := stack(zd, ZD)$ $ZD := csort(ZD, 0)$

Fit a Logfit Function and Straight Line to Magnitude vs. Redshift Data

$zz := ZD^{\langle 0 \rangle}$ $max(zz) = 0.83$ $m_{pk} := ZD^{\langle 2 \rangle}$ $max(m_{pk}) = 23.73$

$ab := logfit(zz, m_{pk}, vg)$ $M(z) := ab_0 \cdot ln(z + ab_1) + ab_2$

$ba := line(log(zz), m_{pk})$ $M_{line}(z) := ba_0 + ba_1 \cdot log(z)$ $ba_1 = 4.803$

Hubble Diagram: Supernova Type 1a Measurement - Effective Magnitude vs. Redshift (z)

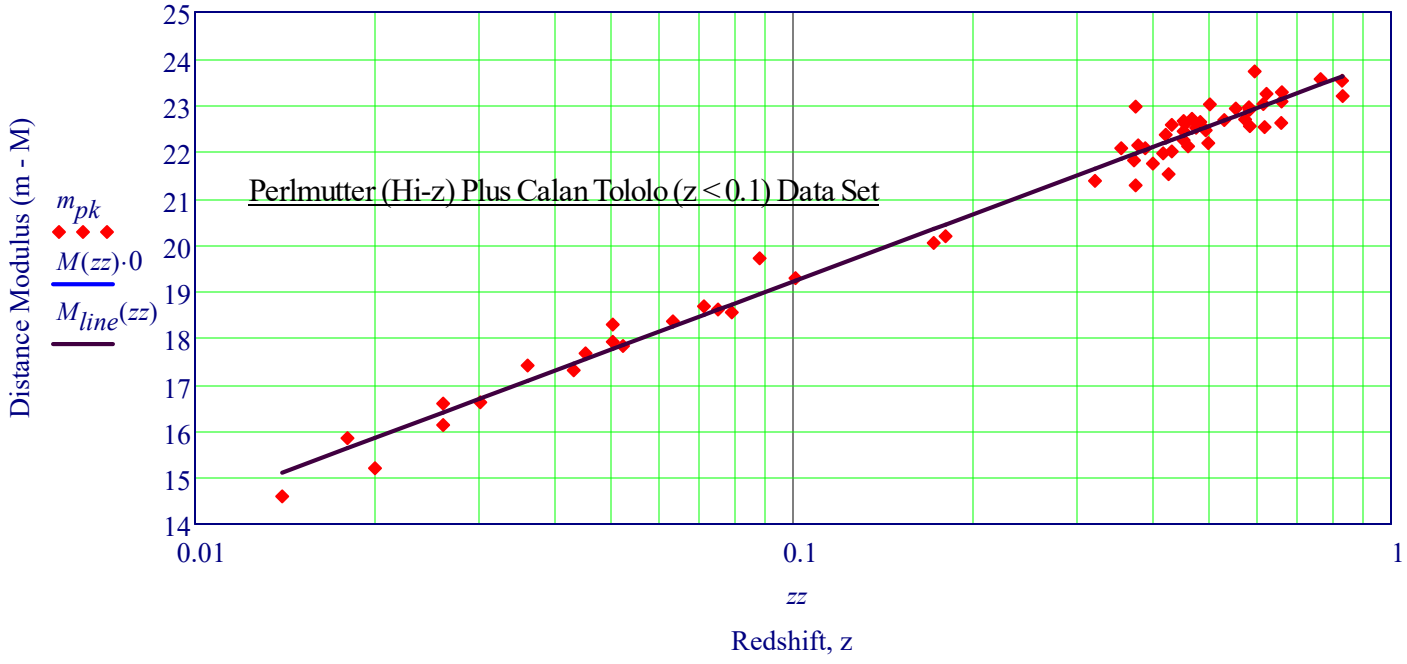

Find the Percent of z > 0.1 Supernovae that are above the Regression Line, Mline

$$PercentAboveMean := \left(\sum_{n=30}^{59} if\left(m_{pk_n} - M_{line}(zz_n) > 0, 1, 0\right) \right) \frac{1}{30}$$

$PercentAboveMean = 56.667 \cdot \%$

This shows that the Velocities of the High z Galaxies are statistically increasing faster than the mean Hubble Constant. **The Expansion is Accelerating.**

XXVIIC. The 5 Year Dark Energy Survey (DESI) and Supernovae - 2024

Refer to the Article:
The Dark Energy Survey (DES): Cosmology Results With ≈1500 New High-redshift Type Ia Supernovae Using The Full 5-year Dataset January 9, 2024 https://arxiv.org/abs/2401.02929

https://skyandtelescope.org/astronomy-news/cosmology/how-strong-is-dark-energy-intriguing-findings-from-new-supernova-catalog/

We have known for nearly 100 years that the universe is expanding. But only at the turn of the 21st century did astronomers discover that the expansion was actually speeding up.
Now, this new study suggests ***that this phenomenon might be weaker than we thought.***
The Previous value for Λ was 69%. This DES Study gives Λ = 65%. See Plot Below.

The largest sample of Type Ia supernovae ever made by a single telescope sheds light on dark energy.

The Dark Energy Survey (DES) was conceived to characterize the properties of dark matter and dark energy with **unprecedented precision and accuracy** through **four primary observational probes** (The Dark Energy Survey Collaboration 2005; Bernstein et al. 2012; Dark Energy Survey Collaboration 2016; Lahav et al.2020).
An example of a supernova discovered by the Dark Energy Survey (DES) within the field covered by one of the individual detectors in the Dark Energy Camera. The supernova exploded in a spiral galaxy with redshift = 0.04528, which corresponds to a light-travel time of about 0.6 billion years. This is one of the nearest supernovae in the sample. In the inset, the supernova is a small dot at the upper-right of the bright galaxy center. ***DES collaboration***

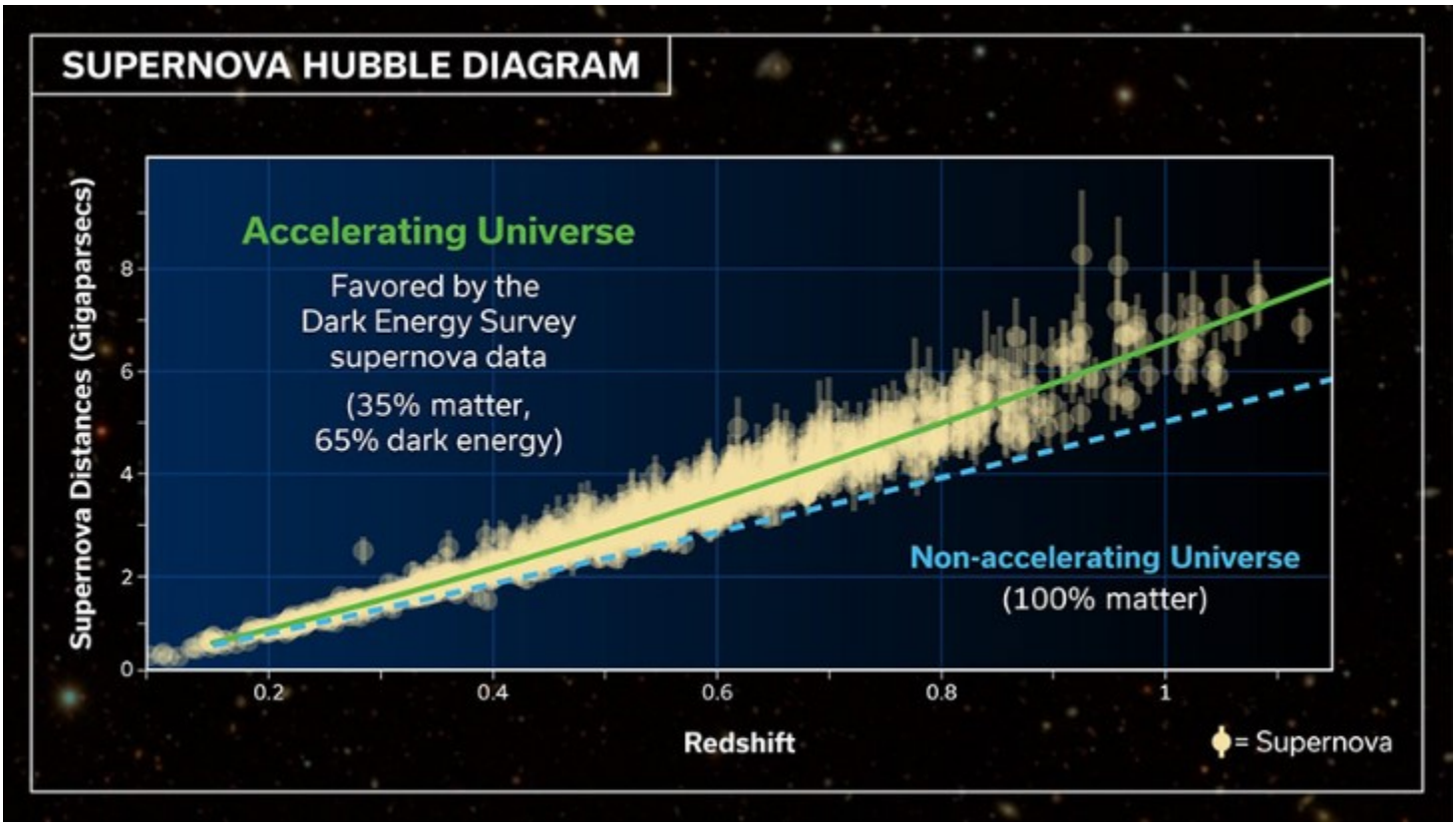

During a five-year survey, astronomers used a special camera mounted on the **Víctor M. Blanco 4-meter Telescope** at Cerro Tololo Inter-American Observatory to discover **1,635 Type Ia supernovae from hundreds of different galaxies** spread over a huge range of distances. The light from these supernovae is anywhere between 1 billion and 9 billion years old. Using the aforementioned standard-candle technique, the team calculated the universe's expansion rate — and **established the first good constraints on dark energy.**

How DESI Contains Expansion History and Dark Enegry

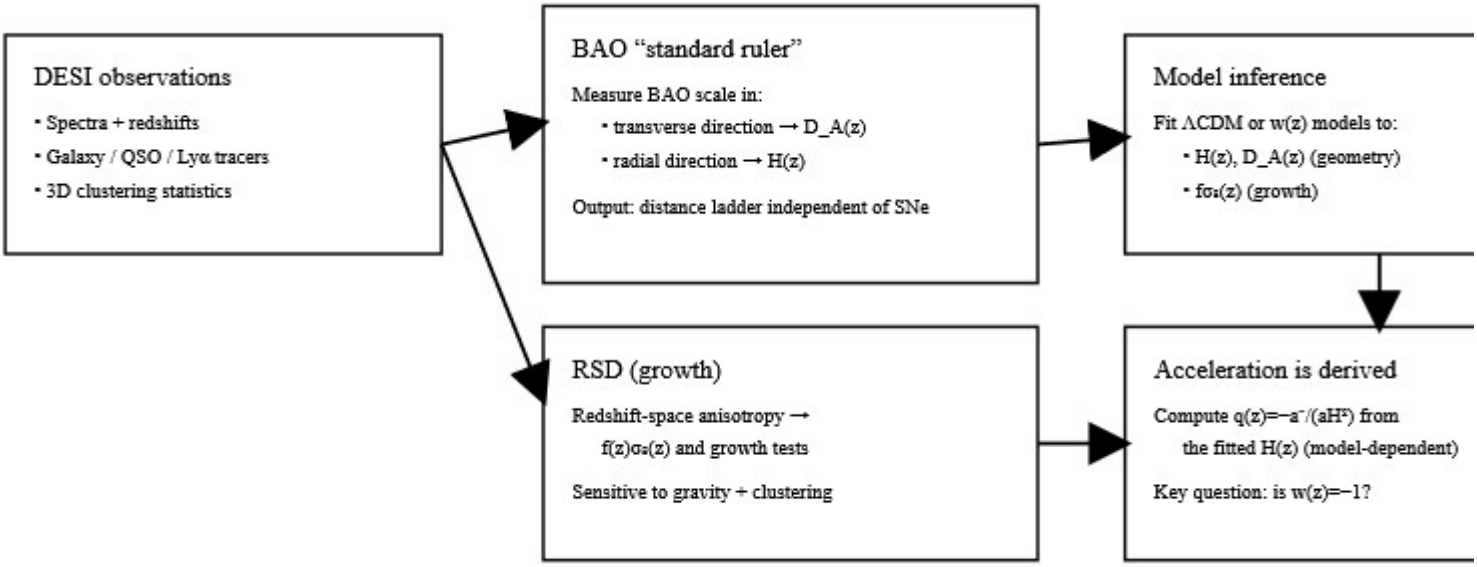

Takeaway: DESI tightly constrains H(z) and D_A(z); "less acceleration" comes from best-fit model comparisons (ΛCDM vs evolving w(z)) across probes.

DESI: BAO/RSD to→ Expansion History to→ Inference: Acceleration or Not

DESI to BAO to Expansion Inferences

This section explains
How DESI observations constrain the cosmic expansion history and how claims about acceleration are inferred.

Result of DESI Survery.pdf

1. DESI Observations
The Dark Energy Spectroscopic Instrument (DESI) measures precise redshifts for galaxies, quasars, and the Lyman-a forest. These observations provide three-dimensional maps of large-scale structure.

2. Baryon Acoustic Oscillations (BAO) — Geometry
DESI measures the BAO feature as a standard ruler in galaxy clustering. The transverse BAO scale constrains the angular-diameter distance $D_A(z)$, while the radial BAO scale constrains the Hubble expansion rate H(z). These measurements provide a distance ladder independent of supernovae.

3. Redshift-Space Distortions (RSD) — Growth of Structure
Anisotropies in redshift space arise from galaxy peculiar velocities. DESI uses these redshift-space distortions to measure the growth rate of structure, typically expressed as $f(z)\sigma_8(z)$. These measurements test gravity and clustering physics.

4. Model Inference
Cosmological models such as ΛCDM or evolving dark energy parameterizations w(z) are fitted simultaneously to H(z), D_A(z), and fs8(z). The choice of model directly affects the inferred expansion history.

5. Acceleration Is Derived, Not Directly Observed
Cosmic acceleration is quantified by the deceleration parameter $q(z) = -(\ddot{a})/(aH^2)$. DESI does not measure $\ddot{a}$ directly. Instead, q(z) is computed from the best-fit H(z) after adopting a cosmological model. Therefore, conclusions about acceleration are model-dependent.

6. Interpretation of Recent DESI Results
DESI BAO measurements are consistent with ΛCDM, but when combined with other probes (CMB, supernovae, weak lensing), the data allow mild deviations from a constant dark-energy equation of state w = -1. These results weaken, but do not eliminate, the evidence for strong late-time acceleration.

Key takeaway: DESI tightly constrains the expansion history H(z). Statements about 'less acceleration' arise from comparing best-fit cosmological models, not from a direct measurement of acceleration itself.

XXVIID. Compare the Theoretical Magnitude-Redshift to Perlmutter 1999 SB 1A

Theoretical Apparent Magnitude-Redshift Relation (Mukhanov)

Physical Foundations of Cosmology, Mukhanov, Equations 2.78 and 2.81

$$\chi_{em}(z, \Omega_m) := \int_0^z \frac{1}{\sqrt{\Omega_m \cdot (1 + z\xi)^3 + (1 - \Omega_m)}}\, dz\xi$$

$$\Phi^2(\chi_{em}) = \begin{cases} \sinh^2 \chi, & k = -1; \\ \chi^2, & k = 0; \\ \sin^2 \chi, & k = +1. \end{cases}$$

Note: For k = 0

$$\Phi(\chi_{em}) = \chi_{em}$$

Then the Theoretical Bolometric Magnitude for k = 0 is Given by:

$$m_{bol}(z, \Omega_m) := 5\, log(1 + z) + 5\, log(\chi_{em}(z, \Omega_m)) + 24$$

$$j := 0 .. 300 \qquad z_j := 10^{0.01 \cdot j - 3}$$

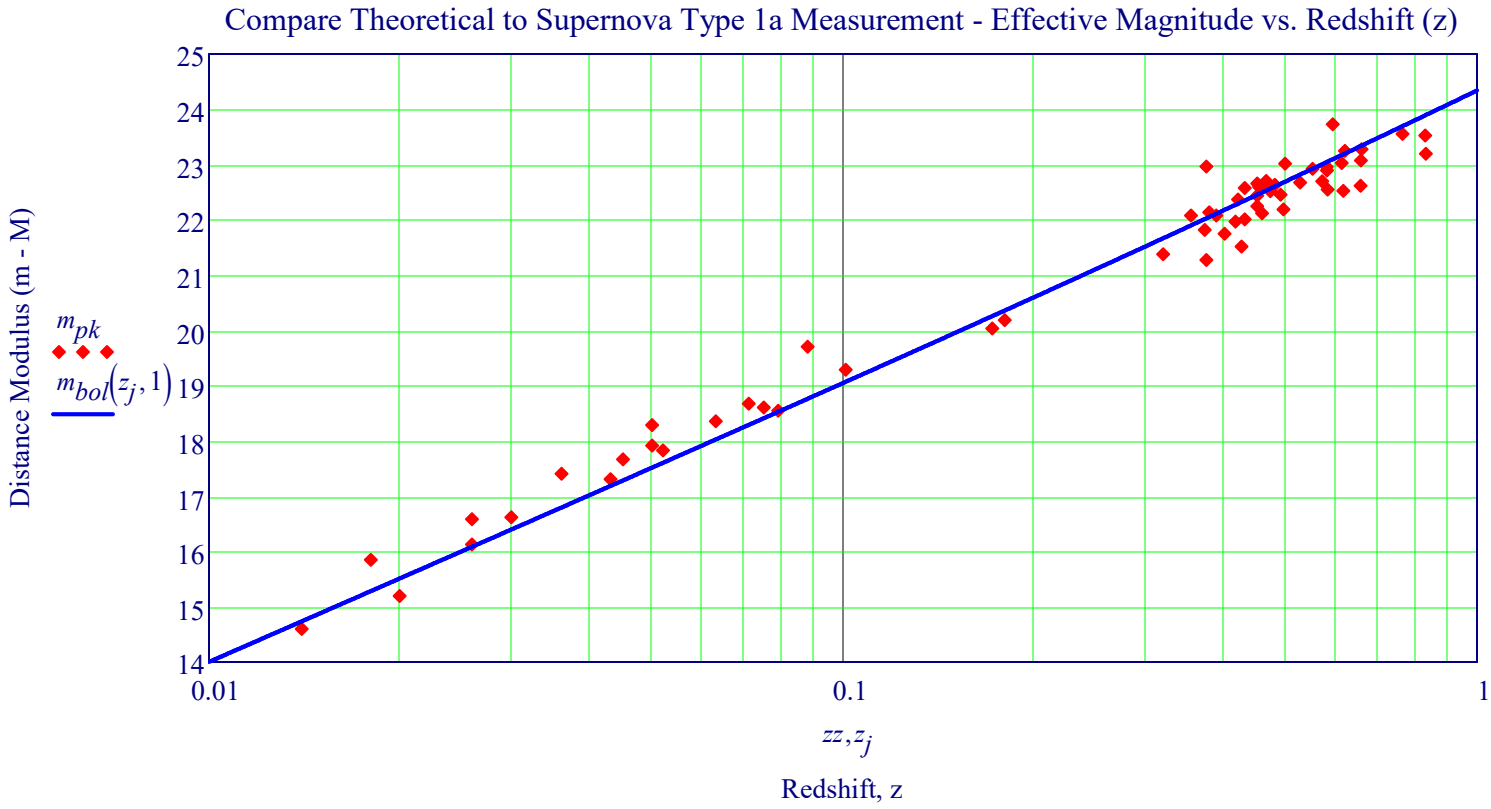

z

Alternative Models for Accelerating Universe

Different model types to quickly navigate the landscape of alternatives to a pure cosmological constant Λ.

⭐ 1. Emergent / "Effective" Dark Energy (No Fundamental DE Field)

These models try to *generate* acceleration from structure, particle-creation effects, or non-standard effective pressures—often without an explicit scalar-field or Λ term.

1.1 Emergent dark energy from new physics

- **Ben-Dayan & Kumar (2023)** — *Emergent Unparticles Dark Energy*, JCAP 12 (2023) 047
  - Unparticle sector produces an effective late-time DE that can fit H_0 & S_8 tensions better than ΛCDM.

1.2 Phenomenological Emergent Dark Energy (PEDE)

- **Hernández-Almada et al. (2024)** — *Phenomenological emergent dark energy in the light of DESI DR1*, PDU 46 (2024)
  - Uses DESI BAO to re-evaluate PEDE vs ΛCDM.

1.3 Emergent DE from structure formation

- **Lapi et al., Part II (2025)** — *Emergent dark energy from structure formation*, JCAP 04 (2025)
  - Structures produce backreaction-like effects that mimic DE, reducing tensions.

1.4 Particle-creation–driven acceleration

- **Lima et al. (2025)** — *Accelerating cosmology without dark energy*, EPJC 85 (2025)
  - Acceleration arises from gravitational particle creation + RRG model; no DE fluid.

⭐ 2. Dynamical Dark Energy ($w(z) \neq -1$)

These explicitly assume DE is a field or fluid with time-varying equation of state—CPL, phantom crossing, etc.

2.1 DESI DR1 → preference for w(z) evolution

- **Giarè et al. (2024)** — *Robust preference for Dynamical Dark Energy*, JCAP 2024
  - Finds ~3σ evidence for evolving w after marginalizing systematics.

2.2 DESI 2024 / DESI + Planck + SNe analysis

- **Roy (2025)** — *Dynamical dark energy in the light of DESI 2024*, PDU 48 (2025)
  - Uses w(a) parameterization showing phantom crossing; reduces H_0 tension.

2.3 DESI DR2 flagship Nature Astronomy paper

- **Gu et al. (2025)** — *Dynamical dark energy in light of DESI DR2*, Nature Astronomy (2025)
  - Shows moderate Bayesian preference for w(z) evolution; strongest mainstream claim against Λ = const.

2.4 Physics-motivated DE families with DESI constraints

- **Lodha et al. (DESI Collaboration, 2025)** — *Physics-focused aspects of dark energy*, PRD 111 (2025)
  - Analyzes thawing, freezing, mirage, and other scalar-field families vs DESI BAO.

⭐ 3. Modified Gravity / Alternative Gravity Theories

These keep some form of DE optional or remove it entirely by modifying the gravitational sector.

3.1 Broad MG approaches to cosmic tensions

- **Di Valentino et al. (eds.) (2024)** — *Special Issue on Modified Gravity*, Universe 10 (2024)
  - Includes f(R), f(Q), scalar–tensor, Galileon, etc., many mimicking accelerations without Λ.

⭐ 4. Challenges / Re-examinations of the Evidence (Systematics-focused)

These do **not** propose new models but question whether the *data* prefers evolving DE or whether systematics mimic it.

4.1 Supernovae systematics may mimic w(z)

- **Efstathiou (2025)** — *Evolving dark energy or supernovae systematics?*, MNRAS 538 (2025)
  - Finds that evolving-DE evidence depends strongly on SN sample.

4.2 Internal consistency of DESI's BAO analysis

- **Wang (2024)** — *Self-consistency of DESI analysis*, arXiv:2404.13833
  - Argues dynamical-DE claims may be sensitive to modeling choices.

⭐ 5. Meta-Analyses / Reviews (Context, not new models)

5.1 Review of w(z) constraints (2023–2024)

- **Escamilla et al. (2024)** — *State of the dark energy equation of state*, JCAP 05 (2024)
  - Summarizes emergent, interacting, scalar-field, and MG models vs current data.

5.2 PDG Dark Energy review

- **Turner & Huterer (2023)** — *Dark Energy*, PDG Review
  - Good baseline: reviews why acceleration is robust but microphysics is open.

🎯 What this organization tells you

1. The "alternative explanation" side:

- Emergent DE papers (Ben-Dayan; Lapi; Lima) aim to remove the need for a cosmological constant.
- Modified-gravity papers (Universe 2024 issue) change Einstein's equations instead of adding DE.

2. The "Λ works but w varies" side:

- DESI DR1/DR2 papers (Giarè, Roy, Gu) provide the strongest statistical hints that $w(z) \neq -1$.

3. The "Check your systematics!" side:

- Efstathiou and Wang caution that some of the evolving-DE signature may be from SN calibration or BAO analysis subtleties.

4. The field is very active:

This is one of the hottest areas in cosmology—2023–2025 saw the strongest challenges to ΛCDM in over a decade.

XXVIII. Lookback Time versus Red Shift and Reconstruction of High Z

$$z = \frac{1}{a} - 1$$

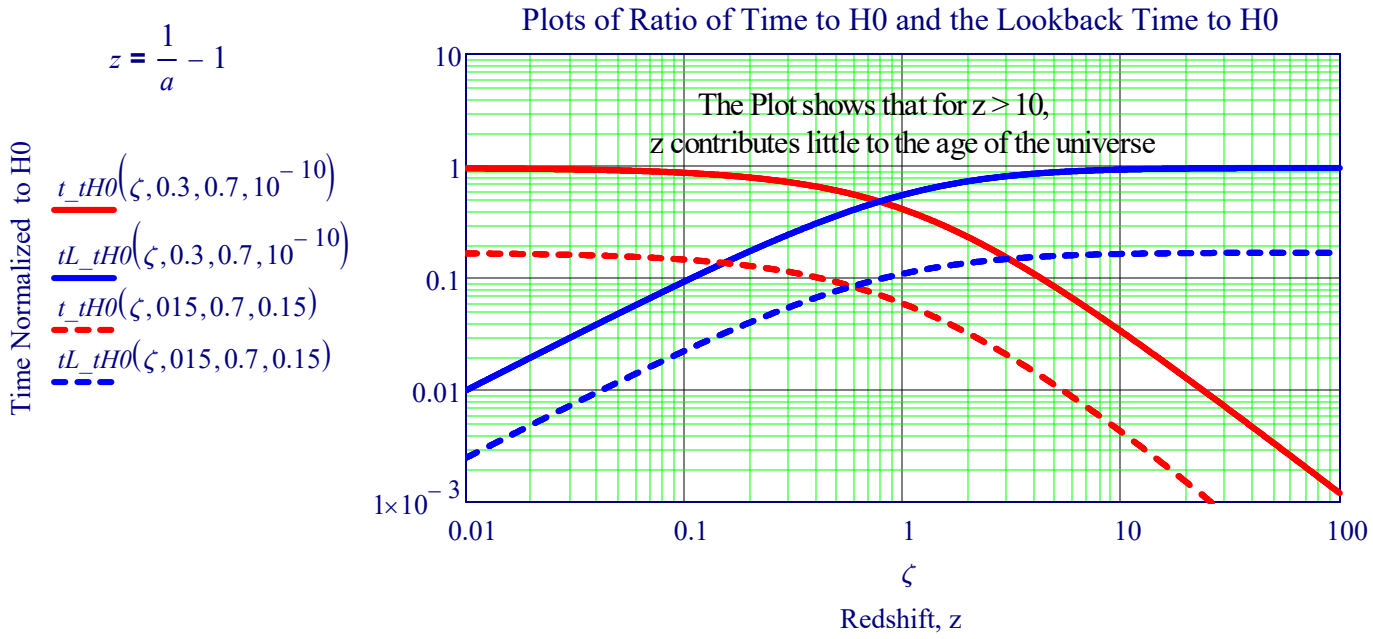

2023 Estimate z=10 is 13.30 Gyr

$t_{BB} := 13.8 Gyr$ $\quad t_{BB} \cdot tL\_tH0(10, 0.3, 0.7, 10^{-10}) = 12.844 \cdot Gyr$

Evolution of the Hubble Factor: Mass Conservation of non-relativistic matter implies $\rho_m \propto a^{-3} = (1+z)^3$. In the ΛCDM model, dark energy is assumed to behave like a cosmological constant: $\rho_\Lambda \propto a^0 = (1+z)^0$. The density of radiation (and massless neutrinos) scales as $\rho_r \propto a^{-4} = (1+z)^4$ because the number density of photons is $\propto a^{-3} = (1+z)^3$ and the mass $E/c^2 = h\nu/c^2$ of each photon scales as $E \propto \lambda^{-1} \propto (1+z)^1 \propto a^{-1}$.

Dynamical Equation Specifying the Evolution of the Hubble Factor of Our Universe

$\Omega_{r0} := 8.7 \times 10^{-5}$ $\quad \frac{H}{H_0} = H\_H0(z) := \sqrt{\Omega_{m0} \cdot (1+z)^3 + \Omega_{\Lambda 0} + \Omega_{r0} \cdot (1+z)^4}$

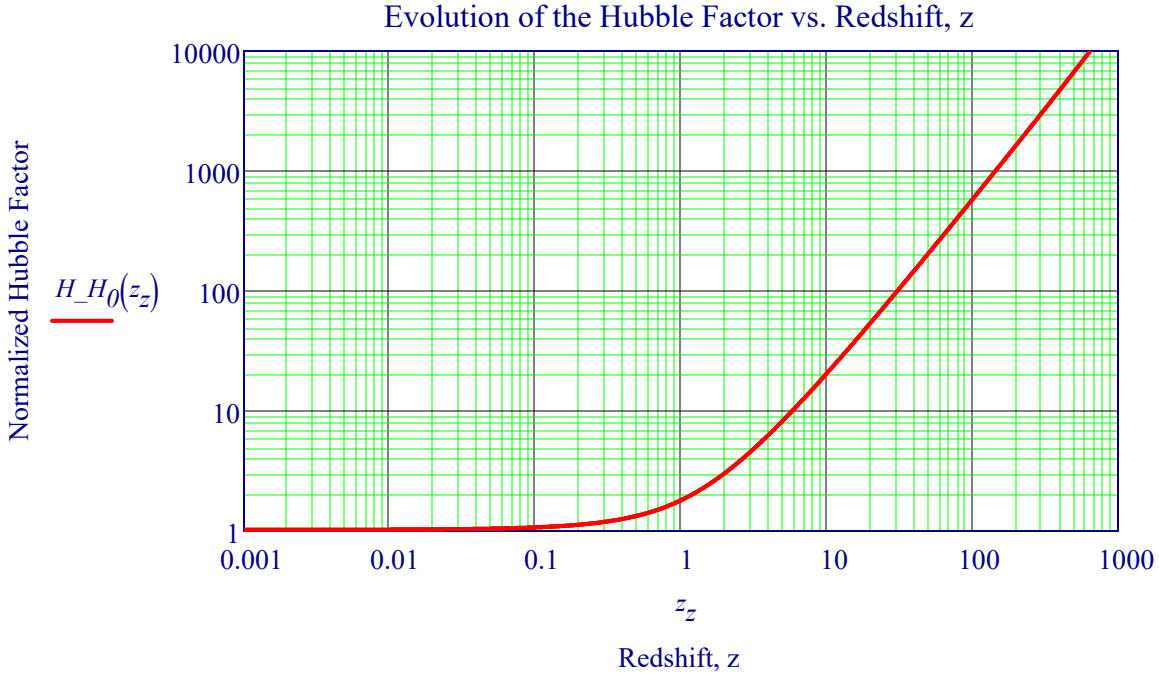

Reconstruction of the Cosmic Equation of State for High Redshift (z = 2 to 5)

Refer to: A. M. Velasquez-Toribio, M. M. Machado & Julio C. Fabris, European Physical Journal, Vol 79, 2018

The accelerated expansion of the universe is one of the biggest problems of cosmology today. Among the different cosmological observables, **the cosmic equation of state (EoS) is of fundamental importance**, as it carries the kinematic and dynamic information of a given cosmological model. The reconstruction of these observables has been widely considered in the literature using different types of cosmological data, such as the following: Supernovae Ia, cosmic background radiation, clusters of galaxies, baryon acoustic oscillations (BAO), Hubble parameter data, $f\sigma_8$, and so on. Nevertheless, the reconstruction of this observable has **not been considered for high redshift**, in principle, **due to the lack of data for any redshift greater than 2.0**. However, this question is currently changing and we can consider **the reconstruction of the EoS (w(z)) for high redshifts**. Understanding in detail how *w(z)* evolves as a function of time is fundamental to know the nature of dark energy.

We use two methods to reconstruct the EoS: the first method makes use of distance measurements from Gamma-Ray Bursts (GRBs) & the second uses simulated data of the Hubble parameter generated by **Sandage–Loeb (SL) effect**. Sandage-Loeb (SL) test method directly measures the expansion history of the universe in the "z desert" of $2 < z < 5$. **In this paper we reconstruct *w(z)* using two model-independent approaches** the comoving distance is related to the luminosity distance by the relation: $D_L = (1+z)D_c$, and the comoving distance as a function of the Hubble parameter is defined by the following expression:

$$D_c = \frac{c}{H_0}\int_0^z \frac{dx}{h(x,\theta)} \qquad D_L = (1+z)D_c$$

where h (z,θ) is the dimensionless Hubble parameter, $H(z)/H_0$. In our case, it is given explicitly by Friedmann Equation

$$h^2(z,\Omega_{m0},\Omega_k) = \left\{\Omega_{m0}(1+z)^3 + \Omega_k(1+z)^2 + (1-\Omega_{m0}-\Omega_k)\exp\left[3\int_0^z \frac{1+w(z')}{1+z'}dz'\right]\right\}.$$

Function of *w(z)*

where Ω_{m0} and Ω_k represent the matter density parameter and curvature respectively. In this paper, we assume that $\Omega_k = 0$, which matches the results of the Planck satellite. To derive from the previous equation, an expression for EoS, is useful. The definition

$$D_c = \frac{1}{\sqrt{-\Omega_k}}\sin\left(\sqrt{-\Omega_k}\int_0^z dz'\frac{H_0}{H(z')}\right) \qquad D_L = (1+z)D_c$$

where we have included the term curvature. We can use this equation above together with the equation of h(z) to **derive the equation of state *w(z)* as a function of *Dc* and its derivatives. *DL(z)* can be inverted to Find *w(z)*:**

$$w(z) = \frac{2(1+z)(1+\Omega_k D_c^2)D_c'' - [(1+z)^2\Omega_k D_c'^2 + 2(1+z)\Omega_k D_c D_c' - 3(1+\Omega_k D_c^2)]D_c'}{3(1+z)^2[\Omega_k + (1+z)\Omega_m]D_c'^2 - (1+\Omega_k D_c^2)D_c'}$$

Derivation w(z) from DL
arxiv.org/abs/0807.4304v1
arxiv/astro-ph/0702670

where D_c' and D_c'' are the derivatives of D_c with respect to z. The ΛCDM Model for h, $h_{\Lambda CDM}(z)$ is:

$$h_{\Lambda CDM}(z) := \sqrt{\Omega_{m0}\cdot(1+z)^3 + \Omega_{r0}\cdot(1+z)^4 + \Omega_{\Lambda 0}} \qquad h_G(z) := 3 + \left[\frac{8.3-3}{3}\cdot(z-2)\right]$$

Below plots shows the simulated data using the Sandage–Loeb effect and reconstructed h(z) (h_G) using a Gaussian process.

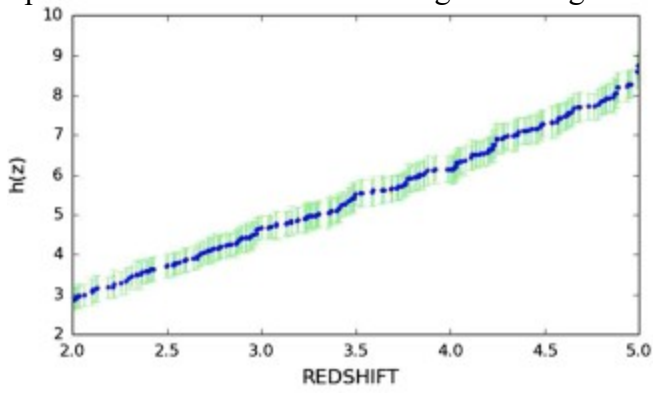

N. Aghanim et al. [Planck Collaboration]. arXiv:1807.06209
P.A.R. Ade, et al. [Planck Collaboration], A&A 594, A13 (2016)

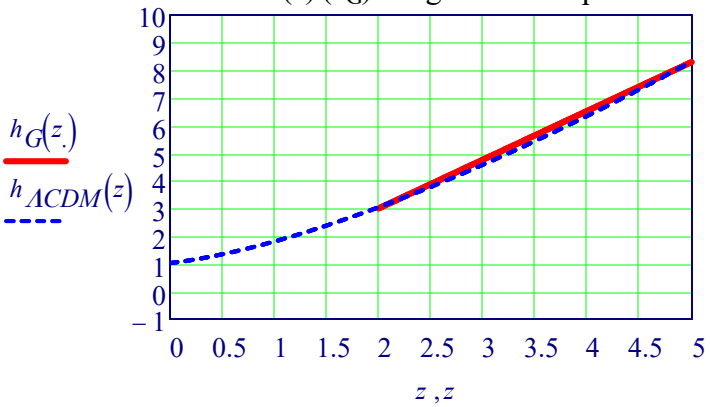

A. Sandage, Astrophys. J. 136, 319 (1962)
Parameter estimation with Sandage-Loeb test, arxiv1407.7123

XXIX. Early Universe Models: Quark-Gluon Plasma

Refer to Section IIC. Hypothetical and Observable Thermal Sequence for the ΛCDM Theory

Quark–Gluon plasma (QGP or quark soup) is a state of matter of Quantum Chromodynamics (QCD) of an interacting localized assembly of quarks and gluons at thermal (local kinetic) and (close to) chemical (abundance) equilibrium. The word plasma signals that free color charges are allowed. It can be said that QGP emerges to be the new phase of strongly interacting matter which manifests its physical properties in terms of nearly free dynamics of practically massless gluons and quarks. Both quarks and gluons must be present in conditions near chemical (yield) equilibrium with their color charge open for a new state of matter to be referred to as QGP.
In the Big Bang theory, quark–gluon plasma filled the entire Universe before matter as we know it was created. Quark–gluon plasma is a state of matter in which the elementary particles that make up the hadrons of baryonic matter are freed of their ***Strong Force*** attraction (deconfinment) for one another under extremely high energy densities.

CERN–2014–001,KEK Proceedings 2013–8, 17 March 2014

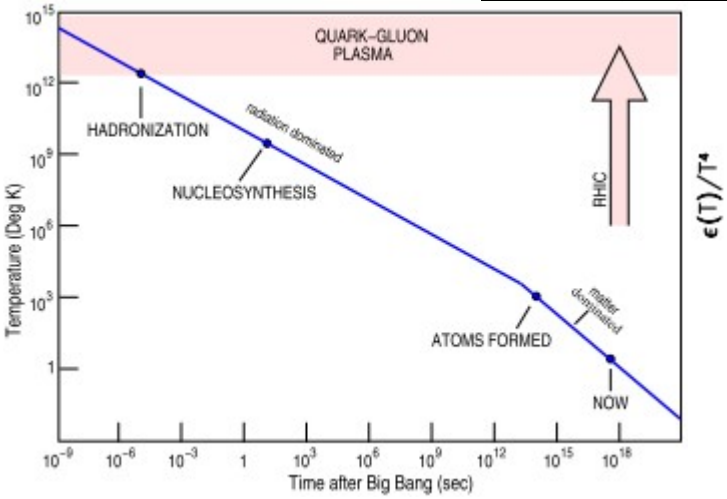

Temperature history of the universe.

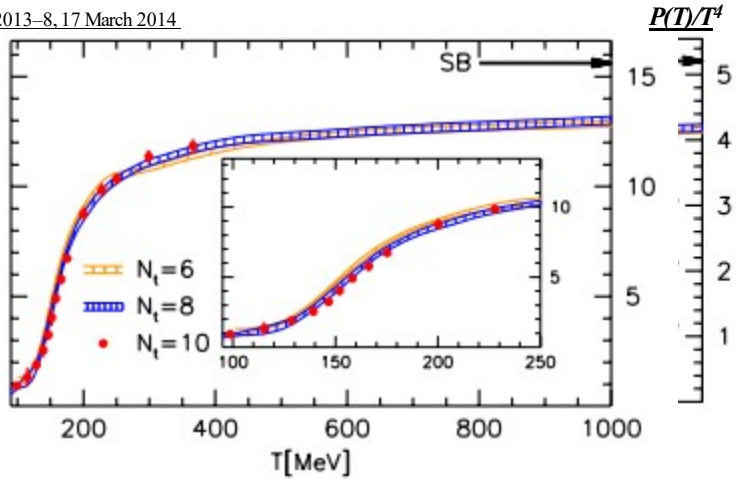

Energy density ***ε(T)*** and Pressure ***P(T)*** normalized by T^4 as a function of temperature (***T***). N_t is the number of lattice points in the temporal direction. The Stefan-Boltzmann (SB) limits are indicated by arrows.

The phase diagram (pressure vs temperature) of water below shows three broad regions separated by phase transition lines, the triple point where all three phases coexist, and the critical point where the vapour pressure curve terminates and two distinct coexisting phases, namely liquid and gas, become identical. The QCD phase diagram is known only schematically, except for the lattice QCD predictions at vanishing or small μB , in particular the prediction of a crossover transition around T ~ 150-170 MeV for vanishing Baryon Chemcial potential μ_B.

Note that both energy density (***ε***) and pressure (P) rise rapidly around T = 160 MeV,

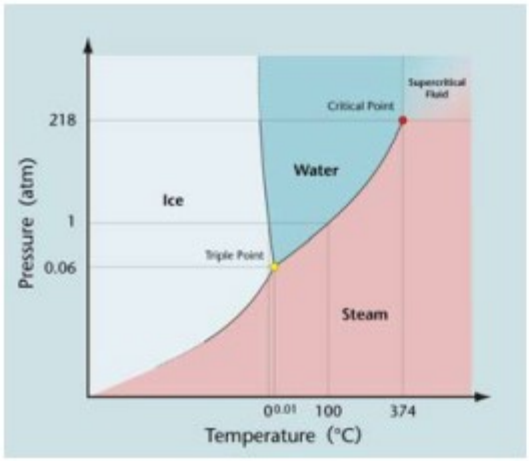

Phase diagram of Water

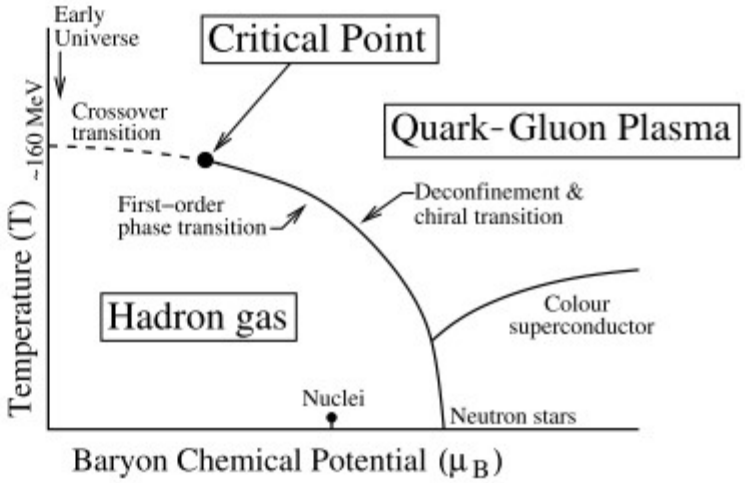

QCD phase diagram.

Early Universe Models: Nucelosynthesis - Metallicity - Population III Stars

Modeling Hydrogen Orbitals (We will use the Maple Programming Language for Model)

$Y(l, m, \theta, \phi)$ is the spherical harmonic or angular part of an orbital, where l is the angular momentum (azimuthal) quantum number and m is the magnetic quantum number. θ is the angle with the z axis in spherical coordinates and ϕ is the angle around the z axis in spherical coordinates. These angles follow the quantum mechanics convention, used here and in the VectorCalculus package, which is different from the math convention used in the rest of Maple.

A d_{z2} orbital has $l = 2$ and $m = 0$ and an angular part that is the spherical harmonic $Y(2, 0, \theta, \phi)$. (This worksheet makes liberal use of atomic variables to make nice looking variables such as d_{z2}, check "Atomic Variables" in the view menu to highlight these.)
The function *cartesian* converts the spherical harmonic to the usual form in terms of x, y, z and r (use the function *fullcartesian* to remove the last r)

> $d_{z2} := Y(2, 0, \theta, \phi);$

$$d_{z2} := \frac{1}{4}\frac{\sqrt{5}\left(3\cos(\theta)^2 - 1\right)}{\sqrt{\pi}}$$

$$-\frac{1}{4}\frac{\sqrt{5}\left(x^2 + y^2 - 2z^2\right)}{r^2\sqrt{\pi}}$$

The plots of orbitals usually seen are just plots of the squares of their angular parts (for contour plots of the wavefunction with both radial and angular parts, see below). Recall again that Maple's (θ, ϕ) is (ϕ, θ) in quantum mechanics, so put ϕ before θ in the plot command. A useful way to color these is by phase. Since this spherical harmonic is real, the phase simply indicates the sign: red for positive (phase = 0), cyan for negative (phase = π).

> $plot3d\left(d_{z2}^2, \phi = 0..2\pi, \theta = 0..\pi, coords = spherical, style = patchnogrid, scaling = constrained, color = \text{argument}\left(d_{z2}\right)/(2\pi), grid = [50, 50], axes = none\right)$

Only the spherical harmonics with $m = 0$ are real. For example, for $l = 2, m = 1$ we have

> $d_1 := Y(2, 1, \theta, \phi)$

$$d_1 := \frac{1}{4}\frac{\sqrt{30}\,\sin(\theta)\cos(\theta)\,e^{I\phi}}{\sqrt{\pi}} \qquad (3.2)$$

The square of the absolute value can be plotted in the same way as above. The colors now show phases other than 0 and π.

> $plot3d\left(|d_1|^2, \phi = 0..2\pi, \theta = 0..\pi, coords = spherical, style = patchnogrid, scaling = constrained, color = \text{argument}\left(d_1\right)/(2\pi), grid = [30, 30], axes = none\right)$

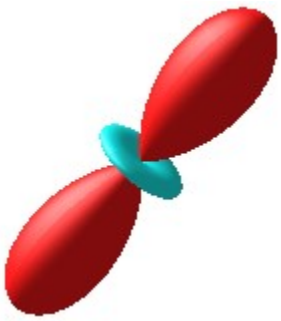

Maple Plots:

The square of the absolute value can be plotted in the same way as the spherical harmonic at the left. The colors now show phases other than 0 and π.

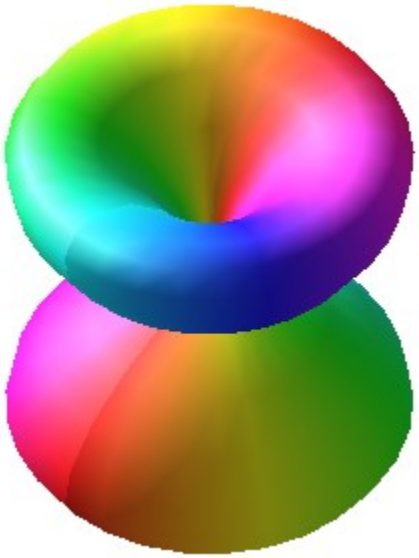

Nucelosynthesis in the Early Universe: Ratio of Neutrons to Protons

Introduction to Cosomology, Ryden

"The basic building blocks for nucleosynthesis are neutrons and protons. As the Universe cools, protons and neutrons become stable particles and they, in turn, bind into nuclei. With a decay time of only fifteen minutes, the existence of a free neutron is as fleeting as fame; once the universe was several hours old, it contained essentially no free neutrons. However, a neutron which is bound into a stable atomic nucleus is preserved against decay. There are still neutrons around today, because they've been tied up in deuterium, helium, and other atoms.

The Boltzmann distribution for the number density of nonrelativistic nuclei of atomic weight A is: $n_A \approx T^{3/2} e^{(\mu A - m A)/k}$.

Given the masses of the particles in Mega Electron Volts (MeV), the number density for neutrons and protons is:"

$MeV := 1.60218 \times 10^{-13} \cdot J$ $\quad m_n := 939.565420 MeV$ $\quad m_p := 938.272088 MeV$ $\quad m_n - m_p = 1.293 \cdot MeV$

$$n_n = g_n \cdot \left(\frac{m_n \cdot k \cdot T}{2\pi\hbar^2} \right)^{\frac{3}{2}} \cdot e^{\frac{-m_n \cdot c^2}{k_b \cdot T}} \qquad n_p = g_p \cdot \left(\frac{m_p \cdot k \cdot T}{2\pi\hbar^2} \right)^{\frac{3}{2}} \cdot e^{\frac{-m_p \cdot c^2}{k_b \cdot T}}$$

Since the statistical weights of protons and neutrons are equal, with $g_p = g_n = 2$, the neutron-to-proton ratio is then given by the equation:

$$Ratio_{n\_p}(T) := \left(\frac{m_n}{m_p} \right)^{\frac{3}{2}} \cdot e^{-(m_n - m_p) \cdot \frac{c_v^2}{k_b \cdot T \cdot K}}$$

These reactions continued until the decreasing temperature and density caused the reactions to become too slow, which occurred at about T = 0.7 MeV (time around 1 second) and is called the freeze out temperature.

Freeze Out Temperature in Kelvin, K

$$T_{Freeze\_Out} := \frac{0.7 \cdot MeV}{k_b \cdot K} = 2.865 \times 10^{68}\, s$$

Ratio of Neutrons to Protons in Early Universe

$Freeze\_Out := Ratio_{n\_p}(T_{Freeze\_Out}) = 0.158$

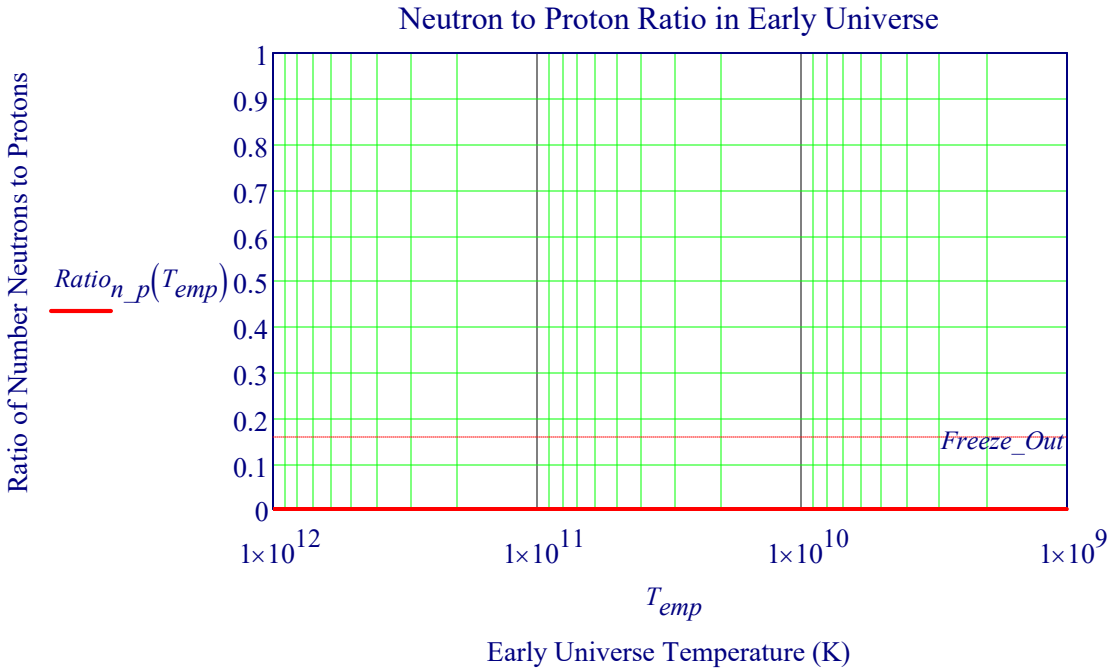

Abundance of the light elements over time

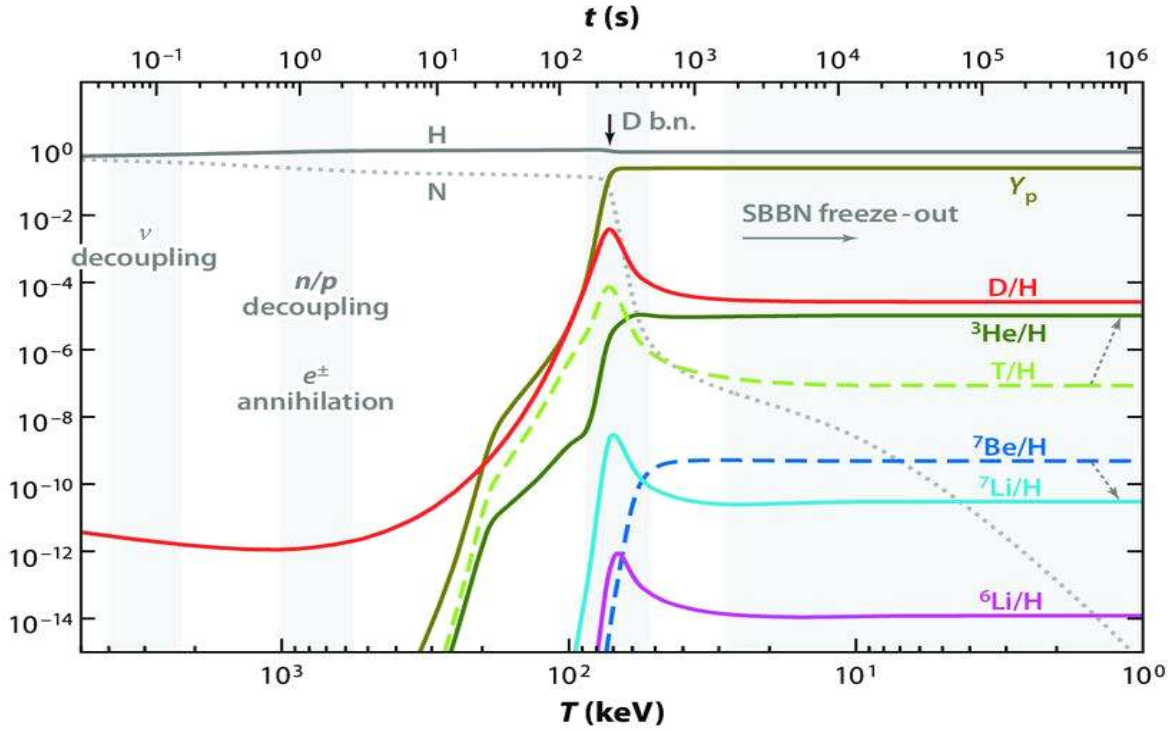

This plot shows the abundance of the light elements over time, as the Universe expands and cools during the various phases of Big Bang Nucleosynthesis. By the time the first stars form, the initial ratios of hydrogen, deuterium, helium-3, helium-4, and lithium-7 are all fixed by these early nuclear processes. *Credit:* M. Pospelov & J. Pradler, Annual Review of Nuclear and Particle Science, 2010

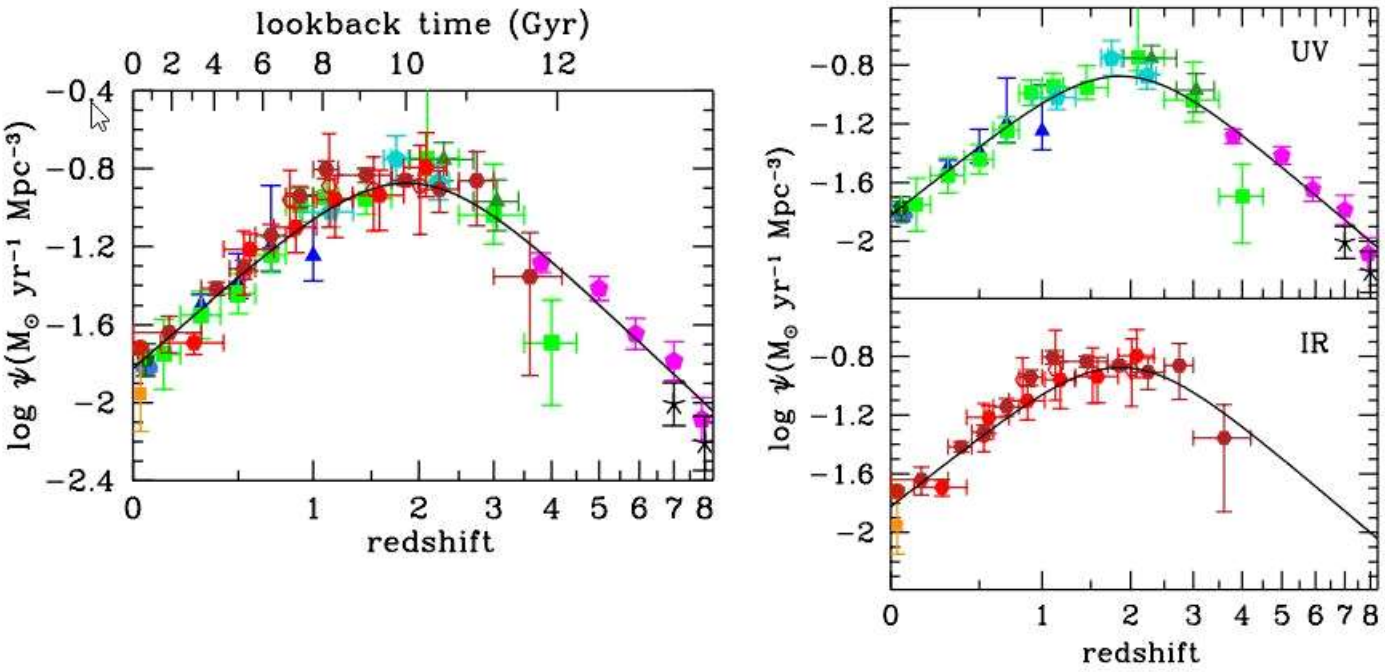

The star-formation rate in the Universe is a function of redshift, which is itself a function of cosmic time. The overall rate, (left) is derived from both ultraviolet and infrared observations, and is remarkably consistent across time and space. Note that star formation, today, is only a few percent of what it was at its peak (between 3-5%), and that the **majority of stars were formed in the first ~5 billion years** of our cosmic history. Only about ~15% of all stars, at maximum, have formed over the past 4.6 billion years, with the cumulative history of star-formation transforming about 1% of all atoms, by mass, into oxygen. *Credit*: P. Madau & M. Dickinson, 2014, ARAA

Metallicity - Population III Stars - JWST

Definition of Metallicity, Z:

The relative abundances of the chemical elements can be measured in a number of astronomical objects, in particular using spectroscopic techniques. **The observed strengths of spectral lines** depend on a variety of factors among which are the chemical abundances of the elements producing those spectral lines.
It is convenient to define the fractions by mass of hydrogen X, of helium Y, and of heavy elements Z.
Therefore, Z = (mass of heavy elements)/(total mass of all nuclei). in some object, objects or region of space. We therefore have $X + Y + Z \equiv 1$.

The most recent determination of the solar $Z(Z_\odot)$ gives a value of 0.0134.

A very small fraction of metals is sufficient to alter the behavior of the star completely.

The more metallic a star, the more opaque it is (since metals absorb radiation), and how opaque it is, in turn, relate to its size, temperature, brightness, life span, and other key properties. Metallicity basically also tells you how the star will die.

Population III Stars

The advancement of observational technologies has brought increasing attention to the study of the first galaxies, black holes, and stars in the early universe. Detection of population III stars is a goal of NASA's James Webb Space Telescope. Among its many grand discoveries set to come, perhaps the greatest of all is the possibility of observing the light from the very first stars in the Universe. These **chemically pristine**, so-called '**Population III'** stars, formed out of the primordial hydrogen and helium (and trace amounts of lithium), and were the first embers to ignite, producers of the starlight that ended the cosmic dark ages and paved the way for cosmic dawn.

Sirius is the star with the highest known metallicity of 0.5, which corresponds to a Fe to H ratio of three times the sun. The search of Population III stars with JWST is actively ongoing. The search is for strongly-lensed extremely metal-poor small mass star clusters of 10^4 $M_\odot$ and with $Z \sim 10^{-3}$ $Z_\odot$.

The Simple Model of Galactic Chemical Evolution

$M_{total} = M_{stars} + M_{gas}$ Therefore the heavy element mass fraction of the gas is

$$Z \equiv \frac{M_{\rm metals}}{M_{\rm gas}}$$

Let the change in M_{stars} and M_{gas} in this time be δM_{stars} and δM_{gas}.
We firstly need to express the change δZ in the metallicity of the interstellar gas in terms of δM_{stars} and δM_g

$$\delta Z = \frac{\delta M_{\rm metals}}{M_{\rm gas}} - Z\frac{\delta M_{\rm gas}}{M_{\rm gas}}$$

We need to distinguish between the the total mass in stars M_{stars} at time t and the total mass that has taken part in **star formation** M_{SF} over all periods up to time t. When a mass δM_{SF} goes into stars during star formation, the total mass in stars will change by amount less than this, because material from the new stars is ejected back into the interstellar gas. So, $\delta M_{SF} > \delta M_{stars}$, and $M_{SF} > M_{stars}$.
Let α be the fraction of mass participating in star formation that remains locked up in long-lived stars (and stellar remnants). So, $\delta M_{stars} = \alpha\, \delta M_{SF}$ (with $0 < \alpha < 1$)
The mass of newly synthesized heavy elements ejected back into the Interstellar Medium, ISM, is proportional to the mass that goes into stars (from the Simple Model assumptions listed above). Let the mass of newly synthesized heavy elements ejected into the ISM be equal to $p\,\delta M_{stars}$, where p is a parameter known as the yield, with p set to be a constant here. This gives

$$Z(t) = -p\,\ln\left(\frac{M_{\rm gas}(t)}{M_{\rm gas}(0)}\right)$$

Since the $M_{gas}(0) = M_{total}(t)$ (a constant) for all t (because we have a closed box that initially contained only gas), we can rewrite this equation using the gas fraction $\mu \equiv M_{gas}(t)/M_{total}(t)$ as $Z(t) = -p \ln \mu$

$$Z = -p \ln\left(\frac{M_{gas}(0) - M_{stars}(t)}{M_{gas}(0)}\right) \quad \text{which rearramges to} \quad \frac{M_{stars}(t)}{M_{gas}(0)} = 1 - e^{-Z(t)/p}$$

This is a prediction of how the fraction of the mass of the volume that is in stars varies with metallicity. $M_{stars}(t)/M_{gas}(0)$ increases from zero at time t = 0, and can become very large if most of the gas is used up in star formation. Today, at time t_1 , we have a metallicity Z_1 and a mass in stars M_{stars1} . Therefore we have

$$\frac{M_{stars}(t)}{M_{stars1}} = \frac{1 - e^{-Z(t)/p}}{1 - e^{-Z_1/p}} \qquad \frac{N(Z)}{N_1} = \frac{1 - e^{-Z(t)/p}}{1 - e^{-Z_1/p}}$$

where N_1 is the value of N(Z) today.

<u>This gives a specific prediction of the number of stars as a function of metallicity</u>

The figure below gives a comparison of the the predicted metallicity distribution from Equation N(Z) with observations of long-lived stars in the solar neighbourhood. The Simple Model prediction is found to be very different to the observed distribution.

<u>The Simple Model predicts a far larger proportion of Metal-Poor Stars than are actuall found.</u>
<u>This has become known as the G dwarf problem.</u>

$$p := 0.010 \qquad Z_1 := 0.017 \qquad \frac{N(Z)}{N_1} = \frac{1 - e^{-Z(t)/p}}{1 - e^{-Z_1/p}} \qquad N_{N1}(Z) := \frac{1 - exp\left(\frac{-Z}{p}\right)}{1 - exp\left(\frac{-Z_1}{p}\right)}$$

<u>The observed iron abundance, [Fe/H], is often regarded as a proxy for the total metallicity, Z, of stars.</u>

<u>Cumulative Metallicity Distribution</u>

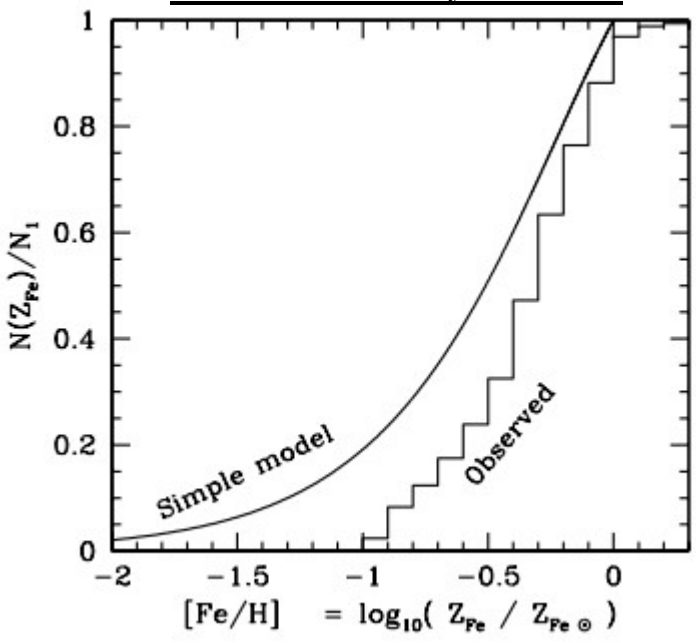

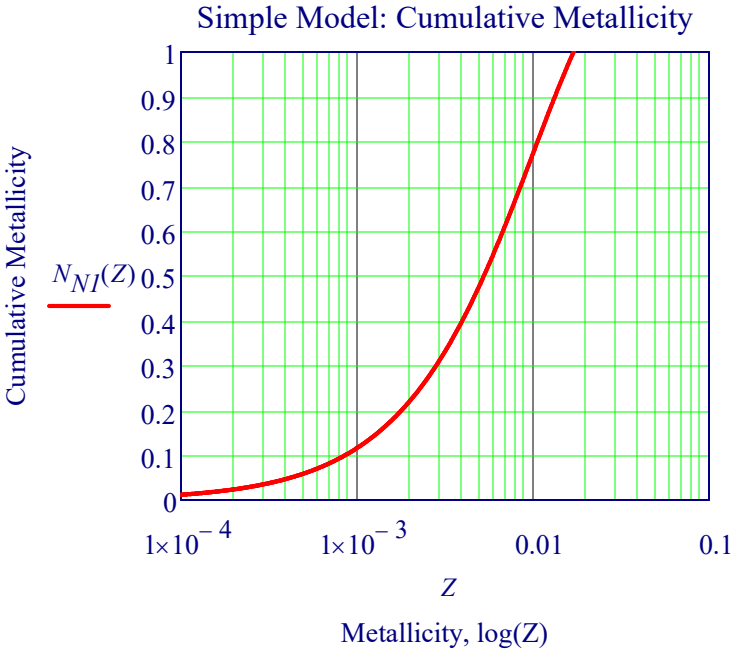

The observed **Cumulative Metallicity** distribution for stars in the solar neighbourhood, compared with the Simple Model prediction for p = 0.010 and $Z_1 = Z_\odot = 0.017$.

[The observed distribution uses data from Kotoneva et al.,M.R.AS, 336, 879, 2002, for stars in the Hipparcos Catalog.]

Population III Stars Metallicity- JWST - Continued
Contrary to Expectations: Metallicity and Mass

JWST found young stars that are hotter and with high metallicity. Some where found with nickel, which is heavier than iron in the periodic table. This came as somewhat of a surprise. The JWST observation of the galaxy **JADES-GS-z14-0** at redshift z=14.32, which is the most distant galaxy observed, shows surprisingly high metal enrichment (**Z ~ 0.05 - 0.2 Z⊙**), indicating a rapid assembly of metals in the early universe and it started galaxy formation very early. It is 325 to 330 million years old (2.1% of Universe Age.) It is also far more massive than expected, M ~ 500 10^6 $M_\odot$.

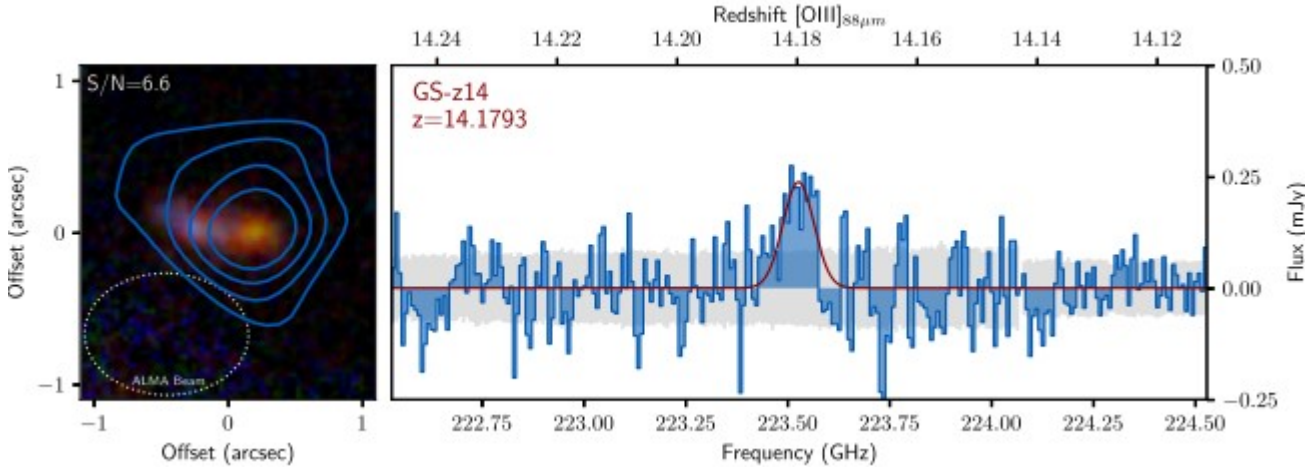

JADES-GS-z14-0 Atacama Large Millimeter/submillimeter Array (**ALMA**), **found an emission line of oxygen**, making this the most distant detection of oxygen, when the Universe was slightly under a mere 300 million years old.
Detection of [OIII] 88μm in JADES-GS-z14-0 at z=14.1793, S. Schouws et. all, March 17, 2025, www.eso.org/public/

Under current cosmological models, all matter created in the Big Bang was mostly hydrogen (75%) and helium (25%), with only a very tiny fraction consisting of other light elements such as lithium and beryllium.

When the universe had cooled sufficiently, the first stars were born as population III stars, without any contaminating heavier metals. This is postulated to have affected their structure so that their stellar masses became hundreds of times more than that of the Sun. In turn, these massive stars also evolved very quickly, and their nucleosynthetic processes created the first 26 elements (up to iron in the periodic table). Many theoretical stellar models show that most high-mass population III stars rapidly exhausted their fuel and likely exploded in extremely energetic pair-instability supernovae. The oldest stars observed thus far, **known as population II, have very low metallicities**; as subsequent generations of stars were born, they became more metal-enriched, as the gaseous clouds from which they formed received the metal-rich dust manufactured by previous generations of stars from population III.
As those population II stars died, they returned metal-enriched material to the interstellar medium via planetary nebulae and supernovae, enriching further the nebulae, out of which the newer stars formed.

These youngest stars, including the Sun, therefore have the **highest metal content,** known as **population I stars**.

Required JWST Instrumentation

Requires ultradeep exposures would be needed to detect ~ 10^5 M⊙ Pop III galaxies at z = 10, with color–colour selections combining JWST/NIR Cam and JWST/MIRI photometry enabling a clean selection of Pop III galaxies at z ≈ 7–8. Fortuitous gravitational Lansing of Pop III galaxies will greatly relax the otherwise demanding integration times needed.
See Section XXIV: Advances in Measurement and Technology for Measuring Hubble Constant

Some Possible Explanations

Any one or combination of these proposed explanations appears feasible: (1) a higher star formation efficiency at that time; (2) a higher percentage of very massive stars at that time; (3) a reduced quantity of dust or the presence of dust with a less dimming effect; and (4) adjustments to our understanding of the properties of dark matter haloes at that time. Spectroscopic follow-up studies for the observed galaxy candidates are ongoing. As research continues, the list of 90 ultrabright galaxies initially thought to have formed early in the cosmic dawn will likely be reduced.

Distribution of Galaxy Rotation in JWST Advanced Deep Extragalactic Survey

The distribution of galaxy rotation in JWST Advanced Deep Extragalactic Survey, Lior Shamir, MNRAS 538, 76–91 (2025) https://doi.org/10.1093/mnras/staf292

Analysis of spiral galaxies by their direction of rotation in JADES

shows that the number of galaxies in that field that rotate in the opposite direction relative to the Milky Way galaxy is ~ 50 per cent higher than the number of galaxies that rotate in the same direction relative to the Milky Way. The analysis is done using a computer-aided quantitative method, but the difference is so extreme that it can be noticed and inspected even by the unaided human eye. These observations are in excellent agreement with deep fields taken at around the same footprint by Hubble Space Telescope and JWST.

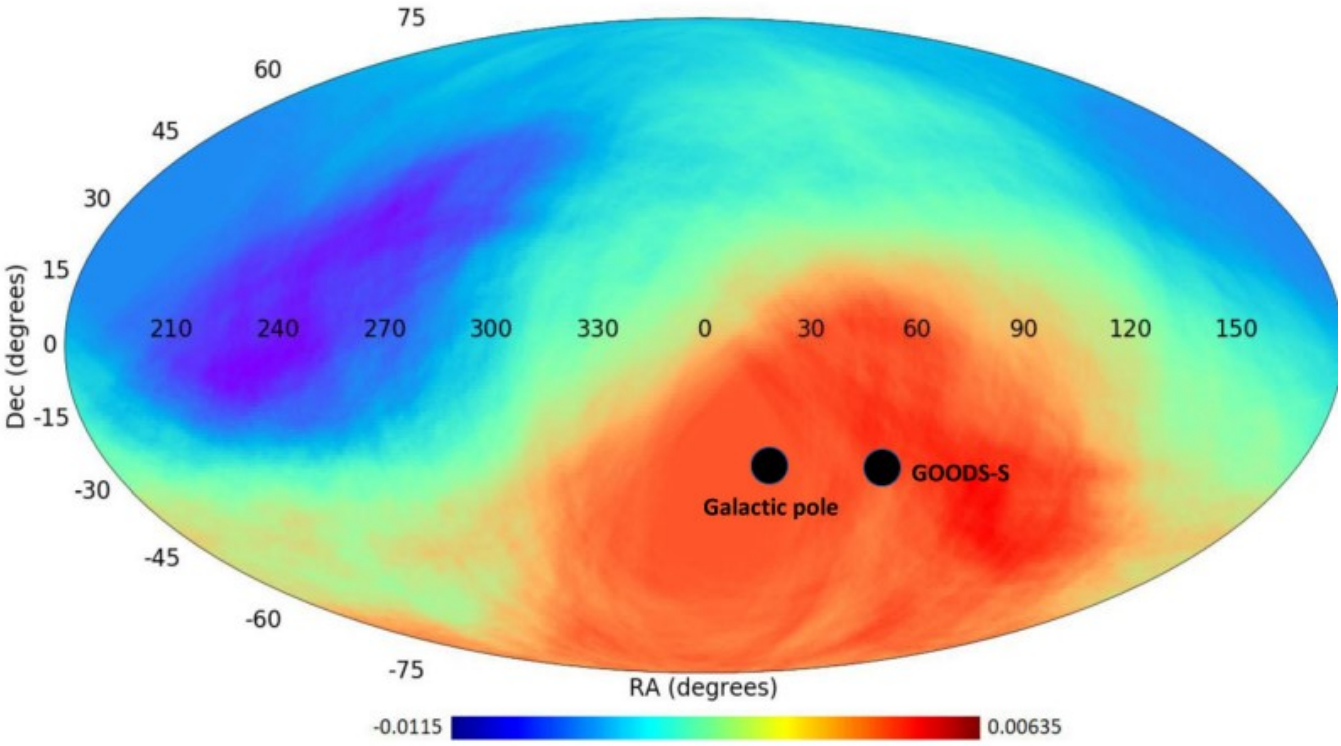

The differences in the number of galaxies with opposite directions of rotations in different parts of the sky as determined by using 1.3×10^6 galaxies imaged by the DESI Legacy Survey (Shamir 2022e).
The location of the GOODS-S field is at a part of the sky with a higher number of galaxies rotating clockwise.

Redshift z	cw	ccw	cw/cw+ccw	p-value
0 - 0.05	3216	3180	0.5003	0.698
0.05 - 0.1	6240	6270	0.498	0.4
0.1 - 0.15	4236	4273	0.496	0.285
0.15 - 0.2	1586	1716	0.479	0.008
0.2 - 0.5	2598	2952	0.469	1.07×10^{-6}
Total	17876	18391	0.493	0.0034

As the above table shows, the asymmetry increases as the redshift gets higher.

The distribution of galaxies rotating clockwise and counterclockwise imaged by SDSS. All galaxies are within the RA range of (120°, 210°). The p-values are the binomial distribution p-value to have such asymmetry or stronger by chance. The table is taken from Shamir (2020) springer.com/article/10.1007/s10509-020-03850-1

XXX. Some Key Problems of the ΛCDM Cosmology

Challenges for ΛCDM: An update, L. Perivolaropoulos and F. Skara, 2022
A Candid Assessment of Standard Cosmology, Fulvio Melia, 2022
https://en.wikipedia.org/wiki/Lambda-CDM_model#cite_note-Planck_2018-19

The standard Hot Big Bang model, in which the **early universe was radiation- dominated**, is not without its flaws. In particular, after the discovery of the cosmic microwave background led to the widespread embrace of the Big Bang, it was realized that the standard Hot Big Bang scenario had **three underlying problems**.

1. **XXX. The flatness problem:** why is the universe so close to being flat today?
   The universe is nearly flat today, and was even flatter in the past?

Λ-CDM Model Parameters to see the Fine Tuning for $\Omega_k \approx 0$.

$\Omega_\Lambda := 0.6842$ $\Omega_m := 0.3158$ $\Omega_k := 1 - \Omega_\Lambda - \Omega_m$ $\Omega_k = 0$

A spatially flat universe $\Omega_K = 0.0007 \pm 0.0019$

The Cosmic Concordance

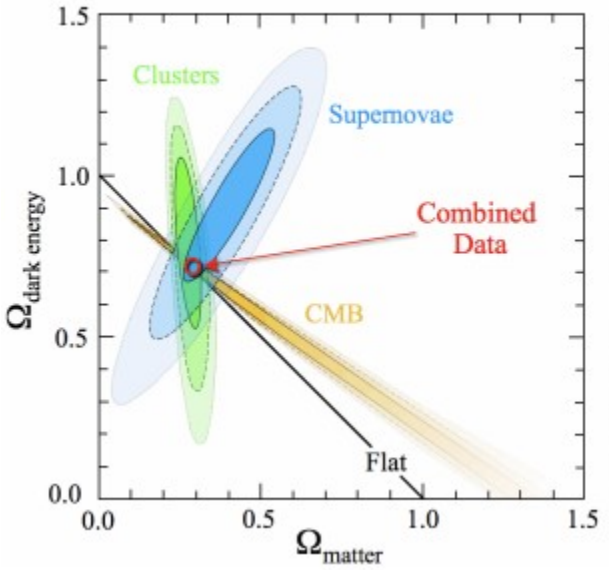

Multiple types of *different*, *independent* measurements and different cosmological probes all agree

(Not all are shown here, e.g., local Ω_m measurements, BAO, BBNS, ages of globular clusters, etc.)

2. **The horizon problem:**
   How comes the CMBR is so uniform?
   "The universe is nearly isotropic and homogeneous today, and was even more so in the past?
3. **Absence of Topological Defects - The monopole problem:**
   where are the copious amounts of magnetic monopoles predicted to exist in the BB cosmology?
4. **Early Structure Formation - Premature formation of Galaxies. High Metallicity.**
5. **Low Entropy - The Second Law of Thermodynamics**
6. **Discrepancy Between Theoretically Estimated and Actual Value of Λ**
7. **Hubble Tension - Difference between Global and Local Determined Values of H_0**
8. **Early Appearance of Super Massive Black Holes**
9. **Violations of Cosmological Principle: Isotropy, Homogeneity, and KBC Void**
10. **Cosmological Lithium Problem: Observable Lithium less than calculated Λ-CDM Model by Factor of 3-4.**
11. **Early Universe High Redshift Galaxies: JWST sees galaxies JADES-GS-z14-0 at redshift of 14.32**
12. **Unfalsifiability: ΛCDM model built upon foundation of conventionalist stratagems: Not Popper Unfalsifiable.**
13. **Electroweak Horizon Problem** - Higgs Particle-->Possible phase transition associated with Grand Unification Theories

XXXI. Three Analyses of the Flatness Problem - The Fine Tuning Problem

A. *An Introduction To Modern Cosmology,* Andrew Liddle
B. *A survey of dark matter and related topics in cosmology,* Bing-Lin Young, Phys. 12(2), 121201 (2017),
C. *Astronomy 275 Lecture Notes,* Edward Wright: Spring 2015, Section 6.1

What is the Flatness Problem?

Recent measurements of the total density of the Universe find $0.95 < \Omega o < 1.05$. This near flatness is a problem because the Friedmann Equation tells us that $\Omega \approx 1$ is a very unstable condition - like a pencil balancing on its point. It is a very special condition that won't stay there long. Here is an example of how special it is. We know that

$(\Omega^{-1} - 1)\,\rho\,R^2 = \text{constant}$. Therefore, we can write,

$$\left(\Omega^{-1} - 1\right)\rho \cdot R^2 = \left(\Omega_0^{-1} - 1\right)\rho_0 \cdot R_0^2$$

where the right hand side is today and the left hand side is at any arbitrary time. We then have,

$$\left(\Omega^{-1} - 1\right) = \left(\Omega_0^{-1} - 1\right)\frac{\rho_0}{\rho}\cdot\left(\frac{R_0}{R}\right)^2$$

redshift is related to the scale factor by $R = Ro/(1+z)$. Consider **the evolution during matter-domination** where $\rho = \rho_o(1+z)^3$. Inserting these we get,

$$\left(\Omega^{-1} - 1\right) = \frac{\left(\Omega_0^{-1} - 1\right)}{1+z}$$

Inserting the current limits on the density of the Universe, **$0.95 < \Omega o < 1.05$**
(for which $-0.05 < (\Omega o^{-1} - 1) < 0.05$),
we get a constraint on the possible values that could have had at redshift, z.

$$\frac{1}{1+\frac{0.05}{1+z}} < \Omega < \frac{1}{1-\frac{0.05}{1+z}} \qquad \Delta\Omega(z,\phi) := \frac{1}{1-\frac{\phi\cdot 0.05}{1+z}}$$

At recombination (when the first hydrogen atoms were formed) $z \approx 10^3$ and the constraint on Ω yields,

$$\Delta\Omega(1000,-1) = 0.99995 \quad < \Omega < \quad \Delta\Omega(1000,1) = 1.00005$$

So the observation that $0.95 < \Omega o < 1.05$ today, means that at a redshift of $z \approx 10^3$ we must have $0.99995 < \Omega < 1.000005$. This range is small... special. However, had to be even more special earlier on. We know that the standard ΛCDM successfully predicts the relative abundances of the light nuclei during nucleosynthesis between ≈ 1 minute and ≈ 3 minutes after the big bang, so let's consider the slightly earlier time, 1 second after the big bang which is about the beginning of the epoch in which we are confident that the Friedmann Equation holds. The redshift was $z \approx 10^{11}$ and the resulting constraint on the density at that time was,

$$\Delta\Omega\left(1\cdot 10^{11},-1\right) = 0.9999999999995 \quad < \Omega < \quad \Delta\Omega\left(1\cdot 10^{11},1\right) = 1.0000000000005$$

This range is even smaller and more special, (although we have **assumed matter domination** for this calculation, at redshifts higher than $z_{eq} \approx 3000$, we have **radiation domination** and $\rho = \rho_o(1+z)^4$. This makes the $1+z$ in the equation a $(1+z)^2$ and requires that early values of be even closer to 1 than calculated here).

To summarize:

$$\begin{aligned} 0.95 &< \Omega_o(z=0) < 1.05 \\ 0.99995 &< \Omega(z=10^3) < 1.000005 \\ 0.9999999999995 &< \Omega(z=10^{11}) < 1.0000000000005 \end{aligned}$$

A. *An Introduction To Modern Cosmology,* Andrew Liddle

The flatness problem is the easiest one to understand. We have learned that the Universe possesses a total density of material, $\Omega_{tot} = \Omega_0 + \Omega_A$, which is close to the critical density. Very conservatively, it is known to lie in the range $0.5 < \Omega_{tot} < 1.5$. In terms of geometry, that means that the Universe is quite close to possessing the flat (Euclidean) geometry. We have seen that the Friedmann equation can be rewritten as an equation showing how Ω_{tot} varies with time. Adding modulus signs to the Friedmann Equation gives:

$$|\Omega_{\rm tot}(t) - 1| = \frac{|k|}{a^2 H^2}$$

We know from this that this that $\boldsymbol{\Omega_{tot}}$ is precisely equal to one, then it remains so for all time. But what if it is not?

Let's consider the situation where we have a conventional Universe (matter or radiation dominated) where the normal matter is more important than the curvature or cosmological constant term. Then we can use the solutions ignoring the curvature term, using equations to find

$a^2H^2 \propto t^{-1}$	radiation domination	$\lvert\Omega_{\rm tot} - 1\rvert \propto t$	radiation domination
$a^2H^2 \propto t^{-2/3}$	matter domination .	$\lvert\Omega_{\rm tot} - 1\rvert \propto t^{2/3}$	matter domination .

In either case, the difference between Ω_{tot} and 1 is an *increasing* function of time. That means that the flat geometry is an unstable situation for the Universe; if there is any deviation from it then the Universe will very quickly become more and more curved. Consequently, for the Universe to be so close to flat even at its large present age means that at very early times it must have been extremely close to the flat geometry.

An alternative way to see this is to remember that the densities of matter and radiation reduce with expansion as l/a^3 and l/a^4 respectively. These are both faster reductions than the curvature term k/a^2. So if the curvature term is not to totally dominate in the present Universe, it must have begun much smaller than the other terms.

The equations for $|\Omega_{tot} - 1|$ derived above stop being valid once the curvature or cosmological constant terms are no longer negligible, since we used the *a(t)* solutions for the flat geometry to derive them. But they are fine to give us an approximate idea of what the problem is. For extra ease let's assume that the Universe always has only radiation in it. Using the equations above, we can ask how close to one the density parameter must have been at various early times, based on the constraint today ($t_o \approx 4 \times 10^{17}$ sec).

- At decoupling ($t \simeq 10^{13}$ sec), we need $|\Omega_{\rm tot} - 1| \leq 10^{-5}$.
- At matter–radiation equality ($t \simeq 10^{12}$ sec), we need $|\Omega_{\rm tot} - 1| \leq 10^{-6}$.
- At nucleosynthesis ($t \simeq 1$ sec), we need $|\Omega_{\rm tot} - 1| \leq 10^{-18}$.
- At the scale of electro-weak symmetry breaking, which corresponds to the earliest known physics ($t \simeq 10^{-12}$ sec), we need $|\Omega_{\rm tot} - 1| \leq 10^{-30}$.

Written out in long hand, that means we know that at nucleosynthesis, an era we are supposed to understand very well indeed, the density parameter must have lain within the range $0.99999999999999999 < \Omega_{tot} < 1.00000000000000001$! Out of all the possible values that it might have had, this seems a very restrictive range. Any other value would lead to a Universe extremely different to that which we see.

The easiest way out of this dilemma is to suppose that the Universe must have precisely the critical density. But on the face of it there seems no reason to prefer this choice over any other. What would be nice would be an explanation of such a value.

Regardless of whether or not we understand the physical origin of these numbers. they are an observed fact. One useful thing they tell us is that the Universe is very close to spatial flatness at decoupling and at nucleosynthesis, which means that it is always a good approximation to set $k = 0$ in the Friedmann equation when describing those phenomena.

B. *A survey of dark matter and related topics in cosmology*

Phys. 12(2), 121201 (2017), Bing-Lin Young

We note that in the very early universe **radiation energy dominates**. Then $H^2(z) \approx (1+z)^4$ which says

$$\Omega_k(z) \approx (1+z)^{-2}\,\Omega_k$$

This gives rise to the well-known flatness problem. For any finite value of the curvature parameter, i.e., any value of Ω_k at the present epoch, the curvature fraction to the effective total energy density is negligibly small at the early universe of $z \gg 1$. Running the argument in the reversed direction with $\Omega_k \approx (1+z)^2\,\Omega_k(z)$, we have

a z^2 growth in the curvature density fraction.

From the fact that the observed matter-energy density today ρ_0 is close to the critical density ρ_c, this requires a very small curvature density fraction in the early universe. This gives raise to a fine tuning problem unless $k = 0$: Furthermore, a finite curvature constant allows the determination of the scale factor at the present time, a_0,

which is unphysical, from the equation

$$\rho_\kappa = \frac{3}{8\pi G_N}\frac{\kappa c^2}{a_o^2} \qquad D_H := \frac{c}{H_0}$$

Critical Density:

$$\Omega_{crit}(h) := 7.5\cdot 10^{21} h^{-1}\cdot M_\odot D_H^{-3}$$

C. Astronomy 275 Lecture Notes: Edward Wright

Edward Wright: Spring 2015, Section 6.1.The Flatness-Oldness Figure 14 (https://astro.ucla.edu/≈wright/)

The expanding universe evolves away from $\Omega_{tot} = 1$:

Note: See the Following Page for more details

***ΩkHR* Equation:**

$$1-\Omega(t) = -\frac{kc^2}{H(t)^2 a(t)^2 R_0^2} = \frac{H_0^2(1-\Omega_0)}{H(t)^2 a(t)^2}$$

$$\left(\frac{H(t)}{H_0}\right)^2 = \frac{\Omega_{r0}}{a^4} + \frac{\Omega_{m0}}{a^3}$$

This creates an enormous fine-tuning problem:

the early universe must have been remarkably close to $\Omega_{tot} = 1$ in order to have $\Omega_{tot} \approx 1$ today!

Just 1 gm/cc out of $447*10^{21}$ gm/cc at 1 ns is the difference between an expanding, flat, or closed universe.

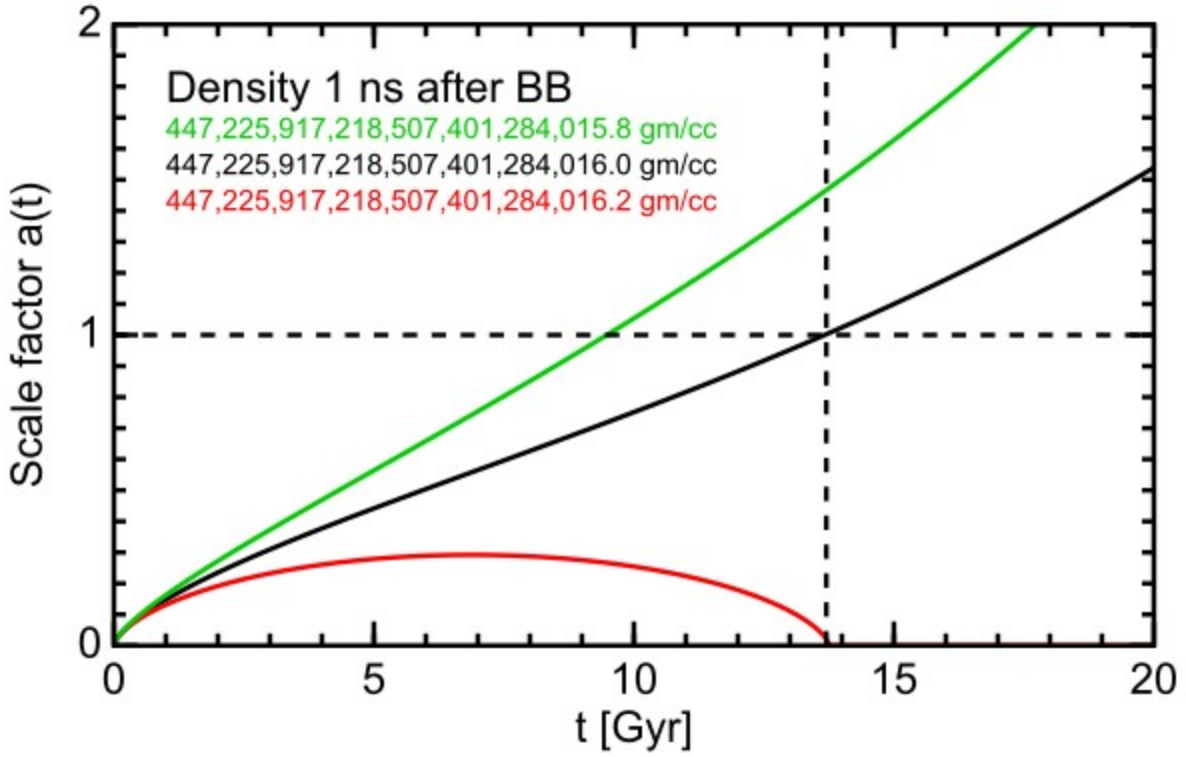

Fine Tuning - The Flatness Problem Details and Calculations

Astronomy 275 Lecture Notes, Edward Wright
https://astro.ucla.edu/~wright/A275.pdf

Refer to: Section 6. Flatness

See Section VI for Energy Equation

Even in the general case with radiation, matter and vacuum densities, the energy equation is still

$$2E_{tot} = v^2 - \frac{8\pi G\rho R^2}{3} = H^2R^2 - \frac{8\pi G\rho R^2}{3} = \text{const}$$

For a Radiation-Dominated critical density Universe, $H_0 = 1/(2*t)$

$$\rho_{crit} = \frac{3\cdot H^2}{8\cdot \pi G} \qquad H = \frac{1}{2t} \qquad \rho_{crit}(t) := \frac{3}{32\pi G\cdot t^2} \qquad \frac{1}{H_0} = 4.344\times 10^{17}\,s$$

Then: $\Omega^{-1} - 1 = \frac{constant}{\rho\cdot a^2}$

Thus to find the value of Density Parameter: **$\Omega^{-1} - 1$**, we need to calculate the density, ρ, during the Planck era.

Planck Time $t_{Pl} = \frac{\hbar}{m_{Pl}c^2}$ $\quad t_{Pl} := \sqrt{\hbar G}\cdot c^{-\frac{5}{2}}$ $\quad t_{Pl} = 13.495\,s\cdot 10^{-44}$

Planck Density $\rho_{Pl} := \frac{3}{32\cdot\pi\cdot G\cdot(t_{Pl})^2}$ $\quad \rho_{Pl} = 2.455\times 10^{94}\,\frac{kg}{m^3}$

Stefan-Boltzmann Law: $P = \varepsilon\,\sigma\,A\,T^4$

For the density at the Planck time this is 2.16×10^{29} gm/cc if $g_{spin} = 106.75$.

But the **current value of ρR^2** is just $\rho_0 = \Omega_0\,\rho_{crit} = 1.8788\,\Omega_0\,h^2\times 10^{-29}$ gm/cc, Ω_0 is the density parameter at present.

Current Energy Density: $u = \frac{g_{spin}}{2}\cdot a\cdot T_0^4$

We can calculate the temperature from: $\rho = \frac{a\cdot g}{2c^2}\cdot T^4$

To find the redshift from Entropy Density, s.

$$s = \frac{4}{3}\cdot\frac{g}{2}\cdot a\cdot T^4 = (1+z)^3\cdot s_o \qquad T_{pl} \approx 10^{32}\,K$$

$$H^2 = \frac{8\pi G}{3}\left(\frac{\pi^2}{30}\right)g_*T^4$$

The Current value of s is s_o $\quad s_o := 2890\cdot k_b\cdot\frac{J}{K}$

The quantity needed to find $\rho R^2 = \rho/(1+z)^2$ in order to find $\Omega - 1$ is given by equation 102 from Astronomy 275 Lecture Notes by Wright.

$$\Omega^{-1} - 1 = \frac{constant}{\rho\cdot a^2} \qquad \frac{\rho}{(1+z)^2} = \left(\frac{3.91}{g}\right)^{\frac{2}{3}}\cdot\left(\frac{a\cdot g\cdot T_o^4\cdot\rho}{2c^2}\right)^{\frac{1}{2}}$$

Calculate Ω required to **get Ω_0 (present density factor) between 0.95 and 1.05** with h = 0.71 and g = 106.75

Finally we get that **at the Planck time** Equation 103 from Astronomy 275:

$$\Omega^{-1} - 1 = \Omega_f(\Omega_0) := 8.7\cdot 10^{-59}\cdot\Omega_0\cdot 0.71^2\cdot\left(\Omega_0^{-1} - 1\right)$$

Then to get Ω_0 between 0.95 and 1.05 for Ω at Planck time

$$\Omega^{-1} - 1 = \Omega_f(0.95) = 0.219\cdot 10^{-59} \qquad \Omega^{-1} - 1 = \Omega_f(1.05) = -0.219\cdot 10^{-59}$$

Evaluating this in the Maple Programming Language to 62 digits gives:

```
Digits := 62;
Ω0.95 := 1 + evalf(0.219*10^(-59));
Ω0.95 := 1.0000000000000000000000000000000000000000000000000000000000000022

Ω1.05 := 1 - evalf(0.219*10^(-59));
Ω1.05 = 0.9999999999999999999999999999999999999999999999999999999999999781
```

Fine Tuning Analogy

The number 10^{-60} is, of course, very tiny. To make an analogy, in order to change the Sun's mass by one part in 10^{60}, you would have to add or subtract two electrons. Our very existence depends on the fanatically close balance between the actual density and the critical density in the early universe.

Thus to get Ω◦ between 0.95 and 1.05 with h = 0.71 and g = 106.75 requires 61 digits of Fine Tuning.

$0.9999999999999999999999999999999999999999999999999999999999999781 < \Omega$ and

$\Omega < 1.0000000000000000000000000000000000000000000000000000000000000022$

The probability for Ω to randomly fall within this narrow window at the Planck Time is astronomically unlikely. Some unknown process must be at work for Ω to be so Finely Tuned.

2. The Cosmological Horizon Problem for the ΛCDM Theory

The universe appears to be homogeneous and isotropic on large scales. According to the COBE measurements,the cosmic background radiation (CBR) is uniform to a part in 10^4 on large scales (from about 10 " to 180 deg). Furthermore, the light element abundance measurements seem to indicate that the observable universe (bounded by the last scattering surface) was homogeneous by the time of nucleosynthesis. Hence, we would **expect the observable universe today (time t_0)** to have **been in causal contact by the time of nucleosynthesis t_n** ; otherwise the initial conditions of the universe would have to be extremely fine tuned in order for the causally disconnected patches to resemble one another as much as they do. However, in a Friedmann Robertson Walker (FRW) universe (a metric of $ds^2 = dt^2 - a(t)^2\, dx^2$) that is matter or radiation dominated, upon naive extrapolation back to the singularity, one finds that there is a finite horizon length at the time of nucleosynthesis. Distant regions of space in opposite directions of the sky are so far apart that, assuming standard Big Bang expansion, they could never have been in causal contact with each other. This is because **the light travel time between them exceeds the age of the universe.**
Hence, for the observable universe to have been **in causal contact** by the time of nucleosynthesis, **the comoving horizon length** must have **been larger than the comoving distance** to the last scattering surface. In other words,

our observable universe today (when appropriately scaled back to the time of nucleosynthesis)
must have fit inside a causal region at the time of nucleosynthesis.

The **comoving size L_0** of the **observable universe today** is

$$L_o = \int_{t_{dec}}^{t_0} \frac{dt}{a(t)}$$

where t_{dec} is the time of the **radiation decoupling** and t_0 is the time today (subscript 0 refers to today).

The **comoving size L_n** of the horizon at the **time of nucleosynthesis**

$$L_n = \int_0^{t_n} \frac{dt}{a(t)}$$

In order to explain causal contact of all points within our observable universe at the time of nucleosynthesis, we require $\mathbf{L_0 < L_n}$. However, this condition is not met in a naive FRW cosmology with matter or radiation domination. Even if we take t_n to be the the time of last scattering of CBR and not the nucleosynthesis time, we still have a horizon problem by a **factor of 10^5** . In **both matter or radiation domination cases**, the time dependence of the scalefactor is a power law with the index less than 1; in a **dust (matter) dominated universe**, $\mathbf{a \propto t^{2/3}}$ and in a **radiation dominated** universe, $a \propto t^{1/2}$. Hence, in the naive FRW cosmology, $L_0 \approx t_0/a_0$ and $L_n \approx t_n/a(t_n)$, such that $L_o > L_n$ while **causal connection requires $\mathbf{L_o < L_n}$.**

This is the horizon problem.
The above XXXII Inflation solves the horizon problem by having a period of accelerated expansion, with

$$\ddot{a} > 0$$

(a period of time when the universe was not dust or radiation dominated).

Can Geodesics in Extra Dimensions Solve the Cosmological Horizon Problem?
Daniel J. H. Chung 1, arXiv:hep-ph/9910235v2 12 Oct 2000
There is a possible non-inflationary solution to the cosmological horizon problem in scenarios in which our observable universe is confined to three spatial dimensions (a three-brane) embedded in a higher dimensional space. A signal traveling along an extra-dimensional null geodesic may leave our three-brane, travel into the extra dimensions, and subsequently return to a different place on our three-brane in a shorter time than the time a signal confined to our three-brane would take. Hence, these geodesics may connect distant points which would otherwise be "outside" the four dimensional horizon (points not in causal contact with one another).

2. The Horizon Problem (See Section V)

Consider matter-only universe:

- Horizon distance $d_H(t) = 3ct$
- Scale factor $a(t) = (t/t_0)\ 2/3$
- Therefore **horizon expands faster than the universe**, so new" objects are constantly coming into view

Consider CMBR:

- It decouples at $1+z \approx 1100$
- i.e., $t_{CMB} = t_0 / 10^{4.5}$
- Then $d_H(t_{CMB}) = 3ct_0 / 10^{4.5}$
- Now this has expanded by a factor of 1000 to $3ct_0 / 10^{1.5}$
- But horizon distance now is $3ct_0$
- So angle subtended on sky by one CMB horizon distance is only $\approx 2°$

Horizons in the Universe

A space-time diagram illustrating the cosmic particle horizon, which defines the observable universe. If we trace our past lightcone back to the big bang, we find the most distant worldline that was ever within our past lightcone. The present distance to this worldline marks the particle horizon limit.

CMBR is Uniform to $\Delta T/T \approx 10^{-6}$

Yet the projected size of the particle horizon at the decoupling was $\approx 2°$ - these regions were causally disconnected - so how come?

=> Patches of CMB sky > 2° apart should not be causally connected!

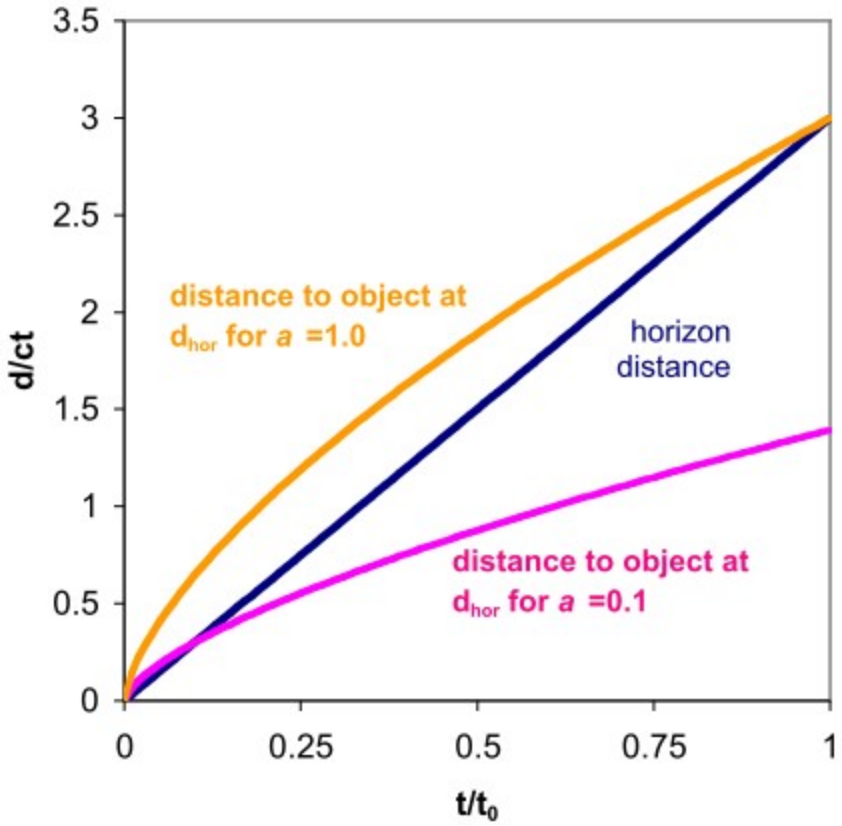

Some Key Problems of the ΛCDM Cosmology - Continued:

3. Origin of Structure
4. Absence of Topological Defects
5. Low Entropy - The Second Law of Thermodynamics
6. Discrepancy Between Theoretically Estimated and Actual Value of Λ
7. The Hubble Tension
8 The Early Appearance of Supermassive Black Holes and Galaxies
9. Violations of Cosmological Principle: Isotropy, Homogeneity, and KBC Void

5. Low Entropy

The CMB blackbody radiation in equilibrium has maximum entropy, with a volume density

$$s_{\mathrm{cmb}} = \frac{4}{3} a_{\mathrm{rad}} T_{\mathrm{cmb}}^{3}$$

in terms of the blackbody temperature T cmb and radiation constant a rad . But while T_{cmb} scales as $(1+z) \approx a(t)^{-1}$ with the expansion of the Universe, any given proper volume V scales as $a(t)^3$. Thus, the total blackbody entropy, $S_{cmb} = S_{emb}$ V, must have remained constant throughout the Universe's history (Frautschi 1982).

The so-called " past hypothesis " conjecture, however, posits that the overall entropy of the observable Universe is increasing monotonically. It must therefore have been significantly lower at earlier times (Layzer 1975; Price 1996; Albert & von Baeyer 2001; Earman 2006) . But this is clearly at odds with the CMB which suggests the Universe was close to thermal and chemical equilibrium — a state of very high entropy — a mere ~ 377,700 yr after the big bang. And if the entropy soon after the big bang was as high as it appears to have been at decoupling (i.e., z dec ~ 1090) , why are we living in a Universe, or a portion thereof, with anomalously low entropy today (Zemansky et al. 1998; Albrecht 2002; Penrose 2004; Egan & Lineweaver 2010) , when physical processes, such as stellar evolution and black hole accretion, are increasing the cosmic entropy everywhere?

This is the conflict known as the " initial entropy problem (IEP).

The standard model currently has no explanation for why the Universe was initially in a very low entropy state (as required by the second law) , and for how the CMB acquired such high entropy so soon after the big bang. Of course, a very low initial entropy by itself is not necessarily the problem. For example, the Universe may have been created from " nothing " and continues to evolve away from that initial state to which it will never return (Vilenkin 1982; Hartle & Hawking 1983; Linde 1984) . The problem emerges when this very low initial entropy is coupled to the subsequent entropy evolution implied by the CMB and what we see today.

The IEP has been one of the most contentious issues in standard cosmology. It remains unsolved. Neither the equilibrium models nor the in fl ationary paradigm can adequately account for the very low initial entropy without relying on a lack of " naturalness. " If the initial state of the Universe was random, characterized by a uniform probability of microstates, it should have been born with maximum entropy, representing thermal equilibrium, not the extremely unlikely low-entropy configuration required by Λ CDM. At face value, the standard model of cosmology thus appears to be inconsistent with the firrst and second laws of thermodynamics, constituting yet another conflict with our fundamental physical theories.

Cosmology and the Arrow of Time: The Second Law of Thermodynamics- One of the Biggest Problems

All the successfull equations of physics are symmetrical in time. Tbey can be used equally well in one direction in time as in the other. The future and the past seem physically to be on a completely equal footing. Newton's Laws, Hamiltons equations, Maxwell's equations, Einstein's general' relativity,'· Dirac's equation, the Schrodinger eqnation . all remain efffectively unaltered if we reverse the direction of time. (Replace the coordinate t which represents time, by -t.) The whole of Classical Physics and part of quantum mechanics is entirely reversible in time.

Our physical understanding actually contains important ingredients other than just equations of time-evolution and some of these do indeed involve time-asymmetries. The most important of these is what is known as the second law of thermodynamics. The low entropy state seems specially ordered, in some manifest way, and the high entropy state, less specially ordered. Define entropy. In rough terms, the entropy of a system is a measure of its manifest disorder. The second law of thermodynamics asserts that the entropy of an isolated system increases with time (or remains constant, for a reversible system).

The concept of phase space or state space is a space in which all possible "states" of a dynamical system or a control system are represented, with each possible state corresponding to one unique point in the phase space. The entropy of a state is a measure of the volume V of the compartment containing the phase-space point which represents the state.

$$\text{Entropy} = k \log V.$$

The number of baryons in the universe is 10^{80}. Now consider the phase space of the entire universe. Each point in the phase space represents a point where there is a different universe. The quantity k is a constant, called Boltzmann's constant. Its value is about 10^{-23} Joules per degree Kelvin. The essential reason for taking a logarithm here is to make the entropy an additive quantity for independent systems.

Putting this together with the Bekenstein-Hawking formula, we find that the entropy of a black hole is proportional to the square of its mass:

$$S_{bh} = m^2 \frac{kG}{h \cdot c}$$

Mass of Sun:

$$M_{\odot} = 1.99 \times 10^{30}\ kg$$

According to a calculation performed in 1929 by Subrahmanyan Chandrasekhar, white dwarfs cannot exist if their masses are more than about 1.4 times the mass of the sun, $1.4\,M_{\odot}$ Note that the Cbandrasekhar limit is not much greater than the sun's mass, whereas many ordinary stars are known whose mass is considerably greater than this value. But there is now a new limit, anaIogus to Chandrasekhar's (referred to as the Landau-Oppenheimer-Volkov limit), whose modem (revised) value is very roughly 2.5 solar masses. The gravitation attraction for a mass greater than this will result in the formation of a black-hole.

Let us consider what was previously thought to supply the largest contribution to the entropy of the universe, namely the 2.7K black-body background radiation. Astrophysicists had been struck by the enormous amounts of entropy that this radiation contains, which is far in excess of the ordinary entropy figures that one encounters in other processes (e.g. in the sun). The background radiation entropy is something like10^8 for every baryon (using natural units, so that Boltzmann's constant, is unity). (In effect, this means that there are 10^8 photons in the background radiation for every baryon.) Thus, with 10^{80} baryons in all, we should have a total entropy of 10^{88}.

The Bekenstein-Hawking formula tells us that the entropy per baryon in a solar mass black hole is about 10^{20} in natmal units so had the universe consisted entirely of solar mass black holes, the total figure would have been very much larger than that given above, namely 10^{100}.

Let us try to be a little more realistic. Rather than populating our galaxies entirely with black holes, let us take them to consist mainly of ordinary stars-some 10^{11} of them and each to have a million (i.e. 10^6) solar-mass black-hole at its core (as might be reasonable for our own Milky Way galaxy). Calculations by Roger Penrose shows that the entropy per baryon would now be actually somewhat larger even than the previous huge figure, namely now 10^{21}, giving a total entropy, in natural umts, of 10^{101}. This figure will give us an estimate of the total phase-space volume V available to the Creator, since this entropy should represent the logarithm of the volume of the (easily) largest compartment. Since 10^{123} is the log of the volume, the volume must be the exponential of 10^{123},

$$V = 10^{10^{123}}$$

6. Discrepancy Between Theoretically Estimated & Actual Value of Λ

A theoretical calculation of the cosmological constant based on a mechanical model of vacuum, Xiao-Song Wang, https://arxiv.org/pdf/2209.10525

In 1917, A. Einstein thought that his equations of gravitational fields should be revised to be

$$R_{\mu\nu} - \tfrac{1}{2} g_{\mu\nu} R + \Lambda g_{\mu\nu} = -\kappa T^{\mathrm{m}}_{\mu\nu},$$

where $g_{\mu\nu}$ is the metric tensor of a Riemannian spacetime, $R_{\mu\nu}$ is the Ricci tensor, $R \equiv g_{\mu\nu} R\mu_{\nu}$ is the scalar curvature, $g_{\mu\nu}$ is the contravariant metric tensor, k is Einstein's gravitational constant, is the energy-momentum tensor of a matter system, Λ is the cosmological constant.

The cosmological constant is a measure of the energy density of the vacuum, which is the lowest energy state.

Theoretical Estimate of Λ

A "natural" Planck system of units expresses everything as combination of fundamental physical constants;
the Planck density is:

$$\rho_{planck} := \frac{2\pi \cdot c^5}{\hbar \cdot G^2} \qquad \rho_{planck} = 5.169 \times 10^{96} \frac{kg}{m^3}$$

The observed value is:

$$\Omega_{vac} := 0.7 \qquad \rho_{crit} := \rho_0$$

$$\rho_{vac} := \Omega_{vac} \cdot \rho_{crit} \qquad \rho_{vac} = 6.051 \cdot 10^{-30} \cdot \frac{gm}{cm^3}$$

This is Off by 123 Orders of Magnitude

- This is modestly called "**the fine-tuning problem**"
  (because it requires a cancellation to 1 part in 10^{123})
- The other "natural" value is zero
- So, lacking a proper theory, physicists just declared the cosmological constant to be zero, and went on…

7. The Hubble H_0 *CMBR* versus *ΛCDM* Tension

Challenges for ΛCDM: An update, L. Perivolaropoulos and F. Skara, arXiv:2105.05208v3 [astro-ph.CO] April 7, 2022

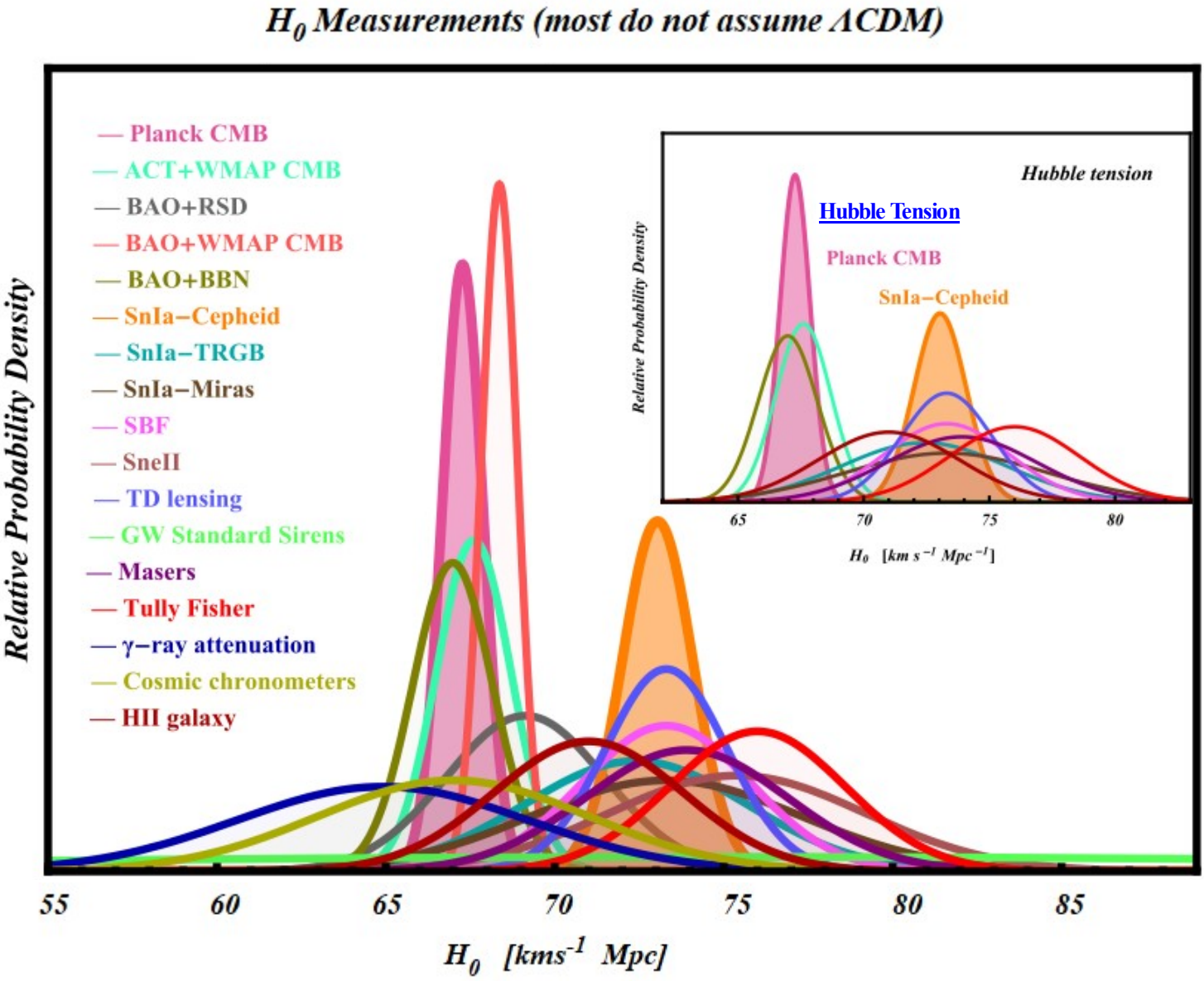

One dimensional relative probability density value of H_0 derived by recent measurements

Notice that the tension is not so much between early and late time approaches but more between approaches that calibrate based on low z (z 0.01) gravitational physics and those that are independent of this assumption.

For example cosmic chronometers and γ-ray attenuation which are late time but independent of late gravitational physics are more consistent with the CMB-BAO than with late time calibrators.

Data Sources: (Planck CMB (Aghanim et al. 2020e), ACT+WMAP CMB (Aiola et al. 2020), BAO+RSD (Wang et al. 2017), BAO+WMAP CMB (Zhang and Huang 2019), BAO+BBN (Addison et al. 2018), SnIa-Cepheid (Riess et al. 2021b), SnIa-TRGB (Jones et al. 2022), SnIa-Miras (Huang et al. 2019), SBF (Blakeslee et al. 2021), SneII (de Jaeger et al. 2022), TD lensing (Wong et al. 2020), GW Standard Sirens (Abbott et al. 2020a), Masers (Pesce et al. 2020), Tully Fisher (Kourkchi et al. 2020), γ-ray attenuation (Zeng and Yan 2019), cosmic chronometers (Yu et al. 2018), HII galaxy (Fern´andez Arenas et al. 2018)). All measurements are shown as Normalized **Gaussian** Cistributions.

8. Early Appearance of Supermassive Black Holes and Galaxies

A Candid Assessmet of Standard Cosmology, Fulvio Melia

The Early appearance of quasars in the ΛCDM Universe (Melia 2018) , such as ULAS J134208.10 + 092838.61 (henceforth **J1342 + 0928**, an ultraluminous supermassive black hole at **redshift z = 7.54**. This object has an inferred mass of M = 7.8 10^8 M and (as we shall see shortly) should have **taken more than 820 Myr** to grow via standard Eddington-limited accretion. **But its redshift suggests we're seeing it only several hundred Myr after Population II and III Supernovae could have created the (presumably) ~ 5 – 25 M_e seed that started its growth to the gargantuan object we see today.**

The growth of black hole seeds (massive or otherwise) is constrained by the maximum luminosity attainable due to the outward radiation pressure on ionized matter under the influence of gravity. The limiting power in hydrogen-rich plasma is known as the Eddington limit, $L_{Edd} \approx 1.3 \times 10^{38}$ (M/M_e) ergs s^{-1} . With an assumed effiiciency, ε, for converting rest-mass energy into radiation, one then infers an accretion rate $\dot{M} = L_{bol}/c^2$, in terms of the bolometric luminosity, L_{bol}. One typically adopts a fiducial value ε = 0.1 to cover the possible variations in basic accretion-disk theory, to arrive at the expression

$$\frac{dM}{dt} = \frac{1.3 \times 10^{38}\ \text{erg s}^{-1}}{\epsilon\, c^2 M_\odot} M$$

(Salpeter 1964; Melia 2013b) , whose solution is known as the Salpeter relation, where M_{seed} ($\sim 5 - 25$ Me) is the seed created at t_{seed}.

$M_{seed} := 5\,M_\odot$

$$M_{Salpeter}(t) := M_{seed} \cdot exp\left[\left[\frac{(t - 820)\cdot Myr}{45 Myr}\right]\right] \qquad M_{Salpeter}(820) = 5 \cdot M_\odot$$

Conventional astrophysics thus predicts that **J1342 + 0928** should have **taken approximately 820 Myr to grow from an initial black hole mass of 10** $M_\odot$ Although mergers in the early Universe (Lippai et al. 2009; Tanaka & Haiman 2009; Hirschmann et al. 2010) might have shortened this growth time, there are limitations to how this mechanism could have worked. Simulations show that the black hole distribution always converges toward a Gaussian, irrespective of how one chooses the initial seed profile. But to comply with the observational constraints, ~ 100 $M_\odot$ seeds must have started forming no later than z ~ 40 (Tanaka & Haiman 2009) , well before the EoR. In addition, seeds must not have formed after z ~ 20 – 30, for then there would be an overproduction of black holes at ~ 10^5 $M_\odot$ to ~ 10^7 $M_\odot$) compared to the data (see, e.g., Figures 5 and 6 in Tanaka & Haiman 2009) . Without this cutoff, the lower mass black holes would be over-represented by a factor ~ 100 – 1000.

The suggestion that early mergers might have critically impacted the formation of supermassive black holes at high-z is therefore inconsistent with our view of how and when Population III stars were born. **The onset of the EoR at t ~ 400 Myr is set by the cooling time to form the first generation of stars, corresponding to z ~ 15** — much later than z ~ 40. And there is no explanation for why these stars then stopped forming below z ~ 20 – 30, even before the EoR started. **One would be forced to hypothesize that some mechanism other than Population III supernovae must have created the massive seeds well before the EoR, requiring new, unknown physics.**

But we simply have no observational evidence for such events occurring prior to z ~15.

An additional problem with the merger scenario is that the halo abundance now appears to have been smaller than previously thought by at least an order of magnitude. Large (4 Mpc^3) high-resolution simulations (Johnson et al. 2013) show that Population III and II star formation overlapped and evolved down to z ~ 6. The enhanced metal enrichment and the feedback radiation — including molecule-dissociating Lyman –Werner photons that destroyed the coolants H_2 and HD required for the condensation of early matter — would have significantly altered the halo and Population III star formation rates. Indeed, both the halo and Population III star formation rates would have been reduced by an order of magnitude at z >= 10 compared to previous, less sophisticated simulations. This net shift reduced the volume density of Population III supernovae, and the density of black hole seeds they produced, at the redshift (z >= 10) when the frequency of mergers among these objects would have mattered most.

The Premature Formation of Galaxies

Interest in the cosmic dawn has also been generated by the recent dramatic discovery of faint galaxies at redshifts well before the end of the EoR. By stretching the imaging capabilities of WFC3/IR on the Hubble Space Telescope (HST), and introducing gravitational lensing techniques, several teams appear to have uncovered galaxies emerging at $z \sim 10 - 12$, a highly surprising result.
It now appears that these primordial galaxies contributed to the re-ionization of the cosmic fluid, and may even have dominated this process. These initial detections by HST have been characterized as an "impossibly early" galaxy problem, but the more recent discovery by the James Webb Space Telescope (JWST), of well-formed ($\sim 10^9\ M_\odot$) galaxies at redshifts extending out to ~ 17, with some confirming ALMA observations have greatly exacerbated this apparent conflict with the standard model. As of this writing, the JWST discoveries are still considered to be primarily candidates, though their photometrically identified redshifts appear to be quite reliable, and follow-up observations will be conducted very shortly. As we shall see, if these turn out to be real, as is highly expected, their implied formation would have begun (and been largely completed) even before Population II and III stars are supposed to have emerged.

Just as we found for the supermassive black holes, **this rapid emergence of high-z galaxies so quickly after the big bang therefore appears to be in conflict with our current understanding of how they evolved.** These two problems are probably not independent of each other. Not surprisingly, one can easily show that the same time-compression problem is responsible for the tension seen between theory and the premature formation of both the early quasars and galaxies.

One can already see from this brief summary, however, that **the rate of growth versus redshift does not appear to be quite right.** Probing more deeply, one infers from the results that the ratio of the doubling time t_{db} (essentially the inverse of the sSFR) to the corresponding cosmic time falls within the range $\sim 0.1 - 0.3$, independently of redshift. For the sake of illustration, let us take the smaller value, which minimizes the growth time. Then, a galaxy with mass $M_* = 10^8\ M_\odot$ at $z = 6$ (i.e., $t_* \sim 900$ Myr in ΛCDM) must have started its assembly at $t_{init} \sim (0.9)^n\ t_*$ where $n = M_*/M_{init})$ log2 is the number of doublings from an initial mass M_{init} at t_{init}. One therefore infers that such galaxies seen at $z = 6$ could have started forming during the transition from Population III to Population II stars (i.e., $t_{init} \sim 230$ Myr) if one conservatively assumes that $M_{init} = 10^4 M_\odot$.
But the timeline breaks down completely if one instead considers the same type of growth rate for a similar galaxy seen at $z = 10$ (i.e., $t_* \sim 550$ Myr in ΛCDM). Such a galaxy must have started growing from an initial condensation of $M_{init} = 10^4\ M_\odot \sim 140$ Myr, well before Population III stars had suffcient time to evolve and explode as supernovae, initiating the subsequent growth of galactic structure. As a specific illustrative example, consider that a $10^9\ M_\odot$ galaxy seen at $z \sim 10.^7$ (i.e., $t_* \sim 490$ Myr), must have started growing at $t \sim 82$ Myr, a situation that simply cannot be reconciled with what must have happened at the dawn of cosmic structure formation. Comparing the time compression problem for quasars with that of galaxies, one draws the interesting conclusion that **stretching the time elapsed per unit of redshift by a factor 2 beyond z ~ 6 would be sufficient to eliminate the tension in both cases.**

XXX. Some Key Problems of the ΛCDM Cosmology - Continued

9. Violations of Cosmological Principle: Isotropy, Homogeneity, and KBC Void
10. Cosmological Lithium Problem: Observable Lithium less than calculated Λ-CDM Model by Factor of 3-4.
11. Early Universe High Redshift Galaxies: JWST sees galaxies JADES-GS-z14-0 at redshift of 14.32
12. Unfalsifiability: ΛCDM model is built upon a foundation of conventionalist stratagems:
Not Popper Unfalsifiable.
13. Electroweak Horizon Problem - Higgs -->Possible phase transition associated - Grand Unification Theories
14. Latest Findings JWST Challenge Cosmology Models - Early Galaxies
15. XXXIII. The Inflation Hypothesis and the Very Early Universe

14. Latest Findings JWST Challenge Cosmology Models - Early Galaxies

Astrophysicists may have an explanation for the James Webb Space Telescope's discovery of a swarm of mysterious early galaxies that threaten to break cosmology.

The ΛCDM Model predicts that, as we look farther and farther back in time — i.e., to greater and greater cosmic distances — that the galaxies we see will be inherently smaller, bluer, less evolved, less rich in heavy elements, and that at some point beyond where we've been able to look, we should cease to see stars or galaxies of any type, as we'll reach the Universe's "dark ages."

Webb finds most distant known galaxies (JADES-GS-z14-0 and z14.32 290 Million Years after Big Bang
Brighter, Larger, Redder, and Younger and Oxygen (indicates 2nd Generation) does not agree with ΛCDM Model.

https://www.livescience.com/space/cosmology/james-webb-telescopes-observations-of-impossible-galaxies-at-the-dawn-of-time-may-finally-have-an-explanation
The galaxies, which the James Webb telescope (JWST) spotted forming as early as 500 million years after the Big Bang, were so bright that they theoretically shouldn't exist: Brightnesses of their magnitude should only come from massive galaxies with as many stars as the Milky Way, yet these early galaxies took shape in a fraction of the time that ours did.

The discovery threatened to upend physicists' understanding of galaxy formation and even the standard model of cosmology. Now, a team of researchers using supercomputer simulations suggest that the galaxies may not be so massive at all — they could just be unusually bright.

Bursts of star formation explain mysterious brightness at cosmic dawn Intense ashes of light, not mass, resolve the puzzle of impossible brightness Peer-Reviewed Publication,NORTHWESTERN UNIVERSITY, 3-OCT-2023
A period that lasted from roughly 100 million years to 1 billion years after the Big Bang, cosmic dawn is marked by the formation of the universe's rst stars and galaxies. Before the JWST launched into space, astronomers knew very little about this ancient time period.

"The JWST brought us a lot of knowledge about cosmic dawn," Sun said. "Prior to JWST, most of our knowledge about the early universe was speculation based on data from very few sources. With the huge increase in observing power, we can see physical details about the galaxies and use that solid observational evidence to study the physics to understand what's happening."

Do JWST's results contradict the Big Bang?
https://bigthink.com/starts-with-a-bang/jwsts-contradict-big-bang/

Many of these early galaxies that JWST is finding have peculiar, puzzling properties about them that appear difficult to reconcile with this theoretical picture that the Universe has painted for us. They appear, for example, to be:

- very massive,
- very bright,
- very rich in heavy elements - High Metallicity. **See Section XXX**,
- very actively forming new stars,
- and very rich in gas.

Prognosis:
There are an enormous number of astrophysical possibilities that invoke no fundamentally new physics that could potentially account for why these galaxies would exist with these large masses and brightnesses.

XXXII. The Inflation Hypothesis and the Very Early Universe[2]

A hypothesis is an educated guess or prediction about the relationship between two variables. It must be a testable statement; something that you can support or falsify with observable evidence. The objective of a hypothesis is for an idea to be tested, not proven.

What is the concept of inflation? In a cosmological context, inflation can most generally be defined as the hypothesis that there was a period, early in the history of our universe, when the expansion was accelerating outward; that is, an epoch when the acceleration equation.

$$\frac{\ddot{a}}{a} = -\frac{4\pi G}{3c^2}(\varepsilon + 3P), \qquad \frac{d}{dt}a = \sqrt{\frac{8\pi G\cdot\rho_\nu}{3}}\cdot a = H_\nu\cdot a$$

tells us that when $P < -\varepsilon/3$. Thus, inflation would have taken place if the universe were temporarily dominated by a component with equation-of-state parameter $w < -1/3$. The simplest implementation of inflation states that the universe was temporarily dominated by a positive cosmological constant Λ_i (with $w = -1$), and thus had an acceleration equation that could be written in the form

$$\frac{\ddot{a}}{a} = \frac{\Lambda_i}{3} > 0$$

the Hubble constant H_i during the inflationary phase was thus constant, with the value $H_i = (\Lambda_i/3)^{1/2}$, and the scale factor grew exponentially with time:

$$a(t) \propto e^{H_i t}.$$

During inflation, the universe is dominated by the vacuum energy. In a time interval, Δt the universe expands by a factor $\exp(H_v \Delta t)$. Define the Doubling Time, t_D, as the time it takes the universe to double in size.

In the early universe, when the scale factor is very small, then mass density ρ_m must be much greater than ρ_v.

Matter density ρ_m is diluted. Then Doubling Time, t_D, is:

$$\rho_\nu := 10^{71}\,\frac{gm}{cm^3} \qquad H_\nu := \sqrt{\frac{8\pi\cdot G\cdot\rho_\nu}{3}}$$

$$e^{H_\nu\cdot t_D} = 2 \qquad t_D := H_\nu^{-1}\cdot log(2, e)$$

$$t_D = 2.931\,s\cdot 10^{-33}$$

To see how a period of exponential growth can resolve the flatness, horizon, and monopole problems, suppose that the universe had a period of exponential expansion sometime in the midst of its early, radiation-dominated phase. For simplicity, suppose the exponential growth was switched on instantaneously at a time t_i, and lasted until some later time t_f, when the exponential growth was switched off instantaneously, and the universe reverted to its former state of radiation-dominated expansion. In this simple case, we can write the scale factor as

$$a(t) = \begin{cases} a_i(t/t_i)^{1/2} & t < t_i \\ a_i e^{H_i(t-t_i)} & t_i < t < t_f \\ a_i e^{H_i(t_f-t_i)}(t/t_f)^{1/2} & t > t_f. \end{cases}$$

Note that the inflationary expansion is **superluminal**: the space can expand much faster than c.

Thus, between the time t_i, when the hypothesized exponential inflation began, and the time t_f, when the inflation stopped, the scale factor increased by a factor

$$\frac{a(t_f)}{a(t_i)} = e^N$$

where N, the number of e-foldings of inflation, would be

$$N \equiv H_i(t_f - t_i)$$

If the duration of inflation, $t_f - t_i$, was long compared to the Hubble time during inflation, then N was large, and the growth in scale factor during a hypothetical inflationary period would be enormous.

For concreteness, let's take one possible model for inflation. This model states that exponential inflation started around the GUT time, $t_i \approx t_{GUT} \approx 10^{-36}$ s, with a Hubble parameter and lasted for N e- foldings, ending at $t_f \approx (N+1)t_{GUT}$. Note that the cosmological constant Λ_i present at the time of inflation in this model was very large compared to the cosmological constant that is present today. Currently, the evidence is consistent with an energy density in Λ of $\varepsilon_{\Lambda,0} \approx 0.69\varepsilon_{c,0} \approx 0.0034$ TeVm^{-3}. To produce exponential expansion with a Hubble parameter Hi $\approx 10^{36}$ s^{-1}, the cosmological constant during inflation would have had an energy density

$$\varepsilon_{\Lambda_i} = \frac{c^2}{8\pi G}\Lambda_i = \frac{3c^2}{8\pi G}H_i^2 \sim 10^{105}\,\text{TeV m}^{-3},$$

over 10^7 orders of magnitude larger.

Prior to the inflationary period, the universe was radiation-dominated. Thus, the horizon distance at the beginning of inflation was

$$d_{\text{hor}}(t_i) = a_i c \int_0^{t_i} \frac{dt}{a_i(t/t_i)^{1/2}} = 2ct_i.$$

The horizon size at the end of inflation was

$$d_{\text{hor}}(t_f) = a_i e^N c \left(\int_0^{t_i} \frac{dt}{a_i(t/t_i)^{1/2}} + \int_{t_i}^{t_f} \frac{dt}{a_i \exp[H_i(t-t_i)]} \right)$$

If N, the number of e-foldings of inflation, is large, then the horizon size at the end of inflation was

$$d_{\text{hor}}(t_f) = e^N c(2t_i + H_i^{-1})$$

An epoch of exponential inflation causes the horizon size to grow exponentially. If inflation started at $t_i \approx 10^{-36}$s, then the horizon size immediately

$$d_{\text{hor}}(t_f) = a_i e^N c \left(\int_0^{t_i} \frac{dt}{a_i(t/t_i)^{1/2}} + \int_{t_i}^{t_f} \frac{dt}{a_i \exp[H_i(t-t_i)]} \right)$$

$$d_{\text{hor}}(t_i) = 2ct_i \approx 6 \times 10^{-28}\,\text{m}.$$

For concreteness, let's assume N = 65 e-foldings of inflation, just a bit more than the minimum of 60 e-foldings required to explain the flatness of today's universe. In this fairly minimal model, if we take the horizon size immediately after inflation was

$$d_{\text{hor}}(t_f) \approx e^N 3ct_i \sim 15\,\text{m}$$

During the brief period of ~ 10^{-34}s that inflation lasts in this model, **the horizon size is boosted exponentially from submicroscopic scales to something the size of a whale**. The exponential increase in the horizon size during inflation is illustrated by the solid line in Figure 10.3. In the post-inflation era, when the universe reverts to being radiation-dominated, the horizon size grows at the rate $d_{hor} \propto a \propto t^{1/2}$, as points that were separated by a distance $d_{hor}(t_f)$ at the end of inflation continue to be carried apart from each other by the expansion of the universe.

In the hypothetical model we've adopted, where inflation started around the GUT time and lasted for N = 65 e-foldings, the scale factor was $a(t_f) \sim 2 \times 10^{-27}$ at the end of inflation, estimated from Equation 10.30. At the time of last scattering, the scale factor was $a(t_{ls}) \approx 1/1090 \approx 9.1 \times 10^{-4}$. Thus, in our model, the horizon distance grew from $d_{hor}(t_f) \sim 15$ m at the end of inflation to $d_{hor}(t_{ls}) \sim 200$ Mpc at the time of last scattering. This is 800 times bigger than the horizon size $d_{hor}(t_{ls}) \approx 0.25$ Mpc that we calculated in the absence of inflation, and is large enough that antipodal points on the last scattering surface are causally connected.

This model states that exponential inflation started around the GUT time, $t_i \approx t_{GUT} \approx 10^{-36}$ s, with a Hubble parameter and lasted for N e- foldings, ending at $t_f \approx (65 + 1) * t_{GUT}$.

$$D_c = \left(\frac{c}{H_0}\right) \int_0^{R_c} \frac{dR}{R^2 \sqrt{\frac{\Omega_\gamma}{R^4} + \frac{\Omega_M}{R^3} + \Omega_\Lambda}}$$

$GUT := 10^{-35}$

og-log Plot of Cosmic Scale Factor of Observable Universe: a(t) vs t (sec)

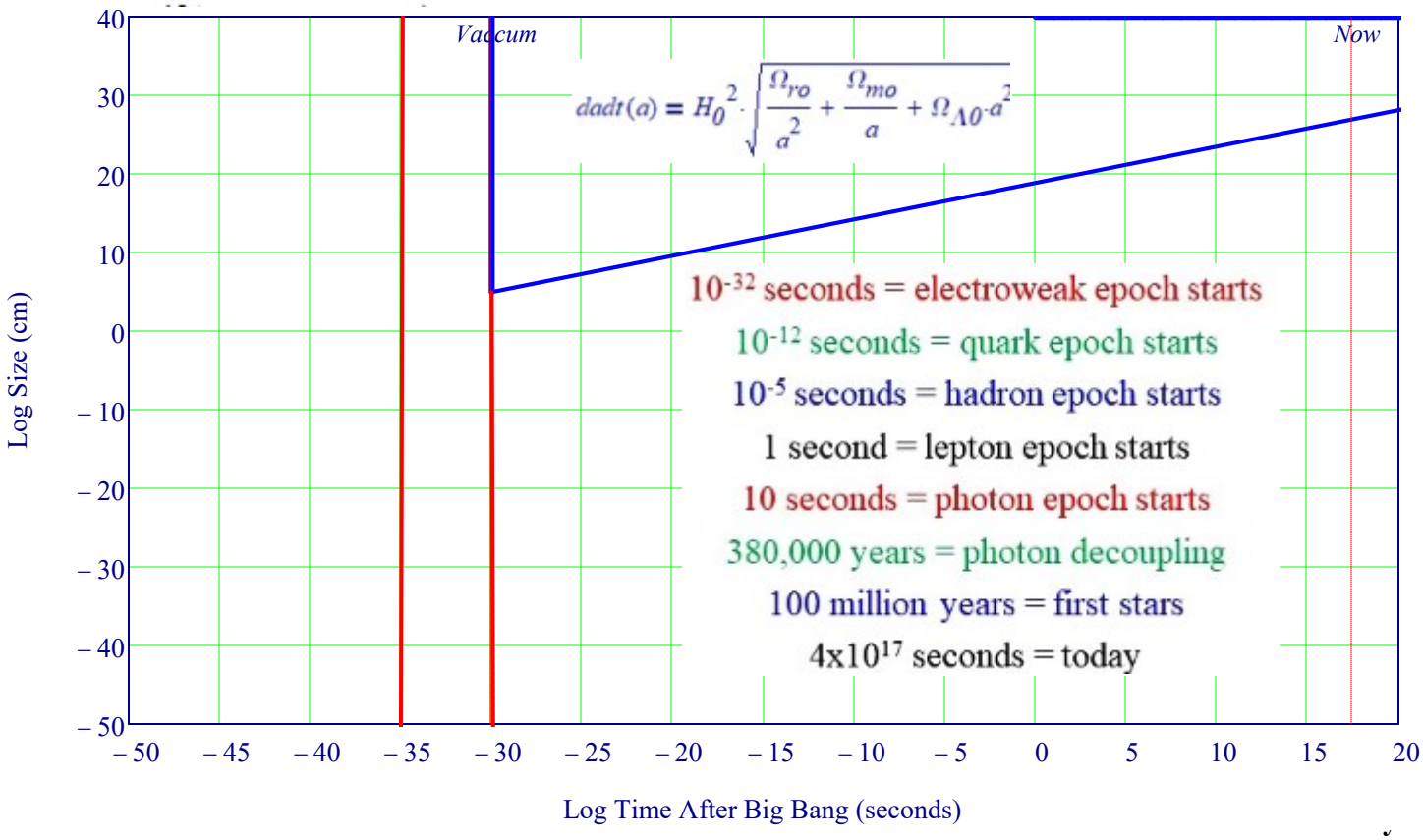

Time after Big Bang (s) $t = \left(\frac{1}{H_0}\right) \int_0^{R_c} \frac{dR}{R \sqrt{\frac{\Omega_\gamma}{R^4} + \frac{\Omega_M}{R^3} + \Omega_\Lambda}}$

The solid line shows the growth of the horizon distance in a universe where exponential inflation begins at $t = 10^{-36}$s and lasts for N = 65 e-foldings. The dashed line, for comparison, shows the horizon distance in a radiation-dominated universe without an inflationary epoch.

Biggest Weakness of The ΛCDM Theory - the Inflation Hypothesis

The Weight of the Vacuum - The Worst Scientific Prediction Ever

• A "natural" Planck system of units expresses everything as combination of fundamental physical constants; the Planck density is: $\rho_{Planck} = c^5 / (hG^2) = 5.15 \times 10^{93}$ g cm^{-3}

• The observed value is: $\rho_{vac} = \Omega_{vac}\, \rho_{crit} \approx 6.5 \times 10^{-30}$ g cm^{-3}

• This is modestly called "the fine-tuning problem" The above shows that it requires a cancellation to 1 part in 10^{123})

• The Physical Origins of the Dark Energy are completely unknown at this time,

The Inflation Hypothesis

The ΛCDM Theory starts with the assumption that the universe sprang from a "singularity". Singularity is a mathematical concept and it has no meaning in the realm of Physics. It may be Mathematics, but it certainly is not Physics. It is disturbing that the two main ingredients in ΛCDM, Cold Dark Matter and Dark Energy, are not understood.

The ΛCDM Theory is based on the concept of Inflation. Inflation postulates that after 10^{-36} seconds that the universe expanded by a factor of a thousand billion billion billion and then at the right moment the inflation stopped. What is the physical mechanism for inflation? An Inflaton field? How did the inflation know when to stop? How could it have stopped everywhere at the same instant.

In order to explain the rotational velocity of galaxies and a few other phenomena, the concepts of dark matter and dark energy were proposed as explanations. The nature of dark matter is unknown and dark energy is presumed to be the cosmological constant. Quantum theory predict that this constant is 10^{120} times larger than the measured value. This has been referred to as the biggest error ever made in science.
The ΛCDM Theory predicts that the initial galaxies that were formed a few millions years after the BB, that galaxies would be formed that would be small in size. Contrary to the predicted, the JWT is finding that there are some large galaxies that were formed at this time.
The Model of GR assumes that the universe is isotropic and homogenous. This may be true locally, but it is not known is this is true in general.
To demonstrate inflation's problems, we will start by following the edict of its proponents: assume inflation to be true without question.

Neil Turok: Physics is in Crisis

Inflation is not a theory. It is a huge collection of models.

During the Planck Era, the symmetry of the matter gets broken due to the curvature of space-time and this is called a trace anomaly. What goes along with this, when you have all these Quantum fields which are describing the matter, so photons, electrons, all of them are associated with a Quantum field. The vacuum field is unable to stand still. The vacuum is not empty. The vacuum consists of all the vibrations of all the fields that you add in the standard model and the problem is those vacuum vibrations should produce huge gravitational waves. "Gravity" detects the energy of the vibrations of particle fields and should produce huge gravitational waves. There have been no primordial gravitational waves detected.

Physicists have essentially been cheating. Taking that vacuum energy of all the fields that we know about and just subtracted it. That is not really consistent. Feynmann acknowledged this. All the great physicists acknowledge this. That what we do is essentially when we do Quantum field Theory and couple it to gravity. This is essentially to cheat.

With Inflation we've found a way around that cheat. We've found a way to cancel the trace anomaly and to cancel the vacuum energy without adding even one particle to the standard model. That mechanism turns out to give fluctuations as a side effect and those fluctuations.
This may match the observations and we then have the best of all possible worlds.

Is the theory at the heart of modern cosmology deeply flawed? Paul J. Steinhardt

https://www.scientificamerican.com/article/cosmic-inflation-theory-faces-challenges/
"One thing it would tell us is that at some time shortly after the big bang there had to have been a tiny patch of space filled with an exotic form of energy that triggered a period of rapidly accelerated expansion ("inflation") of the patch. Most familiar forms of energy, such as that contained in matter and radiation, resist and slow the expansion of the universe because of gravitational self-attraction. Inflation requires that the universe be filled with a high density of energy that gravitationally self-repels, thereby enhancing the expansion and causing it to speed up. It is important to note, however, that this critical ingredient, referred to as inflationary energy, is purely hypothetical; we have no direct evidence that it exists. Furthermore, there are literally hundreds of proposals from the past 35 years for what the inflationary energy may be, each generating very different rates of inflation and very different overall amounts of stretching. Thus, it is clear that inflation is not a precise theory but a highly flexible framework that encompasses many possibilities."

Is the theory at the heart of modern cosmology deeply flawed?
https://www.jstor.org/stable/26002474

Summary:
Highly improbable conditions are required to start inflation. Worse, inflation goes on eternally, producing infinitely many outcomes, so the theory makes no firm observational predictions.
The basic idea of the big bang is that the universe has been slowly expanding and cooling ever since it began some 13.7 billion years ago. This process of expansion and cooling explains many of the detailed features of the universe seen today, but with a catch: the universe had to start off with certain properties.

For instance, it had to be extremely uniform, with only extremely tiny variations in the distribution of matter and energy. Also, the universe had to be geometrically flat, meaning that curves and warps in the fabric of space did not bend the paths of light rays and moving objects. But why should the primordial universe have been so uniform and flat? A priori, these starting conditions seemed unlikely. That is where Guth's idea came in. He argued that even if the universe had started off in total disarray—with a highly nonuniform distribution of energy and a gnarled shape—a spectacular growth spurt would have spread out energy until it was evenly dispersed and straightened out any curves and warps in space.

What gave Guth's idea its appeal was that theorists had already identified many possible sources of such energy. The leading example is a hypothesized relative of the magnetic field known as a scalar field, which, in the particular case of inflation, is known as the "*inflato*n" field.

The inflaton's potential energy can cause the universe to expand at an accelerated rate. In the process, it can smooth and flatten the universe, provided the field remains on the plateau long enough (about 10^{-30} second) to stretch the universe by a factor of 10^{25} or more along each direction. Inflation ends when the field reaches the end of the plateau and rushes downhill to the energy valley below. At this point, the potential energy converts into more familiar forms of energy—namely, the dark matter, hot ordinary matter and radiation that fill the universe today. The universe enters a period of modest, decelerating expansion during which the material coalesces into cosmic structures.

The self-perpetuating nature of inflation is the direct result of quantum physics combined with accelerated expansion. Recall that quantum fluctuations can slightly delay when inflation ends. Where these fluctuations are small, so are their ef affects. Yet the fluctuations are uncontrollably random. In some re regions of space, they will be large, leading to substantial delays.

Inflating points continue to grow and, in a matter of instants, dwarf the well-behaved region that ended inflation on time. The result is a sea of inflating space surrounding a little island filled with hot matter and radiation. What is more, rogue regions spawn new rogue regions, as well as new islands of matter—each a self-contained universe. The process continues ad infinitum, creating an unbounded number of islands surrounded by ever more inflating space.
What does it mean to say that inflation makes certain predictions—that, for example, the universe is uniform or has scale-invariant fluctuations—if anything that can happen wi happen an infinite number of times?

For inflation, the observed outcome depends sensitively on what is the initial state. That defeats the entire purpose of inflation: to explain the outcome no matter what conditions existed beforehand.

The naive theory supposes that inflation leads to a predictable outcome governed by the laws of classical physics. The truth is that quantum physics rules inflation, and anything that can happen will happen. And if inflationary theory makes no firm predictions, what is its point? The underlying problem is that procrastination carries no penalty—to the contrary, it is positively rewarded. Rogue regions that delay ending inflation continue to grow at an accelerating pace, so they invariably take over.

The Big Bang also leads to the conclusion that most of the matter in the universe is not the "normal" atomic matter with which we are familiar. One of the arguments for the Big Bang is that it appears to be able to account for the relative abundance of the "light" chemical elements such as hydrogen, helium, and lithium. However, the nuclear recipe that accounts for the abundance of these light elements also fixes the total number of protons and neutrons (classified as baryons) generated by the Big Bang. Since atoms contain protons and neutrons, atoms are classified as baryonic matter. Observations suggest the possible existence of large amounts of non-luminous dark matter in addition to the luminous matter (stars and luminous gas) that we can observe. The ratio of total matter to visible matter is often claimed to be roughly ten to one, which implies that dark matter would account for about 90 percent of the matter in the universe. Accounting for this "missing" dark matter is quite difficult, which is why both creationist and evolutionist cosmologists have suggested that what we perceive as large amounts of dark matter may actually result from unknown physics

Theorems About Cosmic Origins, Singularities, and Time

Key Theorems Constraining Cosmological Models

Theorem	What It Constrains	Importance Level
Hawking–Penrose	Singularities in GR	Foundational
Borde–Guth–Vilenkin	Past completeness	Foundational
Raychaudhuri	Geodesic focusing	Structural
EGS / Almost-EGS	Geometry from CMB	Observational
Cosmic No-Hair	Inflation outcomes	Dynamical
Etherington	Distance relations	Testable
Sachs–Wolfe	CMB anisotropies	Observational

XXXIII Proof of the Borde-Guth-Vilenkin (BGV) Theorem

The beginning of-the universe.
The Borde Guth Vilenkin Theorem, indefinitely continued into past., Vilenkin,
*I*nference-review.com/ VOL. 1, NO. 4 / OCTOBER 2015

The BGV theorem demonstrates "that **any inflating model that is globally expanding must be geodesically incomplete in the past**".

Was the big bang truly the beginning of the universe? A beginning in what? Caused by what? And determined by what, or whom? These questions have prompted physicists to make every attempt to avoid a cosmic beginning.

Physicists hoped initially that the singularity might be an artifact of Friedmann's simplifying assumption of perfect uniformity, and that it would disappear in more realistic solutions of Einstein's equations. Roger Penrose closed this loophole in the mid-1960s by showing that, under a very general assumption, the singularity was unavoidable. Under the null convergence condition, gravity always forces light rays to converge.
(Mathematically, t**he null convergence condition (NCC) requires** that the Ricci curvature tensor $R_{\mu\nu}$ must satisfy $R_{\mu\nu}N^{\mu}N^{\nu} \geq 0$ for all null vectors N^{μ}. A null vector is a vector of zero norm, $N\mu N\mu=0$. Combined with Einstein's equations, NCC is equivalent to the null energy condition (NEC), requiring that $T_{\mu\nu}N_{\mu}N_{\nu} \geq 0$ for all null N_{μ}, where $T_{\mu\nu}$ is the Einstein Energy-Momentum Tensor.)

$$R_{\mu\nu} - \frac{1}{2}g_{\mu\nu}R = \frac{1}{M_{\rm pl}^2}T_{\mu\nu}$$

Proof

Start with a homogeneous, isotropic, and spatially flat universe with the metric:
This implies that the **density of matter or energy measured by any observer cannot be negative**. The conclusion holds for all familiar forms of classical matter.

$$ds = dt^2 - a^2(t)dx_i dx^i$$

The Hubble expansion rate is $H = a\dot{}/a$, where the dot denotes a derivative with respect to time t. We can imagine that the universe is filled with comoving particles, moving along the timelike geodesics vector x = const. Consider an inertial observer, whose world line is $x_{\mu}(\tau)$, parametrized by the proper time τ. For an observer of mass m, the 4-momentum is $P^{\mu}=m\, dx^{\mu}/d\tau$, so that $d\tau = (m/E)dt$ where $E = P^0 = (p_2+m_2)^{1/2}$ denotes the energy, and p, the magnitude of the 3-momentum. It follows from the geodesic equation of motion that $p \propto 1/a(t)$, so that

$p(t) = [a(t_f)/a(t)]p_f$, where p_f designates the momentum at some reference time t_f.

Thus
$$\int_{t_i}^{t_f} H(\tau)d\tau = \int_{a(t_i)}^{a(t_f)} \frac{mda}{\sqrt{m^2a^2 + p^2a(t_f)}} = F(\gamma_f) - F(\gamma_i) \leq F(\gamma_f)$$

where $t_i < t_f$ is some initial moment.
Note that:

$$F(\gamma) = \frac{1}{2}\ln\left(\frac{\gamma+1}{\gamma-1}\right) \quad \text{where} \quad \gamma = \frac{1}{\sqrt{1-\nu^2}}$$

γ is the Lorentz factor, and $v_{rel} = p/E$ is the observer's speed relative to the comoving particles.

For any non-comoving observer, γ > 1 and F(γ) > 0

The expansion rate averaged over the observer world line can be defined as

$$\text{Define: } H_{\text{av}} = \frac{1}{\tau_{\text{f}} - \tau_{\text{i}}} \int_{t_{\text{i}}}^{\tau_{\text{f}}} H(\tau) d\tau.$$

Assuming that $H_{av} > 0$ and using the first equation, it follows that

$$\tau_{\text{f}} - \tau_{\text{i}} \leq \frac{F(\gamma_{\text{f}})}{H_{\text{av}}}.$$

This implies that any non-comoving past-directed timelike geodesic satisfying the condition $H_{av} > 0$, must have a finite proper length, and so must be past-incomplete.

There is no appealing to homogeneity and isotropy in an arbitrary space-time. Imagine that the universe is filled with a congruence of comoving geodesics, representing test particles and consider a non-comoving geodesic observer described by a world line $x_\mu(\tau)$

Let u_μ and ν^μ designate the 4-velocities of test particles and the observer.
Then the Lorentz factor of the observer relative to the particles is

$$\gamma = u_\mu \nu^\mu$$

To characterize the expansion rate in general space-time, it suffices to focus on test particle geodesics that cross the observer's world line. Consider two such geodesics encountering the observer at times τ and $\tau + \Delta\tau$.
Define the parameter

$$H = \frac{d}{d\tau} F(\gamma(\tau))$$

with $F(\gamma) = 1/\gamma$, and γ defined by

$$H = \lim_{\Delta\tau \to 0} \frac{\Delta u_r}{\Delta r}$$

Clearly, $F(\gamma) > 0$, and the argument goes through as before.

In general relativity, a timelike congruence in a four-dimensional Lorentzian manifold can be interpreted as a family of world lines of certain ideal observers in our spacetime.

A rigorous formulation of the BGV theorem is now possible.
Let λ be a timelike or null geodesic maximally extended to the past, and
let C be a timelike geodesic congruence defined along λ.

A universe that has been expanding on average throughout its history
cannot be infinite in the past but must have a beginning.

**If the expansion rate of $\mathcal{C}$ averaged along λ is positive,
then λ must be past-incomplete.**

Space Time Theorems

I. Theorems About Cosmic Origins, Singularities, and Time

1. Hawking–Penrose Singularity Theorems (1965–1970)

Status: Foundational (more fundamental than BGV)

What they say:

Under very general physical conditions, including reasonable energy conditions and causal structure, spacetime must be geodesically incomplete. In cosmological and gravitational-collapse scenarios, this incompleteness is interpreted as the presence of spacetime singularities.

Why they matter:

These theorems provided the first rigorous demonstration that general relativity predicts its own breakdown under physically realistic conditions. They apply directly to Big Bang cosmology and black hole formation and do not rely on inflationary assumptions.

Relation to BGV:

The Hawking–Penrose theorems rely on stronger energy conditions but are narrower in scope. By contrast, BGV weakens the assumptions while extending applicability to inflationary spacetimes.

---

2. Borde–Guth–Vilenkin (BGV) Theorem (2003)

What it says:

Any universe that has, on average, a positive Hubble expansion along a past-directed timelike or null geodesic is geodesically past-incomplete, regardless of energy conditions.

Why it matters:

This result applies even when the classical energy conditions required by the Hawking–Penrose theorems fail. It encompasses eternal inflation, cyclic models, and emergent-universe scenarios, and it does not assume Einstein's field equations.

Key distinction:

The BGV theorem is kinematic rather than dynamical, relying only on spacetime expansion properties rather than gravitational field equations.

---

3. Raychaudhuri Equation (Theorem-like Role)

Status: Structural backbone of singularity proofs

What it says:

The Raychaudhuri equation governs the evolution of geodesic congruences and shows that, under attractive gravity, initially converging geodesics inevitably focus, leading to caustics and geodesic incompleteness.

Why it matters:

This equation underlies all modern singularity theorems. It connects expansion, shear, vorticity, and energy conditions, and explains why singularities arise generically rather than as exceptional solutions.

In this work:

The Raychaudhuri equation serves as the mathematical engine behind both the Hawking–Penrose and BGV theorems.

II. Theorems That Constrain Cosmological Models

4. Cosmic No-Hair Theorem

What it says:

Universes with a positive cosmological constant evolve toward de Sitter–like states, dynamically suppressing initial anisotropies and inhomogeneities.

Why it matters:

This theorem explains the observed large-scale isotropy of the universe and provides theoretical support for both inflationary dynamics and late-time cosmic acceleration.

Connection to BGV:

The Cosmic No-Hair theorem explains why inflation works locally even if inflationary spacetimes remain past-incomplete globally, as indicated by BGV.

---

5. Ehlers–Geren–Sachs (EGS) Theorem

What it says:

If all fundamental observers measure an exactly isotropic cosmic microwave background, then the spacetime geometry must be Friedmann–Lemaître–Robertson–Walker (FLRW), under mild physical assumptions.

Why it matters:

This theorem provides a direct observational justification for the cosmological principle and links CMB isotropy to large-scale spacetime geometry.

Role in cosmology:

EGS elevates the use of FLRW geometry from a philosophical assumption to an empirical inference.

---

6. Almost–Ehlers–Geren–Sachs (Almost-EGS) Theorem

What it says:

If the cosmic microwave background is nearly isotropic for all observers, then the universe must be close to an FLRW spacetime.

Why it matters:

This theorem extends EGS to realistic observational conditions, where small anisotropies are present, and justifies perturbative treatments of cosmological structure.

Role in cosmology:

Almost-EGS bridges idealized exact results with real CMB measurements.

III. Theorems About Perturbations and Structure Formation

7. Sachs–Wolfe Theorem

What it says:

Gravitational potential fluctuations at the surface of last scattering produce temperature anisotropies in the cosmic microwave background on large angular scales.

Why it matters:

This theorem establishes a direct link between general-relativistic perturbations and observable CMB anisotropies and explains the low-multipole plateau in the CMB temperature power spectrum.

Cosmological significance:

It connects primordial curvature perturbations to late-time observables.

---

8. Weinberg Adiabatic Mode Theorem

What it says:

Certain long-wavelength adiabatic perturbation modes remain conserved outside the cosmological horizon.

Why it matters:

This conservation law justifies extrapolating primordial perturbations from inflationary epochs to recombination and beyond.

Role in cosmology:

The theorem underpins the robustness of inflationary predictions and the near scale-invariance of large-scale structure.

IV. Theorems About Expansion and Distance Measures

9. Etherington Reciprocity Theorem (Distance Duality)

What it says:

In any metric theory of gravity where photon number is conserved, the luminosity distance D_L and angular-diameter distance D_A are related by

$D_L = (1+z)^2 D_A$.

Why it matters:

This theorem links independent cosmological distance measures and provides a powerful observational consistency test.

Observational relevance:

Violations would signal exotic physics such as photon non-conservation or non-metric gravity.

10. Friedmann Theorem (FLRW Uniqueness)

What it says:

Assuming large-scale homogeneity and isotropy, the FLRW metric is the unique solution of Einstein's field equations.

XXXIV. Modified Gravity

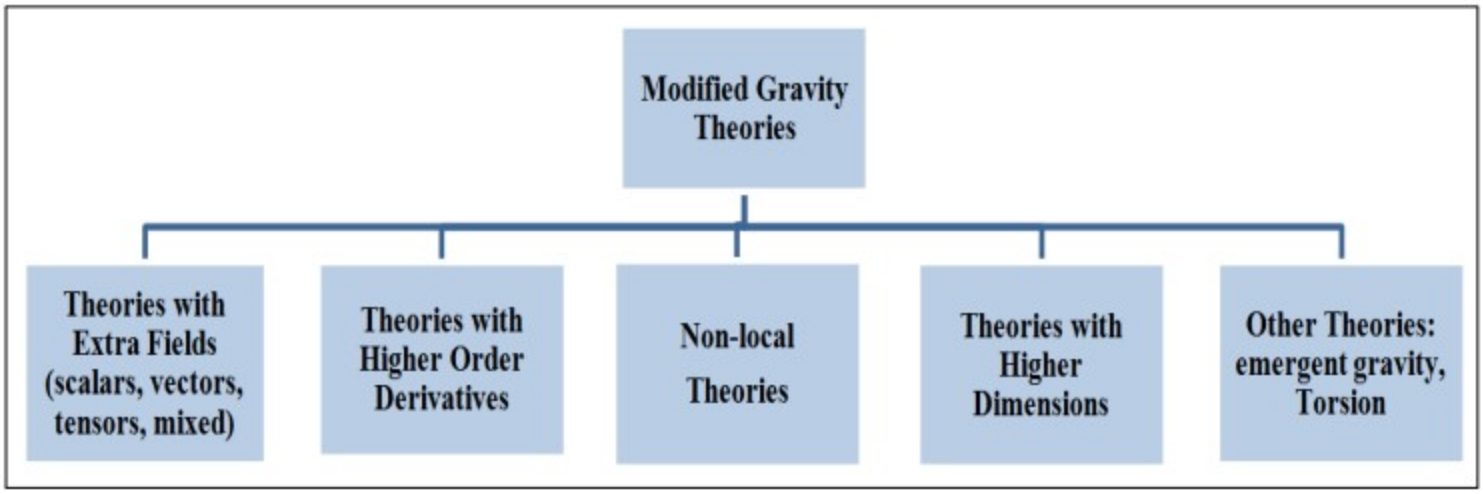

1. $f(R)$ Gravity

Core Idea

$f(R)$ gravity generalizes Einstein's theory by replacing the Ricci scalar R in the Einstein–Hilbert action with a nonlinear function $f(R)$. Instead of gravity being determined purely by spacetime curvature proportional to R, the dynamics now include higher-order curvature effects that become important at cosmological scales.

Mathematical Structure

The action is:

$$S = \frac{1}{16\pi G}\int d^4x\sqrt{-g}\,f(R) + S_{\text{matter}}$$

This leads to fourth-order field equations, introducing an effective scalar degree of freedom often called the *scalaron*.

Cosmological Motivation

Certain choices of $f(R)$ naturally produce late-time cosmic acceleration **without invoking a cosmological constant**. The acceleration arises from modified gravitational dynamics rather than vacuum energy.

Observational Consequences

- Modified growth rate of structure
- Scale-dependent gravitational strength
- Deviations in weak lensing and galaxy clustering
- Can mimic ΛCDM expansion while altering growth

Viability and Challenges

- Must reduce to GR in the Solar System (via *chameleon screening*)
- Many functional forms ruled out by stability and laboratory tests
- Still viable in restricted parameter space

Status

One of the most studied and mathematically well-defined alternatives to ΛCDM.

2. Scalar–Tensor Gravity (Brans–Dicke and Extensions)

Core Idea

Gravity is mediated not only by the metric tensor but also by a scalar field ϕ that modulates the effective gravitational constant:

$$G_{\text{eff}} \propto \frac{1}{\phi}$$

Mathematical Structure

The Brans–Dicke action:

$$S = \int d^4x\sqrt{-g}\left[\phi R - \frac{\omega}{\phi}(\nabla\phi)^2\right] + S_{\text{matter}}$$

Modern versions generalize this to arbitrary coupling functions and potentials.

Cosmological Motivation

- Natural in higher-dimensional and string theories
- Allows time-varying gravitational strength
- Can explain cosmic acceleration through scalar dynamics

Observational Consequences

- Alters expansion history $H(z)$
- Changes growth of structure and lensing kernels
- Strongly constrained by Solar System tests

Viability and Challenges

- Brans–Dicke parameter ω must be very ↓ je ($\omega \gg 10^4$)
- Screening mechanisms required (chameleon, symmetron)

3. DGP Gravity (Extra-Dimensional Gravity)

Core Idea

The universe is a 4-dimensional brane embedded in a 5-dimensional bulk. Gravity behaves as:

- 4D at short distances
- 5D at cosmological scales

Mathematical Structure

The action includes both 4D and 5D Einstein–Hilbert terms:

$$S = M_5^3 \int d^5x\sqrt{-g_5}R_5 + M_4^2 \int d^4x\sqrt{-g_4}R_4$$

Cosmological Motivation

The leakage of gravity into extra dimensions can produce **self-acceleration** without dark energy.

Observational Consequences

- Modified expansion history
- Suppressed growth of structure
- Distinct weak-lensing signatures

Viability and Challenges

- Self-accelerating branch contains ghost instabilities
- Tightly constrained by large-scale structure data

Conceptually influential but largely ruled out in its simplest form.

4. MOND and Relativistic Extensions (TeVeS)

Core Idea

MOND modifies Newton's law at extremely low accelerations:

$$a \ll a_0 \sim 10^{-10}\,\mathrm{m/s^2}$$

This eliminates the need for dark matter in galaxies.

Mathematical Structure

Nonlinear modification of Poisson's equation; relativistic completion achieved via **TeVeS**, which includes:

- Tensor field (metric)
- Vector field
- Scalar field

Cosmological Motivation

- Explains galaxy rotation curves naturally
- Predicts the baryonic Tully–Fisher relation

Observational Consequences

- Excellent galaxy-scale fits
- Weak lensing often requires additional fields or dark components
- Difficulty fitting CMB and large-scale structure

Viability and Challenges

- Struggles at cluster and cosmological scales
- Requires tuning or additional dark fields

Status

Successful phenomenologically at galactic scales; problematic cosmologically.

5. Massive Gravity (and Bimetric Gravity)

Core Idea

The graviton is given a **nonzero mass**, altering gravity on large scales and weakening it at cosmological distances.

Mathematical Structure

Modern ghost-free massive gravity (dRGT) introduces a reference metric $f_{\mu\nu}$ in addition to the physical metric $g_{\mu\nu}$.
Bimetric gravity allows both metrics to be dynamical.

Cosmological Motivation

- Late-time acceleration emerges from graviton mass
- No vacuum energy required

Observational Consequences

- Modified gravitational wave propagation
- Scale-dependent growth of structure
- Strong lensing and ISW effects altered

Viability and Challenges

- Stability constraints are severe
- Parameter space tightly limited by GW observations

Status

Theoretically elegant; observationally constrained but not ruled out.

XXXV. In the Realm of the Hubble tension − a Review of Solutions

arXiv:2103.01183v3 [astro-ph.CO] 5 Jun 2021

The simplest ΓCDM model provides a good fit to a large span of cosmological data but harbors large areas of phenomenology and ignorance. With the improvement of the number and the accuracy of observations, discrepancies among key cosmological parameters of the model have emerged.

The most statistically significant tension is the 4σ to 6σ disagreement between predictions of the Hubble constant, H_0, made by the early time probes in concert with the "vanilla" ΓCDM Cosmological model, and a number of late time, model-independent determinations of H_0 from local measurements of distances and redshifts.

The high precision and consistency of the data at both ends present strong challenges
to the possible solution space and demands a hypothesis with enough rigor to explain multiple observations – whether these invoke new physics, unexpected large-scale structures or multiple, unrelated errors.
We present a summary of the proposed theoretical solutions is presented in the following page.

We classify the many proposals to resolve the tension in these categories:
Early Dark Energy, Late Dark Energy, Dark energy models with 6 degrees of freedom and their extensions, Models with extra relativistic degrees of freedom, Models with Extra Interactions, Unified cosmologies, Modified gravity, Inflationary models, Modified recombination history, Physics of the critical Phenomena, and Alternative proposals. Some are formally successful, improving the fit to the data in light of their additional degrees of freedom, restoring agreement within 1 to 2σ between Planck 2018, using the Cosmic Microwave Background power spectra data, Baryon Acoustic Oscillations, Pantheon SN data, and R20, the latest SH0ES Team measurement of the Hubble constant

($H_0 = 73.2 \pm 1.3$ km s^{-1} Mpc^{-1} at **68% Confidence Level, CL**).

However, there are many more unsuccessful models which leave the discrepancy well above the 3σ disagreement level. In many cases, reduced tension comes not simply from a change in the value of H_0
but also due to an increase in its uncertainty due to degeneracy with additional physics, complicating the picture and pointing to the need for additional probes. While no specific proposal makes a strong case for being highly likely or far better than all others we list some solutions as follows:

Solutions involving

- **early or dynamical dark energy,**
- **neutrino interactions,**
- **interacting cosmologies,**
- **primordial magnetic fields, and**
- **modified gravity**

provide the best options at 68% CL until a better alternative comes along.

In the Whisker Plot below

the cyan vertical band corresponds to the H_0 value from SH0ES Team

($R20$, $H_0 = 73.2 \pm 1.3$ km s^{-1} Mpc^{-1} at 68% CL)

and the light pink vertical band corresponds to the H_0 value as reported by Planck 2018 team.

Alternatives to ΛCDM

Alternative	CMB	H_0 Tension	Structure Formation
Early Dark Energy	Modified power spectrum	Increases H_0	Small effect
Phantom or dynamical Dark Energy	Modified power spectrum	Increases H_0	Small effect
Interactions between Dark Matter and Dark Energy	Modified power spectrum	Can increase H_0	Small effect
Modified Gravity Theories	Departs from ΛCDM	Can increase H_0	Altered growth of structures
Decaying or Self-Interacting Dark Matter	Modified power spectrum	Varied	Can be suppressed

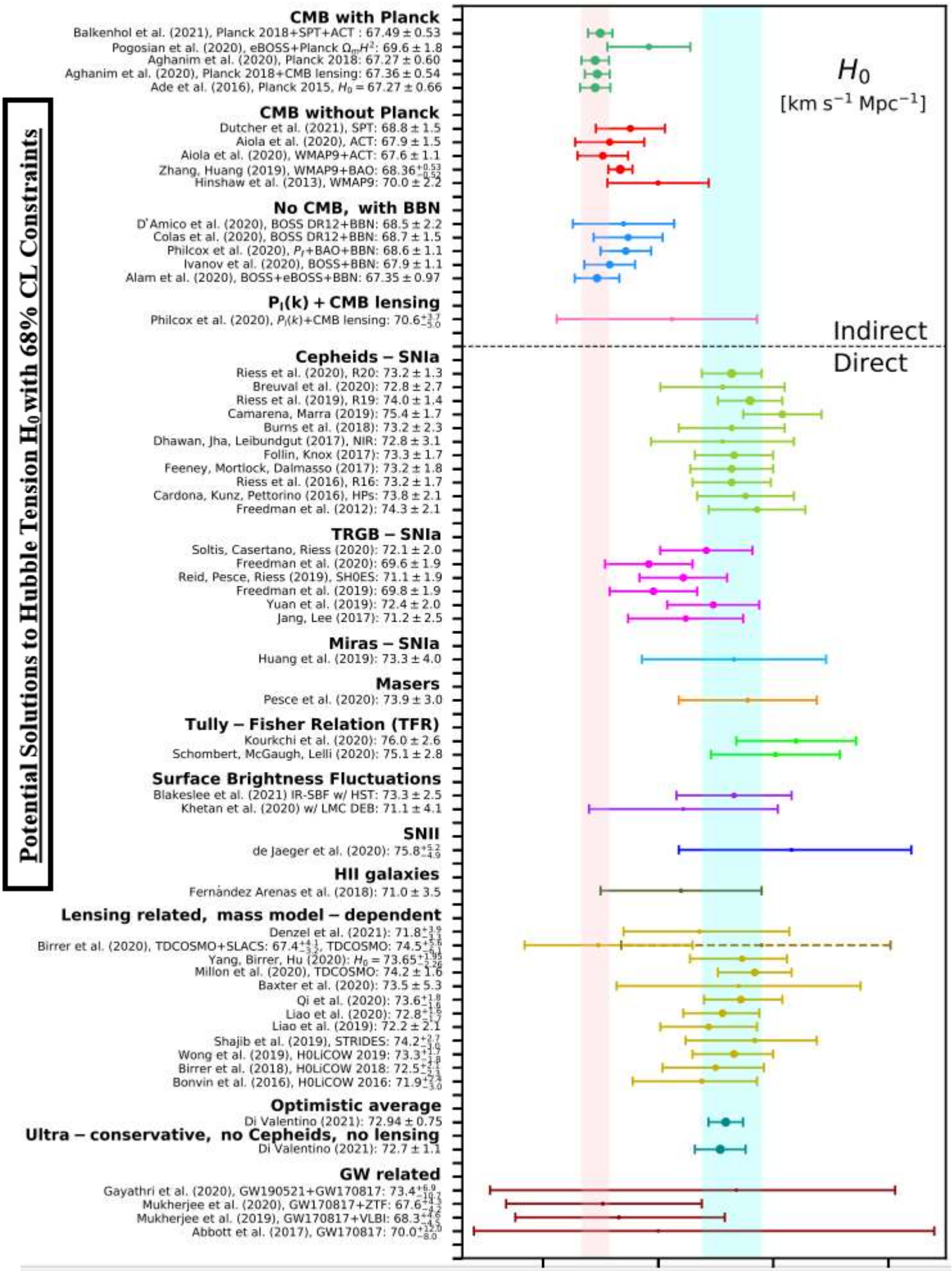
Potential Solutions to Hubble Tension H_0 with 68% CL Constraints
CMB with Planck
Balkenhol et al. (2021), Planck 2018+SPT+ACT : 67.49 ± 0.53
Pogosian et al. (2020), eBOSS+Planck $\Omega_m h^2$: 69.6 ± 1.8
Aghanim et al. (2020), Planck 2018: 67.27 ± 0.60
Aghanim et al. (2020), Planck 2018+CMB lensing: 67.36 ± 0.54
Ade et al. (2016), Planck 2015, H_0 = 67.27 ± 0.66
CMB without Planck
Dutcher et al. (2021), SPT: 68.8 ± 1.5
Aiola et al. (2020), ACT: 67.9 ± 1.5
Aiola et al. (2020), WMAP9+ACT: 67.6 ± 1.1
Zhang, Huang (2019), WMAP9+BAO: $68.36^{+0.53}_{-0.52}$
Hinshaw et al. (2013), WMAP9: 70.0 ± 2.2
No CMB, with BBN
D'Amico et al. (2020), BOSS DR12+BBN: 68.5 ± 2.2
Colas et al. (2020), BOSS DR12+BBN: 68.7 ± 1.5
Philcox et al. (2020), P_l+BAO+BBN: 68.6 ± 1.1
Ivanov et al. (2020), BOSS+BBN: 67.9 ± 1.1
Alam et al. (2020), BOSS+eBOSS+BBN: 67.35 ± 0.97
$P_l(k)$ + CMB lensing
Philcox et al. (2020), $P_l(k)$+CMB lensing: $70.6^{+3.7}_{-5.0}$
H_0
[km s^{-1} Mpc^{-1}]
Indirect
Direct
Cepheids − SNIa
Riess et al. (2020), R20: 73.2 ± 1.3
Breuval et al. (2020): 72.8 ± 2.7
Riess et al. (2019), R19: 74.0 ± 1.4
Camarena, Marra (2019): 75.4 ± 1.7
Burns et al. (2018): 73.2 ± 2.3
Dhawan, Jha, Leibundgut (2017), NIR: 72.8 ± 3.1
Follin, Knox (2017): 73.3 ± 1.7
Feeney, Mortlock, Dalmasso (2017): 73.2 ± 1.8
Riess et al. (2016), R16: 73.2 ± 1.7
Cardona, Kunz, Pettorino (2016), HPs: 73.8 ± 2.1
Freedman et al. (2012): 74.3 ± 2.1
TRGB − SNIa
Soltis, Casertano, Riess (2020): 72.1 ± 2.0
Freedman et al. (2020): 69.6 ± 1.9
Reid, Pesce, Riess (2019), SH0ES: 71.1 ± 1.9
Freedman et al. (2019): 69.8 ± 1.9
Yuan et al. (2019): 72.4 ± 2.0
Jang, Lee (2017): 71.2 ± 2.5
Miras − SNIa
Huang et al. (2019): 73.3 ± 4.0
Masers
Pesce et al. (2020): 73.9 ± 3.0
Tully − Fisher Relation (TFR)
Kourkchi et al. (2020): 76.0 ± 2.6
Schombert, McGaugh, Lelli (2020): 75.1 ± 2.8
Surface Brightness Fluctuations
Blakeslee et al. (2021) IR-SBF w/ HST: 73.3 ± 2.5
Khetan et al. (2020) w/ LMC DEB: 71.1 ± 4.1
SNII
de Jaeger et al. (2020): $75.8^{+5.2}_{-4.9}$
HII galaxies
Fernández Arenas et al. (2018): 71.0 ± 3.5
Lensing related, mass model − dependent
Denzel et al. (2021): $71.8^{+3.9}_{-3.3}$
Birrer et al. (2020), TDCOSMO+SLACS: $67.4^{+4.1}_{-3.2}$, TDCOSMO: $74.5^{+5.6}_{-6.1}$
Yang, Birrer, Hu (2020): $H_0 = 73.65^{+1.95}_{-2.26}$
Millon et al. (2020), TDCOSMO: 74.2 ± 1.6
Baxter et al. (2020): 73.5 ± 5.3
Qi et al. (2020): $73.6^{+1.8}_{-1.6}$
Liao et al. (2020): $72.8^{+1.6}_{-1.7}$
Liao et al. (2019): 72.2 ± 2.1
Shajib et al. (2019), STRIDES: $74.2^{+2.7}_{-3.0}$
Wong et al. (2019), H0LiCOW 2019: $73.3^{+1.7}_{-1.8}$
Birrer et al. (2018), H0LiCOW 2018: $72.5^{+2.1}_{-2.3}$
Bonvin et al. (2016), H0LiCOW 2016: $71.9^{+2.4}_{-3.0}$
Optimistic average
Di Valentino (2021): 72.94 ± 0.75
Ultra − conservative, no Cepheids, no lensing
Di Valentino (2021): 72.7 ± 1.1
GW related
Gayathri et al. (2020), GW190521+GW170817: $73.4^{+6.9}_{-10.7}$
Mukherjee et al. (2020), GW170817+ZTF: $67.6^{+4.3}_{-4.2}$
Mukherjee et al. (2019), GW170817+VLBI: $68.3^{+4.6}_{-4.8}$
Abbott et al. (2017), GW170817: $70.0^{+12.0}_{-8.0}$

Reference List

Foundational Relativity & Cosmology

1. Einstein, A. *The Foundation of the General Theory of Relativity.* Annalen der Physik, 1916.
2. Einstein, A. *Cosmological Considerations on the General Theory of Relativity.* 1917.
3. Schwarzschild, K. *Über das Gravitationsfeld eines Massenpunktes.* 1916.
4. Friedmann, A. *On the Curvature of Space.* Zeitschrift für Physik, 1922.
5. Friedmann, A. *On the Possibility of a World with Negative Curvature.* 1924.
6. Lemaître, G. *Un univers homogène de masse constante et de rayon croissant.* 1927.
7. de Sitter, W. *On Einstein's Theory of Gravitation.* 1917.
8. Weinberg, S. *Gravitation and Cosmology.* Wiley, 1972.
9. Peebles, P. J. E. *Principles of Physical Cosmology.* Princeton Univ. Press, 1993.

Cosmic Expansion, H_0'30, Distance Ladder

10. Slipher, V. *Spectrographic Observations of Nebulae.* Lowell Observatory, 1912.
11. Hubble, E. *A Relation Between Distance and Radial Velocity Among Extra-Galactic Nebulae.* PNAS, 1929.
12. Hubble, E., & Humason, M. *The VelocityDistance Relation.* ApJ, 1931.
13. Sandage, A. *Cosmology: A Search for Two Numbers.* 1970.
14. Hubble Space Telescope Key Project. *A Measurement of the Hubble Constant.* ApJ 553, 2000.
15. Riess, A. G., et al. *Observational Evidence from Supernovae for an Accelerating Universe.* AJ, 1998.
16. Baade, W., & Zwicky, F. *On Supernovae.* 1934.
17. Leavitt, H. S. *Periods of 25 Variable Stars.* 1912.
18. Tully, R. B., & Fisher, J. R. *A New Method of Determining Distances to Galaxies.* 1977.
19. Carroll, B. W., & Ostlie, D. A. *Modern Astrophysics.* 2007.

Cosmic Microwave Background (CMB)

20. Gamow, G. *The Origin of Elements and Separation of Galaxies.* 1948.
21. Alpher, R. A., Bethe, H., & Gamow, G. *Origin of the Chemical Elements.* 1948.
22. Penzias, A. A., & Wilson, R. W. *A Measurement of Excess Antenna Temperature at 4080 Mc/s.* 1965.
23. COBE Collaboration. *Detection of CMB Anisotropies.* 1992.
24. BOOMERanG Collaboration. *Balloon Observations of Millimetric Radiation.* 19982000.
25. MAXIMA Collaboration. *High-Resolution CMB Observations.* 2000.
26. WMAP Collaboration. *Wilkinson Microwave Anisotropy Probe 9-Year Results.* 20032013.
27. Planck Collaboration. *Planck 2018 Cosmological Parameters.* A&A, 2018.

Large-Scale Structure & Galaxy Surveys

28. Sloan Digital Sky Survey (SDSS). *Data Releases on Galaxy Structure.* 2000present.
29. 2dF Galaxy Redshift Survey (2dFGRS). *Two-Degree Field Spectroscopic Survey.* 19952002.
30. Dark Energy Survey (DES). *Five-Year Supernova and Weak Lensing Results.* 2013present.
31. BOSS/eBOSS (SDSS-III/IV). *Baryon Acoustic Oscillations (BAO) Measurements.*
32. Euclid Mission (ESA). *Dark Energy and Structure Formation Mission.* 2023present.

Early Universe Physics & Nucleosynthesis

33. Alpher, R., & Herman, R. *Theory of the Origin of Chemical Elements.* 1950.
34. Mukhanov, V. *Physical Foundations of Cosmology.* Cambridge Univ. Press, 2005.
35. Kolb, E. W., & Turner, M. S. *The Early Universe.* Addison-Wesley, 1990.
36. Particle Data Group (PDG). *Review of Particle Physics.* Annual.

Inflation, ΛCDM Theory, Cosmological Problems

37. Guth, A. H. *Inflationary Universe: A Possible Solution to Cosmological Problems.* 1981.
38. Linde, A. *Chaotic Inflation.* 1982.
39. Borde, A., Guth, A. H., & Vilenkin, A. *Inflationary Spacetimes Are Incomplete.* PRL 90, 2003.
40. Steinhardt, P. J., & Turok, N. *Critiques of Inflation and Cyclic Models.* 2002.
41. Perlmutter, S., et al. *Measurements of Ω and Λ from 42 High-Redshift SNe.* ApJ 517, 1999.
42. Perivolaropoulos, L., & Skara, F. *Challenges for ΛCDM: An Update.* arXiv:2105.05208, 2022.
43. Verde, L., Treu, T., & Riess, A. G. *The Hubble Tension: Current Status.* 2019.
44. Di Valentino, E., et al. *Cosmology Interrogating the Hubble Tension.* 2021.

Dark Matter, Galaxy Rotation Curves

45. Zwicky, F. *The Redshift of Extragalactic Nebulae.* 1933.
46. Rubin, V., & Ford, W. *Rotation of the Andromeda Galaxy.* 1970.
47. Navarro, J. F., Frenk, C. S., & White, S. D. M. *A Universal Density Profile.* ApJ, 1997.
48. Bullock, J., & Boylan-Kolchin, M. *Small-Scale Challenges to ΛCDM.* 2017.

JWST Discoveries & High-Redshift Galaxies

49. JWST Collaboration. *Early Release Science.* 2021present.
50. JADES Collaboration. *Galaxies at z > 1015 Including JADES-GS-z14-0.* 2023.
51. JWST/NIRSpec & NIRCam Instrument Teams. *Spectral and Imaging Constraints on Early Structure.*

Fine Structure Constant & Fundamental Physics

52. Gutiérrez, C. M., & López-Corredoira, M. *Variation of Fine Structure Constant Over Cosmological Times.* ApJ 713, 2010.
53. Uzan, J-P. *Fundamental Constants and Their Variation.* Reviews of Modern Physics, 2003.

Text Books

1. *Redeeming Mathematics,* Vern S. Poythress
2. *Introduction to Cosmology,* B. Ryden, 2006
3. *Cosmological Physics*, Peacock 1990
3. *Cosmological Physics*, Peacock 1990
4. *Physical Foundations of Cosmology*, V. Mukhanov, 2005
5. *Galaxies and Cosmology* - Caltech Lectures, Djorgovski

I. Simple Lunar Trajectories: Kepler's Elliptical Model (Planar Point Mass)

This Section on Kepler is shown for historical interest. Newton's Dynamics is used in all the following Sections

Kepler's E Model (Planar Point Mass 2 Body): **See** the **Glossary** and **Figures** in **last two pages** of this Study

Convert Cartesian Ellipse Eq. in (x,y) to polar (r,v) coordinates $\left(\frac{x}{a}\right)^2+\left(\frac{y}{b}\right)^2=1$ $r(\nu,e):=\frac{a\cdot\left(1-e^2\right)}{1+e\cdot\cos\left(\nu-\frac{\pi}{2}\right)}$

Ellipse is relative to the **focus**

$x(a,\theta):=a\cdot\cos(\theta)$ and $y(b,\theta):=b\cdot\sin(\theta)$

$0\le t<2\pi$ $e=\frac{c}{a}$ $r(x,y):=\sqrt{x^2+y^2}$ and $\theta(x,y):=\operatorname{atan}\left(\frac{y}{x}\right)$

For the moon

$e_m:=.0549$ $d_m:=384400\text{km}$ $d_{ap}:=406603\text{km}$ $m_m:=7.347\cdot10^{22}\text{kg}$ $a_m:=\frac{d_{ap}}{1+e}$ $\mu:=3.986\cdot10^5\frac{\text{km}^3}{\text{sec}^2}$

For the Earth: Mass $m_e:=5.972\cdot10^{24}\text{kg}$ Note: a and b are distances from the center, c

The parameter e is known as the eccentricity. The value of this parameter defines the shape of our orbit. Depending on the value of e there are four kinds of shapes (conic sections), which means there are four kinds of orbits: circle, ellipse, parabola, and hyperbola, for e = 0, < 1, = 1, and > 1, respectively.

$H\equiv1$ $e_e:=.6$ $e_c:=0$ $e_h:=2$ $e_p:=1.000$ $\theta:=0,0.01..2\pi$ $G\cdot m_e=3.985\times10^{14}\frac{\text{m}^3}{\text{s}^2}$

Basics from Newton's Laws: Energy, Momentum, Parameters of Ellipse $r_o:=300\text{km}$ $\phi_o:=0$

$\text{Energy}(v,r):=\frac{v^2}{2}-\frac{\mu}{r}$ $h\left(v_o,r_o,\phi_o\right):=r_o\cdot v_o\cdot\cos\left(\phi_o\right)$ $h=r^2\cdot v\nu^2$ $h_u(p):=\sqrt{\mu\cdot p}$

$p\left(v_o\right):=\frac{h\left(v_o,r_o,\phi_o\right)^2}{\mu}$ $a\left(v_o\right):=\frac{-\mu}{\text{Energy}\left(v_o,r_o\right)}$ $e_{traj}(v,a):=\sqrt{1-\frac{p(v)}{a}}$

Period of Moon Sat Orbit

$T:=2\cdot\pi\cdot\sqrt{\frac{a_m^3}{G\cdot m_e}}=99.98\cdot\text{hr}$

$r_h(\theta,e):=\frac{H}{1+e\cdot\cos\left(\theta+\frac{\pi}{2}\right)}$

If we can Solve for Eccentric Anomaly, E, we get Time of Flight, TOF, t - T

$\cos(\nu)=\frac{p-r}{e\cdot r}$ $\nu(p,r,e):=\operatorname{acos}\left(\frac{p-r}{e\cdot r}\right)$

Recursion for Eccentric Anomaly, M & E (Deg)

mean anomaly M (in deg (0<= M<=360)

$MA\left(M_o,t,t_o\right):=M_o+\sqrt{\frac{\mu}{a_m^3}}\cdot\left(t-t_o\right)$

```
EcA(e, M, dp) :=
    mx_it ← 30
    i ← 0
    K ← π / 180
    del ← 10^(−dp)
    m ← M / 360
    m ← 2·π·(m − floor(m))
    E ← m  if e < 0.8
    E ← π  otherwise
    F ← E − e·sin(m) − m
    while |F| > del ∧ i < mx_it
        E ← E − F / (1 − e·cos(E))
        F ← E − e·sin(E) − m
        i ← i + 1
    E ← E / K
```

Plot of Conic Orbits: c, e, p, h

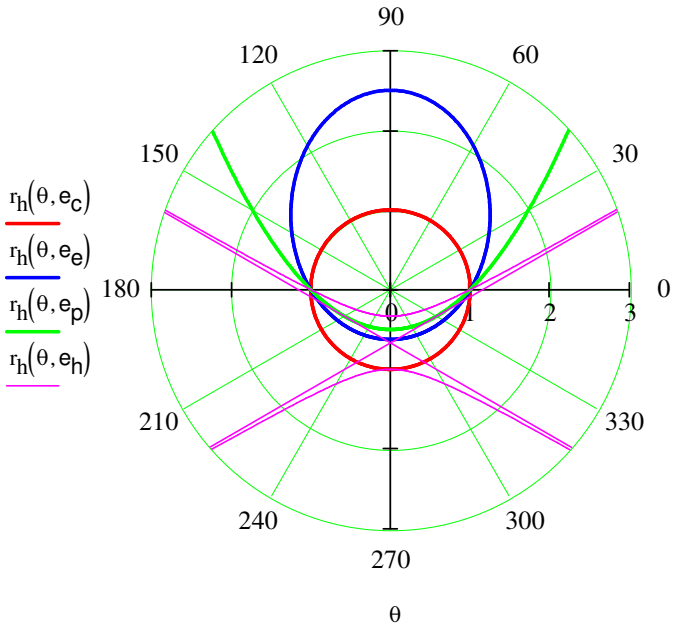

t/T: $\frac{27}{360}=0.075$ $\text{EcA}\left(e_m,27,5\right)=28.501$

Find E and ϕ In Degrees

$\phi(e,\text{EcA}):=90-\frac{180\cdot\operatorname{atan2}\left(\sqrt{1-e^2}\cdot\sin(\text{EcA}),\cos(\text{EcA})-e\right)}{\pi}$

$\phi(0.977,48.43418\cdot\text{deg})=153.029$

The Patched Conic Section Approximation for Finding a Lunar Trajectory

The Patched Conic Method is an Approximation for finding a trajectory by dividing space between the sphere of influence (SOI) of the earth, Lunar Earth Orbit (LEO) and the SOI region of the moon.

When the spacecraft is within the sphere of influence of the moon, only the gravitational force between the spacecraft and the moon is considered, otherwise the gravitational force between the spacecraft and the earth is used. This reduces a complicated n-body problem to multiple two-body problems, for which the solutions are the well-known conic sections of the Kepler orbits. Below is an example composite solution.

See for Example:
Optimal Two-Impulse Trajectories with Moderate Flight Time for Earth-Moon Missions,
Sandro da Silva Fernandes
Mathematical Problems in Engineering
Vol. 2012, Article ID 971983,
or
Bate, R. R., D. D. Mueller, and J. E. White,
Fundamentals of Astrodynamics

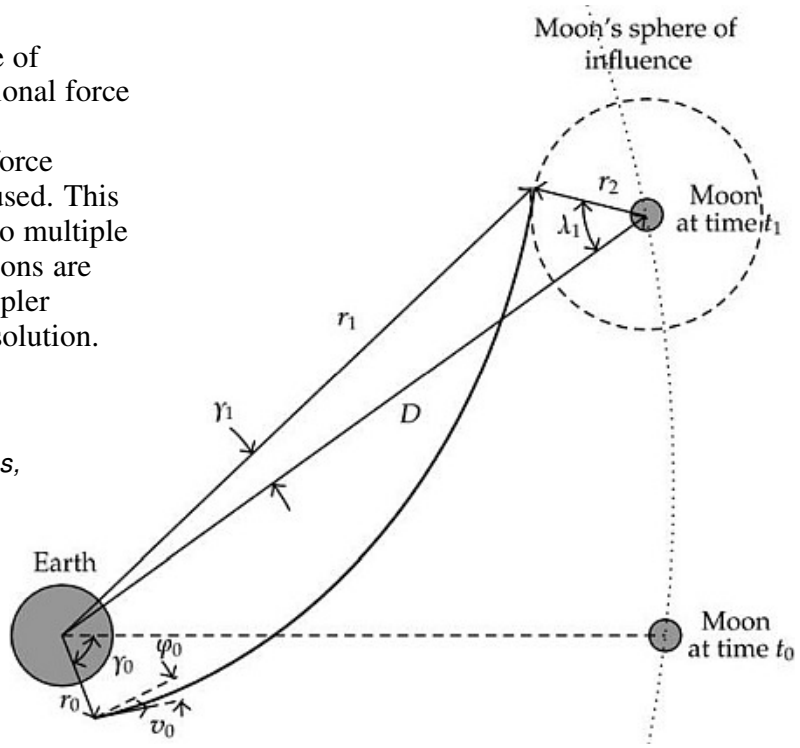

Rather than dealing with large powers of 10, we can use **Astronomical Units**, for distance, velocity, time: AU, VU, TU. Where AU is the mean distance of the earth to the sun and DU is the radius of the earth. TU is the time unit. Then the velocity unit, (VU) is equal to DU/TU.

$DU := 6378.145km$ $AU := 1.496 \cdot 10^8 km$ $kmps := \frac{km}{s}$ $VU := 7.905368kmps$ $TU := 806.8s$ $D := d_m$

Laplace's Equation for Moon's Sphere of Influence:
this is about 1/6 of the distance, D, to the moon

$$R_{sif} := D \cdot \left(\frac{m_m}{m_e}\right)^{0.4} \qquad R_s := 66300km \qquad R_s = 10.395 \cdot DU$$

The conic patched problem for finding a trajectory can be stated as follows:

Given: Initial rocket launch conditions in the earth's sphere of Influence, that is, initial position, velocity, flight path angle, and phase angle: r_0, v_0 ϕ_0, **and** γ_0 ,
The three quntities r_0, v_0 ϕ_0 will give us initial energy and anglular momentum.

Find: Arrival conditions at moon's Sphere of Influence: r_1, v_1 ϕ_1, λ_1. **r_0, v_0 ϕ_0, and λ_1**

The problem with assigning these initial points is that they may not give a satisfactory solution to match the arrival conditions. Our strategy is to use the arrival ange λ_1 to the moon's SOI as one of the independent condition
.

Given the 3 initial conditions and one arrival condition as our **independent variables:**
These will move us into the radius of the moon's sphere of influence. Some trial and error may still be required.

EXAMPLE: See Bate, R. R., D. D. Mueller, and J. E. White, *Fundamentals of Astrodynamics*

Solution: Select the **Apollo 11 Flight Conditions** for initial conditions: r_0, v_0, ϕ_0 and λ_1.

Given: $r_0 := DU + 334km$ $v_0 := 10.6kmps$ $\phi_0 := 0deg$ A reasonable angle to arrive at moon $\lambda_1 := 30deg$

Find: r_1, v_1, ϕ_1, γ_1 (the last symbol, γ, is the Greek letter gamma, the Arrival Phase Angle at the Moon)

Initial Energy and Angular Momentum are $Energy(v_0, r_0) = -0.011 \cdot VU^2$ $h_0 := h(v_0, r_0, \phi_0) = 1.441 \cdot \frac{DU^2}{TU}$

$D = 60.268 \cdot DU$ By the Law of Cosines: $r_1(\lambda_1) := \sqrt{D^2 + R_s^2 - 2D \cdot R_s \cdot \cos(\lambda_1)}$ $r1 := r_1(\lambda_1) = 51.529 \cdot DU$

From Law of Conservation of Energy and Momentum: $E_0 := Energy(v_0, r_0)$ $E_0 = -0.011 \cdot \frac{DU^2}{TU^2}$ $h_1 := h_0$

$v_1(r_1) := \sqrt{2 \cdot \left(E_0 + \frac{\mu}{r_1}\right)}$ $v1 := v_1(r1) = 0.128 \cdot VU$ $v1 := 0.1296VU$ $\phi_1 := acos\left(\frac{h_1}{r1 \cdot v1}\right)$ $\phi_1 = 77.542 \cdot deg$

In order to calculate the **Time of Flight**, TOF, to the moon's SOI, we need to Find:

p, a, e, E_0 and E_1 for the Geocentric Trajectory.

$p := \frac{h_0^2}{\mu} = 2.075 \cdot DU$ $a := \frac{-\mu}{2\,Energy(v_0, r_0)}$ $e := \sqrt{1 - \frac{p}{a}}$ $e = 0.977$ $\nu_1 := \nu(p, r1, e)$ $\nu_1 = 2.956$

$\gamma_1 := asin\left(\frac{R_s}{r1} \sin(\lambda_1)\right) = 5.789 \cdot deg$ $a = 44.698 \cdot DU$ since: $\nu_0 := 0$ $EcA_0 := 0$ $EcA_1 := acos\left(\frac{e + \cos(\nu_1)}{1 + e \cdot \cos(\nu_1)}\right)$

$EcA_1 = 1.728$ $TOF := \sqrt{\frac{a^3}{\mu}} \cdot \left[\left(EcA_1 - e \cdot \sin(EcA_1)\right) - \left(EcA_0 - e \cdot \sin(EcA_0)\right)\right]$ $TOF = 51.132 \cdot hr$

We can use the same procedure at the moon (Selenocentric).
See Section XVI for the Newtonian Gravitational Solution for the Lunar Trajectory.
We need to determine the values of v1 and Rs in units based on the moon's gravitational attraction parameters.
The Angular Velocity of the Moon (ω_m) in its orbit is

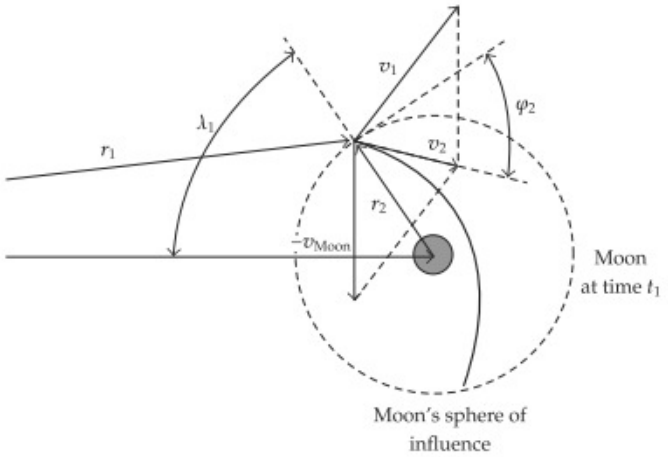

: $\omega_m := 2.649 \cdot 10^{-6} \frac{rad}{s}$ $\omega_m := 2.137 \cdot 10^{-3} \frac{1}{TU}$ $\gamma_0 := \nu_1 - \nu_0 - \gamma_1 - \omega_m \cdot TOF$ $\gamma_0 = 135.637 \cdot deg$

$v_{1m} := 1.024kmps$ $\mu_m := 4093 \frac{km^3}{s^2}$ $v_m := 1.018kmps$ Then $v_{2m} := 1.198kmps$

$\varepsilon_2 := 5.68deg$ $e_m := 2.078$ $r_p := 4105km$ $h_p := 2367km$ $R_s = 10.395 \cdot DU$

$\mu_m := 4.903 \cdot 10^3 \cdot \frac{km^3}{s^2}$

Time of Flight

Develop an algorithm to Calculate Time of Flight

$$\text{TOF}_{alg}(v_0, r_0, \phi_0, \lambda_1) :=$$

$h_0 \leftarrow r_0 \cdot v_0 \cdot \cos(\phi_0)$

$p \leftarrow \dfrac{h_0^{\,2}}{\mu}$

$E_0 \leftarrow \text{Energy}(v_0, r_0)$

$\text{EcA}_0 \leftarrow 0$

$a \leftarrow \dfrac{-\mu}{2E_0}$

$e \leftarrow \sqrt{1 - \dfrac{p}{a}}$

$r1 \leftarrow \sqrt{D^2 + R_s^{\,2} - 2D \cdot R_s \cdot \cos(\lambda_1)}$

$\nu_1 \leftarrow \nu(p, r1, e)$ This gives a different value

$\text{EcA}_1 \leftarrow \text{acos}\left(\dfrac{e + \cos(\nu_1)}{1 + e \cdot \cos(\nu_1)}\right)$

$\text{TOF} \leftarrow \dfrac{\sqrt{\dfrac{a^3}{\mu}} \cdot \left[\left(\text{EcA}_1 - e \cdot \sin(\text{EcA}_1)\right) - \left(\text{EcA}_0 - e \cdot \sin(\text{EcA}_0)\right)\right]}{\text{hr}}$

$A \leftarrow (\text{TOF} \quad e)^T$

$v_0 = 10.846 \cdot \text{kmps}$ $\quad \text{TOF}_{alg}(v_0, r_0, \phi_0, \lambda_1) = \begin{pmatrix} 51.132 \\ 0.977 \end{pmatrix}$

$\text{tof}(v_0) := \text{TOF}_{alg}(v_0, r_0, \phi_0, \lambda_1)_0$ $\quad \text{ecc}(v_0) := \text{TOF}_{alg}(v_0, r_0, \phi_0, \lambda_1)_1$

Initial Conditions: $r_0 = 1.05 \cdot \text{DU}$ $\quad \text{Alititude} := r_0 - 1\text{DU} = 318.907 \cdot \text{km}$ $\quad \phi_0 = 0$

hyperbolic := 1

$v_{inj} := 10.8\text{kmps}, 10.805\text{kmps} .. 11.2\text{kmps}$

Note: As the velocity increases above the minimum 10.8 kmps, the Time of Flight decreases and the trajectory shape changes from Elliptical to Hyperbolic.

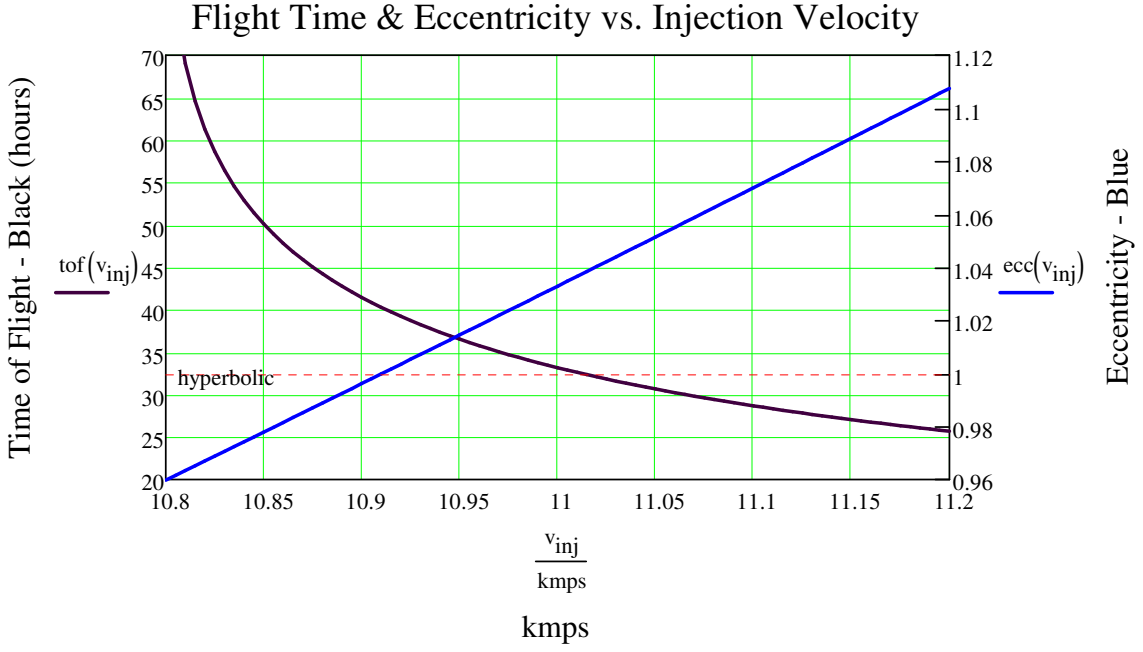

Polar Plot of the Solution for the Patched Conic Lunar Approximation

$\nu := -90.002\text{deg}, -90.001\text{deg} .. 41\text{deg}$ $\quad \chi := 39.5\text{deg}, 39.501\text{deg} .. 360\text{deg}$ $\quad r(\nu) := \frac{a\cdot\left(1-e^2\right)}{1+e\cdot\cos\left(\nu+\gamma_0\right)}$

Note: λ_1 is not = 30 deg $\quad \varphi := 33\text{deg}$ $\quad \text{Earth}(\theta) := 1.5\sin(\theta+\varphi)$ $\quad \theta := 0, 0.001 .. 2\pi$

$r_m := 82$ $\quad a_m := 1.5$ $\quad r_{moon}(\theta,\varphi) := r_m\cdot\cos(\theta-\varphi) + \sqrt{a_m{}^2 - r_m{}^2\sin(\theta-\varphi)^2}$

Radius of Moon Sphere of Influence $\quad r_{msi}(\theta,\varphi) := r_m\cdot\cos(\theta-\varphi) + \sqrt{10.4^2 - r_m{}^2\sin(\theta-\varphi)^2}$

$\xi := 0.05, 0.051 .. \varphi - 0.05$ $\quad r_{m\_path}(\xi) := r_m$

Point of Conic Patch
SpShip := 75.5

$\psi := 0, 0.0017365 .. \varphi$ $\quad r_{line}(\theta) := \frac{0.1}{\sqrt{1-(1\cdot\cos(\theta-\varphi))^2}}$

$\upsilon := 39.5\text{deg}$

Polar Plot: Geocentric Frame - Earth at the Center

From the list of functions shown on the left of the plot below:

r(v) shows the Trajectory Ellipse Conic Ptach in blue, Earth(θ) is at the center in black, $r_{moon}(\theta,\varphi)$ in red is the location of the moon at intercept φ = 33°, $r_{msi}(\theta)$ is the circle in green of the moon's of sphere of influence, $r_{moon}(\theta,0)$ in red is the initial location of the moon at 0°, $r_{m\_path}(\xi)$ is the dotted line path of moon from 0 to φ. r(χ) is the dotted line that shows the elliptical path back to the earth, and r_{line} is the red straight line from earth at center to the moon to show angle λ_1. SpCraft is where SpaceCraft enters the Moon's Sphere of Influence. Point of Conic Patch. Blue dot.

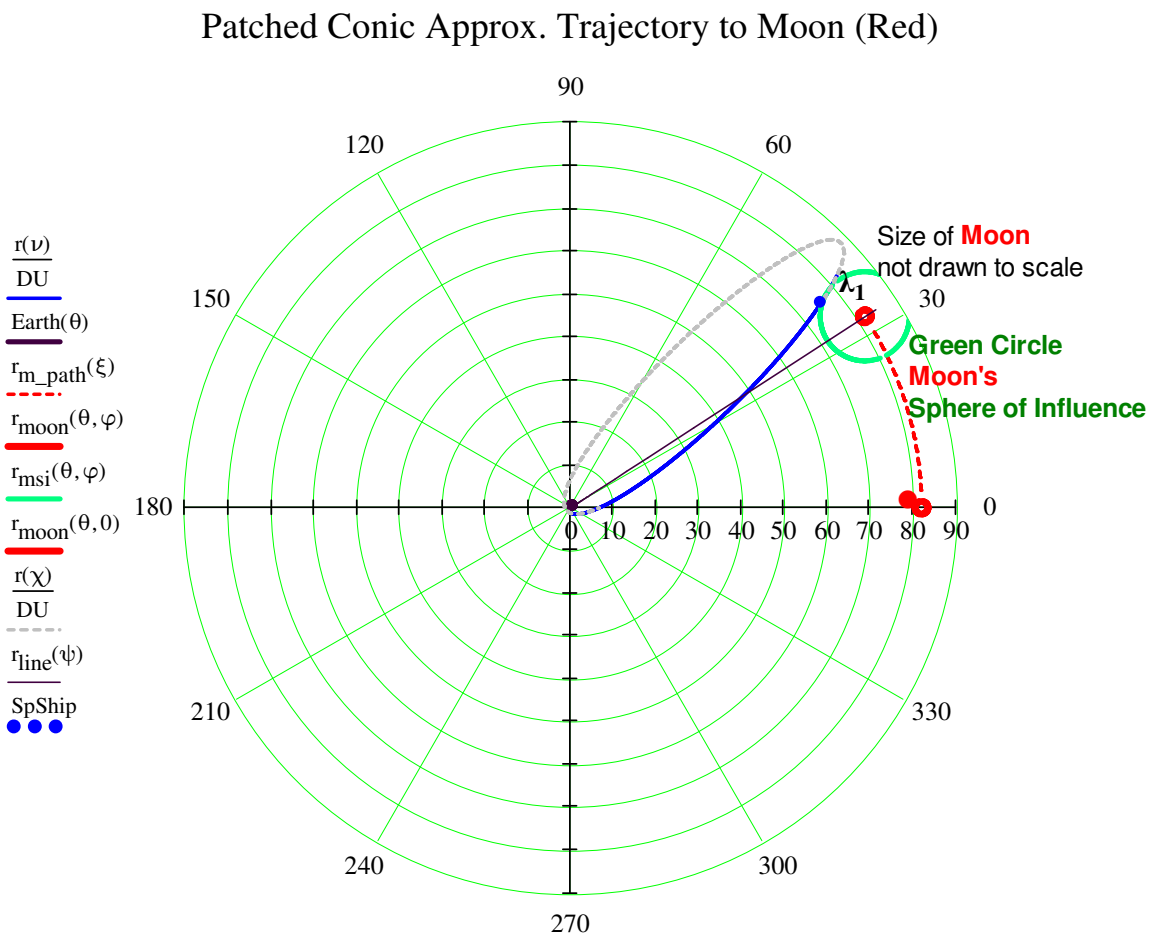

$e := 2.718281828459045$

$\nu, \theta, \xi, \theta, \theta, \theta, \chi, \psi, \upsilon$

IA. Apollo Free Return Trajectory: Simulation for CSM to Moon & Back

Trajectory Model: 3-Body (Earth, Moon, Spacecraft) 2D Planar Point Mass with **Earth at Center**

This 3 body gravitational solution for the FRT uses the Mathcad Differential Equation Solving Methodology discussed:
arXiv:1504.07964
"***Motion of the planets: the calculation and visualization in Mathcad***", Valery Ochkov, Katarina Pisa

The aborted Apollo 13 mission was the only mission to actually turn around the Moon in a free-return trajectory.

Solve the Gravitational and Dynamics Equations for Earth, Moon, & CSM Trajecto

$kg := 1 \quad m := 1 \quad s := 1 \quad N := 1 \quad s := 1 \quad min := 60s \quad hr := 3600s \quad kgf := 9.80665N$

$km := 1000m \quad kmps := km \quad kph := \frac{km}{hr} \quad mph := 0.447 \cdot 10^{-3} kmps \quad G := 6.67384 \cdot 10^{-11} \cdot \frac{N \cdot m^2}{kg}$

Run Simulation for 160 hrs **Apollo 11 Orbit 77 hrs**

$FRAME := 999 \quad n_{ode} := 20000 \quad n := 999 \quad n_{plot} := 10000 \quad t_{end} := \frac{160hr}{n+1} \cdot (FRAME + 1) \quad t_{orb} = 81.44\ hr$

Time of Flight (TOF) = t_{orb}

Trajectory to Moon's Sphere of Influence

Initial x,y Velocity CSM **Radius of Earth** **Apogee to Moon**

$v_{0x} := 6.811kmps \quad v_{0y} := 6.356kmps \quad v_{CSM} := 9.317kmps \quad R_e := 6370km \quad d_{m\_ap} := 405500km$

Define Gravitational and Dynamics Equations for Earth, Moon, and CSM

$$\begin{array}{l} \\ \text{Earth, e} \\ \text{Moon, m} \\ \text{CSM, s} \end{array} \begin{array}{c} \begin{matrix} \text{Mass} & \text{Start position} & & \text{Start Velocity} & \end{matrix} \\ \begin{pmatrix} m_e & x_{e0} & y_{e0} & vx_{e0} & vy_{e0} \\ m_m & x_{m0} & y_{m0} & vx_{m0} & vy_{m0} \\ m_s & x_{s0} & y_{s0} & vx_{s0} & vy_{s0} \end{pmatrix} \end{array} := \begin{pmatrix} 5.972 \cdot 10^{24} kg & 0m & 0m & 0kph & 0kph \\ 7.347 \cdot 10^{22} kg & d_{m\_ap} & 0km & 0kmps & 0.97kmps \\ 13600kg & R_e + 100km & R_e - 100km & v_{0x} & v_{0y} \end{pmatrix}$$

Given **Solve Set of Differential Guidance Equations for 3 Body Problem of Earth, Moon, and CSM**

$x_e(0) = x_{e0} \quad x_{e'}(0) = vx_{e0} \quad y_e(0) = y_{e0} \quad y_{e'}(0) = vy_{e0}$

$$m_e \cdot x_{e''}(t) = \frac{G \cdot m_e \cdot m_m \cdot (x_m(t) - x_e(t))}{\left[\sqrt{(x_e(t) - x_m(t))^2 + (y_e(t) - y_m(t))^2}\right]^3} + \frac{G \cdot m_e \cdot m_s \cdot (x_s(t) - x_e(t))}{\left[\sqrt{(x_e(t) - x_s(t))^2 + (y_e(t) - y_s(t))^2}\right]^3}$$

$$m_e \cdot y_{e''}(t) = \frac{G \cdot m_e \cdot m_m \cdot (y_m(t) - y_e(t))}{\left[\sqrt{(x_e(t) - x_m(t))^2 + (y_e(t) - y_m(t))^2}\right]^3} + \frac{G \cdot m_e \cdot m_s \cdot (y_s(t) - y_e(t))}{\left[\sqrt{(x_e(t) - x_s(t))^2 + (y_e(t) - y_s(t))^2}\right]^3}$$

$x_m(0) = x_{m0} \quad x_{m'}(0) = vx_{m0} \quad y_m(0) = y_{m0} \quad y_{m'}(0) = vy_{m0}$

$$m_m \cdot x_{m''}(t) = \frac{G \cdot m_m \cdot m_e \cdot (x_e(t) - x_m(t))}{\left[\sqrt{(x_m(t) - x_e(t))^2 + (y_m(t) - y_e(t))^2}\right]^3} + \frac{G \cdot m_m \cdot m_s \cdot (x_s(t) - x_m(t))}{\left[\sqrt{(x_m(t) - x_s(t))^2 + (y_m(t) - y_s(t))^2}\right]^3}$$

$$m_m \cdot y_{m''}(t) = \frac{G \cdot m_m \cdot m_e \cdot (y_e(t) - y_m(t))}{\left[\sqrt{(x_m(t) - x_e(t))^2 + (y_m(t) - y_e(t))^2}\right]^3} + \frac{G m_m \cdot m_s \cdot (y_s(t) - y_m(t))}{\left[\sqrt{(x_m(t) - x_s(t))^2 + (y_m(t) - y_s(t))^2}\right]^3}$$

$x_s(0) = x_{s0} \quad x_{s'}(0) = vx_{s0} \quad y_s(0) = y_{s0} \quad y_{s'}(0) = vy_{s0}$

$$m_s \cdot x_{s''}(t) = \frac{G \cdot m_s \cdot m_e \cdot (x_e(t) - x_s(t))}{\left[\sqrt{(x_s(t) - x_e(t))^2 + (y_s(t) - y_e(t))^2}\right]^3} + \frac{G \cdot m_s \cdot m_m \cdot (x_m(t) - x_s(t))}{\left[\sqrt{(x_s(t) - x_m(t))^2 + (y_s(t) - y_m(t))^2}\right]^3}$$

$$m_s \cdot y_{s''}(t) = \frac{G \cdot m_s \cdot m_e \cdot (y_e(t) - y_s(t))}{\left[\sqrt{(x_s(t) - x_e(t))^2 + (y_s(t) - y_e(t))^2}\right]^3} + \frac{G \cdot m_s \cdot m_m \cdot (y_m(t) - y_s(t))}{\left[\sqrt{(x_s(t) - x_m(t))^2 + (y_s(t) - y_m(t))^2}\right]^3}$$

IA. Free Return Trajectory: 3 Body Sim for CSM to the Moon & Back

Trajectory Model: 3-Body (Earth, Moon, Spacecraft) 2D Planar Point Mass with **Earth at Center**

Differential Equation Solver

$$\begin{pmatrix} x_e \\ y_e \\ x_m \\ y_m \\ x_s \\ y_s \end{pmatrix} := \text{Odesolve}\left[\begin{pmatrix} x_e \\ y_e \\ x_m \\ y_m \\ x_s \\ y_s \end{pmatrix}, t, t_{end}, n_{cde}\right]$$

Initial Velocity (km/s) of CSM at an Altitude of 141 km:

$$\sqrt{v_{0x}^2 + v_{0y}^2} = 9.316 \cdot \text{kmps}$$

Distance to the Center of the Moon

$$d_m(t) := \left[\sqrt{(x_m(t) - x_s(t))^2 + (y_m(t) - y_s(t))^2}\right] \qquad \frac{d_m(t_{orb})}{R_m} = 1.619$$

time t_{fly}, just beyond lunar fly by time t_{flydot}

$$t := 0, \frac{t_{end}}{n_{plot}} .. t_{end} \qquad t_{fly} := 0, \frac{t_{end}}{n_{plot}} .. 90hr \qquad t_{fly.} := \frac{x_s(t_{orb})}{R_e}$$

$$vx_s(t) := \frac{d}{dt}x_s(t) \qquad vy_s(t) := \frac{d}{dt}y_s(t) \qquad s(t) := \sqrt{vx_s(t)^2 + vy_s(t)^2}$$

Finding a Free Return Trajectory (FRT) is a little tricky. First, the trajectory must catch the moon at the exact place and time as travels around the earth and then after being swing around by the moon's gravity it must swing back and catch the earth in such a way as to go into earth orbit. This can present a problem for the Differential Equation Solver. This is a three body problem. A change in the CSM's trajectory is influenced by the pull the moon, which in turn is affected by the pull of the earth. The solver can easily fail to converge on a solution. A change in angle by 10 degrees can result in a large change in orbit time of 4.5 days. We also must check that CSM does not crash into moon.

Below is a plot of our FRT solution for the Apollo Trajectory. It shows the CSM's x,y position and velocity from earth to moon and back. .Note the figure 8 orbit of this Free Return. The Apollo 11 flight time to the moon was 77 hours. Our simulation is for 81.4 hours. Because of instabilities, convergence problems, etc. some trial and error was required.

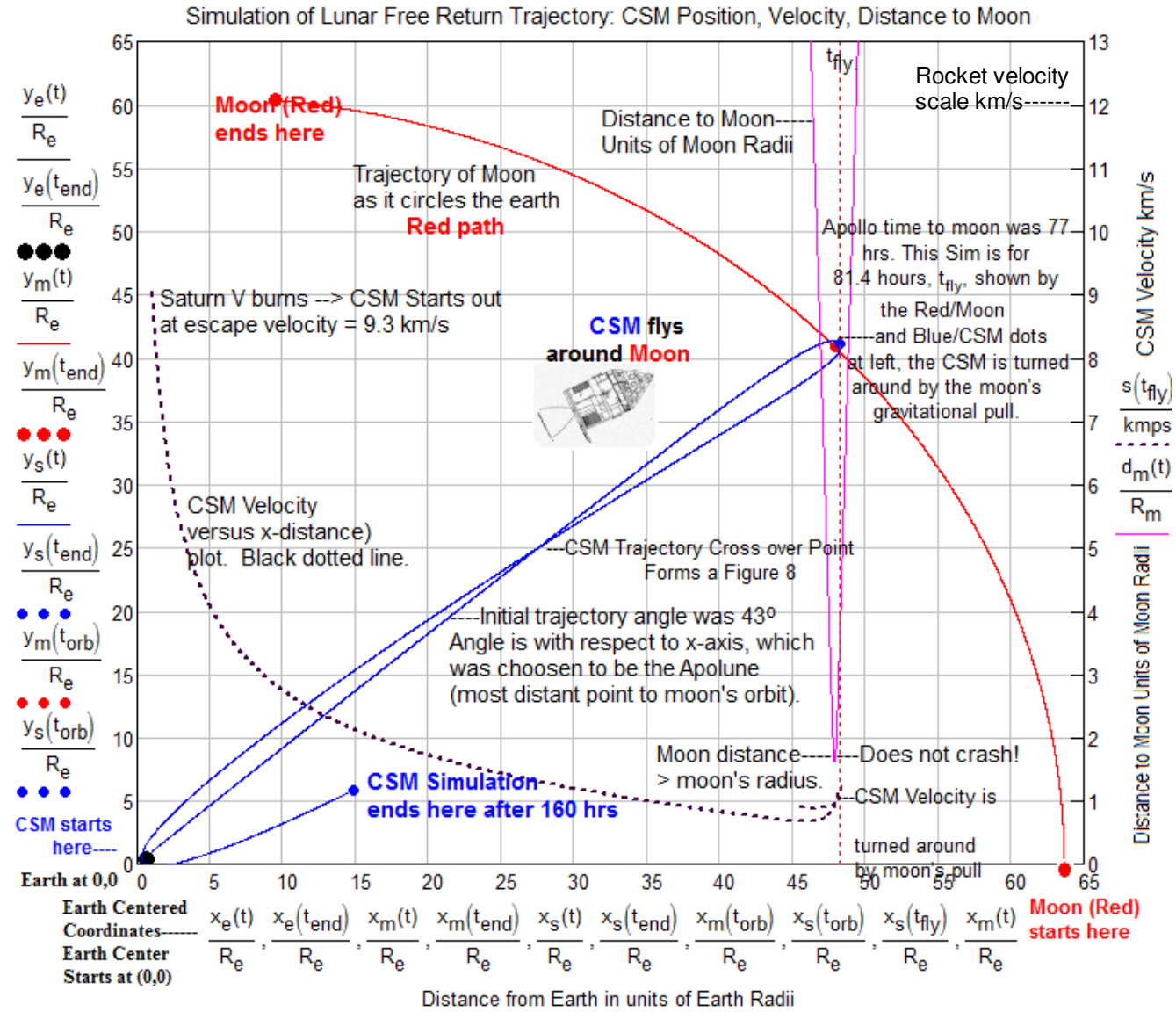

IB. 4-Body Sim of Apollo Free Return Trajectory: CSM to Moon & Back

Trajectory Model: 4-Body (Earth, Moon, Sun, Spacecraft) 2D Planar Point Mass w **Earth at Center**

This Simulation Uses the Mathcad Differential Equation Solving Methodology discussed in: arXiv:1504.07964
"Motion of the planets: the calculation and visualization in Mathcad", Valery Ochkov, Katarina Pisačić

4-Body Reference Frame: Earth and moon are initially at 0,0 and the earth and sun are initially not moving.

$kg := 1 \quad m := 1 \quad s := 1 \quad N := 1 \quad \underset{\sim}{s} := 1 \quad min := 60s \quad hr := 3600s \quad kgf := 9.80665N$

$km := 1000m \quad kmps := km \quad kph := \frac{km}{hr} \quad mph := 0.447 \cdot 10^{-3} kmps \quad n_{plot} := 10000$

Run Simulation for 115 hrs **Apollo 11 Orbit 77 hr**

$FRAME := 999 \quad n_{ode} := 20000 \quad n := 999 \quad t_{end} := \frac{114.5hr}{n+1} \cdot (FRAME + 1) \quad t_{orb} := 58.5hr$

Time of Flight (TOF) = t_{orb}

$G := 6.67384 \cdot 10^{-11} \cdot \frac{N \cdot m^2}{kg}$

Trajectory to Moon's Sphere of Influence Apolune

Initial x,y Velocity CSM	Radius of Earth	Apogee to Moon
$v_{0x} := 7.58kmps$	$R_m := 1737.4km$	$R_e := 6370km$	$d_{m\_ap} := 405500km$
$v_{0y} := 5.5kmps$	$v_{CSM} := \sqrt{v_{0x}^2 + v_{0y}^2}$	$v_{CSM} = 9.365 \cdot kmps$	$d_{e\_ap} := 152 \cdot 10^6 km$
$t_{end} = 114.5hr$			

Define Gravitational and Dynamics Equations for Earth, Moon, and CSM

e is Earth
a is Sun
m is Moon
s is CSM

$$\begin{pmatrix} m_e & x_{e0} & y_{e0} & vx_{e0} & vy_{e0} \\ m_a & x_{a0} & y_{a0} & vx_{a0} & vy_{a0} \\ m_m & x_{m0} & y_{m0} & vx_{m0} & vy_{m0} \\ m_s & x_{s0} & y_{s0} & vx_{s0} & vy_{s0} \end{pmatrix} := \begin{pmatrix} 5.972 \cdot 10^{24} kg & 0m & 0m & 0kph & 0kmps \\ 1.989 \cdot 10^{30} kg & -130 \cdot 10^6 km & -80 \cdot 10^6 km & 0kmps & 0kmps \\ 7.347 \cdot 10^{22} kg & d_{m\_ap} & 0km & 0kmps & 0.97kmps \\ 13600kg & R_e + 110km & R_e - 96km & v_{0x} & v_{0y} \end{pmatrix}$$

Given

Set of Differential Guidance Equations for 4 Body Problem of Earth, Moon, and CSM

$x_e(0) = x_{e0} \quad x_e'(0) = vx_{e0} \quad y_e(0) = y_{e0} \quad y_e'(0) = vy_{e0} \quad x_m(0) = x_{m0} \quad x_m'(0) = vx_{m0} \quad y_m(0) = y_{m0} \quad y_m'(0) = vy_{m0}$

$$m_e \cdot x_e''(t) = \frac{G \cdot m_e \cdot m_m \cdot (x_m(t) - x_e(t))}{\left[\sqrt{(x_e(t) - x_m(t))^2 + (y_e(t) - y_m(t))^2}\right]^3} + \frac{G \cdot m_e \cdot m_s \cdot (x_s(t) - x_e(t))}{\left[\sqrt{(x_e(t) - x_s(t))^2 + (y_e(t) - y_s(t))^2}\right]^3} + \frac{G \cdot m_e \cdot m_S \cdot (x_S(t) - x_e(t))}{\left[\sqrt{(x_e(t) - x_S(t))^2 + (y_e(t) - y_S(t))^2}\right]^3}$$

$$m_e \cdot y_e''(t) = \frac{G \cdot m_e \cdot m_m \cdot (y_m(t) - y_e(t))}{\left[\sqrt{(x_e(t) - x_m(t))^2 + (y_e(t) - y_m(t))^2}\right]^3} + \frac{G \cdot m_e \cdot m_s \cdot (y_s(t) - y_e(t))}{\left[\sqrt{(x_e(t) - x_s(t))^2 + (y_e(t) - y_s(t))^2}\right]^3} + \frac{G \cdot m_e \cdot m_S \cdot (y_S(t) - y_e(t))}{\left[\sqrt{(x_e(t) - x_S(t))^2 + (y_e(t) - y_S(t))^2}\right]^3}$$

$$m_m \cdot x_m''(t) = \frac{G \cdot m_m \cdot m_e \cdot (x_e(t) - x_m(t))}{\left[\sqrt{(x_m(t) - x_e(t))^2 + (y_m(t) - y_e(t))^2}\right]^3} + \frac{G \cdot m_m \cdot m_s \cdot (x_s(t) - x_m(t))}{\left[\sqrt{(x_m(t) - x_s(t))^2 + (y_m(t) - y_s(t))^2}\right]^3} + \frac{G \cdot m_m \cdot m_S \cdot (x_S(t) - x_m(t))}{\left[\sqrt{(x_m(t) - x_S(t))^2 + (y_m(t) - y_S(t))^2}\right]^3}$$

$$m_m \cdot y_m''(t) = \frac{G \cdot m_m \cdot m_e \cdot (y_e(t) - y_m(t))}{\left[\sqrt{(x_m(t) - x_e(t))^2 + (y_m(t) - y_e(t))^2}\right]^3} + \frac{G m_m \cdot m_s \cdot (y_s(t) - y_m(t))}{\left[\sqrt{(x_m(t) - x_s(t))^2 + (y_m(t) - y_s(t))^2}\right]^3} + \frac{G m_m \cdot m_S \cdot (y_S(t) - y_m(t))}{\left[\sqrt{(x_m(t) - x_S(t))^2 + (y_m(t) - y_S(t))^2}\right]^3}$$

$x_s(0) = x_{s0} \quad x_s'(0) = vx_{s0} \quad y_s(0) = y_{s0} \quad y_s'(0) = vy_{s0} \quad x_S(0) = x_{S0} \quad x_S'(0) = vx_{S0} \quad y_S(0) = y_{S0} \quad y_S'(0) = vy_{S0}$

$$m_s \cdot x_s''(t) = \frac{G \cdot m_s \cdot m_e \cdot (x_e(t) - x_s(t))}{\left[\sqrt{(x_s(t) - x_e(t))^2 + (y_s(t) - y_e(t))^2}\right]^3} + \frac{G \cdot m_s \cdot m_m \cdot (x_m(t) - x_s(t))}{\left[\sqrt{(x_s(t) - x_m(t))^2 + (y_s(t) - y_m(t))^2}\right]^3} + \frac{G \cdot m_s \cdot m_S \cdot (x_S(t) - x_s(t))}{\left[\sqrt{(x_s(t) - x_S(t))^2 + (y_s(t) - y_S(t))^2}\right]^3}$$

$$m_s \cdot y_s''(t) = \frac{G \cdot m_s \cdot m_e \cdot (y_e(t) - y_s(t))}{\left[\sqrt{(x_s(t) - x_e(t))^2 + (y_s(t) - y_e(t))^2}\right]^3} + \frac{G \cdot m_s \cdot m_m \cdot (y_m(t) - y_s(t))}{\left[\sqrt{(x_s(t) - x_m(t))^2 + (y_s(t) - y_m(t))^2}\right]^3} + \frac{G \cdot m_s \cdot m_S \cdot (y_S(t) - y_s(t))}{\left[\sqrt{(x_s(t) - x_S(t))^2 + (y_s(t) - y_S(t))^2}\right]^3}$$

$$m_S \cdot x_S''(t) = \frac{G \cdot m_S \cdot m_e \cdot (x_e(t) - x_S(t))}{\left[\sqrt{(x_e(t) - x_S(t))^2 + (y_e(t) - y_S(t))^2}\right]^3} + \frac{G \cdot m_S \cdot m_m \cdot (x_m(t) - x_S(t))}{\left[\sqrt{(x_m(t) - x_S(t))^2 + (y_m(t) - y_S(t))^2}\right]^3} + \frac{G \cdot m_S \cdot m_S \cdot (x_s(t) - x_S(t))}{\left[\sqrt{(x_s(t) - x_S(t))^2 + (y_s(t) - y_S(t))^2}\right]^3}$$

$$m_S \cdot y_S''(t) = \frac{G \cdot m_S \cdot m_e \cdot (y_e(t) - y_S(t))}{\left[\sqrt{(x_e(t) - x_S(t))^2 + (y_e(t) - y_S(t))^2}\right]^3} + \frac{G \cdot m_S \cdot m_m \cdot (y_m(t) - y_S(t))}{\left[\sqrt{(x_m(t) - x_S(t))^2 + (y_m(t) - y_S(t))^2}\right]^3} + \frac{G \cdot m_S \cdot m_S \cdot (y_s(t) - y_S(t))}{\left[\sqrt{(x_s(t) - x_S(t))^2 + (y_s(t) - y_S(t))^2}\right]^3}$$

IB. 4-Body Sim of Apollo Free Return Trajectory: CSM to Moon and Back

Trajectory Model: 4-Body (Earth, Moon, Sun, Spacecraft) 2D Planar Point Mass w **Earth at Center**

Plot for Sim of 4-Body Free Return Traj: CSM to Moon and Back

Differential Equation Solver

$$\begin{pmatrix} \text{Earth} \\ \text{Moon} \\ \text{Space Craft} \\ \text{Sun} \end{pmatrix} \begin{pmatrix} x_e \\ y_e \\ x_m \\ y_m \\ x_s \\ y_s \\ x_a \\ y_a \end{pmatrix} := \text{Odesolve}\left(\begin{pmatrix} x_e \\ y_e \\ x_m \\ y_m \\ x_s \\ y_s \\ x_a \\ y_a \end{pmatrix}, t, t_{end}, n_{ode}\right)$$

Initial Velocity (km/s) of CSM at an Altitude of 141 km:

$$\sqrt{v_{0x}^2 + v_{0y}^2} = 9.365 \cdot \text{kmps}$$

time t_{fly}, just beyond lunar fly by time $t_{flyby\ dot}$

$$t := 0, \frac{t_{end}}{n_{plot}} .. t_{end} \qquad t_{fly} := 0, \frac{t_{end}}{n_{plot}} .. 160\text{hr} \qquad t_{fly.} := \frac{x_s(t_{orb})}{R_e}$$

$$vx_s(t) := \frac{d}{dt} x_s(t) \qquad vy_s(t) := \frac{d}{dt} y_s(t) \qquad s(t) := \sqrt{vx_s(t)^2 + vy_s(t)^2}$$

Distance from Earth to Moon

$$d_{me}(t) := \left[\sqrt{(x_m(t) - x_e(t))^2 + (y_m(t) - y_e(t))^2}\right]$$

Distance to the Center of the Moon

$$d_m(t) := \left[\sqrt{(x_m(t) - x_s(t))^2 + (y_m(t) - y_s(t))^2}\right]$$

$$\frac{d_m(t_{orb})}{R_m} = 3.242$$

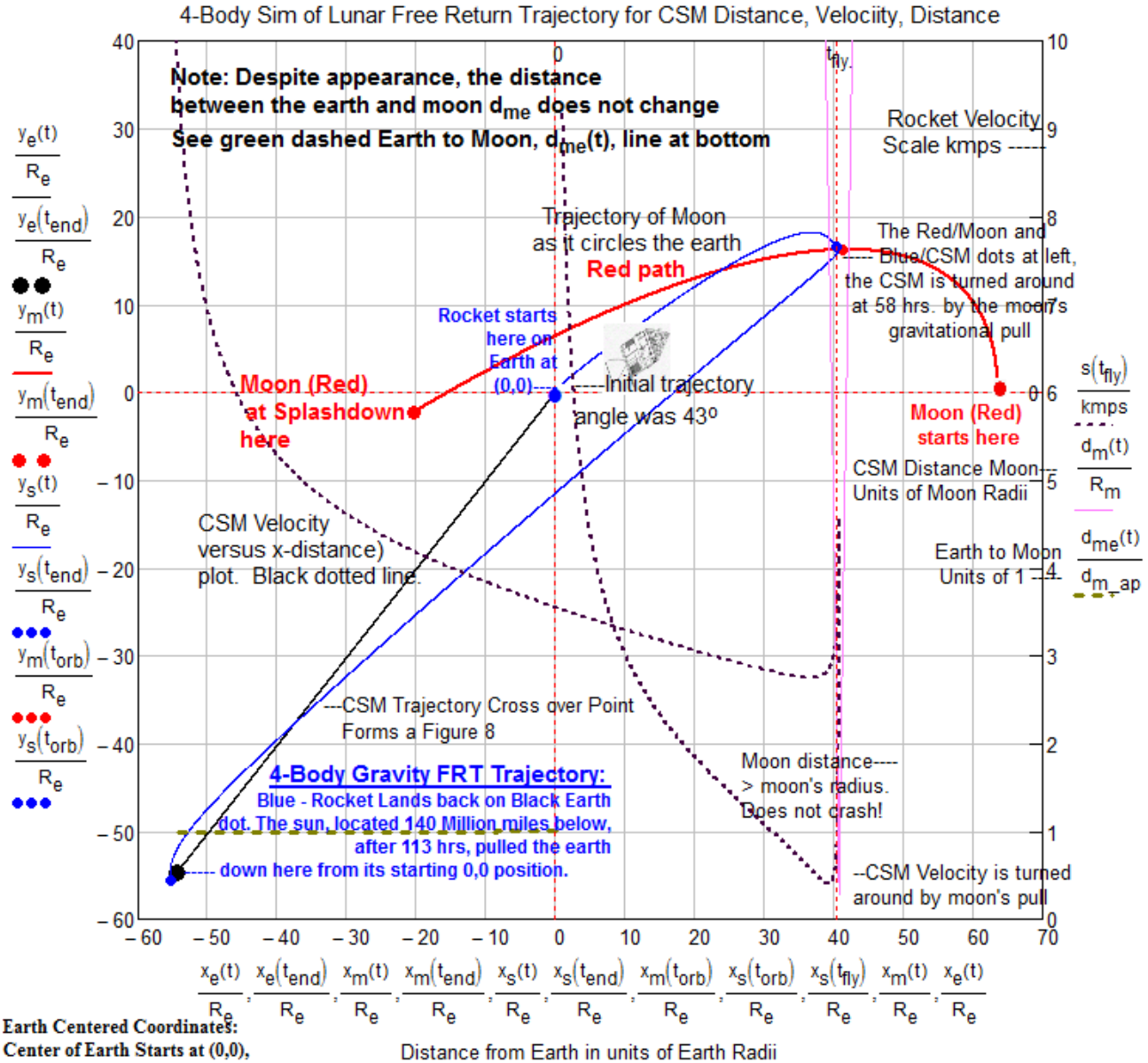

Earth Centered Coordinates: Center of Earth Starts at (0,0), but gravitational pull of sun, 94 million miles below-left of earth pulls the earth down & left from 0,0 so it ends at black dot above. The rocket (blue dot)lands back on earth 114 hours after launch.

Note: The radial velocity of the earth around the sun is 1° every 365 days or 1/365° per day. Our sim runs 114 hrs or 114/24 days. This results in (1/365°) x 114/24 or 7.5°. For the purpose of our illustration, we will ignore this added complexity. Think of this as a rotating reference frame, such as our experience of us living on a rotating earth